Spring 5-2-2022

Jet-Like Correlations in 200GeV Au+Au Collisions

Anthony Hodges

JET-LIKE CORRELATIONS IN $\sqrt{s_{NN}} = 200$ GeV Au+Au COLLISIONS

by

ANTHONY MICHAEL HODGES

A Dissertation Submitted in Partial Fulfillment of the Requirements for the Degree of

Doctor of Philosophy

in the College of Arts and Sciences

Georgia State University

2022

JET-LIKE CORRELATIONS IN $\sqrt{s_{NN}} = 200$ GeV Au+Au COLLISIONS

by

ANTHONY MICHAEL HODGES

Under the Direction of Megan Connors, PhD

ABSTRACT

Ultrarelativistic heavy-ion collisions at the Relativistic Heavy Ion Collider (RHIC) and the Large Hadron Collider (LHC) allow for a novel environment in which to study the fundamental interaction between quarks and gluons, known as the nuclear strong force. The strong force ordinarily confines quarks and gluons ("partons") to the interior of composite particles such as protons and neutrons ("hadrons"), but, in heavy-ion collisions, energy densities become sufficiently high that hadrons effectively melt into a plasma of free partons known as a Quark Gluon Plasma (QGP). Quantifying the properties of the QGP, such as its bulk viscosity, temperature, and entropy-to-shear-viscosity ratio have become key endeavors of high energy nuclear physics in the past two decades. Additionally, quantification of the

strength of the color field (the strong interaction analogy of the electromagnetic field) and how energy permeates through the plasma itself is necessary. This dissertation focuses on the latter set of objectives through the use of an experimental observable known as "jets", which are collimated sprays of particles. Additionally, jets in heavy-ion collisions have been found to have both their momentum and their shape modified relative to jets found in proton-proton collisions, where there is no QGP formation. This jet modification occurs because the parent partons of the jets have themselves been modified by the interaction with the color field inside the QGP. Thus, studying jet modification allows us to quantify properties of the QGP itself. This dissertation presents the results of examining angular correlations between jet fragments and high momentum neutral pions (π^0). Correlating jet fragments to a high momentum π^0 allows for high statistical precision, as neutral pions are one of the most abundant particles created in heavy-ion collisions. A high momentum ($p_T \geq 12$ GeV/c) π^0 can also carry up to 80% of a single jet's momentum, making them very good proxies for the jet itself kinematically. This work will utilize the largest heavy-ion data set available from the PHENIX detector, collected during 2014, containing approximately 20 billion Au+Au events.

INDEX WORDS: Quark-gluon plasma, nuclear physics, PHENIX, jet,
Direct photon-hadron correlation, sPHENIX, hadronic calorimeter

JET-LIKE CORRELATIONS IN $\sqrt{s_{NN}} = 200$ GeV Au+Au COLLISIONS

by

ANTHONY MICHAEL HODGES

Committee Chair:	Megan Connors
Committee:	Xiaochun He
	Murad Sasour
	Fabien Baron

Electronic Version Approved:

Office of Graduate Studies

College of Arts and Sciences

Georgia State University

May 2022

DEDICATION

I dedicate this dissertation to my parents, Becky and Timothy Rice. I cannot put into words the depth of my appreciation for their love and unwavering support over the course of my physics career thus far. I look forward to my continued endeavors in this field with them and their big, furry, canine companions at my side.

ACKNOWLEDGMENTS

I would firstly like to acknowledge my advisor, Megan Connors, for giving me the opportunity to start my Ph.D. career in high energy physics. Additionally, I would like to thank the continuous guidance of Xiaochun He, Murad Sarsour, and Carola Butler over the course of my Ph.D. career. Under this group's supervision, I have gained a multifaceted skill set that spans not only hardware and software knowledge, but also public speaking and mentoring. The multitude of experiences afforded me by the group have made me not just taught me about heavy ion physics, but made me a better scientist and, I hope, person as well. On the other side of this are the PHENIX and sPHENIX collaborations, who granted me multitudes of opportunities to travel to wonderful places, meet wonderful people, experience many new cultures, and represent the collaborations' collective work and progress. Specifically, the PHENIX Speaker's Bureau and the sPHENIX Hadronic Calorimeter Group were critical to these opportunities.

Finally, I must acknowledge the multitude of friends I've made along the way. My fellow graduate students Saif Ali and Uttam Acharya sweated alongside me testing thousands of scintillator tiles over the years, and Ping Wong continues to brighten my dissertation work with quips left in her macro names that I'm still discovering a year after her graduation. And I'm ever thankful to Anant Dabas and Jacob Tutterow for making the grueling summer of 2020 tile testing a little less miserable. Jacob and I also make a mean pair of spellcasters in our Dungeons and Dragons group.

TABLE OF CONTENTS

ACKNOWLEDGMENTS . . . . . **v**

LIST OF TABLES . . . . . **x**

LIST OF FIGURES . . . . . **xiv**

1 Introduction **1**

1.1 The Standard Model of Particle Physics 2

1.1.1 The Nuclear Strong Force and Quantum Chromodynamics 5

1.2 The Quark-Gluon Plasma 11

1.2.1 Creation and Evolution in Heavy-Ion Collisions 12

1.2.2 Experimental Variables and Terminology 14

1.2.3 Probing the Quark-Gluon Plasma 20

1.2.4 Theoretical Modelling 33

1.3 Purpose of This Dissertation 41

2 Heavy-Ion Colliders and Experiments **44**

2.1 The Relativistic Heavy-Ion Collider 44

2.2 PHENIX 46

2.2.1 Beam-Beam Counters 47

2.2.2 Zero-Degree Calorimeters 52

2.2.3 Central Arm Tracking 53

2.2.4 Ring-Imaging Cherenkov Detector 61

2.2.5 Electromagnetic Calorimeter 63

2.2.6 PHENIX Data sets 66

3 π^0-Triggered Two-Particle Correlations: Analysis **69**

3.1 Data Selection 69

3.1.1 Event Selection . . . 70
3.1.2 Single Photon Selection . . . 71
3.1.3 Photon Pair Selection . . . 77
3.1.4 Charged Hadron Track selection . . . 81
3.1.5 Run Selection . . . 85
3.2 Detector Corrections . . . 88
3.2.1 Charged Hadron Tracking Efficiency . . . 89
3.2.2 Acceptance Correction . . . 110
3.3 Background Flow subtraction . . . 117
3.3.1 Charged Hadron v_n Coefficients . . . 119
3.3.2 π^0 v_n Coefficients . . . 120
3.3.3 Background Magnitude Estimation via Absolute Background Subtraction . . . 123
3.3.4 Background Magnitude Estimation via ZYAM . . . 128
3.4 Extracting Physics Quantities . . . 132
3.4.1 Integrated Per-Trigger Yield Modification: $I_{AA}(p_T)$ . . . 133
3.4.2 Differential Per-Trigger Yield Modification: I_{AA} vs. $\Delta\phi$ . . . 133
3.4.3 Differential Per-Trigger Yield Modification: D_{AA} vs. $\Delta\phi$ . . . 133
4 Systematic Uncertainty . . . 135
4.1 Flow Harmonics . . . 135
4.2 ZYAM . . . 137
4.3 Absolute Background Subtraction . . . 138
4.4 Hadron Efficiency . . . 139
4.5 π^0 Combinatorial Background . . . 139
4.6 Propagation of Systematic Uncertainties . . . 147
4.6.1 Flow Harmonics and Background Subtraction . . . 147
4.6.2 Hadron Efficiency Uncertainty . . . 149

4.6.3 Combinatorial Background Uncertainty from π^0 Reconstruction . . . 149
4.6.4 Uncertainty From Baseline $p+p$ Measurements . . . 150
4.7 Summary of Systematic Uncertainties . . . 152
4.7.1 Jet Functions . . . 152
4.7.2 Yields . . . 162
4.7.3 $I_{AA}(p_T)$, I_{AA} vs. $\Delta\phi$, and D_{AA} vs $\Delta\phi$ . . . 164
5 Results . . . 191
5.1 Jet Functions . . . 191
5.2 Yields . . . 193
5.3 Away-side $I_{AA}(p_T)$ . . . 194
5.4 I_{AA} vs. $\Delta\phi$ . . . 195
5.5 $\pi^0 D_{AA}$ vs. $\Delta\phi$ . . . 198
5.6 Direct photon D_{AA} vs. $\Delta\phi$ . . . 199
6 Discussion . . . 203
6.1 Comparisons to Results in Large Nucleus-Nucleus Collisions. . . . 203
6.1.1 Comparison to Previous PHENIX Results . . . 204
6.1.2 STAR Results in 200 GeV $Au+Au$ Collisions . . . 205
6.1.3 ALICE Results from 2.76 TeV $Pb+Pb$ Collisions . . . 206
6.1.4 CMS Results in 5.02 TeV $Pb+Pb$ . . . 207
6.1.5 ATLAS Results in 5.02 TeV $Pb+Pb$ . . . 209
6.2 Comparison to Small System Results . . . 211
7 Future Prospects . . . 213
7.1 Direct Photon-Hadron Correlations . . . 213
7.2 sPHENIX . . . 220
7.2.1 The Hadronic Calorimeter . . . 220
7.2.2 Tile Testing at Georgia State University . . . 224

8 Summary 235

REFERENCES 239

Appendices 245

A Other Available PHENIX Datasets 245

A.1 2014 200 ***GeV*** $Au+Au$ ***Data*** 245

A.2 2015 200 ***GeV*** $p+p$ ***Data*** 245

A.3 2016 200 ***GeV*** $Au+Au$ ***Data*** 246

B Embedding Efficiencies for Runs 10 and Run 11 246

B.1 Run 10 246

B.2 Run 11 248

C Run 10 PC3 Matching Recalibrator in Real Data 249

D Data Table: Coefficients of Flow Harmonics 250

E Data Table: ξ 251

F Data Table: Jet Functions 252

G Data Table: Per Trigger Yields 302

H Data Table: $I_{AA}(p_T)$ 304

I Data Table: I_{AA} **vs.** $\Delta\phi$ 306

J Data Table: $\pi^0 D_{AA}$ **vs.** $\Delta\phi$ 314

K Data Table: Direct photon D_{AA} **vs.** $\Delta\phi$ 322

LIST OF TABLES

Table 1.1 Possible color states for gluons 5

Table 2.1 Summary of PHENIX minimum bias data sets 68

Table 3.1 Summary of cuts applied during particle and event selection 70

Table 3.2 Run Groups 85

Table 3.3 Values for the fit parameters in Eqn. 3.9. 105

Table 4.1 Sources of Systematic Uncertainty and Their Classification 148

Table 4.2 Systematic uncertainity sources for the hadron efficiency calculation. . 149

Table 1 Interpolated charged hadron v_n 250

Table 2 Interpolated π^0 v_2 250

Table 3 Scaling factor g_n^h 250

Table 4 ξ in Run 14 251

Table 5 0–20%, 4.0–5.0 $\otimes$ 0.5–1.0 GeV/c Jet Function 252

Table 6 0–20%, 4.0–5.0 $\otimes$ 1.0–2.0 GeV/c Jet Function 253

Table 7 0–20%, 4.0–5.0 $\otimes$ 2.0–3.0 GeV/c Jet Function 254

Table 8 0–20%, 4.0–5.0 $\otimes$ 3.0–5.0 GeV/c Jet Function 255

Table 9 0–20%, 4.0–5.0 $\otimes$ 5.0–7.0 GeV/c Jet Function 256

Table 10 0–20%, 5.0–7.0 $\otimes$ 0.5–1.0 GeV/c Jet Function 257

Table 11 0–20%, 5.0–7.0 $\otimes$ 1.0–2.0 GeV/c Jet Function 258

Table 12 0–20%, 5.0–7.0 $\otimes$ 2.0–3.0 GeV/c Jet Function 259

Table 13 0–20%, 5.0–7.0 $\otimes$ 3.0–5.0 GeV/c Jet Function 260

Table 14 0–20%, 5.0–7.0 $\otimes$ 5.0–7.0 GeV/c Jet Function 261

Table 15 0–20%, 7.0–9.0 ⊗ 0.5–1.0 GeV/c Jet Function 262
Table 16 0–20%, 7.0–9.0 ⊗ 1.0–2.0 GeV/c Jet Function 263
Table 17 0–20%, 7.0–9.0 ⊗ 2.0–3.0 GeV/c Jet Function 264
Table 18 0–20%, 7.0–9.0 ⊗ 3.0–5.0 GeV/c Jet Function 265
Table 19 0–20%, 7.0–9.0 ⊗ 5.0–7.0 GeV/c Jet Function 266
Table 20 0–20%, 9.0–12.0 ⊗ 0.5–1.0 GeV/c Jet Function 267
Table 21 0–20%, 9.0–12.0 ⊗ 1.0–2.0 GeV/c Jet Function 268
Table 22 0–20%, 9.0–12.0 ⊗ 2.0–3.0 GeV/c Jet Function 269
Table 23 0–20%, 9.0–12.0 ⊗ 3.0–5.0 GeV/c Jet Function 270
Table 24 0–20%, 9.0–12.0 ⊗ 5.0–7.0 GeV/c Jet Function 271
Table 25 0–20%, 12.0–15.0 ⊗ 0.5–1.0 GeV/c Jet Function 272
Table 26 0–20%, 12.0–15.0 ⊗ 1.0–2.0 GeV/c Jet Function 273
Table 27 0–20%, 12.0–15.0 ⊗ 2.0–3.0 GeV/c Jet Function 274
Table 28 0–20%, 12.0–15.0 ⊗ 3.0–5.0 GeV/c Jet Function 275
Table 29 0–20%, 12.0–15.0 ⊗ 5.0–7.0 GeV/c Jet Function 276
Table 30 20–40%, 4.0–5.0 ⊗ 0.5–1.0 GeV/c Jet Function 277
Table 31 20–40%, 4.0–5.0 ⊗ 1.0–2.0 GeV/c Jet Function 278
Table 32 20–40%, 4.0–5.0 ⊗ 2.0–3.0 GeV/c Jet Function 279
Table 33 20–40%, 4.0–5.0 ⊗ 3.0–5.0 GeV/c Jet Function 280
Table 34 20–40%, 4.0–5.0 ⊗ 5.0–7.0 GeV/c Jet Function 281
Table 35 20–40%, 5.0–7.0 ⊗ 0.5–1.0 GeV/c Jet Function 282
Table 36 20–40%, 5.0–7.0 ⊗ 1.0–2.0 GeV/c Jet Function 283
Table 37 20–40%, 5.0–7.0 ⊗ 2.0–3.0 GeV/c Jet Function 284
Table 38 20–40%, 5.0–7.0 ⊗ 3.0–5.0 GeV/c Jet Function 285
Table 39 20–40%, 5.0–7.0 ⊗ 5.0–7.0 GeV/c Jet Function 286

Table 40 20–40%, 7.0–9.0 ⊗ 0.5–1.0 GeV/c Jet Function 287
Table 41 20–40%, 7.0–9.0 ⊗ 1.0–2.0 GeV/c Jet Function 288
Table 42 20–40%, 7.0–9.0 ⊗ 2.0–3.0 GeV/c Jet Function 289
Table 43 20–40%, 7.0–9.0 ⊗ 3.0–5.0 GeV/c Jet Function 290
Table 44 20–40%, 7.0–9.0 ⊗ 5.0–7.0 GeV/c Jet Function 291
Table 45 20–40%, 9.0–12.0 ⊗ 0.5–1.0 GeV/c Jet Function 292
Table 46 20–40%, 9.0–12.0 ⊗ 1.0–2.0 GeV/c Jet Function 293
Table 47 20–40%, 9.0–12.0 ⊗ 2.0–3.0 GeV/c Jet Function 294
Table 48 20–40%, 9.0–12.0 ⊗ 3.0–5.0 GeV/c Jet Function 295
Table 49 20–40%, 9.0–12.0 ⊗ 5.0–7.0 GeV/c Jet Function 296
Table 50 20–40%, 12.0–15.0 ⊗ 0.5–1.0 GeV/c Jet Function 297
Table 51 20–40%, 12.0–15.0 ⊗ 1.0–2.0 GeV/c Jet Function 298
Table 52 20–40%, 12.0–15.0 ⊗ 2.0–3.0 GeV/c Jet Function 299
Table 53 20–40%, 12.0–15.0 ⊗ 3.0–5.0 GeV/c Jet Function 300
Table 54 20–40%, 12.0–15.0 ⊗ 5.0–7.0 GeV/c Jet Function 301
Table 55 Away side yield, 0–20% 302
Table 56 Away side yield, 20–40% 303
Table 57 0–20%, Away side $I_{AA}(p_T)$ 304
Table 58 20–40%, Away side $I_{AA}(p_T)$ 305
Table 59 0–20%, trigger p_T 4.0–5.0 Away–side $I_{AA}(\Delta\phi)$ 306
Table 60 0–20%, trigger p_T 5.0–7.0 Away–side $I_{AA}(\Delta\phi)$ 307
Table 61 0–20%, trigger p_T 7.0–9.0 Away–side $I_{AA}(\Delta\phi)$ 308
Table 62 0–20%, trigger p_T 9.0–12.0 Away–side $I_{AA}(\Delta\phi)$ 309
Table 63 20–40%, trigger p_T 4.0–5.0 Away–side $I_{AA}(\Delta\phi)$ 310
Table 64 20–40%, trigger p_T 5.0–7.0 Away–side $I_{AA}(\Delta\phi)$ 311

Table 65 20–40%, trigger p_T 7.0–9.0 Away–side $I_{AA}(\Delta\phi)$ 312

Table 66 20–40%, trigger p_T 9.0–12.0 Away–side $I_{AA}(\Delta\phi)$ 313

Table 67 0–20%, trigger p_T 4.0–5.0 Away–side $D_{AA}(\Delta\phi)$ 314

Table 68 0–20%, trigger p_T 5.0–7.0 Away–side $D_{AA}(\Delta\phi)$ 315

Table 69 0–20%, trigger p_T 7.0–9.0 Away–side $D_{AA}(\Delta\phi)$ 316

Table 70 0–20%, trigger p_T 9.0–12.0 Away–side $D_{AA}(\Delta\phi)$ 317

Table 71 20–40%, trigger p_T 4.0–5.0 Away–side $D_{AA}(\Delta\phi)$ 318

Table 72 20–40%, trigger p_T 5.0–7.0 Away–side $D_{AA}(\Delta\phi)$ 319

Table 73 20–40%, trigger p_T 7.0–9.0 Away–side $D_{AA}(\Delta\phi)$ 320

Table 74 20–40%, trigger p_T 9.0–12.0 Away–side $D_{AA}(\Delta\phi)$ 321

Table 75 D_{AA} vs. $\Delta\phi$ data points for $2 < \xi < 2.4$ 322

Table 76 D_{AA} vs. $\Delta\phi$ data points for $1.6 < \xi < 2$ 322

Table 77 D_{AA} vs. $\Delta\phi$ data points for $1.2 < \xi < 1.6$ 322

Table 78 D_{AA} vs. $\Delta\phi$ data points for $0.8 < \xi < 1.2$ 322

Table 79 D_{AA} vs. $\Delta\phi$ data points for $0.4 < \xi < 0.8$ 322

Table 80 D_{AA} vs. $\Delta\phi$ data points for $0.0 < \xi < 0.4$ 323

LIST OF FIGURES

Figure 1.1 Stand model of elementary particles which are categorized into quarks (purple), leptons (green) and force carriers (blue). The particle properties such as mass, charge, spin, and name are labeled in each grid [4]. 3

Figure 1.2 Feynman diagrams of strong interactions. Left: quark-gluon interaction. Center and Right: gluon-gluon interactions. 7

Figure 1.3 The coupling constant, α_s, of the strong interaction as a function of squared momentum transfer Q^2 obtained from different experiments [12]. . . 10

Figure 1.4 The phase diagram for QCD as a function of temperature and baryon chemical potential. The different white lines represent phase transitions. The green and purple lines represent regions of the phase space probed by different collider experiments. 11

Figure 1.5 Evolution of heavy-ion collisions [14] 13

Figure 1.6 Depiction of the coordinate system used in heavy-ion collisions. The beam line is directed through the page horizontally along the z-axis, with the positive y-axis pointed upwards, and the positive x-axis directed into the page. 15

Figure 1.7 ((a)) Pseudorapidity η plotted as a function of θ. The blue dot is at (90°,0). ((b)) Translation of common angles into units of pseudorapidity [19] 17

Figure 1.8 Visual representations of N_{Part}, N_{Coll}, and the impact parameter b in heavy-ion collisions [20]. 18

Figure 1.9 Centrality determination via charged particle multiplicity. The bottom x-axis represents the amount of charged tracks measured in the MBD, the y-axis represents the inelastic cross-section, and the top x-axis represents an approximation of the impact parameter in femtometers[22]. 19

Figure 1.10 Cartoon depicting a collision of large nuclei. The left side shows the formation of the Quark-Gluon Plasma with a elliptic shape owed to the initial elliptic shape of the overlap region of the two nuclei. The right picture shows how this spatial anisotropy leads to particles emerging with different momentum due to their interactions with the medium [23]. 20

Figure 1.11 Two-particle correlation results from the ATLAS experiment [24] in (a) $Pb-Pb$ collisions at $\sqrt{s_{NN}} = 5.02$TeV, (b) $p+Pb$ collisions at $\sqrt{s_{NN}} = 5.02$TeV, and (c) $p+p$ collisions at $\sqrt{s_{NN}} = 13$TeV. As the collision systems get larger, the amount of correlations found at large $|\eta|$ away from $(\Delta\phi, \Delta\eta) \approx (0, 0)$ becomes very large due to contributions from ellitpic flow. 21

Figure 1.12 Proton and π^- Directed flow, v_1 as a function of rapidity y in $Au+Au$ collisions at varying center of mass energies. The black stars, red circles, and blue diamonds represent the $0-10\%, 10-40\%$, and $40-70\%$ centrality bins, respectively. Each row is a different center of mass energy [25]. 23

Figure 1.13 v_2 (red), v_3 (blue), and v_4 (ink) for charged hadrons as a function of centrality percentile in 2.76 TEV $Pb+Pb$ collisions [26] 24

Figure 1.14 Monte Carlo simulation showing how a triangular overlap region can occur in the initial stages of heavy ion collisions, thus leading to nonzero v_3 [27]. 24

Figure 1.15 Left: Charged hadron v_2 as a function of p_T and $KE_T$for various hadron species as measured by the PHENIX and STAR experiments in minimum bias $Au + Au$ collisions at 200GeV. Right: v_2 for as function of p_T and KE_T for various hadron species after scaling by the number of constituent quarks for each species [28]. 25

Figure 1.16 R_{AA} as a function of transverse momentum for a variety of particle species in $0-20\%$ 200GeV $Au+Au$ collisions as measured by the PHENIX detector [29]. 28

Figure 1.17 A dijet in $\Delta\phi$ space. The arrows represent different jet fragments, and their magnitude represents their momenta. 29

Figure 1.18 An example of a two-particle correlation measurement made in PYTHIA. (a) Correlations between a trigger particle and associated charged hadrons in $\Delta\phi\Delta\eta$-space. (b) The same correlation measurement, but projected onto the $\Delta\phi$ axis [15] 29

Figure 1.19 Top: Two-particle correlation distributions for minimum bias $d+Au$ collisions (Green), central $d+Au$ collisions (Red), for $p+p$ collisions (Black). Bottom: Comparison of two-particle correlations distributions for central $d+Au$ collisions (Green) to those seen in $p+p$ (Black) and central $Au+Au$ collisions (Red) [30] 30

Figure 1.20 Inclusive photon-hadron (Green diamonds), decay photon-hadron (Red squares), and direct photon-hadron (Black dots) in 200 GeV $p+p$ collisions (Top) and 200 GeV $Au+Au$ collisions (Bottom) [31] 31

Figure 1.21 I_{AA} as a function of the associate hadron p_T^h in four separate direct photon p_T bins, alongside the I_{AA} for hadron-hadron correlations for $5 < p_T^{Trigger} < 10$ GeV/c in the upper left hand panel [31]. 33

Figure 1.22 I_{AA} as a function of ξ in direct photon-hadron correlations in three direct photon momentum ranges. Solid curves are calculations from CoLBT-Hydro[33], and the dashed curve is from a Borghini-Wiedemann modified leading logarithmic approximation (BW-MLLA) calculation [35]. 37

Figure 1.23 Top: Z boson-hadron angular correlations in 5.02TeV $p+p$ collisions (Blue) and 5.02TeV $Pb+Pb$ collisions (Red). Bottom D_{AA} vs. $\Delta\phi$. 39

Figure 2.1 Alternating Gradient Synchrotron (AGS) and RHIC at Brookhaven National Laboratory. 44

Figure 2.2 2011 and onwards configuration of the PHENIX detector. The subsystem of note here is the Silicon Vertex Detector located at the interaction point 46

Figure 2.3 Left: The beam-beam counter in its entirety. The 64 photomultiplier tubes of the BBC are located at the front, and in back are the readout electronics. Right: A single BBC PMT consisting of a 30 mm long quartz Cherenkov radiator connected to a 54 mm long PMT. The whole tube is covered with a hexagonal piece of shielding used to keep out excess light [47]. 47

Figure 2.4 Distribution of the total charge embedded in both the BBC north and south collected over all of Run 16's minimum bias events for $|z| < 30$cm. . . 50

Figure 2.5 Centrality distribution for Run 16's minimum bias data set. 51

Figure 2.6 Number of events in a given centrality range as a function of run number for Run 16's minimum bias data set. 52

Figure 2.7 Depiction of ZDC's and dipole magnets along the beam pipe. The black lines represent the ion beams, and neutron and charged particle trajectories are represented by green and red lines, respectively. Unlike neutrons, charged particle trajectories bend because of the dipole magnet and miss the ZDC's [48]. 53

Figure 2.8 Left: mechanical drawing of the PHENIX Drift Chamber. Center: Drawing of a sector of the drift chamber with 6 layers of wire labelled as X1, X2, U1, U2, V1, and V2. Right: Top view of the wire orientations from three neighboring sectors 55

Figure 2.9 Cartoon of a single track traversing the PHENIX drift chamber. Here one can see depictions of the polar angle ϕ and the inclination angle α 57

Figure 2.10 Cartoon depiction of the location of the PHENIX Pad Chambers (PC1, PC2, and PC3) within the central arms. Distances to interaction point and other measurements of interest are also shown 58

Figure 2.11 Left: PC1 readout pad consisteing of nine pixels grouped together in a staggered configuration. While shown for PC1, the outer pad chambers have similar configurations which accomplish a comparable angular resolution, albeit with larger pixels. Right: pads are arrangement into an inter-locking pattern such that three vertically adjacent pixels form a cell. These cells form the fundamental component of a pad chamber cluster. 59

Figure 2.12 Internal configuration of a PHENIX Pad Chamber panel 60

Figure 2.13 Left: Outer view of the RICH subsystem. Right: Cutaway drawing showing Cherenkov light rays being reflected into the PMT array by a spherical mirror (not depicted). 61

Figure 2.14 Left: Cherenkov light from an electron being focused onto the PMT array by the RICH's mirrors. Right: Rings of Cherenkov light hitting PMT's. In this analysis, if any PMT is fired by a track with momentum beneath 5GeV/c, the track is vetoed. 63

Figure 2.15 Left: A lead-scintillator module with a cutaway through which one can see the four individual towers that compose the modules. Right: Schematic of a lead-glass supermodule composed of 24 individual models. 65

Figure 2.16 Left: Electromagnetic shower initiated by electronic bremsstrahlung. Right: Electromagnetic shower initiated by a photon undergoing pair production. 66

Figure 3.1 Hit maps of clusters within the EMCal for clusters with $3 < E_{Cluster} <$ 7 GeV before the removal of bad towers. The color scale represents how many times a cluster registered within a given tower. Sectors 0 through 5 are lead-scintillator, while sectors 6 and 7 are lead-glass 72

Figure 3.2 Hit maps of clusters within the EMCal for clusters with $7 < E_{Cluster} <$ 12 GeV before the removal of bad towers. The color scale represents how many times a cluster registered within a given tower. Sectors 0 through 5 are lead-scintillator, while sectors 6 and 7 are lead-glass 73

Figure 3.3 Hit maps of clusters within the EMCal for clusters with $3 < E_{Cluster} <$ 7 GeV after the removal of bad towers. The color scale represents how many times a cluster registered within a given tower. Sectors 0 through 5 are lead-scintillator, while sectors 6 and 7 are lead-glass 74

Figure 3.4 Hit maps of clusters within the EMCal for clusters with $7 < E_{Cluster} < 9$ GeV after the removal of bad towers. The color scale represents how many times a cluster registered within a given tower. Sectors 0 through 5 are lead-scintillator, while sectors 6 and 7 are lead-glass 75

Figure 3.5 The impact of each cut on the inclusive photon spectrum in the 0–20% centrality bin. The cuts are applied sequentially going from left to right and top to bottom in the legend. Some cuts can be hidden because their impact is negligible; thus, the next cut sits on top of it. 76

Figure 3.6 The impact of each cut on the inclusive photon spectrum in the 20–40% centrality bin. The cuts are applied sequentially going from left to right and top to bottom in the legend. Some cuts can be hidden because their impact is negligible; thus, the next cut sits on top of it. 77

Figure 3.7 Invariant mass distributions in each π^0 momentum region in the 0–20% (Top) and 20–40% (Bottom) centrality classes. The red solid line represents the total fit to the spectrum, whereas the blue dashed line is the background only. The vertical red dashed lines represent the nominal invariant mass window range of 0.12 GeV/c^2 to 0.16 GeV/c^2, and the vertical blue dashed lines represent the upper and lower sideband regions used to compute the π^0 reconstruction systematic uncertainty, discussed in Sec. 4.5 79

Figure 3.8 π^0 p_T distribution for the 0–20% centrality class (Left) and the 20–40% centrality class (Right) in the Run 14 200 GeV $Au + Au$ data set. 80

Figure 3.9 Impact of different cuts on the raw π^0 spectrum in the 0–20% centrality class 80

Figure 3.10 Impact of different cuts on the raw π^0 spectrum in the 20–40% centrality class 81

Figure 3.11 Spectra of associate hadrons in the Run 14 200 GeV $Au + Au$ data set in the 0–20% (Left) and 20–40% (Right) centrality bins. 83

Figure 3.12 Impact of individual cuts on the associate hadron spectrum in the 0–20% centrality bin. 84

Figure 3.13 Impact of individual cuts on the associate hadron spectrum in the 20–40% centrality bin. 84

Figure 3.14 Summed event-mixing background correlation functions in different run groups. These correlation functions are normalized to 1. 86

Figure 3.15 Distribution of standard deviations for each run in the 2014 data set. A Gaussian fit is used to extract the mean and the standard deviation, σ, in the peak region and is shown by the solid red line. The red dashed line indicates $\mu + 3\sigma$, beyond which a run becomes "bad". 87

Figure 3.16 Examples of bad runs in Run 14. The event-mixing background correlation fucntions from each run (black) and from the corresponding run group (red) are drawn on the left in each panel. The ratio of the two is shown on the right of each panel. 87

Figure 3.17 Number of charged hadron tracks per event as a function run number (top) and number of events as a function of run number (bottom). The blue dashed lines indicate the different run groups. From left to right are groups 0 to group 5. Bad runs are drawn in red. 88

Figure 3.18 Initial kinematics for simulated hadrons used in the efficiency calculation. The z-vertex distribution is based off of real data from the 2014 200 GeV $Au + Au$ data set. 90

Figure 3.19 Left: unweighted input p_T spectrum. Right: input p_T spectrum weighted by fit to published spectrum [51]. The re-weighted distribution also has a much higher bin count to take advantage of the increased simulation statistics used in this efficiency calculation 91

Figure 3.20 Track position distributions for real (blue) and simulated (red) tracks before (Left) and after (Right) normalization to remove differences purely due to statistical differences between the simulated real sets of track data. 93

Figure 3.21 Example fit to the $d\phi$ track matching variable from Run 10's simulation. The blue fit is for the wider Gaussian with width parameter σ_2, and the black curve represents the Gaussian fit to the signal region with width paraemter σ_1. The red curve present is the total fit that contains both signal and background components. 95

Figure 3.22 Fits to the μ and σ of the track matching parameter dz in Run 10 simulation. The red corresponds to negatively charged pions, and the blue corresponds to positively charged pions. 96

Figure 3.23 Fits to the μ and σ of the track matching parameter $d\phi$ in Run 10 simulation. The red corresponds to negatively charged pions, and the blue corresponds to positively charged pions. 97

Figure 3.24 Distributions of the sigmalized dz values in units of $n\sigma$ as a function of p_T^{Hadron} for positive (Blue) and negative (Red) pions in Run 10 simulation. 99

Figure 3.25 Distributions of the sigmalized $d\phi$ values in units of $n\sigma$ as a function of p_T^{Hadron} for positive (Blue) and negative (Red) pions in Run 10 simulation.remo100

Figure 3.26 Left: Number of tracks with a given circular sigma value in different p_T ranges as described in the legend before undergoing the PC3 matching recalibration procedure. Right: Number of tracks with a given circular sigma value in different p_T ranges as described in the legend after undergoing the PC3 matching recalibration procedure. Both come from Run 10 simulation . 101

Figure 3.27 Number of tracks with a given circular sigma value in different p_T ranges as described in the legend before undergoing the PC3 matching recalibration procedure in Run 14 simulation. 101

Figure 3.28 The combined output spectrum for all particle species from simulation. The different spectra show the impact of a given cut on the input spectrum. 102

Figure 3.29 Top: Input (blue) and output (red) particle distributions for all particle species. Bottom: Identified hadron efficiencies. 103

Figure 3.30 Blue: Identified hadron ratios before being scaled by their abundance relative to $\pi^{\pm}$'s. Red: Identified hadron ratios after being scaled by their abundance relative to $\pi^{\pm}$'s. 104

Figure 3.31 Non identified hadron efficiency as a function of hadron p_T. The red curve is the fit to the data points. 105

Figure 3.32 Yield of S-Type tracks in the 0–20% (Left) and 20–40% (Right) centrality bins for Run 14. 107

Figure 3.33 Yield of R-Type tracks in the 0–20% (Left) and 20–40% (Right) centrality bins for Run 14. 108

Figure 3.34 Embedding efficiencies for Run 14 in the 0–20% (Left) and 20–40% (Right) centrality bins for Run 14. 108

Figure 3.35 Embedding efficiencies for Run 10 (Blue), Run 11 (Red) and Run 14 with a stanrd circular track matching cut (Black) and a 1σ circular track matching cut for $p_T^{Track} \geq 5$ GeV/c 110

Figure 3.36 Illustrations of detector acceptance effect on angular correlation measurements. The grey areas represent the PHENIX central arm detectors, the blue arrow represents a trigger particle, and the yellow arrow represents an associated charged track. Left: example of accepted correlation. Right: example of missed correlation where the charged track is missed by the detector because of limited acceptance.. 111

Figure 3.37 Same-event (black dots) and mixed-event (red circles) correlations in the 0–20% centrality class in Run 14. The top set of numbers represent the charged hadron momentum bins, and the righthand set of numbers represent the π^0 momentum bins 113

Figure 3.38 Same-event (black dots) and mixed-event (red circles) correlations in the 20–40% centrality class in Run 14. The top set of numbers represent the charged hadron momentum bins, and the righthand set of numbers represent the π^0 momentum bins 114

Figure 3.39 Correlation functions in Run 14 0–20% after tracking and embedding efficiency and detector acceptance corrections. The top set of numbers represent the charged hadron momentum bins, and the righthand set of numbers represent the π^0 momentum bins 115

Figure 3.40 Correlation functions in Run 14 20–40% after tracking and embedding efficiency and detector acceptance corrections. The top set of numbers represent the charged hadron momentum bins, and the righthand set of numbers represent the π^0 momentum bins 116

Figure 3.41 v_2^h values in different centrality classes. The open circles are from experimental results [56]. The black dots are the merged values from the open circles. 119

Figure 3.42 Merged (solid dots) and interpolated (open circles) v_n^h values. The blue dash lines are the fits of the nominal, upper and lower bounds values of the solid points. 120

Figure 3.43 Merged $v_2^{\pi^0}$ values (black dots) in 0–20% (left) and 20–40% (right) centrality bins. The red and blue data points are the measured values from [58]. 121

Figure 3.44 Merged (dots) and interpolated (circle) $v_2^{\pi^0}$ values in 0–20% (Left) and 20–40% (Right) centrality bins. The red dash lines are the fits of the nominal, upper and lower error bars of the merged $v_2^{\pi^0}$ values. 121

Figure 3.45 g_3 (top row) and g_4 (bottom row) calculated using charged hadron v_n in [56] in different centrality classes. The dash lines are the constant fits and their upper and lower bound values. 123

Figure 3.46 Yield of trigger (top) and associate charged hadrons (bottom) as functions of N_{part} from Run 14 data. 126

Figure 3.47 Yield of trigger (top) and associate particles (bottom) as function of N_{coll} from Run 14 data. 127

Figure 3.48 ξ as a function of centrality in different trigger and associate p_T ranges from Run 14. 128

Figure 3.49 Fits to correlation functions measured in Run 14 in the 0–20% centrality class. 129

Figure 3.50 Fits to correlation functions measured in Run 14 in the 20–40% centrality class. 130

Figure 3.51 Correlation functions (black points), collective flow (red curve) and background level (dashed red line) in the 0-20% centralty class. 131

Figure 3.52 Correlation functions (black points), collective flow (red curve) and background level (dashed red line) in the 20-40% centralty class. 132

Figure 4.1 Example of an invariant mass spectrum. The blue dash line represents the background level, and the red solid line is a fit to both the combinatorial background and the signal. The vertical dashed lines indicate the signal invariant π^0 mass window (red), and side-band mass windows (blue). 140

Figure 4.2 Invariant mass spectra π^0 p_T bins. The total fit to the data is the red solid line, and the solid blue line represents the fit to the background. The dotted lines represent the nominal invariant mass range (red) and the side band windows (blue) used in this analysis. The top row is from the 0–20% centrality class and the bottom row is from the 20–40% centrality class. . . . 141

Figure 4.3 Signal-to-background ratio for reconstructed π^0's as a function of π^0 p_T in the 0–20% (black) and 20–40% centrality classes. 142

Figure 4.4 Near (top) and away-side (bottom) per trigger yields as a function of associate p_T in different trigger p_T bins in 0–20% centrality. Per trigger yields obtained from side-band and π^0 mass peak regions are drawn in red and black, respectively. The ratios of per trigger yields from different mass windows are drawn at the bottom of each panel. 143

Figure 4.5 Near (top) and away-side (bottom) per trigger yields as a function of associate p_T in different trigger p_T bins in 20–40% centrality. See Figure 4.4 for description. 143

Figure 4.6 Relative background π^0 systematic uncertainty as a function of associate p_T in near (top) and away-side (bottom) peaks in the 0–20% centrality class. The trigger p_T is labeled on the top of each panel. 146

Figure 4.7 Relative background π^0 systematic uncertainty as a function of associate p_T in near (top) and away-side (bottom) peaks in the 20–40% centrality class. The trigger p_T is labeled on the top of each panel. 147

Figure 4.8 Jet functions in 0–20% centrality class with systematic uncertainties from only the second order flow harmonic drawn as boxes. 153

Figure 4.9 Jet functions in 02–40% centrality class with systematic uncertainties from only the second order flow harmonic drawn as boxes. 154

Figure 4.10 Jet functions in 0–20% centrality class with systematic uncertainties from only the third order flow harmonic drawn as boxes. 155

Figure 4.11 Jet functions in 20–40% centrality class with systematic uncertainties from only the third order flow harmonic drawn as boxes. 156

Figure 4.12 Jet functions in 0–20% centrality class with systematic uncertainties from only the fourth order flow harmonic drawn as boxes. 157

Figure 4.13 Jet functions in 20–40% centrality class with systematic uncertainties from only the fourth order flow harmonic drawn as boxes. 158

Figure 4.14 Jet functions in 0–20% centrality with systematic uncertainty from ZYAM for $p_T^{Hadron} < 1$ GeV/c and Absolute Background Subtraction for $p_T^{Hadron} > 1$ GeV/c drawn as boxes. 159

Figure 4.15 Jet functions in 20–40% centrality with systematic uncertainty from ZYAM for $p_T^{Hadron} < 1$ GeV/c and Absolute Background Subtraction for $p_T^{Hadron} > 1$ GeV/c drawn as boxes. 160

Figure 4.16 Jet functions in 0–20% centrality with systematic uncertainty from combinatorial π^0 reconstruction process drawn as box. 161

Figure 4.17 Jet functions in 20–40% centrality with systematic uncertainty from combinatorial π^0 reconstruction process drawn as box. 162

Figure 4.18 Relative uncertainties in away-side yield in 0–20% centrality. 163

Figure 4.19 Relative uncertainties in away-side yield in 20–40% centrality. 164

Figure 4.20 Relative uncertainties from various sources on the away-side I_{AA} in the 0–20% centrality class. 165

Figure 4.21 Relative uncertainties from various sources on the away-side I_{AA} in 20–40% centrality class. 166

Figure 4.22 Away-side I_{AA} vs. $\Delta\phi$ in the 0–20% centrality class with only the systematic uncertainty arising from, σ^{f2}, the second order flow harmonics drawn. 167

Figure 4.23 Away-side I_{AA} vs. $\Delta\phi$ in the 20–40% centrality class with only the systematic uncertainty arising from, σ^{f2}, the second order flow harmonics drawn. 168

Figure 4.24 Away-side I_{AA} vs. $\Delta\phi$ in the 0–20% centrality class with only the systematic uncertainty arising from, σ^{f3}, the third order flow harmonics drawn. 169

Figure 4.25 Away-side I_{AA} vs. $\Delta\phi$ in the 20–40% centrality class with only the systematic uncertainty arising from, σ^{f3}, the third order flow harmonics drawn. 170

Figure 4.26 Away-side I_{AA} vs. $\Delta\phi$ in the 0–20% centrality class with only the systematic uncertainty arising from, σ^{f4}, the fourth order flow harmonics drawn. 171

Figure 4.27 Away-side I_{AA} vs. $\Delta\phi$ in the 20–40% centrality class with only the systematic uncertainty arising from, σ^{f4}, the fourth order flow harmonics drawn. 172

Figure 4.28 Away-side I_{AA} vs. $\Delta\phi$ in the 0–20% centrality class with only the systematic uncertainty arising from underlying event subtraction drawn. . . 173

Figure 4.29 Away-side I_{AA} vs. $\Delta\phi$ in the 20–40% centrality class with only the systematic uncertainty arising from the underlying event subtraction drawn. 174

Figure 4.30 Away-side I_{AA} vs. $\Delta\phi$ in the 0–20% centrality class with only the systematic uncertainty arising from the π^0 reconstruction process drawn. . . 175

Figure 4.31 Away-side I_{AA} vs. $\Delta\phi$ in the 20–40% centrality class with only the systematic uncertainty arising from the π^0 reconstruction process drawn. . . 176

Figure 4.32 Away-side I_{AA} vs. $\Delta\phi$ in the 0–20% centrality class with only the systematic uncertainty arising from the $p+p$ baseline drawn. 177

Figure 4.33 Away-side I_{AA} vs. $\Delta\phi$ in the 20–40% centrality class with only the systematic uncertainty arising from the $p+p$ baseline drawn. 178

Figure 4.34 Away-side D_{AA} vs. $\Delta\phi$ in the 0–20% centrality class with only the systematic uncertainty arising from, σ^{f2}, the second order flow harmonics drawn. 179

Figure 4.35 Away-side D_{AA} vs. $\Delta\phi$ in the 20–40% centrality class with only the systematic uncertainty arising from, σ^{f2}, the second order flow harmonics drawn. 180

Figure 4.36 Away-side D_{AA} vs. $\Delta\phi$ in the 0–20% centrality class with only the systematic uncertainty arising from, σ^{f3}, the third order flow harmonics drawn. 181

Figure 4.37 Away-side D_{AA} vs. $\Delta\phi$ in the 20–40% centrality class with only the systematic uncertainty arising from, σ^{f3}, the third order flow harmonics drawn. 182

Figure 4.38 Away-side D_{AA} vs. $\Delta\phi$ in the 0–20% centrality class with only the systematic uncertainty arising from, σ^{f4}, the fourth order flow harmonics drawn. 183

Figure 4.39 Away-side D_{AA} vs. $\Delta\phi$ in the 20–40% centrality class with only the systematic uncertainty arising from, σ^{f4}, the fourth order flow harmonics drawn. 184

Figure 4.40 Away-side D_{AA} vs. $\Delta\phi$ in the 0–20% centrality class with only the systematic uncertainty arising from underlying event subtraction drawn. . . 185

Figure 4.41 Away-side D_{AA} vs. $\Delta\phi$ in the 20–40% centrality class with only the systematic uncertainty arising from the underlying event subtraction drawn. 186

Figure 4.42 Away-side D_{AA} vs. $\Delta\phi$ in the 0–20% centrality class with only the systematic uncertainty arising from the π^0 reconstruction process drawn. . . 187

Figure 4.43 Away-side D_{AA} vs. $\Delta\phi$ in the 20–40% centrality class with only the systematic uncertainty arising from the π^0 reconstruction process drawn. . . 188

Figure 4.44 Away-side D_{AA} vs. $\Delta\phi$ in the 0–20% centrality class with only the systematic uncertainty arising from the $p+p$ baseline drawn. 189

Figure 4.45 Away-side D_{AA} vs. $\Delta\phi$ in the 20–40% centrality class with only the systematic uncertainty arising from the $p+p$ baseline drawn. 190

Figure 5.1 π^0–hadron jet functions measured in 200 GeV $Au+Au$ collisions in the 0–20% centrality class. p_T^{Trig} increases as one goes from the top of set of plots to the bottom, and p_T^{Hadron} increases as one goes from left to right. ± 6.9 scale uncertainty not shown. 192

Figure 5.2 π^0–hadron jet functions measured in 200 GeV $Au+Au$ collisions in the 20–40% centrality class. p_T^{Trig} increases as one goes from the top of set of plots to the bottom, and p_T^{Hadron} increases as one goes from left to right. ± 6.9 scale uncertainty not shown. 193

Figure 5.3 Integrated away-side yields in 200 GeV $Au+Au$ collisions in the 0–20% (Black) and 20–40% (Red) centrality classes. The $p+p$ baseline is plotted in blue for reference. 194

Figure 5.4 Away-side I_{AA} as a function of the associate hadron momentum measured in 0–20% (Black) and 20–40% centrality classes. 195

Figure 5.5 The I_{AA} vs. $\Delta\phi$ for the 4–5 GeV/c π^0 momentum bin. The points here are from the 0.5–1 associate hadron momentum bin. 196

Figure 5.6 The I_{AA} vs. $\Delta\phi$ for the 4–5 GeV/c π^0 momentum bin. There are multiple hadron momentum ranges which are defined by the legend. 197

Figure 5.7 The I_{AA} vs. $\Delta\phi$ for the 4–5 GeV/c π^0 momentum bin. There are multiple hadron momentum ranges which are defined by the legend. 197

Figure 5.8 Top: Folded per-trigger yields versus $\Delta\phi$ from 200 GeV 0–20$ $Au+Au$ (Black) and $p+p$ (Blue) collisions. Each column is a different π^0 momentum bin, and the associate hadron momentum ranges between 0.5–1 GeV/c. Bottom: D_{AA} vs. $\Delta\phi$. 199

Figure 5.9 Top: Folded per-trigger yields versus $\Delta\phi$ from 200 GeV 20–40% $Au+Au$ (Black) and $p+p$ (Blue) collisions. Each column is a different π^0 momentum bin, and the associate hadron momentum ranges between 3–5 GeV/c. Bottom: D_{AA} vs. $\Delta\phi$. 199

Figure 5.10 Direct photon-hadron jet functions in 0–40% 200 GeV $Au+Au$ collisions (Black) and 200 GeV $p+p$ collisions (Blue) [34] for $5 < p_T^\gamma < 9$ GeV/c. Only the away-side ($\pi/2 < \Delta\phi < \pi$) is shown here to correspond to the D_{AA} vs. $\Delta\phi$ shown in Fig. 5.11. The dashed line represents zero. 200

Figure 5.11 D_{AA} vs. $\Delta\phi$ for direct photon-hadron correlations in 0–40% 200 GeV $Au+Au$ collisions $5 < p_T^\gamma < 9$ GeV/c. 201

Figure 6.1 Comparison of this analysis's $I_{AA}(p_T)$ result (red) to the published result in the 0–20% centrality class. 205

Figure 6.2 Comparison of this analysis's $I_{AA}(p_T)$ result (red) to the published result (black) in the 20–40% centrality class. 205

Figure 6.3 Left: The away-side I_{AA} as a function of p_T^{Hadron} from 200 GeV $Au+Au$ collisions measured by the PHENIX experiment. Right: The away-side I_{AA} as a function of z_T from 200 GeV $Au+Au$ collisions measured by the STAR experiment [60]. The I_{AA} from π^0-hadron and direct photon–hadron correlations are drawn in blue and red, respectively. 206

Figure 6.4 Left: The away-side I_{AA} as a function of p_T^{Hadron} from 200 GeV $Au+Au$ collisions measured by the PHENIX experiment. Right: Away-side I_{AA} as a function of p_T from 2.76 TeV $Pb+Pb$ data from ALICE experiment [61]. The results from π^0-hadron and hadron-hadron correlations are drawn in red and black, respectively. 207

Figure 6.5 D_{AA} vs. $\Delta\phi$ as measured via Z–hadron correlations 5.02TeV $Pb+Pb$ collisions by the CMS experiment. The top set of plots shows the per-trigger yield of hadrons correlated to a Z boson in $Pb+Pb$ (red) and baseline $p+p$ (blue) collisions. Each coloumn of plots represents a different centrality class. The bottom row is the $D_{AA} = Y_{PbPb} - Y_{pp}$. 209

Figure 6.6 ATLAS I_{AA} as a function of associate hadron momentum for 3 Z boson momentum ranges: 15–30 GeV/ (Green), 30–60 GeV/c (Red), and $>$ 60 GeV/c (Orange). Hybrid models with (solid bands with color corresponding to Z momentum range) and without (cross-hatched bands with color corresponding to Z momentum range) are also included. 210

Figure 6.7 Away-side I_{dA} as a function of z_T in 200 GeV $d+Au$ collisions [65]. . 212

Figure 7.1 The probability weighting function giving the probability that a given π^0 will have a decay daughter with $5 < p_T^\gamma < 7$ GeV/c. 214

Figure 7.2 Top: Integrated yields of hadrons associated with direct photons with $5 < p_T^\gamma < 9$ GeV/c in n 200 GeV $Au+Au$ (Black), $d+Au$ (Pink), and $p+p$ (Blue) collisions. Bottom: I_{AA} and I_{dA} in 200 GeV $Au+Au$ and $d+Au$ collisions. The radius of the isolation cones used in the $p+p$ and $d+Au$ collisions is shown next to their respective legend entries, along with their offset along the ξ-axis, which is done for visual clarity. 217

Figure 7.3 Direct photon I_{AA} in 200 GeV $Au+Au$ collisions in three direct photon momentum windows. Each window shows the I_{AA} calculated with an integration range of $|\Delta\phi - \pi| < \pi/2$ (black), $|\Delta\phi - \pi| < \pi/3$ (blue), and $|\Delta\phi - \pi| < \pi/6$ (red). 218

Figure 7.4 Cross-section of the sPHENIX detector currently under construction at Brookhaven National Laboratory 221

Figure 7.5 A) The sPHENIX barrel. B) Going from inner to oute radius: the electromagnetic calorimeter, followed by the inner hadronic calorimeter, which serves as its support structure, and the outer hadronic calorimeter. The small dotted lines represent particle trajectories. One can also see the relative tilt of the inner and outer hadronic calorimeters, which is chosen to ensure that particles strike at least four scintillator tiles. C) A sector of the outer hadronic calorimeter in building 1008. While the blue paint also makes it look cool, the paint is also there to prevent the steel from rusting. Photos courtesy of Xiaochun He. 222

Figure 7.6 Depiction of the projective tilt in the outer (Top) and inner (Bottom) hadronic calorimeters. 223

Figure 7.7 A) Reconstructed energy as a function of input energy for different combinations of calorimetry subsystems. The EMCal, inner HCal, and outer HCal's combined response is shown in black. Response from just the inner and outer HCals is in red, and the response of just the outer HCal is in blue. First-order polynomial fits to the data are shown using the same color scheme. B) Energy resolution for various calorimetry subsystem combinations as a function of the input energy. The EMCal, inner HCal, and outer HCal's combined response is shown in black. Response from just the inner and outer HCals is in red, and the response of just the outer HCal is in blue. 224

Figure 7.8 Pallets of tiles at GSU, ready to be unpacked and tested. 225

Figure 7.9 Top: The tile dimension checker fitted with pegs for the B25 tile shape. Bottom: A B25 fitted into the dimension checker 227

Figure 7.10 Left: Glass gauge for checking a tile's thickness. Right: A Z01 tile being inserted into the gauge. One can see the blue mark on the tile's ID sticker, indicating that it did not fit smoothly through the thickness gauge. . 228

Figure 7.11 Configuration of a standard test with eight inner tiles sandwiched between two inner tile reference tiles. 229

Figure 7.12 Landau fit to an ADC distribution. The text near the peak of the distribution denotes the location of the "Most Probable Value" (MPV) for the distribution. 230

Figure 7.13 Final performance ratio distributions for the outer (Left) and inner (Right) HCal tiles tiles. 231

Figure 7.14 Installation of the BABAR magnet into the sPHENIX cradle. 234

Figure 1 Left: Yields of high momentum ($p_T^{\pi^0} > 6$ GeV/c) π^0's from the Minimum Bias (Black) and ERT (Red) data sets. Right: Number of π^0's in the ERT set divided by the same quantity from the Minimum Bias set. 245

Figure 2 Left: Yield of S-Type tracks from the Run 10 embedding procedure in the 0–20% centrality bin. Right: Yield of R-Type tracks from the Run 10 embedding procedure in the 0–20% centrality bin. 246

Figure 3 Left: Yield of S-Type tracks from the Run 10 embedding procedure in the 20–40% centrality bin. Right: Yield of R-Type tracks from the Run 10 embedding procedure in the 20–40% centrality bin. 247

Figure 4 Left: Run 10 embedding efficiency in the 0–40% centrality bin. Right: Run 10 embedding efficiency in the 20–20% centrality bin. 247

Figure 5 Left: Yield of S-Type tracks from the Run 11 embedding procedure in the 0–20% centrality bin. Right: Yield of R-Type tracks from the Run 11 embedding procedure in the 0–20% centrality bin. 248

Figure 6 Left: Yield of S-Type tracks from the Run 11 embedding procedure in the 20–40% centrality bin. Right: Yield of R-Type tracks from the Run 11 embedding procedure in the 20–40% centrality bin. 248

Figure 7 Left: Run 11 embedding efficiency in the 0–40% centrality bin. Right: Run 11 embedding efficiency in the 20–40% centrality bin. 249

Figure 8 Number of tracks within a given circular sigma for Run 10 (Left) and for Run 14 (Right) 249

CHAPTER 1

Introduction

Heavy ion physics occupies a unique sector of the soundscape that is high energy physics, itself a branch of nuclear physics. If particle physics, grounded in decades of experimentation and theory surrounding lower multiplicity $p + p$ and low-energy, fixed-target collisions, is classic rock, then heavy ion physics is technical death metal. The high multiplicity of particles in the final state, the presence of a hot, dense medium known as the Quark Gluon Plasma (QGP), and the long range spatial correlations that arise due to the collision geometry create a cacophonous discord, the inner workings of which are difficult to tease out both experimentally and theoretically. However, before we broach the daunting subject of heavy ion heavy metal, we must first start with a little music theory. Much like heavy metal owes its existence to jazz and blues, heavy ion physics is routed in understanding the Nuclear Strong Force, which is modelled mathematically by Quantum Chromodynamics (QCD). This introductory chapter will also include how the nuclear strong force fits into our understanding of fundamental physics as a whole: the Standard Model of Particle Physics.

1.1 The Standard Model of Particle Physics

The Standard Model of Particle Physics encompasses three of the four fundamental forces of nature. These three are the electromagnetic force, described by Quantum Electrodynamics (QED), the weak interaction, described by the unified electro-weak theory (EWT) [1–3], and the nuclear strong force, described by Quantum Chromodynamics (QCD). Gravity, the final remaining force, is best described by Einstein's Theory of General Relativity and is currently incompatible with quantum field theory. It is predicted that the gravitational force should be mediated by the exchange of a massless, spin 2 boson known as the graviton, but searches for such a particle have yet to yield results consistent with this prediction.

The Standard Model also currently includes fundamental particles that can interact with one another via the three forces listed above. Figure 1.1 details their various properties, including mass, electric charge, and spin. The top six, purple boxes represent the six flavors of quarks in the Standard Model, increasing in mass as you go from left to right. This mass increase is also denoted by the "generation" numbers above each column of quarks. Quarks are spin 1/2 fermions, carry a fraction of the electric charge, e, and can interact weakly by undergoing flavor-changing interactions mediated by the Z^0 and $W^{\pm}$ bosons. This last interaction gives rise to the phenomenology of radioactivity in elements such as potassium-40.

Located in the green boxes beneath the quarks lay the second class of fermions, known as leptons, the most familiar of which is the electron. Electrons are most commonly found in atomic orbitals and their configuration in these orbitals give rise to the chemical properties

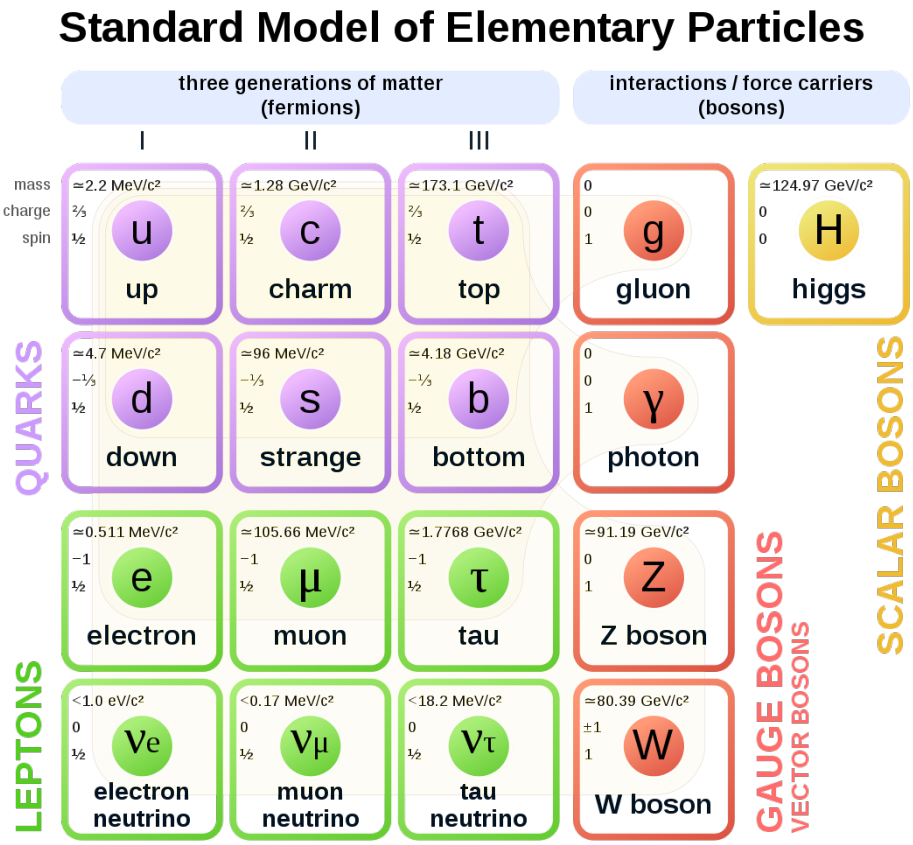

Figure 1.1: Stand model of elementary particles which are categorized into quarks (purple), leptons (green) and force carriers (blue). The particle properties such as mass, charge, spin, and name are labeled in each grid [4].

of the individual elements on the periodic table. To the right of the electron, again with increasing mass, lay the muon and the tau lepton. Each has the same spin and charge as the electron, but with heavier masses, 105.66 MeV/c^2 and 1.7768 GeV/c^2, respectively, compared to the electron's 0.511 MeV/c^2 [5]. This increased mass makes muons and tau leptons rarer particles, with their primary creation mechanisms being violent nuclear reactions in Earth's atmosphere or in powerful particle colliders. Both also have extremely short liftetimes before weakly decaying into less massive leptons.

There also exists an associated electron neutrino, muon neutrino, and tau nuetrino beneath their more massive namesakes. Neutrinos, broadly, facilitate the conservation of lepton numbers during weak nuclear interactions. Additionally, neutrinos are nearly massless and carry no electric nor color charge, making them nearly impossible to detect. It was believed for quite some time that neutrinos were massless; however, new insight has led scientists to believe that not only to neutrinos have mass [6], but the different neutrino flavors might oscillate between these different mass eigenstates [7]. Additionally, the study of neutrinos may serve as a way to capture certain phenomena that would challenge our current understanding of the laws of nature. The observation of neutrino-less double beta decay, for instance, would provide counter-evidence to the notion that lepton number is a conserved quantity. Indeed, a large part of neutrino physics is focused on probing physics "Beyond the Standard Model" (BSM) by probing unique symmetry violations.

On the right side of table in Fig. 1.1 are the gauge bosons, mediators of the interactions permitted by the Standard Model. All are spin 1, given them the designation of "vector" boson, with the exception of the recently discovered Higgs boson, which is a spinless "scalar" boson. The gluon and photon (denoted g and γ, respectively) mediate the strong and electromagnetic interactions. The neutral Z and charged W bosons mediate the weak force, facilitating flavor changing interactions involving quarks and leptons. And, finally, the mass of fundamental particles is determined via their interaction with the Higgs boson and its underlying field. It's important to note that the Higgs mechanism is responsible for only the mass of the fundamental particles listed in the table. The mass of composite particles like

hadrons is achieved through the quantum chromodynamical binding energy of the constituent quarks.

1.1.1 The Nuclear Strong Force and Quantum Chromodynamics

Quantum Chromodyanmics (QCD) is the mathematical framework that describes the strong nuclear interaction between quarks and gluons, heretofore referred to as "partons." QCD is explained best by comparing and contrasting it with Quantum Electrodynamics (QED). Like in QED, the nuclear strong force is mediated by a massless, spin-1 boson known as the gluon, and the gluon is exchanged by the quanta of the underlying field of the strong force, quarks, the same way photons are exchanged by electrons and other electrically charged particles. The analogy begins to fray slightly with the fact there are six color charges in QCD (red, grean, blue and their anti-colors), as opposed to the two electric charges in QED (positive and anti-positive, also referred to by some as "negative"). Where things really begin to diverge, however, is with the fact that the gluon is not neutral with respect to its conserved current like the photon is. The gluon can occupy one of eight color states, known as the "color octet" that is laid out in Table 1.1.

Table 1.1: Possible color states for gluons

$(r\bar{b}+b\bar{r})/\sqrt{2}$	$-i(r\bar{b}+b\bar{r})/\sqrt{2}$
$(r\bar{g}+g\bar{r})/\sqrt{2}$	$-i(r\bar{g}+g\bar{r})/\sqrt{2}$
$(b\bar{g}+g\bar{b})/\sqrt{2}$	$-i(b\bar{g}+g\bar{b})/\sqrt{2}$
$(r\bar{r}+b\bar{b})/\sqrt{2}$	$(r\bar{r}+b\bar{b}-2g\bar{g})/\sqrt{6}$

Mathematically, this divergence from QED is evident in a comparison between the two

theories' Lagrangians, shown in Eqn. 1.1 and 1.2 below [8, 9].

$$\mathcal{L}_{\text{QCD}} = \sum_q \bar{\psi}_{q,a} \left(i\gamma^\mu \partial_\mu \delta_{ab} - g_s \gamma^\mu t^C_{ab} A^C_\mu - m_q \delta_{ab} \right) \psi_{q,b} - \frac{1}{4} G^A_{\mu\nu} G^{A\mu\nu} \tag{1.1}$$

$$\mathcal{L}_{\text{QED}} = \bar{\psi}(i\gamma^\mu \delta_\mu - m)\psi - \frac{1}{4} F_{\mu\nu} F^{\mu\nu} \tag{1.2}$$

In both equations, ψ represents a fermion field (specifically with color charge a in the case of QCD), γ^μ represent the Dirac matrices, m the fermion mass, and δ_μ the gauge covariant derivative. In Eqn. 1.1, g_s is the QCD coupling constant, A^C_μ corresponds to the gluon field, where the variable C goes from 1 to 8 to account for the 8 gluon color states as shown in 1.1, and the term t^C_{ab} represents the 8 3×3 special unitary matrices that are the generators of $SU(3)$, the underlying symmetry group of QCD. The final two terms in both the equations, $G^a_{\mu\nu}$ and $F_{\mu\nu}$, describe the strength of boson field of each theory, and therein lies the unique property of the gluon. The definition of these terms is the following:

$$G^a_{\mu\nu} = \partial_\mu \mathcal{A}^a_\nu - \partial_\nu \mathcal{A}^a_\mu - g_s f_{ABC} \mathcal{A}^b_\mu \mathcal{A}^c_\nu \tag{1.3}$$

$$F_{\mu\nu} = \partial_\mu A_\nu - \partial_\nu A_\mu \tag{1.4}$$

Here, $\mathcal{A}$ represents the strength of the field tensor, g_s represents the QCD coupling strength, f_{ABC} represents what are known as structure constants of SU(3), the underlying symmetry group of QCD (in contrast to QED, which is decsribed by a U(1) symmetry). And, indeed, Eqns. 1.1 and 1.4 have similar leading terms, but the structure functions of the former arise

because of the non-Abelian (or non-commutative) nature of SU(3). These non-zero structure functions, in turn, do not eliminate the trailing $g_s \mathcal{A}^b_\mu \mathcal{A}^c_\nu$ terms, which, therefore, allows for non-zero gluon-gluon interactions in QCD's mathematical description of the nuclear strong force. Examples of quark-quark, quark-gluon, and gluon-gluon interactions are shown in 1.2

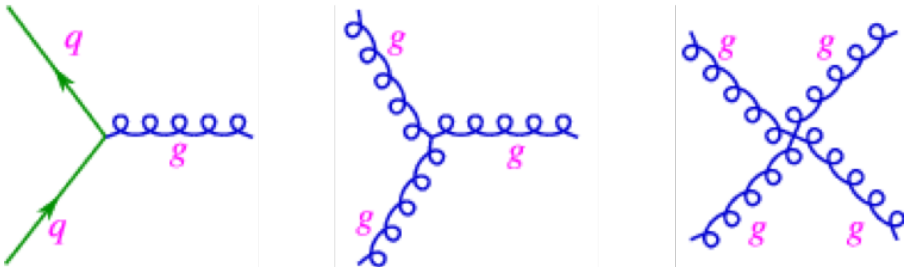

Figure 1.2: Feynman diagrams of strong interactions. Left: quark-gluon interaction. Center and Right: gluon-gluon interactions.

Confinement and Asymptotic Freedom

Turning to the quarks themselves, specifically two quarks interacting such as in the formation of the meson, we have the following effective potential between the quark-anti-quark pair given by Eqn. 1.5 [10]:

$$V(r) = -\frac{a}{r} + br \tag{1.5}$$

By applying the relationship that the force produced by a given potential is proportional to the negative gradient of the potential, one can see that the first term in Eqn. 1.5 becomes repulsive, albeit it dies off very quickly because of its $1/r$ dependence. This term implies that quarks experience a repulsive force when very close to one another, preventing hadrons from collapsing in on themselves. Upon examining the second term, however, we see that at

larger r, the force felt by strong interacting particles is constant as a function of the distance between them. This means that the amount of energy stored between a quark-antiquark pair grows linearly with the distance between them. Eventually, it becomes more energetically favorable to spawn another quark-antiquark out of the QCD vacuum, thus creating two mesons, rather than allowing the original two quarks to become further separated and/or isolated. The fact that the most energetically favorable states are tightly bound hadrons leads to the property of the nuclear strong force known as "confinement," which is the observation that there are no free partons at everyday length and energy scales.

The phrase "everyday length and energy scales" might immediately elicit the follow-up question: "what happens at very uncommon length and energy scales"? For this, we must turn back to quantum field theory, specifically at the parameter g in Eqn. 1.3, which is also sometimes written as α_s. This parameter is known as the coupling constant, which, broadly, describes the strength of a given interaction between two field quanta. The larger this number, the stronger the interaction, and vice versa. In a field theory such as QED, the coupling constant is:

$$\alpha_{QED} = \frac{e^2}{4\pi\epsilon_0\hbar c} \approx 1/137 \tag{1.6}$$

Where e is the electron charge, ϵ_0 is the vacuum permitivity of free space, $\hbar$ is the reduced Panck's constant, and c is the speed of light. One can see this expression has no explicit dependence on, say, the scale at which we probe the field theory (e.g. with a high-frequency or high-momentum probe for instance). The coupling for QCD, however, has two explicit

dependencies on such scale-like quantities, as one can see in Eqn. 1.7[11].

$$\alpha_s(Q^2) = \frac{\alpha_s(\mu^2)}{1 + \frac{33-2N_f}{12\pi} \cdot \alpha_s(\mu^2) \ln \frac{Q^2}{\mu^2}}, \tag{1.7}$$

Here, Q^2 is the momentum transfer between two strongly interacting objects, μ is the QCD scale, and N_f is the number of flavors. The dependence on Q^2 and μ^2 leads to the coupling of the nuclear strong force decreasing at increasing momentum transfer and decreasing length scales, respectively. Physically, α_s becomes smaller when using high energy probes to probe the field theory (large Q^2), or when the distance between strongly interacting particles becomes exceedingly small (small μ^2). Thus, the nuclear strong force has what is known as a "running coupling." Experimental validation of this aspect of the nuclear strong force's coupling's behavior can be seen in 1.3 [12], where the measured α_s is plotted as a function of momentum transfer, Q.

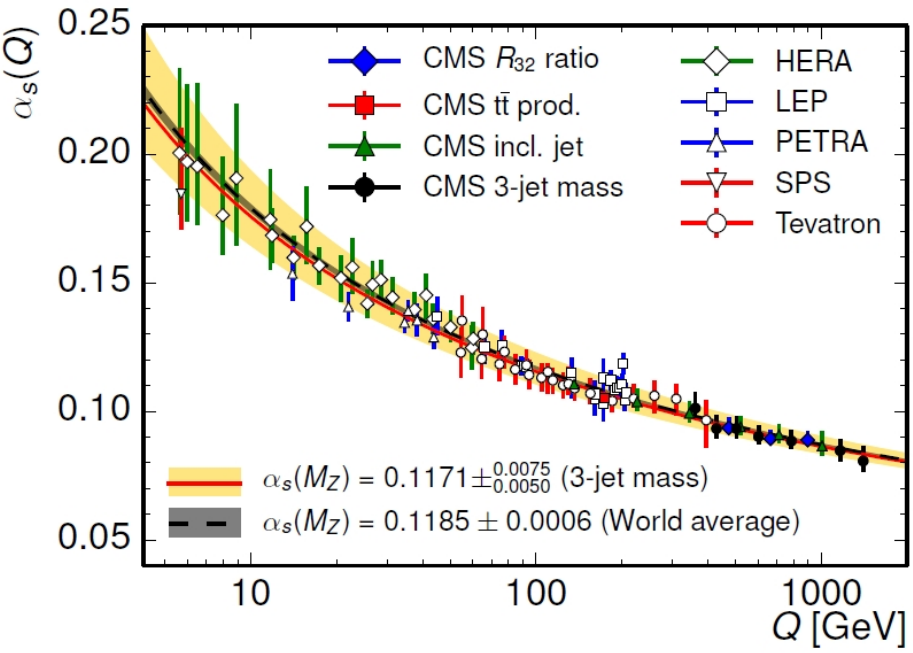

Figure 1.3: The coupling constant, α_s, of the strong interaction as a function of squared momentum transfer Q^2 obtained from different experiments [12].

Because of the limiting behaviors of the QCD coupling, the nuclear strong force is predicted to exhibit what is known as "asymptotic freedom," wherein the coupling between the field quanta grows so week that they gain their own degrees of freedom, rather than be confined to the interior of hadrons. The next section details the creation and probing of this exotic state of matter composed of deconfined partons known as the Quark Gluon Plasma (QGP).

1.2 The Quark-Gluon Plasma

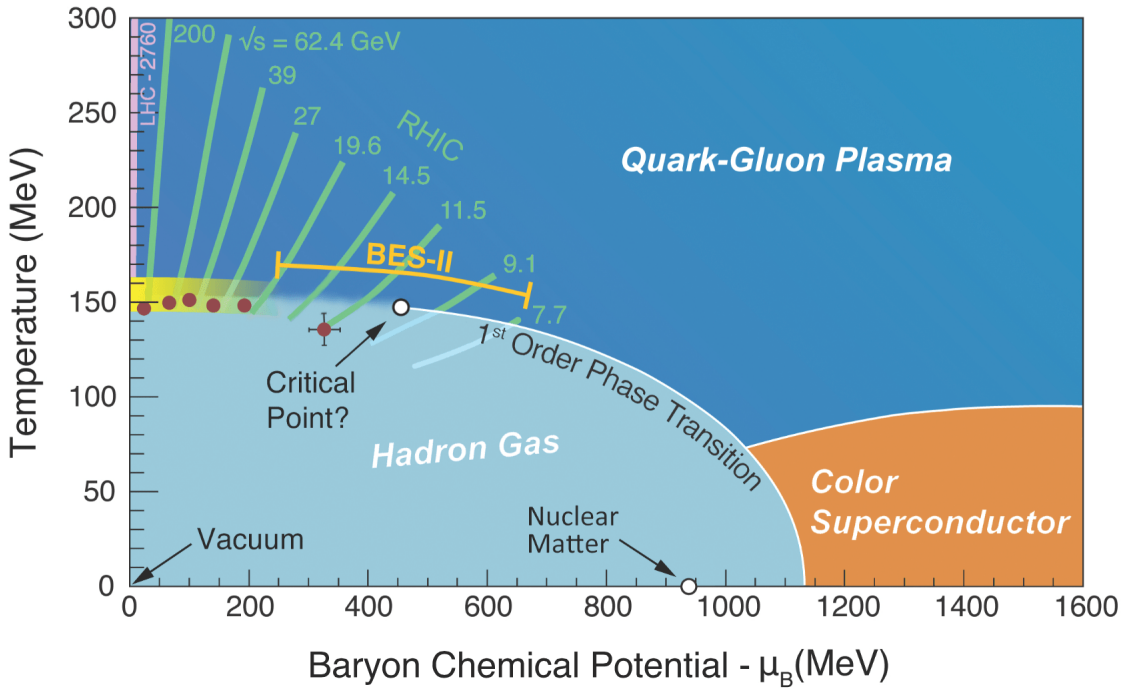

Figure 1.4: The phase diagram for QCD as a function of temperature and baryon chemical potential. The different white lines represent phase transitions. The green and purple lines represent regions of the phase space probed by different collider experiments.

QCD predicts that at extremely high energies and extremely small length scales, the effective coupling between strongly interacting partons should diminish significantly, allowing for a novel state of matter composed of deconfined quarks and gluons. Fig. 1.4 shows the phase diagram for strongly interacting matter. Ordinary hadronic matter lives in the light blue region labelled "Hadron Gas," which includes nuclear matter (the "stuff" that makes up our everyday existence) at an appropriately high μ_B. At the so-called "critical temperature," however, a phase transition occurs, and hadronic matter melts in an extremely dense, extremely hot state of deconfined partons, the Quark-Gluon Plasma. Current estimations of

the critical temperature and energy density to achieve this phase transition are 170 MeV and 1 GeV/fm^3, respectively [13]. The QGP itself is of immense interest to the nuclear physics community as it offers a unique environment in which to study the nuclear strong force.

1.2.1 Creation and Evolution in Heavy-Ion Collisions

In order to probe the QGP sector of the QCD phase diagram, one must have a way of reliably creating one in a laboratory setting. In order to reliably create this deconfined state of quarks and gluons, large nuclei such as gold and lead are accelerated up to a significant fraction of the speed of light and collided in particle colliders such as the Relativistic Heavy Ion Collider located at Brookhaven National Laboratory in Long Island, New York, and the Large Hadron Collider in Geneva, Switzerland. The facilities, known as synchrotrons, create sufficient energy densities via ultra-relativistic collisions to create Quark-Gluon Plasmas such that they can be created and studied repeatedly. Fig. 1.5 [14] shows how heavy-ion collisions evolve over time, and the individual stages of the evolution of the collision shall be discussed here.

The Initial State

The initial state (or "initial conditions" as labelled in 1.5) contains the initial distributions of partons before any collision processes have taken place. At this point, the target nuclei have been accelerated to a significant portion of the speed of light, and, thus, appear to be shaped like pancakes in the laboratory reference frame.

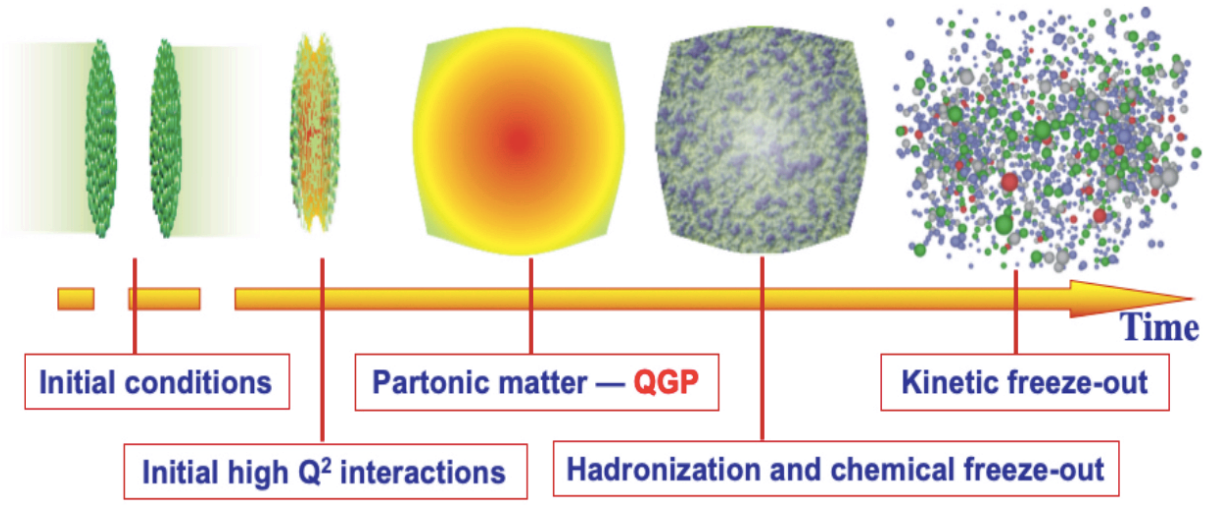

Figure 1.5: Evolution of heavy-ion collisions [14]

Initial Hard Scatterings

The second phase of heavy-ion collisions contains collisions with very large momentum transfer (large Q^2) between individual partons. These violent, partonic collisions are known as hard scatterings, and the hard-scattered partons that are produced in this process will eventually go on to fragment and hadronize into a distribution of high-momentum particles known as a jet. However, before fragmentation, hard-scattered partons will interact with the medium, losing energy to it as they do so. Thus, the jets measured in heavy-ion collisions appear to be modified with respect to their hadron yield and their shape when compared to jets in proton-proton collisions, where no medium is formed.

Quark-Gluon Plasma

After the initial set of high-Q^2 collisions, temperatures and energy densities become sufficiently high that the colliding nuclei melt, creating a dense soup of deconfined partons known as the Quark-Gluon Plasma. It is at this point that the evolution of the medium is

governed by viscous hydrodynamics and jet-medium interactions. This phase lasts on the order of 1–10fm/c (which converts to 3×10^{-24}–3×10^{-23} seconds), but is sensitive to the initial conditions of the collision such as center of mass energy [15].

Hadronization

Hadronization refers to the non-perturbative process by which quarks transform into states with net-zero color charge (hadrons). This phase occurs after the QGP has expanded and cooled, which means conditions are no longer extreme enough to allow for partonic degrees of freedom.

Chemical Freeze-Out

This is the final stage of the collision where the final-state particle distributions are reached. Here, all hadronization and decay processes that can be seen within an experiment have finished [16–18].

1.2.2 Experimental Variables and Terminology

Here we will detail specialized terminology that will be used in the remainder of the dissertation. To begin, we shall define the laboratory coordinate system. Fig. 1.6 shows the coordinate system inside the lab frame. The beams of colliding particles are directed along the z-axis, perpendicular to which is the xy-plane. It is typical, when discussing particle collisions, to use a mish-mash of Cartesian and cylindrical coordinates. The angle θ is defined as the inclination angle from the z-axis (also referred to as the polar angle), and the angle ϕ is the polar coordinate in the xy-plane. Furthermore, given a particle with momentum

four-vector $p = p(E, p_x, p_y, p_z)$, a particle's momentum that is directed into the xy-plane (it's transverse momentum), p_T, is defined by 1.8. This quantity will occur frequently in the course of this dissertation.

$$p_T = \sqrt{p_x^2 + p_y^2} \tag{1.8}$$

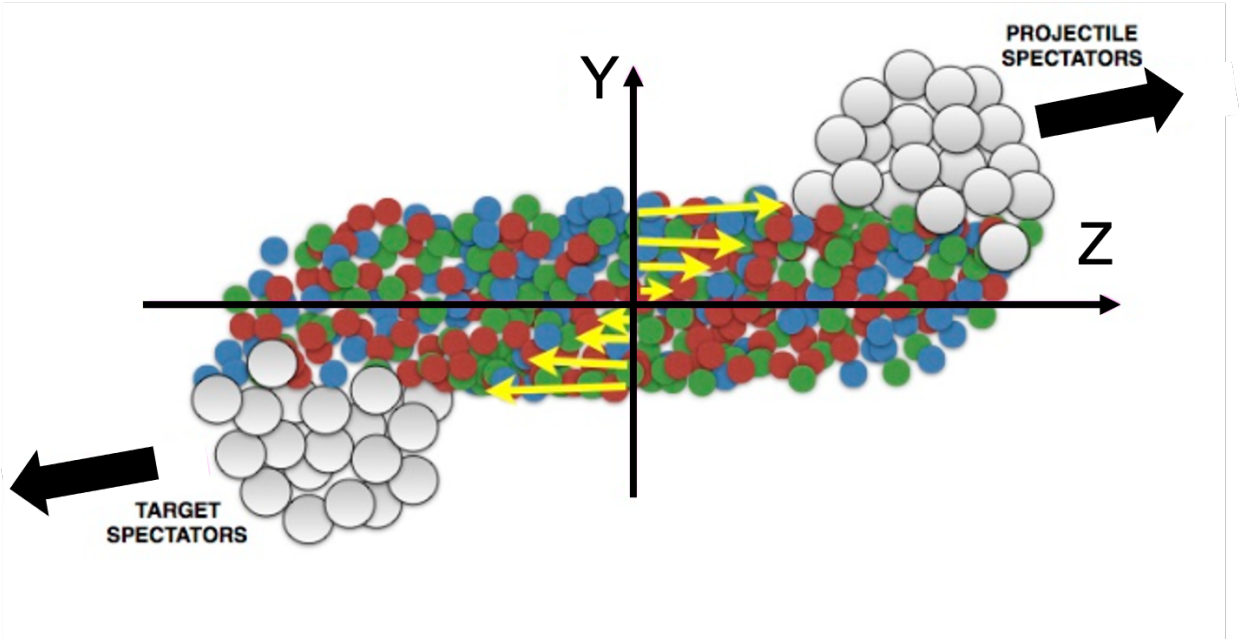

Figure 1.6: Depiction of the coordinate system used in heavy-ion collisions. The beam line is directed through the page horizontally along the z-axis, with the positive y-axis pointed upwards, and the positive x-axis directed into the page.

However, it must be noted that the above coordinate system is not Lorentz invariant. That is to say, upon transformation from reference frame X to frame X' under coordinate transformation λ, a given set of coordinates (e.g. (x, y, z)) may not be the same in each frame. Thus, we introduce two special variables in particular to quantify the polar angle θ.

The first is known as "rapidity", denoted by y, and is defined in Eqn. 1.9 below.

$$y = \frac{1}{2} \ln \frac{E + p_z}{E - p_z} \tag{1.9}$$

Where E is a particle's energy, and p_z is a particle's momentum along the z-axis. It should be noted that rapidity itself is not Lorentz invariant, but rapidity gaps, Δy, are. In order to develop a purely Lorentz-invariant analogue for the polar angle, we turn to psuedorapidity, η. Given the mass-energy relation,

$$E^2 = m^2 + p^2 \tag{1.10}$$

where m is the particle's rest mass, and we have used natural units such that $c = \hbar = 1$, we can substitute the fact that $p_z = p \cos\theta$ and Eqn. 1.10 into the definition of rapidity from Eqn. 1.9. This gives

$$y = \frac{1}{2} \ln \frac{\sqrt{m^2 + p^2} + p \cos\theta}{\sqrt{m^2 + p^2} - p \cos\theta}. \tag{1.11}$$

For the case where $p \gg m$, as is such in relativistic particle collisions, Eqn. 1.11 reduces to:

$$\begin{aligned} y &= \frac{1}{2} \ln \frac{p + p \cos\theta}{\sqrt{p - p \cos\theta}} \\ y &= \frac{1}{2} \ln \frac{1 + \cos\theta}{\sqrt{1 - \cos\theta}} \\ y &= -\frac{1}{2} \ln \frac{1 - \cos\theta}{\sqrt{1 + \cos\theta}}. \end{aligned} \tag{1.12}$$

From here, we perform a trigonometric substitution inside the natural logarithm to arrive at the definition of psuedorapity in Eqn. 1.13.

$$\eta = -\frac{1}{2} \ln \frac{\theta}{2} \tag{1.13}$$

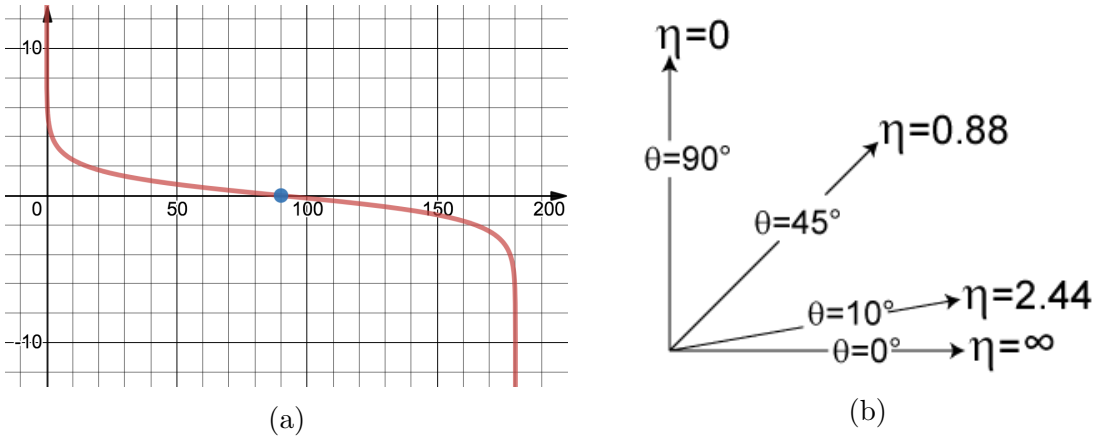

(a) (b)

Figure 1.7: (a) Pseudorapidity η plotted as a function of θ. The blue dot is at (90°,0). (b) Translation of common angles into units of pseudorapidity [19]

Centrality

When colliding two spherical objects in general, one can discuss what's known as the "impact parameter," b, which is the distance between the center of each projectile measured in the plane perpendicular to their trajectory. In heavy-ion collisions, the impact parameter plays a direct role in determining the severity of QGP medium-induced effects seen on an event-by-event basis. As the impact parameter shrinks, the number of nucleons taking part in the collision, or "participant nucleons", N_{Part}, increases, along with the number of binary collisions (collisions between individual nucleons), N_{Coll}, thus raising the energy density,

leading to a more violent QGP fireball. Conversely, "spectator" nucleons are those that are not directly involved in the collisions. They "witness" it (hence the term "spectator") but are not actually struck by another nucleon themselves. The distinction, as well as a visualization of the impact parameter, is illustrated in Fig. 1.8.

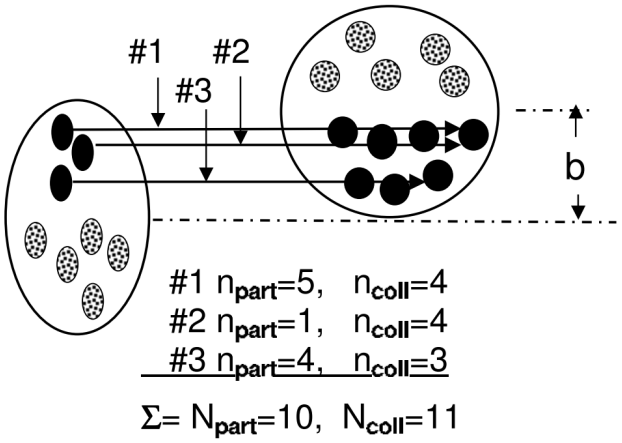

Figure 1.8: Visual representations of N_{Part}, N_{Coll}, and the impact parameter b in heavy-ion collisions [20].

Inversely, when the impact parameter is very large, there are more spectators, less participants, and thus a less severe amount medium-induced modifications. Despite its importance, however, the impact parameter is impossible to measure in real events. Thus, the notion of centrality is introduced to categorize events as a proxy for the impact parameter. Each experiment defines centrality in a way that is specific to its own minimum bias detector's (MBD) capability, and is expounded upon in detail in Sec. 2.2.1.1. In order to tether what the minimum bias detector measures back to the actual impact parameter in a meaningful way, though, the MBD's signal is compared to the Glauber Monte Carlo model[21], which allows a mapping between a quantity such as the number of charged particles measured in

an event to the impact parameter, as shown in Fig. 1.9. One can think of the Glauber Model as a mapping that takes one from the bottom x-axis of N_{ch} to the top x-axis of N_{Part} and the impact parameter, b.

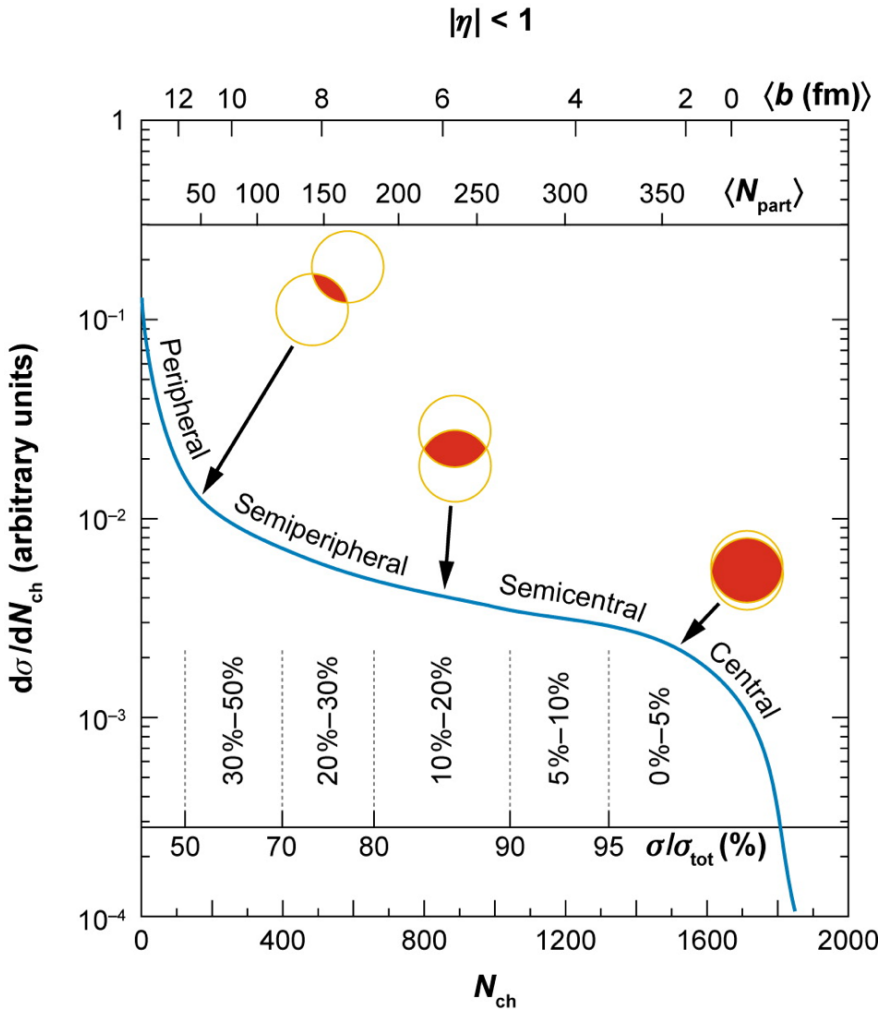

Figure 1.9: Centrality determination via charged particle multiplicity. The bottom x-axis represents the amount of charged tracks measured in the MBD, the y-axis represents the inelastic cross-section, and the top x-axis represents an approximation of the impact parameter in femtometers[22].

1.2.3 Probing the Quark-Gluon Plasma

There are two primary experimental observables that validate the hypothesis that QGP is created inside ultra-relativistic heavy-ion collisions. One is the observation of long-range spatial correlations between particles that emerge from heavy-ion collisions known as "flow", and the other is the modification in the yield of high momentum particle formations known as jets.

1.2.3.1 Collective Flow

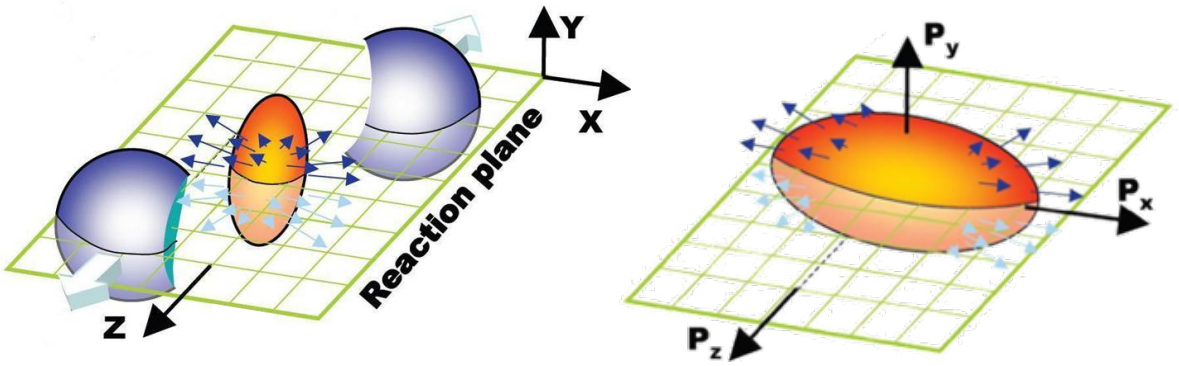

Figure 1.10: Cartoon depicting a collision of large nuclei. The left side shows the formation of the Quark-Gluon Plasma with a elliptic shape owed to the initial elliptic shape of the overlap region of the two nuclei. The right picture shows how this spatial anisotropy leads to particles emerging with different momentum due to their interactions with the medium [23].

In heavy-ion collisions, the spatial overlap of the two colliding nuclei need not be perfectly circular as was discussed when defining the notion of centrality. This spatial anisotropy in the initial state of the collision then leads to a momentum anisotropy in the final state as particles undergo medium-interactions along differing path lengths. Fig. 1.10 depicts the creation of the QGP medium and how its shape is owed to the shape of the collision

geometry and how this spatial anisotropy is transferred into a momentum anisotropy in the final state. Experimentally, collective flow in heavy-ion collisions can be measured via multi-particle correlations, in which a particle is chosen as a "trigger" particle, and the angular separation between it and other particles in the event, $\Delta\phi$, is recorded. These correlations can be analyzed via Fourier decomposition given by Eqn. 1.14. A hallmark feature of these correlations is that they are long-range in nature, meaning they span a long range in pseudorapidity, whereas correlations due to jets alone do not. This is shown in 1.11, where one can see that the number of correlations at large η away from the near-side peak at $(\Delta\phi, \Delta\eta) \approx (0, 0)$ grows as the system size increases. This phenomenon is often referred to as the "ridge".

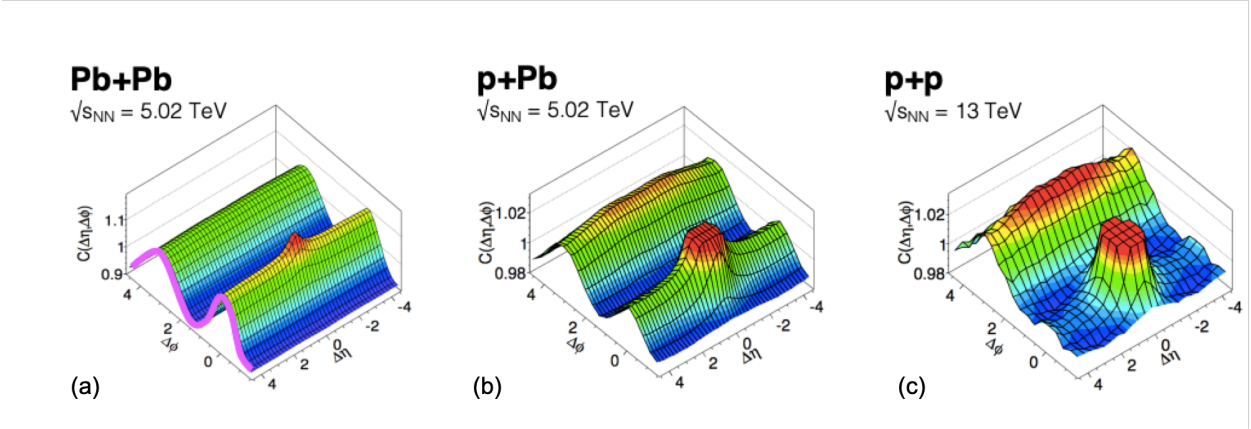

Figure 1.11: Two-particle correlation results from the ATLAS experiment [24] in (a) $Pb-Pb$ collisions at $\sqrt{s_{NN}} = 5.02$TeV, (b) $p + Pb$ collisions at $\sqrt{s_{NN}} = 5.02$TeV, and (c) $p + p$ collisions at $\sqrt{s_{NN}} = 13$TeV. As the collision systems get larger, the amount of correlations found at large $|\eta|$ away from $(\Delta\phi, \Delta\eta) \approx (0, 0)$ becomes very large due to contributions from ellitpic flow.

$$\frac{N_{Particles}}{d\phi} \propto 1 + 2\sum_{n=1}\langle v_n\rangle \cos(n[\phi - \psi_n]) \tag{1.14}$$

Spatial relations measured via multi-particle correlations are analyzed by decomposing them via Fourier decomposition, shown in Eqn 1.14. Here, $N_{Particles}/d\phi$ represents the number of particles at a given azimuthal angle, ϕ. The v_n terms are often referred to as "flow harmonics" and they quantify the relative strength of each of the different modes (e.g. v_1, v_2, v_3, etc.). The v_n values, thus, determine the shape of the udnerlying event in azimuth. Lastly, ψ_n represents the n^{th}-order reaction plane angle. The reaction plane angle is measured in the experiment in the xy-plane by measuring the spatial density of spectator particles.

While only the four harmonics, v_{1-4}, will play a role in this dissertation, it should be possible to measure an arbitrarily high n^{th} order harmonic given a large enough sample set. The first harmonic v_1 is called "directed flow," and it arises from participating nucleons in each of the target nuclei pushing back on each other in opposite directions along the beam line. Because this effect is primarily directed along the beamline, and, thus, large $|\eta|$, the effect at mid-rapidity ($|\eta| \approx 0$) is negligible, as is shown in Fig. 1.12 [25].

The second harmonic, v_2 is referred to as "elliptic flow" and owes its name to the elliptical shape of the overlap region of the collision as shown in Fig. 1.10. Initially, elliptic flow was thought to be the primary source of flow at mid-rapidity, with higher order odd terms (e.g. v_3) thought to be zero, and higher order even terms (e.g. v_4) thought to be negligible. However, this conclusion proved to be erroneous, as shown in Fig. 1.13 [26] where a non-zero

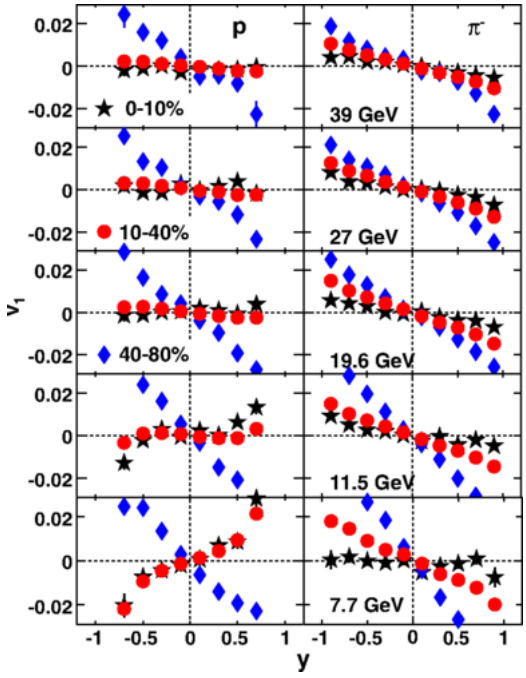

Figure 1.12: Proton and π^- Directed flow, v_1 as a function of rapidity y in $Au+Au$ collisions at varying center of mass energies. The black stars, red circles, and blue diamonds represent the $0-10\%, 10-40\%$, and $40-70\%$ centrality bins, respectively. Each row is a different center of mass energy [25].

v_3 can be seen. It can also been seen that v_4 in the most central collisions is about 25% as large as v_2, which is not negligible.

While the existence of higher order even flow harmonics can be understood as perturbations to the underlying elliptic shape, non-zero v_3 comes from event-by-event fluctuations in the collision geometry that results in triangular shaped collision areas. Thus, v_3 is often referred to as "triangular flow". An example of how nucleonic fluctuations in the initial state can cause triangular overlap regions is shown in Fig. 1.14 [27].

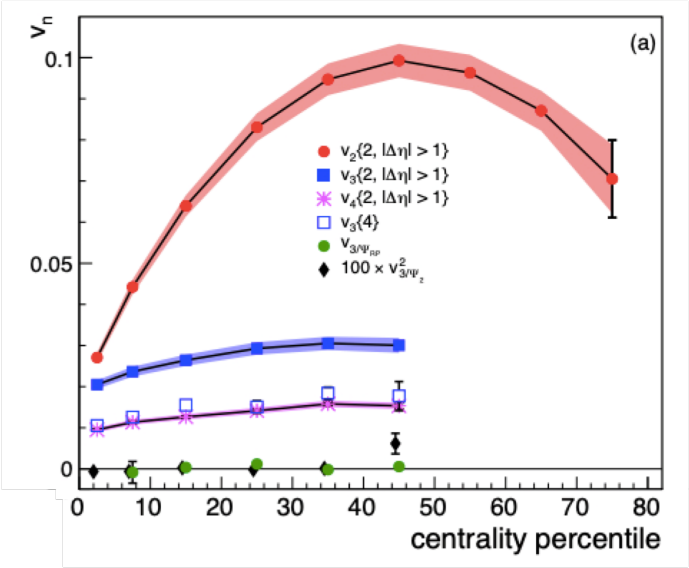

Figure 1.13: v_2 (red), v_3 (blue), and v_4 (ink) for charged hadrons as a function of centrality percentile in 2.76 TEV $Pb + Pb$ collisions [26]

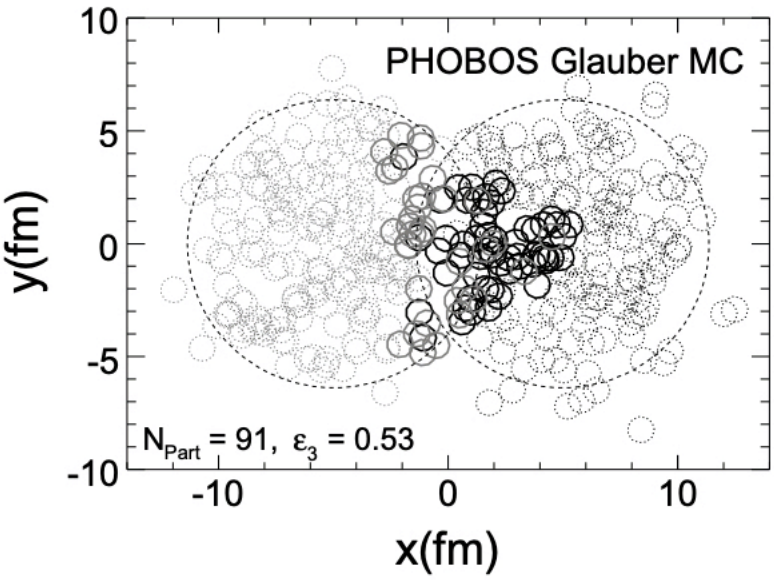

Figure 1.14: Monte Carlo simulation showing how a triangular overlap region can occur in the initial stages of heavy ion collisions, thus leading to nonzero v_3 [27].

There is one characteristic of collective flow that makes it a hallmark signature of the Quark-Gluon Plasma, though, and that is the phenomenon of constituent quark scaling.

Fig. 1.15 [28] shows the elliptic flow, v_2 as a function of both transverse momentum p_T and transverse kinetic energy KE_T for several particle species which includes both mesons and baryons. One can see that for $p_T \gtrsim 2$ GeV/c and for $KE_T \gtrsim 1$ GeV, the v_2 measurements begin to split, with the protons, lambda, and Ξ baryons having a higher v_2 than the pions, kaons, and K^0_s (sometimes referred to as "k-short") mesons. However, one can see that in the left panel, when looking at the quantity v_2/n_q, which is the elliptic flow harmonic divided by the number of constituent valence quarks for a given species, this difference disappears, and the flow measurements across both baryons and mesons converge. This phenomenon of the constituent quark scaling of v_2 provides the evidence that it is, in fact, the quarks inside the QGP itself that are flowing, and so the observation of the azimuthal anisotropy of final state hadrons is an emergent phenomenon born of the flowing of free quarks.

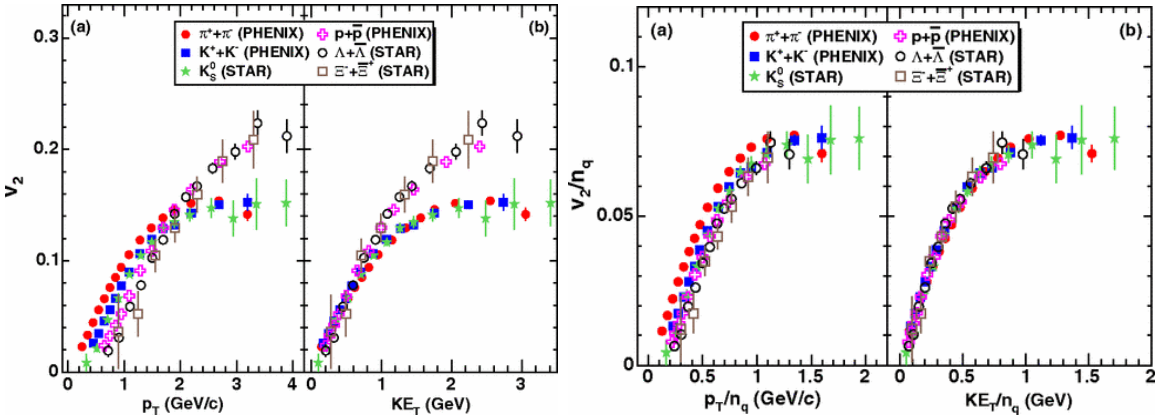

Figure 1.15: Left: Charged hadron v_2 as a function of p_T and $KE_T$for various hadron species as measured by the PHENIX and STAR experiments in minimum bias $Au + Au$ collisions at 200GeV. Right: v_2 for as function of p_T and KE_T for various hadron species after scaling by the number of constituent quarks for each species [28].

1.2.3.2 Jet Modification

The second indicator of the presence of the QGP in heavy-ion collisions is the phenomenon of jet modification. As mentioned previously, hard-scattered partons lose energy to the QGP, and this energy loss results in modifications to both the shape and yield of jets in heavy-ion collisions relative to jets in $p+p$ collisions. From these studies, information about the medium, such as the the energy loss per unit path length, given by the parameter $\hat{q}$, can be extracted. The total energy lost by a parton traversing a path of length L is $\hat{q}L$. Mathematically, $\hat{q}$ is defined by Eqn. 1.15.

$$\hat{q} = \rho \int q_T^2 \frac{d\sigma}{dq_T^2} dq_T^2 \tag{1.15}$$

Here, ρ represents the density of partons in the medium, σ represents the cross-section of interaction between two medium constituents, and q_T^2 is the momentum transfer exchanged during parton-medium interactions. The study of jet modification in heavy-ion collisions is one of the best avenues by which to extract $\hat{q}$, though, in principle, experimentally, only the total energy loss $\hat{q}L$ is feasible, as the exact path-length of the parton through the medium is never known. Extraction of this quantity is done by modelling partonic interactions in-medium and then comparing the results of these models to results obtained from experiment.

Modification to Single Particle Yields: R_{AA}

Historically, the observation of jet quenching was first seen via the observable R_{AA} [29], which is defined as in Eqn. 1.16

$$R_{AA} = \frac{1}{\langle N_{coll}^{AA} \rangle} \frac{N_{AA}}{N_{pp}} \ . \tag{1.16}$$

Here, N_{coll}^{AA} is the number of binary collisions in $A + A$ collisions, and N_{AA} and N_{pp} are the yields of a given particle species as in $A + A$ and $p + p$ collisions, respectively. Put simply, the R_{AA} quantifies the extent to which a $A + A$ event is the superposition of numerous $p + p$ collisions. An $R_{AA} = 1$ is consistent with no modification, whereas an $R_{AA} < 1$ and $R_{AA} > 1$ are consistent with a suppression and enhancement, respectively, in the yield of a given particle species. Fig. 1.16 shows the R_{AA} as a function of p_T for several particle species as measured in the 10% most central 200 GeV $Au + Au$ collisions. One can see at high p_T a suppression in the yield of high momentum particles which are likely part of a jet.

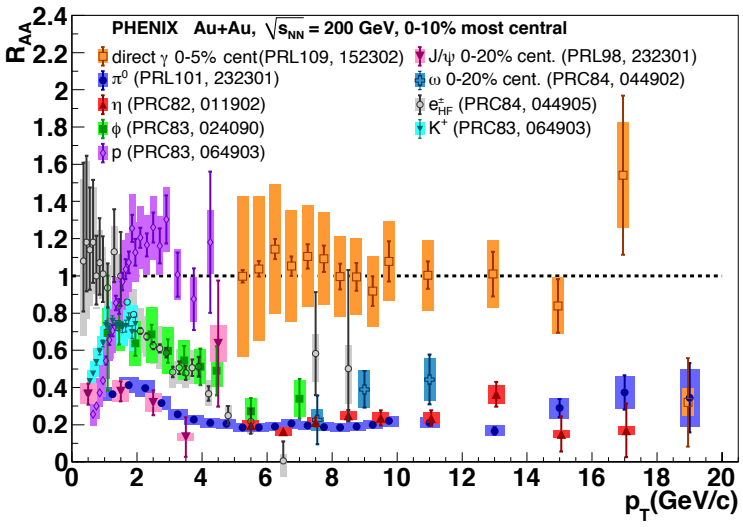

Figure 1.16: R_{AA} as a function of transverse momentum for a variety of particle species in $0-20\%$ 200GeV $Au+Au$ collisions as measured by the PHENIX detector [29].

Two-Particle Correlations

Studies of jet properties can also be carried out by two-particle correlations just as flow studies are. Here, the trigger particle is usually chosen to be a particle likely to be a high-p_T fragment of a jet, and the azimuthal separation between the trigger particle and the other associated hadrons in the event is measured, as shown schematically in 1.17 [15]. Correlations due to the underlying event are then subtracted, leaving only correlations due to jets. This results in two prominent peaks in $\Delta\phi$ space, where $\Delta\phi = \phi^{Trigger} - \phi^{Hadron}$. One occurs at $\Delta\phi \approx 0$ and the other at $\Delta\phi \approx \pi$, known as the near and away-side peaks, respectively. An example of this in $p+p$ collisions simulated via PYTHIA is shown in Fig.1.18 [15]. One of the chief advantages of the method of two-particle correlations over measuring fully reconstructed jets is that there is no constraint or requirement placed on the away-side jet or its constituents, thus allowing for an more unbiased measurement.

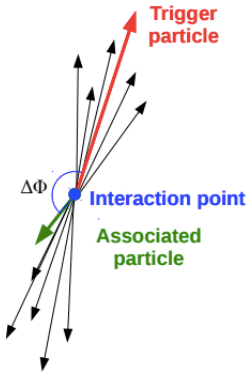

Figure 1.17: A dijet in $\Delta\phi$ space. The arrows represent different jet fragments, and their magnitude represents their momenta.

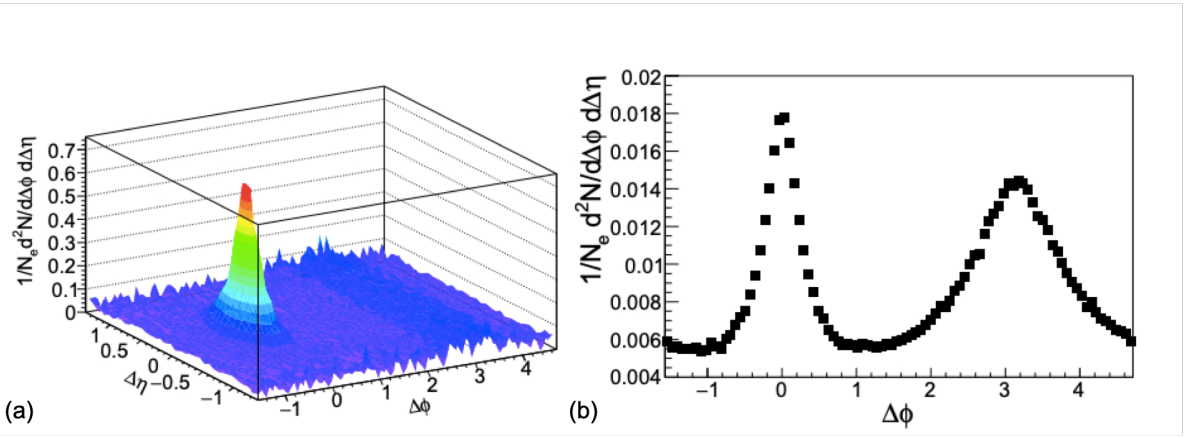

Figure 1.18: An example of a two-particle correlation measurement made in PYTHIA. (a) Correlations between a trigger particle and associated charged hadrons in $\Delta\phi\Delta\eta$-space. (b) The same correlation measurement, but projected onto the $\Delta\phi$ axis [15]

As discussed earlier, jets in heavy-ion collisions have been modified because of interactions between their parent partons and the QGP. This modification is seen by the disappearance of the away-side peak in two-particle correlations as one looks at the yield of high-momentum jet fragments. The suppression in the angular yield of high-momentum hadrons relative to those measured in $p + p$ collisions can be seen in Fig. 1.19 [30]. Here, one clearly sees a

suppression in the yield of high-momentum associate hadrons in $Au + Au$ collisions relative to those in $p + p$ collisions. As hard partons traverse the medium, they lose energy to it in accordance with Eqn. 1.15, and this partonic energy loss leads to the creation of fewer high momentum state hadrons.

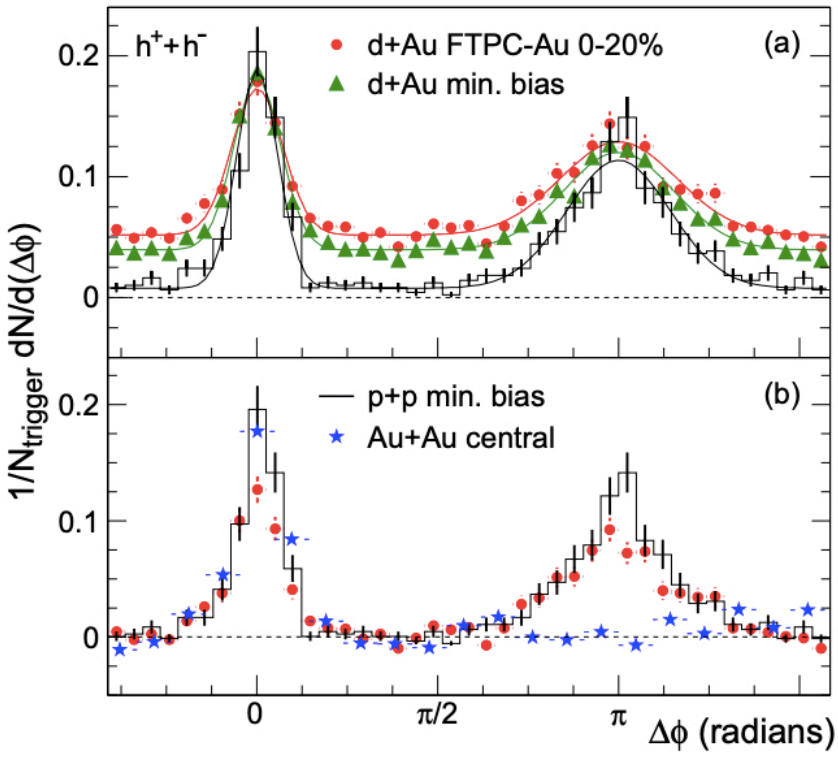

Figure 1.19: Top: Two-particle correlation distributions for minimum bias $d + Au$ collisions (Green), central $d + Au$ collisions (Red), for $p + p$ collisions (Black). Bottom: Comparison of two-particle correlations distributions for central $d + Au$ collisions (Green) to those seen in $p + p$ (Black) and central $Au + Au$ collisions (Red) [30]

The results shown in Fig. 1.19 are for hadron-hadron correlations, but current endeavors using two-particle correlations include using neutral bosons such as direct photons as the trigger particle, as they are color neutral and, thus, do not interact with the medium, which

is best demonstrated by the R_{AA} of direct photons being consistent with 1 across a wide p_T range as shown in Fig. 1.16. Fig. 1.20 [31] shows inclusive photon-hadron, decay photon-hadron, and direct photon-hadron correlations as a function of the separation angle, $\Delta\phi$, in both 200 GeV $p+p$ collisions and 200 GeV $Au+Au$ collisions. One of the most noticeable features of direct photon-hadron correlations is that the yield about the near-side is consistent with zero to within uncertainty after the subtraction of correlations from decay photon-hadron sources, showing that direct photons appear isolated in $\Delta\phi$ space.

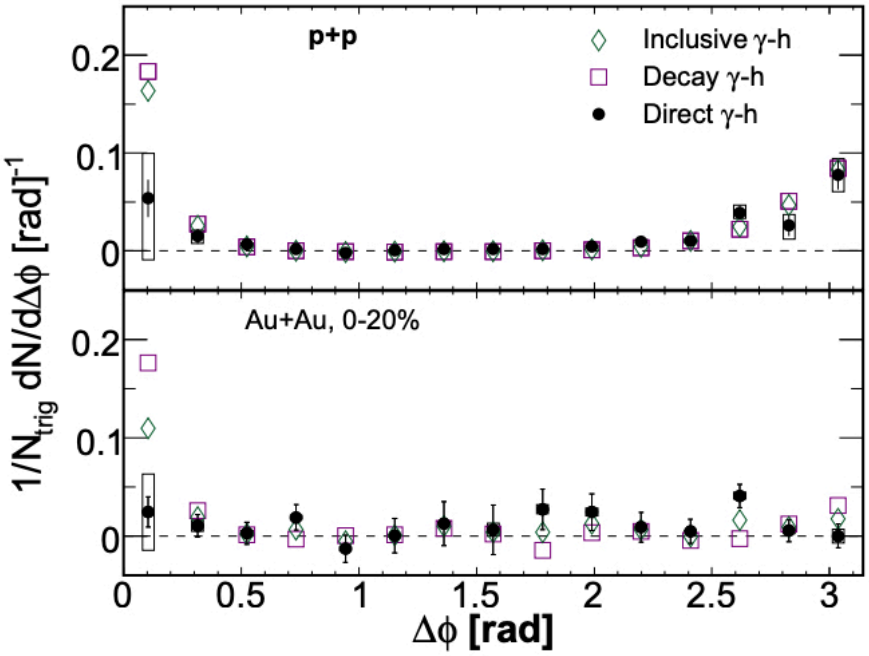

Figure 1.20: Inclusive photon-hadron (Green diamonds), decay photon-hadron (Red squares), and direct photon-hadron (Black dots) in 200 GeV $p+p$ collisions (Top) and 200 GeV $Au+Au$ collisions (Bottom) [31] .

One of the quantities of interest extracted from two-particle correlations is the I_{AA}, which is defined as the ratio of the integrated, per-triggger yields in $A+A$ collisions to that in $p+p$

as shown in Eqn. 1.17.

$$I_{AA} = \frac{Y_{AA}}{Y_{pp}} \tag{1.17}$$

As with the R_{AA}, an I_{AA} consistent with 1 means there is no modification to the per-trigger yield, whereas $I_{AA} < 1$ and $I_{AA} > 1$ mean a suppression and enhancement in the per-trigger yield, respectively. Fig. 1.21 shows the I_{AA} as a function of the associate hadron p_T in four direct photon p_T bins, alongside the I_{AA} for hadron-hadron correlations for $5 < p_T^{Hadron} <$ 10 GeV/c. Here one can see a suppression in the yield of associate hadrons in each direct photon momentum range. One of the primary efforts of the field currently is to increase the statistical precision of these neutral boson-hadron correlations by measuring them in larger and larger data sets.

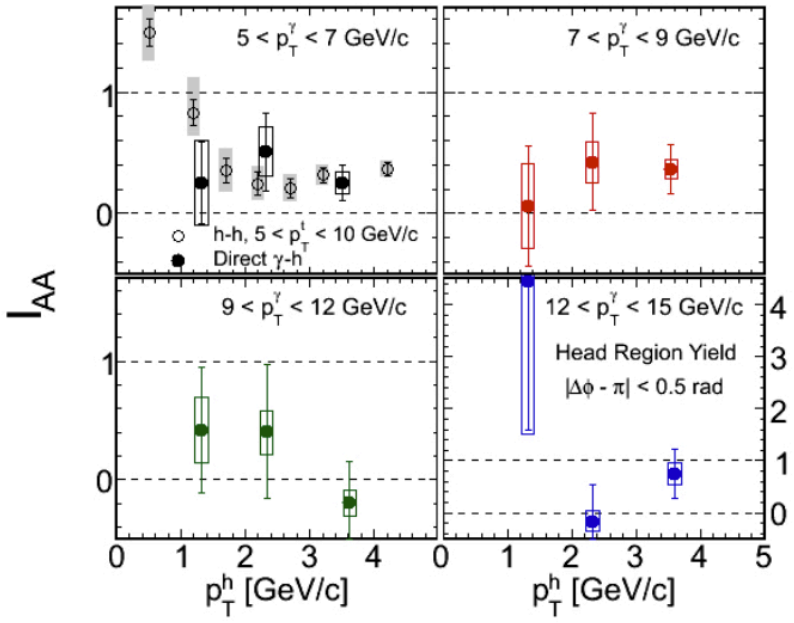

Figure 1.21: I_{AA} as a function of the associate hadron p_T^h in four separate direct photon p_T bins, alongside the I_{AA} for hadron-hadron correlations for $5 < p_T^{Trigger} < 10$ GeV/c in the upper left hand panel [31].

1.2.4 Theoretical Modelling

The Fragmentation Function

Mathematically, jet production follows the following scheme: consider two nuclei, A and B, with partons a and b, respectively. In the collision between nucleus A and B, their partons, a and b, have some probability, $d\sigma_{ab\to cX}$, to scatter off one another and create partons c and X (where X denotes a parton not of interest). Parton c then will go through fragmentation, thus producing a hadron, h. The differential cross-section of this process is given in Eqn. 1.18.

$$d\sigma = \sum_{a,b,c} \int\int\int f_a^A(x_a) f_b^B(x_b) \cdot d\sigma_{ab\to cX} \cdot D_c^h(z) dx_a dx_b dz \ . \tag{1.18}$$

Eqn. 1.18 has three sets of terms of note:

- $f_a^A(x_a) f_b^B(x_b)$ are the initial parton distribution functions (PDF's) of nucleus A and B. They are functions of the variable x_a (x_b), which encodes the fraction of the nucleus's momentum that is carried by parton a (b).

- $d\sigma_{ab\to cX}$ is the differential cross-section of the scattering process $a + b \to c + X$ as described above.

- $D_c^h(z)$ is the fragmentation function, which gives the probability with which a parton, c will fragment into a hadron h with momentum fraction $z = p^{Hadron}/p^{Parton}$.

While it is possible to calculate the cross-section $d\sigma_{ab\to cX}$, the parton distribution functions and fragmentation functions can only be measured experimentally at this point in time, owing to the highly non-perturbative nature of QCD. The PDF's encode information about the initial state and, thus, any PDF-dependent modification between $p+p$ and $A+A$ collisions can be classified as a cold matter effect (i.e. an effect solely due to the presence of a nucleus in the collision rather than the formation of QGP medium). Energy loss due to interactions with the QGP, however, modify the fragmentation by inducing a shift relative to the $p + p$ fragmentation function, and this shift is proportional to the fractional energy loss, $-\frac{\Delta E}{E}$. Thus, the modified momentum fraction, z', in $A + A$ collisions is

$$z' = \frac{z}{1 - \frac{\Delta E}{E}} \ . \tag{1.19}$$

Which will then yield a modified fragmentation function that has been shifted accordingly

$$D_c^h(z') = D_c^h(\frac{z}{1-\frac{\Delta E}{E}}) \ . \tag{1.20}$$

Thus, one can see that the jet modification seen in $A + A$ collisions is an expression of a modification to the fragmentation measured in $A + A$ collisions relative to that measured in $p+p$ collisions [32]. Experimentally, one can let a high p_T trigger particle stand in for the p_T of the parton and measure the yield of associate hadrons via two-particle correlations. In this way, the observable I_{AA} as defined in Eqn. 1.17 is approximately related to the fragmentation function as follows:

$$I_{AA} = \frac{Y_{AA}}{Y_{pp}} \approx \frac{D_{AA}(z)}{D_{pp}(z)} \ . \tag{1.21}$$

CoLBT-Hydro

Modeling jet energy loss due to medium interactions depends upon two factors. One is the radiative energy loss per unit length travelled in the medium, and the second is the response from the medium to the energy embedded in it by the hard-scattered parton. One such model that includes both processes is the Linear Boltzman Transport model that has been coupled with a hydrodynamic evolution [33]. In CoLBT-Hydro, jet propagation through the medium is governed by a linear Boltzmann equation, and energy lost to jet-medium interactions appears in the form of soft gluon radiation. Additionally, in this model, the QCD coupling constant, α_s, is set to $\alpha_s = g^2/4\pi$, where g again is the gluon interaction

strength.

Jet propagation is then coupled to the hydrodynamic evolution of the medium by adding a source term to the hydrodynamic equation given in Eqn. 1.22.

$$\partial_\mu T^{\mu\nu} = 0 \rightarrow \partial_\mu T^{\mu\nu} = j^\nu \tag{1.22}$$

Here, the insertion source term, j_ν drives the coupling of the evolution of the jet and medium via $(3+1)$–D hydrodynamic equations. In the course of solving the equations, both jet propagation via LBT and the hydrodynamic evolution of the medium are handled simultaneously. That is to say that for every time step $\Delta\tau$, energy from a radiating parton is carried out according to the Linear Boltzmann Equation, and the local temperature and fluid velocity of the medium are obtained from Eqn. 1.22.

A comparison between CoLBT-Hydro calculations and recent PHENIX direct photon-hadron correlation results [34] can be seen in Fig. 1.22 for $0-40\%$ 200 GeV $Au+Au$ collisions. Here, the I_{AA} is plotted as a function of ξ, which is defined as

$$\xi = -\ln(z_T) = -\ln(p_T^{Hadron}/p_T^{Trigger}) \tag{1.23}$$

As both ξ and z_T relate the associate hadron momentum to the trigger particle's momentum (which is meant to serve as a proxy for the parton momentum), they are often referred to as "fragmentation variables". For reference, a high ξ value relates to a low associate hadron momentum, and a low ξ value relates to a high associate hadron momentum. One can see

in Fig. 1.22 that the CoLBT-Hydro model has excellent qualitative agreement with the data for the 5–7 and 7–9 GeV/c direct photon momentum bins, especially in the enhancement regime at high ξ, where models that fail to include medium response tend to fail to reproduce phenomena measured at low momentum. A lack of statistics in data for the highest direct photon momentum bin, 9–12 GeV/c makes comparison between the model and data difficult, however.

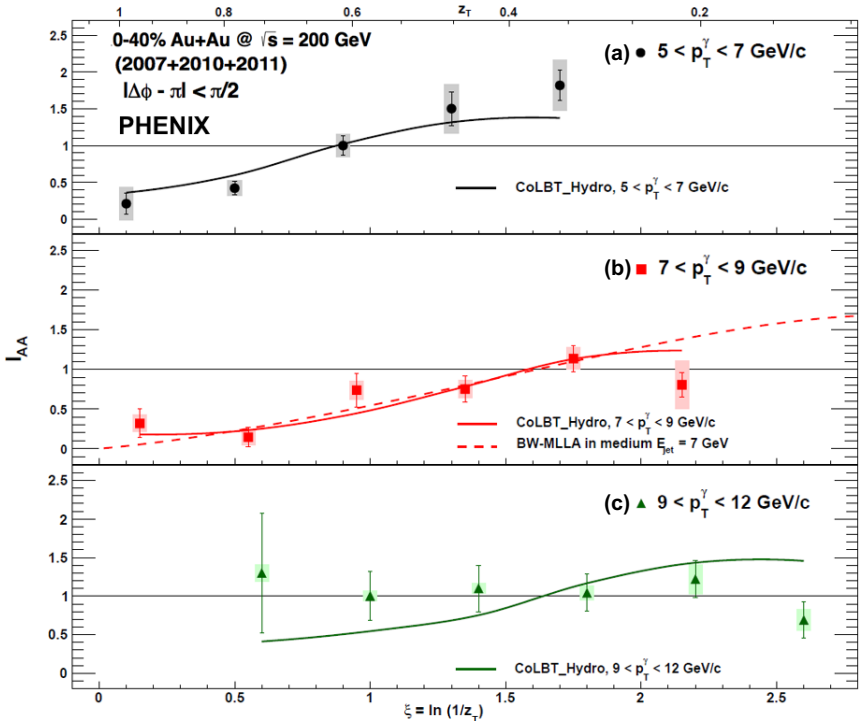

Figure 1.22: I_{AA} as a function of ξ in direct photon-hadron correlations in three direct photon momentum ranges. Solid curves are calculations from CoLBT-Hydro[33], and the dashed curve is from a Borghini-Wiedemann modified leading logarithmic approximation (BW-MLLA) calculation [35].

The Hybrid Model

Another model that attempts to include medium response as a mechanism for jet modification is the Hybrid model [36]. This model used a hybrid strong and weak coupling approach

to the phenomenon of jet quenching. That is to say that different physics process are treated with methods appropriate for their appropriate coupling strengths. Hard processes, such as the evolution of the jet through the medium, are treated with perturbative QCD (pQCD), as they are expected to be weakly coupled. However, processes involving the soft radiation radiated by this parton are treated as being strongly coupled and are treated via holographic calculations from AdS/CFT [37]. The primary feature of this model is that the energy lost by hard partons to the medium appears as a "wake" in the medium, similar to how a ballistic projectile through water creates a wake. Energy loss in this model is governed by Eqn. 1.24.

$$\frac{1}{E_{\text{in}}}\frac{dE}{dx} = -\frac{4}{\pi}\frac{x^2}{x_{\text{stop}}^2}\frac{1}{\sqrt{x_{\text{stop}}^2 - x^2}} \tag{1.24}$$

Here, E_{in} is the initial parton energy (specifically a hard-scattered quark that is modelled as a string a la string theory), x represents the distance travelled by the quark, and x_{Stop} represents the total distance travelled by the quark. A primary consequence of this equation is that $E \to 0$ as $x \to x_{Stop}$. The maximal stopping distance allowed by this theory is

$$x_{\text{stop}}^{\text{Max}} = \frac{1}{2\kappa_{\text{sc}}}\frac{E_{\text{in}}^{1/3}}{T^{4/3}} \tag{1.25}$$

Where κ_{sc} is dimensionless constant and T is the QGP temperature. A comparison between the the Hybrid model and CMS Z boson-hadron correlations 0–30% 5.02 TeV $Pb + Pb$ collisions is shown in Fig. 1.23. The top row shows the angular correlations, whereas the bottom row shows the D_{AA}, which is the difference, rather than the quotient, of the integrated

yields in $A+A$ and $p+p$ (i.e. $D_{AA} = Y_{AA} - Y_{pp}$). For D_{AA}, a value of zero is consistent with no modification, whereas positive and negative values indicate enhancement and suppression, respectively, relative to the $p+p$ baseline. Two calculations are made for this comparison, one with the wake mechanism, and one without. One can see that for $\Delta\phi \approx \pi$ (i.e. near the away-side jet peak), the model that includes the wake has excellent agreement with the data in the 0–30% centrality bin, whereas the model without the wake fails to describe the data. The model also under-shoots the data in the more peripheral 30–50% centrality bin. A calculation for CoLBT-Hydro is also shown, although it appears to over-shoot the data in the 0–30 centrality bin, and under-shoot it in the 30–50% centrality bin.

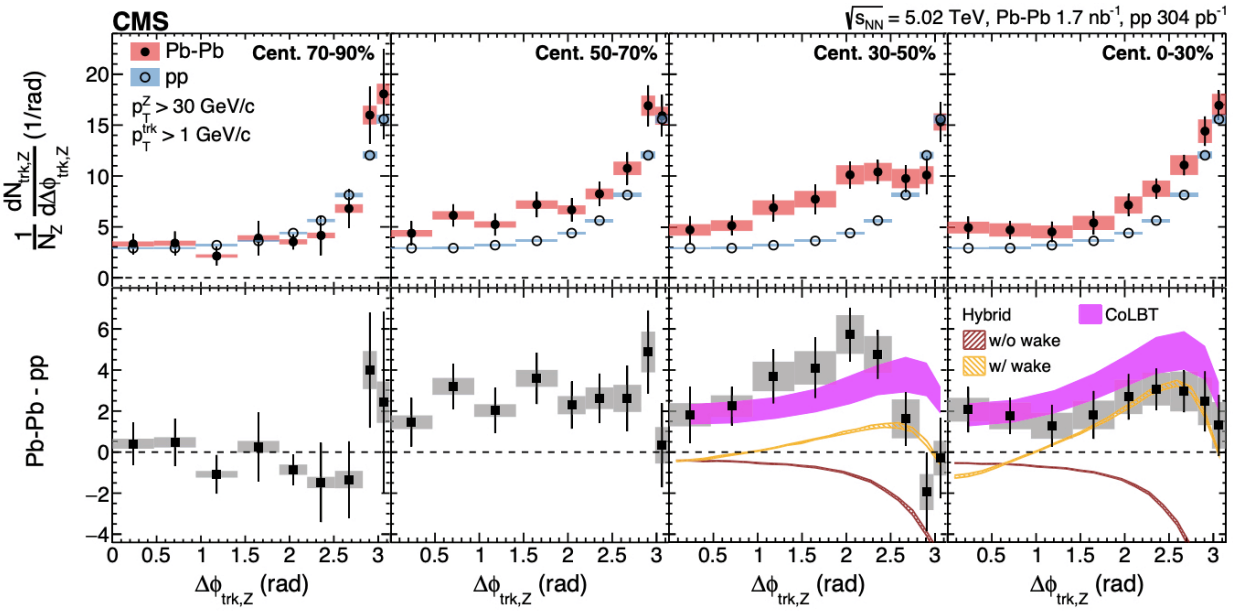

Figure 1.23: Top: Z boson-hadron angular correlations in 5.02TeV $p+p$ collisions (Blue) and 5.02TeV $Pb+Pb$ collisions (Red). Bottom D_{AA} vs. $\Delta\phi$.

In conclusion, theoretical models have come far in describing the complicated intermingling of jet-medium interactions. However, there remains much progress to be made, and

this progress must be guided by rigorous comparison to data from experiment, and highly differential (i.e. divided into many bins) measurements are the key to discriminating against models with subtle differences. The results obtained for this dissertation will to provide such measurements.

1.3 Purpose of This Dissertation

Though the PHENIX detector completed its data taking mission in 2016, there remain several large data sets left to analyze. Two such data sets are the 200 GeV $Au+Au$ sets taken in 2014 and 2016. This dissertation will extract π^0 triggered two-particle correlation measurements from the 2014 data set. Results measured in the 2014 dataset will utilize the same procedures as those in [38] in terms the raw data analysis, and the same procedure for subtracting the underlying event will be used, with the exception of the use of a different method to calculate the background magnitude for the lowest hadron momentum bin ($p_T^{Hadron} < 1$ GeV/c). Previous PHENIX π^0-hadron correlation results such as in [39] only subtracted underlying event contributions from the second-order flow harmonic, assuming the third-order harmonic, v_3, to be zero, and the fourth order, v_4, to be negligible. However, as discussed earlier, the odd-numbered harmonics are, in fact, not zero, and can leave behind a sizeable amount of contamination when not accounted for during the underlying event subtraction.

Additionally, the I_{AA} measured with respect to $\Delta\phi$ was measured in [38] and allows quantification of jet modification at the substructure level, a type of measurement usually attributed to full-jet reconstruction, using two-particle correlations. The observable is extracted by dividing the jet functions point-by-point in $\Delta\phi$ space, rather than by integrating the entire away-side region and taking the ratio of the resultant integrated yields. While the increased size of the 2014 data set does improve the statistical precision of the observable, the I_{AA} vs. $\Delta\phi$ measurement is still susceptible to zero or near-zero values in the $p + p$ baseline.

Thus, a complementary result, the D_{AA} vs. $\Delta\phi$ is introduced in this dissertation. The D_{AA} is defined as the difference, rather than the quotient, between the per-trigger yields in $Au+Au$ collisions, Y_{AA} and the same quantity in baseline $p+p$ collisions, Y_{pp}. The principle benefit of this observable is that it can probe modification to the $Au+Au$ per-trigger yields at wider angles relative to the away-side jet peak where values in the $p+p$ jet function become very close to zero. This causes both the central values to fluctuate and the statistical and systematic uncertanties to grow very large in the I_{AA} vs. $\Delta\phi$. The D_{AA}, however, is immune from this effect.

This dissertation follows the following order. Chapter 2 will detail the Relativistic Heavy Ion Collider (RHIC) located at Brookhaven National Laboratory, its European contemporary experiment the Large Hadron Collider (LHC) located at CERN, and the PHENIX detector located at the 8 o'clock position on the RHIC beamline. Chapter 3 will discuss the analysis process used to analyze the raw data taken by PHENIX, as well as the process of extracting the π^0-hadron correlations, including the corrections applied to the data due to detector effects. One of these corrections, the correction for the occupancy effect seen in heavy-ion collisions, has been done for the first time in nearly a decade for this type of analysis, and so particular attention will be paid to its documentation. In chapter 4, we will discuss the systematic uncertainties associated with each result and their sources, which will then be followed by a discussion of the results themselves in Chapter 5. These results will then be compared to contemporary experiments at both RHIC and the LHC and model calculations in Chapter 6. Finally, the dissertation will conclude in Chapter 7 by discussing the current

status of the sPHENIX detector, a next-generation jet and heavy flavor detector designed as the successor experiment to PHENIX, as well as opportunities to make highly precise direct photon-hadron correlations with PHENIX's 2014 and 2016 data sets.

CHAPTER 2

Heavy-Ion Colliders and Experiments

2.1 The Relativistic Heavy-Ion Collider

If heavy-ion collisions are heavy metal concert, then high-energy particle colliders such as the Relativistic Heavy Ion Collider (RHIC) are their venues. RHIC began its operation in 2000 with four experiments: PHENIX [40], BRAHMS [41], PHOBOS [42], and STAR [43]. BRAHMS, PHOBOS, and PHENIX finished their data taking missions in 2006, 2009, and 2016, respectively, but the STAR experiment continues to take data, focusing on taking advantage of RHIC's Beam Energy Scan program in 2019 and 2020, and now focusing on forward upgrade implementation for RHIC's 2022 data taking run.

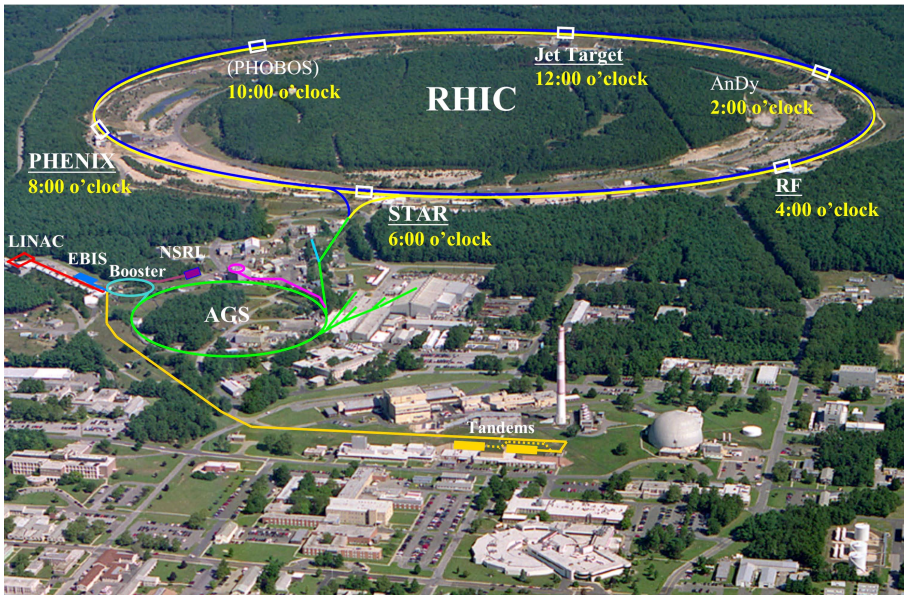

Figure 2.1: Alternating Gradient Synchrotron (AGS) and RHIC at Brookhaven National Laboratory.

A primary advantage of the RHIC facility is its ability to collide a multitude of beam

species at a wide variety of center of mass energies, spanning $\sqrt{s_{NN}} = 7.7$ GeV in heavy and light-ion systems, to $\sqrt{s_{NN}} = 510$ GeV for $p+p$ collisions. While the industry standard heavy-ion collision species at RHIC is 200 GeV $Au+Au$ collisions, the facility is also capable of creating $U+U$, $Cu+Cu$, $Al+Al$, and $Cu+Au$ collisions on the heavy-ion side, and to further probe the QCD phase diagram, RHIC is also capable of creating many mixed collisions as well to, allowing for more precise exploration of the QCD phase diagram shown in Fig 1.4. To this end, RHIC can also collide $d+Au$, ^3He+Au, $p+Au$, and $p+Al$ beams. Indeed, measurements of multi-particle correlations in the latter three collision species at 200 GeV yielded evidence for collective flow in small systems [44].

Before beams of any species can be collided, they must pass through a series of facilities shown in Fig. 2.1. Firstly, ion of various species are produced via the Electron Beam Ion Source (EBIS). These ions are then fed into Linear Accelerators (LINACs), where they are then passed on to the Booster Synchrotron. It is here that the ions receive their first large kick to approximately 37% speed of light [45]. From the Booster Synchrotron, ions are then injected into the Alternate Gradient Synchrotron, where they then are accelerated to approximately 99.7% speed of light [45]. Finally, the beams are transferred into RHIC, where they are then separated into bunches. Bunch sizes vary depending on collision systems, but in the case of $Au+Au$ collisions, a beam is separated into 112 bunches containing 1.1 billion ions [46]. This results in a luminosity of $2\times10^{26}\text{cm}^{-2}\text{s}^{-1}$. Additionally, the RHIC rings contain magnet known as "Siberian Snakes", which allows for the creation of spin-polarized proton beams. Polarized proton collisions are critical to the RHIC spin physics

program, which seeks to understand the spin structure of the proton.

2.2 PHENIX

The PHENIX (**P**ioneering **H**igh-**E**nergy **N**uclear **I**nteraction E**X**periment) detector is a general-purpose particle detector which sat at the 8 o'clock position on the RHIC beamline from 2000 until it completed its data taking mission in 2016, when it was dismantled to make way for its successor experiment, sPHENIX. The PHENIX detector is shown in its Run 11 configuration in Fig. 2.2, beyond which it was not changed in a way relevant to this dissertation. The detector itself contains two large central arm spectrometers at mid rapidity which contain the Drift Chambers, Pad Chambers, Ring Imagine Cherenkov Detectors, Beam-Beam Counters, and the Electromagnetic Calorimeters. These subsystems, along with the central magnet, play critical roles in this dissertation's analysis and will have their own sections detailing their functionality and purpose.

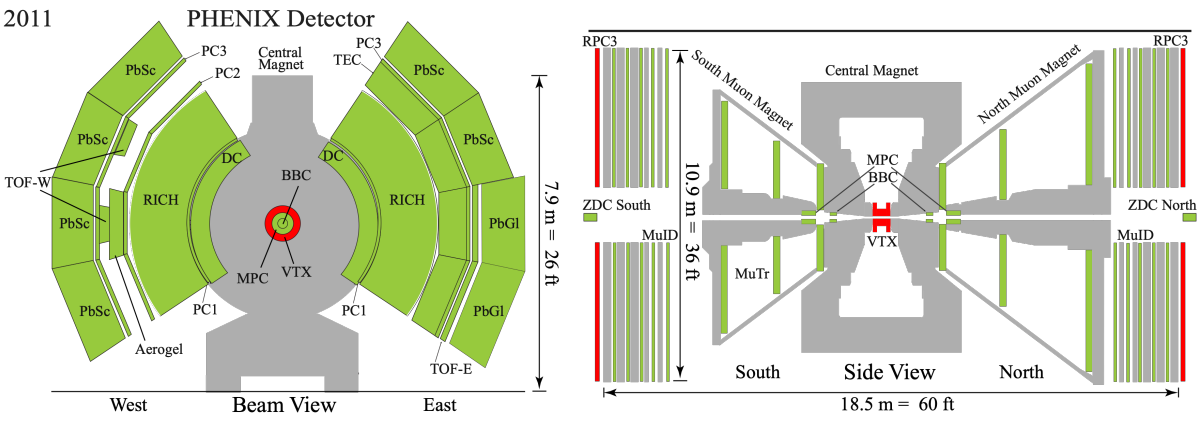

Figure 2.2: 2011 and onwards configuration of the PHENIX detector. The subsystem of note here is the Silicon Vertex Detector located at the interaction point

2.2.1 Beam-Beam Counters

The Beam-Beam Counters (BBC) [47] are a pair of detectors that sit at the north and south end of the beam line 1.44 meters from the interaction point, covering $3.0 \leq |\eta| \leq 3.9$ in psuedorapidity and 2π in azimuth. They are composed of sixty-four photomultiplier tubes (PMT's) each, and their primary function is event categorization according to parameters such as the event z-vertex, centrality, collision time, and event plane. Each tube has a 30 mm long quartz Cherenkov radiator at the front and is covered by a metal shell to prevent light leakage [47].

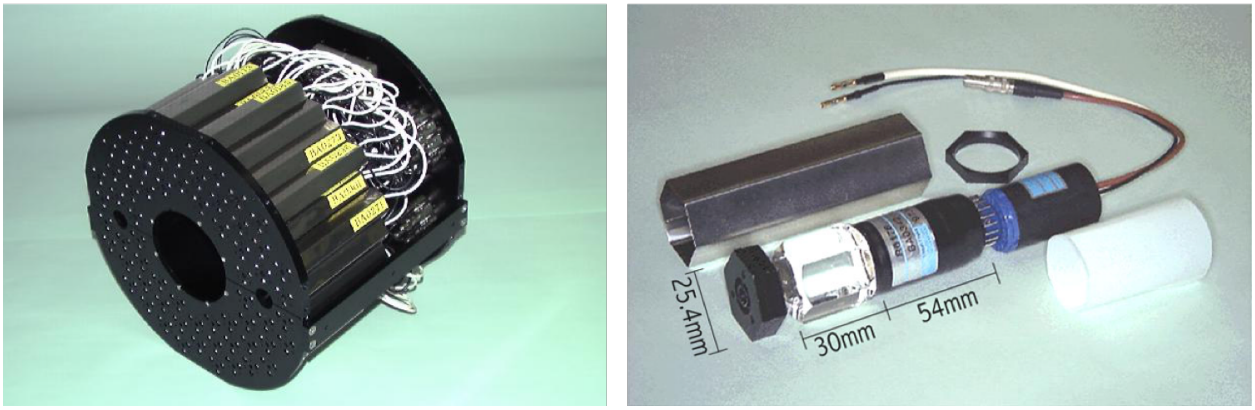

Figure 2.3: Left: The beam-beam counter in its entirety. The 64 photomultiplier tubes of the BBC are located at the front, and in back are the readout electronics. Right: A single BBC PMT consisting of a 30 mm long quartz Cherenkov radiator connected to a 54 mm long PMT. The whole tube is covered with a hexagonal piece of shielding used to keep out excess light [47].

Event categorization starts with determining the event timing itself. Particles from the collision arrive at the two BBC's asymmetrically because every collision is not centered perfectly at $z = 0$. Thus there are two initial timing parameters, T_N and T_S, the initial timing of the event as measured by the North and South BBC arms, respectively. T_N and

T_S are calculated according to the following Eqn. 2.1:

$$T_{S/N} = \frac{1}{m}\sum_{i=1}^{m} T_i \ , \tag{2.1}$$

Here, m is the number of fired PMT tubes, and T_i is the hit time of the i^{th} fired PMT tube. Using these arrival times, the collision time T_0 can be estimated using Eqn. 2.2:

$$T_0 = \frac{T_s + T_N + 2L/c}{2}, \tag{2.2}$$

Where $L = 144$ cm is the distance from BBC to the interaction region and c is the speed of light. Finally, the z-vertex (z_0) of the position can be calculated as:

$$z_0 = \frac{T_S - T_N}{2} \times c \tag{2.3}$$

2.2.1.1 Centrality Determination

Additionally, the BBC's serve as PHENIX's minimum bias detector and is estimated via simulation to have an efficiency of 93% in 200 GeV Au+Au collisions. And, as PHENIX's minimum bias detector, the BBC determines each event's centrality categorization by measuring charged particle multiplicities as described in 1.2.2. PHENIX's minimum bias criteria is as follows:

- More than one PMT in either north or south BBC must be struck

- The reconstructed z-vertex must be within $\pm$30cm of the interaction region ($z = 0$).
- The north and South zero-degree calorimeters must measure non-zero energy.
- There must be a successfully reconstructed z-vertex from the zero degree calorimeters.

Initially, an analysis of Run 16 was the target of this dissertation. As such, to become familiar with the PHENIX software infrastructure and as a service task for the PHENIX collaboration, the centrality reclibration was carried out for it. The first step in the process is to measure the charged measured in the BBC's across all events in Run 16 that have been tagged as minimum bias. The charge is collected in sixty separate 1cm z-vertex bins for the final calibration. The resultant charge distribution integrated over all z-vertex bins can be seen in Fig. 2.4. Corrections for drifts in the gain supplied to the BBC north and south are also applied by dividing each charge entry by the mean charge for a given data-taking time window (also referred to as a "run" with a lower-case "r", formally defined in Sec 3.1.5).

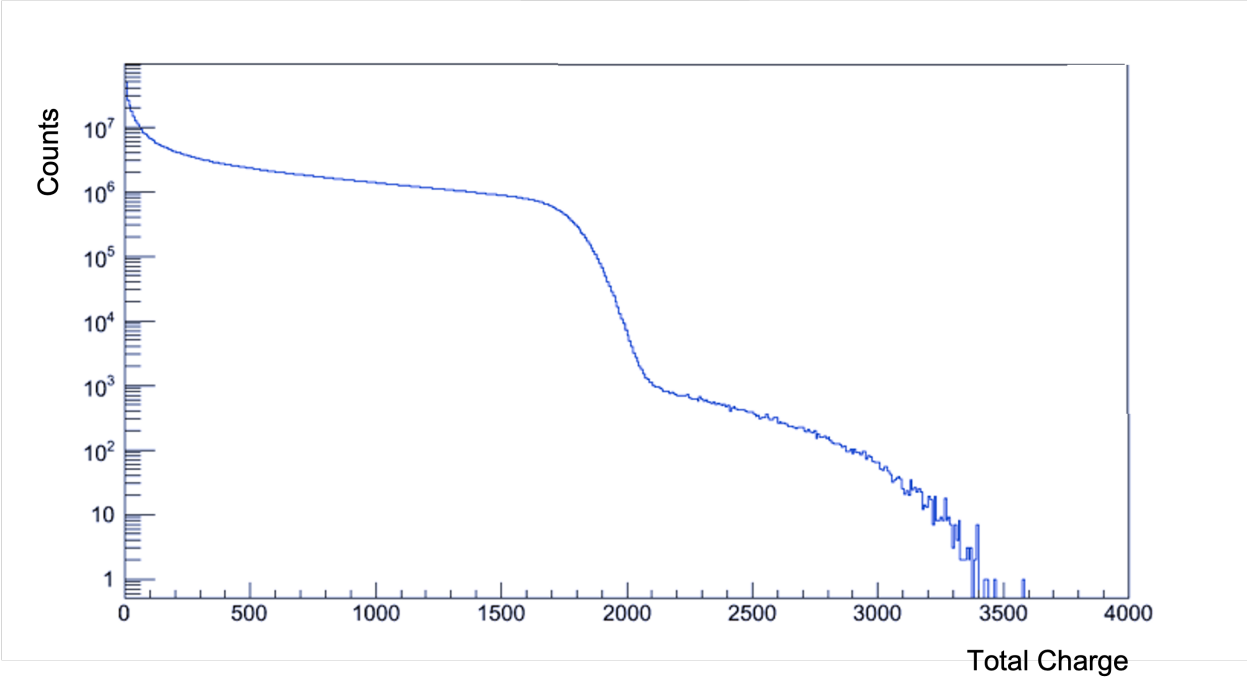

Figure 2.4: Distribution of the total charge embedded in both the BBC north and south collected over all of Run 16's minimum bias events for $|z| < 30$cm.

Next, this charge distribution is broken apart into 1% quantiles such that the number of events in each quantile is the same. Thus, the same fraction of the inelastic cross section is sampled in centrality ranges of the same size. This results in Fig. 2.5, which is a distribution of the number of events in each centrality bin. The distribution is flat as desired, meaning the process has been carried out successfully. This calibration is one of the first steps towards making a data set usable to other collaboration members.

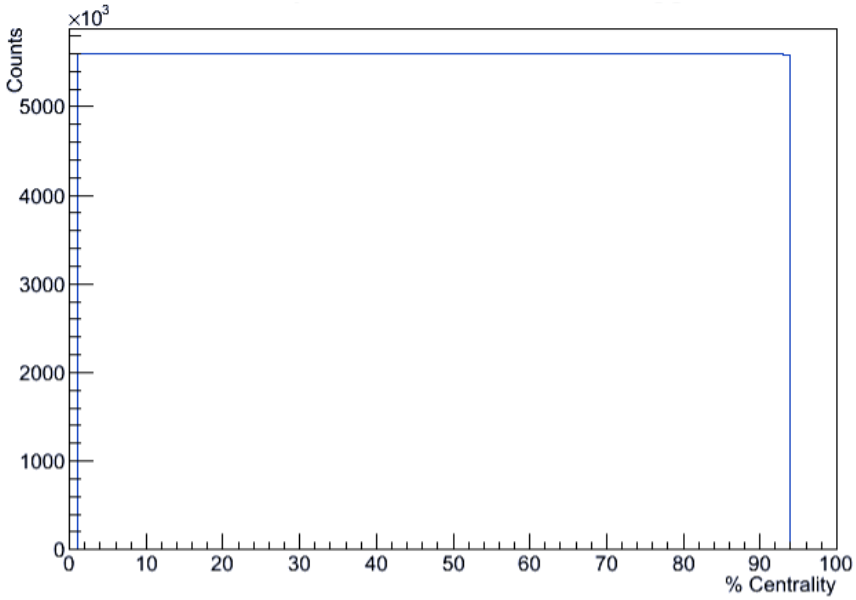

Figure 2.5: Centrality distribution for Run 16's minimum bias data set.

To cross-check the result, the number of events that fall within a given centrality range in each run is calculated. The expectation is that for a flat distribution such as in Fig. 2.5, the number of events that fall within a centrality percentile, Δc, is equal to $(\Delta c)(N_{Events})$ (for $0 < \Delta c < 1$). For example, for 100 events, one expects there to 25 events in the 0–25% and 25–50% centrality classes, or 15 events in the 30–45% centrality class, etc. The cross-check is shown in Fig. 2.6, which shows that the number of events per quantile agrees to within the standard deviation of the expected value of $(\Delta c)(N_{Events})$ over the course of Run 16 and for centrality bins that span from the most central (0–5%) to the peripheral (80–93%), thus meaning that the calibration process was a success.

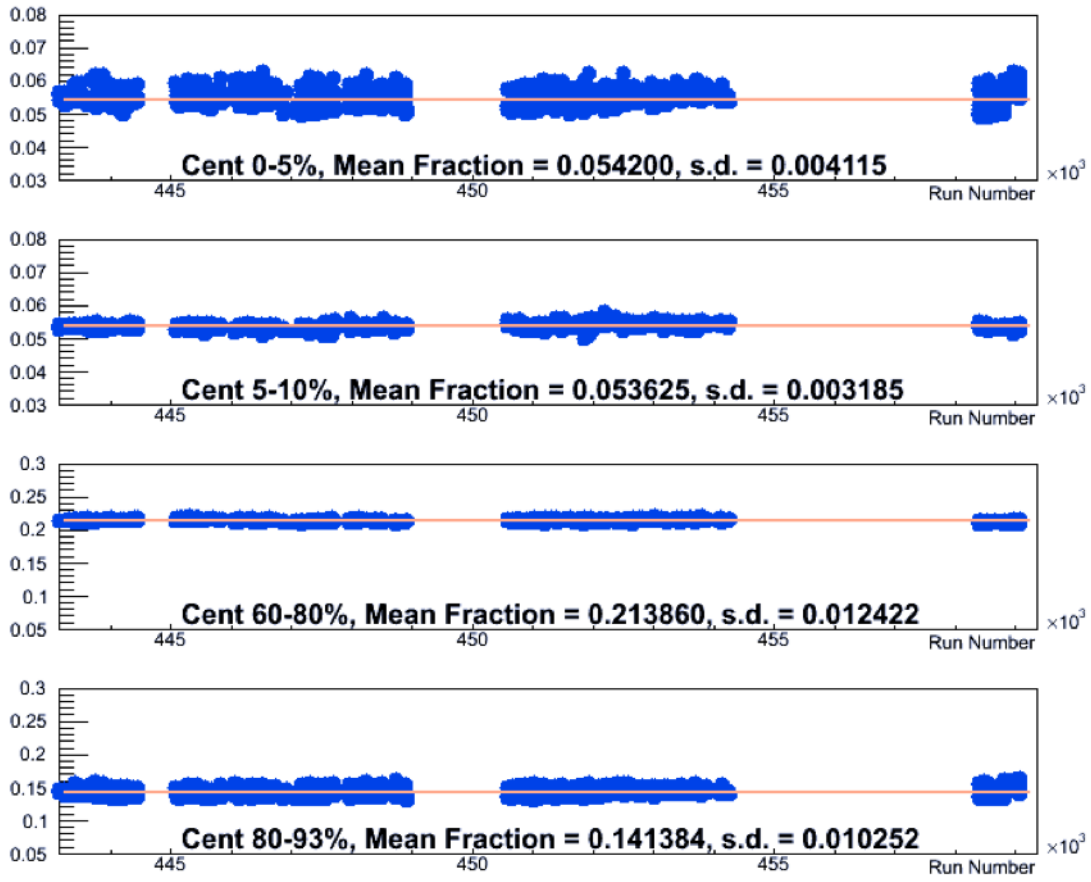

Figure 2.6: Number of events in a given centrality range as a function of run number for Run 16's minimum bias data set.

2.2.2 Zero-Degree Calorimeters

The zero-degree calorimeters (ZDC) [48] are a pair of hadronic calorimeters located in the North and the South arms, at a distance of 18 m from the interaction region. The ZDC's are dedicated to neutron measurements which can be used to measure event centrality and z-vertex position; though, their primary purpose in this analysis is to work in tandem with the BBC's for the purpose of background reduction during centrality determination as described in the previous section.

A dipole magnet sits in front of each ZDC arm and magnets are responsible for shielding the ZDC's from charged particles, which are bent away from the ZDC's upon encountering the dipole's magnetic fields. Thus, only neutral particles, neutrons in this particular case, arrive at the ZDC's. The z-vertex of the event can be measured by the ZDC in the same fashion as the BBC's by using Equation (2.3).

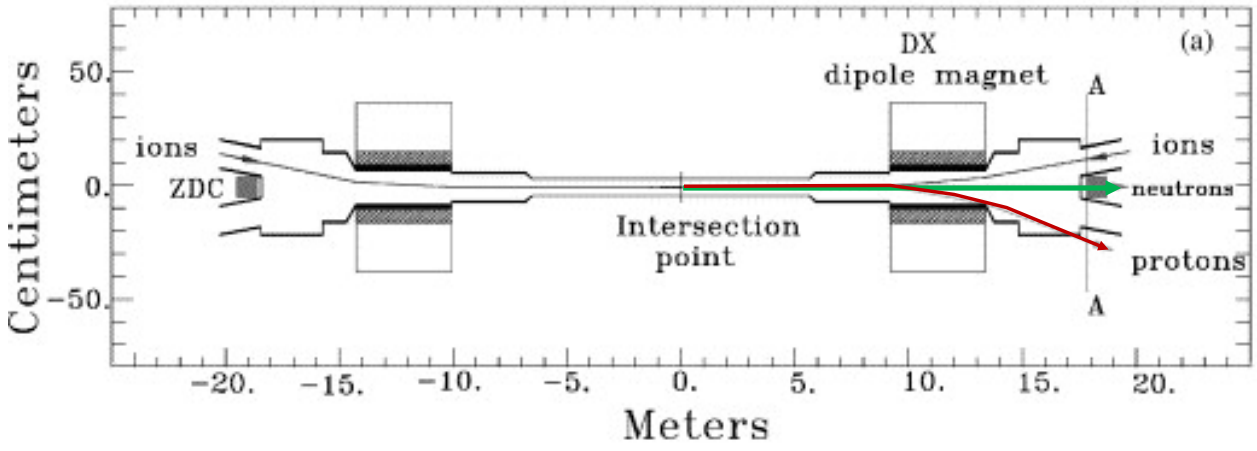

Figure 2.7: Depiction of ZDC's and dipole magnets along the beam pipe. The black lines represent the ion beams, and neutron and charged particle trajectories are represented by green and red lines, respectively. Unlike neutrons, charged particle trajectories bend because of the dipole magnet and miss the ZDC's [48].

2.2.3 Central Arm Tracking

The primary subsystems responsible for the reconstruction of tracks created by charged particles are the PHENIX Drift Chambers (DCH) and Pad Chambers (PC) [49]. These two subsystems, along with the electromagnetic calorimeter discussed in Sec. 2.2.5, cover π radians in azimuth and ± 0.35 units in psuedorapidity, the former dimension giving PHENIX it's iconic shape with a gap at the 12 and 6 o'clock positions. Charged particles created in

particle collisions streak through the gas-filled volume of the drift chamber, ionizing atoms in their path. This ionization causes electron-ion pairs to form along the path of the track. An electric field inside the drift chamber then guides the ions and electrons towards anode and cathode wires in the drift chamber, respectively. The drift chamber will then use the hit information to reconstruct the track via combinatorial Hough Transform (CHT). Inter-subsystem track matching between the drift chambers, pad chambers, and electromagnetic calorimeters is also used to reduce the number of fake tracks. In this method, tracks reconstructed in the drift chamber are matched to hits in the pad chamber or, in the event of dead pixels in the pad chambers, a tower of the electromagnetic calorimeter, confirming that they've been seen in multiple parts of the detector.

2.2.3.1 Drift Chamber

The Drift Chamber is the first step in track reconstruction. As outlined above, it is a gaseous volume filled with 50% Argon and 50% Ethane and a large assortment of wires which are struck by ions produced when charged tracks traverse the drift chambers. These wires are categorized into U, V, and X categories based on how they are arranged in the Drift Chamber. The X layer wires cross the drift chamber in straight lines (parallel to the beamline), whereas the U and V layers do so at angles, as shown in Fig. 2.8. While the bulk of the heavy lifting in terms of track reconstruction is done by the X layers, the U and V layers help refine the tracking information along the z-direction. In total, the PHENIX drift chambers carry a total of 12,800 wires.

As mentioned above, when charged particles pass through the drift chamber, they cause

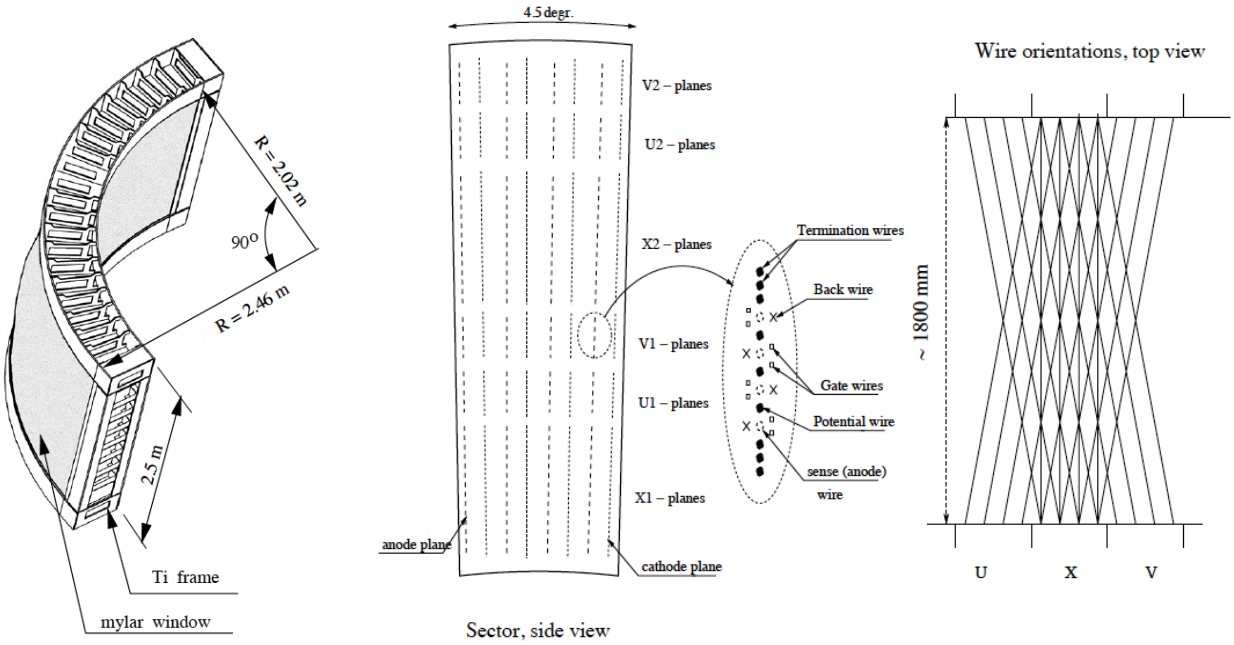

Figure 2.8: Left: mechanical drawing of the PHENIX Drift Chamber. Center: Drawing of a sector of the drift chamber with 6 layers of wire labelled as X1, X2, U1, U2, V1, and V2. Right: Top view of the wire orientations from three neighboring sectors

cascades of ions and electrons to strike wires in the U, V, and X layers. What results, then, is a complex network of hit information from multiple different tracks with different momenta and trajectories. This hit information is then fed through a Combinatorial Hough Transform to reconstruct the tracks and recover information such as their momentum. In general, the goal of a Hough Transform is to probabilistically identify lines from sets of points. Here these points are the hits in the drift chamber distributed in the $x - y$ plane. Each pair of points (x_i, y_i) in this space can be transformed into a line, and these lines populate a unique vector space known as a "feature space," which, in the study of pattern recognition, is a vector space composed of n-dimensional vectors composed of information that describes a given set of data. The slopes and y-intercepts of these lines are the components of these

vectors, but because high momentum tracks appear straight in the drift chamber, this causes a singularity where $m = 0$ corresponds to too many tracks to allow for faithful reconstruction. Thus, the Hough Transform is slightly modified so that the lines are parameterized in polar coordinates:

$$r(\theta) = x_i \cos\theta + y_i \sin\theta \tag{2.4}$$

In this way, we can have a unique representation for the line for each set of points when we constrain $0 < \theta < \pi$. If a set of points lies along a line $y_i = mx_i + b$, then it constrains the parameterization given in Eqn. 2.4 to:

$$r(\theta) = x_i \cos\theta + (mx_i + b) \sin\theta \tag{2.5}$$

There is a point of intersection for the whole family of curves given by Eqn. 2.5, and it is the point where $\cos\theta + m \sin\theta = 0$. Sampling many $r - \theta$ pairs will eventually result in a peak in the feature space, which uniquely identifies the line. However, using a simple Hough Transform such as the one listed above is computationally expensive and leads to the reconstruction of many false tracks. Thus, a Combinatorial Hough Transform (CHT), in which one considers pairs of ordered pairs instead of singular points, is used. In PHENIX, the CHT considers pairs of X1 and X2 drift chamber hits and bins them into a two-dimensional histogram $\phi - \alpha$ histogram, where ϕ is the polar coordinate and α, which, as depicted in Fig. 2.9, is the inclination angle from a track to a given reference line in the DCH. One

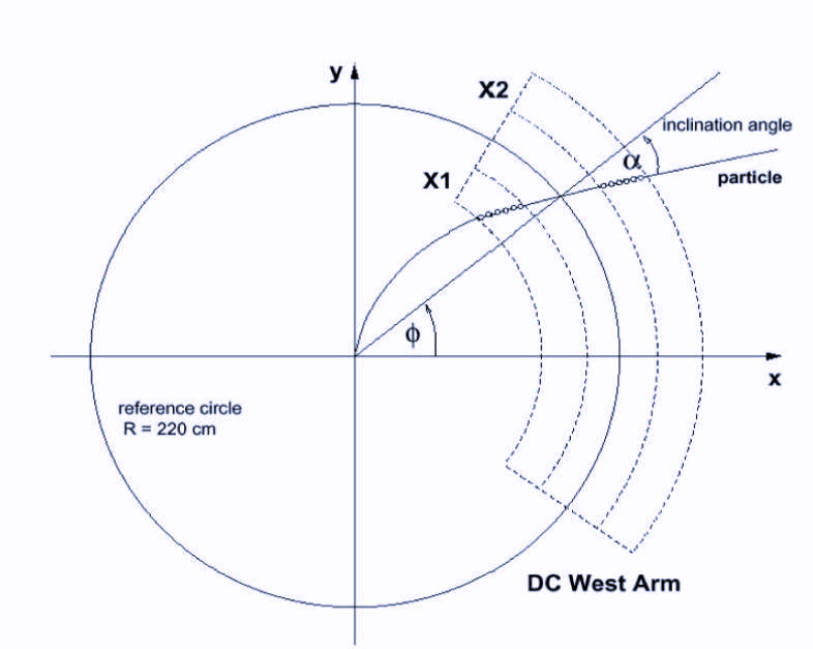

Figure 2.9: Cartoon of a single track traversing the PHENIX drift chamber. Here one can see depictions of the polar angle ϕ and the inclination angle α

important thing to point out is that although tracks in PHENIX are bent by the detector's interior magnet, once they reach the DCH, they become straight as they exit the magnetic field, thus permitting use of the CHT as outlined above. Additionally, reconstructed tracks are required to be confirmed by the Pad Chamber 1 (PC1) subsytem.

Final track candidates are chosen when a peak in the $\alpha - \phi$ histogram mentioned above rises above a certain threshold. The momentum of these tracks is then derived from the inclination angle α from the following relation:

$$\alpha \approx \frac{K}{p_T} \tag{2.6}$$

Where K is the integrated field strength and p_T is the transverse momentum of the track.

2.2.3.2 The Pad Chambers

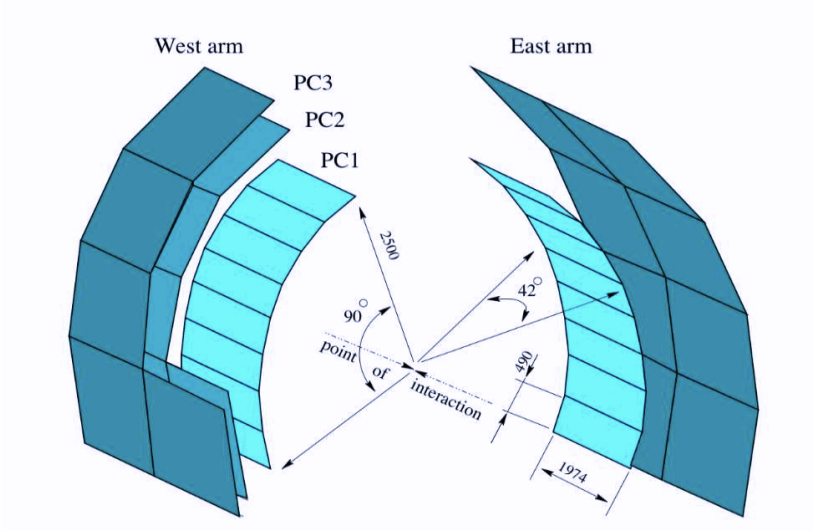

Figure 2.10: Cartoon depiction of the location of the PHENIX Pad Chambers (PC1, PC2, and PC3) within the central arms. Distances to interaction point and other measurements of interest are also shown

The Pad Chambers (PC1, 2, and 3) are the back-up singers for the Drift Chambers, composed of multiwire proporotional chambers, the Pad Chambers provide supplemental tracking information. As mentioned above, the first Pad Chamber (PC1) is the innermost chamber and is used in track reconstruction where its primary role is to provide information on a track candidate's z coordinate. PC2 is only located in the west arm of the detector and is not used in this analysis. PC3 however, plays a role in providing "track-matching" information, whereby tracks reconstructed in the Drift Chambers are matched to hits in PC3, and such inter-subsystem track information is used to improve the purity of the track sample. Each track will then have a certain amount of mismatch in its spatial coordinates (in centimeters) between the Drift and Pad Chambers (denoted dz and $d\phi$ for such quantities in the z and ϕ

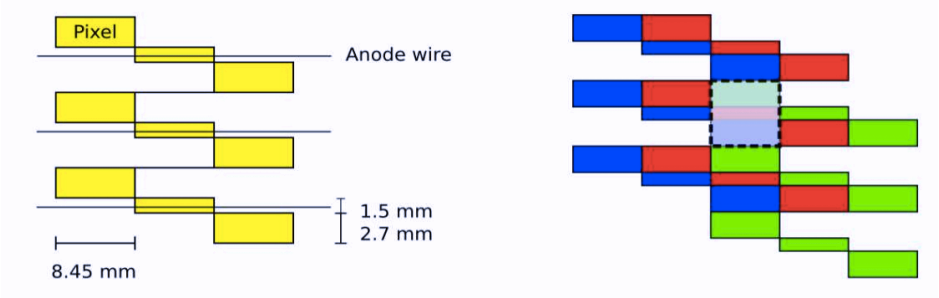

Figure 2.11: Left: PC1 readout pad consisteing of nine pixels grouped together in a staggered configuration. While shown for PC1, the outer pad chambers have similar configurations which accomplish a comparable angular resolution, albeit with larger pixels. Right: pads are arrangement into an inter-locking pattern such that three vertically adjacent pixels form a cell. These cells form the fundamental component of a pad chamber cluster.

directions, respectively). These values are collected for all tracks, and the resulting distributions are fitted with a Gaussian. For this analysis, cuts are made on the standard deviation of the the dz and $d\phi$ distributions, σ_{dz} and $\sigma_{d\phi}$, and this will be further discussed in the Analysis chapter of this dissertation. Depictions of the Pad Chambers and their location in the central arms can be seen in Fig. 2.10.

The individual Pad Chambers consist of a single plane of anode and field wires immersed in a gas mixture (50% ethane and 50% Argon like the drift chambers) that are sandwiched between cathode planes. One of these cathode planes is solid copper, and the other planes is segmented into pixels as shown in Fig. 2.12. These pixels are then combined into groups of three to form one cell. In order to be recorded, signal from a hit must be received by each of the three pixels in a cell to reduce electronic background. This configuration is shown in Fig. 2.11. This signal is then sent to the ReadOut Card (ROC) for amplification.

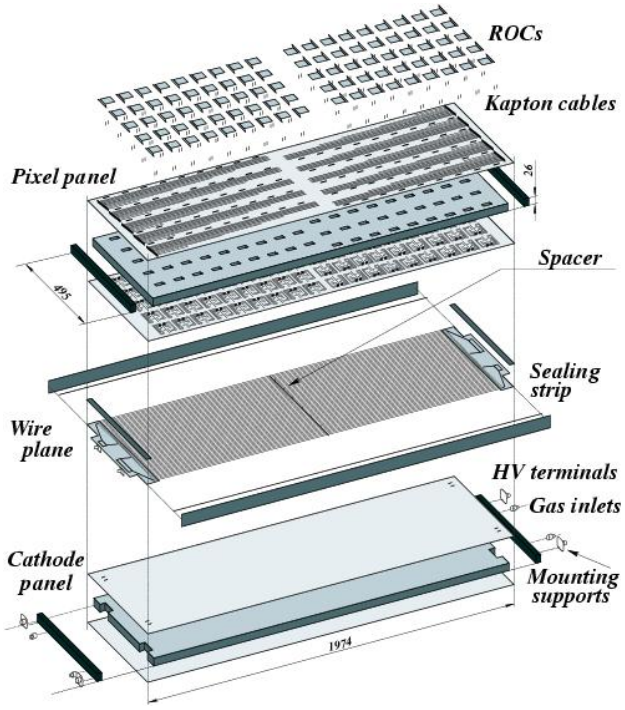

Figure 2.12: Internal configuration of a PHENIX Pad Chamber panel

Structurally, the inner pad chamber (PC1) is supported by its stiff honeycomb-like interior rather than in actual frame. This design is chosen to reduce the PC1's radiation thickness because it resides on the interior of the central arm, close to the interaction region. To provide stability, PC1 is actually glued shut, meaning that it, unlike the drift chambers, for instance, cannot be re-opened for repairs. PC2 and PC3, however, are further away from the interaction region and have fiberglass frames. Lastly, all reconstructed tracks are assigned a quality number depending on the number of hits in the U, V, and X layers of the drift chambers and information from the first pad chamber with 63 and 31 being the best and second best qualities, respectively.

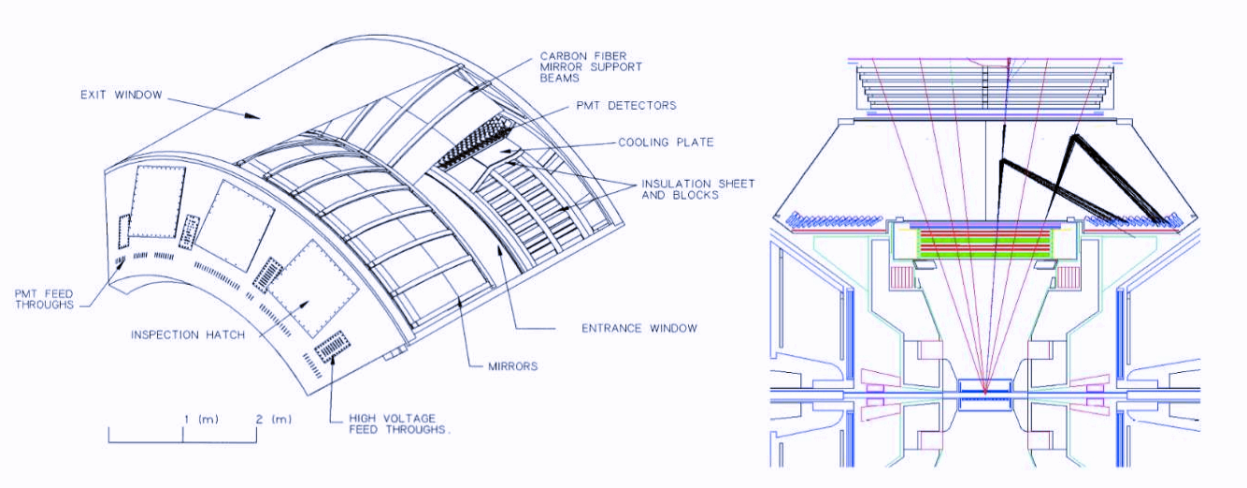

Figure 2.13: Left: Outer view of the RICH subsystem. Right: Cutaway drawing showing Cherenkov light rays being reflected into the PMT array by a spherical mirror (not depicted).

2.2.4 Ring-Imaging Cherenkov Detector

The Ring-Imaging Cherenkov Detector (RICH) sits behind the drift chamber and first pad chamber. Its primary role is to allow for discrimination between electrons and other charged particles. In the case of this analysis, the RICH is used to veto electrons from the charged particle pool so that only charged hadrons remain. A visual overview of the RICH subsystem is shown in Fig. 2.13

The primary phenomonon exploited by the RICH is Cherenkov radiation. Cherenkov radiation is produced when a charged particle traverses a dielectric medium at a speed faster than the speed of light in that medium. Mathematically, this threshold is expressed as:

$$\beta > \frac{1}{n} \tag{2.7}$$

Where $\beta = \frac{v}{c}$ and n is the index of refraction of a given medium. When a charged particle

passes through a dielectric material (often referred to as a radiator) with a velocity that satisfies Eqn. 2.7, molecular dipoles within the material are disturbed by the fast moving electromagnetic field produced by the incoming charged particle. Upon their return to equilibrium, they release a wave of radiation in the short visible and near UV wavelength range. Ordinarily ($\beta < 1/n$), the light released by these dipoles destructively interferes with itself and effectively dissipates. However, past this threshold, the light interferes constructively, causing the radiator to emit Cherenkov radiation along the trajectory of the particle, similar to a Mach cone that appears when objects travel faster than the speed of sound in an atmosphere. This radiation appears at an angle, θ_c, to the charged particle's trajectory, and this angle is governed by Eqn. 2.8.

$$\cos\theta_c = \frac{1}{\beta n} \tag{2.8}$$

PHENIX's RICH detectors use CO_2 as a radiator, which has an index of refraction of $n = 1.000410$, which corresponds to a threshold momentum of 0.02 GeV/c for electrons, whereas charged pions will begin to trigger the rich at 4.7 GeV/c. In spite of CO_2's lower Cherenkov photon yield versus, say, Ethane, the 4.7 GeV/c threshold is also higher than Ethane's threshold momentum, allowing for greater pion/electron separation. Because this analysis makes use of charged pions above the RICH's threshold momentum, however, RICH information for charged tracks above 5 GeV/c is not used.

In practice, each PHENIX RICH subsystem uses a spherical mirror to reflect Cherenkov light into an array of 1280 PMT's (2560 total in both arms). This allows for the Cherenkov

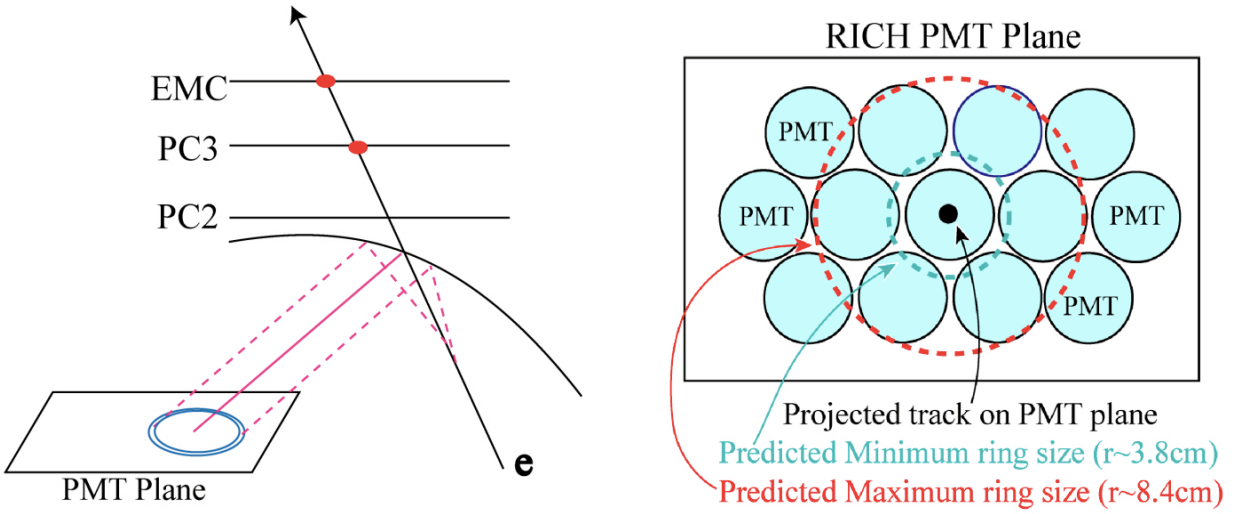

Figure 2.14: Left: Cherenkov light from an electron being focused onto the PMT array by the RICH's mirrors. Right: Rings of Cherenkov light hitting PMT's. In this analysis, if any PMT is fired by a track with momentum beneath 5GeV/c, the track is vetoed.

light from a radiating charged track to be focused into a ring whose radius is independent of the emission point, but instead dependent only on the momentum of the radiating particle. A cartoon of this is shown in Fig. 2.14. Typical ring sizes are about 12 cm.

2.2.5 Electromagnetic Calorimeter

One of PHENIX's most critical subsystems is its electromagnetic calorimeter subsystem. The EMCal is responsible primarily for measuring the energy and position of photons and electrons, and it can also be used as a back-up for the PC3 for track matching in the event of dead cells in the PC3. The EMCal is composed of six lead-scintillator (PbSc) and two lead-glass (PbGl) sectors, as shown in Fig. 2.2. Via test beam measurements, the energy resolution of the PbSc and PbGl sectors were measured to be $8.1\%/\sqrt{E} \otimes 2.1\%$ and $5.9\%/\sqrt{E} \otimes 0.8\%$, with timing resolutions of 100 ps and $200 - 400$ ps, respectively. One of the key advantages

of the PHENIX EMCal is its granularity, which allows for reconstruction of neutral pions (π^0's) from pairs of photons (as opposed to by cluster shape) reliably up to 20 GeV/c, thus making it a centerpiece of this dissertation's analysis.

The PbSc design is known as a Shashlik-type (Russian for "skewer") sampling calorimeter comprised of alternating layers of lead and scintillator. The scintillator is composed of polystyrene containing an organic scintillator known as POPOP and a fluorescent additive p-Terphenyl, which a large light yield (∼12500 photons/GeV/tower). The base unit of the calorimeter sectors are called towers, which contains 66 sampling layers that have been skewered together by wavelength shifting fibers, which themselves are responsible for carrying signal photons to the readout electronics. Four towers are then grouped together into a module, 36 of which form a supermodule, 18 of which will form one sector. This configuration is shown on the left side of Fig. 2.15.

The PbGl modules, by contrast, are large glass blocks containing 51% PbO. The blocks are wrapped in aluminized mylar for light isolation and then grouped into 6-by-4 tower supermodules. The finer segmentation of the PbGl sectors leads to improved position and energy resolution; however, the timing resolution is worse because of its sensitivity to hadronic interactions.

Both towers function using the phenomenon of electromagnetic showers, which are produced via two primary interactions of particles with the EMCal: those arising from photons, and those arising from electrons and positrons. As $e^{\pm}$'s pass through the calorimeter, their trajectories are bent by the positively charged nuclei within the lead atoms, causing them

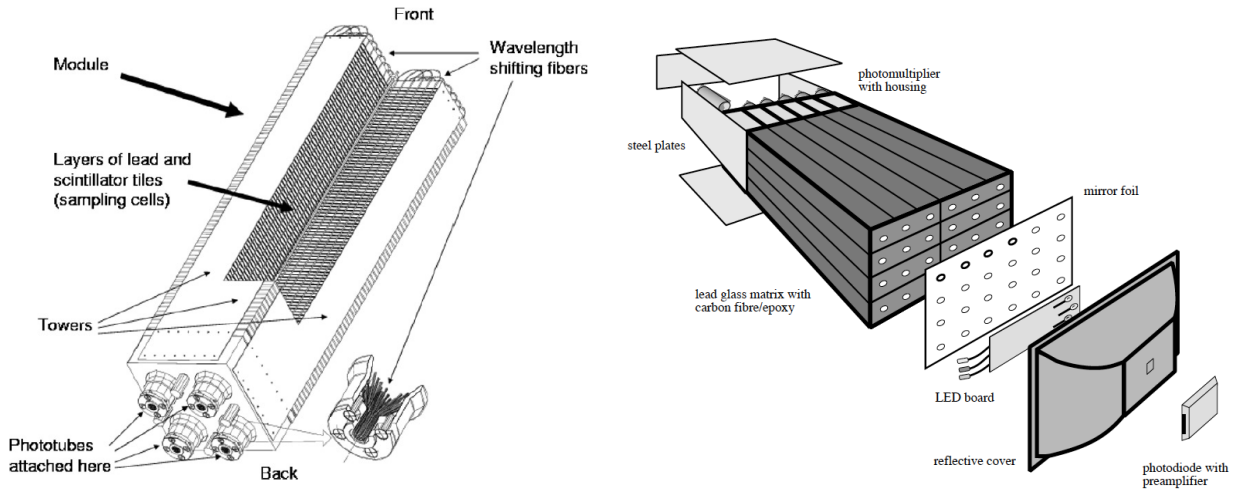

Figure 2.15: Left: A lead-scintillator module with a cutaway through which one can see the four individual towers that compose the modules. Right: Schematic of a lead-glass supermodule composed of 24 individual models.

to radiate photons via bremsstrahlung (German: "breaking radiation"). For photons, electromagnetic showers are begun when a photon similarly passes near a positively-charged lead nucleus, causing it to undergo pair production, whereby an electron-positron pair are produced, which then go on to further shower via the same principle that applies when you begin with an individual electron or positron. Additionally, because the photons and $e^{\pm}$'s that enter the calorimeter typically have above several hundred MeV's worth of energy, the showering processes typically repeat themselves a number of times, leading to a electromagnetic cascade of $e^{\pm}$'s and photons. Both of these process are illustrated in Fig. 2.16. Additionally, because electromagnetic showers produced by photons and $e^{\pm}$'s have slightly different profiles, a cut on the shower shape allows one to discriminate between photons, electrons, and positrons.

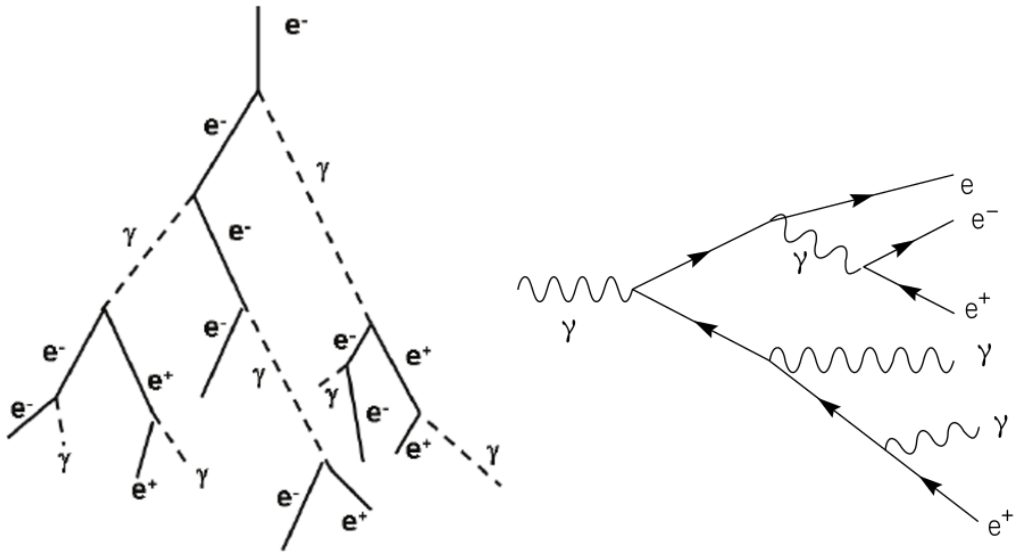

Figure 2.16: Left: Electromagnetic shower initiated by electronic bremsstrahlung. Right: Electromagnetic shower initiated by a photon undergoing pair production.

2.2.6 PHENIX Data sets

A list of data samples taken by the PHENIX detector is shown in Table 2.1, and the data sets used in this analysis, specifically, are highlighted in yellow. PHENIX took data for a wide variety of collisions and center-of-mass energies. Collecting data a various center of mass energies was the focus of the RHIC Beam Energy Scans (BES) in an effort to search for the QCD critical point. Additionally, a parallel effort included holding the center-of-mass energy constant while changing the collision systems, which eventually lead to the discovery of both elliptic and triangular flow in small systems [44] by the PHENIX collaboration. The bread-and-butter collision-type measured by PHENIX, however, is $Au + Au$ collisions at $\sqrt{s_{NN}} = 200$ GeV and their accompanying $p + p$ baseline.

Improving the statistical precision of PHENIX measurements is composed of two strategies. The first is to simply take more data during the RHIC operational periods. This has

culminated in two large-statistics data sets, Run 14 and Run 16. Results from Run 14 will be presented in this dissertation, but, unfortunately, Run 16 was not fully ready for analysis at the same time as Run 14. The second strategy is to combine results from new data sets with those from older data sets. The original intention of this dissertation was to combine new π^0-hadron correlation results from Run 14 (the largest PHENIX 200 GeV $Au+Au$ data set) with those from Runs 10 and 11 reported in [38]. Unfortunately, problems arose with Run 10's PC3 matching recalibrator, meaning a re-measurement of the results would be in order. Thus, the results in this dissertation from Run 14 will serve as the baseline to be combined with future analyses from Run 16.

Table 2.1: Summary of PHENIX minimum bias data sets

Run Number	Year	Species	C.M. energy (GeV)	Number of events	integrated Luminosity (b^{-1})
1	2000	$Au+Au$	130	10 M	1 μ
2	2001–2	$Au+Au$	200	170 M	24 μ
		$p+p$	200	3.7 B	0.15 p
3	2002–3	$d+Au$	200	5.5 B	2.74 n
		$p+p$	200	6.6 B	0.35 p
4	2003–4	$Au+Au$	200	1.5 B	241 μ
		$Au+Au$	62.4	58 M	9 μ
5	2005	$Cu+Cu$	200	8.6 B	3 n
		$Cu+Cu$	62.4	400 M	0.19 n
		$Cu+Cu$	22.4	9 M	2.7 μ
		$p+p$	200	85 B	3.8 p
6	2006	$p+p$	200	233 B	10.7 p
		$p+p$	62.4	28 B	0.1 p
7	2007	$Au+Au$	200	5.1 B	813 μ
8	2008	$d+Au$	200	160 B	80 n
		$p+p$	200	115 B	5.2 p
9	2009	$p+p$	500	3.08 B	14 p
		$p+p$	200	9.36 B	16 p
10	2010	$Au+Au$	200	8.2 B	1.3 m*
		$Au+Au$	62.4	700 M	0.11 n
		$Au+Au$	39	250 M	40 μ
		$Au+Au$	7.7	1.6 M	0.26 μ
11	2011	$p+p$	500	594 B*	27 p
		$Au+Au$	19	13 M	2.17 μ*
		$Au+Au$	27	2.2 B*	5.2 μ
		$Au+Au$	200	5.7 B*	915 μ
12	2012	$p+p$	200	4.5 B	9.24 p
		$p+p$	510	4.2 B	30.03 p
		$Cu+Au$	200	6.8 B	2.8 n
		$U+U$	192	3 B	171.19 μ
13	2013	$p+p$	510	15 B	156.49 p
14	2014	$He+Au$	200	2.8 B	134 n
		$Au+Au$	15	15 M	44.2 μ
		$Au+Au$	200	19.9 B*	2.56 n
15	2015	$p+p$	200	4 B*	59.91 p
		$p+Al$	200	2 B*	691 n
		$p+Au$	200	3.7 B*	206.2 n
16	2016	$Au+Au$	200	14.3 B	2.3 m*
		$d+Au$	20	1.0 B*	
		$d+Au$	39	2.0 B*	
		$d+Au$	62	0.93 B*	
		$d+Au$	200	1.5 B*	286 p*

* Estimated values

CHAPTER 3

π^0-Triggered Two-Particle Correlations: Analysis

As mentioned earlier in Sec. 1.2.3.2, two-particle correlations involves measuring the angular correlations between a high-momentum jet proxy and charged hadrons in a given event. In this analysis, the π^0 serves as the jet proxy, or trigger particle. π^0's in PHENIX are reconstructed by combinatorially pairing photons together and selecting on those that pass a series of quality cuts, including restricting their reconstructed invariant mass to a range centered about the π^0's measured mass of approximately 135 MeV/c^2. The angle between the trigger π^0's and charged hadrons is then measured, yielding a correlation function, which is then corrected for detector inefficiencies and acceptance deficiencies. Finally, the underlying event accounting for flow is subtracted, leaving behind only correlations between particles associated with jets. From the jet functions, we then extract physics quantities. Plots and data shown in this chapter will be from the 2014 PHENIX 200 GeV Au+Au data set, though Sec. 3.2 will make reference to the 2010 and 2011 200 GeV $Au + Au$ data sets as well.

3.1 Data Selection

Cuts are applied on events, EMCal clusters, reconstructed π^0's, and charged tracks. After passing all the cuts described in Table 3.1, the data are binned in centrality percentile, π^0 p_T, and charged hadron p_T. Furthermore, a run-by-run quality assurance, detailed in Sec. 3.1.5, is also performed to remove so-called "bad runs" from the data. These bad runs are typically the result of fluctuations in the performance of different PHENIX subsystems that either go away or are repaired over the course of data taking.

Table 3.1: Summary of cuts applied during particle and event selection

Cut		Criteria
Event	z-vertex	$\|\text{zvtx}\| \leq 10$ cm
	Centrality Bins	0–20%, 20–40%
Single Photon	Tower Cuts	Reject clusters from identified bad towers
		Reject clusters in towers located next to bad towers
		Reject clusters located in towers at the edge of the EMCal
	Energy	$E \geq 1$ Gev
	Shower Shape Cut	Reject clusters that are 2% least likely to be a photon
		using photon probability $< 2\%$ cut or photons that
		fail dispersion cut in the PbGl sectors
	Charged Track Veto	Reject clusters within 8 cm of a charged track projection
		from the PC3 to the EMCal
Photon Pairs	Proximity	Both photons are in the same arm of the EMCal
	Total Energy	$E_{Total} = E_{\gamma_1} + E_{\gamma_2} \geq 4$ GeV
	Energy Asymmetry	$\alpha \leq 0.15 + 0.85(\frac{E_{\pi^0}-4)^2}{1.25})$
	Invariant Mass Cut	$0.12 \leq m_{\gamma\gamma} \leq 0.16$ GeV
	Momentum Bins	4–5 GeV/c, 5–7 GeV/c, 7–9 GeV/c
		9–12 GeV/c, 12–15 GeV/c
Charged Tracks	Track Quality	Reconstructed tracks must have
		a hit in both X1 and X2 planes of the DC,
		a hit in either U or V plane of the DC, and a hit in PC1
	Electron Rejection	Reject tracks with $p_T < 5$ GeV/c that trigger the RICH
	Track Matching	$\sqrt{\sigma^2_{d\phi} + \sigma^2_{dz}} < 2$ for $p_T < 5$
		$\sqrt{\sigma^2_{d\phi} + \sigma^2_{dz}} < 1$ for $p_T \geq 5$
	Momentum Bins	0.5–1 GeV/c, 1–2 GeV/c, 2–3 GeV/c
		3–5 GeV/c, 5–7 GeV/c

3.1.1 Event Selection

To make sure that the final particles fall within the PHENIX pseudorapidity acceptance ($\eta \leq 0.35$), the absolute value of each event z-vertex is required to less than 10 cm. This z-vertex cut is tighter than in years past (which were typically set at ± 30 cm) as a large

fraction of the events in the minimum bias data set fall within this narrower window to make them fall within the acceptance of the silicon vertex detector. Furthermore, this analysis focuses on two centrality bins, 0–20% and 20–40%, to study the potential impact of system size on medium-induced jet modification.

3.1.2 Single Photon Selection

Single photon selection begins with individual clusters reconstructed by the EMCal. Clusters located in predetermined bad regions of the EMCal are rejected fiducially. These include dead and malfunctioning towers found during production of the raw data. Additionally, towers in a three by three square around these dead towers are also rejected. This expanded exclusion zone accounts for the fact that electromagnetic clusters will sometimes span multiple towers. Thus, removing the towers around a given bad tower ensures that no clusters associated with that bad tower will be used in the analysis. Additionally, the two towers closest to the EMCal's edge are also excluded for a similar reason. Towers near the edge of the EMCal's acceptance can possibly "leak" a portion of the cluster's energy outside of the EMCal, meaning that the cluster's energy does not accurately reflect the energy of the original photon or electron. We also reject clusters with an energy beneath 1 GeV to mitigate noise.

A cut on the frequency of hits in a given tower is done to mask "hot towers", which might also be malfunctioning by falsely reporting hits. To create this list of hot towers, data from the entire run is used to measure the average number of clusters per tower. After the removal of outlier towers, the standard deviation of this distribution is calculated, and towers having a number of hits exceeding a certain multiple of the standard deviation are excluded from

this analysis. This analysis, in particular, uses a 4σ cut-off. The impact of the hot tower cut can be seen in Figs. 3.1 through 3.4. All towers bordering hot towers are also masked.

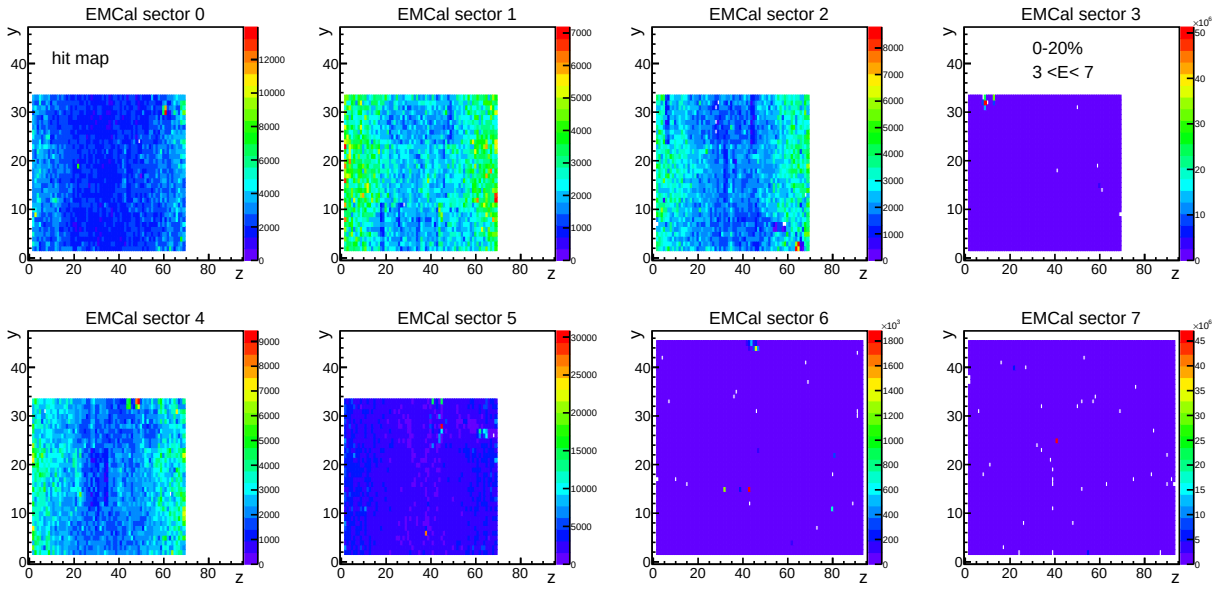

Figure 3.1: Hit maps of clusters within the EMCal for clusters with $3 < E_{Cluster} < 7$ GeV before the removal of bad towers. The color scale represents how many times a cluster registered within a given tower. Sectors 0 through 5 are lead-scintillator, while sectors 6 and 7 are lead-glass

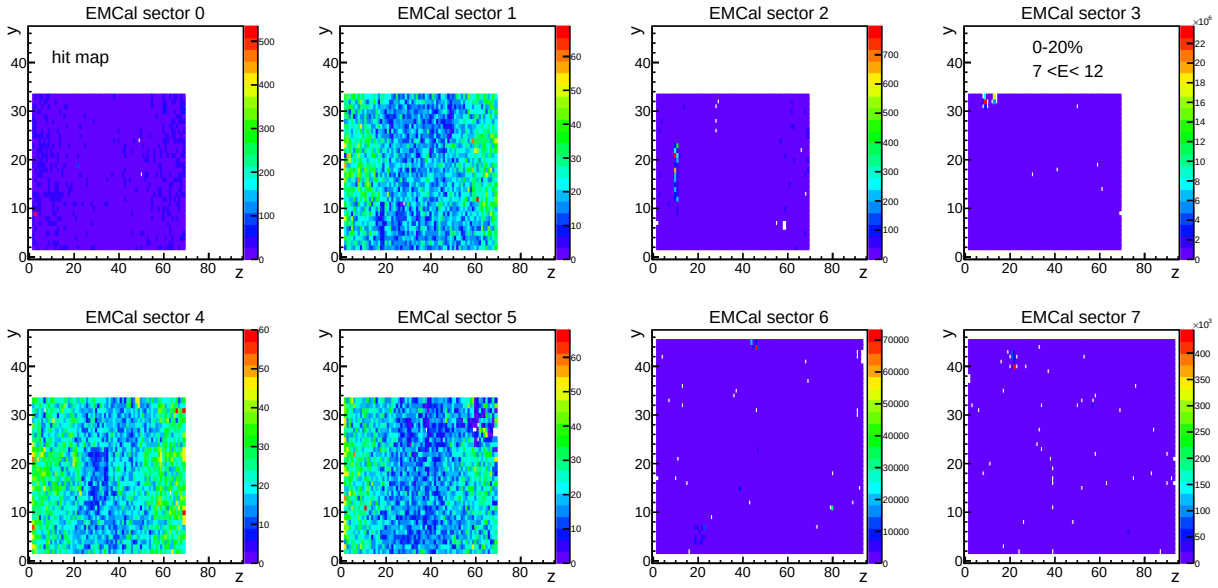

Figure 3.2: Hit maps of clusters within the EMCal for clusters with $7 < E_{Cluster} < 12$ GeV before the removal of bad towers. The color scale represents how many times a cluster registered within a given tower. Sectors 0 through 5 are lead-scintillator, while sectors 6 and 7 are lead-glass

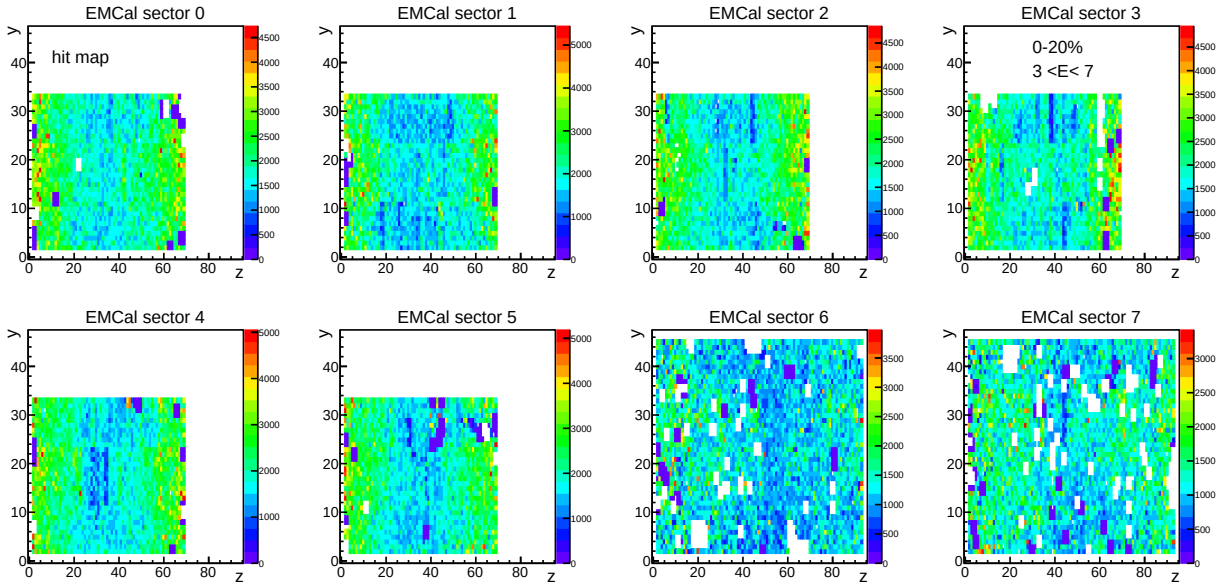

Figure 3.3: Hit maps of clusters within the EMCal for clusters with $3 < E_{Cluster} < 7$ GeV after the removal of bad towers. The color scale represents how many times a cluster registered within a given tower. Sectors 0 through 5 are lead-scintillator, while sectors 6 and 7 are lead-glass

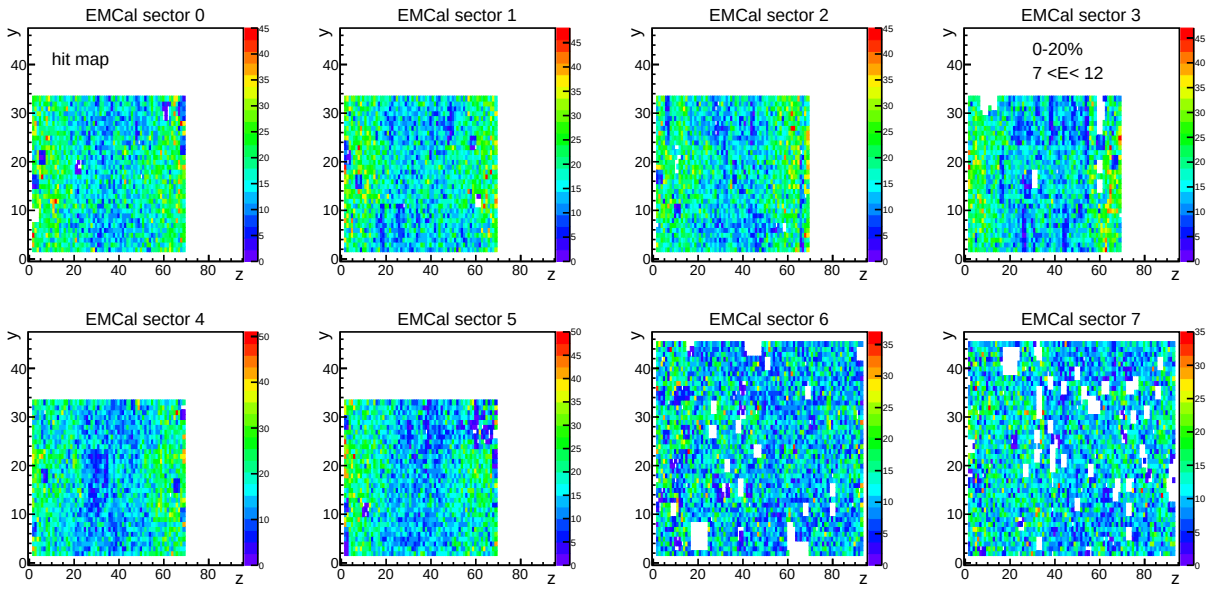

Figure 3.4: Hit maps of clusters within the EMCal for clusters with $7 < E_{Cluster} < 9$ GeV after the removal of bad towers. The color scale represents how many times a cluster registered within a given tower. Sectors 0 through 5 are lead-scintillator, while sectors 6 and 7 are lead-glass

A cut on the shape of the cluster itself is also applied. Idealized reference clusters based on photon showers are created in simulation, and clusters from real data are then compared to them. A cut is then applied to remove the clusters that are within the least likely probability to be a photon. The value cut on is a confidence level, thus, the requirement that the photon probability be $< 2\%$ means that 2% of real photons are removed by this cut. A specialized dispersion cut developed specifically for the PbGl sectors is also used, though its functionality is the same: to cut on the profile of electromgatic clusters.

Finally, a cut must be applied to prevent hadrons that have deposited energy into the EMCal from being considered as photons. To do this, positional information from both the pad chambers and the EMCal is combined, and the distance from the nearest pad chamber

hit and the EMCal cluster of interest is calculated. The basic idea is to exclude any cluster which has an associated pad chamber hit within a certain radius. In this case, the exclusion zone, adopted from [50], is circular with a radius of 8 cm. That is to say, clusters are rejected if there is a charged track projection within 8 cm of a cluster. The effect of the sequential application of each cut on the raw, black single photon spectrum can be seen in Figs. 3.5 for the 0–20% centrality bin and 3.6 for the 20–40% centrality bin. Cutting out bad towers (going from magenta to grey spectra) is the most impactful cut and does the most to give the inclusive spectrum the steeply falling feature typically associated with particle spectra.

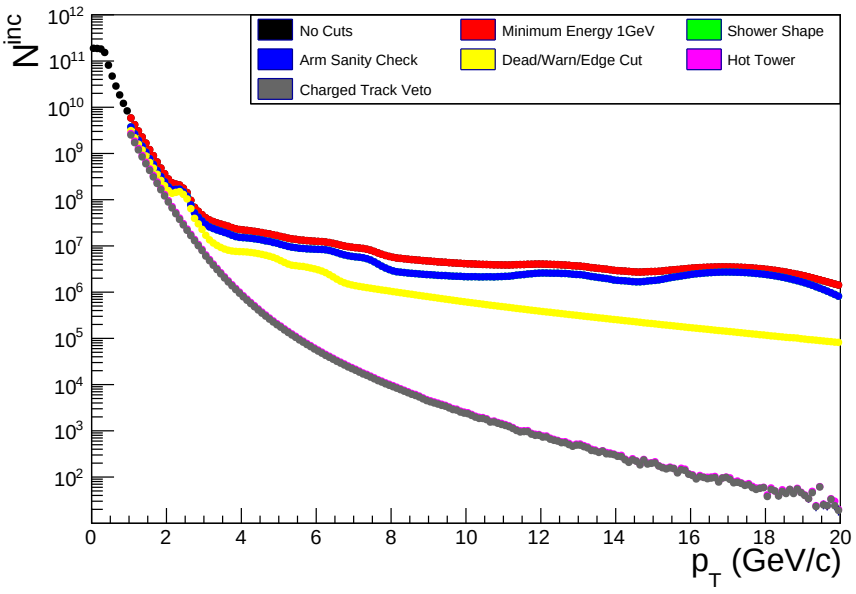

Figure 3.5: The impact of each cut on the inclusive photon spectrum in the 0–20% centrality bin. The cuts are applied sequentially going from left to right and top to bottom in the legend. Some cuts can be hidden because their impact is negligible; thus, the next cut sits on top of it.

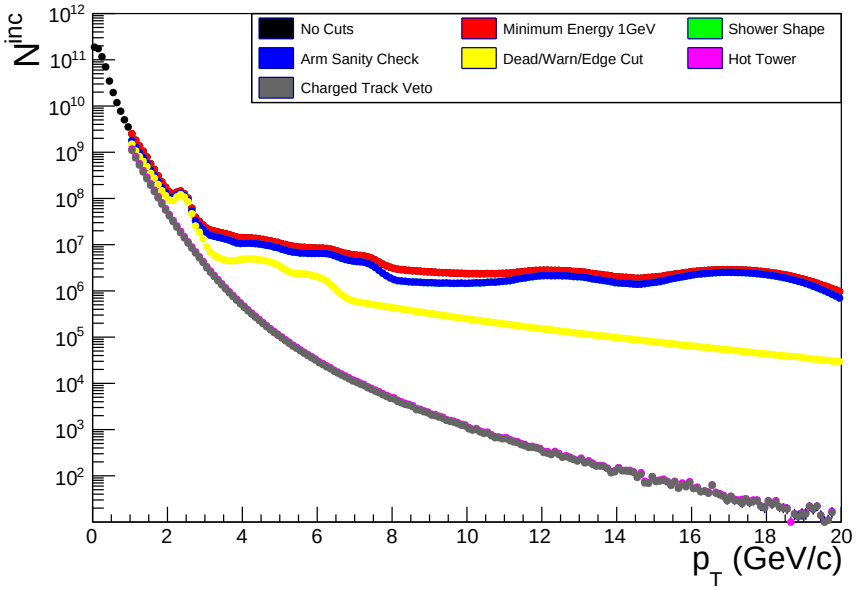

Figure 3.6: The impact of each cut on the inclusive photon spectrum in the 20–40% centrality bin. The cuts are applied sequentially going from left to right and top to bottom in the legend. Some cuts can be hidden because their impact is negligible; thus, the next cut sits on top of it.

3.1.3 Photon Pair Selection

Clusters that pass all cuts detailed in the previous sections can then be used to reconstruct π^0's via combinatorial pairing process. In accordance with the cuts listed in Table 3.1, the decay photon pair must be detected in the same EMCal arm, the total energy of the photon pair, $E_{total} = E_{\gamma 1} + E_{\gamma 2}$, must be at least 4 GeV, and, to help reject fake π^0's, an energy asymmetry cut is applied on the photon pairs that have total energy less than 5.25 GeV. The energy asymmetry is defined by Eqn. 3.1.

$$\alpha = \frac{|E_{\gamma 1} - E_{\gamma 2}|}{E_{\gamma 1} + E_{\gamma 2}} \ . \tag{3.1}$$

Where E_γ is the energy of a given photon used in the π^0 reconstruction process. The asymmetry cut requires that α satisfy the following constraint for $E_{\pi^0} \leq 5.25$ GeV:

$$\alpha \leq 0.15 + 0.85 \left[\frac{E_{total} - 4}{1.25} \right]^2 . \tag{3.2}$$

Next, the mass of the reconstructed π^0 is calculated with the formula given by Eqn. 3.3:

$$m_{\pi^0} = \sqrt{2E_{\gamma 1}E_{\gamma 2}\cos(1-\psi)} , \tag{3.3}$$

Here, ψ is the open angle between the photon pair. The spectra of reconstructed π^0 masses measured in Run 14 are shown in Fig. 3.7. Although Fig. 3.7 shows π^0 candidates with masses from 0–0.2 GeV/c^2, only π^0 candidates with mass between 0.12 GeV/c^2 and 0.16 GeV/c^2 are used as trigger particles.

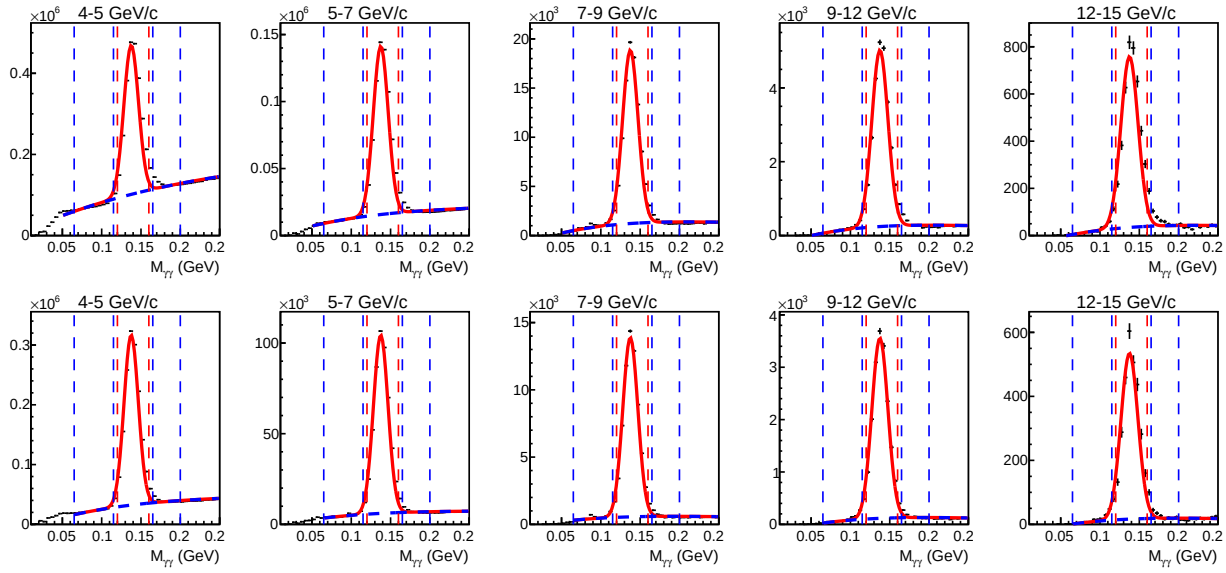

Figure 3.7: Invariant mass distributions in each π^0 momentum region in the 0–20% (Top) and 20–40% (Bottom) centrality classes. The red solid line represents the total fit to the spectrum, whereas the blue dashed line is the background only. The vertical red dashed lines represent the nominal invariant mass window range of 0.12 GeV/c^2 to 0.16 GeV/c^2, and the vertical blue dashed lines represent the upper and lower sideband regions used to compute the π^0 reconstruction systematic uncertainty, discussed in Sec. 4.5

The true π^0 mass is measured to be 134.98 MeV/c^2 [5], but, because of detector smearing, true π^0's reconstructed by the detector may not have this exact value for their mass. Accepting π^0 candidates from the invariant mass ranges listed above accounts for this smearing effect. Finally, as this is a jet modification analysis, π^0's that serve as trigger particles must have a momentum between 4 and 15 GeV/c to increase the likelihood that they are associated with or are the leading hadron of a jet. The π^0 momentum distributions for Run 14 are shown in Fig. 3.8. The most noticeable feature of the spectrum is the plateau-like structure at low $p_T^{\pi^0}$, which is caused by the asymmetry cut. The impact of individual cuts specific to the π^0's can be seen in Figs. 3.9 and 3.10.

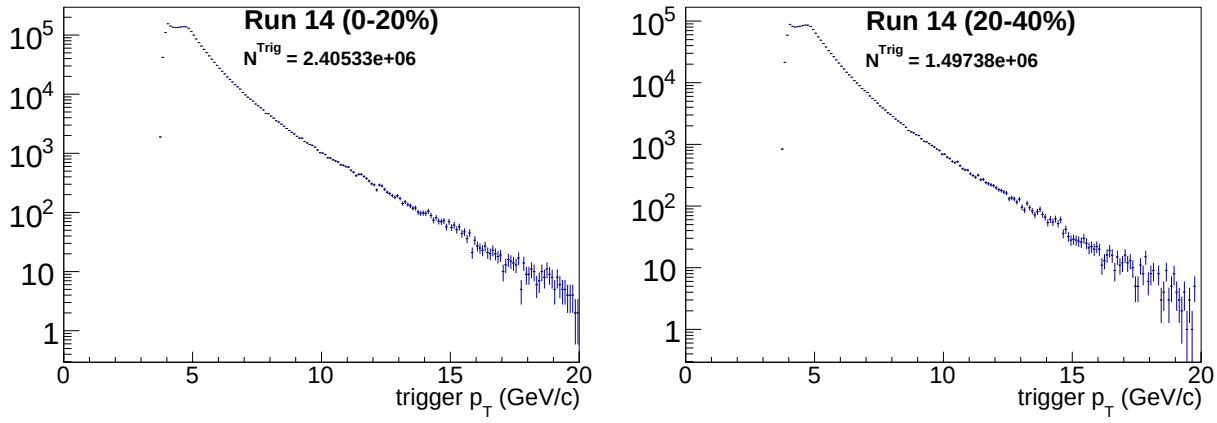

Figure 3.8: π^0 p_T distribution for the 0–20% centrality class (Left) and the 20–40% centrality class (Right) in the Run 14 200 GeV $Au + Au$ data set.

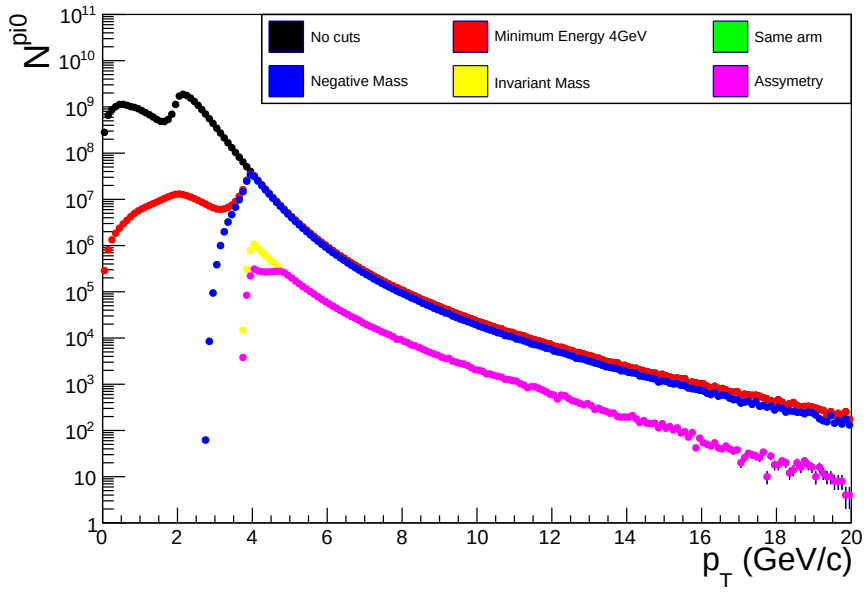

Figure 3.9: Impact of different cuts on the raw π^0 spectrum in the 0–20% centrality class

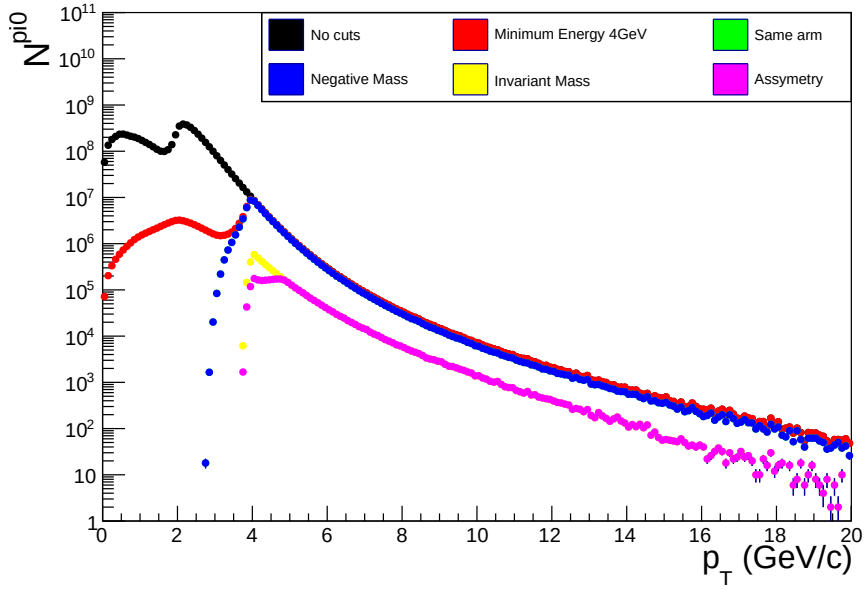

Figure 3.10: Impact of different cuts on the raw π^0 spectrum in the 20–40% centrality class

3.1.4 Charged Hadron Track selection

Charged track measurements are made via charged hadron reconstruction carried out by the drift and first pad chambers, as detailed in Sec. 2.2.3. Additionally, the third pad chamber plays a role in track matching, whereby a reconstructed track's trajectory is projected outwards towards the third pad chamber via track model and is matched to an actual hit in the drift chamber. The distances from the projected track and the actual hit in the pad chamber in ϕ and z are denoted $d\phi$ and dz, respectively. While one can impose cuts on these raw track matching variables themselves, it is instead helpful to cut on their sigmalized versions, $\sigma_{d\phi}$ and σ_{dz}. Because the distributions of the raw track matching distributions change according to momentum, cuts on the raw variables themselves would have to be as well. However, the calibration process for sigamlization removes this p_T dependence, allowing one set of

parameters to be used at all momenta. For this analysis, a so-called "circular" sigma value is used, as defined by Eqn. 3.4.

$$\sigma_{circular} = \sqrt{\sigma_{d\phi}^2 + \sigma_{dz}^2} \ . \tag{3.4}$$

This value must be less than 2 for $p_T < 5$ GeV/c, and less than 1 for $p_T \geq 5$ GeV/. The cut becomes tighter above 5 GeV/c to compensate for the fact that the RICH is no longer used above that threshold because it begins firing on charged hadrons as well as electrons, causing the efficiency to rapidly drop. To reject electrons, a RICH veto cut is applied on tracks with $p_T < 5$ GeV/c. Any track associated with a fired RICH PMT is rejected. All tracks must also pass a track "quality" cut as well, having a track quality of either 63 or 31. These values correspond to the requirements presented in Table 3.1, with a quality value of 63 being the highest quality possible, and 31 being the second highest.

Lastly, this analysis considers tracks with momentum within 0.5–7 GeV/c to be used as associate hadrons. Although one can, in principle, measure charged hadrons up to 10 GeV/c, both [51] and [39] note that a large background begins to contaminate the charged track pool in this region because of in-flight decays of others hadrons such as Kaons, as well as the presence of electrons which can be incorrectly reconstructed as high momentum hadrons. Hence, a top momentum of 7 GeV/c is used. The momentum distributions of the associated tracks are shown in Fig. 3.11. The steep drop at 5 GeV/c in Fig. 3.11 is caused by the tightening of the track matching cut from 2 σ to 1 σ.

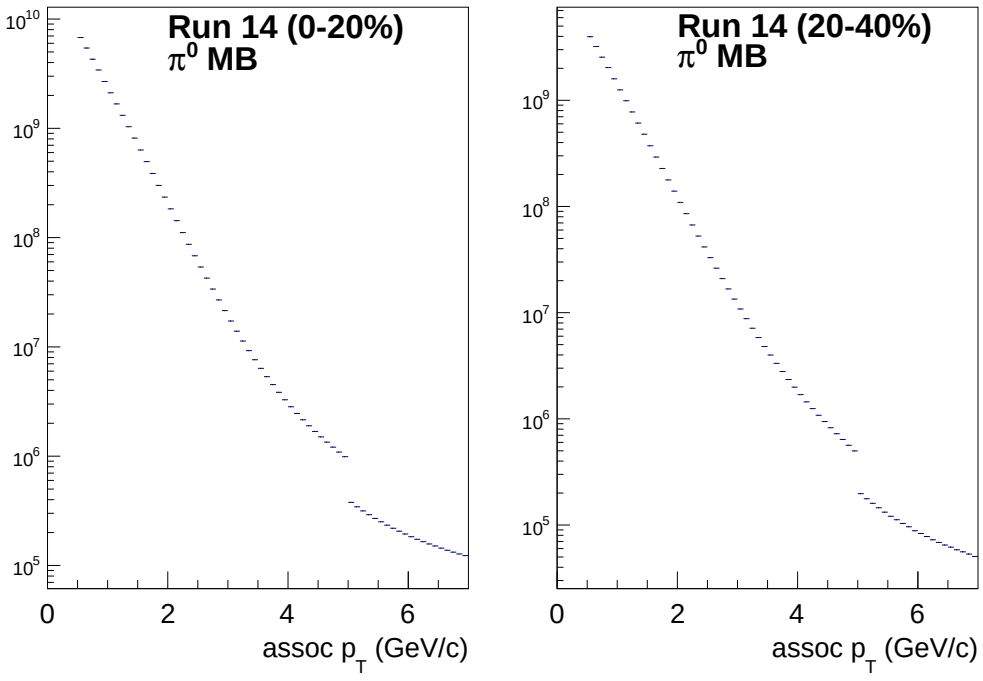

Figure 3.11: Spectra of associate hadrons in the Run 14 200 GeV $Au + Au$ data set in the 0–20% (Left) and 20–40% (Right) centrality bins.

Figs. 3.12 and 3.13 are the impact of individual cuts on the associate hadron spectrum. One can see that the track matching cut is the most severe, especially above 5 GeV/c where it is tightened from 2 σ to 1 σ.

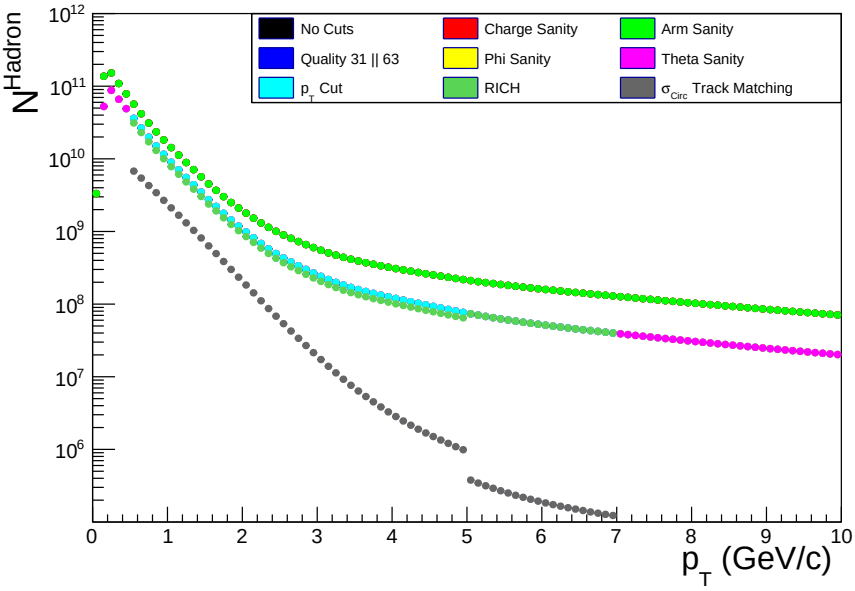

Figure 3.12: Impact of individual cuts on the associate hadron spectrum in the 0–20% centrality bin.

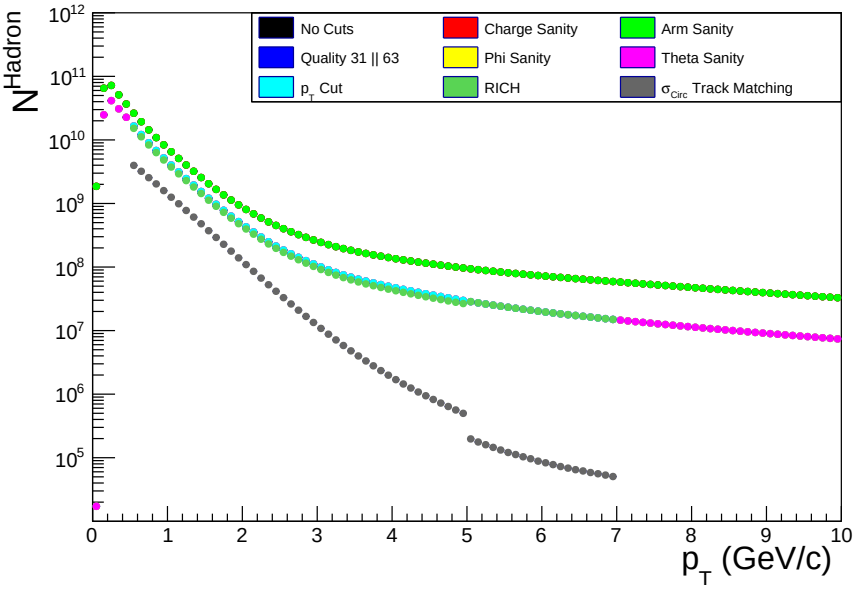

Figure 3.13: Impact of individual cuts on the associate hadron spectrum in the 20–40% centrality bin.

3.1.5 Run Selection

PHENIX data is collected in data-collecting sessions called "runs" (with a small "r", not to be confused with "Run" as in the run year, e.g. "Run 14") which last for roughly 60 minutes. The detector setup and performance can change between or during these runs and cause a variation in detector efficiency and acceptance. Therefore, a run-by-run quality assurance process is performed to remove runs that deviate too far from the average behavior of the Run as a whole. The process for Run 14's run QA is reviewed here.

Following previous analyses [50, 34], good runs are determined by considering the correlation functions used for the event-mixing correction detail in Sec. 3.2.2, which are sensitive to detector acceptance effects. Run 14's runs are separated into six groups as shown in table 3.2. Group 3, which is relatively smaller, exists because of the unique shape of the background correlation functions in that group 3. Comments in the PHENIX run control log also show there were issues in the west arm drift chamber in runs 409697, 409698, 409699, and 409714, and these issues induce a specific feature on the away-side peak of the correlation functions of group 3 (see figure 3.14). Additionally, two runs, 409459 and 409714, are excluded from the analysis because of a malfunction in how information from the drift chambers is encoded and decoded. The event-mixing background correlation functions are summed for each group

Table 3.2: Run Groups

Group	Run Numbers
0	405863 – 406500
1	406501 – 407000
2	407001 – 409690
3	409691 – 410500
4	410501 – 413300
5	413301 – 414988

and then normalized to 1 as shown in Fig. 3.14. Next, the background correlation functions for each run in a given run groups is compared to the summed correlation function for that group by taking the ratio of the two. Under ideal circumstances, this ratio would be consistent with 1 across all $\Delta\phi$; however, variations in run conditions give a distribution of ratios, as shown in Fig. 3.15. Runs with a deviation 3 times or higher than the run group average are rejected. In total, of Run 14's 1069 runs, 995 survive the QA process and make it on to the good run list.

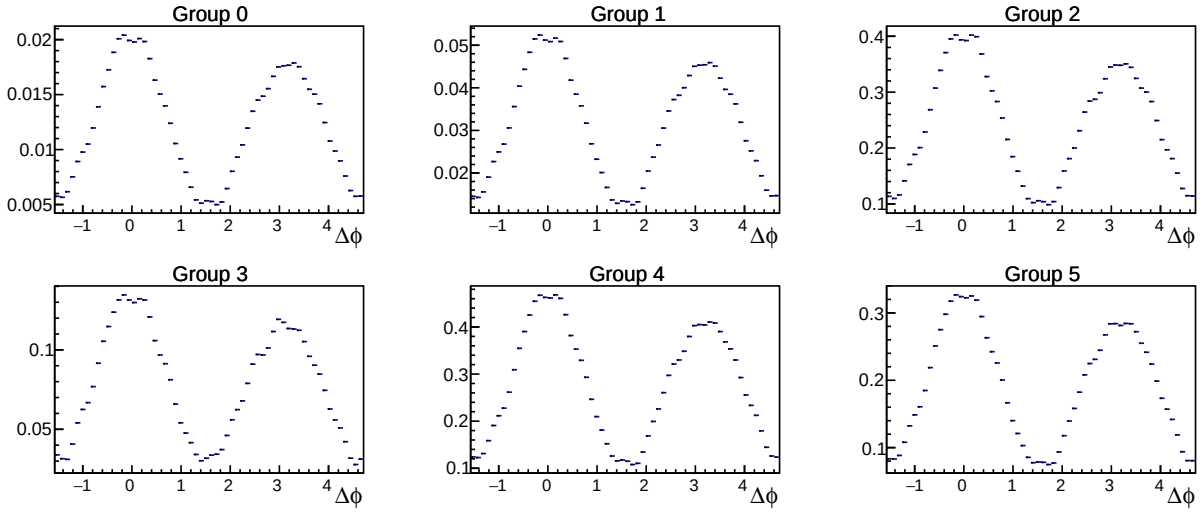

Figure 3.14: Summed event-mixing background correlation functions in different run groups. These correlation functions are normalized to 1.

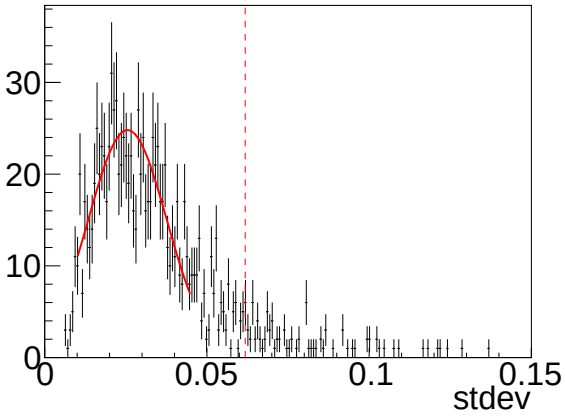

Figure 3.15: Distribution of standard deviations for each run in the 2014 data set. A Gaussian fit is used to extract the mean and the standard deviation, σ, in the peak region and is shown by the solid red line. The red dashed line indicates $\mu + 3\sigma$, beyond which a run becomes "bad".

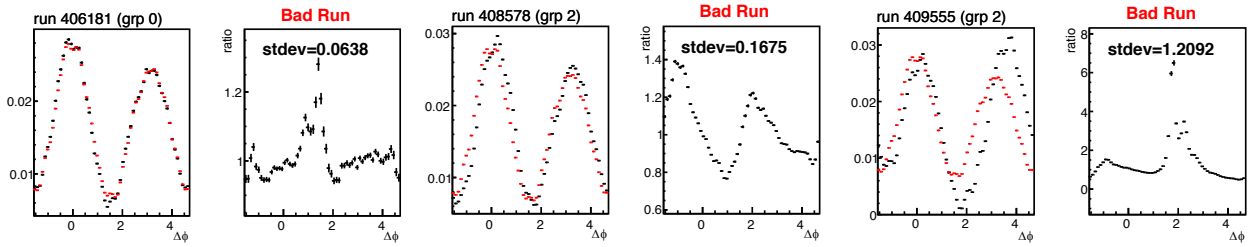

Figure 3.16: Examples of bad runs in Run 14. The event-mixing background correlation fucntions from each run (black) and from the corresponding run group (red) are drawn on the left in each panel. The ratio of the two is shown on the right of each panel.

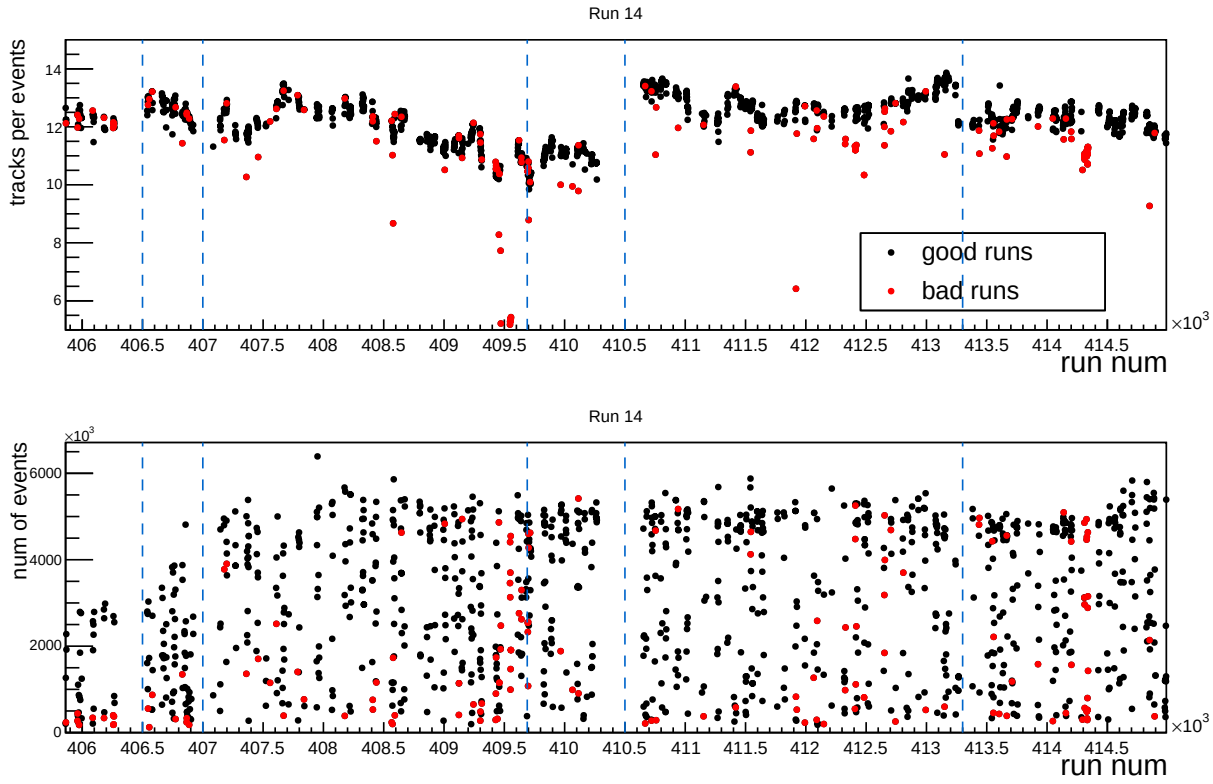

Figure 3.17: Number of charged hadron tracks per event as a function run number (top) and number of events as a function of run number (bottom). The blue dashed lines indicate the different run groups. From left to right are groups 0 to group 5. Bad runs are drawn in red.

3.2 Detector Corrections

Corrections for detector inefficiencies and acceptance limitations must be made before one can extract physics quantities. This section details corrections for the efficiency of the tracking system, inefficiencies due to the occupancy effect, and correlations caused by the shape of the detector itself.

3.2.1 Charged Hadron Tracking Efficiency

The combination of detectors used for charged hadron track reconstruction do not have a 100% efficiency, as one might expect of any measurement device. The efficiency of the tracking system, $\epsilon_{Tracking}$, must be calculated, and its inverse, $\epsilon^{-1}_{Tracking}$ applied to the per-trigger yields to account for correlations missing due to the tracking system's efficiency. The tracking efficiency is calculated in a specialized GEANT3 [52]-based simulation of the PHENIX detector known as PISA (**P**HENIX **I**ntegrated **S**imulation **A**pplication). Positive and negative protons, kaons, and pions ($1,000,000$ of each) are sent through a GEANT mock-up of the detector, and their interactions with the detector are recorded. Tracks from simulation are then analyzed in the same manner as those reconstructed in real data, and the same cuts detailed in 3.1.4 are applied to see how many survive from the original input sample. The tracking efficiencies are calculated for the kaons, protons, and pions separately and as a function of p_T, and then combined after being weighted by their relative abundance, as measured in [53].

3.2.1.1 Input Particle Distributions

$1,000,000$ positive and negative protons, pions, and kaons are created with the following kinematics, which are shown in Fig. 3.18:

- $0.25 \leq p_T \leq 10$ GeV/c
- $|\eta| < 0.4$
- $0 \leq \phi \leq 2\pi$
- $|z| \leq 12$cm

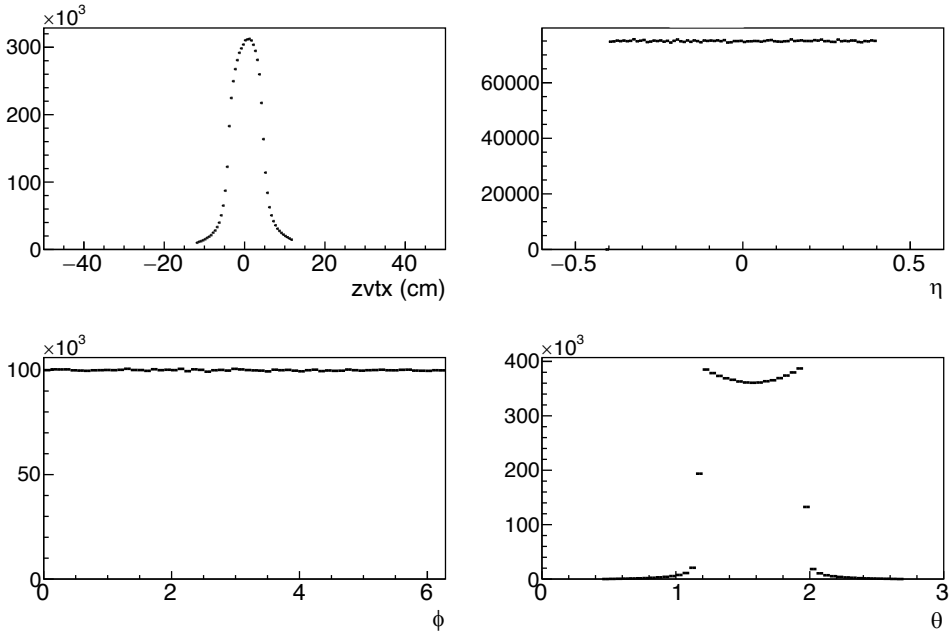

Figure 3.18: Initial kinematics for simulated hadrons used in the efficiency calculation. The z-vertex distribution is based off of real data from the 2014 200 GeV $Au + Au$ data set.

The kinematic ranges for the p_T, pseudorapidity, and z-vertex extend outside the ranges used in this analysis, but this is to prevent so-called "edge effects." Ordinarily, the slight mis-reconstruction of a particle's kinematic information can yield a value slightly higher or lower than its truth value. Near the center of a distribution, such bin migration is basically cancelled out because these reconstructed values have an equal chance of migrating up or down a bin. However, near the edges, this effect is one-sided, and can lead to artificial inefficiencies. Thus, we extend the kinematic range of the input particles to avoid this effect.

Real data is used to influence the input particle distributions in two ways. Firstly, the z-vertex distributions shown in Fig. 3.18 are created by drawing from real data from Run 14. In reality, there is a slight z-vertex dependence to the detector's efficiency, and in real data, one

samples the center of the detector ($z \approx 0$ cm) more so than the rest. Thus, re-weighting the input particles' z-vertex distribution gives a better approximation of the average detector efficiency seen in real data. Secondly, the input p_T distributions are weighted by a fully corrected, published spectrum measured in [51], and this is done to preserve momentum resolution effects. The weighted momentum spectrum can be seen in Fig. 3.19 below. The effects of applying the standard analysis cuts on the z-vertex, pseudorapidity, and azimuthal angle are also shown.

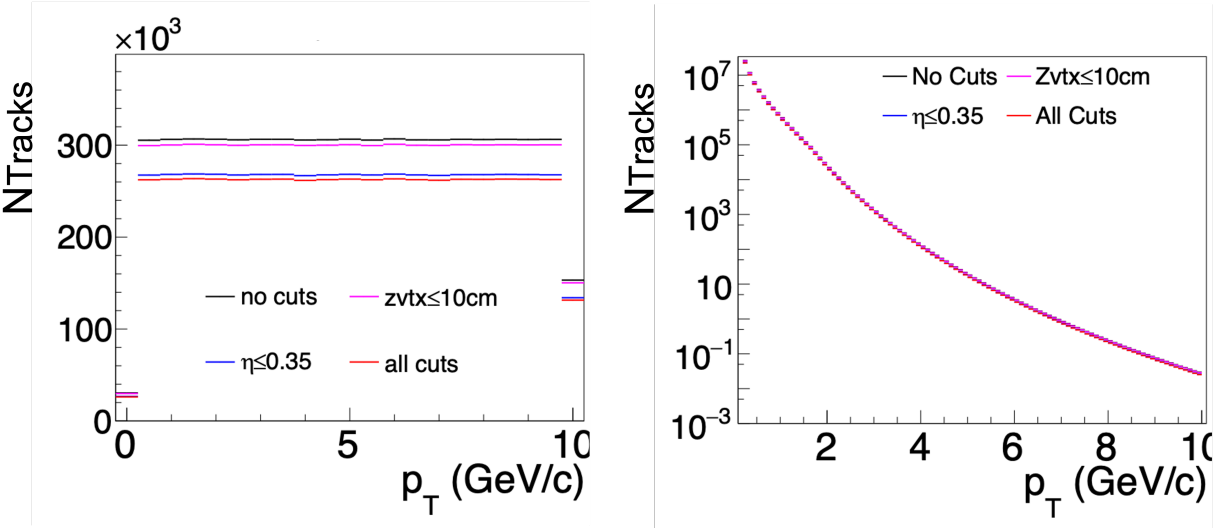

Figure 3.19: Left: unweighted input p_T spectrum. Right: input p_T spectrum weighted by fit to published spectrum [51]. The re-weighted distribution also has a much higher bin count to take advantage of the increased simulation statistics used in this efficiency calculation

3.2.1.2 Modelling the PHENIX Detector in Simulation

As mentioned before, the status of the drift and pad chambers changes from run year to run year. Thus, it is important to model these changes in simulation. Firstly, a representative run is chosen whose track yield closely matches the mean track yield for the entire set of runs of a given year of data taking. Then, a mock production of the raw data is performed

to extract information on the drift and pad chambers. More specifically, the single wire efficiencies are calculated for the drift chambers, and dead cell and readout card lists are made for the pad chambers. The single wire efficiency is calculated for a given wire by comparing how many reconstructed tracks a given wire in the drift chamber did see and how many its neighbors saw. If a given wire played a part in reconstructing far fewer tracks than its neighboring wires, its single wire efficiency is accordingly reduced.

Fig. 3.20 shows a comparison of the number of reconstructed tracks as a function of position in both simulation and in real data. In a perfect world, the overlap between the red and blue distributions would be perfect. However, several hurdles make this nearly impossible. Fluctuations in the state of the detector aside, the simulacrum of the detector in PISA usually will not match real data 100% due to smearing effects and mismatches between in live and dead areas between the simulation's detector and the real one. The extent of this inaccuracy, called the scale uncertainty, is quantified by finding regions of the phase space where the behavior of the detector and simulation are identical. Here, we assume any difference is due to A) a difference in statistics and B) a pure difference between simulation and data. In order to isolate B, we normalize the integrals of this region in simulation and real data together to remove effects from source A. Then, the remaining difference in coverage is the scale uncertainty, which is measured by calculating the ratio of the newly normalized distributions. The scale uncertainty for Run 14 is measured to be 5%.

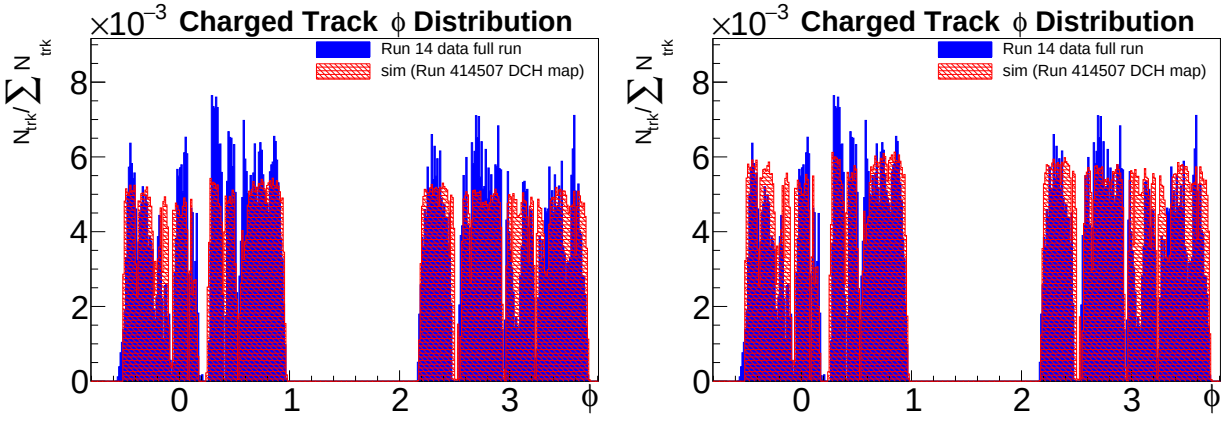

Figure 3.20: Track position distributions for real (blue) and simulated (red) tracks before (Left) and after (Right) normalization to remove differences purely due to statistical differences between the simulated real sets of track data.

Lastly, Run 14 is unique in comparison to previous analyses in the fact that it uses track matching from the EMCal when information from the PC3 is unavailable. The majority of the tracks used in this analysis are confirmed by the PC3 with a ratio of approximately 12:1 when compared to tracks confirmed by the EMCal. However, this ratio was found to be closer to almost 1:1 in simulation, owing to the lack of a proper EMCal dead map in simulation. The over-idealized EMCal also drove up the scale uncertainty to about 12%. As such, it was decided that EMCal track matching would be disabled in simulation, despite its use in the analysis on real data. This is justified though, because results derived without the EMCal in simulation are more similar to what is seen in real data than vice-versa, as quantified by the lower scale uncertainty obtained when not using EMCal track matching.

3.2.1.3 PC3 Track Matching Recalibration

As is used in real data, a cut on the circular sigma track matching value of a given track is used. However, the population of tracks that exist in simulation may not share the same recalibration parameters that those in real data do. Initially, the single particle correction process was to be done for Runs 10, 11, and 14 for the purpose of eventually combining the π^0-hadron results across all three runs, but because of a bug found in Run 10's track matching recalibrator and Run 11's lack of statistical impact, they were discarded from the data pool. However, we demonstrate the PC3 track matching recalibration procedure on Run 10 here (Run 10 is chosen as Run 14's correction did not require this process). To begin, each simulation track's dz and $d\phi$ values are measured in 0.25 GeV/c momentum slices beginning at 0.5 GeV/c. These distributions are then fit with a double Guassian whose form is given by Eqn. 3.5.

$$dx = \frac{A_1}{\sigma_1\sqrt{2\pi}} e^{\frac{-(x-\mu_1)^2}{\sigma_1^2}} + \frac{A_2}{\sigma_2\sqrt{2\pi}} e^{\frac{-(x-\mu_2)^2}{\sigma_2^2}} \tag{3.5}$$

The double Gaussian accounts for a narrow, signal distribution and a wider, background distribution. Here, $A_{1,2}, \mu_{1,2}$, and $\sigma_{1,2}$ are the amplitude, mean, and width of the distributions, and 1 denotes the signal Gaussian, whereas 2 denotes the background distribution. A sample fit to the $d\phi$ distribution for positive pions with $0.5 \leq p_T \leq 0.75$ GeV/c is shown in Fig.3.21. While it suffices to perform the recalibration for just one particle species, it must be done for both positive and negative charges, as their behavior in the ϕ direction is

different because of interactions with the magnetic field.

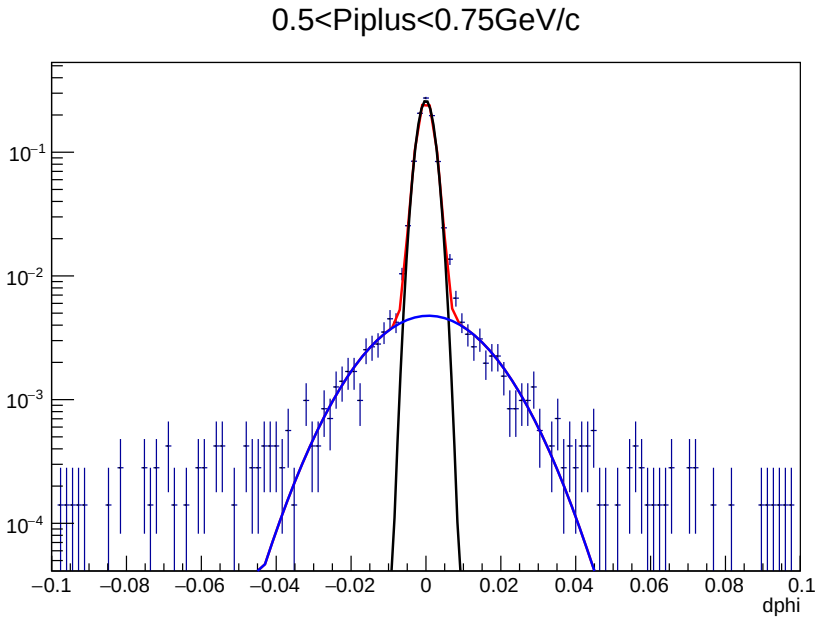

Figure 3.21: Example fit to the $d\phi$ track matching variable from Run 10's simulation. The blue fit is for the wider Gaussian with width parameter σ_2, and the black curve represents the Gaussian fit to the signal region with width paraemter σ_1. The red curve present is the total fit that contains both signal and background components.

Once the mean and width for each $d\phi$ and dz distribution are extracted, they are plotted as a function of the hadron p_T and fitted by Eqn. 3.6, where A, B, C, and D are fitting parameters, and n is allowed to be positive, negative, or fractional depending on what gives the best fit. Results to the fits for both positive and negative pions are shown in Figs. 3.22 and 3.23. It should be noted that in some regions, where statistical uncertainties dominate, the simplest fit form (a straight line) is chosen.

$$y(p_T) = A + \frac{B}{p_T} + \frac{C}{p_T^n} + Dp_T \tag{3.6}$$

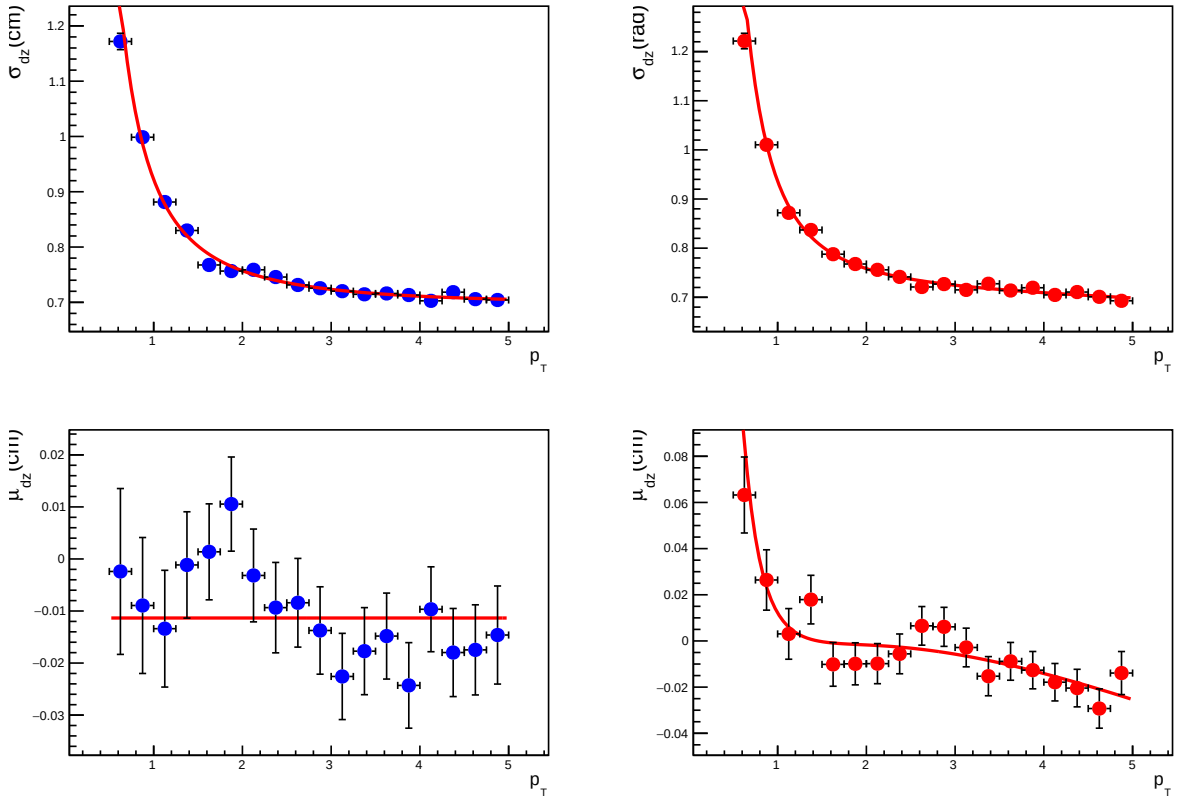

Figure 3.22: Fits to the μ and σ of the track matching parameter dz in Run 10 simulation. The red corresponds to negatively charged pions, and the blue corresponds to positively charged pions.

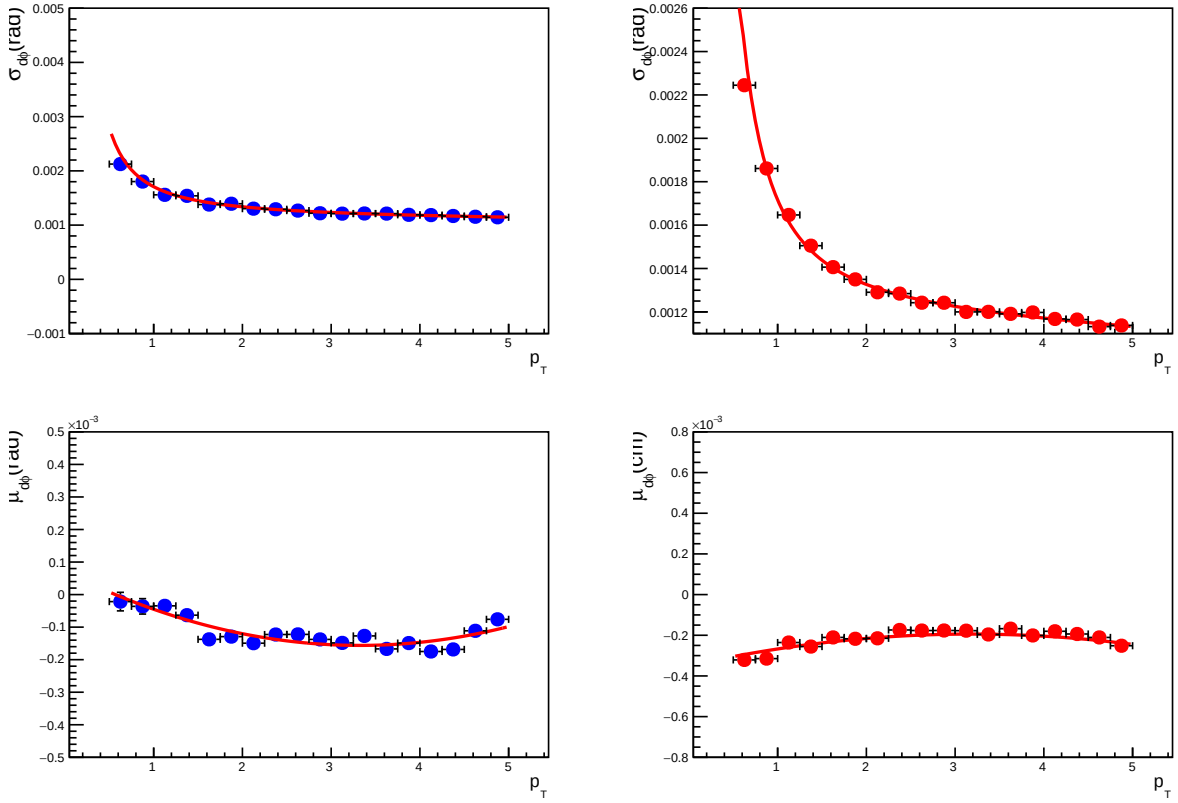

Figure 3.23: Fits to the μ and σ of the track matching parameter $d\phi$ in Run 10 simulation. The red corresponds to negatively charged pions, and the blue corresponds to positively charged pions.

And these fits are stored and placed in a local recalibrator for use in simulation. The recalibrator then uses the fits to calculate the sigmalized variables used in the circular sigma cut defined in Table 3.1 according to the following formulae in Eqns. 3.7 and 3.8.

$$n\sigma_{d\phi} = \frac{d\phi - \mu_{d\phi}}{\sigma_{d\phi}} \tag{3.7}$$

$$n\sigma_{dz} = \frac{dz - \mu_{dz}}{\sigma_{dz}} \tag{3.8}$$

To cross-check the recalibration, distributions of the sigmalized variables are extracted, fit with Eqn. 3.5, and the means and widths are again extracted as a function of p_T. A successful recalibration results in a $\sigma_{d\phi}$ distribution with mean of 1 and standard deviation 1, and a σ_{dz} with a mean of 0 and a standard deviation of 1 as well. Figs. 3.24 and 3.25 shows the result of the recalibration for the sigamlized distributions of σ_{dz} and $\sigma_{d\phi}$. It can be seen that there is still some deviation from the proscribed values given above, and the error bars presented are grossly overestimated by the fitting software. In spite of this, however, the location of the central values is consistent with documented PC3 track matching results for Runs 11 and 14. A similar exercise for Run 14 was also attempted; however, it was found that the initial sigmalized variable distributions were almost fully calibrated, as shown below in Fig. 3.27.

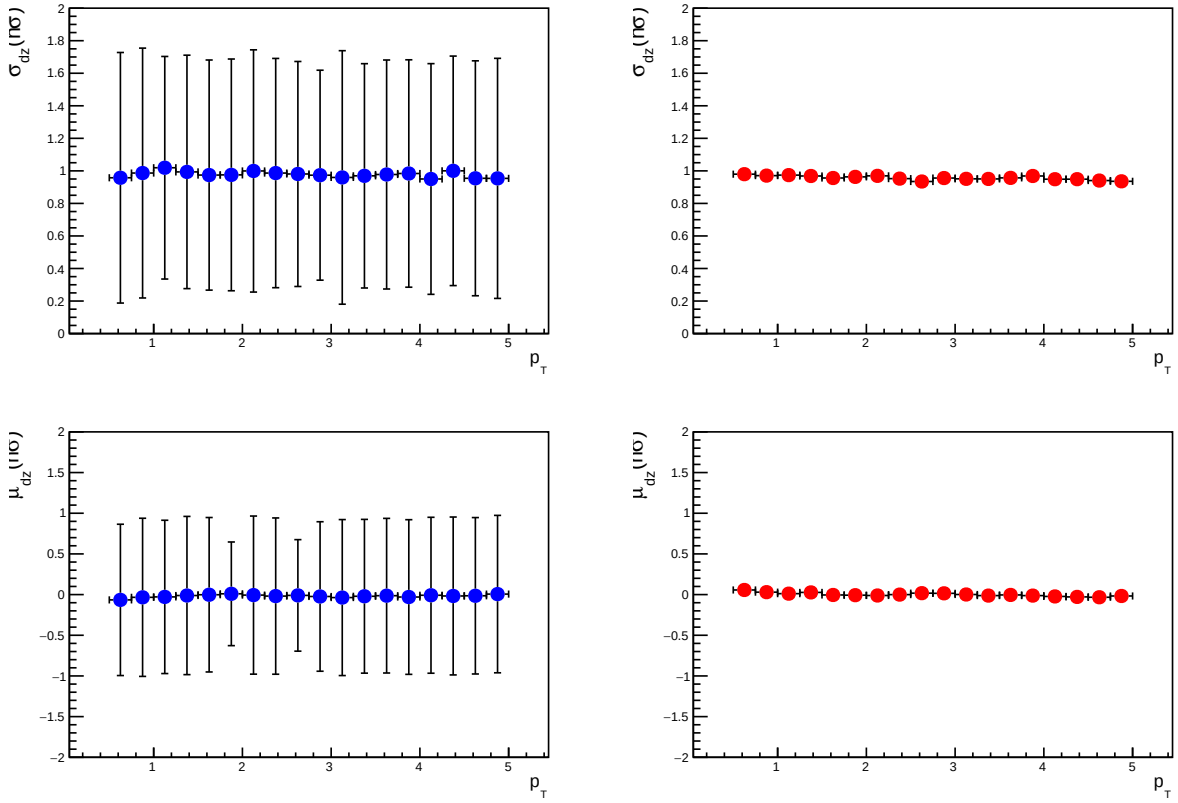

Figure 3.24: Distributions of the sigmalized dz values in units of $n\sigma$ as a function of p_T^{Hadron} for positive (Blue) and negative (Red) pions in Run 10 simulation.

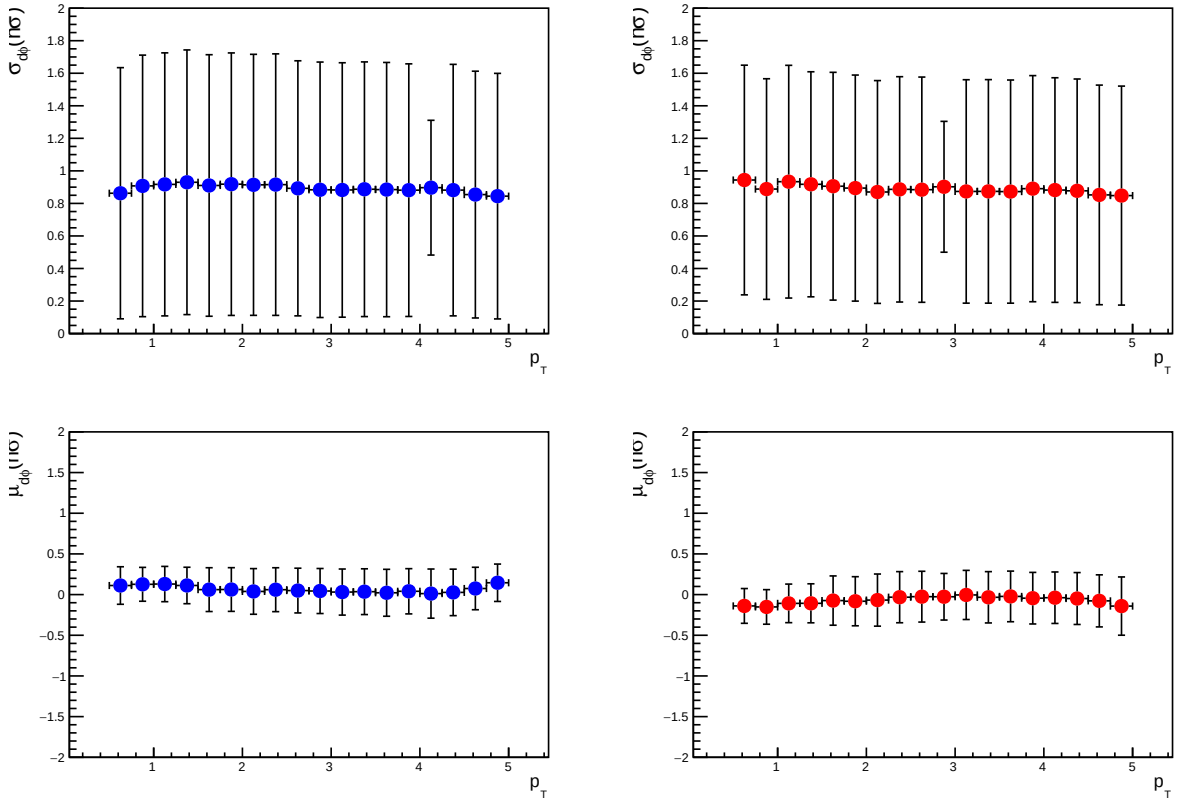

Figure 3.25: Distributions of the sigmalized $d\phi$ values in units of $n\sigma$ as a function of p_T^{Hadron} for positive (Blue) and negative (Red) pions in Run 10 simulation.remo

One final cross-check is also performed on the actual value that is cut on, the circular σ value. Fig. 3.26 shows a distribution of circular $\sigma_{Circ} = \sqrt{pc3^2_{d\phi} + pc3^2_{dz}}$ before and after the PC3 matching recalibration process for Run 10 for several momentum bins. As this distribution is the quadrature convolution of two distributions with mean zero and standard deviation 1 and mean 0, the result distribution has a peak of about $\sqrt{\pi/2)}$ or about 1.25. One can see that the calibration process shifts the distribution to the right slightly to the proscribed value.

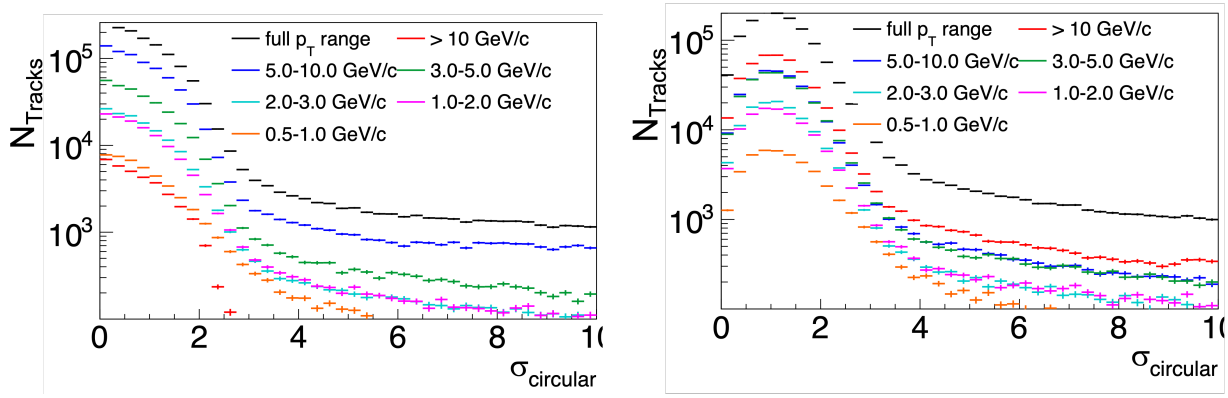

Figure 3.26: Left: Number of tracks with a given circular sigma value in different p_T ranges as described in the legend before undergoing the PC3 matching recalibration procedure. Right: Number of tracks with a given circular sigma value in different p_T ranges as described in the legend after undergoing the PC3 matching recalibration procedure. Both come from Run 10 simulation

Additionally, Fig. 3.27 shows the same distribution, uncalibrated, for Run 14. As it bore the same features as the calibrated distribution seen in Fig. 3.26 it was decided to forego the re-calibration process for it in favor of the one already in place.

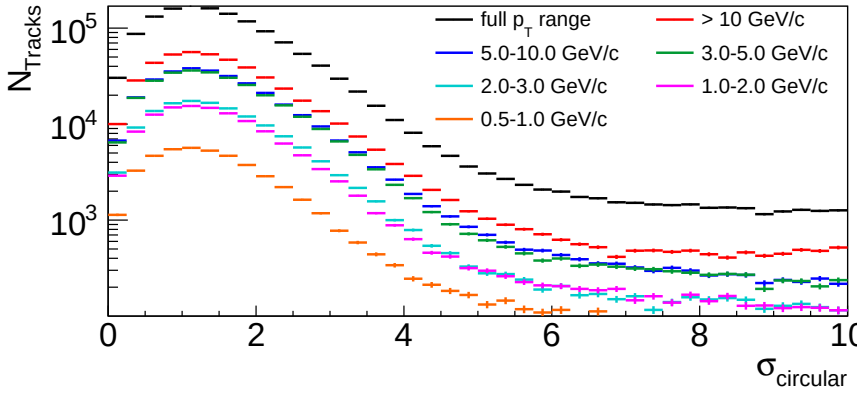

Figure 3.27: Number of tracks with a given circular sigma value in different p_T ranges as described in the legend before undergoing the PC3 matching recalibration procedure in Run 14 simulation.

3.2.1.4 Output Spectra and Identified Particle Ratios

A plot showing the impact of all cuts on the simulated spectrum can be seen in Fig. 3.28. As with cuts on the associate hadrons in real data shown in Figs. 3.12 and 3.13, the track matching requirement is the most stringent. Additionally, one can see large spikes in the spectra, and these occur when a low momentum particle, which carries a large weight, is mis-reconstructed as a high momentum particle and is then re-weighted according to its parent particle's momentum. The Δp_T cut removes this non-physical effect, however.

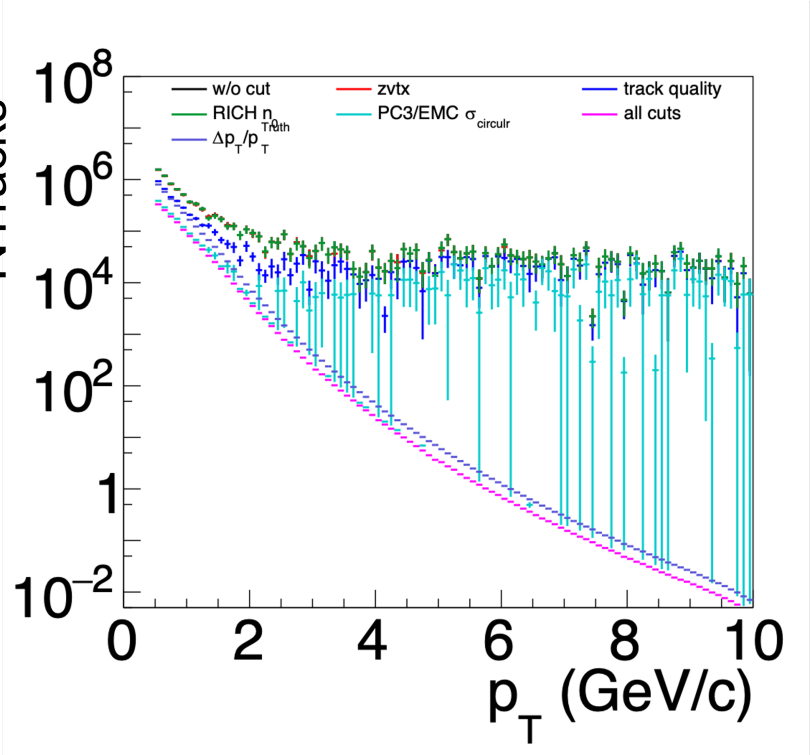

Figure 3.28: The combined output spectrum for all particle species from simulation. The different spectra show the impact of a given cut on the input spectrum.

The output spectra are then divided by the input spectrum from Fig. 3.19 on a species-by-species basis, yielding the efficiency for a given particle species, shown in Fig. 3.29. Next,

the species are weighted by their abundance in 200 GeV $Au + Au$ collisions as measured in [53] as shown in red in Fig. 3.30 and then combined into the total efficiency shown in Fig. 3.31.

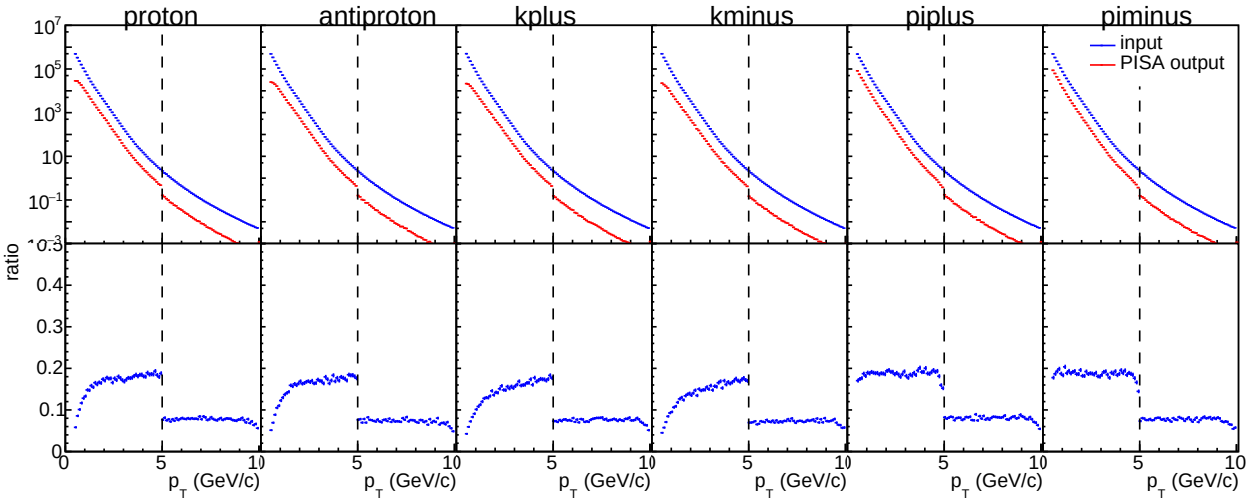

Figure 3.29: Top: Input (blue) and output (red) particle distributions for all particle species. Bottom: Identified hadron efficiencies.

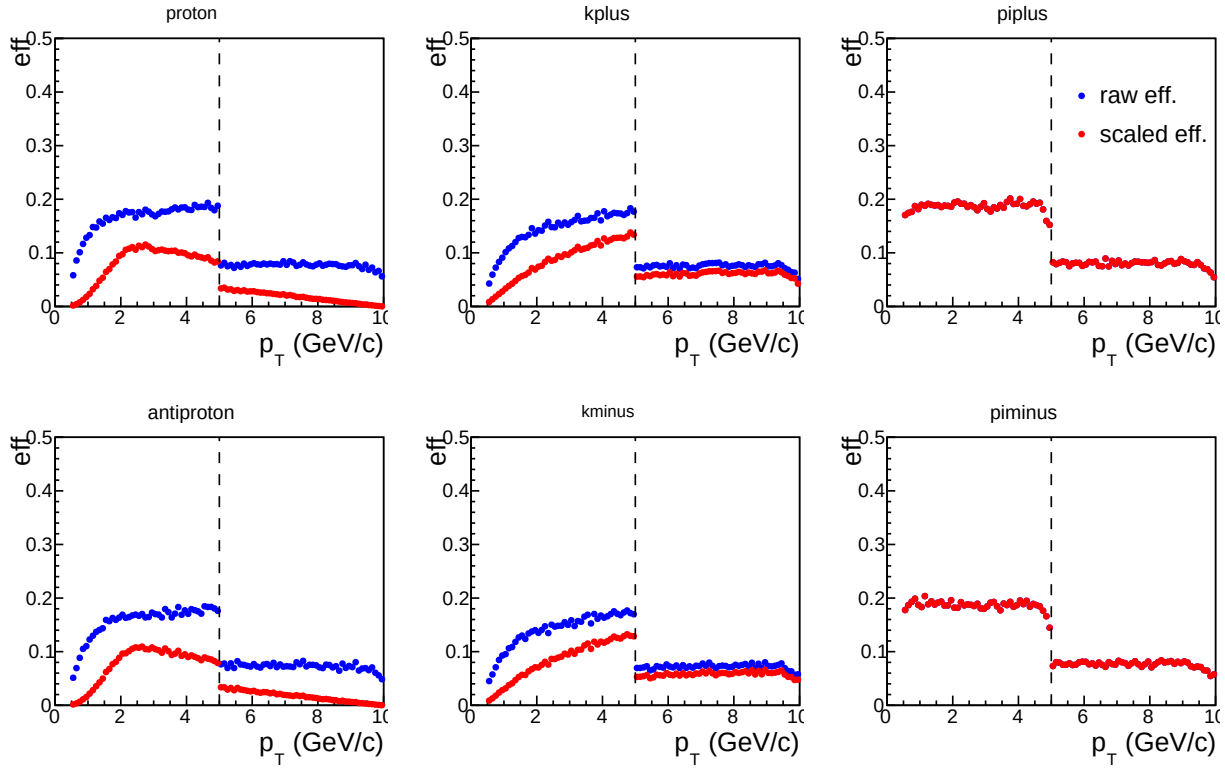

Figure 3.30: Blue: Identified hadron ratios before being scaled by their abundance relative to $\pi^{\pm}$'s. Red: Identified hadron ratios after being scaled by their abundance relative to $\pi^{\pm}$'s.

The final hadron efficiency is calculated by combining the identified hadron efficiencies calculated in Fig. 3.30 and then fitting with a function of the form seen in Eqn.3.9.

$$\epsilon(p_T) = A + Be^{Cp_T} + D + Ee^{Fp_T} \tag{3.9}$$

Where A through F are fitting parameters. C and F, in particular, are allowed to float between negative and positive values to facilitate fit convergence. The result of the fit to the simulation data can be seen in Fig. 3.31. A constant fit is used for the $p_T > 5$ GeV/c region. Additionally, the fit to the $p_T > 5$ GeV/c region only extends to 8 GeV/c to avoid

edge effects that can be seen at $p_T \approx 9 - 10$ GeV/c.

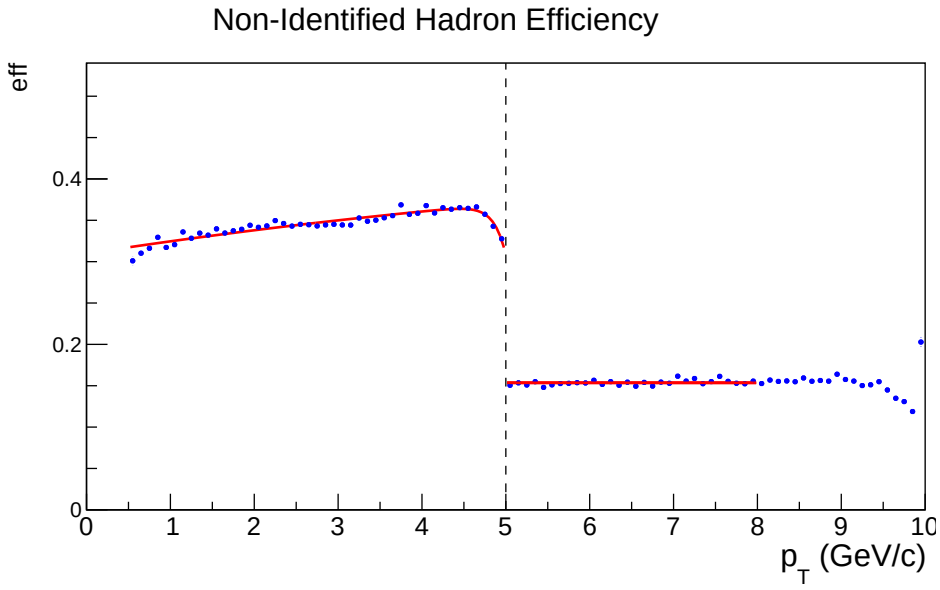

Figure 3.31: Non identified hadron efficiency as a function of hadron p_T. The red curve is the fit to the data points.

Hadron Momentum (GeV/c)	Fit Parameter					
	A	B	C	D	E	F
0.25–5	.0356	-0.144	-0.109	0.098	-3.46*10^{-17}	7.03
5–8	1.54					

Table 3.3: Values for the fit parameters in Eqn. 3.9.

3.2.1.5 The Occupancy Correction

Because of the higher multiplicity of tracks in heavy-ion collisions versus proton-proton collisions and because the tracking system has a finite spatial resolution, tracks can interfere with the reconstruction of other tracks, thus lowering the tracking system's overall efficiency. This phenomenon is known as the occupancy effect, and while it is negligible in p+p collisions, the high multiplicity environment of $A + A$ collisions demands a separate correction for

it. The methods mentioned previously to calculate the tracking efficiency only involve the reconstruction of a single track, and, thus, do not account for the occupancy effect.

In order to correct for the occupancy effect in high multiplicity $A+A$ collisions, a process known as embedding must be used. Embedding is a process whereby hits in the tracking system from simulated tracks are "embedded" into hits from real data. The number of tracks lost due to the occupancy effect is thus estimated by measuring how many tracks are lost during the embedding process. Three classes of tracks are introduced for this procedure, and their details are outlined below.

- G-Type tracks: these are the original Monte Carlo tracks generated by EXODUS, a monte carlo particle generator. They have not interacted with anything in simulation.

- S-Type tracks: these are tracks that have been fired through PISA and then reconstructed. S-Type tracks are used in the calculation of the single particle tracking efficiency, which is the ratio of S to G-type tracks.

- R-Type tracks: these are tracks that have been reconstructed after hits from S-Type tracks have been embedded in real data. They are matched back to the Monte Carlo track by a dominant contributor algorithm, which requires that at least 50% of the hits used to reconstruct the track came from its parent G-Type track.

With the track definitions outlined above, the so-called embedding efficiency can be calculated as the ratio of R-Type tracks to S-Type tracks. It should be noted though, that one can calculate the total single particle correction from dividing the R-Type track yields

by the G-Type track yields. However, for this study, in order to quantify the impact of the installation of the SVX on the magnitude of the occupancy effect, the tracking and embedding efficiencies are calculated separately. Both S-Type and R-Type tracks are required to pass the same cuts as tracks used in analyzing real data along with the additional constraints that:

- The original G-Type track identified as the dominant contributor must have a been a first-generation particle.
- At least two hits in the drift chamber's X1 and X2 layers are required, in addition to the requirement of having a track quality value of 31 or 63.

The impact of tracking cuts on S-Type and R-Type tracks is shown in Figs. 3.32 and 3.33 below. For both types of tracks, the PC3 matching cut is the most severe, as is the case in the single particle efficiency study.

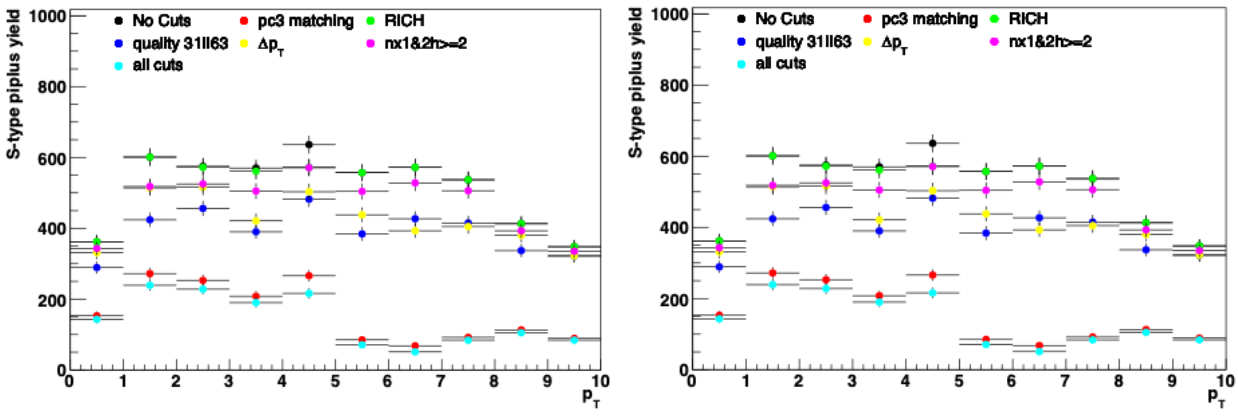

Figure 3.32: Yield of S-Type tracks in the 0–20% (Left) and 20–40% (Right) centrality bins for Run 14.

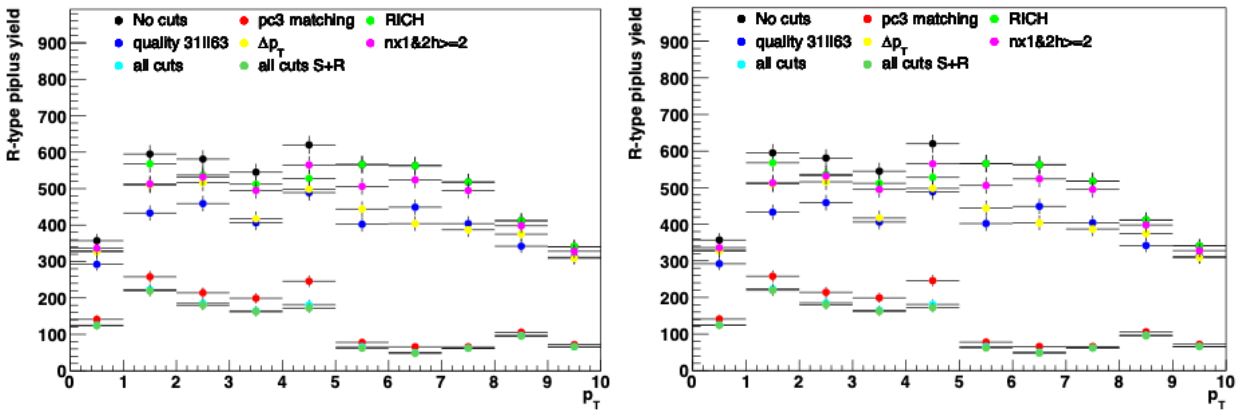

Figure 3.33: Yield of R-Type tracks in the 0–20% (Left) and 20–40% (Right) centrality bins for Run 14.

The total embedding efficiency, the ratio of R-Type tracks to S-Type tracks is shown in Fig. 3.34. The two regions (above and below $p_T = 5$ Gev/c are fit with a simple straight line. Firstly, the statistical uncertainties are slightly too large to permit more complicated fits with much faith. Secondly, it was found that over-fitting the region slightly below 5 Gev/c resulted in an over-correction of the hadron spectrum when the full efficiency and occupancy correction was applied.

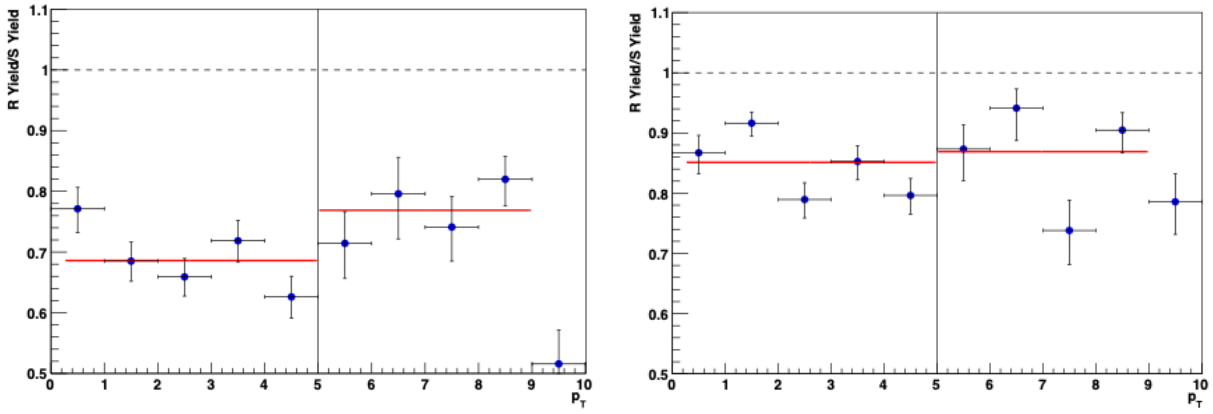

Figure 3.34: Embedding efficiencies for Run 14 in the 0–20% (Left) and 20–40% (Right) centrality bins for Run 14.

The embedding efficiency for Runs 10 and 11 were also calculated, and their accompanying S and R-type track yields are located in App. B. The embedding efficiencies for Runs 10, 11, and 14 are shown in Fig. 3.35. The "hybrid" in "Run 14 w/ Hybrid Matching Cut" refers to the track matching cut used in this analyis that changes to 1σ at $p_T^{Hadron} = 5$ Gev/c, whereas the curved labelled "Run 14" uses a 2σ cut throughout, allowing one to gauge the impact of tighter track matching cuts on the embedding efficiency. Two interesting things become apparent. Firstly, as shown when examining the Run 14 embedding efficiency with and without the tighter track matching cut at high p_T, one finds that the embedding efficiency actually *increases* with a tighter cut. One possible explanation for this phenomenon is that when applying a tighter cut, one is selecting on a purer selection of tracks that are more likely to survive the embedding process.

Secondly it was initially posited that the installation of the SVX before Run 11 would contribute to a lower embedding efficiency because the denser silicon of the SVX would lead to a higher production of conversion electrons, thus increasing the occupancy effect. However, the embedding efficiencies for Runs 10, 11, and 14 are all found to be consistent to within the 5% uncertainty attributed the procedure in studies for [39]. However, the consistency of the embedding efficiencies does not necessarily provide proof that the SVX does *not* increase the yield of conversion electrons, only that the tracking system is relatively agnostic to this increase.

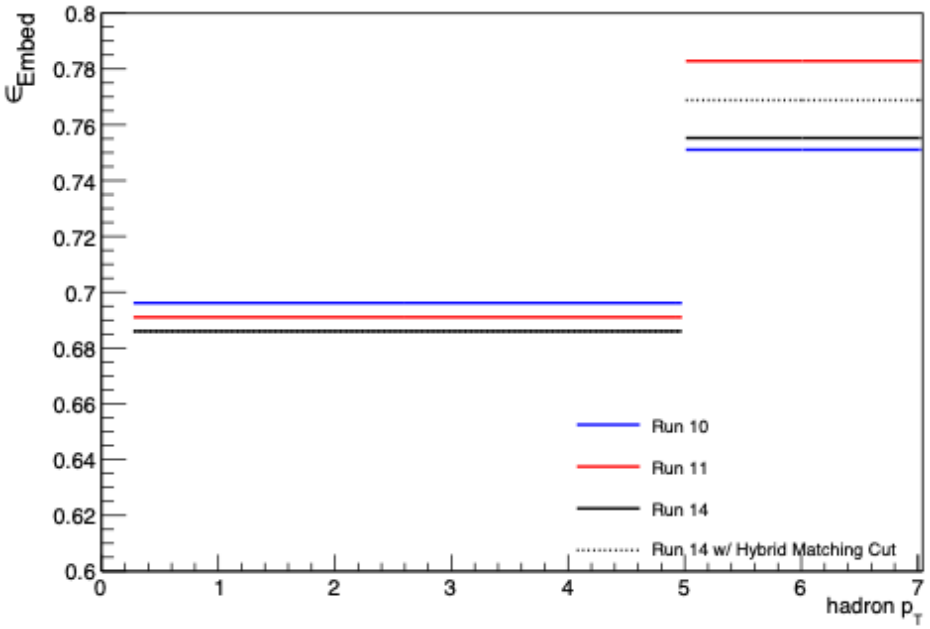

Figure 3.35: Embedding efficiencies for Run 10 (Blue), Run 11 (Red) and Run 14 with a stanrd circular track matching cut (Black) and a 1σ circular track matching cut for $p_T^{Track} \geq$ 5 GeV/c

3.2.2 Acceptance Correction

Although the gaps at the 12 and 6 o'clock positions of PHENIX give the detector its iconic blueprint, they can also induce biases in the correlations. Essentially, because of PHENIX's acceptance, one is simply less likely to measure trigger and associate pairs with an opening angle near 90°, as illustrated in Fig. 3.36. Additionally, holes in the drift and pad chambers can also induces biases towards or against certain correlations angles. In essence, certain features of the measured correlation function can be caused by gaps in the detector's acceptance, rather than physics processes.

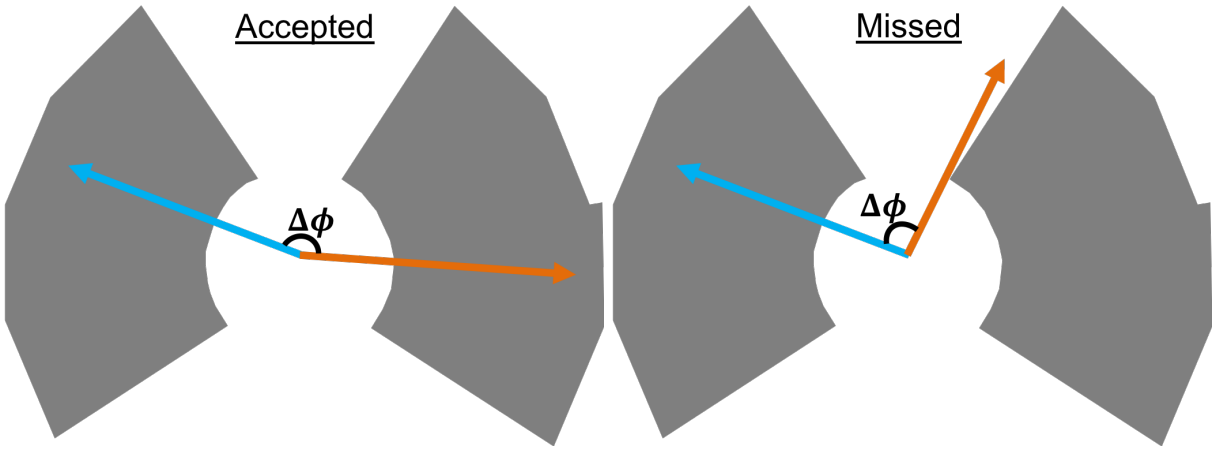

Figure 3.36: Illustrations of detector acceptance effect on angular correlation measurements. The grey areas represent the PHENIX central arm detectors, the blue arrow represents a trigger particle, and the yellow arrow represents an associated charged track. Left: example of accepted correlation. Right: example of missed correlation where the charged track is missed by the detector because of limited acceptance..

To correct for these features, the process of event mixing is used. In event mixing, a trigger particle is paired with charged hadrons from different events, thereby intentionally creating correlation functions consisting entirely of acceptance-driven correlations. These mixed-event correlations are then corrected for tracking inefficiencies much like the same-event pairs are, normalized per-trigger, and then normalized to 2π. This normalization is used because for a detector with perfect acceptance, one expects a unitary correlation function with the property given in Eqn. 3.10.

$$\int_{-\pi/2}^{3\pi/2} d(\Delta\phi) = 2\pi. \tag{3.10}$$

In the absence of acceptance-induced biases, one expects an equal probability of measuring any given correlation angle. Finally, it is assumed the entire correlation signal is a convo-

lution of the same-event foreground and mixed-event background distributions, and so, the foreground distributions are divided by the background distributions after having been fully normalized and separated into the correct trigger and charged hadron momentum ranges. Example distributions are shown for Run 14 in Figs 3.37 and 3.38. For the sake of presentation, the foreground distributions are scaled to meet the near-side peak's height. The fully acceptance, efficiency, and occupancy corrected correlation functions are then shown in Fig. 3.39 and 3.40.

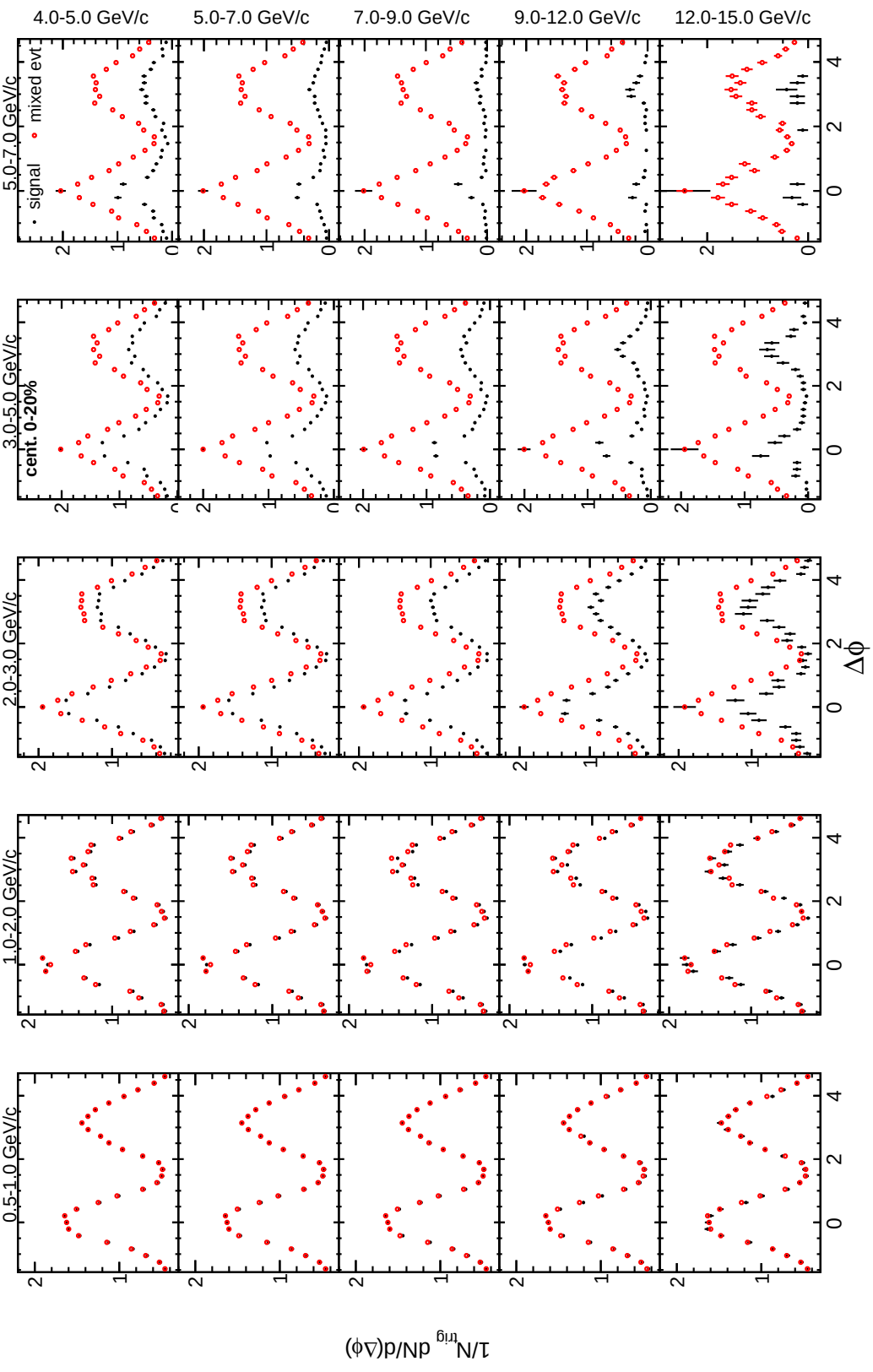

Figure 3.37: Same-event (black dots) and mixed-event (red circles) correlations in the 0–20% centrality class in Run 14. The top set of numbers represent the charged hadron momentum bins, and the righthand set of numbers represent the π^0 momentum bins

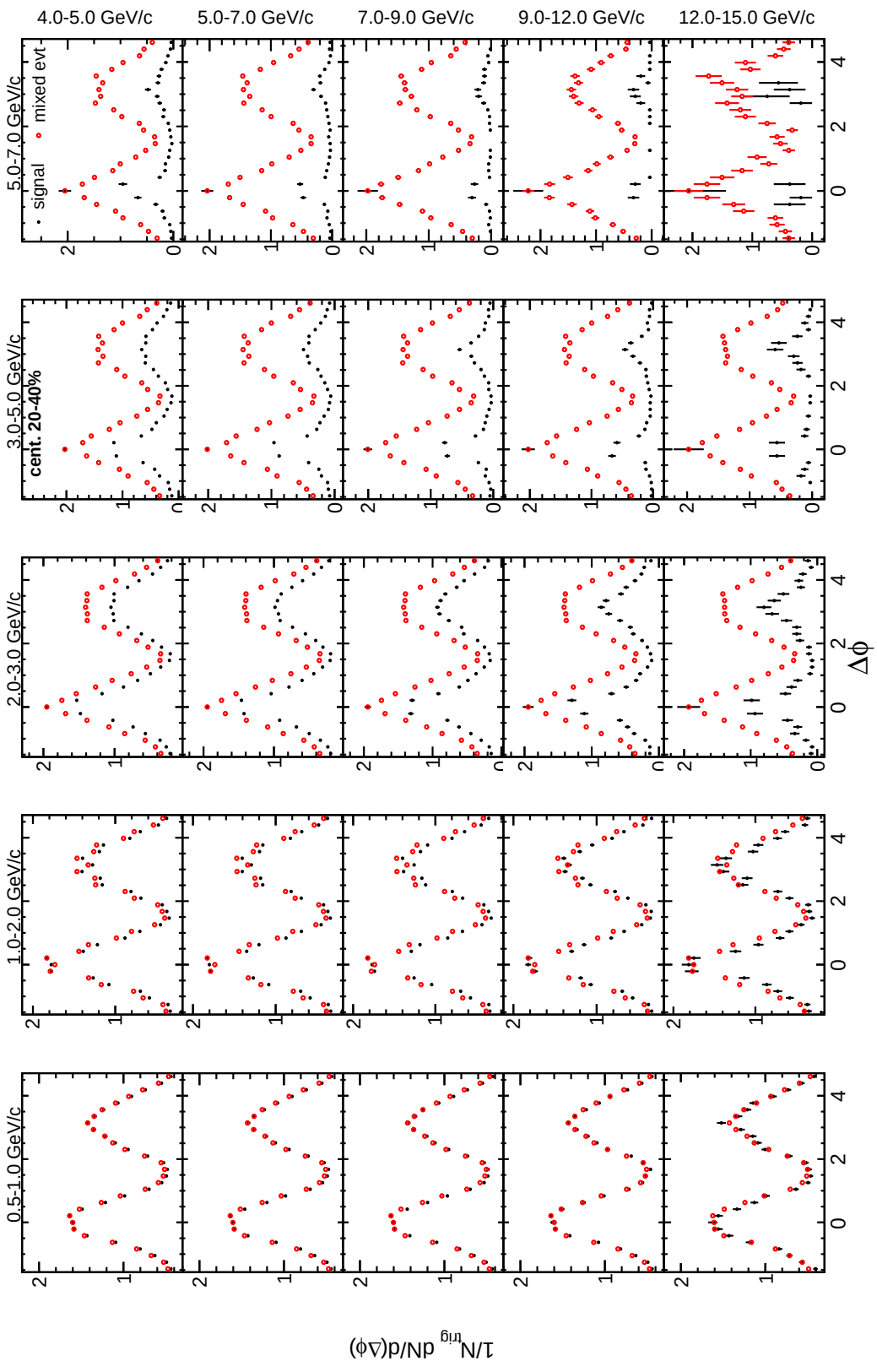

Figure 3.38: Same-event (black dots) and mixed-event (red circles) correlations in the 20–40% centrality class in Run 14. The top set of numbers represent the charged hadron momentum bins, and the righthand set of numbers represent the π^0 momentum bins

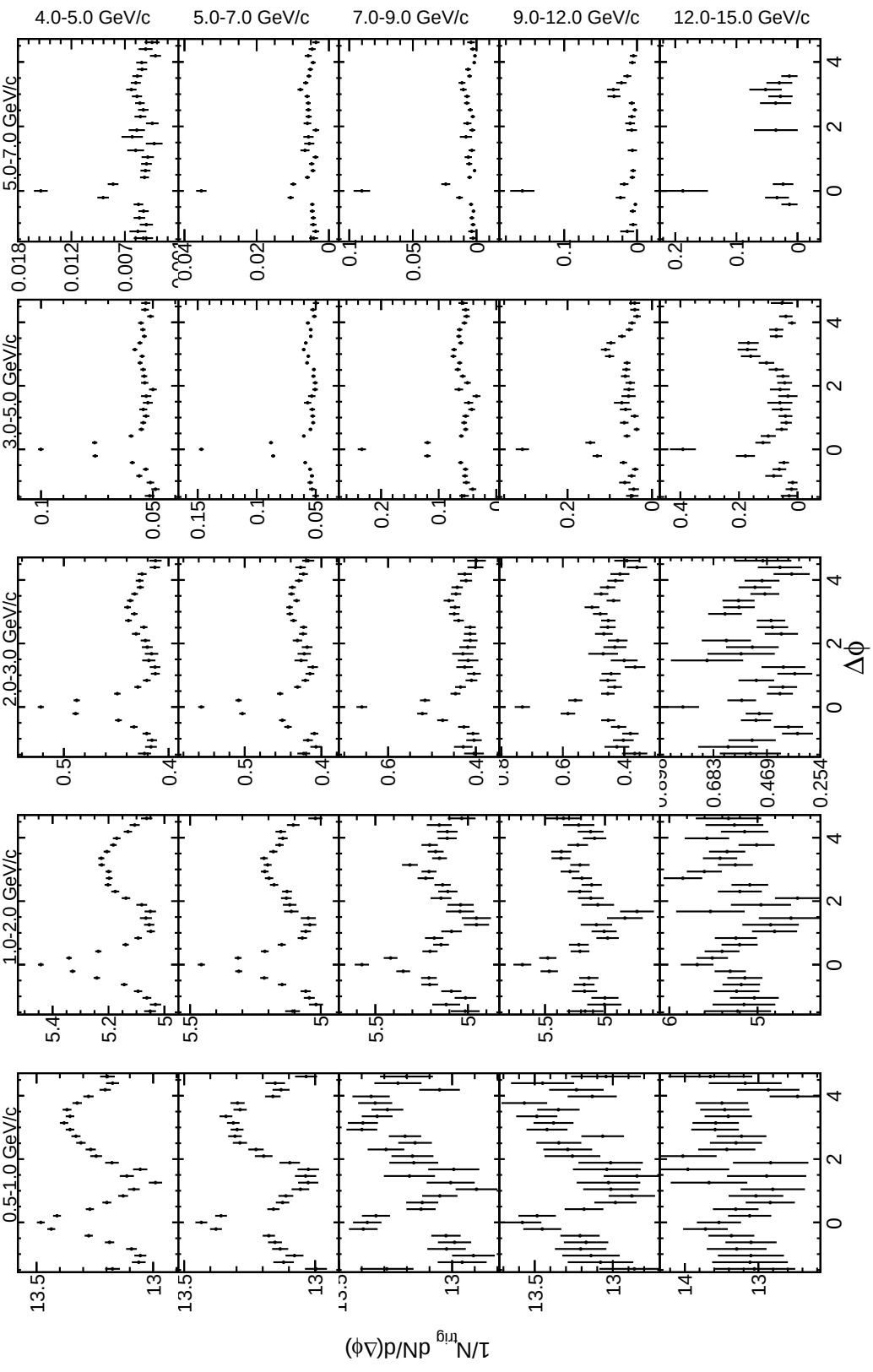

Figure 3.39: Correlation functions in Run 14 0–20% after tracking and embedding efficiency and detector acceptance corrections. The top set of numbers represent the charged hadron momentum bins, and the righthand set of numbers represent the π^0 momentum bins

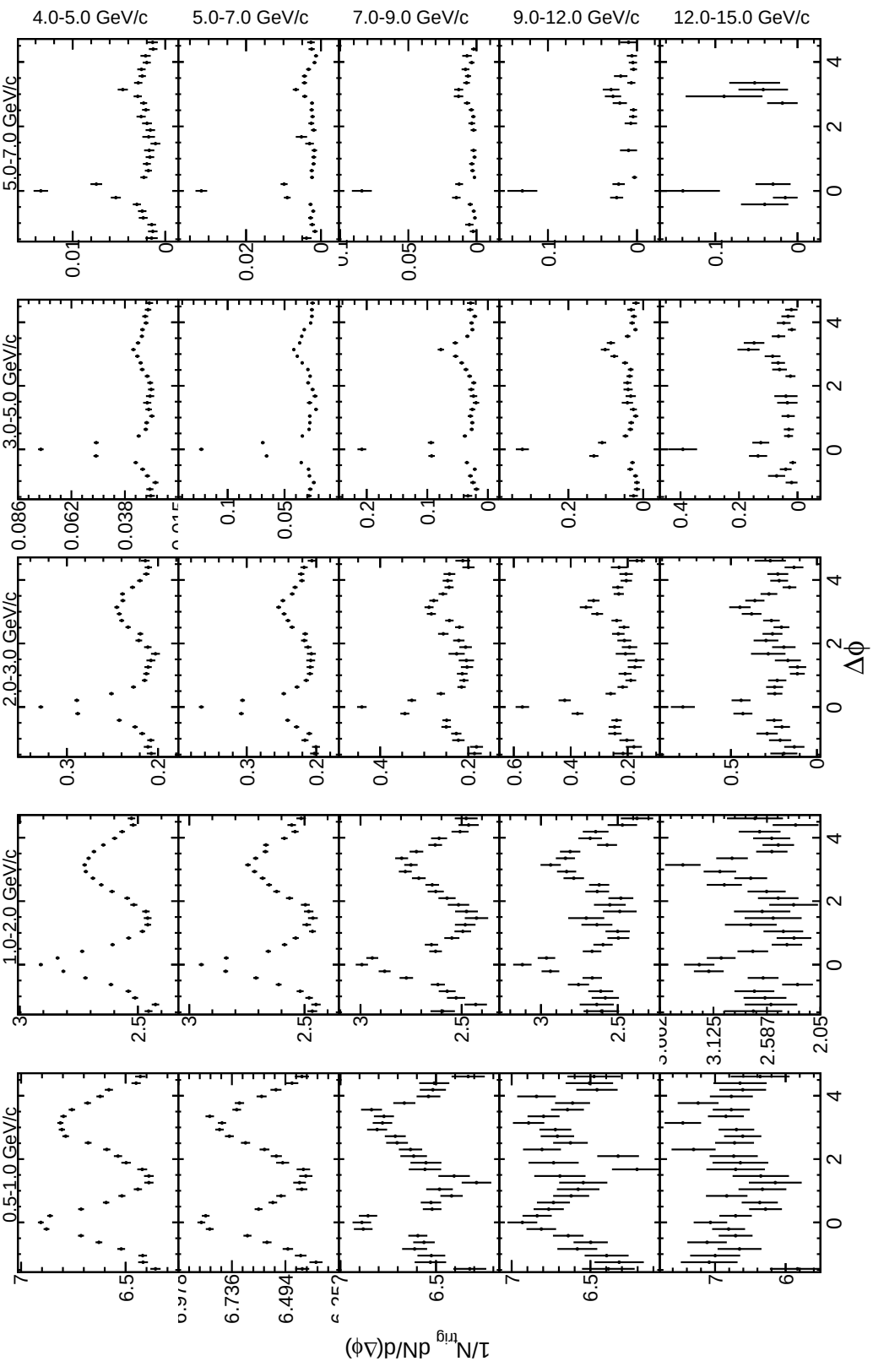

Figure 3.40: Correlation functions in Run 14 20–40% after tracking and embedding efficiency and detector acceptance corrections. The top set of numbers represent the charged hadron momentum bins, and the righthand set of numbers represent the π^0 momentum bins

3.3 Background Flow subtraction

The signal extracted via two-particle correlations is comprised of two components. The first is correlations that arise due to jets, which is the physics this analysis aims to study. There are, however, particles that are paired together by other physical processes unrelated to jets. In $p+p$ collisions, this pairs add a flat background to the correlation function, which is subtracted off using a method known as ZYAM (**Z**ero **Y**ield **A**t **M**inimum), the underlying principle of which is that there should exist a region (typically about $\Delta\phi \approx \frac{\pi}{2}$) where the jet function should be zero. The correlation function measured in $p+p$ collisions is thus fitted, and the background level, b, is extracted directly from the fit and then subtracted off as a flat line in $\Delta\phi$ space, thus yielding correlations due only to jet interactions. However, this process is complicated in heavy-ion collisions, for not only is the background much larger, it is also correlated via spatial anisotropies in the initial state of the collision as detailed in Sec. 1.2.3.1. This is known as the "two-source" model for correlations in particle collisions and is given mathematical form by Eqn. 3.11.

$$\frac{dN_{Corr}}{d\Delta\phi} = \frac{dN_{Jet}}{d\Delta\phi} + \frac{dN_{Background}}{d\Delta\phi} \tag{3.11}$$

Here, N_{Corr} is the total number of correlated pairs, N_{jet} are pairs correlated through jet interactions and $N_{Background}$ are pairs correlated through some background mechanism. Additionally, $d\Delta\phi$ normalizes the histogram by the $\Delta\phi$ bin width. The quantity of interest to us, of course, is $\frac{dN_{Jet}}{d\Delta\phi}$, which can be extracted intuitively by subtracting the $\frac{dN_{Background}}{d\Delta\phi}$ from

the $\frac{dN_{Corr}}{d\Delta\phi}$ term, as shown in Eqn. 3.12.

$$\frac{dN_{Jet}}{d\Delta\phi} = \frac{dN_{Corr}}{d\Delta\phi} - \frac{dN_{Background}}{d\Delta\phi} \tag{3.12}$$

As discussed in Sec. 1.2.3.1, collective flow can be expanded to a Fourier series

$$\frac{dN_{flow}}{d\Delta\phi} = b\Big[1 + 2\sum\langle v_n\rangle \cos\left(n\cdot\Delta\phi\right)\Big] \,, \tag{3.13}$$

Here, b is the background level, which is calculated using the Absolute Background Subtraction method 3.3.3 for $p_T^{Hadron} > 1$ GeV/c. For $p_T^{Hadron} < 1$ GeV/c, the ZYAM method is used, as detailed in Sec 3.3.4. Several experimental results [39, 54, 55] show that the $\langle v_n\rangle$ term in 3.13 can actually be factored as $\langle v_n^{\pi^0}\rangle\langle v_n^h\rangle$ which are the n^{th} order flow harmonic coefficients for π^0's and charged hadrons, respectively.

v_1, which is directed along the longitudinal direction and approximately zero at midrapidty, can be ignored. For this analysis, coefficients 2 through 4 are considered, and the influence of the higher order harmonics is considered negligible. Then, equation 3.13 can be rewritten as:

$$\frac{dN_{flow}}{d\Delta\phi} = b\Big[1 + 2\sum_{n=2}^{4}\langle v_n^{\pi^0}\rangle\langle v_n^h\rangle \cos\left(n\cdot\Delta\phi\right)\Big] \,. \tag{3.14}$$

3.3.1 Charged Hadron v_n Coefficients

v_2^h, v_3^h, and v_4^h values for inclusive charged hadrons in the momentum range of 0.5–10 GeV/c come from previous PHENIX measurements [56]. The charged hadron v_n values from [56] were then merged into a $0-20\%$ and a $20-40\%$ centrality bin for use in [38] as shown in Fig. 3.41, and are re-used here. After the v_n values are merged into the correct centrality bins, the v_n distributions are then fit with Eqn. 3.15 so that values between the published data can then be interpolated.

$$v_n(p_T) = A \cdot e^{-(\frac{B-p_T}{C})^2} + \left(D - E \cdot e^{-F \cdot p_T}\right) \ . \tag{3.15}$$

Evaluation points are chosen from the average of this analysis's measure charged hadron spectrum, and are shown in Fig. 3.42 as open circles. This procedure is also carried out for the charged hadron v_3 and v_4. The v_n values extracted from this method then serve as inputs into Eqn. 3.14.

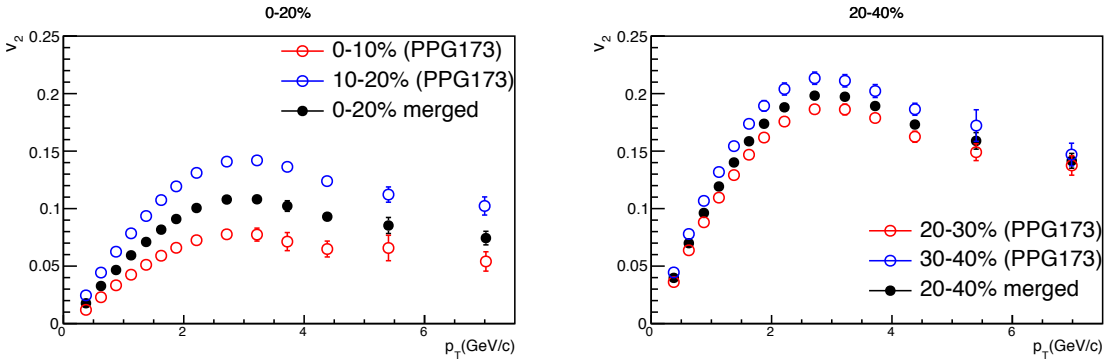

Figure 3.41: v_2^h values in different centrality classes. The open circles are from experimental results [56]. The black dots are the merged values from the open circles.

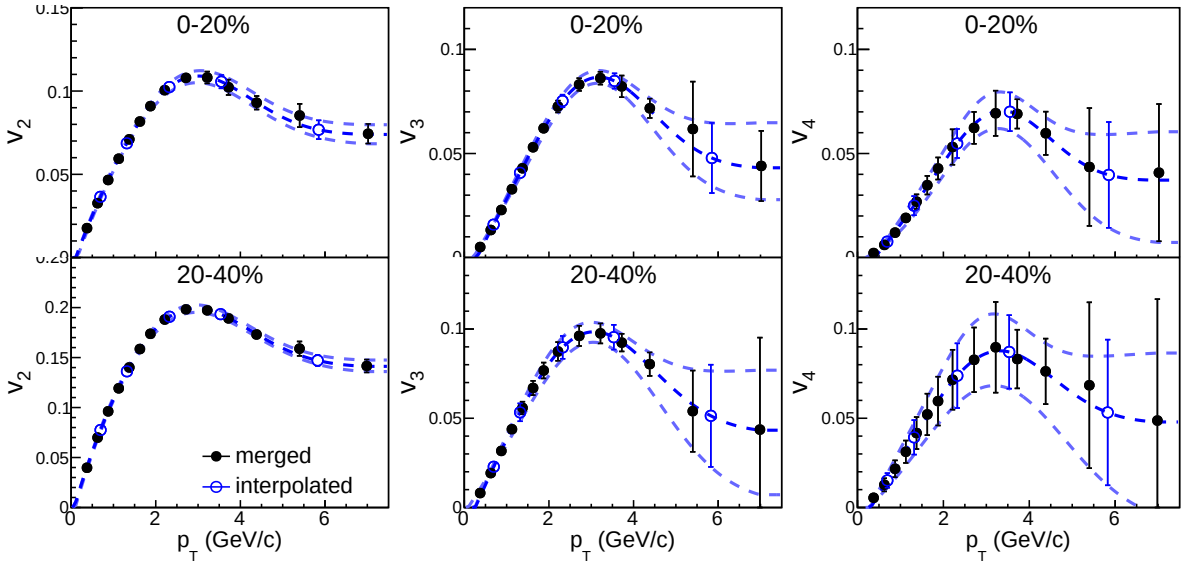

Figure 3.42: Merged (solid dots) and interpolated (open circles) v_n^h values. The blue dash lines are the fits of the nominal, upper and lower bounds values of the solid points.

3.3.2 π^0 v_n Coefficients

The first PHENIX two-particle correlation analysis to subtract the 3^{rd} and 4^{th} flow harmonics was [38], and this subtraction was meant to increase the purity of the measured jet signal, which it did greatly over the previous published result in [39]. However, one of the problems that arose was the lack of measured π^0 v_3 and v_4 results from either PHENIX or STAR in the momentum ranges needed. Thus, another method, known as acoustic scaling [57] was employed and will be detailed in the next section. The process begins as it does with the charged hadron v_n calculations, with the published π^0 v_2 results being merged into a $0-20\%$ and a $20-40\%$ centrality bin. From there, they are fit with Eqn. 3.15 and evaluated at the mean hadron p_T as measured in the analysis. The result of this process is shown in Fig. 3.43.

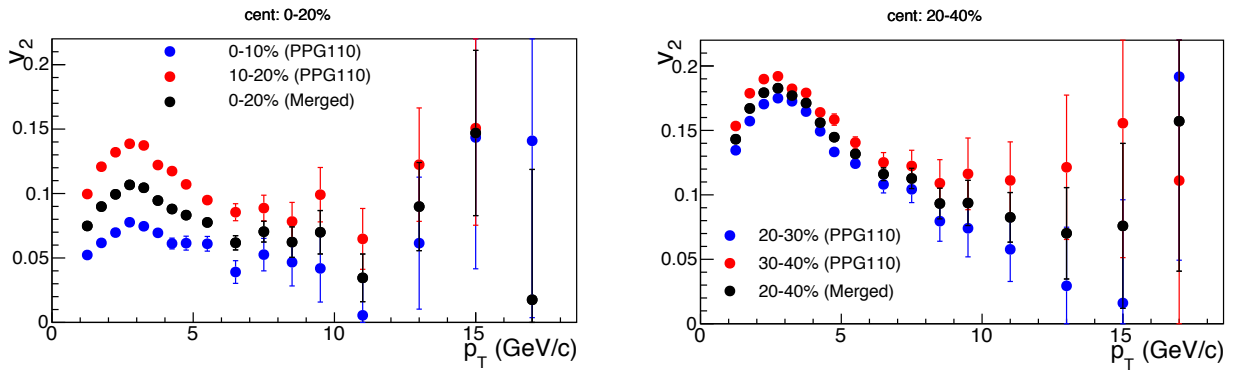

Figure 3.43: Merged $v_2^{\pi^0}$ values (black dots) in 0–20% (left) and 20–40% (right) centrality bins. The red and blue data points are the measured values from [58].

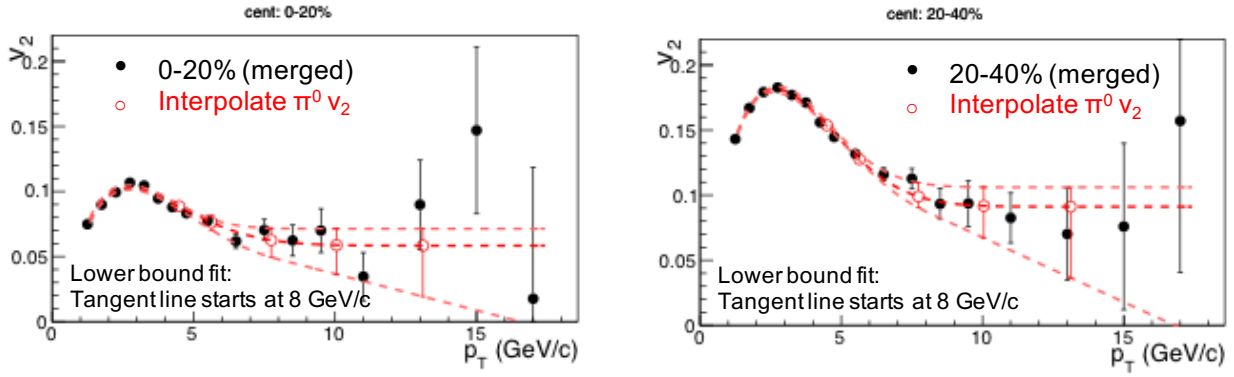

Figure 3.44: Merged (dots) and interpolated (circle) $v_2^{\pi^0}$ values in 0–20% (Left) and 20–40% (Right) centrality bins. The red dash lines are the fits of the nominal, upper and lower error bars of the merged $v_2^{\pi^0}$ values.

Acoustic Scaling

As mentioned earlier, there are no published π^0 v_3 or v_4 measurements from RHIC experiments, so, in order to subtract these harmonics, a method known as acoustic scaling is employed. Acoustic scaling is the observation that the different flow harmonics that can be related by Eqn. 3.16.

$$g_n^h = \frac{v_n^h}{(v_2^h)^{n/2}} \tag{3.16}$$

Thus, by simply rearranging the terms, one can isolate the harmonic of interest and calculate it from a given species' v_2 value and its measured g_n value. One aspect of interest of the g_n values is that they appear to be flat in p_T up to about 10 GeV/c as shown in [57]. Thus, with the data at hand, we can calculate the g_n values for the charged hadrons according to Eqn. 3.16. Then, because of their similar composition and mass, these charged hadron g_n values are used to calculate the missing π^0 v_3 and v_4 values, as shown in Eqn. 3.17. Here, we assume that $g_n^h \approx g_n^{\pi^0}$ due to the similar mass and composition of the three types of pions. Applying equation (3.16) again to estimate neutral pion $v_3^{\pi^0}$ and $v_4^{\pi^0}$ gives

$$v_n^{\pi^0} = g_n^h (v_2^{\pi^0})^{n/2}. \tag{3.17}$$

Fig. 3.45 shows the g_n^h values that are calculated using Eqn. 3.16 using the published v_n^h values from [56]. Because g_n^h is approximately constant in 0–10 GeV/c a flat line is used to fit the data and extract the average g_n^h values. The uncertainties of g_n^h are derived from the fit uncertainties. Finally, $v_3^{\pi^0}$ and $v_4^{\pi^0}$ are estimated using Eqn. 3.17 in conjunction with the g_n^h values from Figure 3.45.

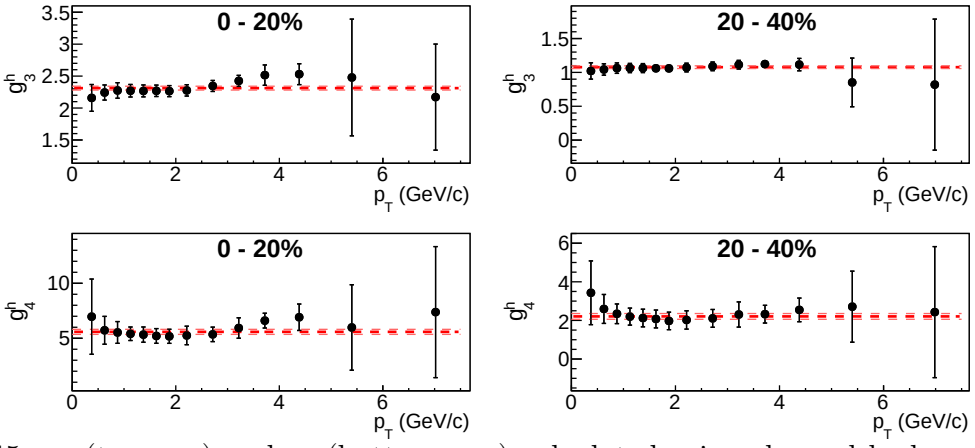

Figure 3.45: g_3 (top row) and g_4 (bottom row) calculated using charged hadron v_n in [56] in different centrality classes. The dash lines are the constant fits and their upper and lower bound values.

3.3.3 Background Magnitude Estimation via Absolute Background Subtraction

With its shape in $\Delta\phi$ space now characterized by the flow harmonics extracted in the previous section, it is now time to calculate the magnitude of the background, denoted as b. In this analysis for $p_T^{Hadron} > 1$ GeV/c, a method known as Absolute Background Subtraction [59] is used to estimate b. The power of this method over ZYAM is that the method is not affected by statistical fluctuations in the correlation function which can effect the the extraction of the background magnitude via fitting. Instead, the background level is calculated assuming that it is combinatoric in nature. That is to say, the number of correlated pairs in an event should scale combinatorially in relation to the number of hadrons and trigger particles in the event. This is encoded in 3.18:

$$b_0 = \frac{\langle n^{AB} \rangle_{\text{mixed}}}{\langle n^A \rangle \langle n^B \rangle_{\text{mixed}}} \ , \tag{3.18}$$

Here, b_0 is the initial background estimate, n^A is the yield of trigger particles (here π^0's), n^B is the yield of associate particles (here, charged hadrons), and n^{AB} is the number of pairs. This ratio tells you the extent to which the number of possible particle combinations ($\langle n^A \rangle \langle n^B \rangle_{\text{mixed}}$) seen in an event exceeds that which arises from trigger-associate particle pairs alone ($\langle n^{AB} \rangle_{\text{mixed}}$). To avoid biasing this calculation towards background levels when only jets are present, correlations measured for the event-mixing process are used, and hadrons from events where trigger particles may not be present are also used. This has the added benefit of simplifying Eqn. 3.18 to Eqn. 3.19 as the use of mixed-event background correlations means the background is solely dependent on the number of background triggers and background pairs and is maximally decorrelated from the jet correlation signal. Next, the initial background estimate, b_0, is multiplied by the centrality correction factor, ξ, giving the total background level, b, in Eqn. 3.20.

$$b_0 = \frac{\langle n^{AB} \rangle_{\text{mixed}}}{\langle n^A \rangle_{\text{mixed}}} \tag{3.19}$$

$$b = \xi b_0 \ , \tag{3.20}$$

ξ is called the centrality correction factor because it accounts for the fact that the background level actually changes smoothly as a function of event centrality. Thus, when looking over a large centrality range (e.g. the 0–20% and 20–40% centrality bins used in this analysis), there is a chance to under or over-estimate the background level. The mathematical definition of ξ is given in Eqn. 3.21. ξ is calculated as the ratio of the mean trigger and associate yields $\langle n^A n^B \rangle$ to the mean number of combinatorial pairs $\langle n^A \rangle \langle n^B \rangle$.

$\langle n^A n^B \rangle$ and $\langle n^A \rangle \langle n^B \rangle$ both depend on the number of binary collisions, N_{coll}, and number of participants, N_{part}. Therefore, they can be estimated in small centrality windows (5% is used for this calculation) using the probability, w^{glaub}, of N_{coll} (N_{part}) yielding a certain number of trigger and asociate particles in a certaint centrality range, as calculated from the Glauber Monte Carlo model [22]. This gives rise to the computational form of (3.21), which can be expressed as (3.22). The summation over i denotes a sum over different centrality bins.

$$\xi = \frac{\langle n^A n^B \rangle}{\langle n^A \rangle \langle n^B \rangle} \tag{3.21}$$

$$= \frac{\sum w_i^{glaub} n_i^A n_i^B}{\sum w_i^{glaub} n_i^A \times \sum w_i^{glaub} n_i^B} \ . \tag{3.22}$$

In order to find n_i^A and n_i^B, distributions n^A and n^B as functions of N_{coll} and N_{part} are fitted with Equations 3.23 and 3.24 over the N_{coll} and N_{part} regions which correspond to the

centrality classes 0–20% and 20–40%. This fitting procedure is shown in Figs. 3.46 and 3.47.

$$n^{A/B} = \gamma \tan^{-1}(\beta N^{\alpha}_{part/coll}) \tag{3.23}$$

$$n^{A/B} = \gamma(1 - e^{\beta N^{\alpha}_{part/coll}}) \tag{3.24}$$

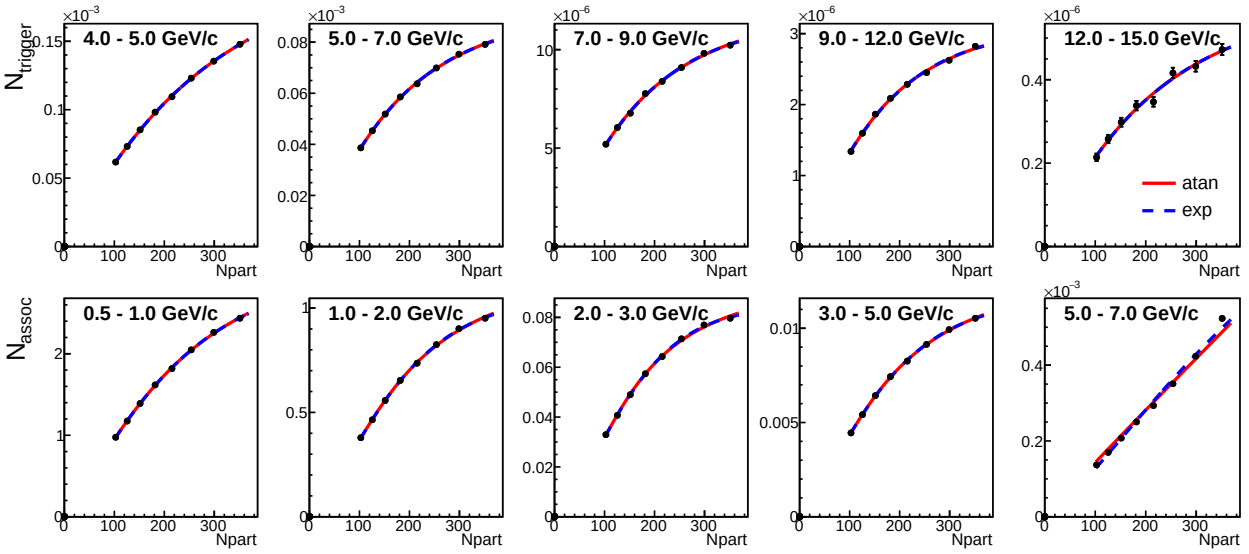

Figure 3.46: Yield of trigger (top) and associate charged hadrons (bottom) as functions of N_{part} from Run 14 data.

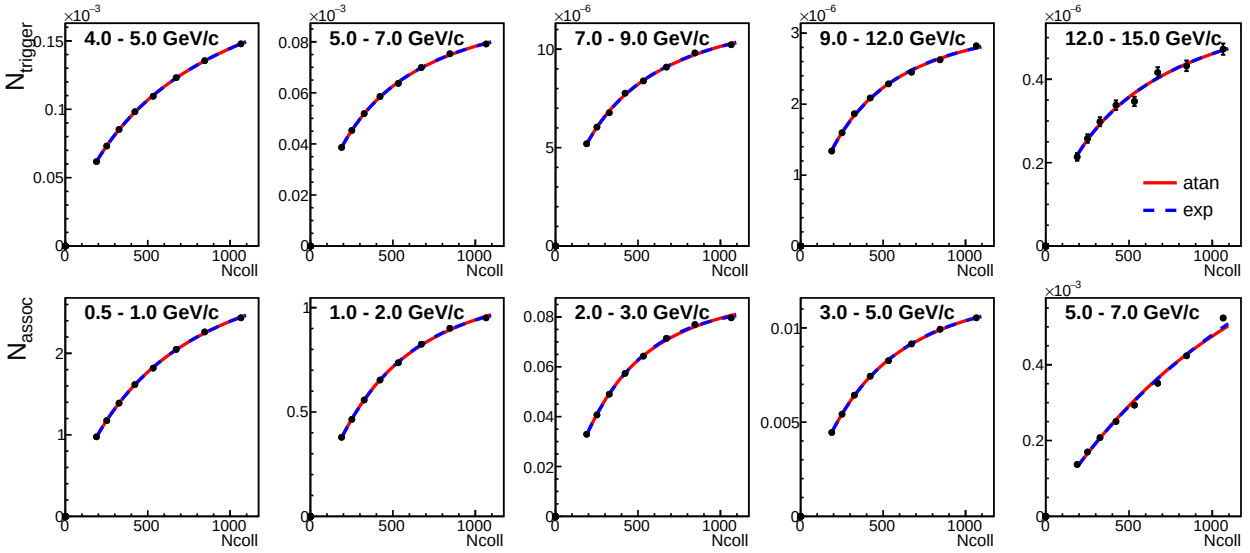

Figure 3.47: Yield of trigger (top) and associate particles (bottom) as function of N_{coll} from Run 14 data.

Equations 3.23 and 3.24 are chosen for how well they fit the data across a large N_{Part} and N_{Coll} range. However, this results in a total of four fits for determining ξ values using equation 3.22. The final ξ values, therefore, are the average of the calculations using these different fits, and the variance in the ξ values given by the different fits is assigned as an uncertainty on the final value. The ξ values used in this analysis for Run 14 are shown in Figure 3.48. The different panels correspond to π^0 momentum bins, and the colored points correspond to charged hadron momentum bins. The points between 0–20% are the ξ values used in that centrality bin, but are spaced out for visibility, and the same applies to the ξ values between 20–40%.

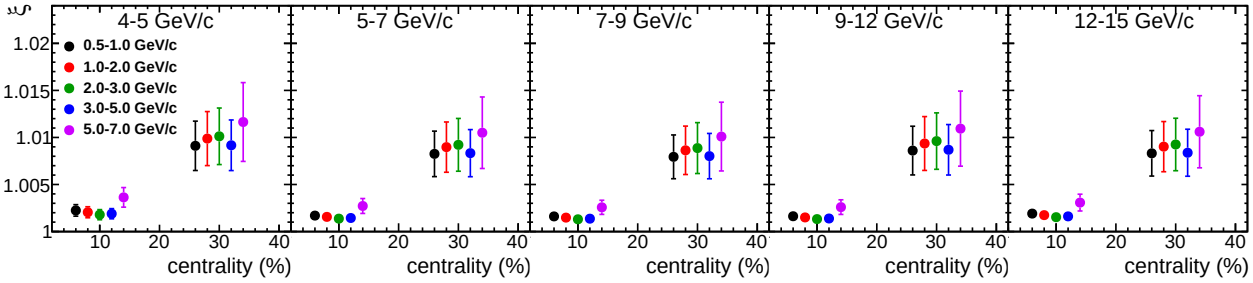

Figure 3.48: ξ as a function of centrality in different trigger and associate p_T ranges from Run 14.

3.3.4 Background Magnitude Estimation via ZYAM

In the course of this analysis, it was found that Absolute Background Subtraction over-subtracts significantly in the lowest p_T hadron bin, 0.5–1 GeV/c. This over-subtraction leads to substantial disagreement with previous measurements and leads to negative per-trigger yields, which are un-physical. To account for this, ZYAM is adopted in this bin alone. Subtraction via ZYAM is done by fitting the entire correlation function with a fit of the following form

$$f(\Delta\phi) = Ae^{-\frac{(\Delta\phi)^2}{B}} + Ce^{-\frac{(\Delta\phi-\pi)^2}{D}} + E(1 + 2\sum_{2}^{4}\langle v_n^{Trig}\rangle\langle v_n^{Hadron}\rangle \cos(n\Delta\phi)) \tag{3.25}$$

The variables A, B, C, and D are fitting parameters that pertain to the Gaussian-like structure of the correlation function. Because we constrain the fit by using real values for the $\langle v_n^{Trig}\rangle\langle v_n^{Hadron}\rangle$ terms, parameter E is thus the background magnitude b. Fits to the correlation functions in the 0.5–1 GeV/c p_T^{Hadron} bin can be seen in Figs. 3.49 and 3.49 below. Here, the method runs into trouble in the higher p_T^{Trig} bins where the correlation function is dominated by statistical uncertainty, and this will lead to large systematic uncertainty on

physics results extracted from these bins. However, the method is very robust at low p_T^{Trig} where there are much smaller statistical error bars.

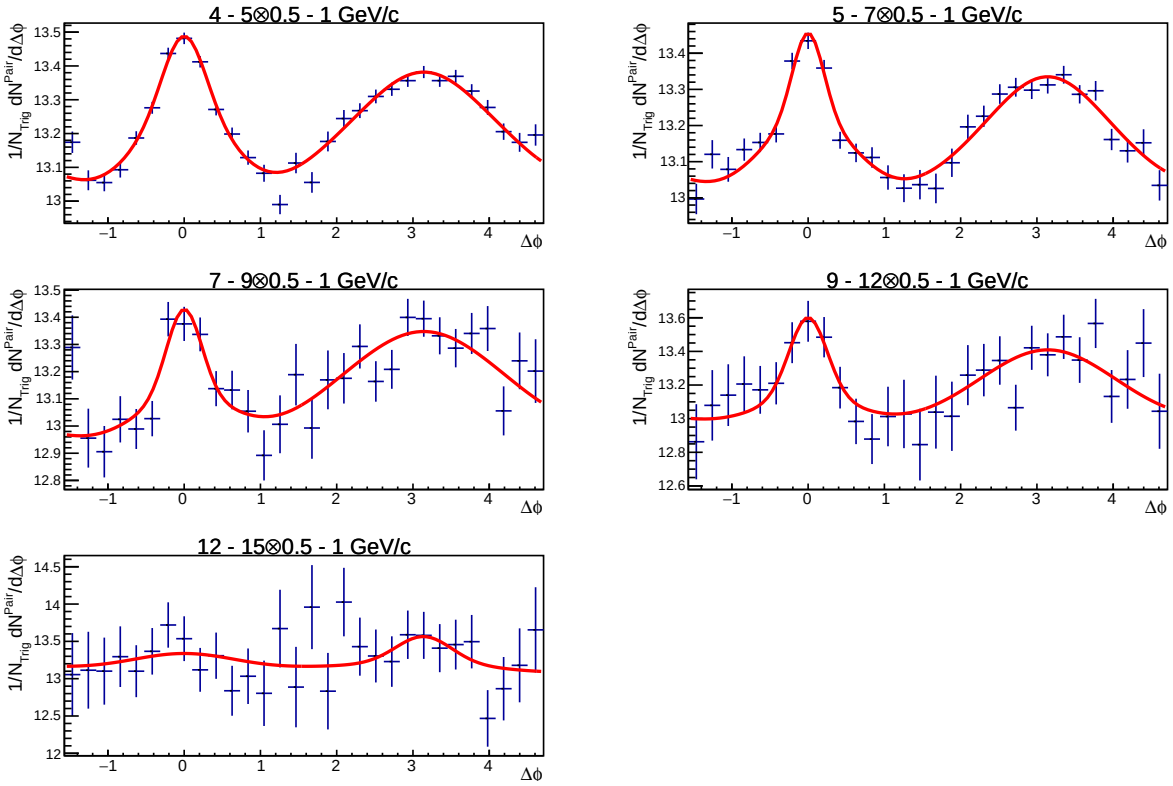

Figure 3.49: Fits to correlation functions measured in Run 14 in the 0–20% centrality class.

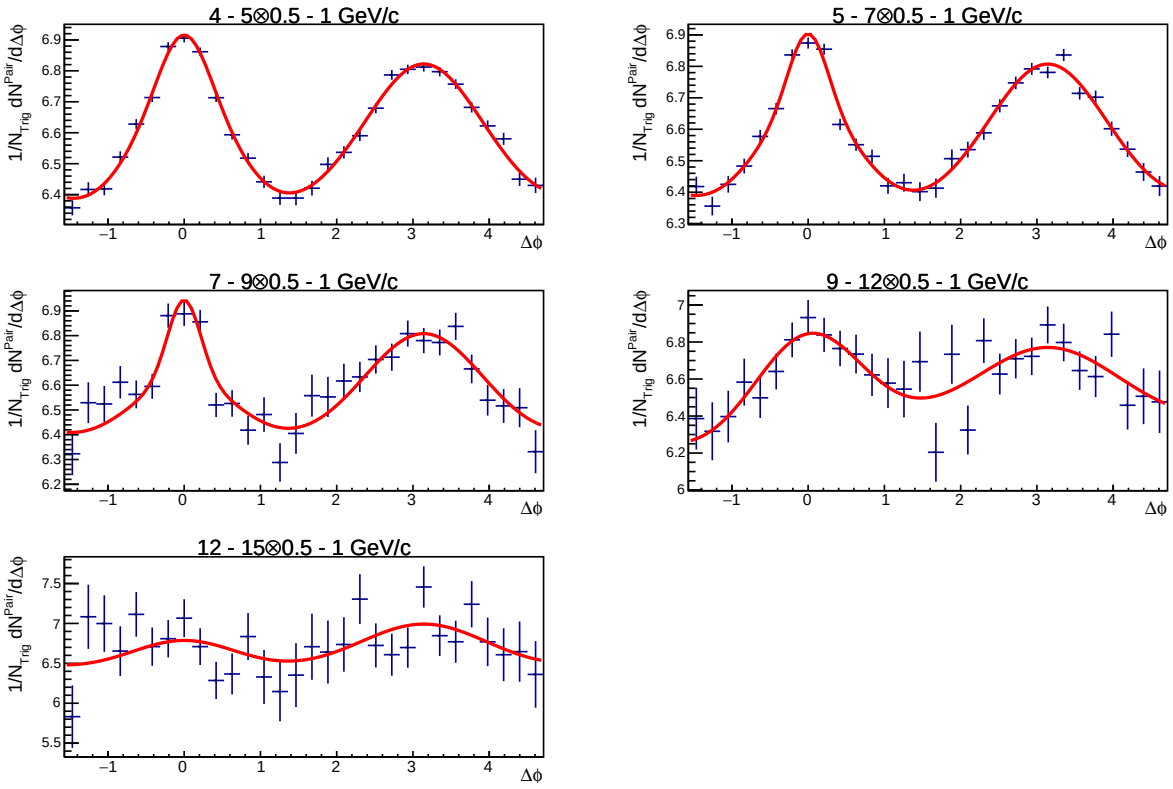

Figure 3.50: Fits to correlation functions measured in Run 14 in the 20–40% centrality class.

The correlation functions and the background correlations due to collective flow scaled by b computed by ZYAM and Absolute Background Subtraction are shown in Figs. 3.51 and 3.52. The fully subtracted jet functions can be seen in Sec. 5 with full systematic uncertainties in Figs. 5.1 and 5.2.

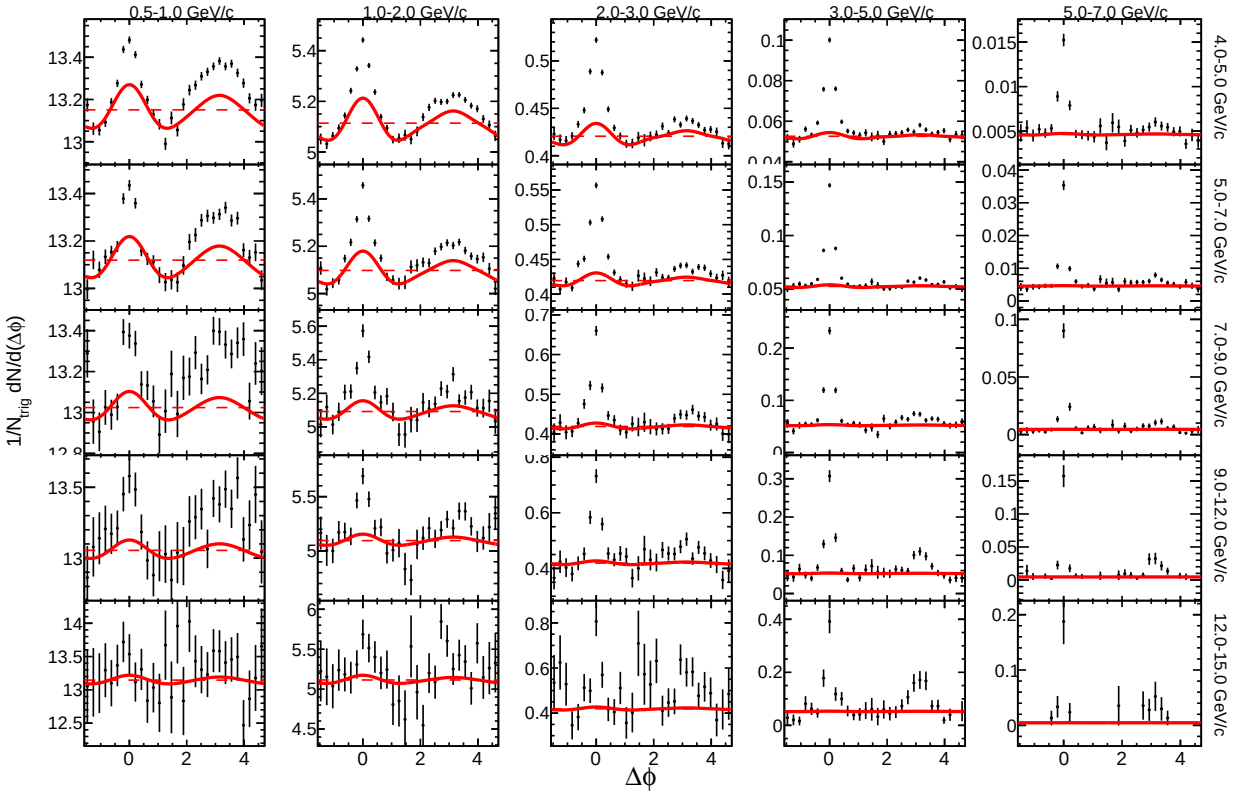

Figure 3.51: Correlation functions (black points), collective flow (red curve) and background level (dashed red line) in the 0-20% centralty class.

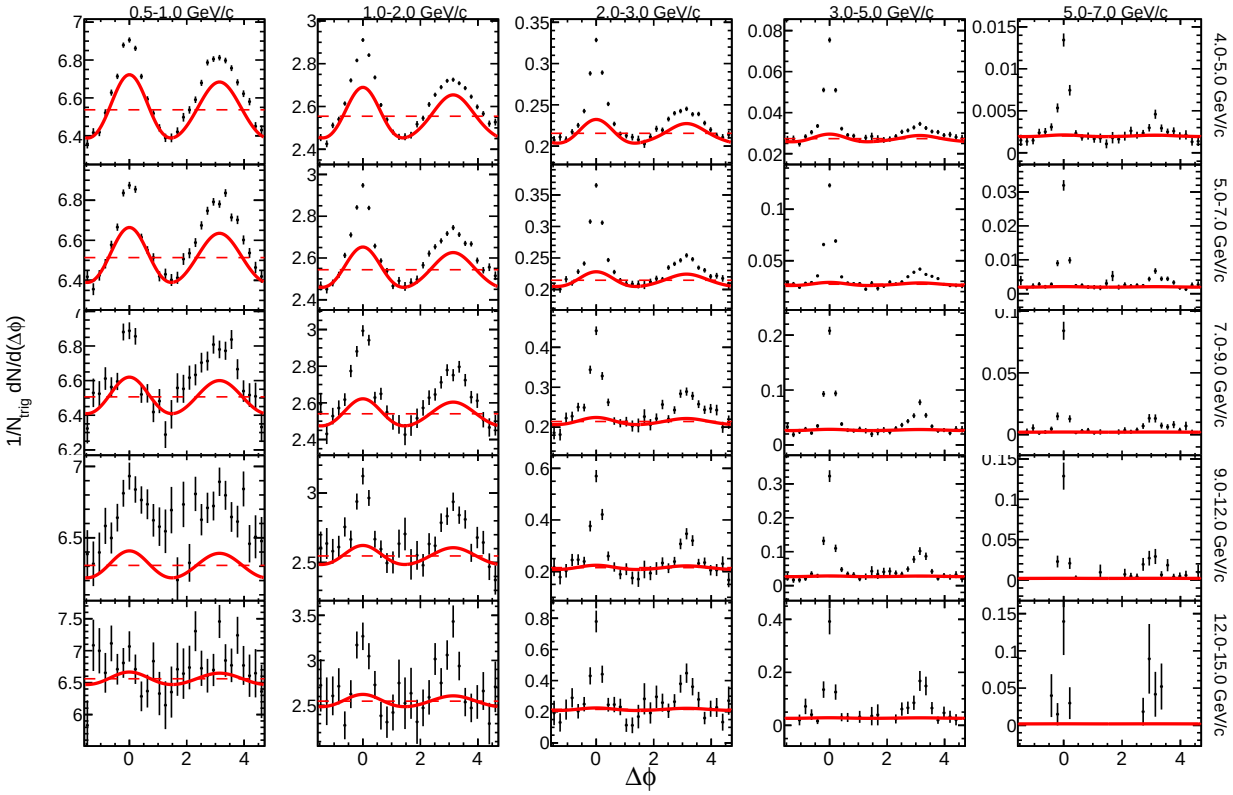

Figure 3.52: Correlation functions (black points), collective flow (red curve) and background level (dashed red line) in the 20-40% centralty class.

3.4 Extracting Physics Quantities

Subtraction of the underlying event due to collective flow yields jet functions, which themselves measure the spatial correlation between particles correlated by jet interactions. These jet functions are the source of the physics results below.

3.4.1 Integrated Per-Trigger Yield Modification: $I_{AA}(p_T)$

I_{AA} is defined as the ratio of the integrated per trigger yields in $Au+Au$ to those in baseline $p+p$ collisions, as per Eqn. 3.26.

$$I_{AA} = \frac{Y_{AA}}{Y_{pp}} \ . \tag{3.26}$$

Y_{AA} and Y_{pp} are the integrated per-trigger yields extracted from the jet functions in $Au+Au$ and $p+p$ collisions, respectively. They are defined as per Eqn. 3.27.

$$Y = \frac{1}{N_{trig}} \int_{\Delta\phi^-}^{\Delta\phi^+} \frac{dN_{jet}}{d\Delta\phi} d\Delta\phi \ , \tag{3.27}$$

Here $\Delta\phi^{\pm}$ is the integration range which is $[\pi - \frac{\pi}{2}, \pi + \frac{\pi}{2}]$ for the away-side peak. I_{AA} can also be computed for the near-side, but this is not extracted for this analysis.

3.4.2 Differential Per-Trigger Yield Modification: I_{AA} *vs.* $\Delta\phi$

The I_{AA} can also be calculated point-by-point in $\Delta\phi$ space by directly dividing the $Au+Au$ jet function by the $p+p$ jet function. This measurement offers a way to quantify modification of the jet structure via two-particle correlations, something usually only attributed to full-jet reconstruction studies.

3.4.3 Differential Per-Trigger Yield Modification: D_{AA} *vs.* $\Delta\phi$

The quantity D_{AA} is defined as the difference between the $Au+Au$ jet functions and the $p+p$ jet functions, rather than the quotient. This observable is introduced in this analysis

to probe jet structure modification like the I_{AA} vs. $\Delta\phi$ observable, but with the benefit of not being effected by division by near-zero yields in the $p+p$ jet functions. This immunity allows the D_{AA} to more reliably (i.e., with smaller uncertainties) probe jet modification further away from the away-side jet peak than the I_{AA} vs. $\Delta\phi$ can.

CHAPTER 4

Systematic Uncertainty

Systematic uncertainties are to quantify how changes in the input parameters (e.g. cuts or v_n values) change the final result. There are five source of systematic uncertainty associated with this analysis. They are:

- The v_n coefficients which can vary between their upper and lower bounds as presented in their original measurements.
- The uncertainty on the centrality bias correction factor ξ that results from the four methods used to calculate it.
- Uncertainties resulting from the hadron efficiency and occupancy corrections.
- The uncertainty arising from the combinatorial method used to reconstruct trigger π^0's
- Systematic uncertainties associated with the baseline $p+p$ measurement done in [39].

This chapter will detail the first four of these five.

4.1 Flow Harmonics

The systematic uncertainty associated with the different flow harmonics arise from the uncertainties reported in [56, 58], as well as the uncertainties calculated for the acoustic scaling

method used to generate the higher order π^0 v_n coefficients.

$$\begin{aligned}\text{Flow}(\Delta\phi) &= 1 + 2[v_2^{\pi^0} v_2^h \cos(2\Delta\phi) + v_3^{\pi^0} v_3^h \cos(3\Delta\phi) + v_4^{\pi^0} v_4^h \cos(4\Delta\phi)] \\ &= 1 + 2[v_2^{\pi^0} v_2^h \cos(2\Delta\phi) + g_3 (v_2^{\pi^0})^{3/2} v_3^h \cos(3\Delta\phi) + g_4 (v_2^{\pi^0})^{4/2} v_4^h \cos(4\Delta\phi)] \ .\end{aligned} \tag{4.1}$$

To find the systematic uncertainty, σ^{f_n}, contributed by the variation of a given order flow harmonic, the corresponding $v_n^{\pi^0}$ and v_n^h terms are set to their upper and lower bound values in Eqn. (4.1), and the systematic uncertainty for a give harmonic is the absolute value of the difference between the nominal result and the varied result. This process is done independently for the upper and lower bound and is done one at a time for $n = 2, 3, 4$ for both the π^0 and charged hadron coefficients. The total uncertainty is evaluated as the quadrature sum of the contributions from each harmonic.

The systematic uncertainty associated with the v_n values tends to be largest at low p_T and decreases at high p_T as the underlying event becomes smaller. The uncertainties associated with the v_n coefficients are generally less than 5% across the different observables. However, one can see a spike in their magnitude in some bins (e.g. the 9–12$\otimes$0.5–1 GeV/c $p_T^{Trig} \otimes p_T^{Assoc}$ bin, as shown in Fig. 4.18). These large increases in the relative uncertainties from the v_n values stems from the use of ZYAM to estimate the underlying event magnitude b. As v_n values are varied to calculate the systematic uncertainties, the b value extracted from ZYAM can also change as fits to the correlation function change, thus driving a larger discrepancy between the nominal and varied results, which yields a larger systematic uncertainty. One

can see this effect does not occur when Absolute Background Subtraction is employed as the background magnitude stays constant during the v_n variance, and the relative uncertainties can be less than 1% on quantities like the integrated yields and I_{AA}.

4.2 ZYAM

ZYAM is used to estimate the background magnitude for the lowest p_T^{Hadron} bin ($0.5 < p_T^{Hadron} < 1$ GeV/c) to avoid the over-subtraction that was encountered when employing Absolute Background Subtraction. To calculate the uncertainty arising from ZYAM, the nominal correlation functions are fit with Eqn. 3.25, but this time the value b is varied between its upper and lower bounds as determined by the errors on the fit. At low $p_T^{\pi^0}$. Thus, Eqn. 3.25 becomes Eqn. 4.2.

$$f(\Delta\phi) = Ae^{-\frac{(\Delta\phi)^2}{B}} + Ce^{-\frac{(\Delta\phi-\pi)^2}{D}} + (E \pm \sigma_{fit})(1 + 2\sum_{2}^{4}\langle v_n^{Trig}\rangle\langle v_n^{Hadron}\rangle \cos(n\Delta\phi)) \quad (4.2)$$

Because the uncertainty on the fit is directly related to the statistical errors in the correlation functions, the systematic due to ZYAM at low $p_T^{\pi^0}$ is not terribly egregious at around 10% and is even lower in some observables compared to the uncertainty from ξ reported in [38]. However, at high $p_T^{\pi^0}$, the method runs into trouble at the statistical error in the correlation functions increases rapidly. The uncertainty quickly jumps to as high as 50% on quantities like the integrated yields, although this is in the 12–15$\otimes$0.5–1 GeV/c $p_T^{Trig}\otimes p_T^{Hadron}$ momentum bin, which is not used to derive later observables. For quantities like the I_{AA}, which is calculated for $p_T^{\pi^0} < 12$ GeV/c, the uncertainty from ZYAM is a large, but more reasonable

20%. Lastly, the other major pitfall of the ZYAM method is the fact that it can influence other observables' uncertainties as well. Because the E term in Eqn. 3.25 is allowed to vary in the calculation of the other uncertainties, a larger variance can occur between the nominal and varied values. It is for this reason that estimating the background level using ZYAM is the largest contributor to the systematic uncertainty in the 0.5–1 GeV/c associate hadron momentum bin.

4.3 Absolute Background Subtraction

The systematic uncertainty arising from the Absolute Background Subtraction method comes from the calculation of the ξ, the centrality bias correction factor. ξ is extracted via fitting trigger and charged hadron distributions as a function of N_{Coll} and N_{Part} via two equations, Eqn. (3.23) and Eqn. (3.24). While the average value is used as the nominal value for ξ, the deviation between them is assigned as a systematic uncertainty.

The uncertainty arising from ξ takes over as the dominant contributor to the total relative uncertainty, but with a number of caveats. It's most dominant contribution can be seen in the integrated yields and I_{AA} in the 4–5 $\otimes$ 0.5–1 GeV/c $p_T^{Trig} \otimes p_T^{Hadron}$ bin, where it's almost 20% in the 20–40% centrality bin. However, it should be noted that the relative uncertainty arising from ξ decreases exponentially as one increases either the trigger momentum or the associate hadron momentum, quickly becoming less than a percent.

4.4 Hadron Efficiency

There are six sources of systematic uncertainty in the single particle efficiency and occupancy corrections.

- The momentum resolution of the central arm tracking systems.
- The PC3 track matching done specifically for the efficiency calculation.
- The embedding procedure.
- The procedure of merging the charged hadron-to-pion ratios from [53].
- The statistical uncertainty from the simulated sample size of charged tracks.

The total systematic arising from the single particle corrections is thus the quadrature sum of all these uncertainties. Furthermore, this uncertainty is presented as a band at the right end of the line at $y = 0$ of a given observable for quotients like the I_{AA}, and quoted as a raw uncertainty for observables like the jet functions and D_{AA}. This presentation is due to the uncertainty's classification as a Type-C uncertainty, which can be applied uniformly point-by-point. The values from each of these sources is given in Table. 4.2.

4.5 π^0 Combinatorial Background

As mentioned in Chap. 3, all photons that pass the single particle cuts listed in Table. 3.1 as paired combinatorially to create π^0 trigger candidates. However, while this method will reconstruct true π^0's, it can also reconstruct fake π^0's as well, which are impossible to

distinguish from real π^0's as they pass all the same cuts. Therefore, it is necessary to assign a systematic uncertainty which accounts for the presence of fake π^0's in the trigger pool. Fig. 4.1 shows an example of an invariant mass distribution. The signal region is highlighted in red and is shown sitting above a combinatoric background which is shaded in green.

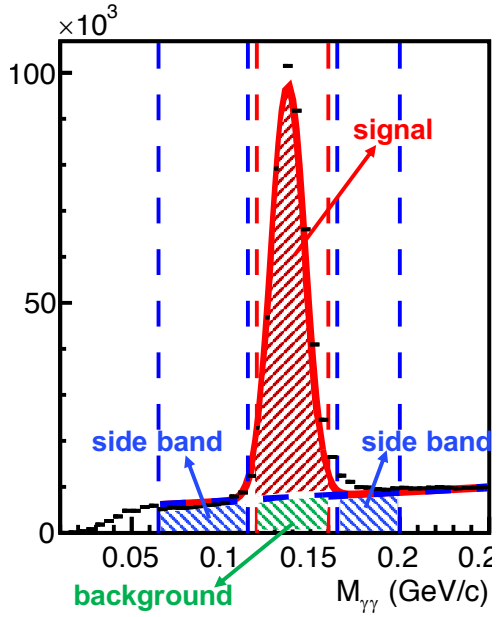

Figure 4.1: Example of an invariant mass spectrum. The blue dash line represents the background level, and the red solid line is a fit to both the combinatorial background and the signal. The vertical dashed lines indicate the signal invariant π^0 mass window (red), and side-band mass windows (blue).

The first step is to quantify a signal-to-background ratio. This calculation is done by fitting the invariant mass spectrum with a Gaussian to account for the signal region and a 4^{th} order polynomial to account for the background. The polynomial terms alone are then integrated in the signal region 0.12–0.16 GeV/c^2, and this quantity is subtracted off the integral of the entire fit in the same region, quantifying the signal term. The more the π^0 mass peak stands out above the background, the larger this term, and the smaller the total

systematic, and vice versa. Fits to the invariant mass spectra can be seen in Fig. 3.7, which is reposted here as Fig. 4.2, and the π^0 signal-to-background ratio is plotted as a function of the π^0 p_T in Fig. 4.3.

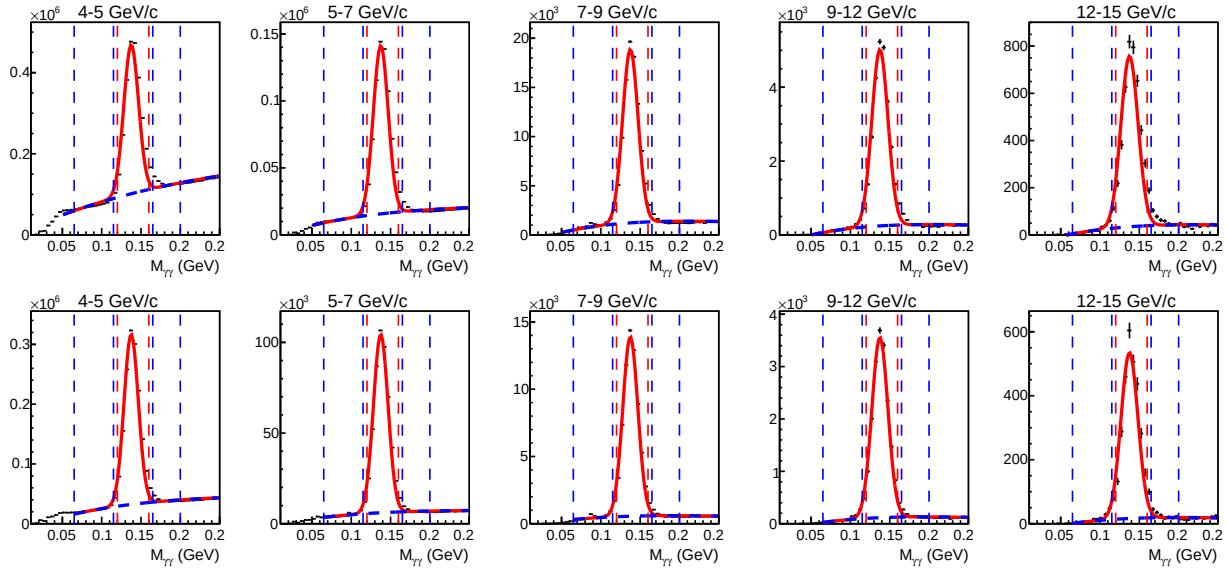

Figure 4.2: Invariant mass spectra π^0 p_T bins. The total fit to the data is the red solid line, and the solid blue line represents the fit to the background. The dotted lines represent the nominal invariant mass range (red) and the side band windows (blue) used in this analysis. The top row is from the 0–20% centrality class and the bottom row is from the 20–40% centrality class.

Next, one must quantify how the choice of invariant mass window effects the per-trigger yield of hadrons. Ideally, even using fake π^0's should not change the number of hadrons that can be paired with any given trigger particle. But in practice this is not necessarily true. Thus, extraction of the jet functions is performed with two "side band" invariant mass windows, and the difference in the per-trigger yields between correlations in the side band and those in the nominal invariant mass regions is measured. The lower side band window used in this analysis is 0.08–0.11 GeV, while the upper side band is 0.165–0.2 GeV. The ratio

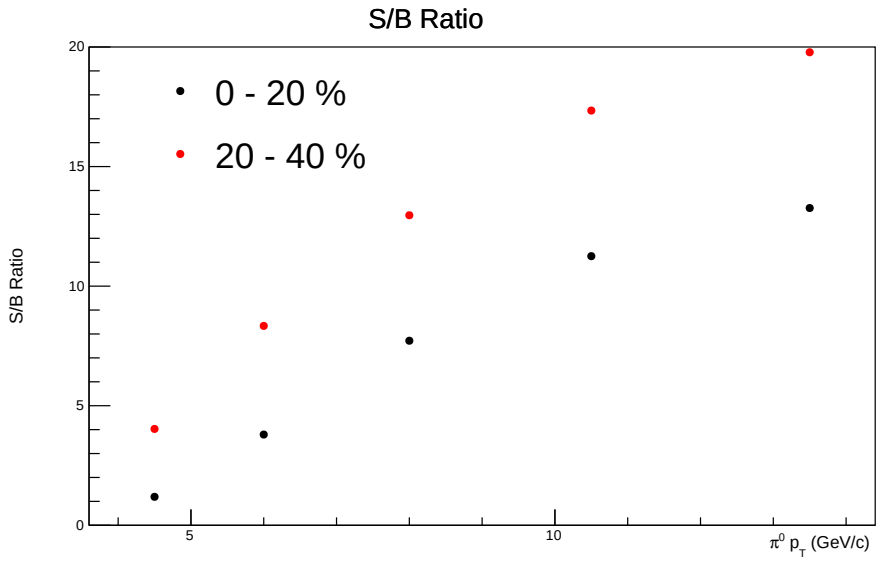

Figure 4.3: Signal-to-background ratio for reconstructed π^0's as a function of π^0 p_T in the 0–20% (black) and 20–40% centrality classes.

of the combined sideband per-trigger yields to the same quantity in the nominal invariant mass window is shown in Fig. 4.4 and Fig. 4.5 for the 0–20% and 20–40% centrality classes, respectively.

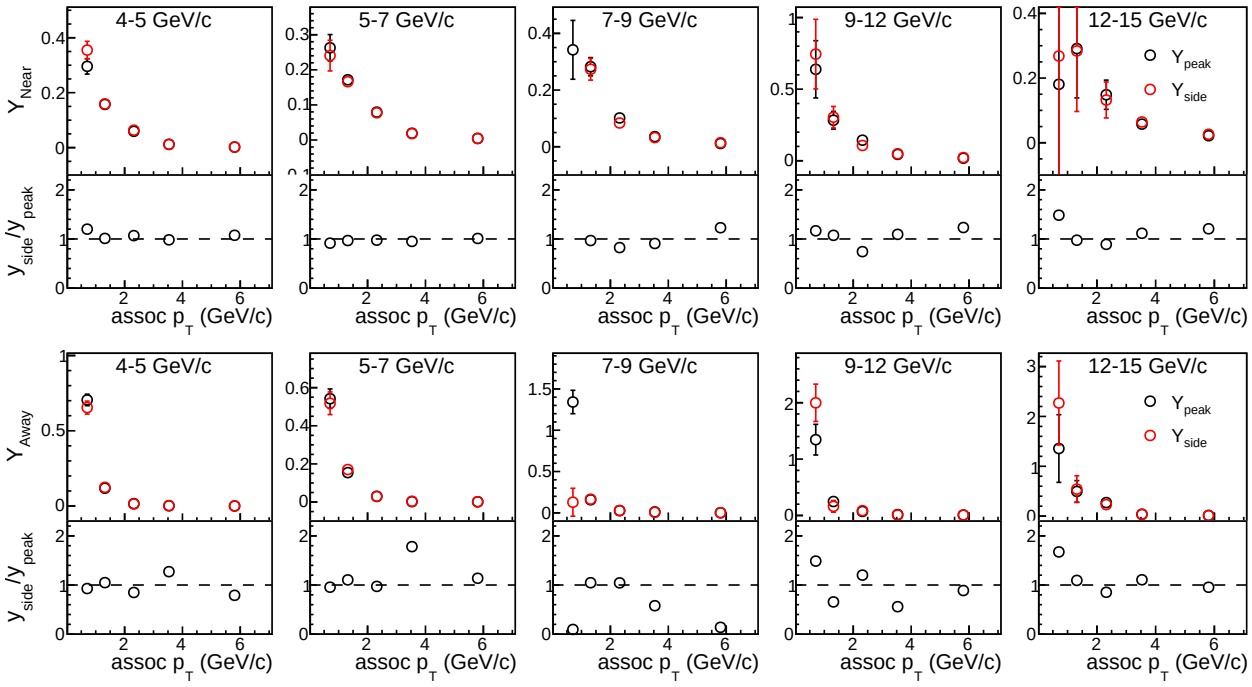

Figure 4.4: Near (top) and away-side (bottom) per trigger yields as a function of associate p_T in different trigger p_T bins in 0–20% centrality. Per trigger yields obtained from side-band and π^0 mass peak regions are drawn in red and black, respectively. The ratios of per trigger yields from different mass windows are drawn at the bottom of each panel.

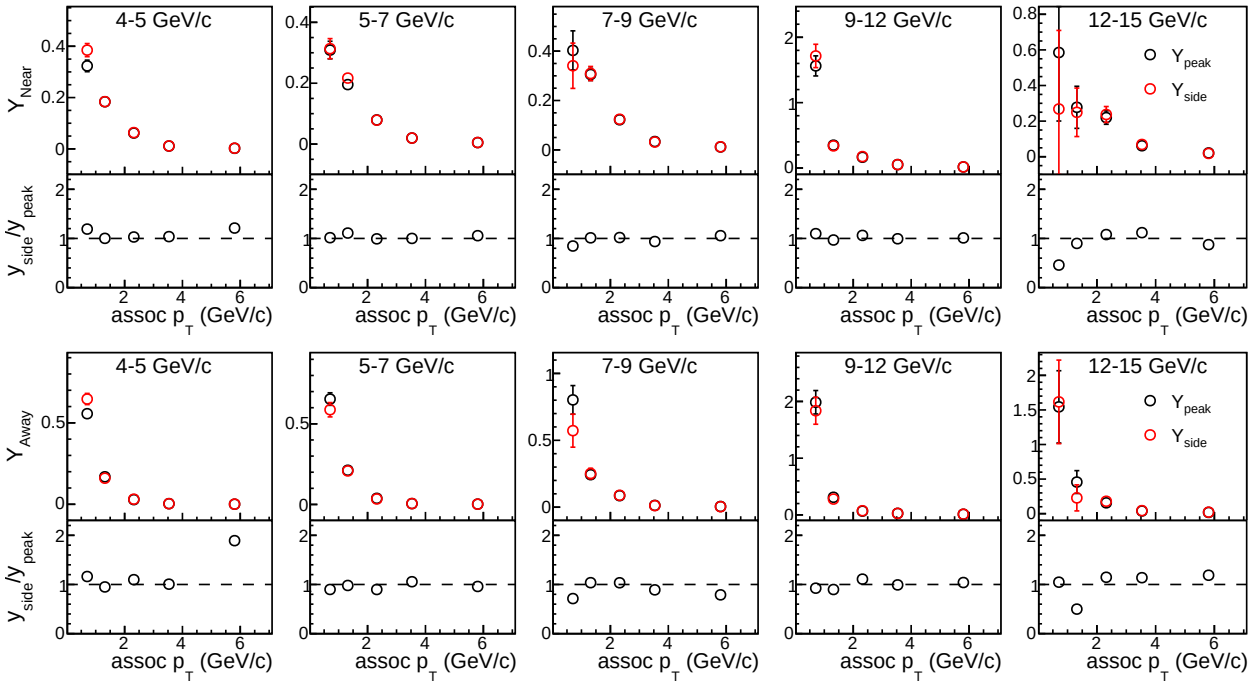

Figure 4.5: Near (top) and away-side (bottom) per trigger yields as a function of associate p_T in different trigger p_T bins in 20–40% centrality. See Figure 4.4 for description.

Both the signal-to-background ratio and the per-trigger yields extracted from the side-band regions are then fed into Eqn. 4.6, which we begin deriving with Eqn. 4.3. The total relative systematic uncertainty for the π^0 reconstruction procedure is defined as

$$\frac{\sigma_Y^{\pi^0}}{Y_{peak}} = \frac{Y_{true} - Y_{peak}}{Y_{peak}}, \tag{4.3}$$

where, σ_{π^0} is the uncertainty of the per-trigger yield. Y_{peak} is the per-trigger yield from the inclusive π^0 trigger candidate pool that falls within the nominal invariant mass window of 0.12–0.16 GeV/c^2. Y_{true} is the same quantity, but for "real" π^0's. However, as mentioned before, there is no true way to differentiate the terms Y_{peak} and Y_{true} in data. To turn the right-hand side into something usable, we start with Eqn. 4.4, which we will then rarrange to isolate the Y_{True} term:

$$\begin{aligned} N_{Peak}Y_{Peak} &= N_{True}Y_{True} + N_{BG}Y_{BG} \\ N_{True}Y_{True} &= N_{Peak}Y_{Peak} - N_{BG}Y_{BG} \\ Y_{True} &= \frac{N_{FG}}{N_{True}}Y_{FG} - \frac{N_{BG}}{N_{True}}Y_{BG} \end{aligned} \tag{4.4}$$

N_{Peak}, N_{True}, and N_{BG} are the number of reconstructed π^0's found in the nominal invariant mass region, the number of true π^0's, and the number of fake π^0's, respectively. Furthermore, Y_{BG} is the per-trigger yield of these fake π^0's. Again, because we do not make an attempt to discriminate between real and fake π^0's in the nominal mass region, Y_{BG} cannot be measured independently. Instead, it is approximated by the per-trigger yield of π^0's with masses that

fall in the side-band regions of the invariant mass spectrum. Thus, Eqn. 4.4 becomes Eqn. 4.5.

$$Y_{True} = \frac{N_{Peak}}{N_{True}} Y_{Peak} - \frac{N_{BG}}{N_{True}} Y_{Side} \ . \tag{4.5}$$

Substituting Eqn. 4.5 into Eqn. 4.3 then yields

$$\begin{aligned} \frac{\sigma_Y^{\pi^0}}{Y_{Peak}} &= \frac{\frac{N_{Peak}}{N_{True}} Y_{Peak} - \frac{N_{BG}}{N_{True}} Y_{Side} - Y_{Peak}}{Y_{Peak}} \\ &= \frac{(\frac{N_{Peak}}{N_{True}} - 1) Y_{Peak} - \frac{N_{BG}}{N_{True}} Y_{Side}}{Y_{Peak}} \\ &= \frac{\frac{N_{Peak} - N_{True}}{N_{True}} Y_{Peak} - \frac{N_{BG}}{N_{True}} Y_{Side}}{Y_{Peak}} \ . \end{aligned}$$

Then, because $N_{Peak} = N_{True} + N_{BG}$, we have

$$\begin{aligned} \frac{\sigma_Y^{\pi^0}}{Y_{Peak}} &= \frac{\frac{N_{BG}}{N_{True}} Y_{Peak} - \frac{N_{BG}}{N_{True}} Y_{Side}}{Y_{Peak}} \\ &= \frac{N_{BG}}{N_{True}} \cdot \frac{Y_{Peak} - Y_{Side}}{Y_{Peak}} \\ &= \frac{1}{N_{True}/N_{BG}} \cdot \left(1 - \frac{Y_{Side}}{Y_{Peak}}\right) \end{aligned} \tag{4.6}$$

Here, the term N_{true}/N_{BG} is the signal-to-background ratio that is measured as mentioned above by carefully dissecting the invariant mass spectrum in the nominal invariant mass window. Finally, the last two terms, Y_{Peak} and Y_{Side}, are directly measurable as well. As stated before, in the ideal case Y_{Side} and Y_{Peak} are approximately the same, as using fake or

real π^0's should not, in principle, change the number of associated hadrons, given that both real and fake π^0's are required to pass the same cuts, making it likely that they're both jet constituents.

The relative systematic uncertainty, $\sigma_Y^{\pi^0}/Y_{peak}$ is plotted as a function of the associate hadron momentum in Figs. 4.6 and 4.7 for both the near and the away-side. The main trend to observe is that the uncertainty is generally smaller in the 20–40% centrality class ($\sim 5\%$ maximum at low p_T^{Hadron} than in more central 0–20% collisions. This decrease in the uncertainty arises because the overall particle multiplicity, and thus, the potential background, is smaller in the 20–40% centrality bin.

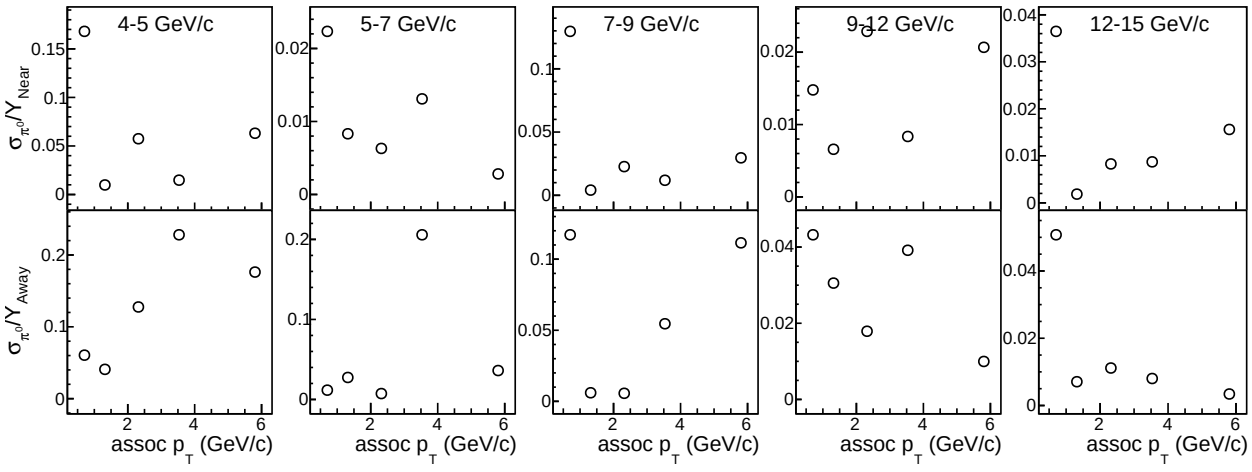

Figure 4.6: Relative background π^0 systematic uncertainty as a function of associate p_T in near (top) and away-side (bottom) peaks in the 0–20% centrality class. The trigger p_T is labeled on the top of each panel.

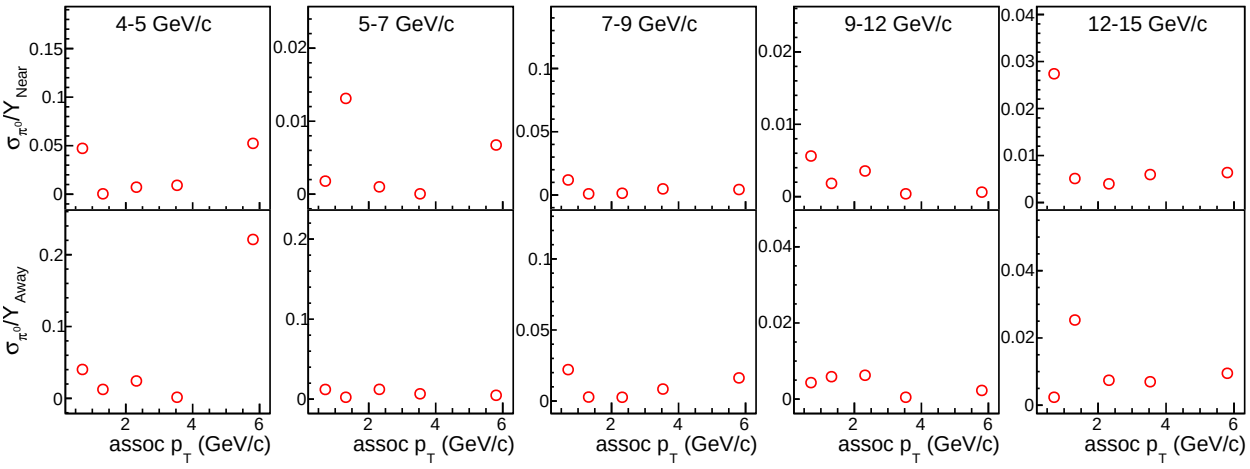

Figure 4.7: Relative background π^0 systematic uncertainty as a function of associate p_T in near (top) and away-side (bottom) peaks in the 20–40% centrality class. The trigger p_T is labeled on the top of each panel.

4.6 Propagation of Systematic Uncertainties

4.6.1 Flow Harmonics and Background Subtraction

The absolute uncertainties that arise from the flow harmonics and Absolute Normalization are obtained by evaluating the jet function at their upper, lower, and nominal values. The differential from each source is the systematic associated with that source. The two notable exceptions are the π^0 combinatoric systematic uncertainty and those arising from the $p+p$ baseline. To combine the systematics, all are added in quadrature

$$\sigma^{total} = \sqrt{\sum (\sigma^i)^2} \tag{4.7}$$

where σ^i is the systematic uncertainty from the i^{th} source.

Systematic uncertainties are categorized according to PHENIX convention into three cate-

gories:

- **Type A**: These uncertainties are completely uncorrelated point-to-point (such as statistical uncertainties) and are propagated via quadrature addition of the errors themselves for simple sums such as the integrated yields or D_{AA} and quadrature sums of the relative yields for ratios such as the I_{AA}

- **Type B**: These uncertainties are correlated point-to-point, meaning that if one data point in the measurement moves upwards, the ones near it will do the same. For instance, when increasing the v_2 to its upper bound, all the points in the jet function will be shifted downwards.

- **Type C**: These uncertainties arise from the uniform application of scale factors and are displayed separately where necessary.

The different systematic uncertainties in this analysis are classified in Table 4.1.

Table 4.1: Sources of Systematic Uncertainty and Their Classification

Quantity	Uncertainty						
	σ^{f2}	σ^{f3}	σ^{f4}	$\sigma^{\xi/ZYAM}$	σ^{π^0}	σ^{pp}	σ^{H}
Jet Function	B	B	B	B	B		C
Jet width	B	B	B	B			
Per trigger yields	B	B	B	B	B		C
Away-side $I_{AA}(p_T)$		B		B	B	B	C
Away-side $I_{AA}(\Delta\phi)$	B	B	B	B	C	B	C

B: Correlated systematic uncertainty

C: global scale uncertainty

4.6.2 Hadron Efficiency Uncertainty

The uncertainty arising from the hadron efficiency is treated as a Type-C uncertainty as was done in [39] and displayed as either a number near the expository text on a plot (e.g. on the jet functions) or as a blue bar on plots taking the ratio of two quantities (e.g. the $I_{AA}(p_T)$ or versus $\Delta\phi$). The systematic uncertainty arising from the tracking efficiency and occupancy correction is 6.9%, and is a combination of several sources, as detailed in Sec. 4.4. Table 4.2 shows the magnitude of these individual contributors, along with the total systematic.

Table 4.2: Systematic uncertainity sources for the hadron efficiency calculation.

	Single Particle Correction Systematic Uncertainties					
	Detector Reproduction in Simulation	Statistical Error	Identified Hadron Ratios	Momentum Resolution	PC3 Matching Recalibration	Total (Maximum)
Run 14	5%	<1%	<3%	2%	3%	6.9%

4.6.3 Combinatorial Background Uncertainty from π^0 Reconstruction

The uncertainty arising from the combinatorial π^0 reconstruction process is applied on all quantities derived from the per-trigger yields extracted from the jet functions. Thus, the uncertainties on the yields are as follows:

$$\frac{\sigma_{jet}^{\pi^0}}{\text{jet}} = \frac{\sigma_{Y}^{\pi^0}}{Y}$$
$$\sigma_{jet}^{\pi^0} = \frac{\sigma_{Y}^{\pi^0}}{Y} \cdot \text{jet} \tag{4.8}$$

and similarly, for quantities such as the I_{AA} and D_{AA},

$$\sigma^{\pi^0}_{I/D} = \frac{\sigma^{\pi^0}_{Y}}{Y} \cdot I/D_{AA} \ . \tag{4.9}$$

4.6.4 Uncertainty From Baseline $p+p$ Measurements

Here we consider the impact of the systematic uncertainty arising from the $p+p$ baseline and its impact on two quantities, the I_{AA} and the D_{AA}, which must be considered separately because they are a quotient and a difference, respectively.

For the I_{AA}, the impact of the $p+p$ systematic begins with considering a downwards fluctuation on the I_{AA}, $I_{AA} - \sigma_I^{pp-}$, caused by an upwards fluctuation from the baseline, $\frac{Y_{AA}}{Y_{pp}+\sigma_Y^{pp+}}$. The impact is then propagated through analytically to the result given by

$$\begin{aligned}
I_{AA} - \sigma_I^{pp-} &= \frac{Y_{AA}}{Y_{pp} + \sigma_Y^{pp+}} \\
\sigma_I^{pp-} &= I_{AA} - \frac{Y_{AA}}{Y_{pp} + \sigma_Y^{pp+}} \\
&= I_{AA} - \frac{Y_{AA}}{Y_{pp}} \cdot \frac{Y_{pp}}{Y_{pp} + \sigma_Y^{pp+}} \\
&= I_{AA}\Big[1 - \frac{Y_{pp}}{Y_{pp} + \sigma_Y^{pp+}}\Big] \\
&= I_{AA} \cdot \frac{Y_{pp} + \sigma_Y^{pp+} - Y_{pp}}{Y_{pp} + \sigma_Y^{pp+}} \\
&= I_{AA} \cdot \frac{\sigma_Y^{pp+}}{Y_{pp} + \sigma_Y^{pp+}} \ .
\end{aligned} \tag{4.10}$$

The same procedure can be used to derive the impact from a downwards fluctuation in the

baseline that results in an upwards fluctuation of the I_{AA}, and the absolute uncertainty on the I_{AA} arising from $p+p$ can be summarized by

$$\sigma_I^{pp\pm} = I_{AA} \cdot \frac{\sigma_Y^{pp\mp}}{Y_{pp} \mp \sigma_Y^{pp\mp}} \tag{4.11}$$

For the D_{AA}, a similar method is applied. We again consider an upwards fluctuation in the D_{AA} caused by a downwards fluctuation in the baseline.

$$\begin{aligned}
D_{AA} - \sigma_D^{pp-} &= Y_{AA} - (Y_{pp} + \sigma_Y^{pp+}) \\
-\sigma_D^{pp-} &= -D_{AA} + (Y_{AA} - (Y_{pp} + \sigma_Y^{pp+})) \\
\sigma_D^{pp-} &= D_{AA} - (Y_{AA} - (Y_{pp} + \sigma_Y^{pp+})) \\
\sigma_D^{pp-} &= D_{AA} - Y_{AA} + Y_{pp} + \sigma_Y^{pp+} \\
\sigma_D^{pp-} &= D_{AA} - D_{AA} + \sigma_Y^{pp+} \\
\sigma_D^{pp-} &= \sigma_Y^{pp+}
\end{aligned}$$

Thus,

$$\sigma_D^{pp\pm} = \sigma_Y^{pp\mp} \tag{4.12}$$

Here, we can see that the propagation of the baseline's uncertainty through to the D_{AA} amounts to a simple addition in quadrature.

4.7 Summary of Systematic Uncertainties

The following plots display the individual contributions of each systematic uncertainty on each measurement. The nominal values and their statistical uncertainties are in black, and the systematic uncertainty on display will be represented by red boxes. In general, systematic uncertainty arising from ξ, ZYAM, and the π^0 reconstruct process are the primary contributor (though their dominance is p_T dependent), especially in per trigger yields and I_{AA}.

4.7.1 Jet Functions

The systematic uncertainties on the jet functions arising from multiple sources are shown in Figs 4.8 to 4.17. One can see that overall, the systematic uncertainties are rather small, with the exception for the lowest hadron p_T bin. Here, the use of ZYAM leads to larger systematic uncertainties over Absolute Background Subtraction (even in plots for the systematics due to the v_n values) for two reasons. Firstly, with increasing trigger momentum comes increasing statistical uncertainty, which the ZYAM level is particularly sensitive to. Secondly, because the ZYAM level is allowed to float when evaluating the systematics from the v_n terms, leading to under or over-subtraction and, thus, a larger deviation from the nominal.

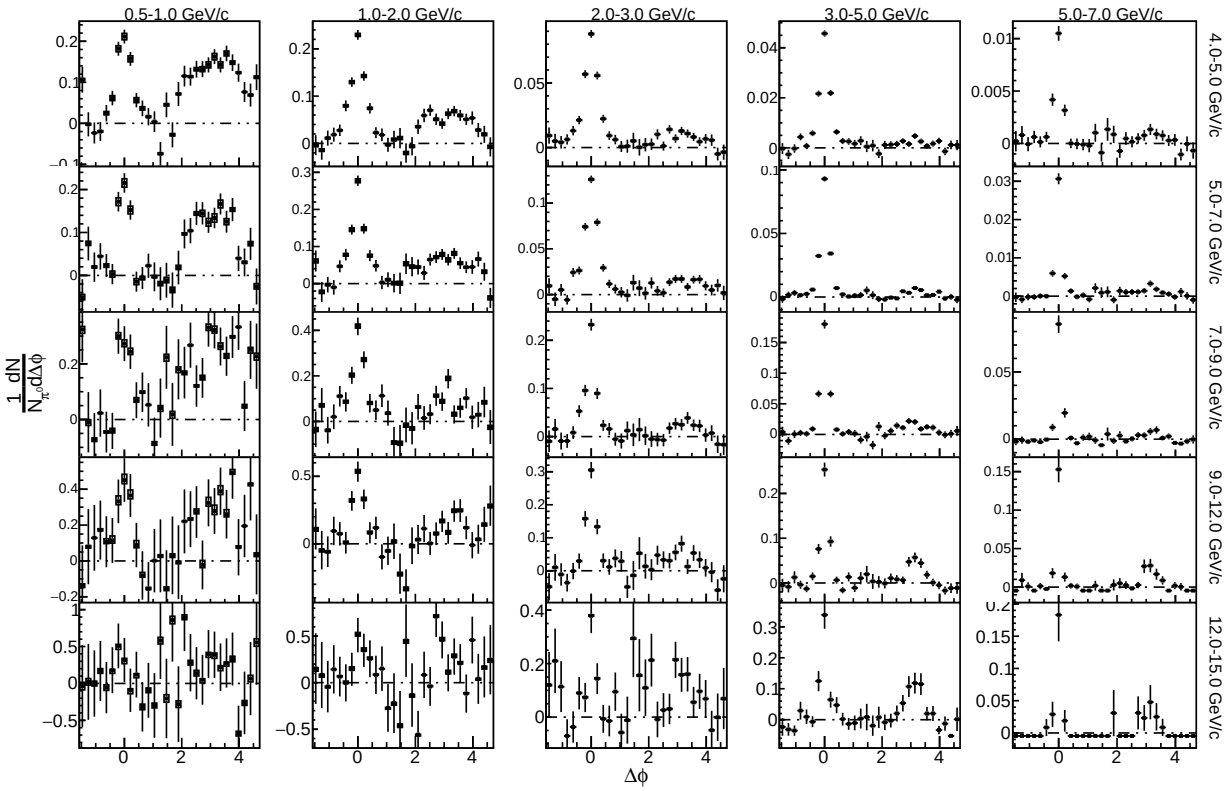

Figure 4.8: Jet functions in 0–20% centrality class with systematic uncertainties from only the second order flow harmonic drawn as boxes.

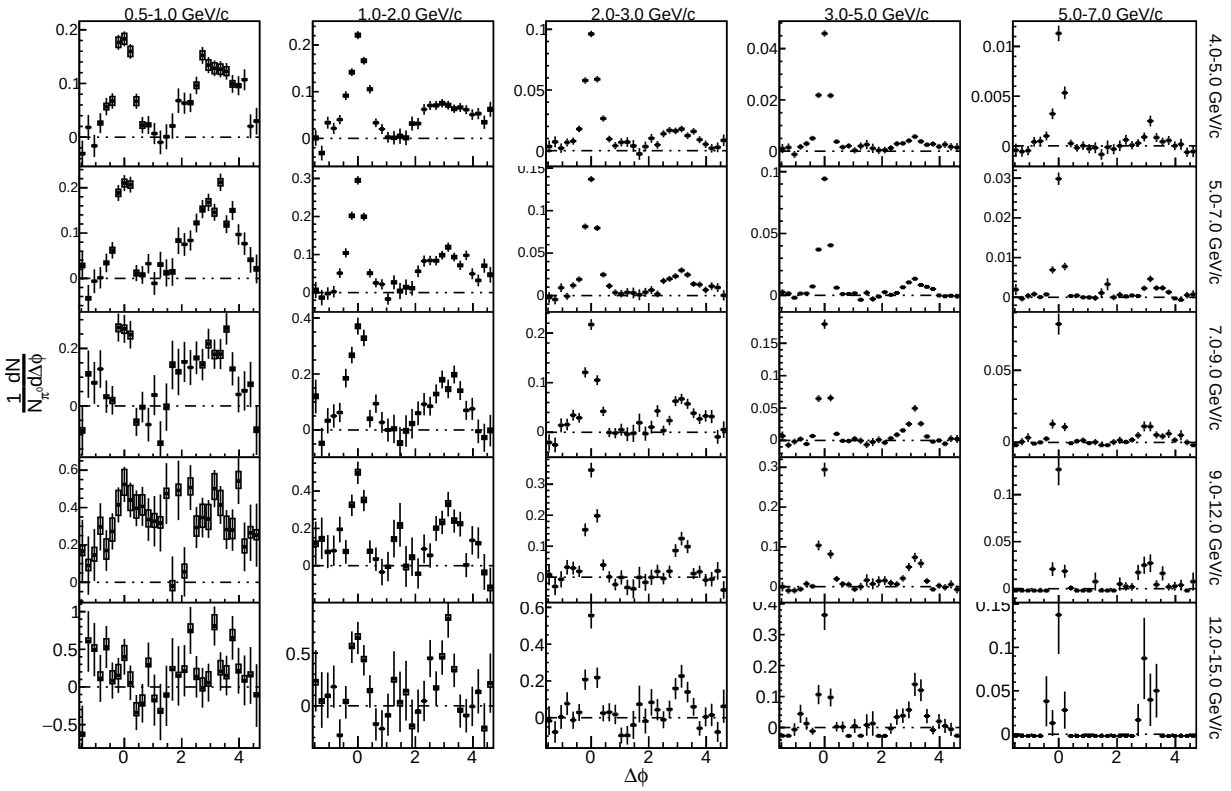

Figure 4.9: Jet functions in 02–40% centrality class with systematic uncertainties from only the second order flow harmonic drawn as boxes.

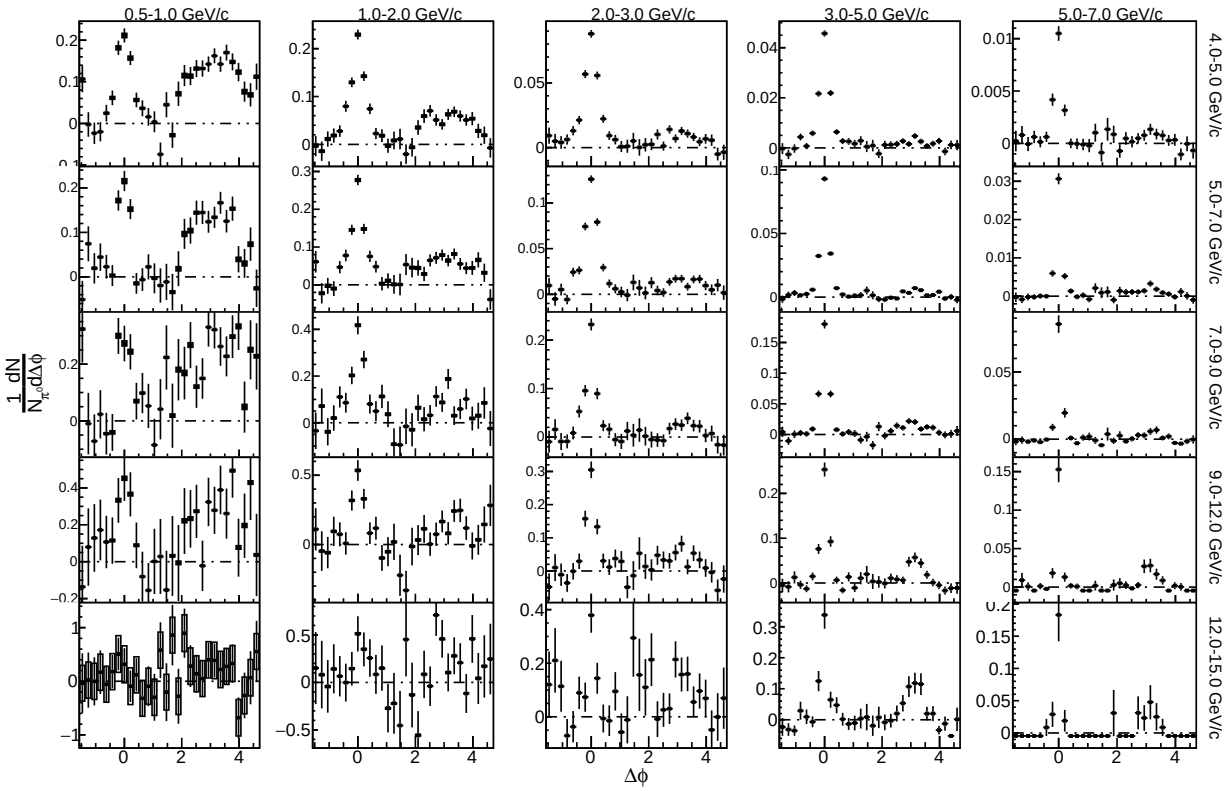

Figure 4.10: Jet functions in 0–20% centrality class with systematic uncertainties from only the third order flow harmonic drawn as boxes.

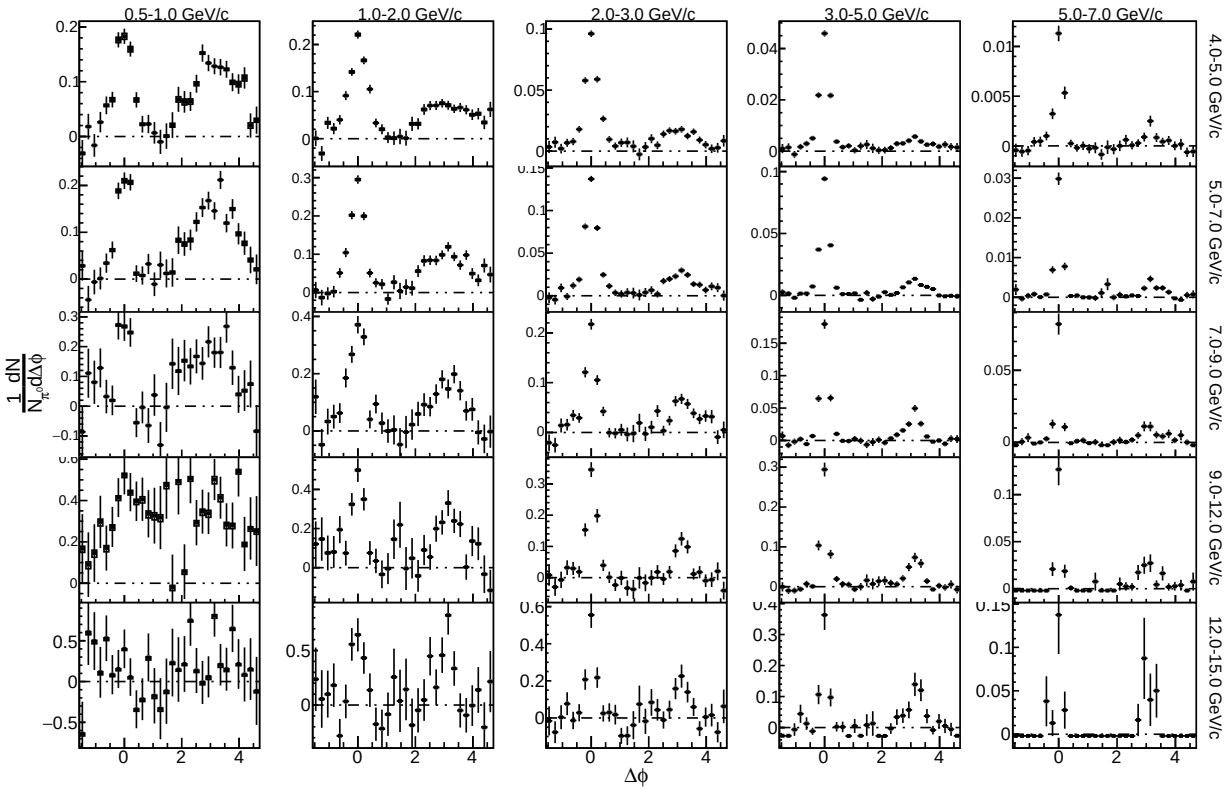

Figure 4.11: Jet functions in 20–40% centrality class with systematic uncertainties from only the third order flow harmonic drawn as boxes.

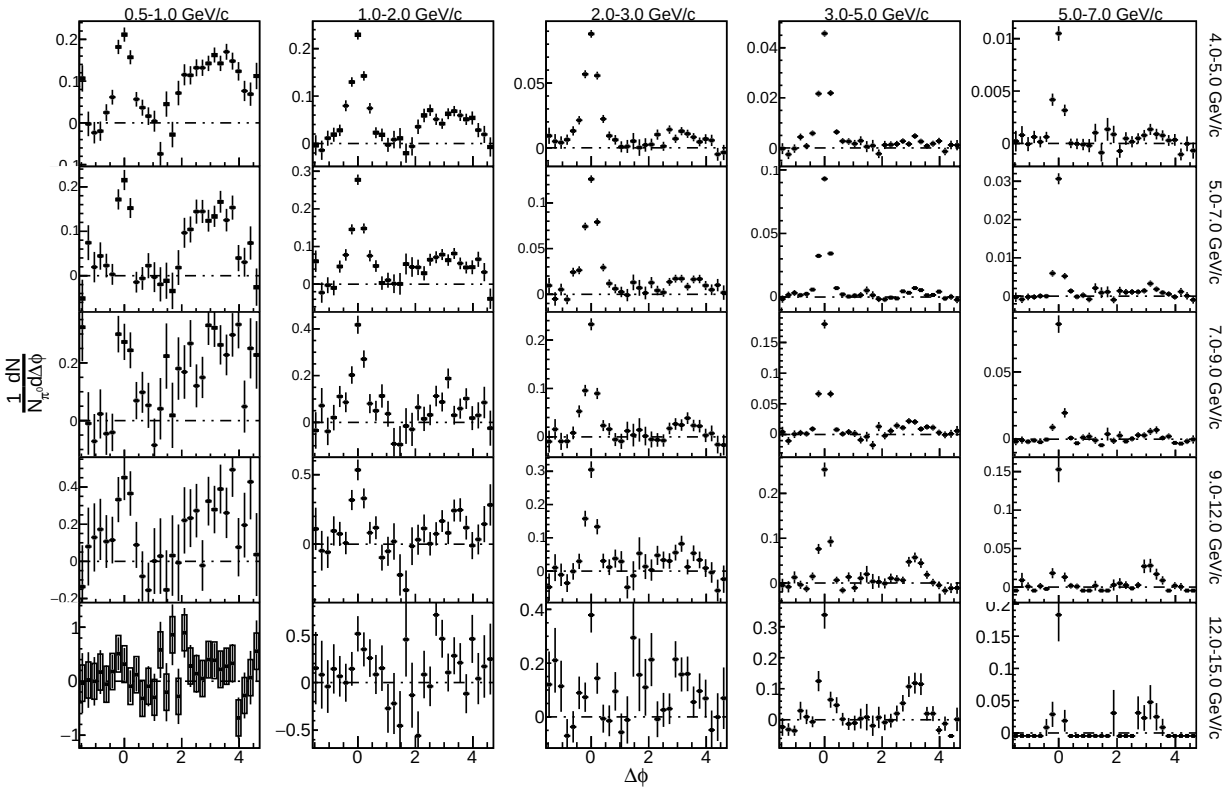

Figure 4.12: Jet functions in 0–20% centrality class with systematic uncertainties from only the fourth order flow harmonic drawn as boxes.

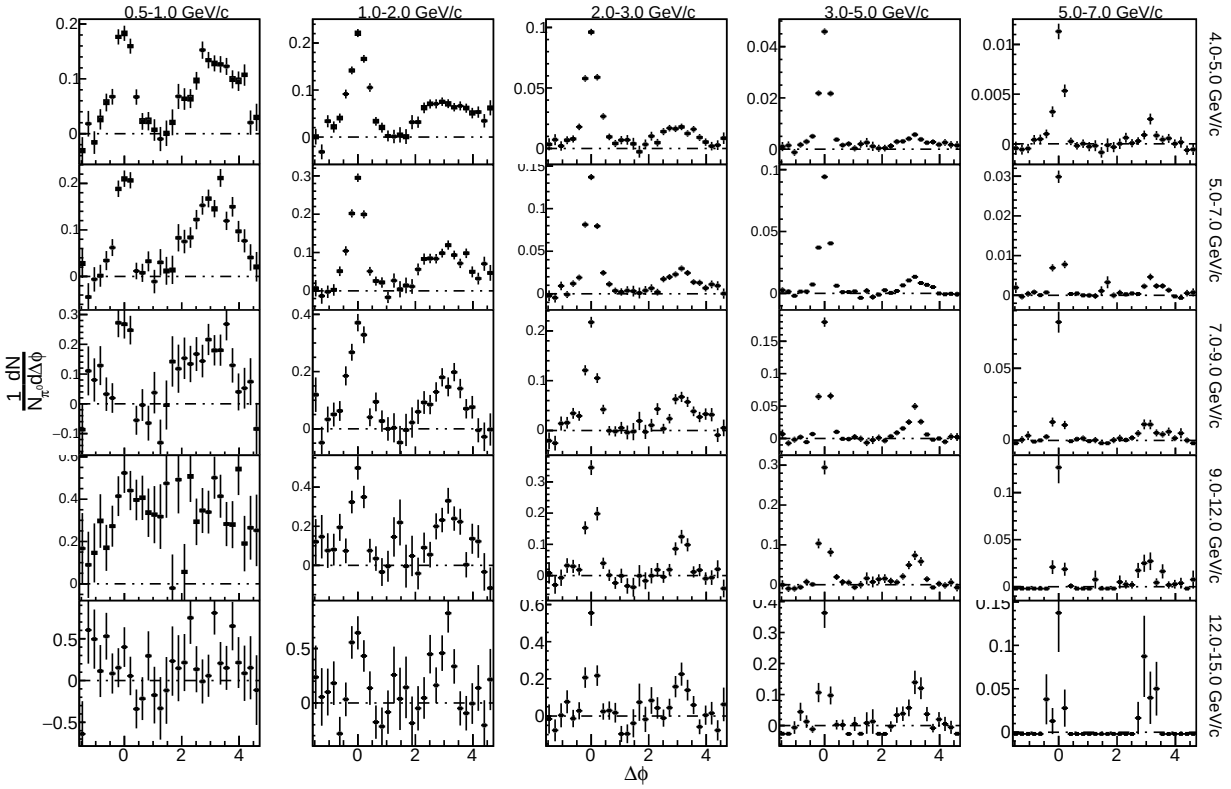

Figure 4.13: Jet functions in 20–40% centrality class with systematic uncertainties from only the fourth order flow harmonic drawn as boxes.

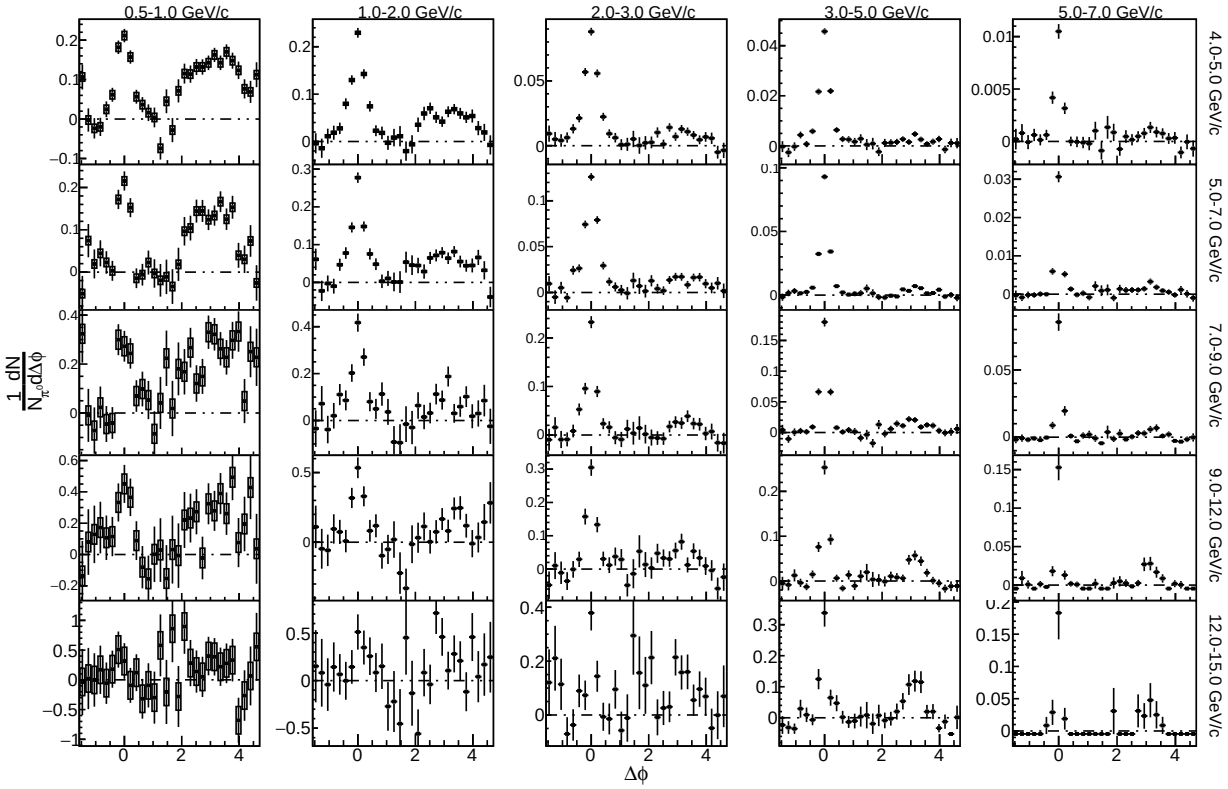

Figure 4.14: Jet functions in 0–20% centrality with systematic uncertainty from ZYAM for $p_T^{Hadron} < 1$ GeV/c and Absolute Background Subtraction for $p_T^{Hadron} > 1$ GeV/c drawn as boxes.

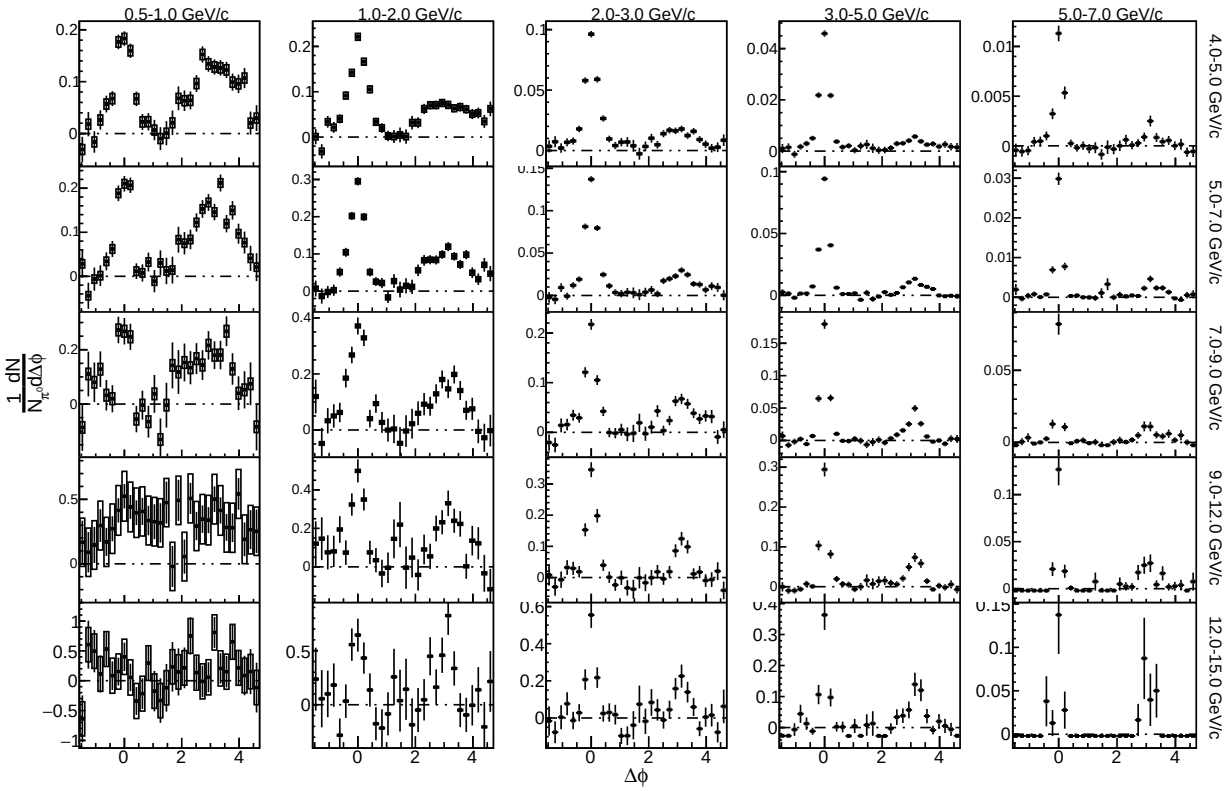

Figure 4.15: Jet functions in 20–40% centrality with systematic uncertainty from ZYAM for $p_T^{Hadron} < 1$ GeV/c and Absolute Background Subtraction for $p_T^{Hadron} > 1$ GeV/c drawn as boxes.

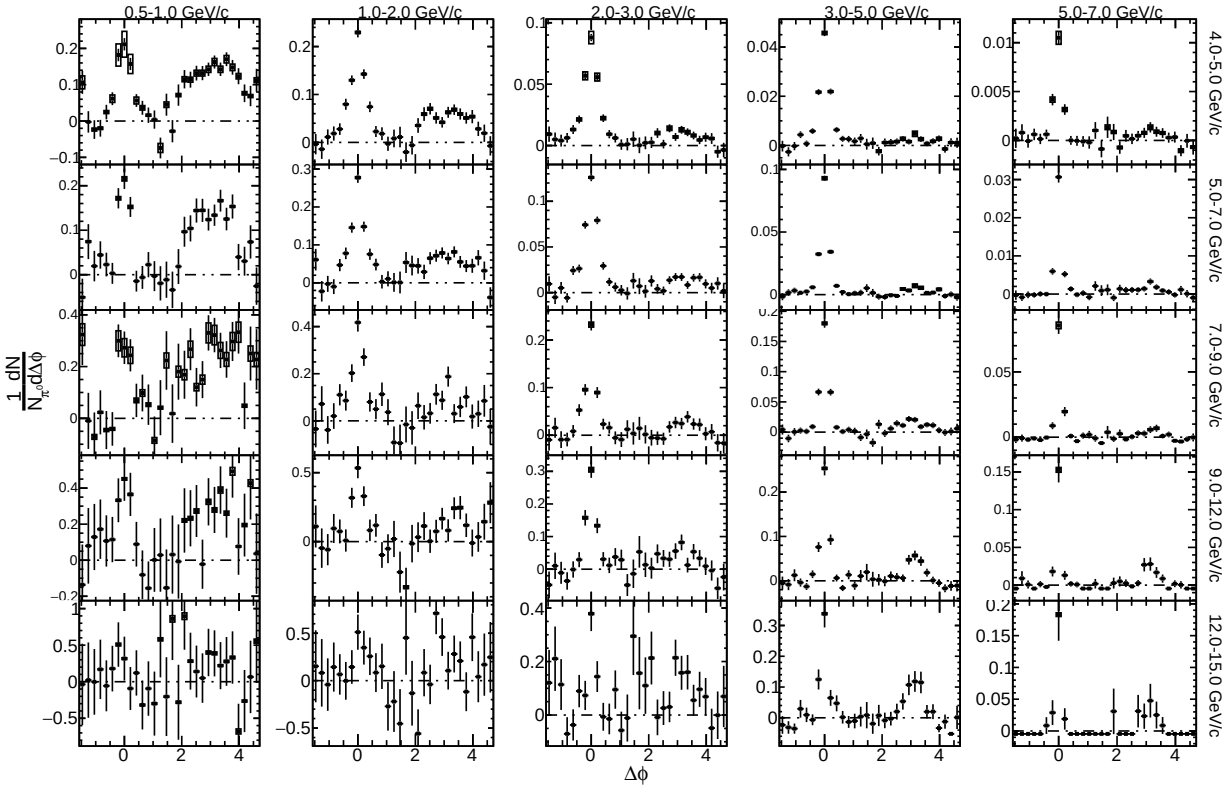

Figure 4.16: Jet functions in 0–20% centrality with systematic uncertainty from combinatorial π^0 reconstruction process drawn as box.

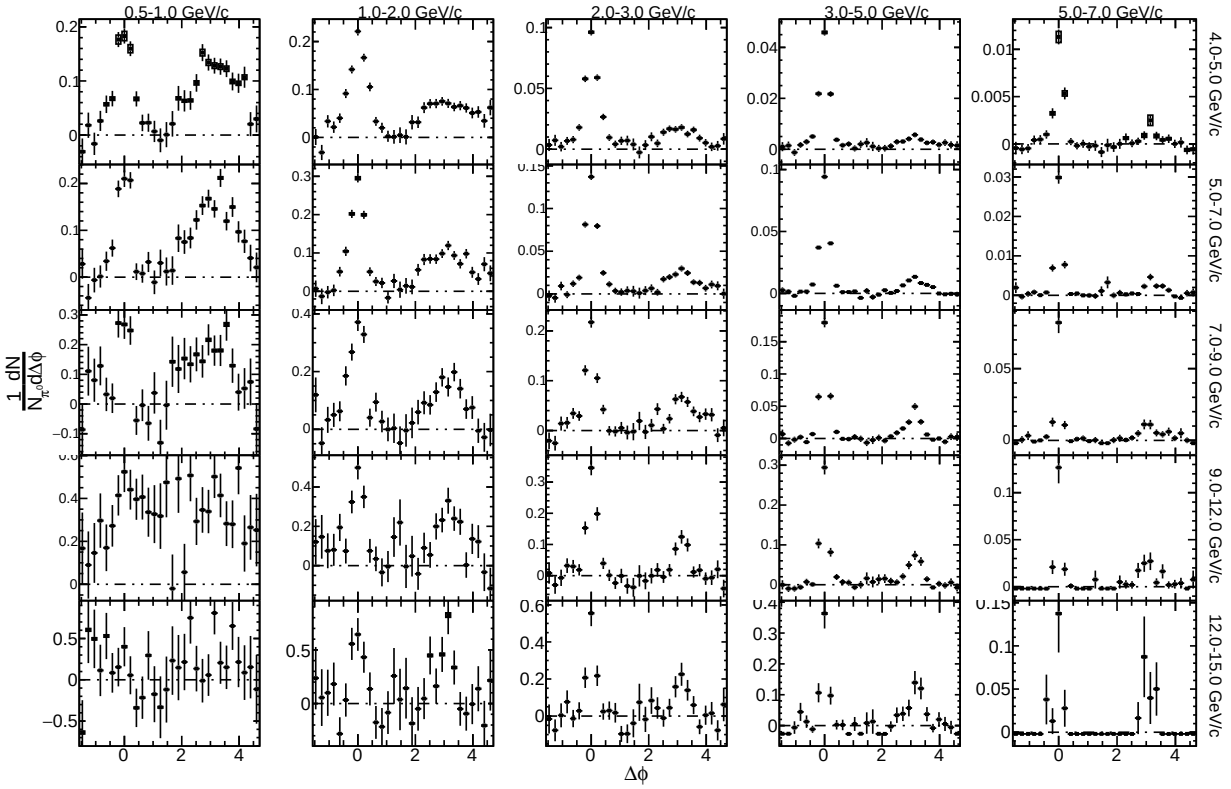

Figure 4.17: Jet functions in 20–40% centrality with systematic uncertainty from combinatorial π^0 reconstruction process drawn as box.

4.7.2 Yields

The systematics on the away-side yields are shown in Figs.4.18 and Figure 4.19. One can see behaviors similar to those of the systematics on the jet functions, and we display them here for the integrated yields to serve as a proxy for the systematics on the D_{AA} vs. $\Delta\phi$ later. It should be noted that the systematic on the even-order harmonics is zero, owing to their symmetry about the away-side peak, as described by Eqn.4.13:

$$\int_{\pi/2}^{3\pi/2} \cos(2n\cdot\phi)d\phi = \frac{1}{2n}\left[\sin(2n\cdot\frac{3\pi}{2}) - sin(2n\cdot\frac{\pi}{2})\right] = 0 \tag{4.13}$$

This only holds for bins where the background level is calculated via Absolute Background Subtraction, though, as the estimation of the underlying event magnitude is completely divorced from the v_n terms, whereas with ZYAM, this is no longer true. This is because the ZYAM level itself is allowed to change in between the upper, lower, and nominal v_n value. Hence, while contributions from directly changing the v_2 and v_4 values might cancel, the resultant ZYAM levels leave a residual systematic.

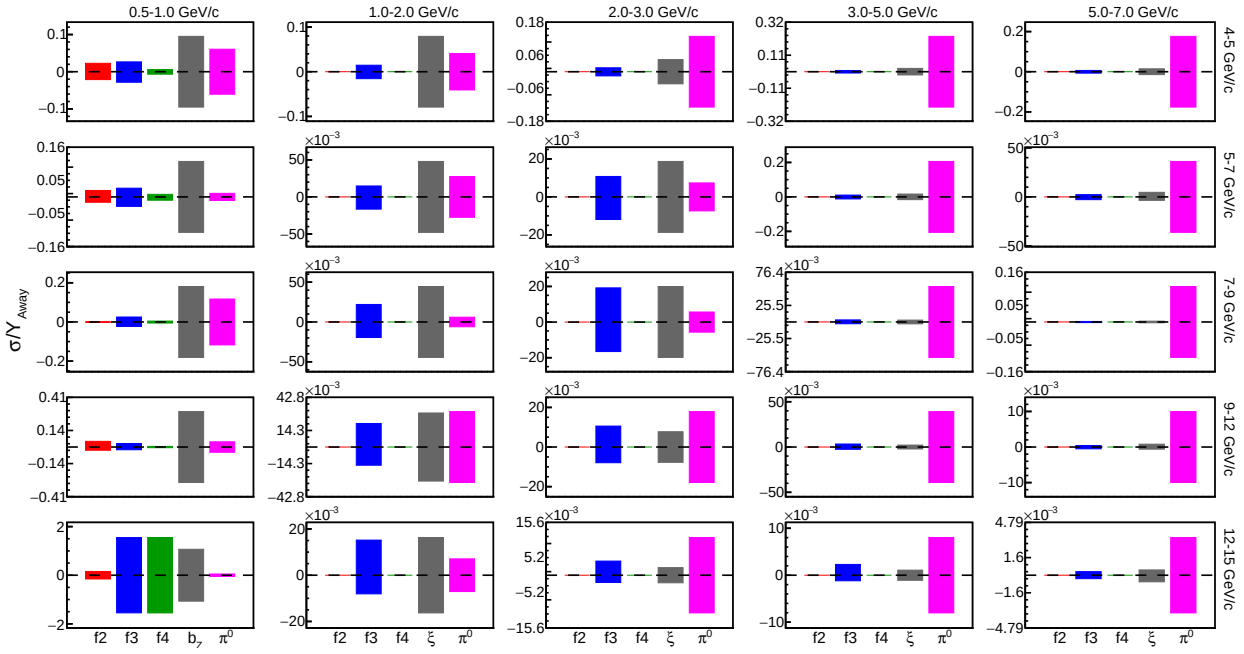

Figure 4.18: Relative uncertainties in away-side yield in 0–20% centrality.

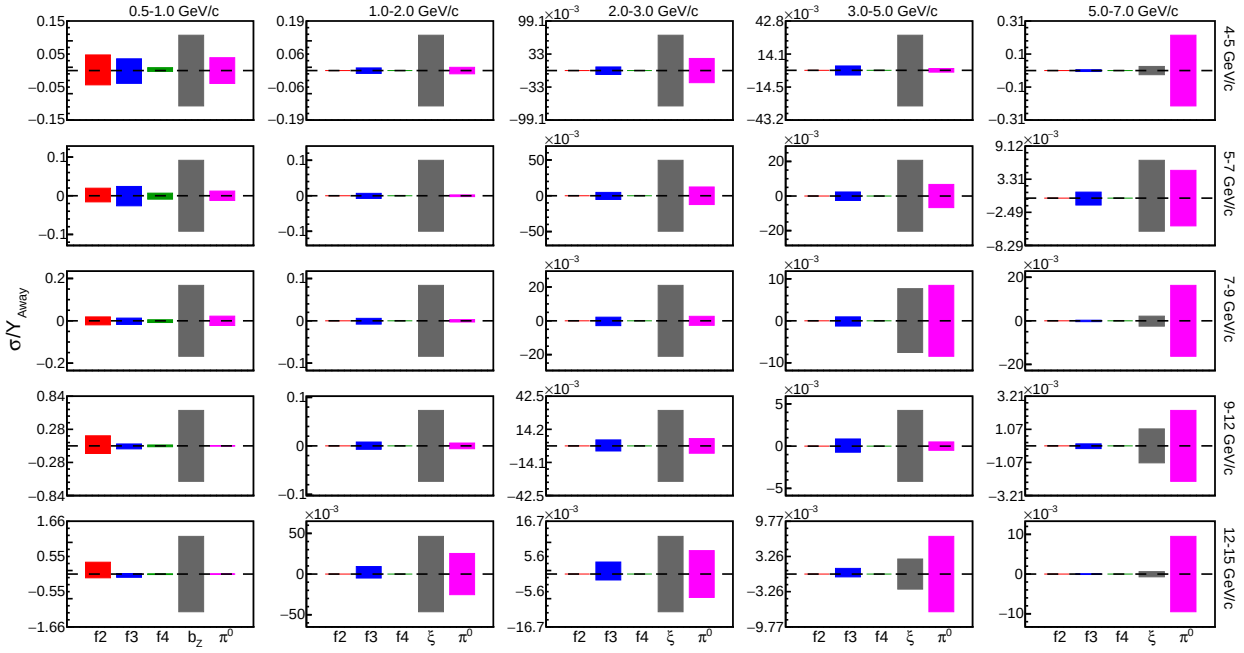

Figure 4.19: Relative uncertainties in away-side yield in 20–40% centrality.

4.7.3 $I_{AA}(p_T)$, I_{AA} *vs.* $\Delta\phi$, *and* D_{AA} *vs* $\Delta\phi$

Figs. 4.20 to Fig. 4.21 are the systematic uncertainty contributions to the $I_{AA}(p_T)$ from various sources. At low hadron p_T, uncertainties on the estimation of the background level via ZYAM dominate. This then switches to the systematic arising from calculating ξ for $p_T^{Hadron} > 1$ GeV/c. As per the previous sections, the even ordered flow harmonics do not contribute to the systematic uncertainties for $p_T^{Hadron} > 1$ GeV/c.

Finally, the systematic uncertainties on I_{AA} vs. $\Delta\phi$ from different sources are shown separately in Figs. 4.22 to 4.33 which show the individual magnitudes of the different systematic uncertainty sources on the I_{AA} versus $\Delta\phi$, and Figs. 4.34 to 4.45 are the same for the D_{AA} versus $\Delta\phi$. One can see that the primary advantage that D_{AA} has over I_{AA} when being shown against $\Delta\phi$ is that the D_{AA} is less affected by regions where the $p+p$ yields are

close to zero, which cause the statistical and systematic uncertainties to increase rapidly as one moves further away from the away-side jet peak.

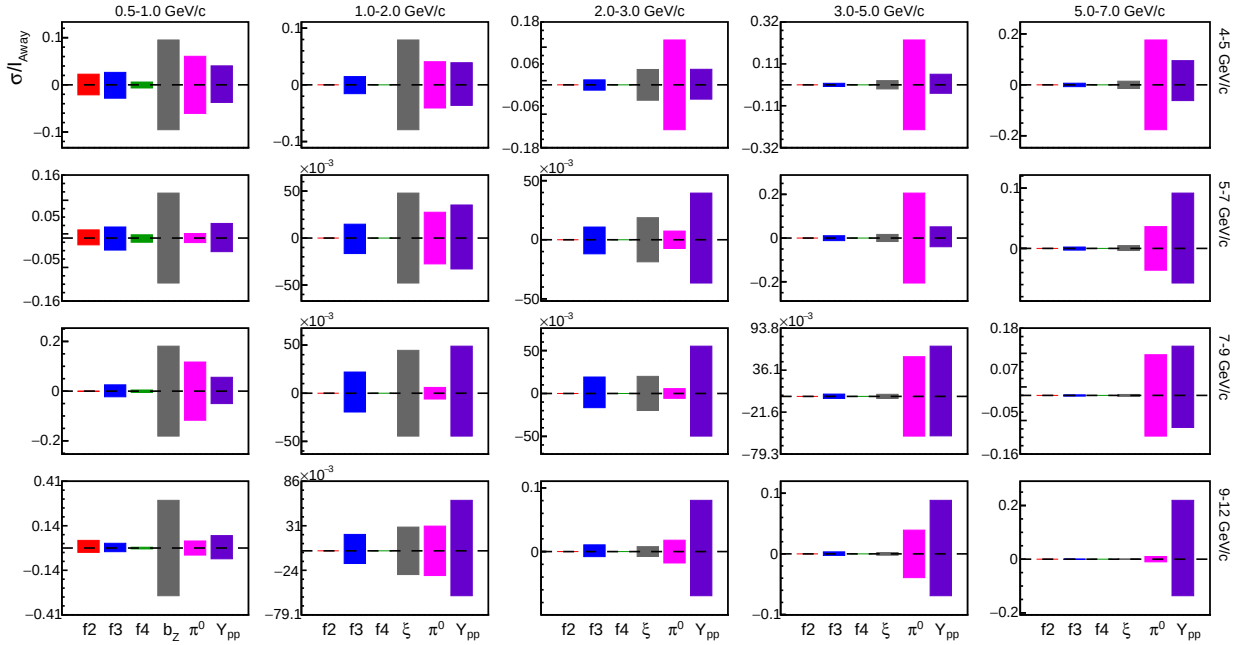

Figure 4.20: Relative uncertainties from various sources on the away-side I_{AA} in the 0–20% centrality class.

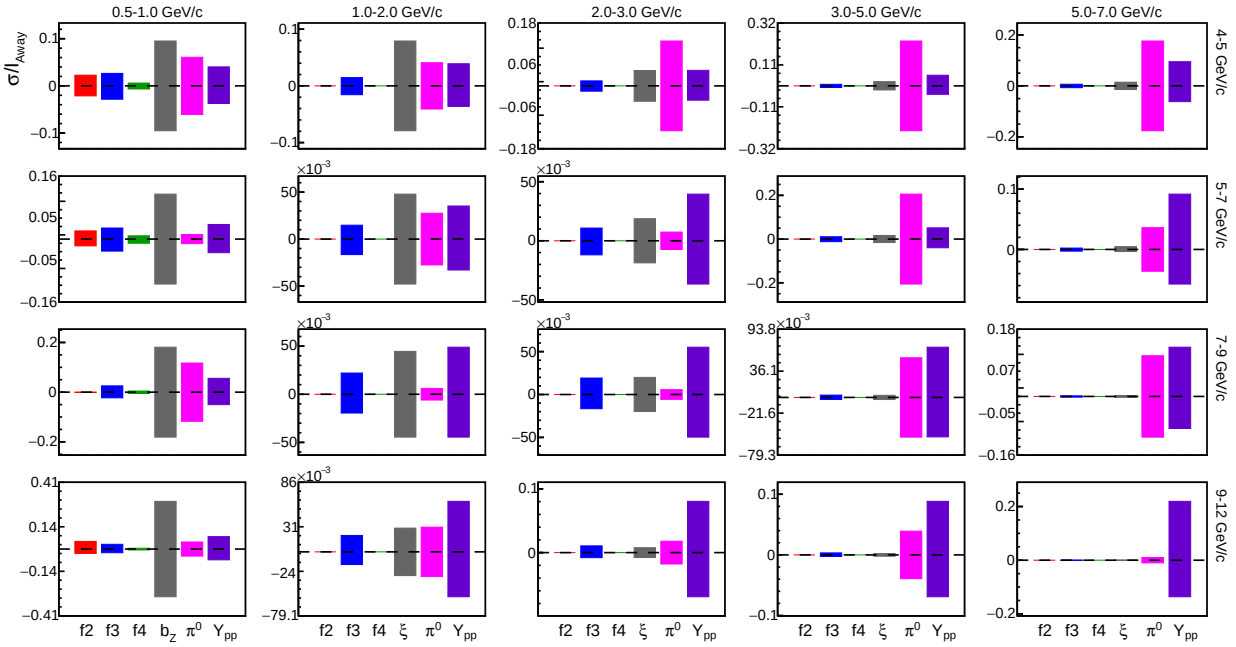

Figure 4.21: Relative uncertainties from various sources on the away-side I_{AA} in 20–40% centrality class.

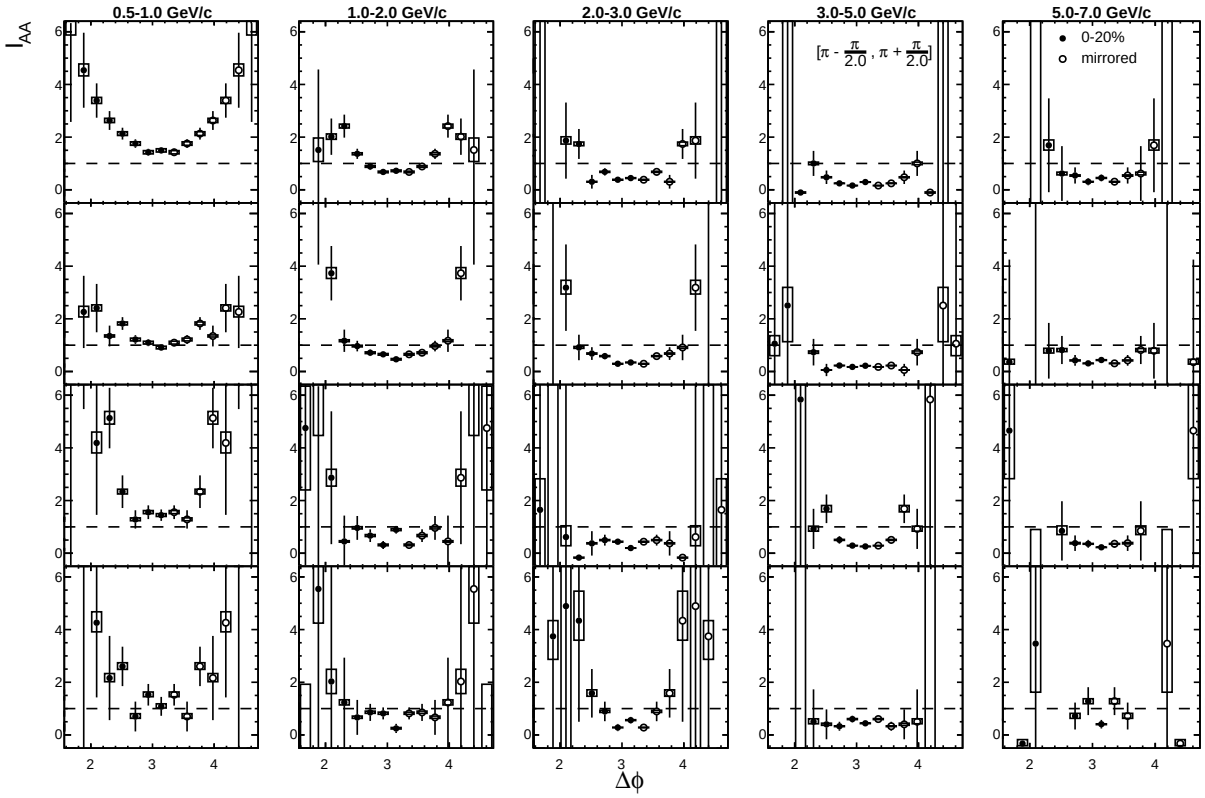

Figure 4.22: Away-side I_{AA} vs. $\Delta\phi$ in the 0–20% centrality class with only the systematic uncertainty arising from, σ^{f2}, the second order flow harmonics drawn.

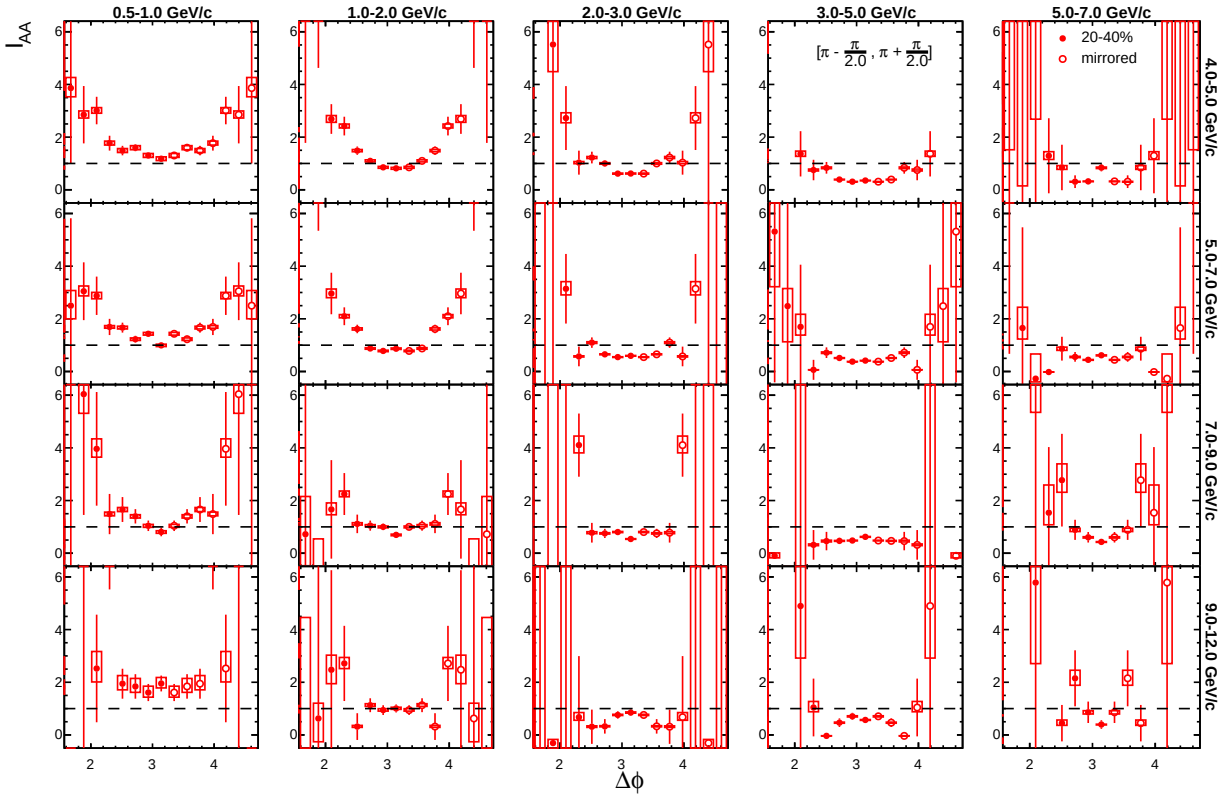

Figure 4.23: Away-side I_{AA} vs. $\Delta\phi$ in the 20–40% centrality class with only the systematic uncertainty arising from, σ^{f2}, the second order flow harmonics drawn.

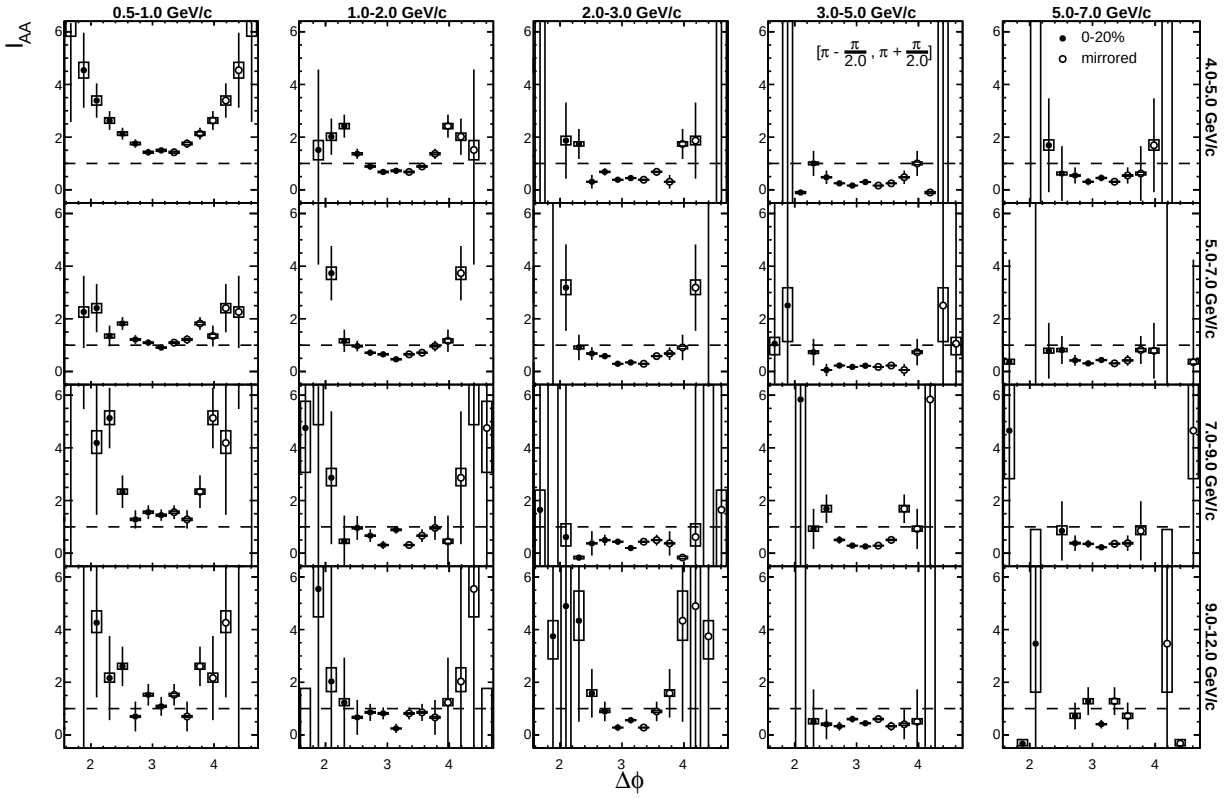

Figure 4.24: Away-side I_{AA} vs. $\Delta\phi$ in the 0–20% centrality class with only the systematic uncertainty arising from, σ^{f3}, the third order flow harmonics drawn.

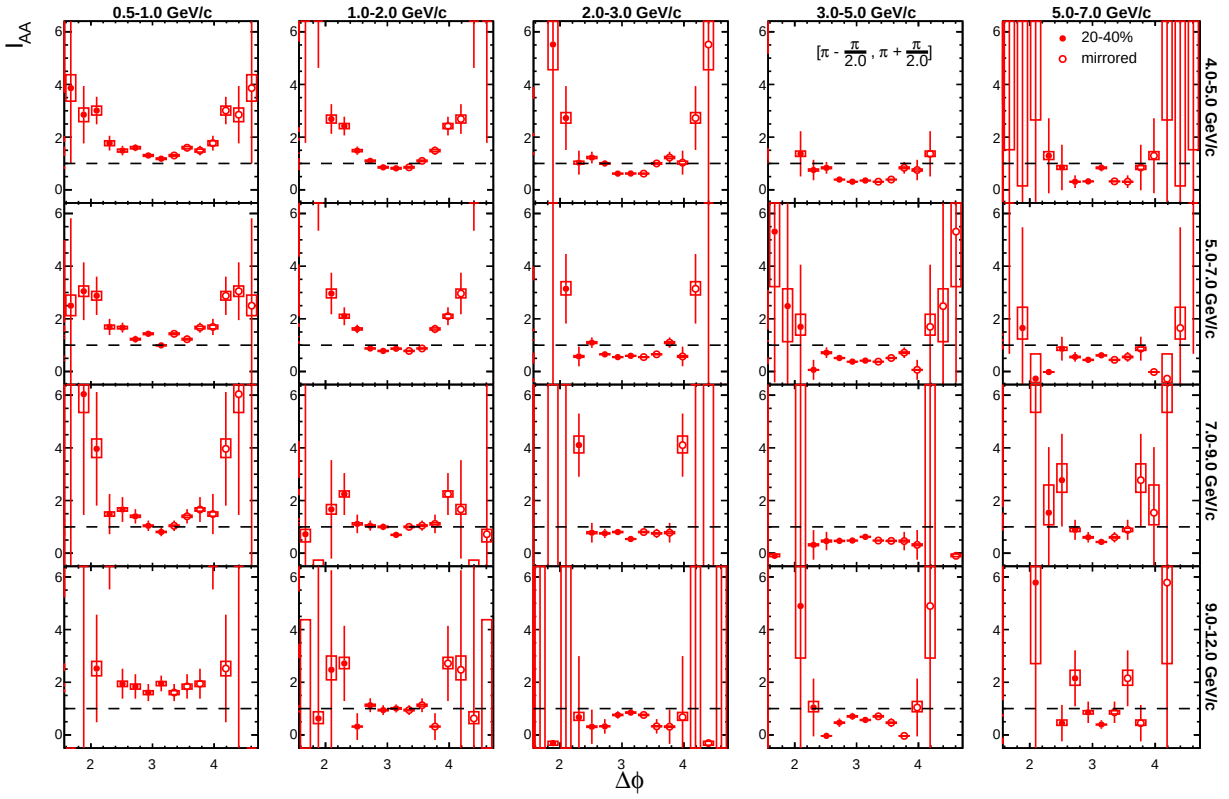

Figure 4.25: Away-side I_{AA} vs. $\Delta\phi$ in the 20–40% centrality class with only the systematic uncertainty arising from, σ^{f3}, the third order flow harmonics drawn.

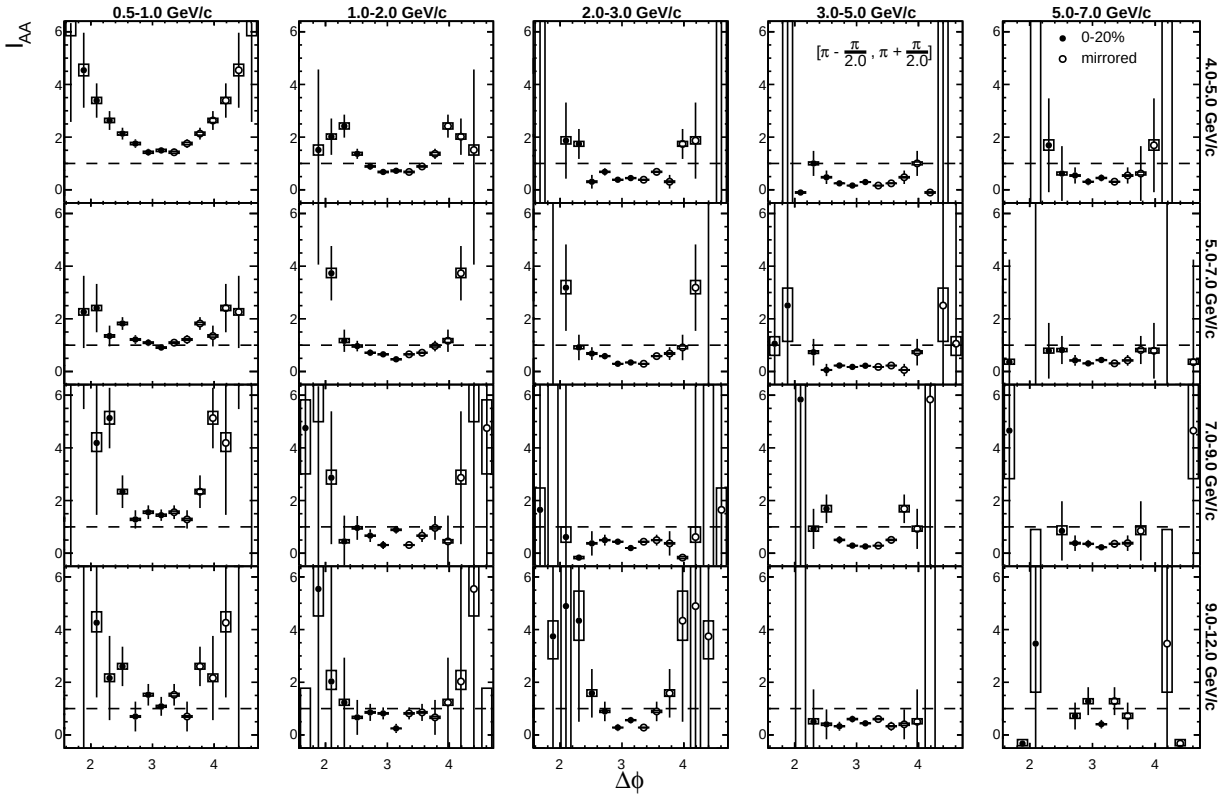

Figure 4.26: Away-side I_{AA} vs. $\Delta\phi$ in the 0–20% centrality class with only the systematic uncertainty arising from, σ^{f4}, the fourth order flow harmonics drawn.

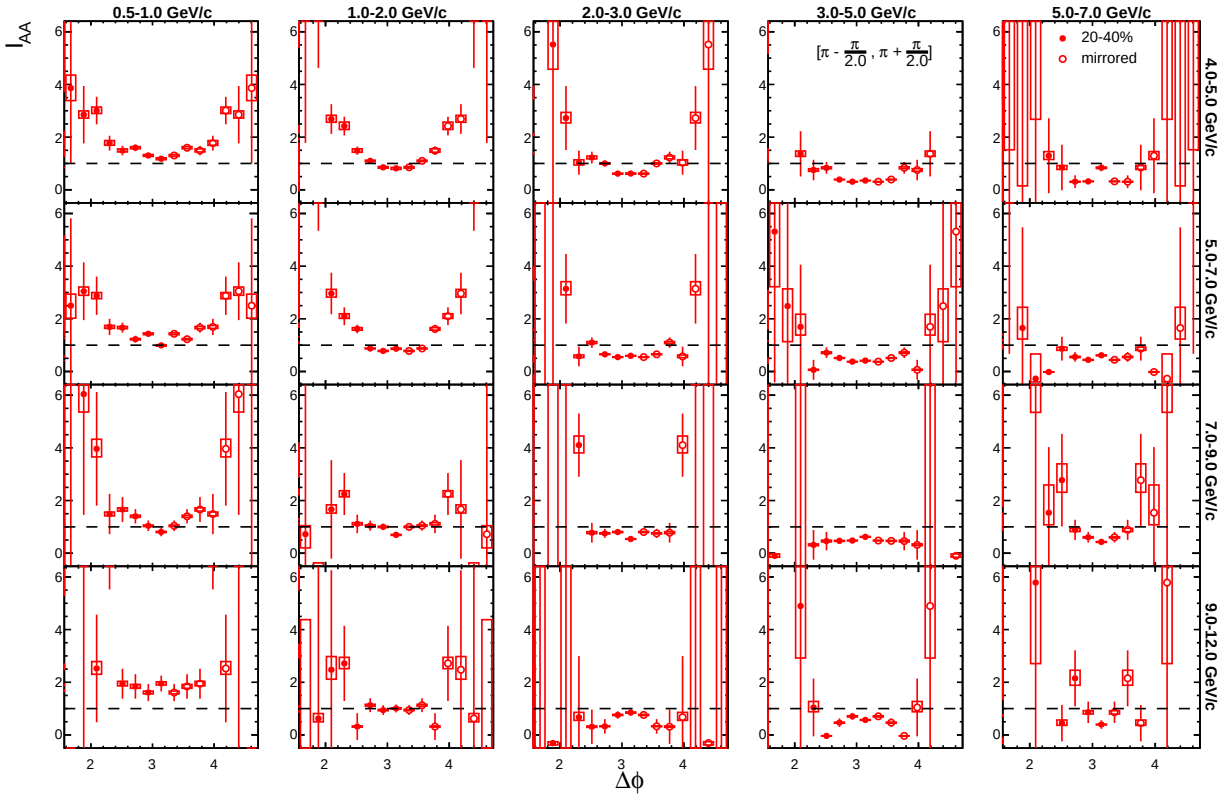

Figure 4.27: Away-side I_{AA} vs. $\Delta\phi$ in the 20–40% centrality class with only the systematic uncertainty arising from, σ^{f4}, the fourth order flow harmonics drawn.

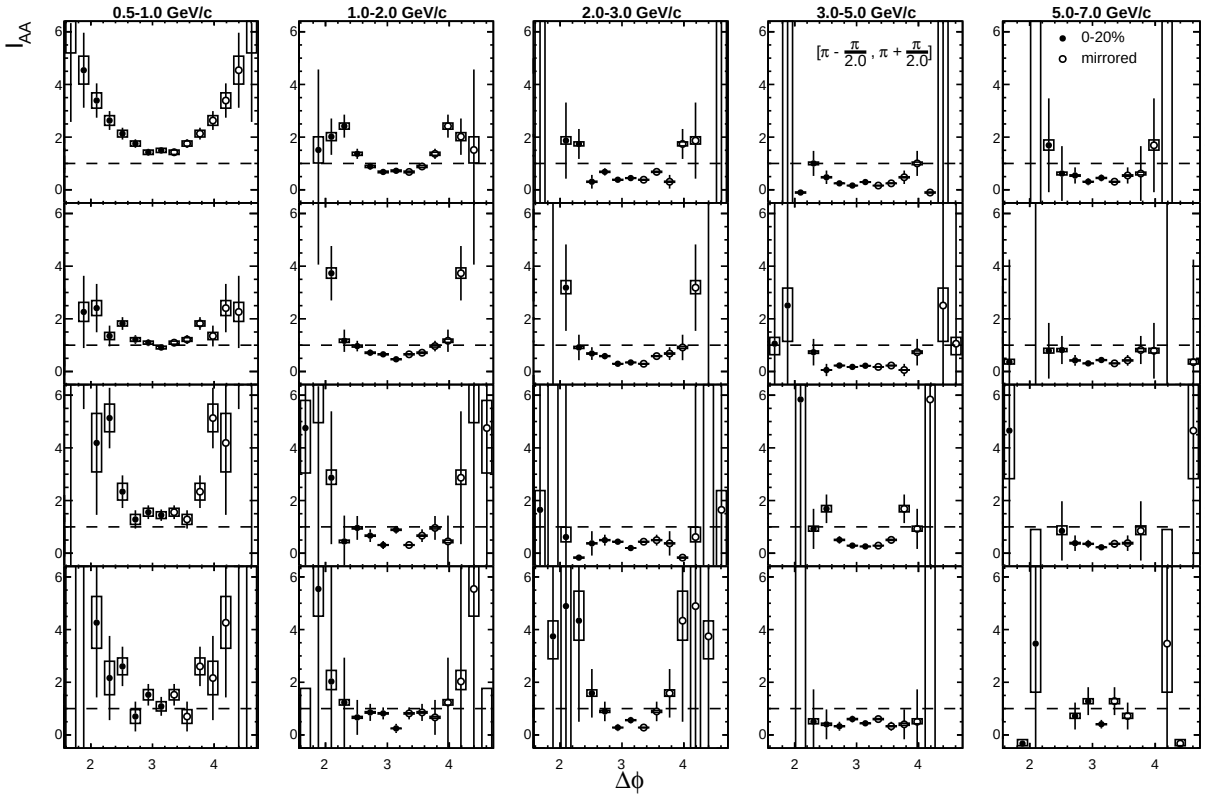

Figure 4.28: Away-side I_{AA} vs. $\Delta\phi$ in the 0–20% centrality class with only the systematic uncertainty arising from underlying event subtraction drawn.

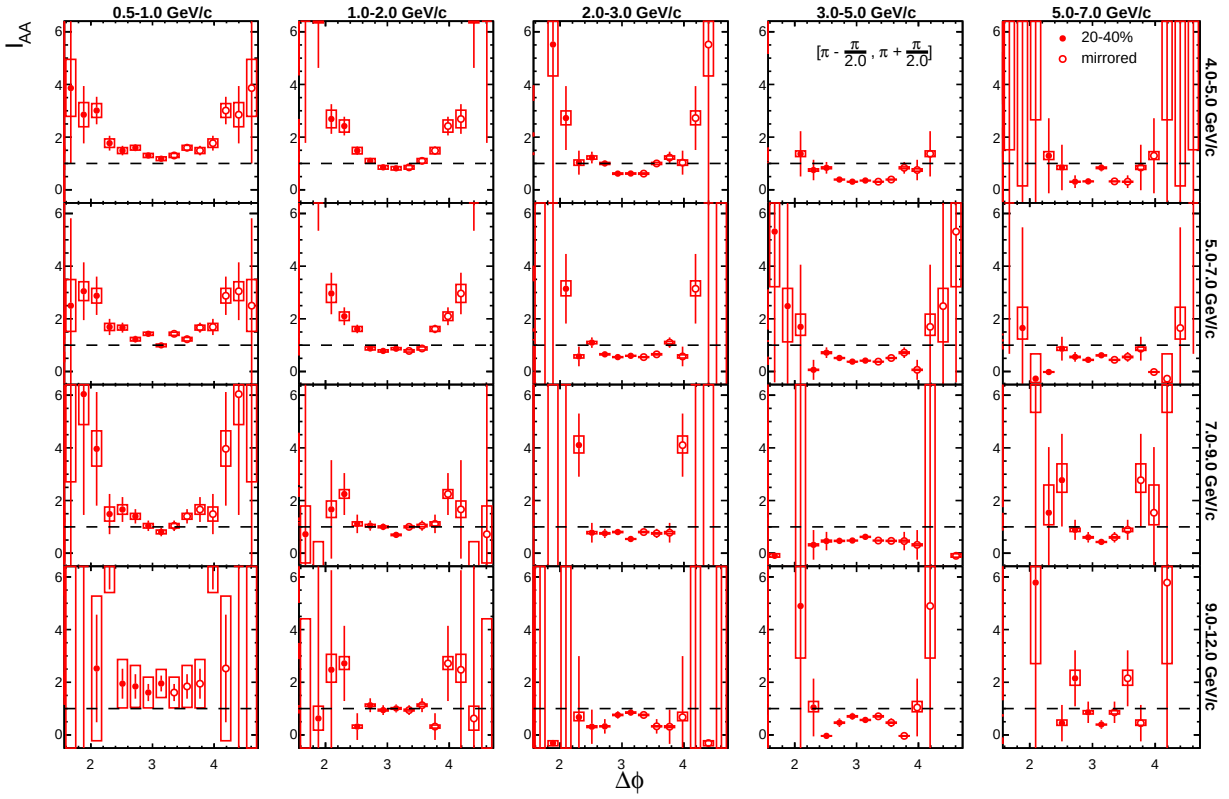

Figure 4.29: Away-side I_{AA} vs. $\Delta\phi$ in the 20–40% centrality class with only the systematic uncertainty arising from the underlying event subtraction drawn.

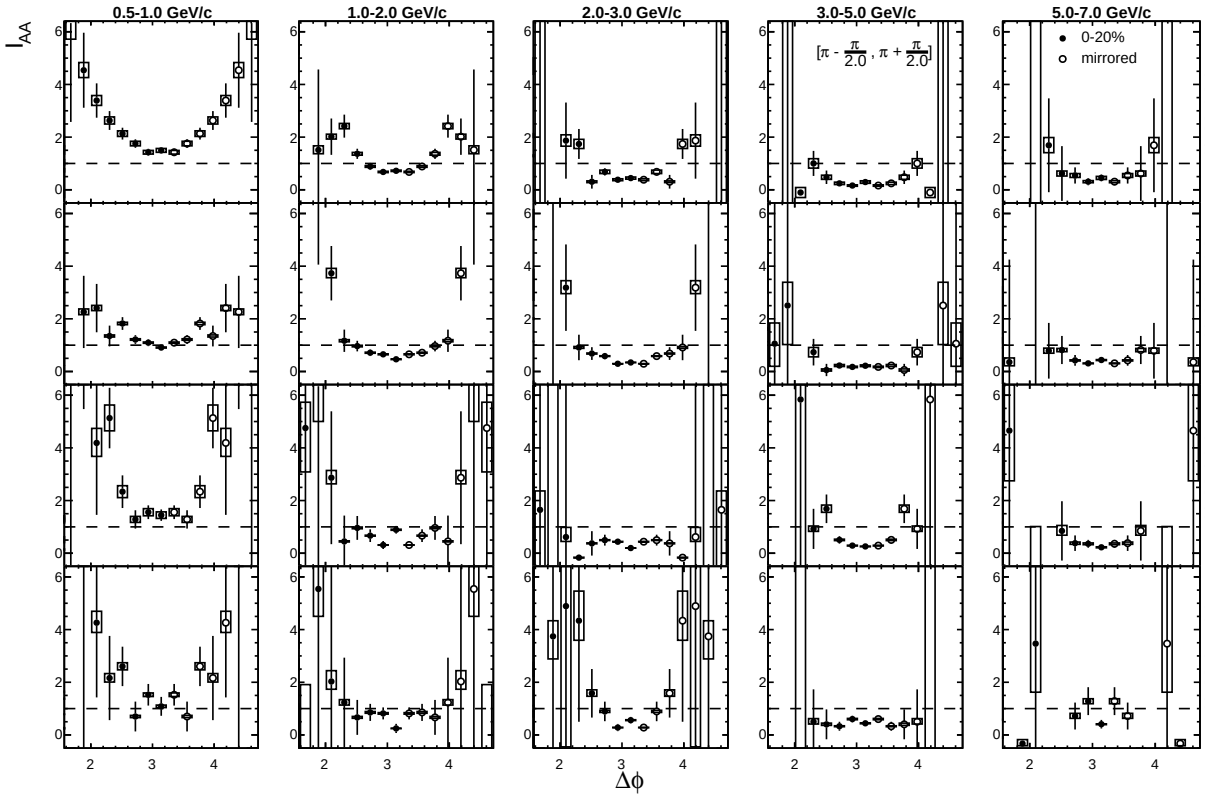

Figure 4.30: Away-side I_{AA} vs. $\Delta\phi$ in the 0–20% centrality class with only the systematic uncertainty arising from the π^0 reconstruction process drawn.

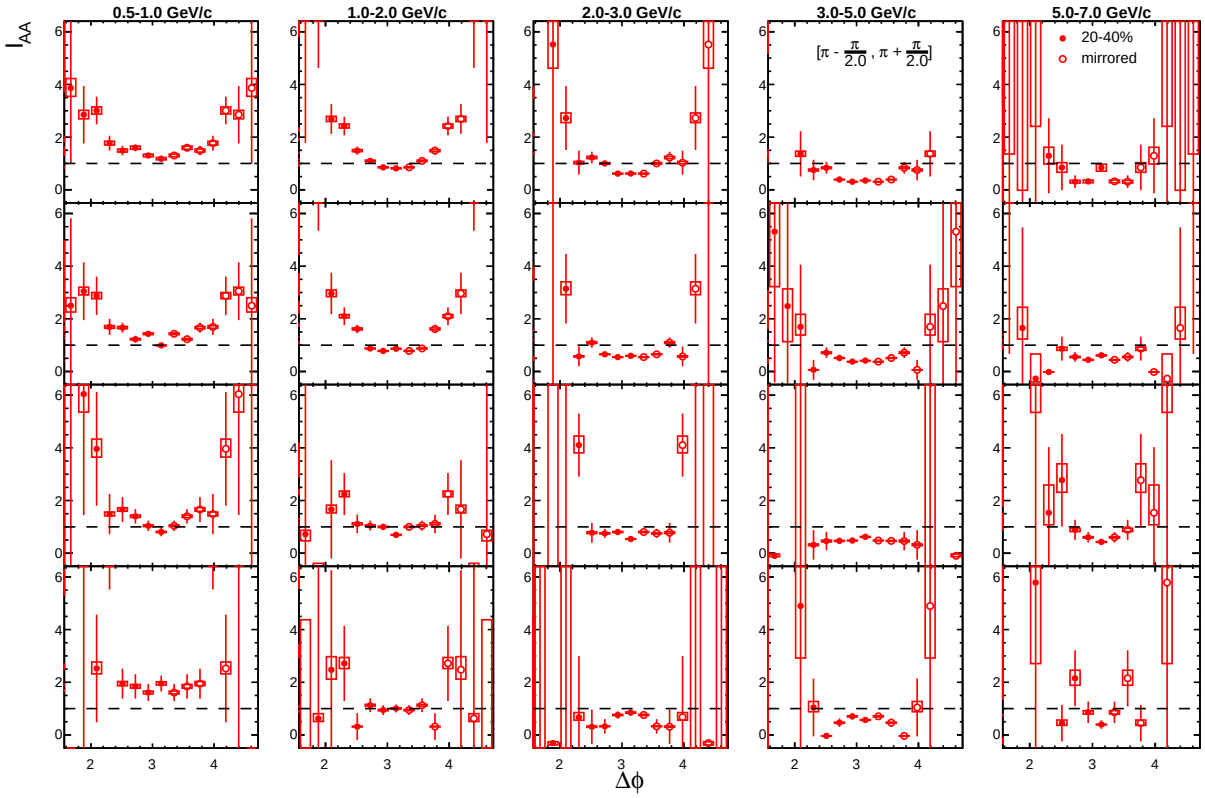

Figure 4.31: Away-side I_{AA} vs. $\Delta\phi$ in the 20–40% centrality class with only the systematic uncertainty arising from the π^0 reconstruction process drawn.

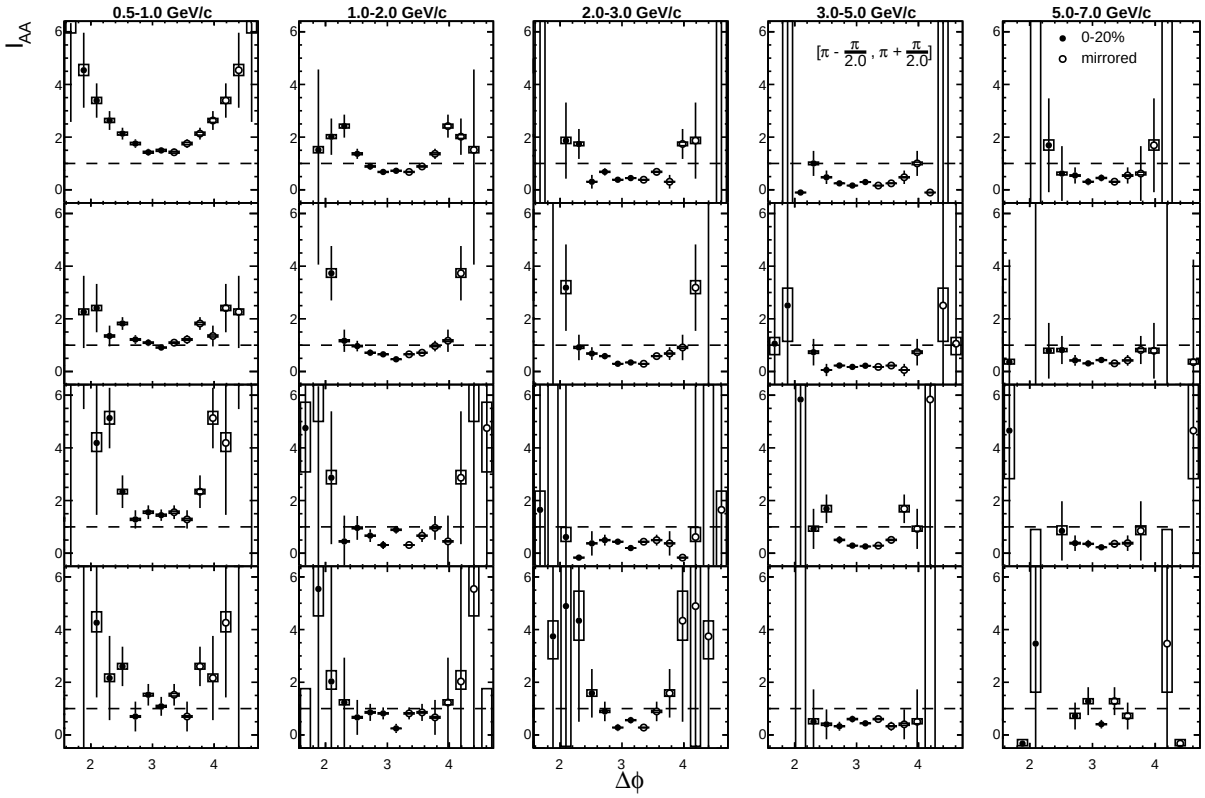

Figure 4.32: Away-side I_{AA} vs. $\Delta\phi$ in the 0–20% centrality class with only the systematic uncertainty arising from the $p+p$ baseline drawn.

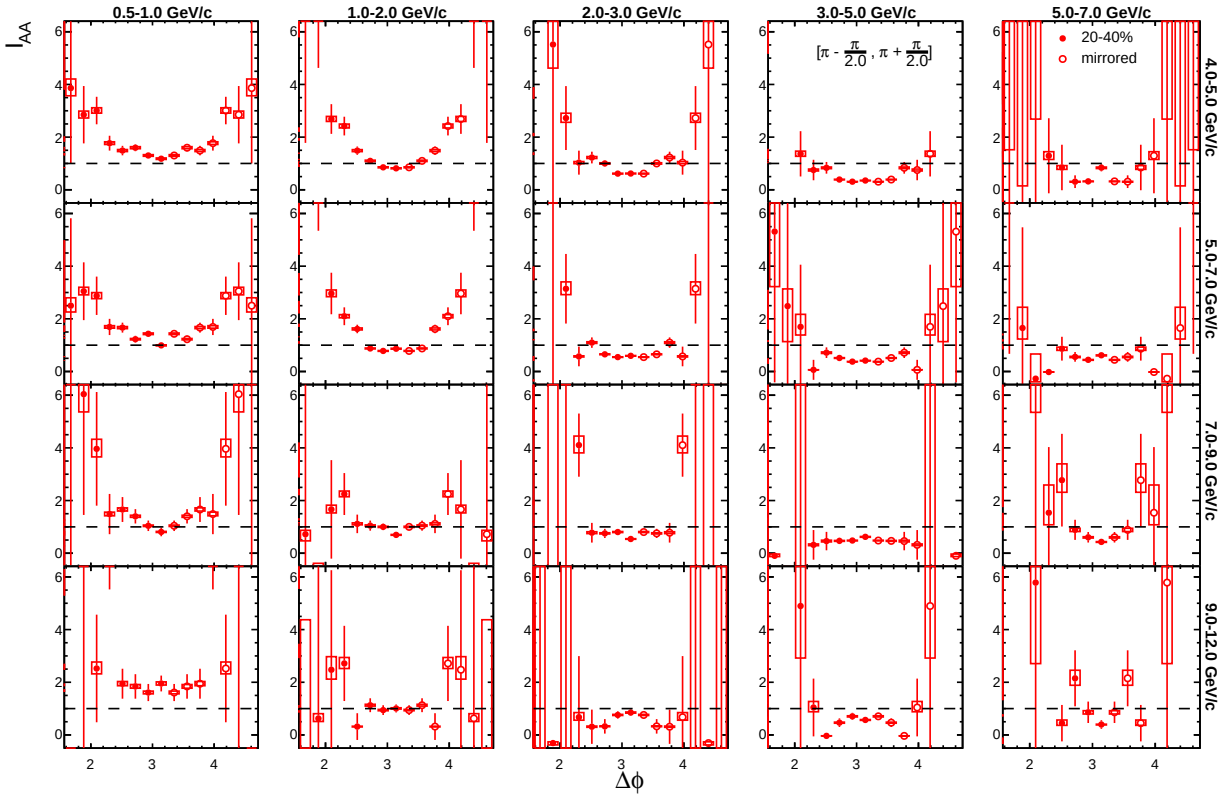

Figure 4.33: Away-side I_{AA} vs. $\Delta\phi$ in the 20–40% centrality class with only the systematic uncertainty arising from the $p+p$ baseline drawn.

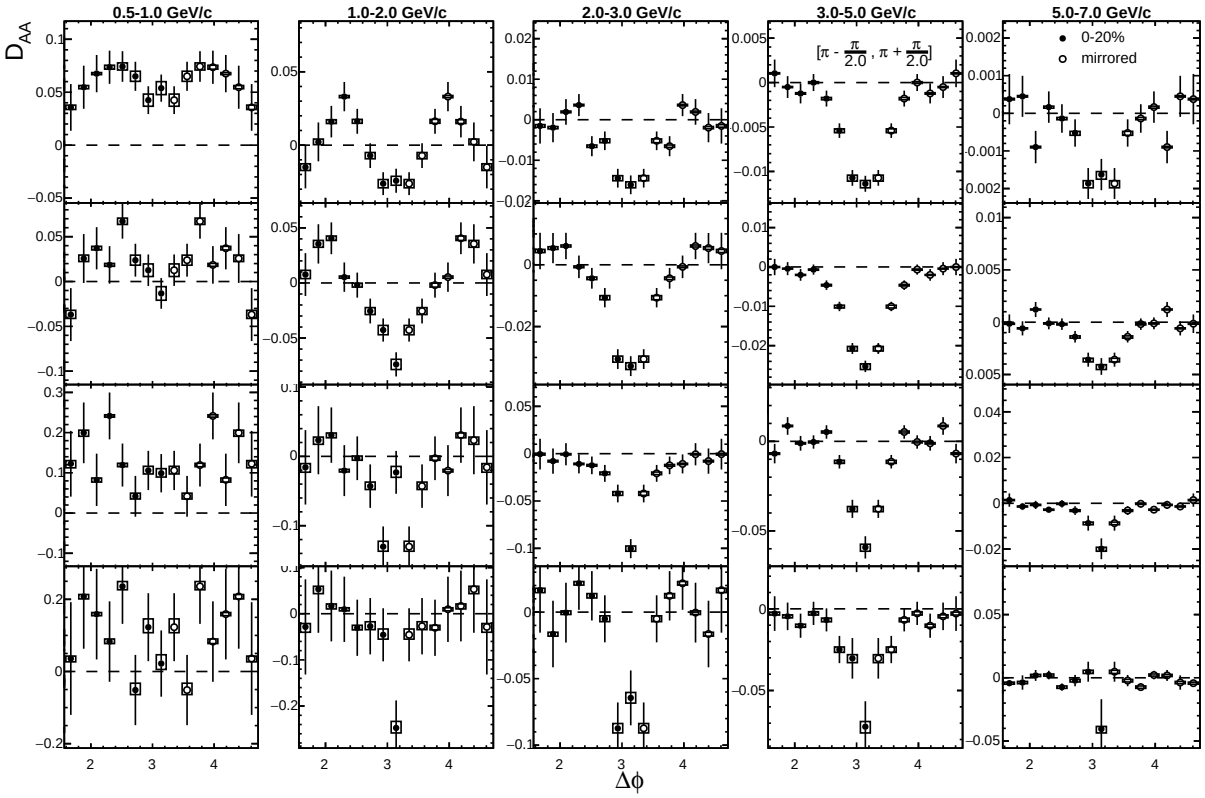

Figure 4.34: Away-side D_{AA} vs. $\Delta\phi$ in the 0–20% centrality class with only the systematic uncertainty arising from, σ^{f2}, the second order flow harmonics drawn.

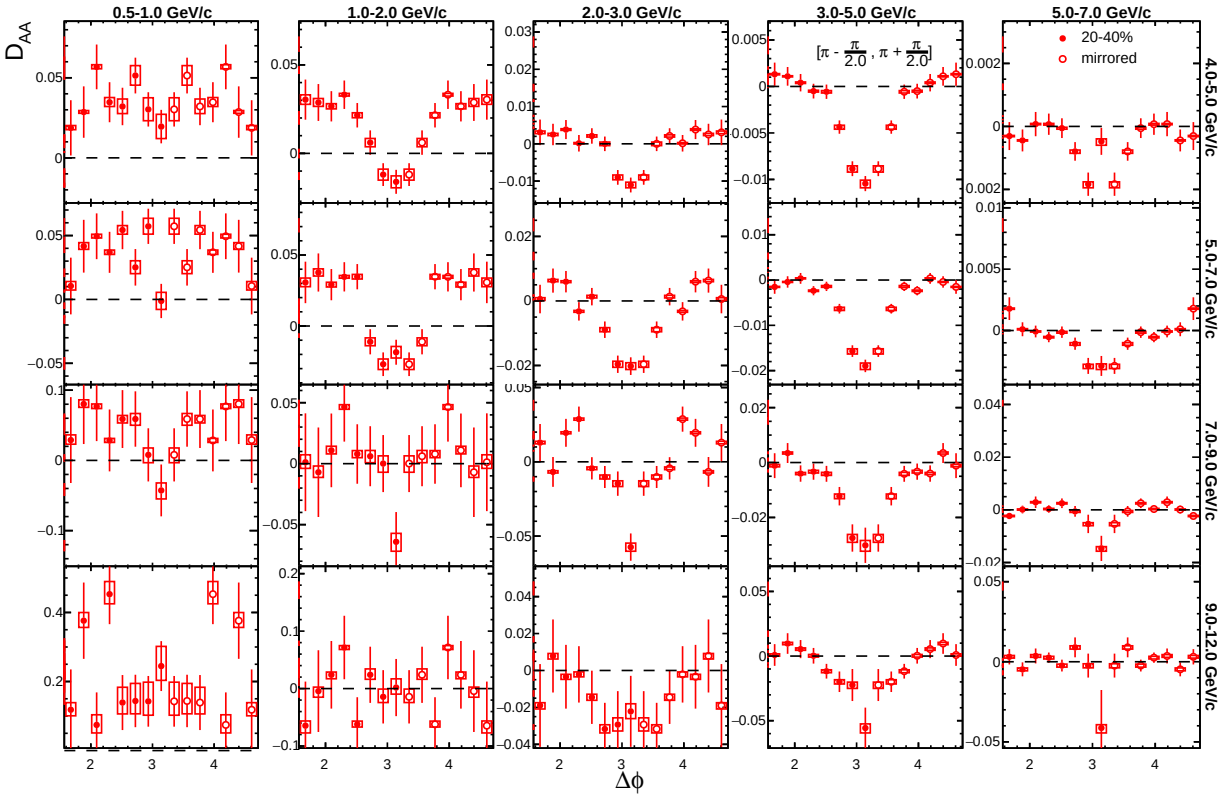

Figure 4.35: Away-side D_{AA} vs. $\Delta\phi$ in the 20–40% centrality class with only the systematic uncertainty arising from, σ^{f2}, the second order flow harmonics drawn.

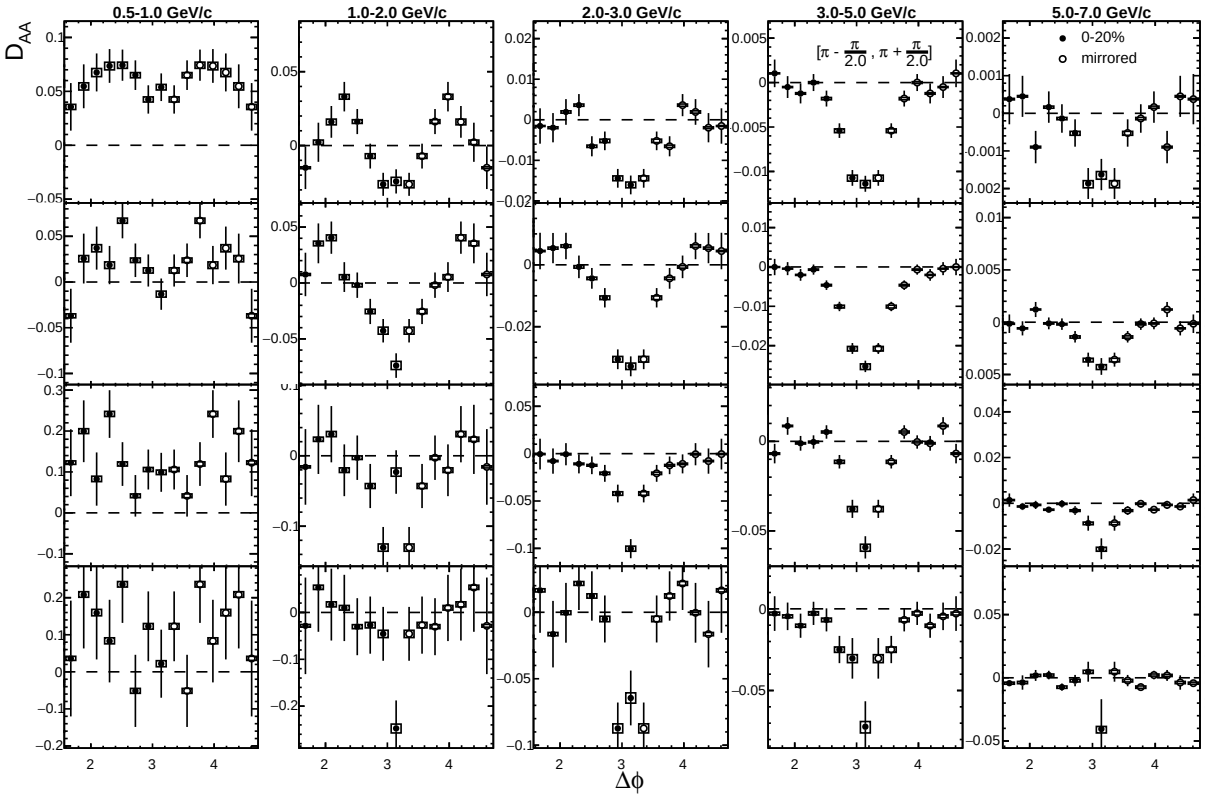

Figure 4.36: Away-side D_{AA} vs. $\Delta\phi$ in the 0–20% centrality class with only the systematic uncertainty arising from, σ^{f3}, the third order flow harmonics drawn.

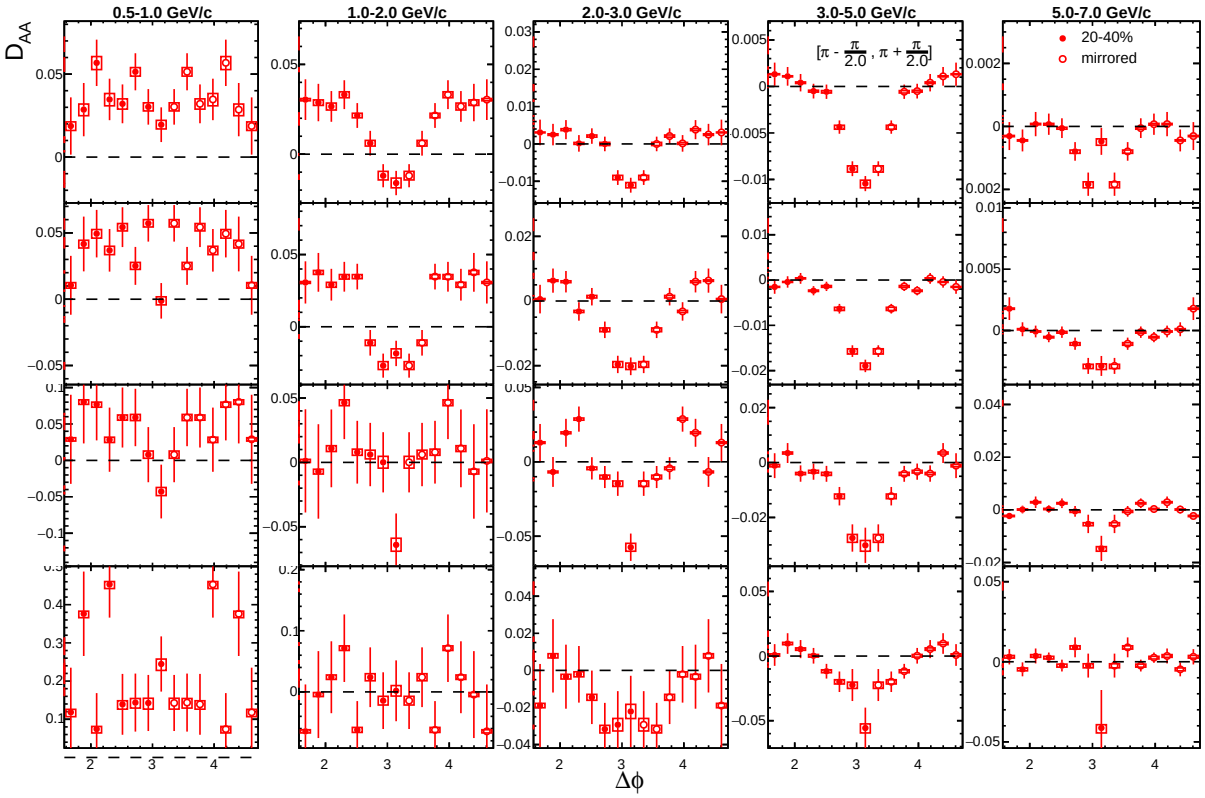

Figure 4.37: Away-side D_{AA} vs. $\Delta\phi$ in the 20–40% centrality class with only the systematic uncertainty arising from, σ^{f3}, the third order flow harmonics drawn.

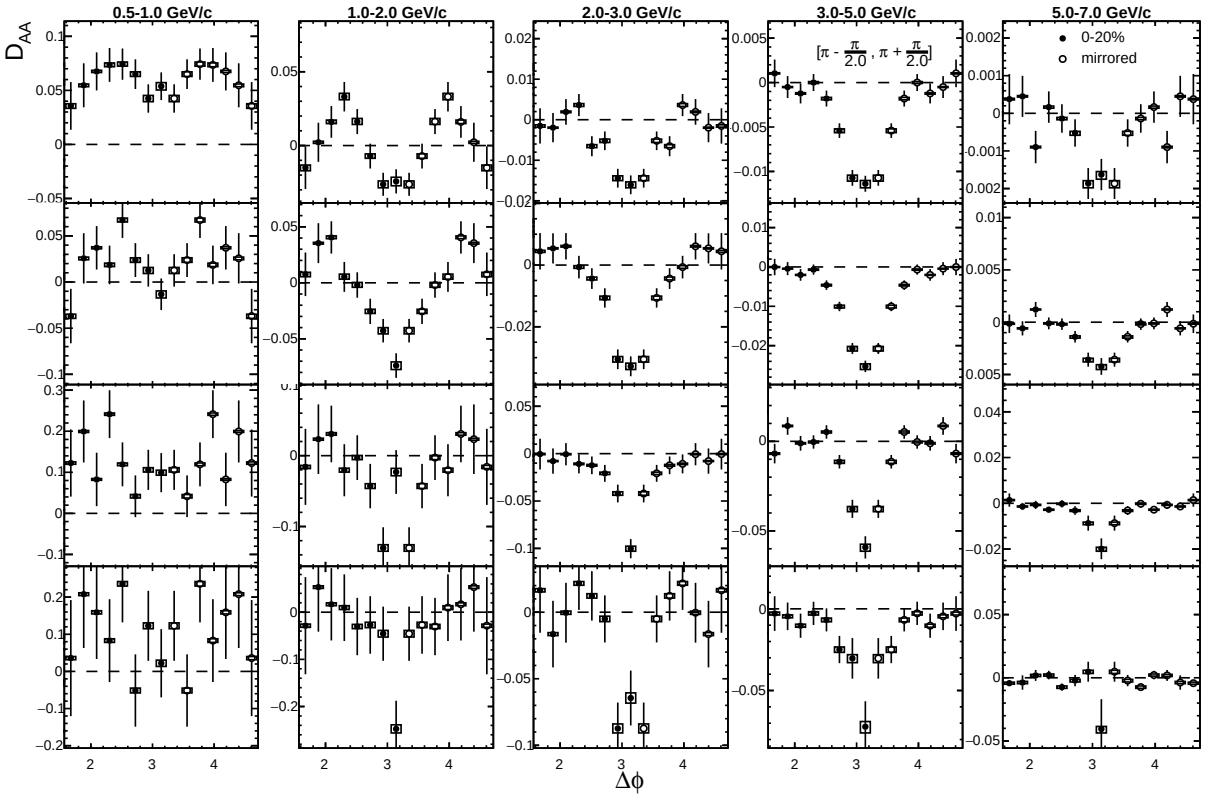

Figure 4.38: Away-side D_{AA} vs. $\Delta\phi$ in the 0–20% centrality class with only the systematic uncertainty arising from, σ^{f4}, the fourth order flow harmonics drawn.

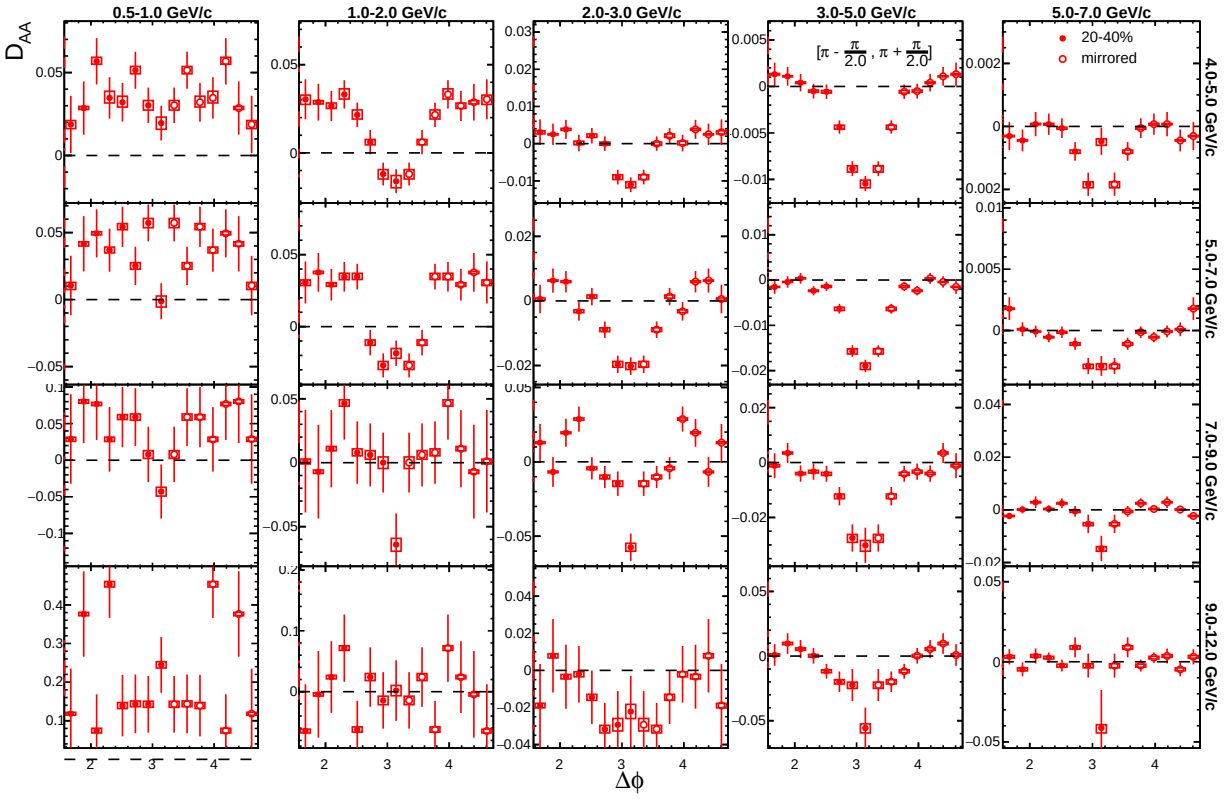

Figure 4.39: Away-side D_{AA} vs. $\Delta\phi$ in the 20–40% centrality class with only the systematic uncertainty arising from, σ^{f4}, the fourth order flow harmonics drawn.

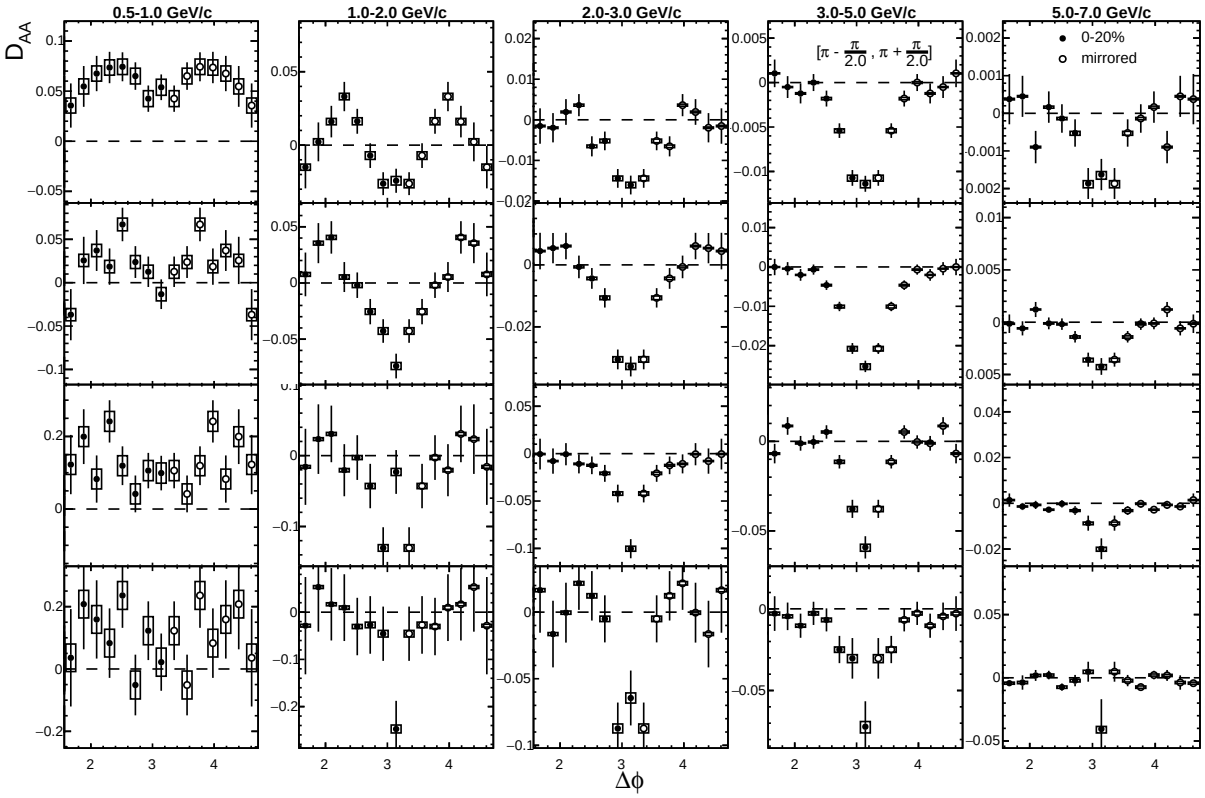

Figure 4.40: Away-side D_{AA} vs. $\Delta\phi$ in the 0–20% centrality class with only the systematic uncertainty arising from underlying event subtraction drawn.

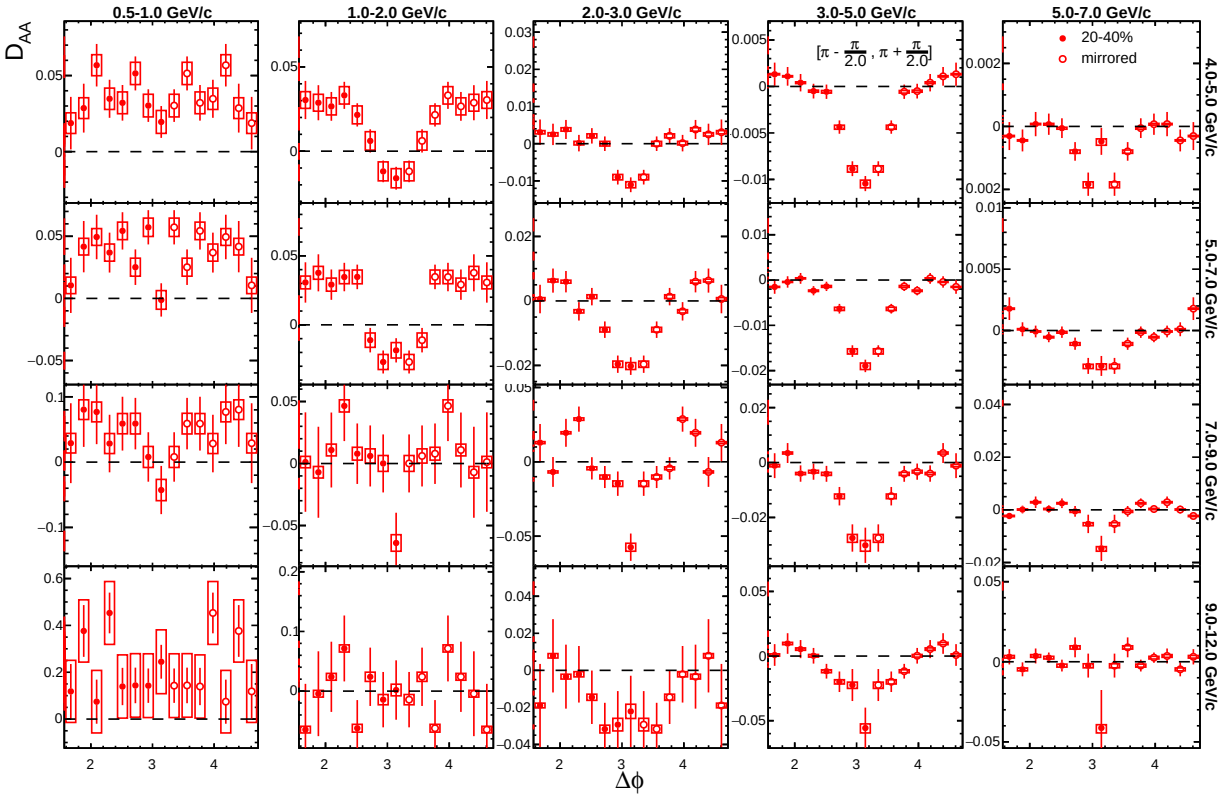

Figure 4.41: Away-side D_{AA} vs. $\Delta\phi$ in the 20–40% centrality class with only the systematic uncertainty arising from the underlying event subtraction drawn.

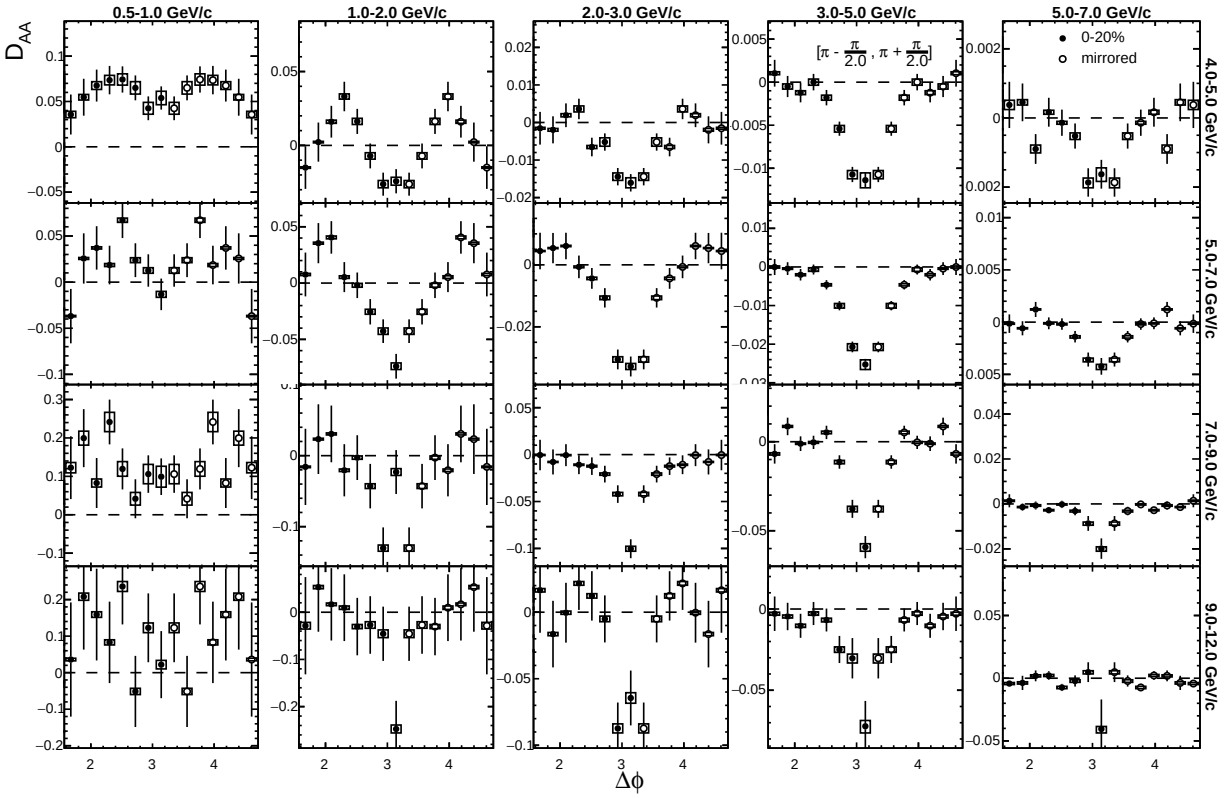

Figure 4.42: Away-side D_{AA} vs. $\Delta\phi$ in the 0–20% centrality class with only the systematic uncertainty arising from the π^0 reconstruction process drawn.

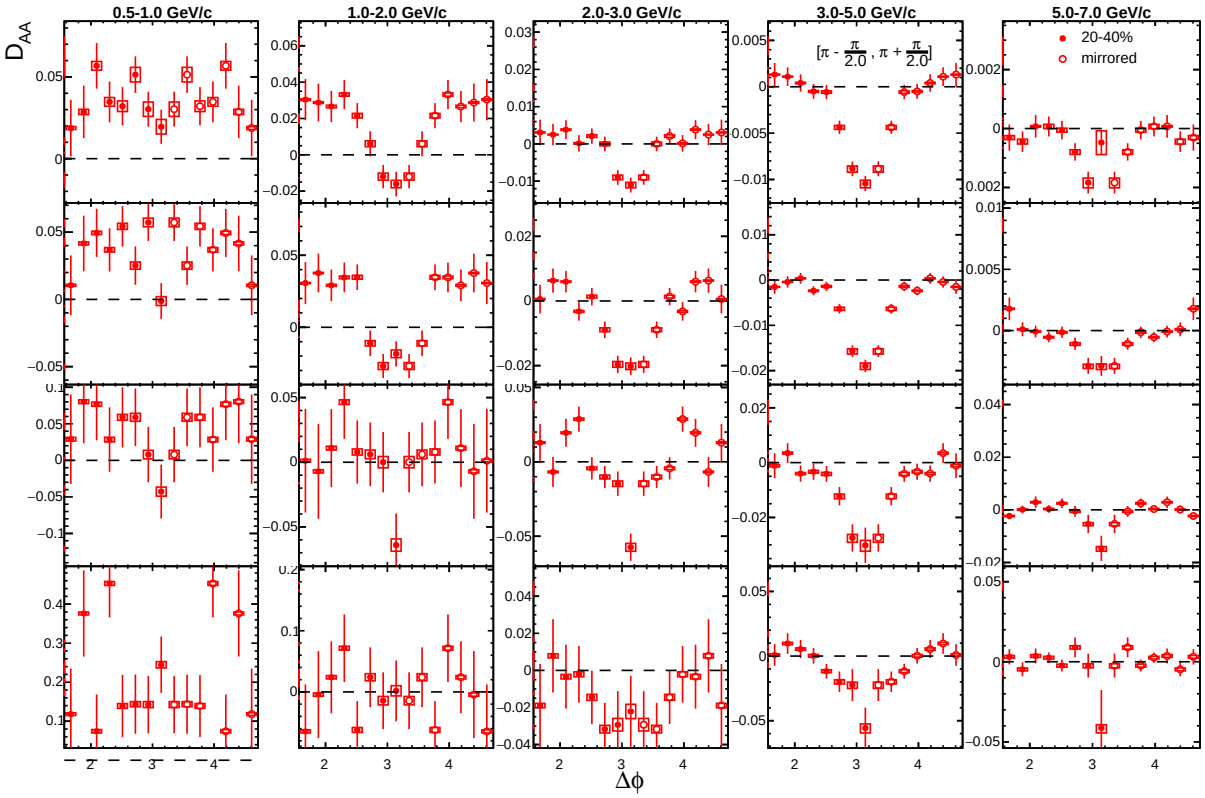

Figure 4.43: Away-side D_{AA} vs. $\Delta\phi$ in the 20–40% centrality class with only the systematic uncertainty arising from the π^0 reconstruction process drawn.

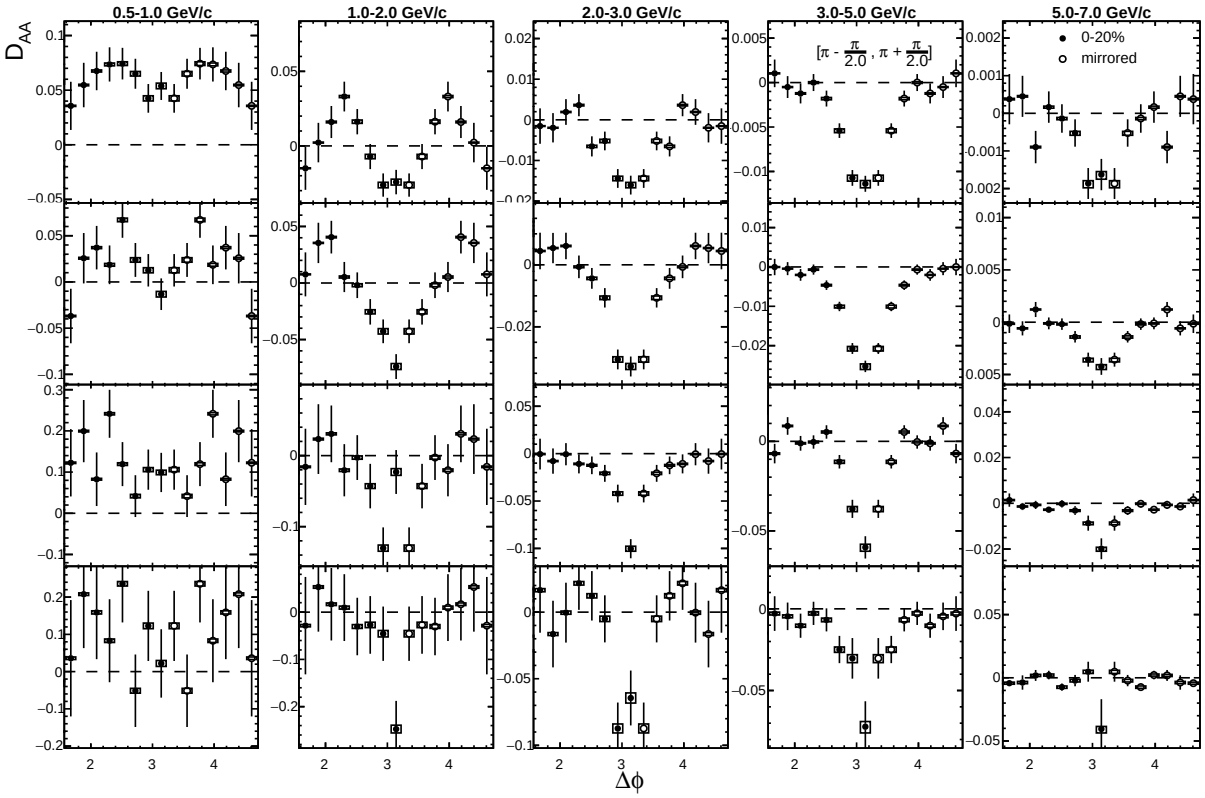

Figure 4.44: Away-side D_{AA} vs. $\Delta\phi$ in the 0–20% centrality class with only the systematic uncertainty arising from the $p+p$ baseline drawn.

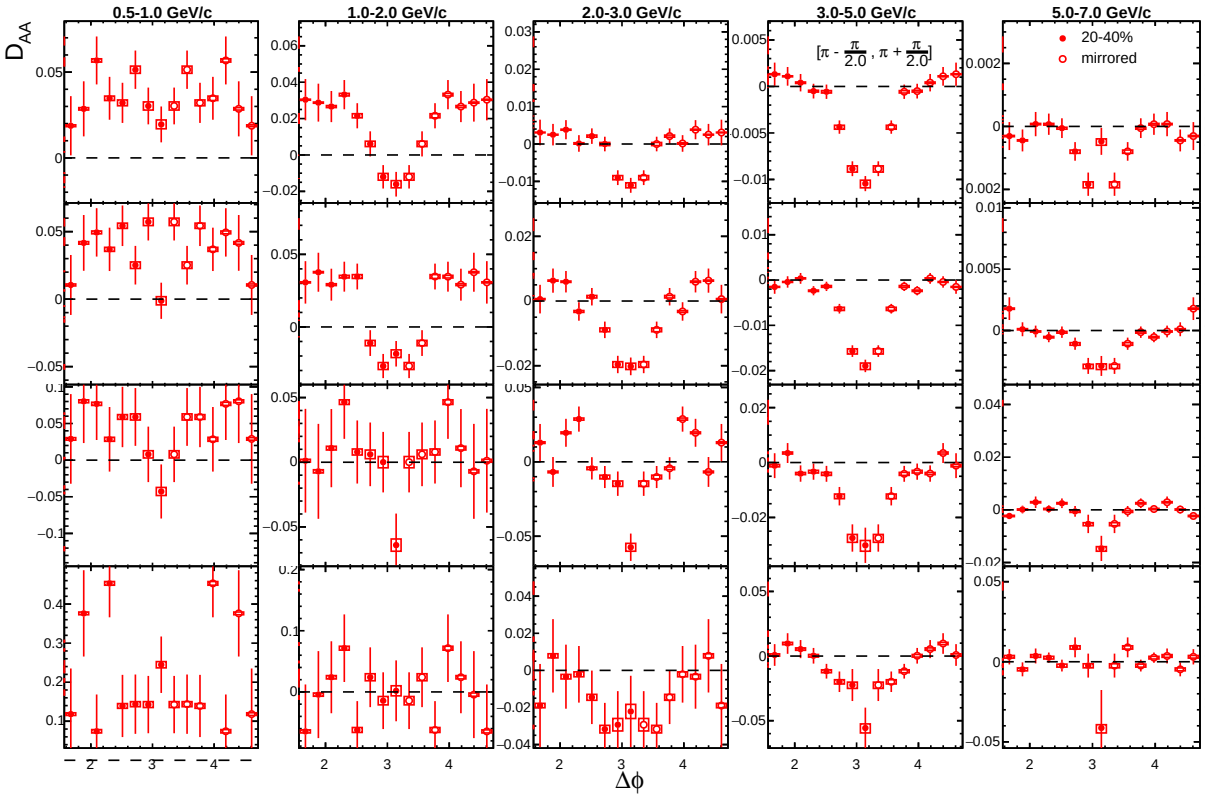

Figure 4.45: Away-side D_{AA} vs. $\Delta\phi$ in the 20–40% centrality class with only the systematic uncertainty arising from the $p+p$ baseline drawn.

CHAPTER 5

Results

This chapter details the results of this analysis from the PHENIX 2014 200 GeV $Au + Au$ data set only. Over the course of the analysis, it was discovered that the 2010 200 GeV $Au + Au$ data set had a faulty PC3 matching recalibrator, which is discussed in App. C. Fixing the recalibrator and re-analyzing Runs 10 and 11 would be a dissertation unto itself, and, so, Run 10 was dropped from the analysis. This left only the 2011 200 GeV $Au + Au$ data set, which contained only roughly 20% of the 2014's overall statistics, and so, to avoid amassing any further systematic uncertanties that might arise from combining the two runs, the results shown here are solely from the 2014 200 GeV $Au + Au$ data set.

5.1 Jet Functions

Jet functions quantify the per-trigger yields of charged hadrons as a function of $\Delta\phi$. They are characterized by two primary structures: one peak at $\Delta\phi \sim 0$ and one at $\Delta\phi \sim \pi$. The first is known as the near-side peak, and $\Delta\phi = 0$ is where the trigger π^0 resides. Thus the associate hadrons in this region are likely from the same jet as the trigger π^0 itself. The region about $\Delta\phi \sim \pi$ is known as the away-side peak. The two peaks are the result of the formation of a dijet pair due to the fragmentation of a hard-scattered parton and its recoil partner. The π^0–hadron jet functions measured in 200 GeV $Au + Au$ collisions are shown in Figs. 5.1 and 5.2. One can see a decrease in the away-side peak relative to the near-side as well as what appears to be a collimation of the near-side peak as one looks at bins with higher and higher p_T^{Hadron}.

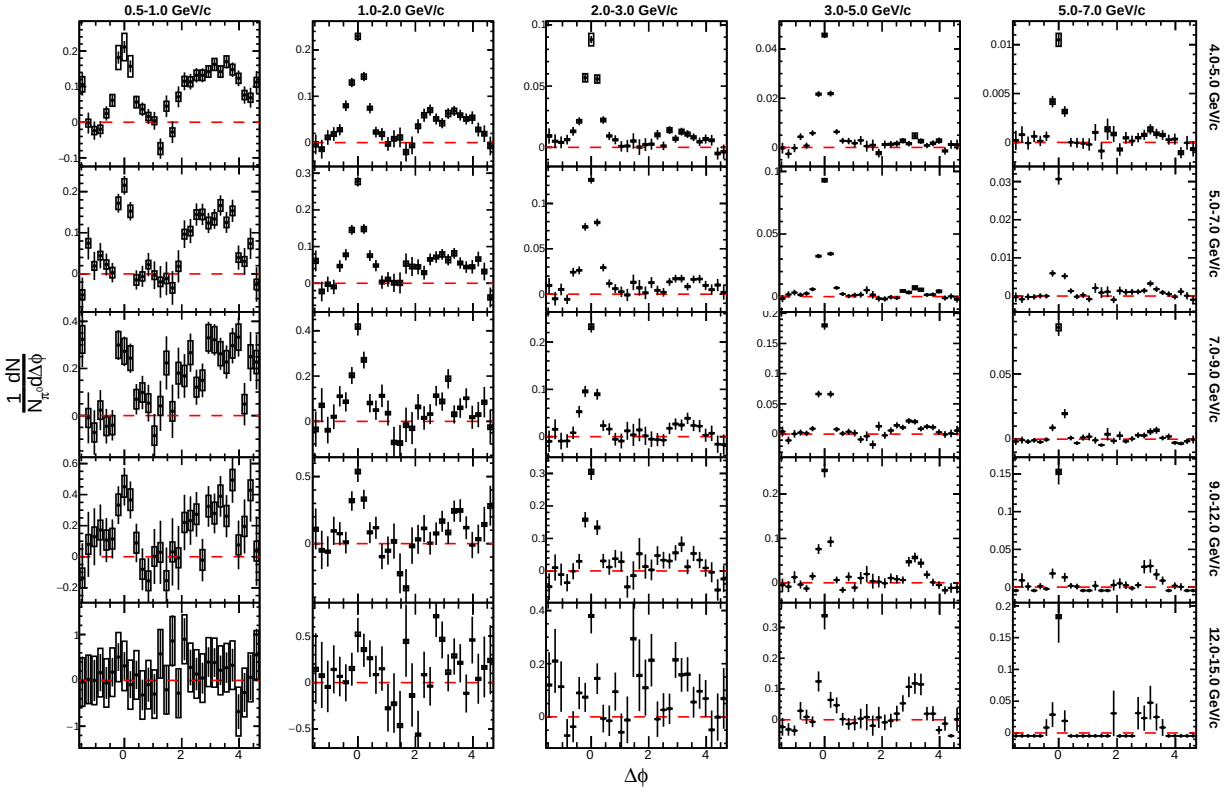

Figure 5.1: π^0–hadron jet functions measured in 200 GeV $Au + Au$ collisions in the 0–20% centrality class. p_T^{Trig} increases as one goes from the top of set of plots to the bottom, and p_T^{Hadron} increases as one goes from left to right. ± 6.9 scale uncertainty not shown.

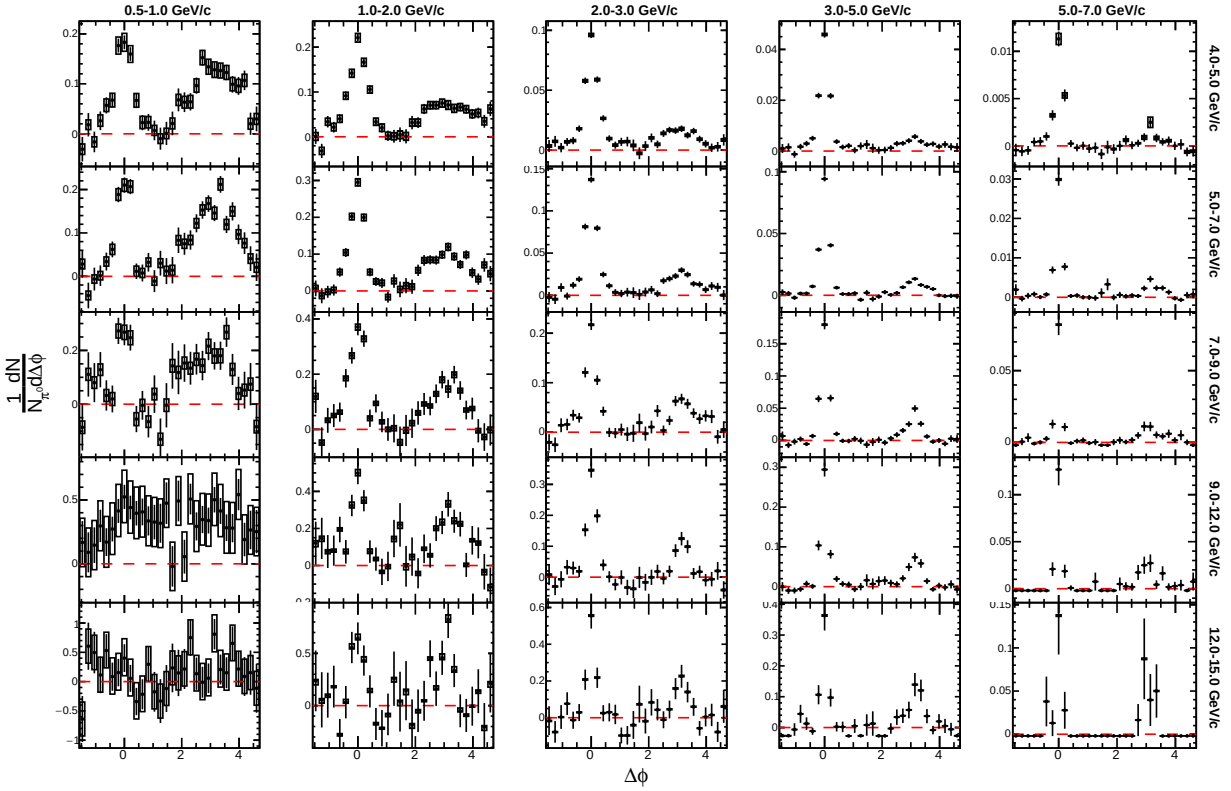

Figure 5.2: π^0–hadron jet functions measured in 200 GeV $Au+Au$ collisions in the 20–40% centrality class. p_T^{Trig} increases as one goes from the top of set of plots to the bottom, and p_T^{Hadron} increases as one goes from left to right. ±6.9 scale uncertainty not shown.

5.2 Yields

The integrated away-side yields in each p_T^{Trig} bin as a function of the associate hadron p_T is plotted in Fig. 5.3. The integral for the yields is computed over the range $|\Delta\phi - \pi| < \pi/2$, thus encompassing the entire away-side jet peak. The integrated yield decreases as a function of the associate hadron p_T in all cases (i.e., the $p+p$ baseline and the $Au+Au$ in the 0–20% and 20–40% centrality bins). Additionally, one can see that the integrated yields in the 20–40% centrality bin are consistently higher or at least equal to those in the 0–20% centrality bin within uncertainty. This difference in the yields occurs because a larger QGP is formed in

more central collisions, leading to a larger path length traversed by hard-scattered partons, thus resulting in a greater energy loss and lower hadron yield. One can note a substantial dip in the integrated away-side yields in the 7–9 $\otimes$ 3–5 GeV/c $p_T^{Trig} \otimes p_T^{Hadron}$ bin, occurring in both the 0–20% and 20–40% centrality bins. This dip arises from over-subtraction in that particular bin, and at high p_T, the integrated yields are particularly sensitive to over-subtraction as they are already quite small. This point, however, when propagated to the $I_{AA}(p_T)$ still has decent agreement with the published result's 0–20% to within statistical uncertainty, as shown in Fig. 6.1. The comparison is still good in the 20–40%, but it must noted that the comparison is less concrete as the published result uses a 20–60% centrality range.

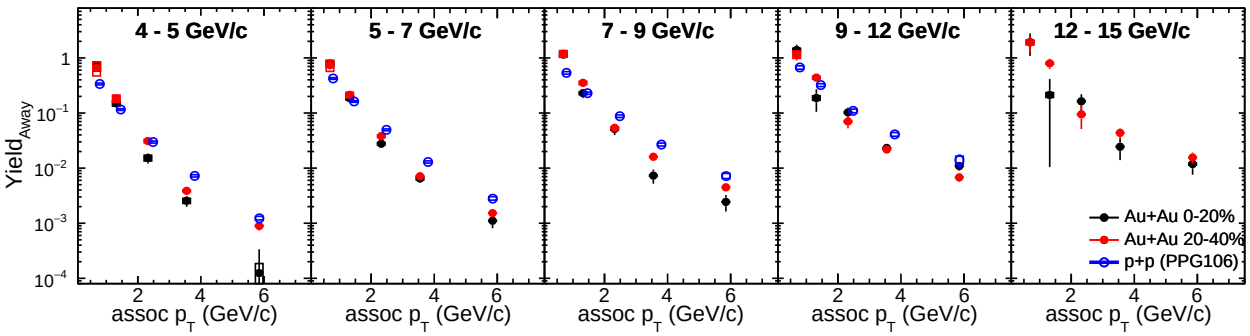

Figure 5.3: Integrated away-side yields in 200 GeV $Au + Au$ collisions in the 0–20% (Black) and 20–40% (Red) centrality classes. The $p + p$ baseline is plotted in blue for reference.

5.3 Away-side $I_{AA}(p_T)$

The $I_{AA}(p_T)$ is defined as the ratio between the integrated per-trigger yield of the jet functions in $A + A$ collisions, Y_{AA}, to that in baseline $p + p$ collisions, Y_{pp}, and is used to quantify modification to the per trigger yields of jets in collisions where a QGP is formed relative to one where no QGP is formed. Here, Y_{AA} and Y_{pp} are calculated by integrating the away-side

peak about the interval $|\Delta\phi - \pi| < \pi/2$. The results, shown in Fig. 5.4, show the I_{AA} as a function of the associate hadron p_T in four π^0 momentum bins and in two centrality bins. One can observe a suppression in the yield of high momentum hadrons and an enhancement in the yield of low momentum hadrons in each bin, with a cross-over point occurring at approximate 1.5 GeV/c in each bin. Lastly, one can see that the modification in the 0–20% bin is more severe on average than that measured in the 20–40% centrality bin. This difference in modification might stem from a difference in the size of QGP produced in 0–20% versus 20–40%, leading to partons in the more central bin to traverse a longer path-length on average, thus suffering more energy loss.

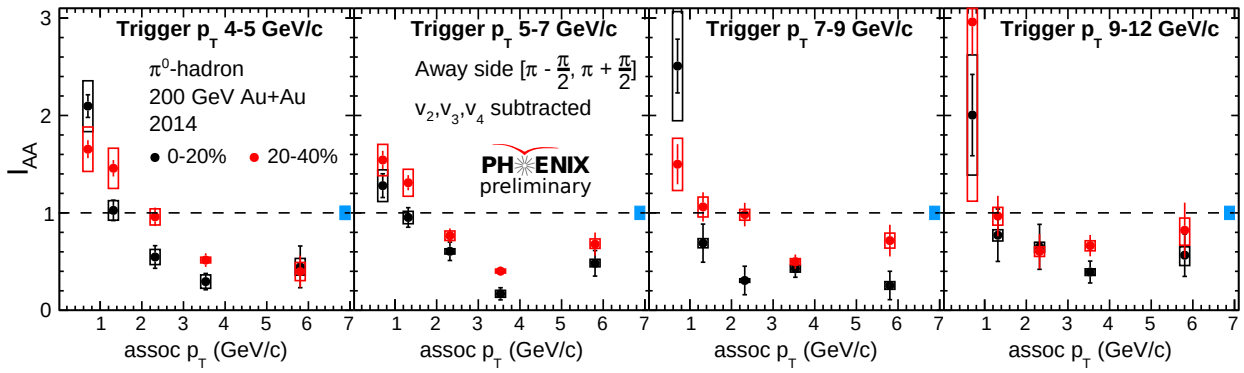

Figure 5.4: Away-side I_{AA} as a function of the associate hadron momentum measured in 0–20% (Black) and 20–40% centrality classes.

5.4 I_{AA} vs. $\Delta\phi$

In an effort to probe jet structure modification, the I_{AA} versus $\Delta\phi$ was first extracted in [38]. To measure this observable, the jet functions in $Au+Au$ collisions are divided point-to-point by the jet functions in $p+p$ collisions. The I_{AA} vs. $\Delta\phi$ from the 2014 PHENIX 200 GeV $Au+Au$ data set in the 0–20% centrality class for $4 < p_T^{\pi^0} < 5$ GeV/c is shown in Figs. 5.5

to 5.7, where each colored set of points represents a different hadron momentum bin. Like with the $I_{AA}(p_T)$, there is an enhancement in the yield of low momentum particles, but the I_{AA} vs. $\Delta\phi$ shows clearly that the excess soft particles appear predominantly at wide angles relative to the away-side jet peak as in Fig. 5.5. Additionally, in the lowest associate hadron momentum bin, this soft particle enhancement is seen at all angles across the away-side peak. As one looks at higher and higher associate hadron momentum bins, the I_{AA} vs. $\Delta\phi$ shows that the region near the away-side peak $|\Delta\phi - \pi| \approx \pi$ sees a suppression in the yield first as in Fig. 5.6. In the highest associate hadron momentum range seen in Fig. 5.7, the yields are suppressed flatly across $\Delta\phi$ to within uncertainty.

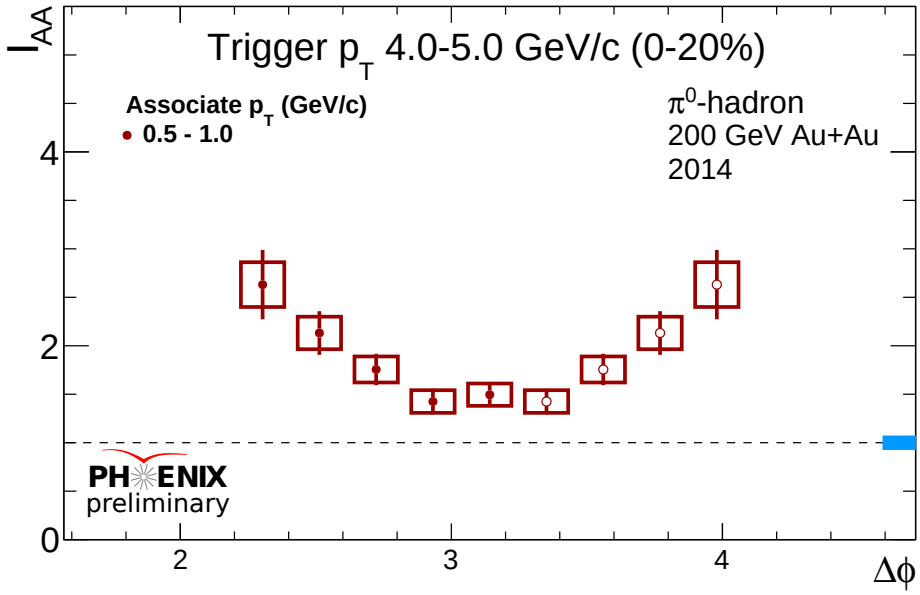

Figure 5.5: The I_{AA} vs. $\Delta\phi$ for the 4–5 GeV/c π^0 momentum bin. The points here are from the 0.5–1 associate hadron momentum bin.

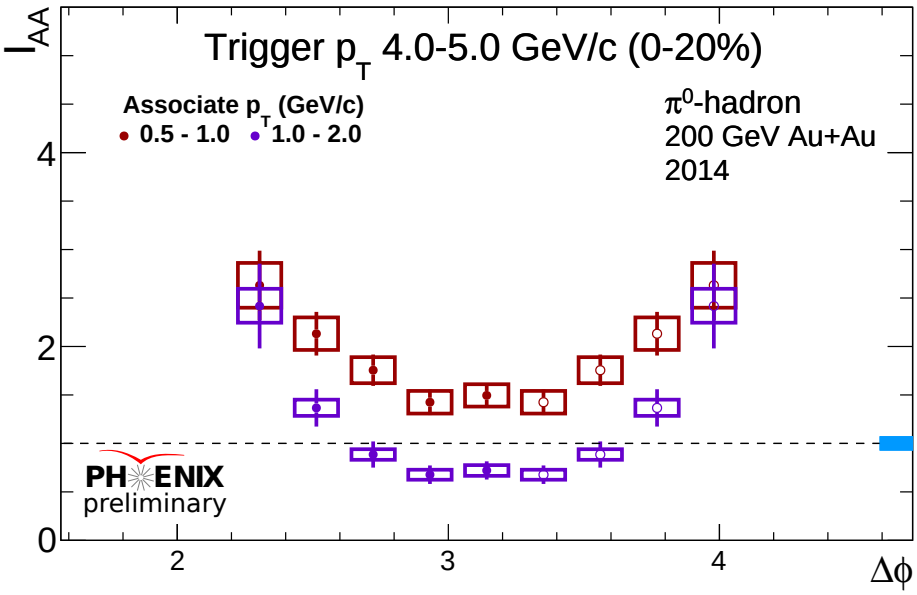

Figure 5.6: The I_{AA} vs. $\Delta\phi$ for the 4–5 GeV/c π^0 momentum bin. There are multiple hadron momentum ranges which are defined by the legend.

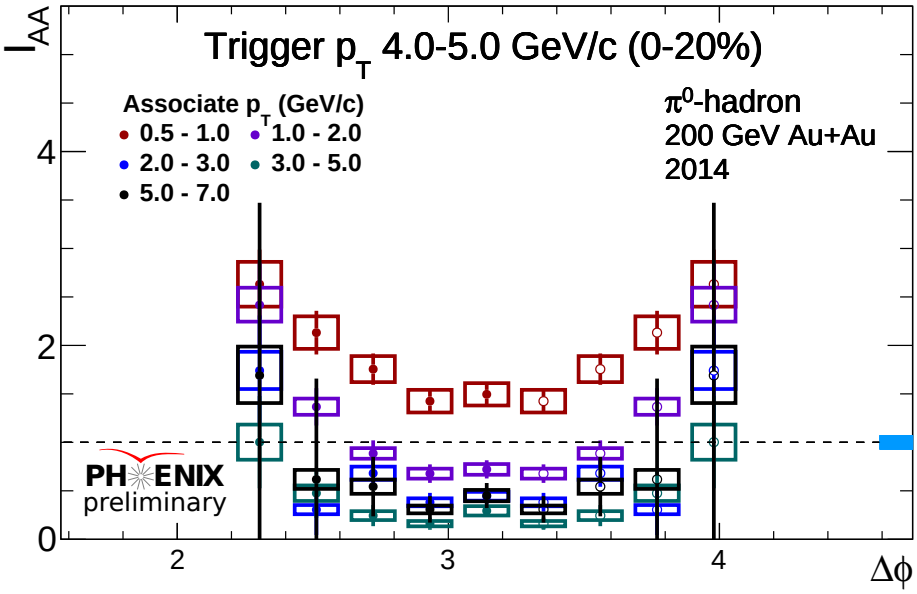

Figure 5.7: The I_{AA} vs. $\Delta\phi$ for the 4–5 GeV/c π^0 momentum bin. There are multiple hadron momentum ranges which are defined by the legend.

5.5 $\pi^0 D_{AA}$ vs. $\Delta\phi$

One major pitfall of the I_{AA} vs. $\Delta\phi$ observable shown above is that it is very sensitive to near-zero points in the $p+p$ baseline as one measures further and further away from the away-side jet peak. This leads to large central values as well as large statistical and systematic uncertanties. In order to combat this, the D_{AA} vs. $\Delta\phi$ has been measured for the first time from the PHENIX collaboration in this dissertation. D_{AA} is defined as the difference, rather than the quotient, of the integrated yields in $Au+Au$ and those in $p+p$. The D_{AA} vs. $\Delta\phi$ is plotted in Figs. 5.8 and 5.9, and one can see that the measurement can go out to $\pi/2$ away from the away-side peak without its uncertainties blowing up. Similar to the I_{AA} vs. $\Delta\phi$, the D_{AA} vs. $\Delta\phi$ shows an enhancement in the yield of soft parts that is more prominent away from the away-side jet peak as seen in Fig. 5.8. However, one can also see a diminishment in this enhancement as one approaches $\Delta\phi \approx \pi/2$, which appears to follow naturally from the fact that both the $Au+Au$ and $p+p$ per-trigger yields trend towards zero in this region. Additionally, Fig. 5.9 further corroborates that the region closest to the jet peak suffers the most severe suppression at high p_T^{Hadron}. Finally, one can see that due to how differential the measurements are in both charged hadron and π^0 momentum space and its increased coverage in $\Delta\phi$ space, the D_{AA} vs. $\Delta\phi$ is an excellent candidate to test the physics presented in [36] shown in Fig. 6.5.

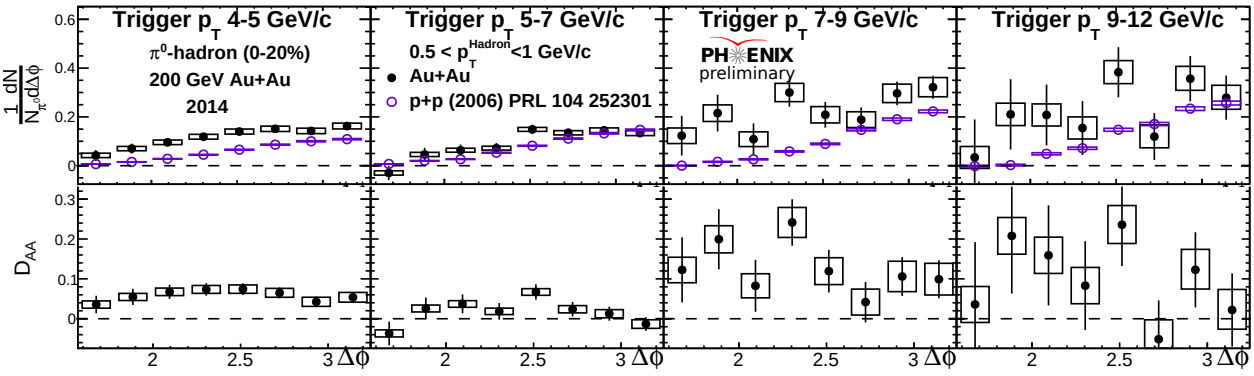

Figure 5.8: Top: Folded per-trigger yields versus $\Delta\phi$ from 200 GeV 0–20\$ $Au + Au$ (Black) and $p + p$ (Blue) collisions. Each column is a different π^0 momentum bin, and the associate hadron momentum ranges between 0.5–1 GeV/c. Bottom: D_{AA} vs. $\Delta\phi$.

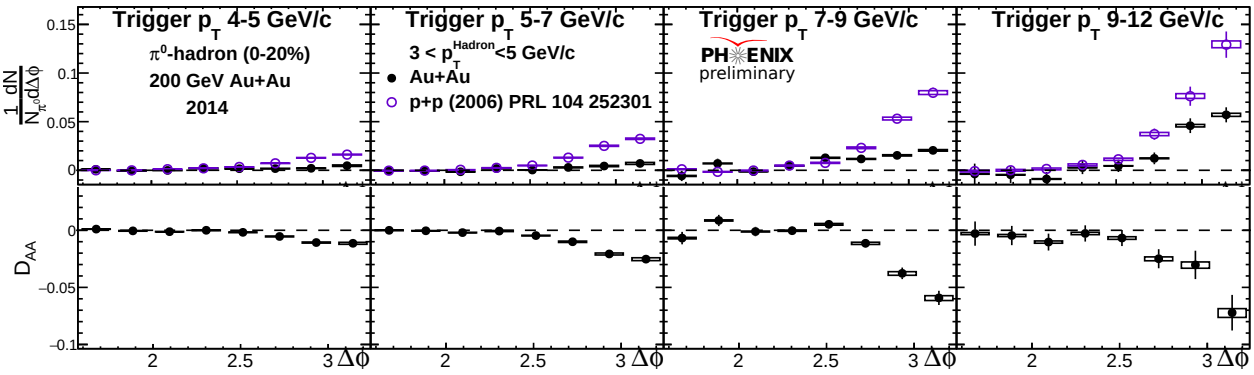

Figure 5.9: Top: Folded per-trigger yields versus $\Delta\phi$ from 200 GeV 20–40% $Au + Au$ (Black) and $p + p$ (Blue) collisions. Each column is a different π^0 momentum bin, and the associate hadron momentum ranges between 3–5 GeV/c. Bottom: D_{AA} vs. $\Delta\phi$.

5.6 Direct photon D_{AA} vs. $\Delta\phi$

A calculation of the D_{AA} vs. $\Delta\phi$ using the jet functions published in [34] is shown in Fig. 5.11, with the jet functions used in their calculations shown in Fig. 5.10.

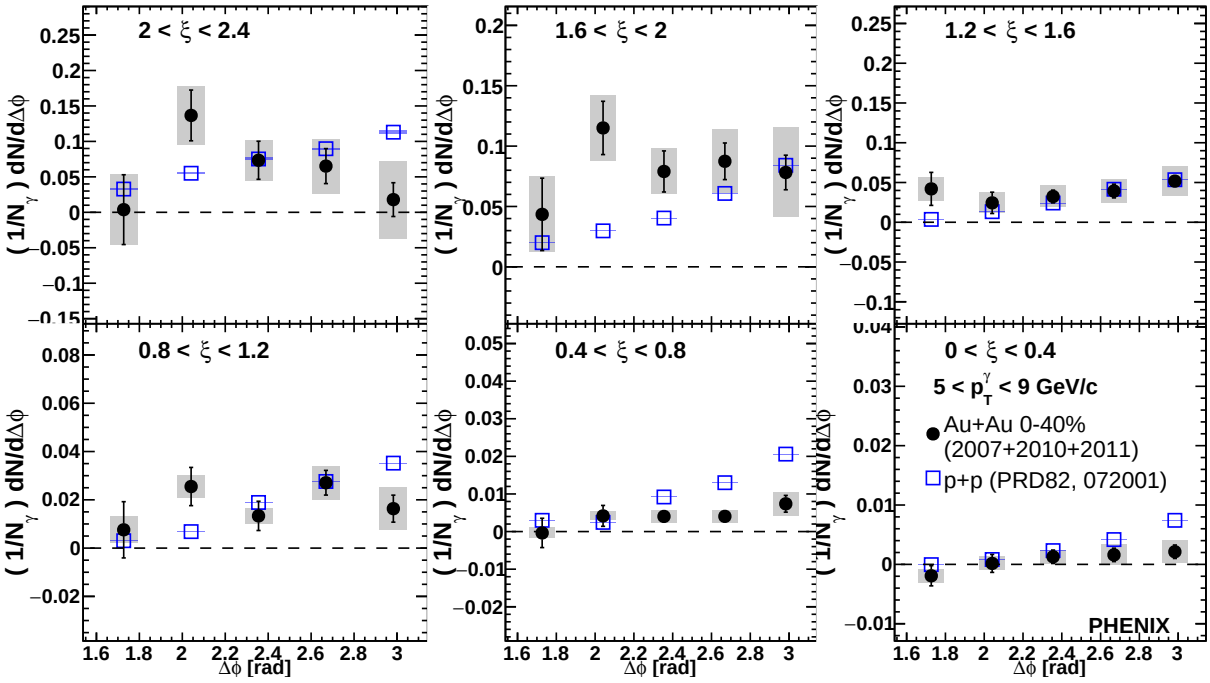

Figure 5.10: Direct photon-hadron jet functions in 0–40% 200 GeV $Au + Au$ collisions (Black) and 200 GeV $p + p$ collisions (Blue) [34] for $5 < p_T^{\gamma} < 9$ GeV/c. Only the away-side ($\pi/2 < \Delta\phi < \pi$) is shown here to correspond to the D_{AA} vs. $\Delta\phi$ shown in Fig. 5.11. The dashed line represents zero.

As with the D_{AA} vs. $\Delta\phi$ measurement made with π^0-triggered correlations, the differential per-trigger yields of the $p + p$ jet function are subtracted from those in the $Au + Au$ jet functions, yielding the D_{AA} vs. $\Delta\phi$ for direct photon-hadron correlations, shown in Fig. 5.11.

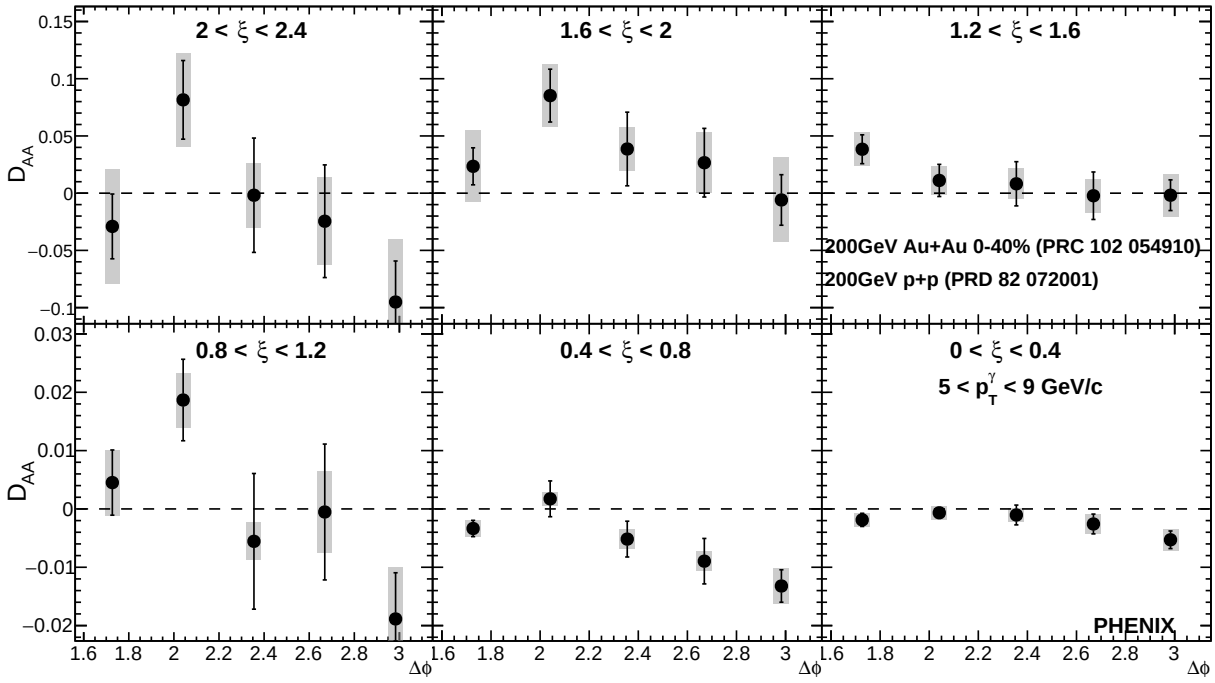

Figure 5.11: D_{AA} vs. $\Delta\phi$ for direct photon-hadron correlations in 0–40% 200 GeV $Au + Au$ collisions $5 < p_T^{\gamma} < 9$ GeV/c.

One can see similar behaviors between the direct photon and π^0-triggered D_{AA} vs. $\Delta\phi$ measurements. A hint of enhancement can be seen in the highest ξ (lowest p_T) bins of the direct photon-hadron measurement in Fig. 5.11. Additionally, one can see a similar suppression in the yield of low ξ (high p_T) particles that appears to be most apparent near the away-side peak ($\Delta\phi \approx \pi$). The combined statistics of later PHENIX data sets (e.g. Run 14 and Run 16) should allow several improvements to this measurements. The number of bins in $\Delta\phi$ space can be increased, and the analysis might have the statistical precision to look at the 0–20% and 20–40% centrality bins separately as was done for the π^0 result. Ultimately, the similarity in the behavior seen in the D_{AA} vs. $\Delta\phi$ measurements in both the π^0 and direct photon-triggered correlations offer a valuable cross-check on one another.

The direct photon-triggered correlations are a well-calibrated probe for studying jet energy loss, but the rarity make the statistical precision of their measurement suffer. Whereas using π^0's as a jet proxy in two-particle correlations allows for highly precise measurements at the cost of some smearing of the relationship between the π^0's momentum and the recoil jet's momentum due to both near and away-side jets' having suffered in-medium energy loss.

CHAPTER 6

Discussion

This dissertation has expanded upon π^0-triggered two-particle correlations presented in both [39] and [38]. As in Ping Wong's thesis, the studies detailed here improve upon the previously published results by subtracting the 3^{rd} and 4^{th} collective flow harmonics, thus allowing for a more precise measurement of modification to the away-side peak's per-trigger yield of charged hadrons and its shape relative to what is measured in baseline $p + p$ collisions. Additionally, this analysis introduces the first measurement of D_{AA} versus $\Delta\phi$ at PHENIX, which improves upon the I_{AA} versus $\Delta\phi$ as it is impervious to fluctuations caused by the differential yields in the $p+p$ baseline approaching zero. The results from this analysis take advantage of PHENIX's largest data set of 200 GeV $Au + Au$ collisions from the 2014 RHIC run. This chapter will compare the results from this analysis to other experiment results, and discuss the implications of any agreements and discrepancies.

6.1 Comparisons to Results in Large Nucleus-Nucleus Collisions.

This section will show comparisons between the $Au+Au$ results from this analysis and results from PHENIX's sibling RHIC experiment, STAR, as well as results from experiments at the LHC. As PHENIX and STAR are meant to be complementary experiments, comparison between the two experiments' results is important for validation. Comparisons to $Pb + Pb$ results will also be shown in an attempt to qualitatively infer how jet modification depends on system size and center of mass energy.

6.1.1 Comparison to Previous PHENIX Results

This analysis serves as an update to PHENIX's previous published π^0-hadron correlation measurements presented in [39]. Compared to the data set used in the publication, the 2014 200 GeV $Au+Au$ data set contains 4.1 times as many events overall, and is the largest 200 GeV $Au+Au$ data set available from PHENIX. In addition to the increased statistics, this analysis also subtracts off the v_2, v_3, and v_4 components of the underlying event due to flow, whereas the published result subtracts off v_2 only. And lastly, ZYAM is used to estimate the magnitude of the underlying event in the $0.5-1$ GeV/c hadron momentum bin, whereas the published result uses Absolute Background Subtraction across all $p_T^{Trig} \otimes p_T^{Hadron}$ momentum bins.

The difference between this analysis and that carried out in [39] is best exemplified in a comparison of the $I_{AA}(p_T)$ results shown In Figs. 6.1 and 6.2. The starkest difference can be seen in the 0–20% centrality bin, where the subtraction of the higher order flow harmonics correlates directly to larged amount of underlying event being subtracted off and, hence, a lower integrated yield, which manifests itself as a lower I_{AA} at low p_T^{Hadron}. At high p_T^{Hadron} where the underlying event is smaller, however, one can see that the two analyses begin to converge. Additionally, there is great agreement between the two analyses when comparing the semi-central bins (20–40% in this analysis and 20–60% in [39]), which implies that the measurement is less sensitive to the subtraction of the higher order flow harmonics in these centrality regions.

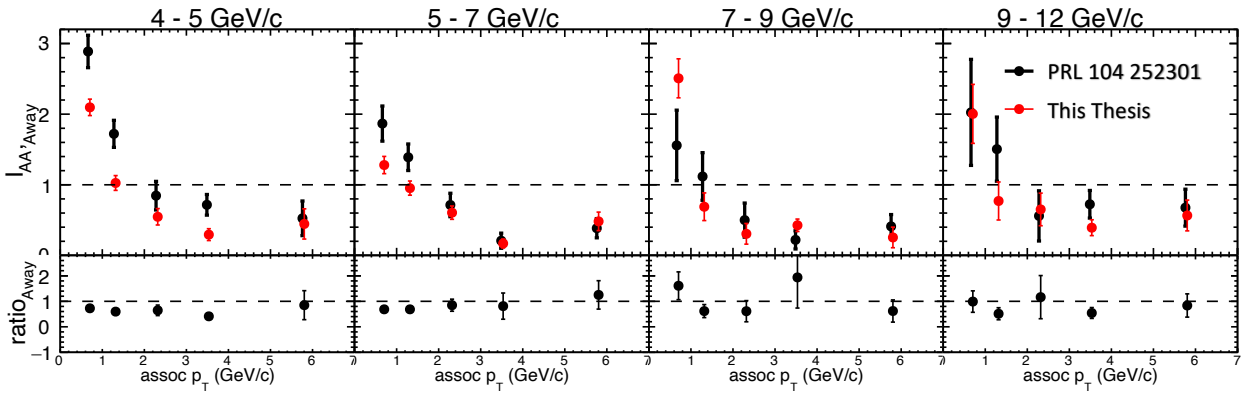

Figure 6.1: Comparison of this analysis's $I_{AA}(p_T)$ result (red) to the published result in the 0–20% centrality class.

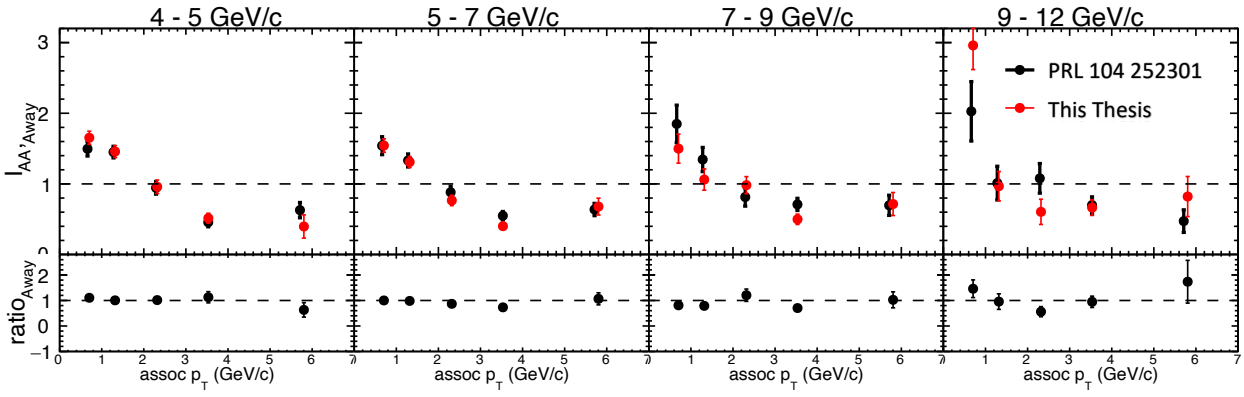

Figure 6.2: Comparison of this analysis's $I_{AA}(p_T)$ result (red) to the published result (black) in the 20–40% centrality class.

6.1.2 STAR Results in 200 *GeV* $Au + Au$ *Collisions*

Fig. 6.3 below shows the I_{AA} as a function of $z_T = p_T^{Hadron}/p_T^{Trig}$ for both π^0–hadron and direct photon–hadron correlations in 200 GeV $Au + Au$ collisions as measured by the STAR (**S**olenoidal **T**racker **A**t **R**HIC) experiment. As the I_{AA} measured in this dissertation is a function of the associate hadron's p_T, the points between the PHENIX and STAR measurement cannot be overlaid, but can be compared side-by-side. In particular, one should compare the STAR result to the 9–12 GeV/c π^0 momentum bin in the 0–20% centrality bin.

Additionally, the STAR result's kinematic reach for the charged hadron extends down to 1.2 GeV/c, whereas this dissertation's result extends down to 0.5 GeV/c, meaning that the STAR result is comparable to this dissertation's result starting at the 1–2 GeV/c in Fig. 4.20. Qualitatively the PHENIX result appears to measure a suppression in the conditional yield of charged hadrons in this region, whereas STAR measures an enhancement of about 20%, although [60] does note that the enhancement in this region is small relative to the systematic uncertainty, which is dominated by the π^0 reconstruction process, the uncertainty for which in this analysis is relatively small in the 9–12 GeV/c π^0 momentum bin.

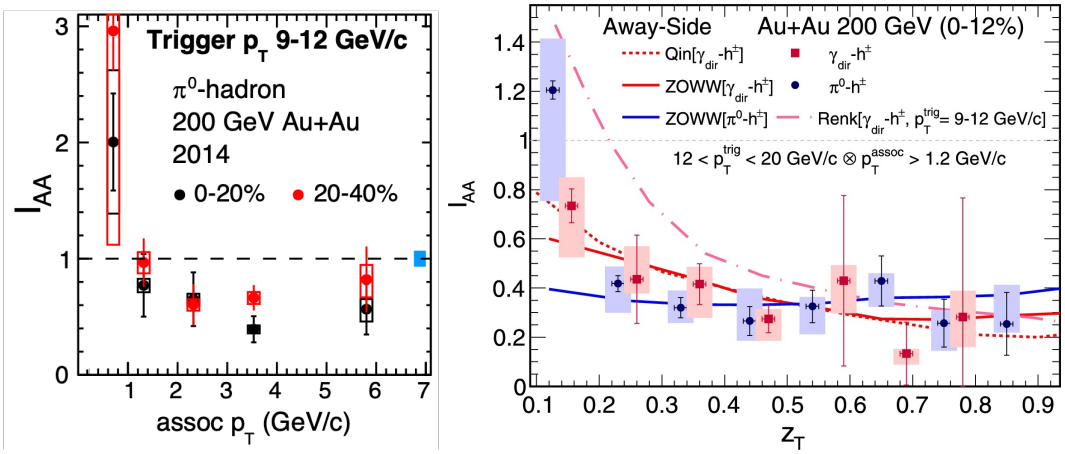

Figure 6.3: Left: The away-side I_{AA} as a function of p_T^{Hadron} from 200 GeV $Au+Au$ collisions measured by the PHENIX experiment. Right: The away-side I_{AA} as a function of z_T from 200 GeV $Au+Au$ collisions measured by the STAR experiment [60]. The I_{AA} from π^0-hadron and direct photon–hadron correlations are drawn in blue and red, respectively.

6.1.3 ALICE Results from 2.76 *TeV* $Pb+Pb$ *Collisions*

The ALICE (**A** **L**arge **I**on **C**ollision **E**xperiment) experiment at the LHC focuses on measuring $Pb+Pb$ collisions at 2.76 and 5.02 TeV center of mass energies. In Fig. 6.4 is the away-side I_{AA} as a function of the associate hadron p_T. Both the ALICE result and this

dissertation's result both measure a suppression in the yield of high momentum associate hadrons and an enhancement in the yield of low momentum associate hadrons. Of particular note is that the transition point from suppression to enhancement occurs at lower p_T^{Hadron} in this dissertation's result, which appears to occur around 1.2 GeV/c bins, than in the ALICE result, where it appears to occur around 3.5 GeV/c. One possible explanation for this phenomenon is that the larger center of mass energy at the LHC allows for the creation of hard-scattered partons with higher initial momentum. These higher momentum partons will thus radiate more energetic "soft" radiation, thus moving the cross-over point higher along p_T^{Hadron} axis.

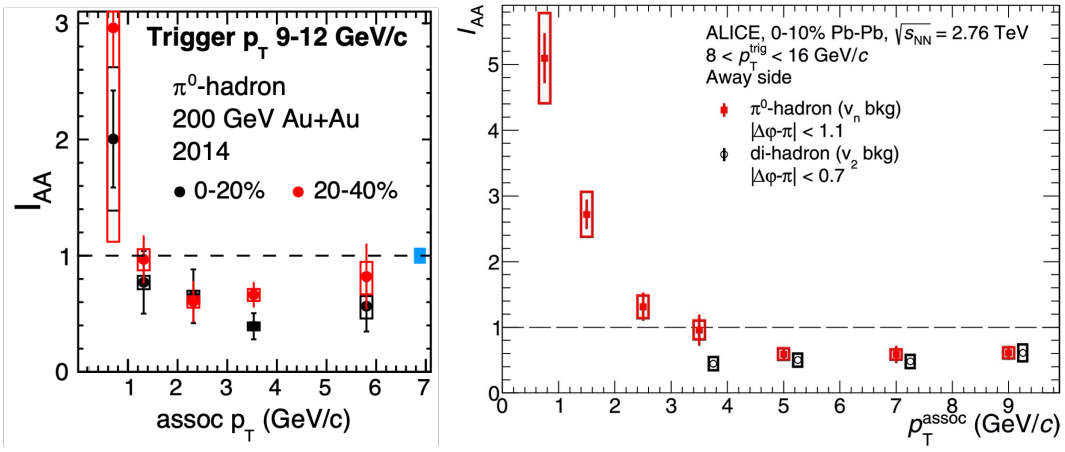

Figure 6.4: Left: The away-side I_{AA} as a function of p_T^{Hadron} from 200 GeV $Au+Au$ collisions measured by the PHENIX experiment. Right: Away-side I_{AA} as a function of p_T from 2.76 TeV $Pb+Pb$ data from ALICE experiment [61]. The results from π^0-hadron and hadron-hadron correlations are drawn in red and black, respectively.

6.1.4 CMS Results in 5.02 *TeV* $Pb+Pb$

The CMS (**C**ompact **M**uon **S**olenoid) solenoid experiment at the LHC has recently measured the D_{AA} versus $\Delta\phi$ [62]. In the CMS study, however, charged hadrons in an event are

correlated to a Z boson rather than a π^0. Z bosons, like direct photons, are color neutral, and, thus, the QGP medium is transparent to them, making them another well-calibrated probe for studying jet modification in heavy-ion collisions. Z bosons are reconstructed via their $Z \rightarrow e^+ + e^-$ and $Z \rightarrow \mu^+ + \mu^-$ decay channels, a method that has the added benefit of a higher signal-to-background ratio at low p_T^Z than the extraction of direct photons. Fig. 6.5 shows the CMS D_{AA} result in 5.02 TeV $Pb + Pb$ collisions for $p_T^Z > 30$ GeV/c and for $p_T^{Hadron} > 1$ GeV/c. Looking specifically at the 0-30% centrality bin at the top right and its associated D_{AA} result beneath, this bin appears to have good qualitative agreement with this dissertation's lower $p_T^{\pi^0} \otimes p_T^{Hadron}$ momentum bins, but it should be pointed out that the measurement made via π^0–hadron correlations is much more differential in p_T because of the relative abundance of trigger π^0's. Theory calculations in Fig. 6.5 are from CoLBT+Hydro [63] calculations discussed in Sec. 1.2.4 and from a hybrid model [36] which propagates energy lost by hard partons as a "wake" through the medium. Focusing on the latter model, one can see that the calculation labelled "wake" seems to have good agreement with the CMS D_{AA}. This agreement can be attributed to the fact that the calculation done for the "w/ wake" curve includes medium response to the energy radiated by partons experiencing energy loss in the form of a wake of low momentum particles. Because the CMS data is measured in one large momentum bin for the associate hadrons, low momentum phenomenology dominates as it is more abundant.

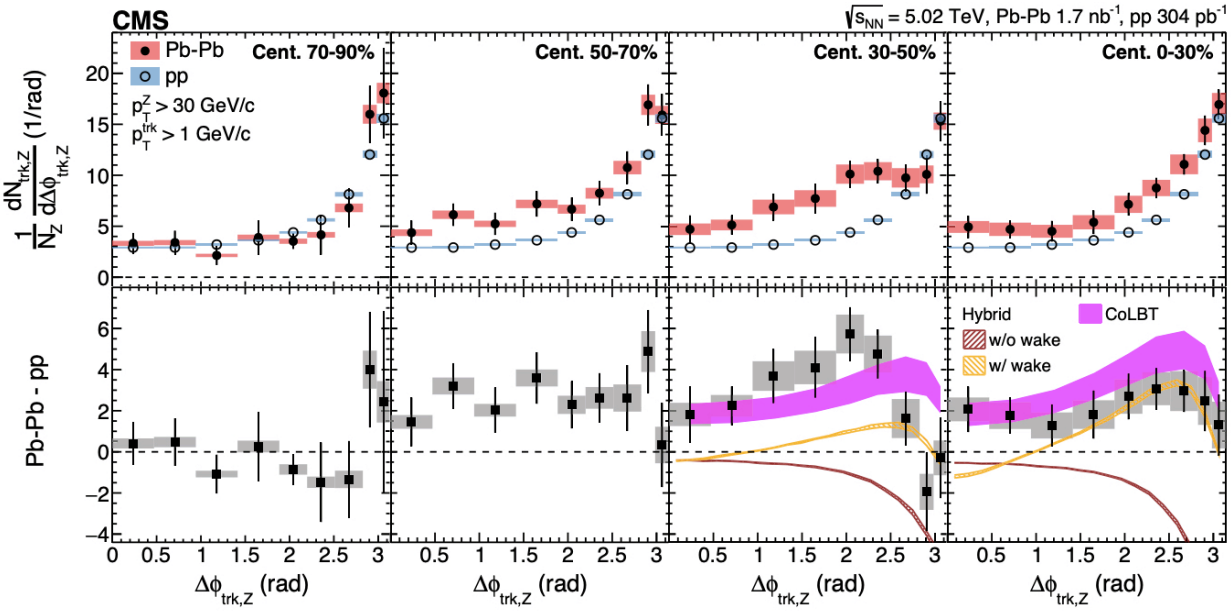

Figure 6.5: D_{AA} vs. $\Delta\phi$ as measured via Z–hadron correlations 5.02TeV Pb+Pb collisions by the CMS experiment. The top set of plots shows the per-trigger yield of hadrons correlated to a Z boson in $Pb+Pb$ (red) and baseline $p+p$ (blue) collisions. Each coloumn of plots represents a different centrality class. The bottom row is the $D_{AA} = Y_{PbPb} - Y_{pp}$.

6.1.5 ATLAS Results in 5.02 *TeV* $Pb+Pb$

The ATLAS (**A** **T**oroidal **L**HC **A**pparatu**S**) experiment additionally has measured jet modification via Z boson hadron correlations [64]. Fig. 6.6 shows the I_{AA} as a function of the associate hadron p_T for three Z boson momentum ranges. The measurement shows a suppression in the yield of high momentum associate hadrons across all p_T^Z, and an enhancement in the yield of low momentum associate hadrons for $p_T^Z > 30$ GeV/c. Model predictions from the Hybrid model with and without a medium response in the form of a wake of low-momentum particles are also presented for each Z boson momentum bin. Both sets of calculations properly account for the depletion of high momentum particles, but only the set which includes the wake mechanic are able to reproduce the enhancement seen

at low momentum. However, it should be noted that the calculations with the wake still seem to have difficulty accurately predicting the turnover point between suppression and enhancement, and fail to describe the lowest Z momentum bin at low hadron momentum.

Compared to the PHENIX results from the 0–20% centrality bin shown in Fig. 5.4, the $I_{AA}(p_T)$ result in this dissertation does not measure an apparent trend in suppression levels that depends on the trigger particle's momentum. It also measures a marked enhancement in the yield of low momentum particles in each π^0 momentum bin, while the ATLAS $I_{AA}(p_T)$ measurement seems to measure a slight suppression in the yield of low momentum particles in its 15–30 GeV/c momentum bin.

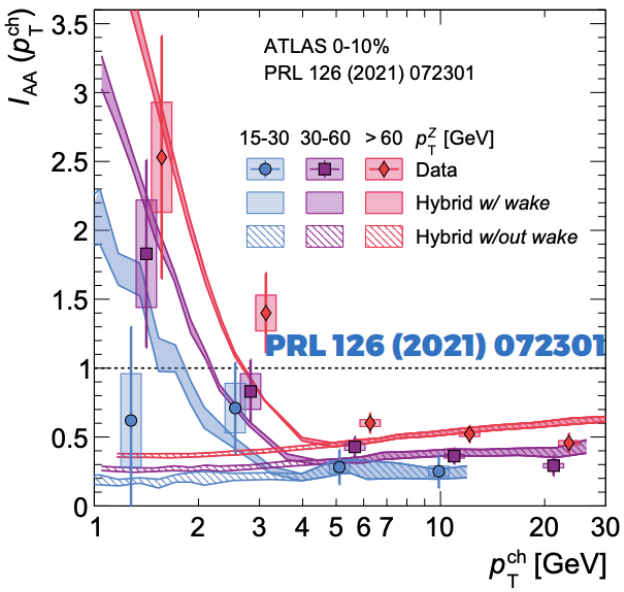

Figure 6.6: ATLAS I_{AA} as a function of associate hadron momentum for 3 Z boson momentum ranges: 15–30 GeV/ (Green), 30–60 GeV/c (Red), and $>$ 60 GeV/c (Orange). Hybrid models with (solid bands with color corresponding to Z momentum range) and without (cross-hatched bands with color corresponding to Z momentum range) are also included.

6.2 Comparison to Small System Results

The original purpose of studying jet modification in small systems was to quantify the impact of cold matter effects. Cold matter effects, loosely, are effects that change the final measurement of an observable (such as the I_{AA}), but are not due to the presence of a QGP medium. They are effects that appear simply because one is colliding two nuclei instead of two protons. It should be noted, though, that recent results [44] shows nonzero collective flow in these small systems, suggesting the presence of a QGP medium, thus muddying the idea that small systems can always be used to isolate these cold nuclear matter effects. Nevertheless, these systems can useful in gauging how the size of the medium created correlates to the magnitude of jet modification measured.

Fig. 6.7 shows the I_{dA} for π^0–hadron correlations measured in 200 GeV d+Au collisions as a function of $z_T = p_T^{Hadron}/p_T^{Trig}$ for both the near and away-side. On the away-side, one can see a clear suppression at high z_T, corresponding to high momentum associate hadrons. At low z_T, one additionally measures a statistically significant enhancement, but this deviation from unity does not exceed the systematic uncertainty of the measurement. Nevertheless, this result does show jet modification in small systems.

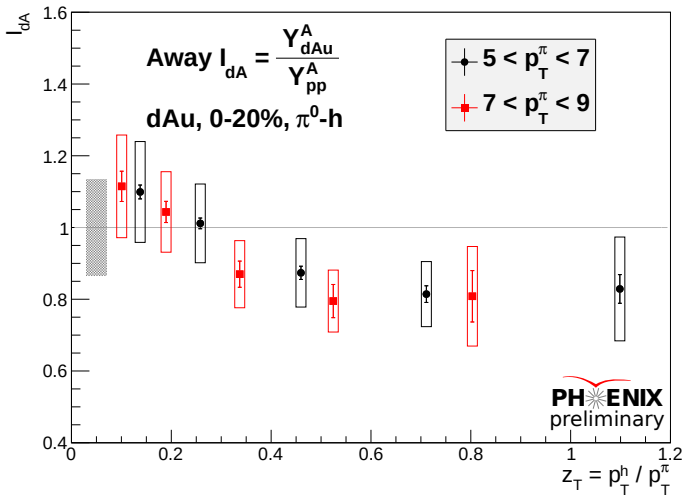

Figure 6.7: Away-side I_{dA} as a function of z_T in 200 GeV $d + Au$ collisions [65].

In conclusion, one can see that the magnitude of the modification (i.e. how far the points deviate from 1) measured by the I_{dA} result is smaller than that seen in large system results. Coupled with evidence from [44], this could mean that the smaller modification is due to the fact that the medium created in small systems collisions is smaller, thus leading to a smaller path-length probed by hard partons and, thus, smaller energy loss. Ultimately, however, the large systematic uncertainties in Fig. 6.7 make drawing a definite conclusion difficult.

CHAPTER 7

Future Prospects

While the studies contained in this dissertation were painstakingly performed and exhausting in their meticulousness, there still remains much work to do in the field of jet physics.

7.1 Direct Photon-Hadron Correlations

Firstly, efforts are fully underway to extend results from this π^0-hadron correlation analysis to the 2016 200 GeV $Au + Au$ data set. Once that is accomplished, it will be time to return to the Run 14 data set analyzed in this dissertation to extract the direct photon-hadron correlations. These correlations are often referred to as the "golden channel" of jet energy loss studies because the direct photon trigger acts as a well-calibrated probe since, to leading order, it approximates the energy of the recoil jet very well. The first step in extracting these correlations will be to map the π^0-hadron correlations to the decay photon-hadron correlations using a decay probability distribution which gives the probability that a given photon came from the decay of a neutral pion. These correlations are measured simultaneously with the single photon-hadron correlations shown in. Mathematically, the single photon and decay photon-hadron yields are related via Eqn. 7.1 below:

$$Y_{Decay} = \frac{\int \rho(p_{T_{\pi^0}} \to p_{T_\gamma})\epsilon^{-1}(p_{T_{\pi^0}})N_{\pi^0-h}dp_{T_{\pi^0}}}{\int \rho(p_{T_{\pi^0}} \to p_{T_\gamma})\epsilon^{-1}(p_{T_{\pi^0}})N_{\pi^0}dp_{T_{\pi^0}}} \tag{7.1}$$

The two pieces of note in the above equation are ρ, which gives the probability that a given single photon came from a π^0 decay, and the second is ϵ, the π^0 reconstruction efficiency. For

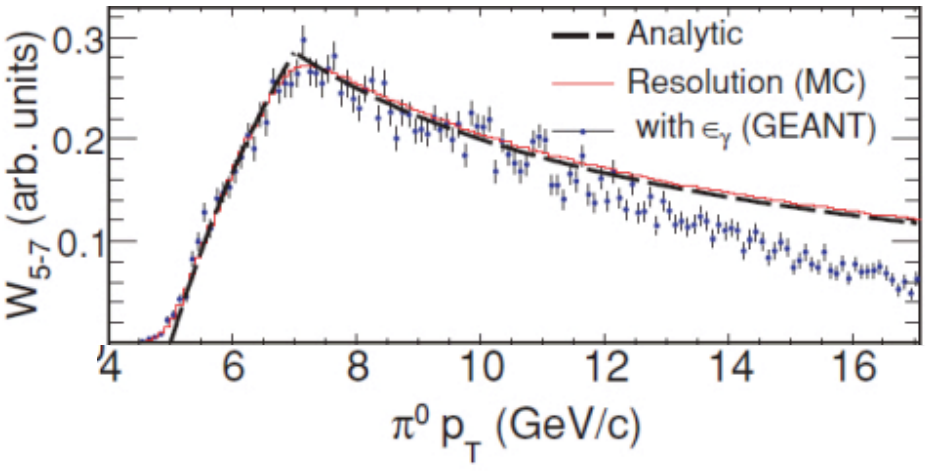

Figure 7.1: The probability weighting function giving the probability that a given π^0 will have a decay daughter with $5 < p_T^\gamma < 7$ GeV/c.

previous analyses, such as that in [34], ρ is calculated by simulating π^0 decays via Monte-Carlo. The resultant distributions of this process are shown in Fig. 7.1. The data points are the results of the Monte Carlo, which includes smearing due to simulated detector effects. The dashed black line is from calculation, the red line is from simulation with no simulated detector response, and the data points are from simulation with simulated detector effects.

After estimating the contribution from decay photon-hadron correlations, they can then be subtracted from the inclusive photon-hadron correlations to yield the direct photon-hadron correlations via a statistical subtraction procedure. The total yield of hadrons associated to high momentum photons is given by Eqn. 7.2.

$$N_{Inclusive}Y_{Inclusive} = N_{Direct}Y_{Direct} + N_{Decay}Y_{Decay} \tag{7.2}$$

where N represents the total number of direct, decay, and inclusive photon triggers, and

Y represents the per-trigger yield of hadrons for a given trigger photon type. Rearranging Eqn. 7.2 to isolate the per-trigger yield of direct photons yields we find

$$Y_{Direct} = \frac{R_\gamma Y_{Inclusive} - Y_{Decay}}{R_\gamma - 1}. \tag{7.3}$$

Here, we have introduced the observable R_γ, which is defined as

$$R_\gamma = \frac{N^\gamma_{Inclusive}}{N^\gamma_{Decay}} \tag{7.4}$$

and has been measured independently. In order to cover the momentum range used in this analysis, the R_{gamma} result from PHENIX's Run 7 data set and used in [50] will need to be used. After performing the statistical subtraction procedure outline in Eqn. 7.3, one will have extracted the jet functions for the direct photon-hadron correlations, which can then be used to extract the same observables shown in Sec 5. The ability to compare π^0 and direct photon-triggered correlations will be a powerful tool, as it creates another handle on the path-length dependence of the energy loss suffered by hard partons due to medium interactions. One would expect that, because they do not suffer energy loss as they traverse the QGP, direct photons should have no preferential depth or geometry by which they emerge from the medium, especially at high p_T. Neutral pion triggers, however, are born from the fragmentation of strongly interacting partons, and so the requirement for them to serve as high momentum trigger particles might bias one's π^0 sample towards those whose parent parton underwent little to no energy loss. This phenomenon (referred to surface bias) tells

us nothing about the path length traverse by the recoil parton and might even force it to suffer an even greater amount of energy loss as it traverses a significant portion of the QGP away from its partner.

7.1.0.1 Previous PHENIX Direct Photon-Hadron Correlation Results

In preparation for extraction of the direct photon-hadron correlations from the 2014 200 GeV Au+Au data set, a similar set of results was published from the 2007, 2010, and 2011 200 GeV $Au + Au$ and $d + Au$ data sets [34], creating a highly differential set of measurements. [34]'s publication had originally stalled during internal review, but efforts over the course of this dissertation satisfied the PHENIX collaboration's internal review process, leading to the paper's publication in 2020. The integrated yields of direct photon-associated hadrons, I_{AA}, and I_{dA} as function of ξ for direct photon triggered correlations in 200 GeV $Au + Au$ and $d + Au$ collisions is shown in Fig. 7.2.

The behavior of the I_{AA} in Fig. 7.2 matches the behavior with those measured in Figs. 4.20 and 4.21, whereby we see suppression in the yield of high-momentum (low ξ) particles, and an enhancement in the yield of low-momentum (high ξ) particles relative to the yields in the $p + p$ baseline. The I_{dA} measurement, however, finds no significant deviation (to within both statistical and systematic uncertainty) from the $p + p$. This lack of modification is an interesting juxtaposition to the discovery of flow in small systems measured in [44]. This phenomenon might be explained by the creation of a QGP medium that is small enough such that it is missed or only very lightly traversed by hard partons, resulting in negligible energy loss.

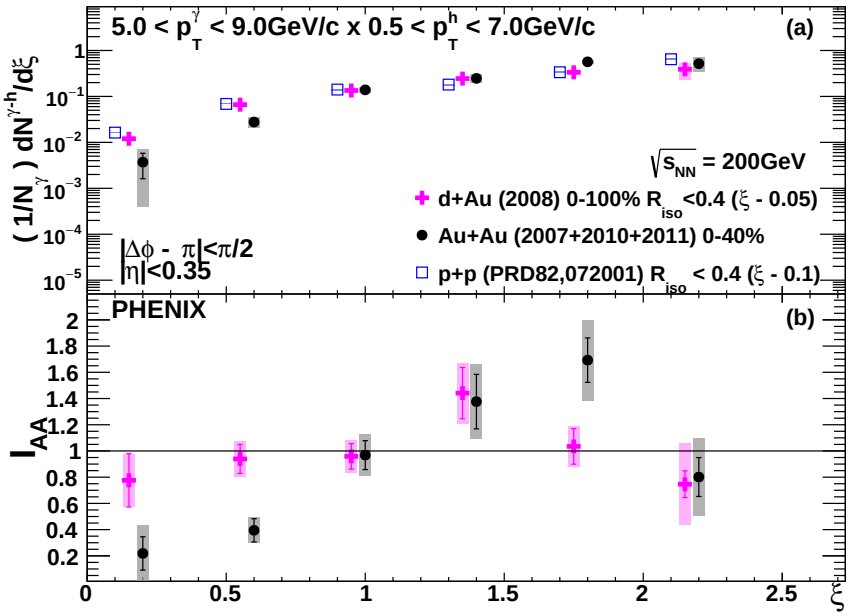

Figure 7.2: Top: Integrated yields of hadrons associated with direct photons with $5 < p_T^{\gamma} < 9$ GeV/c in n 200 GeV $Au+Au$ (Black), $d+Au$ (Pink), and $p+p$ (Blue) collisions. Bottom: I_{AA} and I_{dA} in 200 GeV $Au+Au$ and $d+Au$ collisions. The radius of the isolation cones used in the $p+p$ and $d+Au$ collisions is shown next to their respective legend entries, along with their offset along the ξ-axis, which is done for visual clarity.

Fig. 7.3 shows again the direct photon I_{AA} in 200 GeV $Au+Au$ collisions, but this time varies the range over which the integrated range is calculated. One can see that, in the $5 < p_T^{\gamma}, 7$ direct photon bin, especially, the enhancement measured in $Au+Au$ has a large dependence on how large the angle of integration is. It can be see that the enhancement is widest for the largest opening angle (black points) and smallest (almost non-existent) for the narrowest opening angle (red). This is consistent with the I_{AA} measurement made as a function of $\Delta\phi$ shown in Fig. 5.5, where the softest particles see a significant enhancement to their yields that is most prominent at wide angles to the away-side jet peak ($\Delta\phi \approx \pi$). Additionally, the suppression in the yield of high momentum associated particles seems

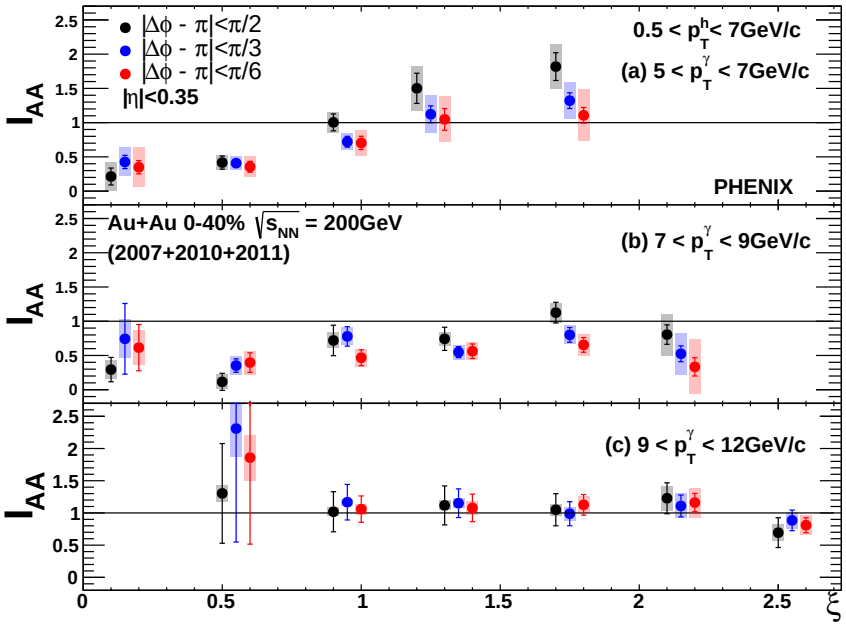

Figure 7.3: Direct photon I_{AA} in 200 GeV $Au + Au$ collisions in three direct photon momentum windows. Each window shows the I_{AA} calculated with an integration range of $|\Delta\phi - \pi| < \pi/2$ (black), $|\Delta\phi - \pi| < \pi/3$ (blue), and $|\Delta\phi - \pi| < \pi/6$ (red).

agnostic to the integration range in Fig. 7.3, and, correspondingly see the same suppression level at all $\Delta\phi$ in Fig. 5.7.

Both Fig. 7.3 and Fig. 7.2 show that the crossover point from suppression to enhancement as a function of ξ does not occur at a fixed value of ξ, whereas measurements from π^0-triggered correlations as a function of the associate hadron momentum do appear to have a fixed transition point. This is currently best understood by understanding the suppression as being a response from the medium to the energy embedded in it. The fixed transition of the transition point along the p_T axis would appear to mean that the medium re-emits the energy lost to it in a fixed momentum range that is independent of the parent parton's momentum. This, in turn, suggests that the enhancement measured at high ξ is due to a

response from the medium to the energy embedded in it, rather than a modification to the parent parton's fragmentation function.

Lastly, it should be noted that the statistical error bars in Fig. 7.3 and Fig. 7.2 are quite large, and this is despite using three runs and an expanded centrality range of $0-40\%$. The analysis of the combined $\sim$30 billion events from the 2014 and 2016 should offer enough statistical power to break this apart into a measurement done in the $0-20\%$ and $20-40\%$ centrality bins while either keeping the relative statistical uncertainty the same, or possibly even decreasing it. Additionally, these measurements will be made as a function of p_T rather than ξ to explore the behavior and location of the transition point in the I_{AA}. A measurement of the I_{AA} as a function of $\Delta\phi$ for direct photon-hadron correlations will also be an immensely important measurement as the first direct photon-tagged, substructure-like measurement by PHENIX.

7.2 sPHENIX

In addition to the work done with data taken by the PHENIX detector, a substantial amount of work was done for the preparation of a new particle detector, PHENIX's successor experiment, sPHENIX. sPHENIX is a next-generation, precision jet and upsilon detector scheduled to begin taking data in 2023. It is the successor experiment to the PHENIX experiment and will take its place at the 8 o'clock position on the RHIC beamline. A schematic of the sPHENIX detector is shown in Fig. 7.4. Charged particle tracking is handled by a combination of the MAPS (Monolithic Active Pixel Sensor) Vertex Dectector (MVTX), Time Projection Chamber (TPC), and the Intermediate Tracker (INTT), with emphasis put on the ability to accurately and reliably reconstruct charged tracks emerging from secondary decay vertices due to heavy flavor decays. Secondly, calorimetry is handled by the Electromagnetic Calorimeter (EMCal), which is responsible for measuring the energy of electrons and photons, and the Inner and Outer Hadronic Calorimeters (oHCAl and iHCal), which are responsible for measuring the energy of both neutral and charged hadrons. sPHENIX's calorimetry subsytems are critical in its role in making unbiased, fully-reconstructed jet measurements, and the hadronic calorimeters in particular will be the focus of this section.

7.2.1 The Hadronic Calorimeter

The sPHENIX haronic calorimeters are composed of scintillating tiles sandwiched between layers of metal absorber plates. These plates are made of aluminum in the iHCal, which will be situated inside the central magnet, and steel in the oHCal. Each tile in the HCal

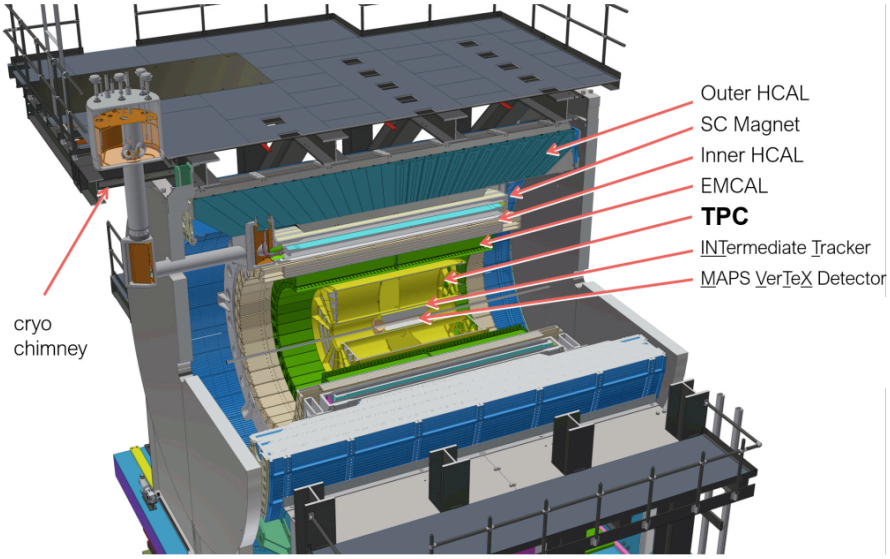

Figure 7.4: Cross-section of the sPHENIX detector currently under construction at Brookhaven National Laboratory

is composed primarily of polystyrene with an organic scintillator mixed in, allowing it to release light when struck by a charged particle. This scintillation light is then captured by a wavelength-shifting fiber and routed to one end of the tile, where a Silicon Photomultiplier (SiPM) resides. In order to reduce the amount of readout electronics needed, signals from sets of tiles called towers are aggregrated into one and readout as a single signal. These towers are composed of four tiles in the inner HCal, and five in the outer HCal. The physical positioning of the tiles within the detector along with breakdowns of the number of tiles and readout components for the outer HCal is shown in Fig. 7.5.

As noted in Fig. 7.5, the tiles of the hadronic calorimeters are tilted in ϕ to ensure that particles embed energies in multiple tiles. Additionally, the shape of the tiles changes as a function of their location in pseudorapidity, as shown in Fig. 7.6. This shape change accounts for the fact that particles leave the interaction region leave at different angles. Thus, making

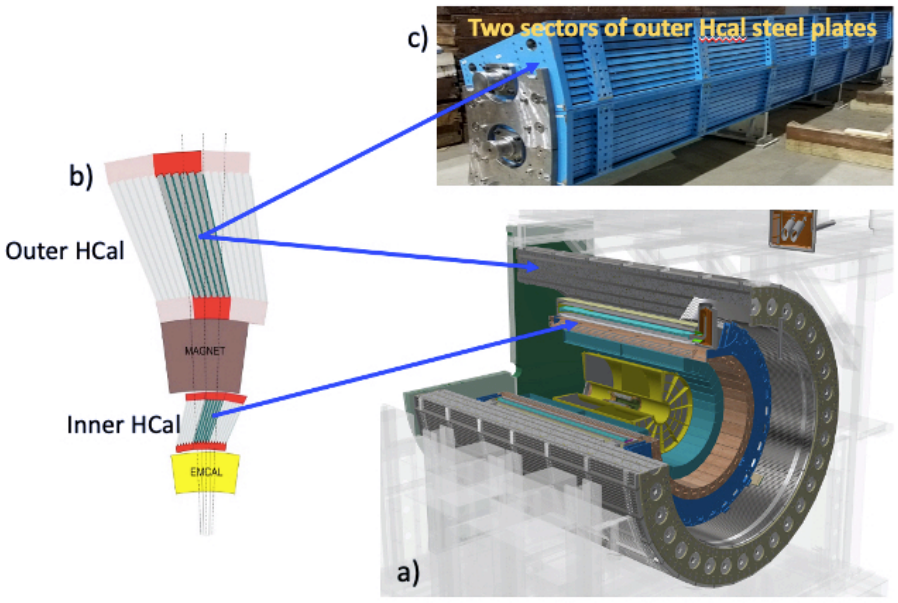

Figure 7.5: A) The sPHENIX barrel. B) Going from inner to oute radius: the electromagnetic calorimeter, followed by the inner hadronic calorimeter, which serves as its support structure, and the outer hadronic calorimeter. The small dotted lines represent particle trajectories. One can also see the relative tilt of the inner and outer hadronic calorimeters, which is chosen to ensure that particles strike at least four scintillator tiles. C) A sector of the outer hadronic calorimeter in building 1008. While the blue paint also makes it look cool, the paint is also there to prevent the steel from rusting. Photos courtesy of Xiaochun He.

the tiles projective in η increases the path length travelled through the tiles by the particles, improving the chances that the energy in a given hadronic shower will be relegated to a single tower.

Extensive testing of the hadronic calorimeter subsytems was carried out via prototypes using test beams at Fermi National Accelerator Laboratory (also known as Fermi Lab) near Batavia, Illinois. Test beam procedures at Fermi Lab allow for the characterization of a given detector's performance by particle beams of a known energy through it and measuring the detector's response. Fig. 7.7 shows the energy resolution as a function of the input for different combinations of calorimetry subsystems, along with fits to the data, from which

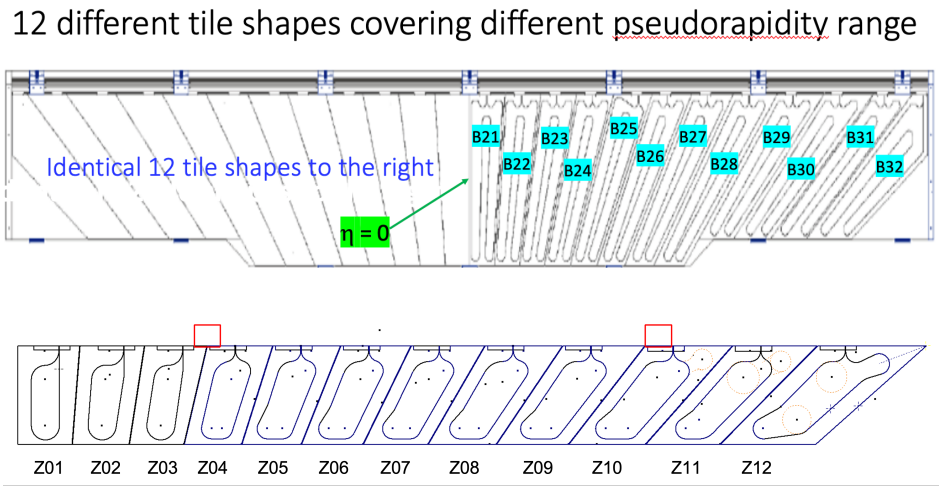

Figure 7.6: Depiction of the projective tilt in the outer (Top) and inner (Bottom) hadronic calorimeters.

the energy resolution and response linearity, both key physics performance parameters, can be determined. For the hadronic calorimetry system in paricular, it was found that the subsystem's resolution was $74.9\%/\sqrt{E}$ when using the inner and outer hadronic calorimeters, which meet the project's requirement of having a hadronic energy resolution of less than $100\%/\sqrt{E}$.

While the energy resolution of the hadronic calorimeters was already shown to have met the project's intended goal, it was questioned if the overall performance could be improved. At the time of the test beams, it was noticed that the response of individual scintillator tiles within the HCal could vary quite significantly. Thus, if tiles of vastly different performance characteristics were placed in the same tower together, the accuracy of the reconstructed jet energy would suffer. Therefore, a plan was put forward to characterize the performance of each scintillator tile before its placement into the detector in order to guide their placement into towers.

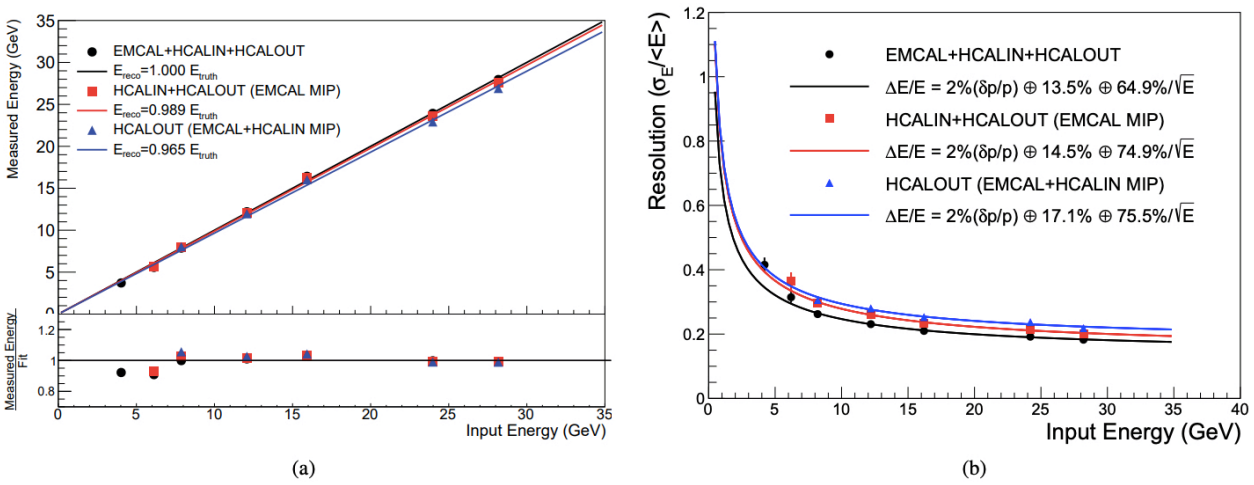

Figure 7.7: A) Reconstructed energy as a function of input energy for different combinations of calorimetry subsystems. The EMCal, inner HCal, and outer HCal's combined response is shown in black. Response from just the inner and outer HCals is in red, and the response of just the outer HCal is in blue. First-order polynomial fits to the data are shown using the same color scheme. B) Energy resolution for various calorimetry subsystem combinations as a function of the input energy. The EMCal, inner HCal, and outer HCal's combined response is shown in black. Response from just the inner and outer HCals is in red, and the response of just the outer HCal is in blue.

7.2.2 Tile Testing at Georgia State University

7.2.2.1 Tile Production and Initial Quality Checks

The scintillating tiles for the hadronic calorimeters are produced by a Russian company named UNIPLAST. There, individual tiles are cut from a $\sim$ 9 meter-long slab of extruded scintillating plastic. The individual tile shapes are then milled via CNC from the extruded slab, after which workers smooth the sides of the tiles by cutting off excess plastic manually. Next, the tiles are submerged in a special liquid for a brief period of time, which deposits onto them a white coating, which helps prevent scintillation light from leaking out. Then, a routing for the wavelength-shifting fiber is cut into the tile, and a wavelength-shifting fiber is

Figure 7.8: Pallets of tiles at GSU, ready to be unpacked and tested.

installed by hand. A special optical glue is then used to cement the fiber into place. Finally, the tiles are wrapped in a layer of Tyvek and a layer of Tedlar. The former is again to help prevent light leaker, and the latter is give the tiles a smooth exterior so they can easily slide into the metal of the calorimeters. Fiducial checks on the tiles' light yields are also performed, and low performing tiles are not shipped to GSU.

The tiles arrive at GSU in large shipping pallets containing roughly 18 boxes each. The pallets are broken downa and the boxes moved to a storage space near the lab where they will be tested. Upon unboxing the tiles undergo three quality control checks. The first is an initial inspection by eye on the overall quality of the tile. Records are kept of any tiles that are damaged or malformed (e.g., having torn wrapping or a significant warp). Next, tiles are passed through a glass dimension checker to test the thickness of the tiles shown in Fig. 7.10.

Special care is taken not to force the tiles through the thickness gauge if met with resistance, as the gap in the thickness corresponds to the tile's thickness when wrapped. Next the tiles are placed into a dimension checker, shown in Fig. 7.9, made especially for this project in a collaborative effort between GSU's machine shop and BNL. The dimension checker is a large slab of aluminum with dozens of holes drilled into it at fixed positions. Each of the wholes has a number that corresponds to a certain tile shape, and when all wholes of a given number are filled with the provided metal pins, they outline the shape of that tile. Tiles are then placed within the dimension checker to see if they fit snugly within the pegs. This assures that the longitudinal dimensions of the tile are within specification.

Finally, two reference tiles are selected at random to serve as dummy reference tiles. These serve as the trigger for the CAEN DT-5702 readout system that records the tiles' light output. 8 standard tests, as outlined below, are performed, and the light output from each tile is calculated relative to the dummy reference tiles. Then, two tiles whose light yield is closest to the average are chosen. This is done to select tiles whose performance reflects the population of the tiles from the beginning, thus minimizing the need for re-calibrations down the line.

7.2.2.2 Relative Light Yield Characterization

In order to characterize the relative performance of the hadronic calorimeter's scintillating tiles, the response of the tiles to being struck by cosmic ray muons is measured for a period of twenty minutes for the outer HCal tiles and thirty minutes for the inner HCal tiles. The time difference is to account for the difference in cosmic ray flux due to the difference in surface

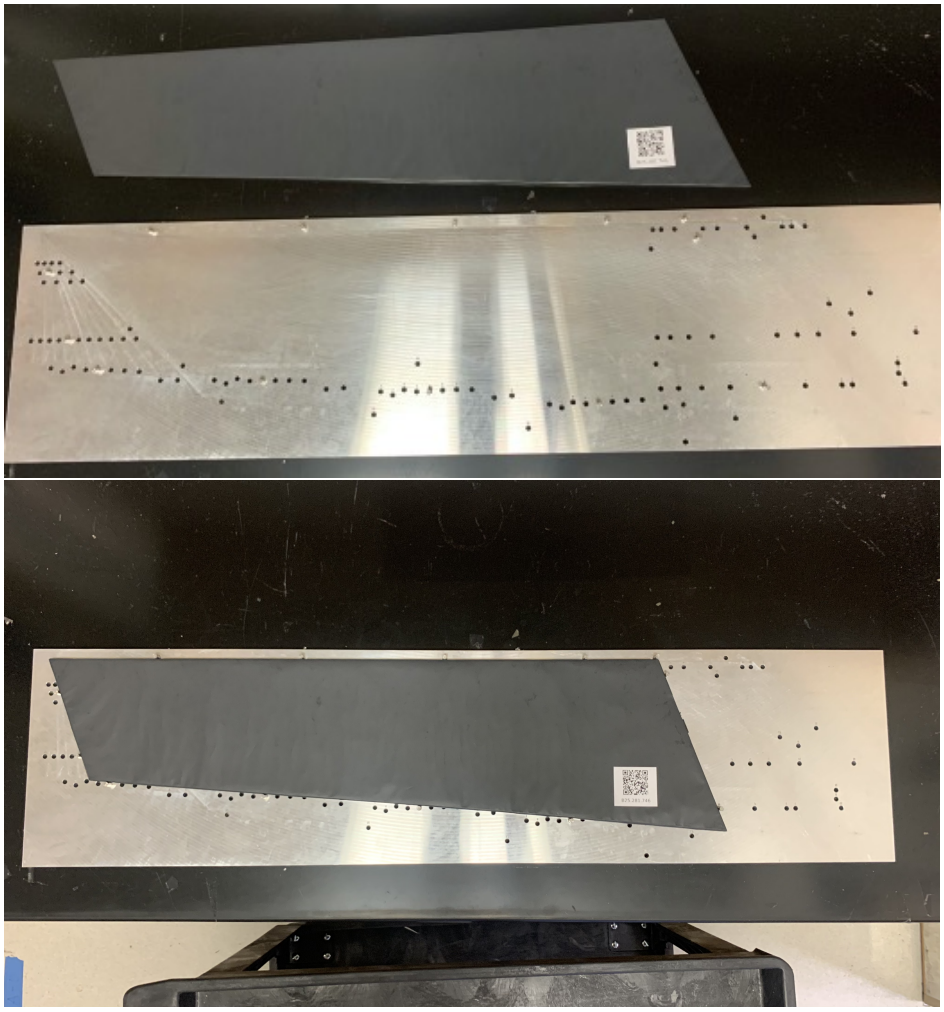

Figure 7.9: Top: The tile dimension checker fitted with pegs for the B25 tile shape. Bottom: A B25 fitted into the dimension checker

area between the inner and outer tiles. In order to measure this response, the tiles are placed into a test stand, which was designed jointly between GSU and Brookhaven National Laboratories and is shown in Fig. 7.11 during a test of inner tiles. Initial prototypes of the test stand were made at GSU in the course of study for this thesis over the course of many tests with pre-production tiles, and these tests helped inform the specifications for the final version of the test stand.

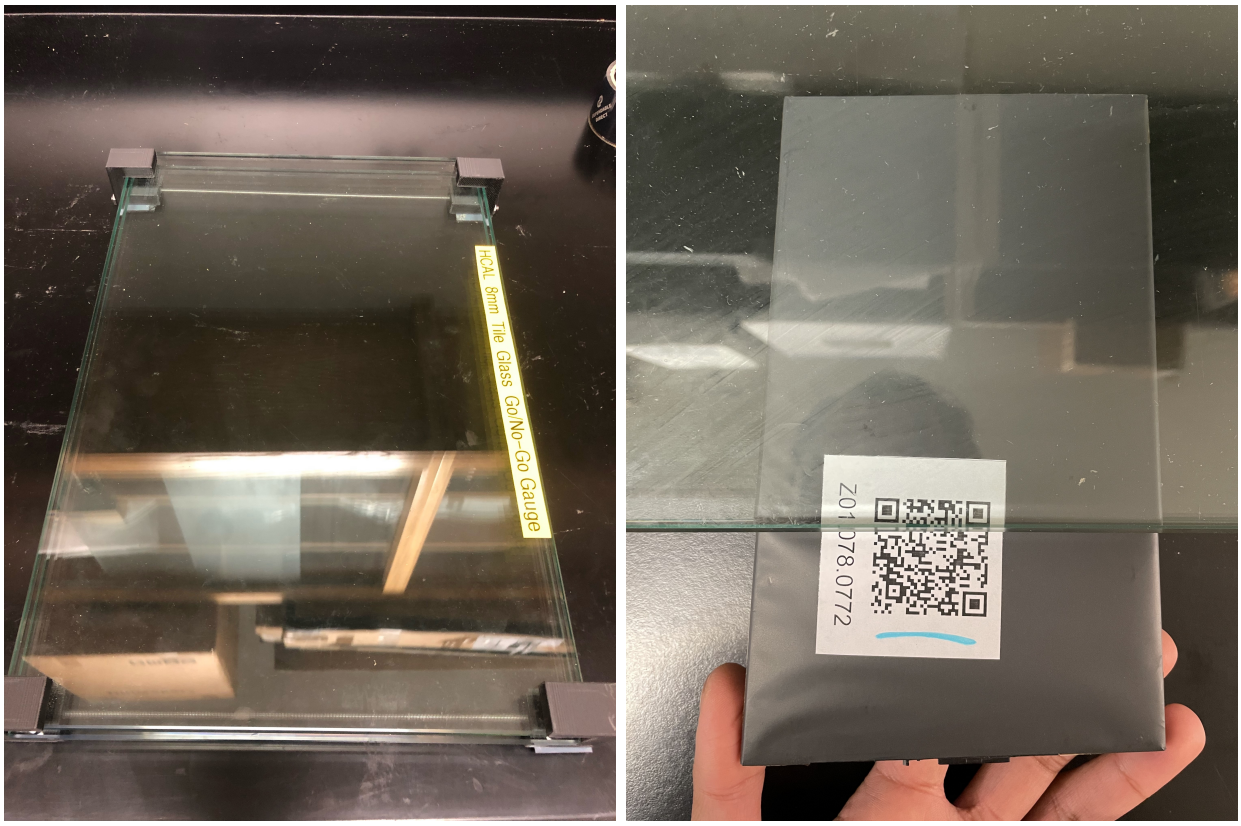

Figure 7.10: Left: Glass gauge for checking a tile's thickness. Right: A Z01 tile being inserted into the gauge. One can see the blue mark on the tile's ID sticker, indicating that it did not fit smoothly through the thickness gauge.

Tiles are tested eight at a time as shown in Fig. 7.11. As cosmic rays strike the tile, they cause it to scintillate, and this scintillation light is then captured captured by a wavelength shifting fiber embedded in the tile, which then routes it to an SiPM at the base of the tile. The signal from the SiPM is then recorded by a CAEN DT-5702 unit, which records the magnitude of the analogue-to-digital conversion (ADC) signal. The standard test length was determined by collecting data for increasingly longer time intervals until such a point that fluctuations in the measured MPV were negligible. Additionally, the threshold value on the CAEN unit was found by varying it until the tests measured a muon flux of approximately

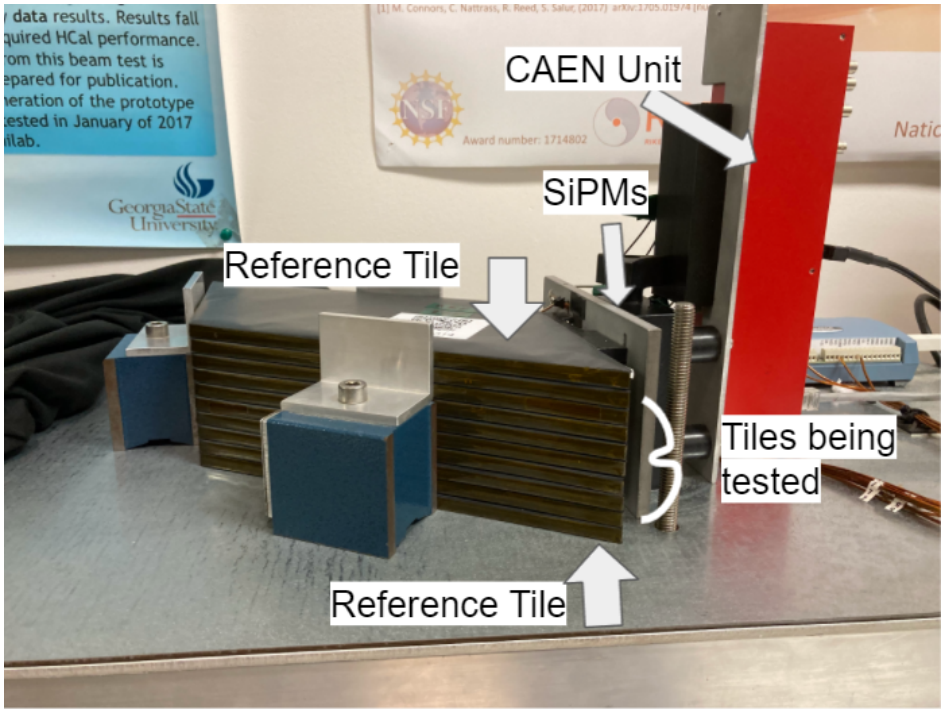

Figure 7.11: Configuration of a standard test with eight inner tiles sandwiched between two inner tile reference tiles.

$\frac{1}{3}$ the sea-level flux of 1 count per minute per square centimeter. Over the course of the test length, histograms for each tile are filled with these ADC values, eventually forming a Landau distribution. This distribution is then fit with a Landau function, which is a probability density function defined by Eqn. 7.5

$$p(x) = \frac{1}{\xi}\phi(\lambda) \tag{7.5}$$

Where ϕ is defined by

$$\phi(\lambda) = \frac{1}{2\pi i}\int_{c-i\infty}^{c+i\infty} e^{\lambda s + s\log s} ds \tag{7.6}$$

And $\lambda = (x - x_0)/\xi$, where x is the ADC value, ξ is the width parameter which is analagous to the Gaussian standard deviation, σ, and x_0 is the location parameter which is analogous to the Gaussian mean, μ. An example of this fit to data collected during a test is shown in Fig. 7.12. The key parameter to extract from the Landau fit is the "Most Probable Value" (MPV) of the distribution, which is the location along the ADC axis of the peak.

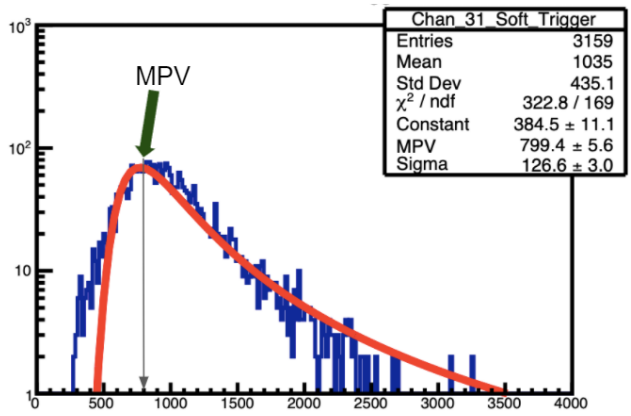

Figure 7.12: Landau fit to an ADC distribution. The text near the peak of the distribution denotes the location of the "Most Probable Value" (MPV) for the distribution.

The MPV is then used as a proxy for the average light yield of a given tile and compared to the MPV's of a set of reference tiles that are included in every test and serve as triggers for the CAEN unit, thus giving rise to the Performance Ratio, defined by Eqn. 7.7. The performance ratio then allows us to compare the relative light yields for all tiles of a given type and then sort them into towers such the variance in performance between tiles in a given tower is minimized.

$$PR = \frac{MPV_{Tile}}{< MPV_{Refs} >} \tag{7.7}$$

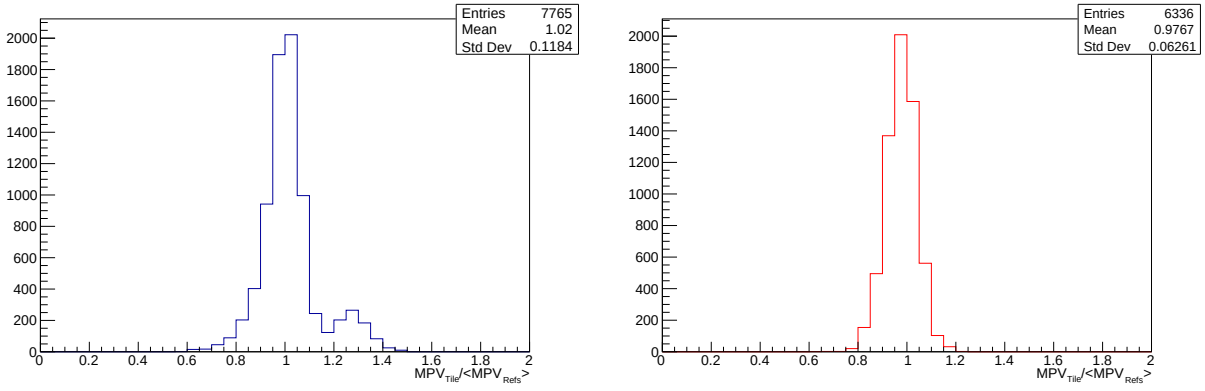

Figure 7.13: Final performance ratio distributions for the outer (Left) and inner (Right) HCal tiles tiles.

Fig. 7.13 shows the final distribution of performance ratios for the outer and inner tiles. The distributions for both the inner and outer tiles are peaked about 1 with a modest standard deviation. These distributions have been corrected for inter-channel performance variance, which were developed over the course of this dissertation. Code for this correction, as well as for other studies by undergraduates and graduate students alike that were peer-mentored over the course the pursuit of this PhD. have resulted in a robust suite of code maintained on GitHub, as well. The mean and deviation of the final performance ratio distributions tell us that the tiles in both calorimeters are very self-similar, which will make their assortment into towers much easier than if the distributions were extremely wide. One might notice the small peak around 1.25 in the outer tiles' PR distribution. During the production of the B24 tiles, there was a marked decrease in the quality of the fiber embedded in the tiles, making them more prone to crazing and light leaks. These tiles with sub par fibers made up the first batch of tiles sent to GSU, and, thus, is the batch reference tiles were

selected from. Later on the issue was rectified, which means that later tiles had a higher light output on average, thus creating a secondary peak.

7.2.2.3 Impact of the COVID-19 Pandemic

In the early months of 2020, the first rapid onset of the COVID-19 pandemic began. While the pandemic spent January and February relegated off the mainland United States, by March, American COVID cases were on the rise, prompting a shut-down of Georgia State University, and, thus, a halt on the tile testing. Similar measures were taken at Brookhaven National Laboratory, and construction on the sPHENIX detector halted altogether for a approximately three months. Beginning in June of 2020, however, laboratories at GSU began to reopen with new safety guidelines. The GSU HCal lab, in particular, adopted social distancing and mask and glove wearing policies to ensure the safety of the students working in the lab. Additionally, whereas in the early phases of the tile testing project as many as twelve graduate and undergraduate students could be on hand at any given time, this number was restricted to two for safety. In spite of these restrictions, however, tile testing resumed in June of 2020, and the project quickly regained traction. Through the hard work of a dedicated team of undergraduate and graduate students, including the author himself, the tile testing project ultimately succeeded in testing all hadronic calorimeter tiles and successfully shipping them to BNL, where they are currently being installed. Although the pursuit extracting direct photon-hadron correlations from PHENIX's Run 14's data set had to be abandoned in part due to the pandemic, that sPHENIX remains on schedule means there will be many more opportunities for photon-jet measurements in the author's future.

7.2.2.4 Current sPHENIX Project Status

Ultimately, the tile testing project at Georgia State University was a wonderful success. Every tile currently being installed in the outer and inner hadronic calorimeters has an associated performance ratio attached to it that is used to help sort it into a tower with tiles of a similar performance ratio. This sorting will help decrease the uncertainty on the reconstructed energy in a given tower, which, in theory, should help drive down the constant (also called the stochastic) term in the energy resolution shown in Fig. 7.7. In total, 6,336 inner HCal tiles were tested, with 99.6% having a performance ratio higher than 0.8. During the pre-production phase of the outer HCal tile testing, 1,506 tiles were tested, with a 98.1% yield of good tiles, and, finally, during the full production phase of the outer HCal tile testing, 6,218 tiles were tested, with a 98.6% yield of good tiles. Installation of the tiles into sPHENIX is also well underway, as evidenced by Fig. 7.14, where one can see the BABAR magnet's installation into the sPHENIX cradle. The outer hadronic calorimeter can be seen directly beneath where the magnet is being installed, capped with black end-pieces. Furthermore, the sPHENIX project as a whole is on-time and is still scheduled to take its first round of data in the spring of 2023. That this start date has not changed is due to the immense work of all the students, faculty, technicians, and engineers that make up the collaboration, and indeed, the family of the sPHENIX experiment.

Figure 7.14: Installation of the BABAR magnet into the sPHENIX cradle.

CHAPTER 8

Summary

This dissertation focuses on two endeavours to study the phenomenon of jet modification that arises in ultra-relativistic nucleus-nucleus collisions. The first is the study of π^0–hadron correlations in 200 GeV Au+Au collisions measured by the PHENIX detector, and the second is the robust and rigorous testing of the sPHENIX hadronic calorimeter's scintillating tiles. The end goal of these studies is to provide robust, experimental results that can offer insights into the quantification of the properties of the Quark-Gluon Plasma such as its transport coefficients via comparison to theoretical models.

The π^0–hadron jet functions are extracted by subtracting off angular correlations from collective flow, up to the fourth harmonic. The away-side jet peak of the jet functions are integrated, and this quantity, Y_{AA}, when divided by the same quantity in baseline $p+p$ collisions, yields the I_{AA}. The I_{AA} in both the 0–20% and 20–40% centrality bins shows a suppression in the yield of high momentum charged hadrons, that eventually transfers to an enhancement in the yield of low momentum particles. This is consistent with partonic energy loss due to medium interactions in the form of soft gluon radiation. The energy loss leads to the detection of fewer high momentum particle associated with the jet, and a larger quantity of soft particles relative to baseline $p+p$ measurements.

The I_{AA} result is then extended by dividing the jet functions point-by-point in $\Delta\phi$ space, which allows quantification of jet modification at the sub-structure level. The I_{AA} vs. $\Delta\phi$ measurement shows again a suppression in the yield of high momentum associate hadrons,

and it further shows that this suppression is most severe and begins to develop first near the core of the away-side jet as one goes to higher and higher associate hadron momentum. Furthermore, as one goes to lower associate hadron momentum, the I_{AA} vs. $\Delta\phi$ shows that the "skirt" of the jet (i.e. regions further away from the away-side jet peak) are the first to see the enhancement in the yield of soft particles, and that the enhancement is consistently largest at these large angles. This latter phenomenon is consistent with the concept that jets in heavy-ion collisions are measured to be broader than their counterparts in $p+p$ collisions (broader here meaning their particle distributions are more widely distributed spacially). The I_{AA} vs. $\Delta\phi$ measurement cements the idea that this broadening occurs because of an excess of soft particles at the periphery of the jet.

The primary pitfall of the I_{AA} vs. $\Delta\phi$ as an observable, however, is its sensitivity to near-zero quantities that occur in the $p+p$ jet function as one moves further and further away from the away-side jet peak. These quantities lead to large statistical and systematic uncertainties that restrict the range of the observable to the region closest to the away-side peak before the uncertainties grow unreasonably large. To combat this, the observable D_{AA} vs. $\Delta\phi$ has been measured. This observable is the difference, rather than the quotient, of the $Au+Au$ and $p+p$ jet functions point-to-point in $\Delta\phi$ space. With reduced uncertainties, the D_{AA} vs. $\Delta\phi$ observable is able to probe further away from the away-side jet peak, which will allow it to better constrain theoretical models such as those discussed in Sec. 5.5. Phenomenologically, this obersable is consistent with the I_{AA} vs. $\Delta\phi$ result in that it observes a suppression in the yield of high momentum associate hadrons that is strongest near the core of the away-side

jet peak, and it also sees an enhancement in the yield of low momentum particles that grows as one moves away from the away-side jet peak. As one approaches the region $|\Delta\phi - \pi| \approx \pi$, this enhancement begins to decrease. Comparisons to the model calculations discussed in Sec. 5.5 are necessary to fully understand the mechanisms at work, however. In particular, the D_{AA} vs. $\Delta\phi$ measurement presented in this thesis would be an excellent tool to elucidate the relationship between the "wake" and "no wake" modes presented by the Hybrid model due to how differential in bother trigger and associate hadron momentum it is.

The results presented in this dissertation offer a highly differential framework for theoretical comparisons owing to the high statistics data set used which was taken by the PHENIX detector in 2014, which, in turn, will allow for the nuclear physics community to further quantify aspects of the Quark Gluon Plasma. Further efforts to provide rigorous and high statistics measurements are currently ongoing on two fronts. The first by other members of the PHENIX collaboration to extract direct photon-hadron correlations from the 2016 data set taken by PHENIX. As discussed in Chap.7, direct photon-hadron correlations are "golden channel" for jet modification studies as the medium is essentially transparent to the direct photon, allowing it to escape the medium unmodified, making it an excellent proxy for the total energy of the recoil jet's energy to leading order. Looking towards the (now very near) future, sPHENIX, the successor experiment to PHENIX, will be capable of making high-precision measurements of jets and upsilons when it begins its data taking mission in 2023. To this end, the nuclear physics group at Georgia State University took a leading role in the assembly of the sPHENIX Hadronic Calorimeter, a subsytem that is criticial to sPHENIX's

goal of making unbiased jet measurements. My fellow graduate students and I tested and quantified the relative light yield of the inner and outer hadronic calorimeter's over $15,000$ scintillator tiles with the end goal being to improve the subsystem's response by grouping tiles with similar performance together. Despite a major setback on account of the global COVID-19 pandemic, we accomplished our goal of testing all tiles for the hadronic calorimeter while inducing no delays to the project overall. sPHENIX's outer hadronic calorimeter is currently fully assembled and installed with the inner hadronic calorimeter not far behind. Ultimately, ours efforts were an immense success.

As is the case with many projects and endeavors, time remains the scarcest of resources. As sPHENIX grows closer and closer to data taking, so too does its need for person-power grow, prompting the last remaining PHENIX analyzers to switch their focus to sPHENIX. A similar phenomenon will occur shortly after sPHENIX's brief three-year data taking run, whereby focus, energy, and person power will shift to the conversion of the Relativistic Heavy-Ion Collider to the Electron-Ion Collider, a next generation collider that will allow precision measurements of the structure of the interior of hadrons. The ever-forward march of time might seem daunting, but it is proof that our efforts in our field still yield forward progress. This dissertation's results will serve as a benchmark for the measurement of even more impressive results from the PHENIX collaboration and, indeed, are part of the reason why sPHENIX's physics mission remains intact. It is a small, but mighty step in helping the field to accomplish its goal of understanding the cacophonous soundscape, the sonorous heavy metal mash-up that are the nuclear strong force and quantum chromodynamics.

REFERENCES

[1] S.L. Glashow, The renormalizability of vector meson interactions, Nucl. Phys. 10 (1959) 107–117. doi:10.1016/0029-5582(59)90196-8.

[2] A. Salam, Weak and Electromagnetic Interactions, Conf. Proc. C 680519 (1968) 367–377. doi:10.1142/9789812795915_0034.

[3] S. Weinberg, A model of leptons, Phys. Rev. Lett. 19 (1967) 1264–1266. doi:10.1103/PhysRevLett.19.1264.

[4] D. I. Kazakov, The higgs boson is found: what is next?, Physics-Uspekhi 57 (9) (2014) 930–942. doi:10.3367/ufne.0184.201409j.1004.

[5] J. Beringer, et al., Review of particle physics, Phys. Rev. D 86 (2012) 010001. doi:10.1103/PhysRevD.86.010001.

[6] F. Capozzi, E. Lisi, A. Marrone, D. Montanino, A. Palazzo, Neutrino masses and mixings: Status of known and unknown 3 ν parameters, Nuclear Physics B 908 (2016) 218–234. doi:10.1016/j.nuclphysb.2016.02.016.
URL https://doi.org/10.1016%2Fj.nuclphysb.2016.02.016

[7] K. Olive, Review of particle physics, Chinese Physics C 40 (10) (2016) 100001. doi:10.1088/1674-1137/40/10/100001.
URL https://doi.org/10.1088/1674-1137/40/10/100001

[8] K. N. and, Review of particle physics, Journal of Physics G: Nuclear and Particle Physics 37 (7A) (2010) 075021. doi:10.1088/0954-3899/37/7a/075021.
URL https://doi.org/10.1088/0954-3899/37/7a/075021

[9] M. E. Peskin, D. V. Schroeder, An Introduction to Quantum Field Theory, Westview Press, 1995, reading, USA: Addison-Wesley (1995) 842 p.

[10] S. Narison, QCD as a Theory of Hadrons: From Partons to Confinement, Cambridge University Press, 2004. doi:10.1017/CBO9780511535000.

[11] A. Deur, S. J. Brodsky, G. F. de Téramond, The QCD running coupling, Progress in Particle and Nuclear Physics 90 (2016) 1–74. doi:10.1016/j.ppnp.2016.04.003.
URL https://doi.org/10.1016%2Fj.ppnp.2016.04.003

[12] V. Khachatryan, et al., Measurement of the inclusive 3-jet production differential cross section in proton–proton collisions at 7 tev and determination of the strong coupling constant in the tev range, The European Physical Journal C 75 (5) (2015) 186. doi:10.1140/epjc/s10052-015-3376-y.

[13] S. Sarkar, et al., The Physics of the Quark-Gluon Plasma, Springer, Berlin, Heidelberg,

2010. doi:10.1007/978-3-642-02286-9.

[14] Z.-T. Liang, M. A. Lisa, X.-N. Wang, Global polarization effect in the extremely rapidly rotating qgp in hic (2019). arXiv:1912.07822.

[15] M. Connors, et al., Jet measurements in heavy ion physics, Rev. Mod. Phys. 90 (2018) 025005. doi:10.1103/RevModPhys.90.025005.

[16] J. Adam, et al., Production of light nuclei and anti-nuclei in *pp* and pb-pb collisions at energies available at the cern large hadron collider, Phys. Rev. C 93 (2016) 024917. doi:10.1103/PhysRevC.93.024917.
URL https://link.aps.org/doi/10.1103/PhysRevC.93.024917

[17] J. Adams, et al., Experimental and theoretical challenges in the search for the quark–gluon plasma: The star collaboration's critical assessment of the evidence from rhic collisions, Nuclear Physics A 757 (1) (2005) 102–183, first Three Years of Operation of RHIC. doi:https://doi.org/10.1016/j.nuclphysa.2005.03.085.
URL https://www.sciencedirect.com/science/article/pii/S0375947405005294

[18] Z. Fodor, S. Katz, Critical point of qcd at finite t and μ, lattice results for physical quark masses, Journal of High Energy Physics 2004 (04) (2004) 050–050. doi:10.1088/1126-6708/2004/04/050.
URL https://doi.org/10.1088/1126-6708/2004/04/050

[19] J. Wok, Pseudorapidity (2007).
URL https://commons.wikimedia.org/w/index.php?curid=5970403

[20] A. S. Carroll, et al., PHOBOS at RHIC: Some global observations, Pramana 61 (5) (2003) 865–876. doi:10.1007/BF02704455.

[21] V. Franco, R. J. Glauber, High-energy deuteron cross sections, Phys. Rev. 142 (1966) 1195–1214. doi:10.1103/PhysRev.142.1195.

[22] M.L. Miller, et al., Glauber modeling in high-energy nuclear collisions, Annual Review of Nuclear and Particle Science 57 (1) (2007) 205–243. doi:10.1146/annurev.nucl.57.090506.123020.

[23] X. Wei, PHENIX Reaction Plane Detector (2007).
URL https://www.bnl.gov/rhic/news/061907/story2.asp

[24] G. Aad, et al., Observation of long-range elliptic azimuthal anisotropies in $\sqrt{s} = 13$ and 2.76 tev *pp* collisions with the atlas detector, Phys. Rev. Lett. 116 (2016) 172301. doi:10.1103/PhysRevLett.116.172301.
URL https://link.aps.org/doi/10.1103/PhysRevLett.116.172301

[25] L. Adamczyk, et al., Beam-energy dependence of the directed flow of protons, antiprotons, and pions in au+au collisions, Phys. Rev. Lett. 112 (2014) 162301. doi:10.1103/PhysRevLett.112.162301.

[26] K. Aamodt, et al., Higher harmonic anisotropic flow measurements of charged particles in pb-pb collisions atsNN=2.76 TeV, Physical Review Letters 107 (3) (jul 2011). doi:10.1103/physrevlett.107.032301.
URL https://doi.org/10.1103%2Fphysrevlett.107.032301

[27] B. Alver, G. Roland, Collision-geometry fluctuations and triangular flow in heavy-ion collisions, Phys. Rev. C 81 (2010) 054905. doi:10.1103/PhysRevC.81.054905.
URL https://link.aps.org/doi/10.1103/PhysRevC.81.054905

[28] A. Adare, et al., Scaling properties of azimuthal anisotropy in Au + Au and Cu + Cu collisions at $\sqrt{s_{\rm NN}}$ = 200 GeV, Phys. Rev. Lett. 98 (2007) 162301. doi:10.1103/PhysRevLett.98.162301.

[29] D. Sharma, Measurement of light mesons by the PHENIX experiment at the RHIC, J. Phys. G38 (2011) 124082. doi:10.1088/0954-3899/38/12/124082.

[30] J. Adams, et al., Evidence from d + Au measurements for final-state suppression of high-p_T hadrons in Au + Au collisions at rhic, Phys. Rev. Lett. 91 (2003) 072304. doi:10.1103/PhysRevLett.91.072304.
URL https://link.aps.org/doi/10.1103/PhysRevLett.91.072304

[31] A. Adare, et al., Photon-hadron jet correlations in p+p and au+au collisions at $\sqrt{s_{NN}}$ = 200gev, Physical Review C 80 (2) (aug 2009). doi:10.1103/physrevc.80.024908.
URL https://doi.org/10.1103%2Fphysrevc.80.024908

[32] A. Majumder, A comparative study of jet-quenching schemes, Journal of Physics G: Nuclear and Particle Physics 34 (8) (2007) S377–S387. doi:10.1088/0954-3899/34/8/s25.

[33] W. Chen, S. Cao, T. Luo, L.-G. Pang, X.-N. Wang, Effects of jet-induced medium excitation in γ-hadron correlation in a+a collisions, Physics Letters B 777 (2018) 86–90. doi:https://doi.org/10.1016/j.physletb.2017.12.015.
URL https://www.sciencedirect.com/science/article/pii/S0370269317309929

[34] U. Acharya, et al., Measurement of jet-medium interactions via direct photon-hadron correlations in Au + Au and d + Au collisions at $\sqrt{s_{NN}}$ = 200 gev, Phys. Rev. C 102 (2020) 054910. doi:10.1103/PhysRevC.102.054910.
URL https://link.aps.org/doi/10.1103/PhysRevC.102.054910

[35] N. Borghini, U. Wiedemann, Distorting the hump-backed plateau of jets with dense

QCD matter, (2005). arXiv:hep-ph/0506218.

[36] J. Casalderrey-Solana, D. C. Gulhan, J. G. Milhano, D. Pablos, K. Rajagopal, Angular structure of jet quenching within a hybrid strong/weak coupling model, Journal of High Energy Physics 2017 (3) (mar 2017). doi:10.1007/jhep03(2017)135.
URL https://doi.org/10.1007%2Fjhep03%282017%29135

[37] P. M. Chesler, K. Rajagopal, Jet quenching in strongly coupled plasma, Physical Review D 90 (2) (jul 2014). doi:10.1103/physrevd.90.025033.
URL https://doi.org/10.1103%2Fphysrevd.90.025033

[38] C.-P. Wong, π^0-hadron correlations in 200gev $au + au$ collisions, PhD dissertation, Georgia State University (2020).
URL https://scholarworks.gsu.edu/phy_astr_diss/122

[39] A. Adare, et al., Transition in yield and azimuthal shape modification in dihadron correlations in relativistic heavy ion collisions, Phys. Rev. Lett. 104 (2010) 252301. doi:10.1103/PhysRevLett.104.252301.

[40] K. Adcox, et al., Formation of dense partonic matter in relativistic nucleus–nucleus collisions at rhic: Experimental evaluation by the phenix collaboration, Nuclear Physics A 757 (1) (2005) 184 – 283, first Three Years of Operation of RHIC. doi:https://doi.org/10.1016/j.nuclphysa.2005.03.086.

[41] I. Arsene, et al., Quark–gluon plasma and color glass condensate at rhic? the perspective from the brahms experiment, Nuclear Physics A 757 (1) (2005) 1 – 27, first Three Years of Operation of RHIC. doi:https://doi.org/10.1016/j.nuclphysa.2005.02.130.

[42] B. Back, et al., The phobos perspective on discoveries at rhic, Nuclear Physics A 757 (1) (2005) 28 – 101, first Three Years of Operation of RHIC. doi:https://doi.org/10.1016/j.nuclphysa.2005.03.084.

[43] J. Adams, et al., Experimental and theoretical challenges in the search for the quark–gluon plasma: The star collaboration's critical assessment of the evidence from rhic collisions, Nuclear Physics A 757 (1) (2005) 102 – 183, first Three Years of Operation of RHIC. doi:https://doi.org/10.1016/j.nuclphysa.2005.03.085.

[44] Aidala, C. and others, Creation of quark–gluon plasma droplets with three distinct geometries, Nature Physics 15 (2019) 214. doi:0.1038/s41567-018-0360-0.

[45] R. Vogt, Chapter 1 - kinematics and invariants, in: R. Vogt (Ed.), Ultrarelativistic Heavy-Ion Collisions, Elsevier Science B.V., Amsterdam, 2007, pp. 3 – 24. doi:https://doi.org/10.1016/B978-044452196-5/50001-3.

[46] Collider–Accelerator Department of RHIC, Relativistic heavy ion collider (rhic) configuration manual (2006).
URL https://www.bnl.gov/cad/accelerator/docs/pdf/RHICConfManual.pdf

[47] M. Allen, et al., Phenix inner detectors, Nuclear Instruments and Methods in Physics Research Section A: Accelerators, Spectrometers, Detectors and Associated Equipment 499 (2003) 549. doi:/10.1016/S0168-9002(02)01956-3.

[48] C. Adler, et al., The rhic zero-degree calorimeters, Nuclear Instruments and Methods in Physics Research Section A: Accelerators, Spectrometers, Detectors and Associated Equipment 499 (2) (2003) 433 – 436, the Relativistic Heavy Ion Collider Project: RHIC and its Detectors. doi:10.1016/j.nima.2003.08.112.

[49] K. Adcox, et al., Phenix central arm tracking detectors, Nuclear Instruments and Methods in Physics Research Section A: Accelerators, Spectrometers, Detectors and Associated Equipment 499 (2) (2003) 489 – 507, the Relativistic Heavy Ion Collider Project: RHIC and its Detectors. doi:10.1016/S0168-9002(02)01952-6.

[50] S. S. Adler, et al., Dense-medium modifications to jet-induced hadron pair distributions in Au + Au collisions at $\sqrt{s_{NN}} = 200$ GeV, Phys. Rev. Lett. 97 (2006) 052301. doi:10.1103/PhysRevLett.97.052301.

[51] S. S. Adler, et al., High-p_T charged hadron suppression in Au+Au collisions at $\sqrt{s_{NN}} =$ 200 GeV, Phys. Rev. C 69 (2004) 034910. doi:10.1103/PhysRevC.69.034910.
URL https://link.aps.org/doi/10.1103/PhysRevC.69.034910

[52] R. Brun, et al., GEANT3 users guide, CERN DD/EE/84-1 (1985).

[53] A. Adare, et al., Spectra and ratios of identified particles in au+au and d+au collisions at $\sqrt{s_{NN}} = 200$ gev, Phys. Rev. C 88 (2013) 024906. doi:10.1103/PhysRevC.88.024906.
URL https://link.aps.org/doi/10.1103/PhysRevC.88.024906

[54] J. Adam, et al., Jet–like correlations with neutral pion triggers in pp and central pb–pb collisions at 2.76 TeV, Physics Letters B 763 (2016) 238 – 250. doi:10.1016/j.physletb.2016.10.048.

[55] L. Adamczyk, et al., Jet–like correlations with direct–photon and neutral–pion triggers at $\sqrt{s_{NN}} = 200$ GeV, Physics Letters B 760 (2016) 689 – 696. doi:10.1016/j.physletb.2016.07.046.

[56] A. Adare, et al., Measurement of two–particle correlations with respect to second– and third–order event planes in Au + Au collisions at $\sqrt{s_{NN}} = 200$ GeV, Phys. Rev. C 99 (2019) 054903. doi:10.1103/PhysRevC.99.054903.

[57] R. A. Lacey, et al., Scaling of the higher-order flow harmonics: implications for initial-eccentricity models and the viscous horizon, , arXiv:1105.3782 (2011).

[58] A. Adare, et al., Azimuthal anisotropy of π^0 production in Au+Au collisions at $\sqrt{s_{NN}} = 200$ GeV: Path-length dependence of jet quenching and the role of initial geometry, Phys. Rev. Lett. 105 (2010) 142301. doi:10.1103/PhysRevLett.105.142301.

[59] A. Sickles, et al., Extraction of correlated jet pair signals in relativistic heavy ion collisions, Phys. Rev. C 81 (2010) 014908. doi:10.1103/PhysRevC.81.014908.

[60] L. Adamczyk, et al., Jet-like correlations with direct-photon and neutral-pion triggers at snn=200 gev, Physics Letters B 760 (2016) 689 – 696. doi:10.1016/j.physletb.2016.07.046.

[61] J. Adam, et al., Jet-like correlations with neutral pion triggers in pp and central pb–pb collisions at 2.76 tev, Physics Letters B 763 (2016) 238 – 250. doi:10.1016/j.physletb.2016.10.048.

[62] A. M. Sirunyan, et al., Using z boson events to study parton-medium interactions in pb-pb collisions, Phys. Rev. Lett. 128 (2022) 122301. doi:10.1103/PhysRevLett.128.122301.
URL https://link.aps.org/doi/10.1103/PhysRevLett.128.122301

[63] W. Chen, S. Cao, T. Luo, L.-G. Pang, X.-N. Wang, Medium modification of γ-jet fragmentation functions in pb+pb collisions at lhc, Physics Letters B 810 (2020) 135783. doi:https://doi.org/10.1016/j.physletb.2020.135783.
URL https://www.sciencedirect.com/science/article/pii/S0370269320305864

[64] G. Aad, et al., Medium-induced modification of z-tagged charged particle yields in Pb + Pb collisions at 5.02 tev with the atlas detector, Phys. Rev. Lett. 126 (2021) 072301. doi:10.1103/PhysRevLett.126.072301.
URL https://link.aps.org/doi/10.1103/PhysRevLett.126.072301

[65] A. Pun, Gamma–hadron and related two–particle azimuthal correlations results in phenix, in: Proceedings of the 13th International Workshop in High pT Physics in the RHIC and LHC Era, Proceedings of Science, 2019, p. 1.
URL https://pos.sissa.it/355/001/pdf

[66] C. Aidala, et al., Nonperturbative transverse-momentum-dependent effects in dihadron and direct photon-hadron angular correlations in $p + p$ collisions at $\sqrt{s} = 200$ GeV, Phys. Rev. D 98 (2018) 072004. doi:10.1103/PhysRevD.98.072004.

Appendix

A Other Available PHENIX Datasets

The PHENIX experiment still has a wealth of data at its disposal for further analyses. This section will delve into the prospects of analyzing more recent data sets, as well as any anticipated difficulties.

A.1 2014 200 *GeV* $Au+Au$ *Data*

The results in this dissertation focus on using the Minimum Bias portion of PHENIX's 2014 200 GeV $Au+Au$ data set. However, there is another set of data that fire the EMCal-RICH Trigger which detects events that contain high energy electromagnetic signals. While this data set has some overlap with the Minimum Bias data set, this overlap can be accounted for, and the unique events in the ERT data set can be used to bolster that of the Minimum Bias. As this analysis focuses on reconstructing high momentum neutral pions to serve as trigger particles, the ERT can help substantially improve the number of trigger particles available for correlation measurements. However, one must develop a protocol during event mixing to mix π^0's from ERT events only with hadrons from Minimum Bias events to avoid biasing the correction. Fig. 1 shows the yield of neutral pion triggers in both data sets. One can see that there is at least a 20% increase in the yield of high momentum π^0's in the ERT data set. Assuming the two data sets are completely unique, this increase is roughly 120%.

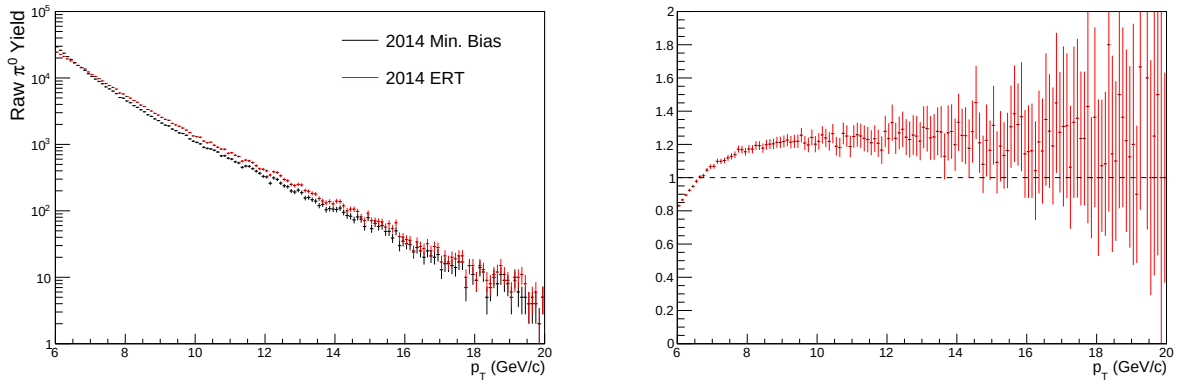

Figure 1: Left: Yields of high momentum ($p_T^{\pi^0} > 6$ GeV/c) π^0's from the Minimum Bias (Black) and ERT (Red) data sets. Right: Number of π^0's in the ERT set divided by the same quantity from the Minimum Bias set.

A.2 2015 200 *GeV* $p+p$ *Data*

π^0-hadron correlations in 200 GeV $p+p$ collisions from PHENIX's 2015 data set have already been measured and published in [66]. The 2015 200 $p+p$ data set is PHENIX's most recent data set and could serve as an updated baseline with increased statistics over the current baseline from [39]. However, one major hurdle is that it was discovered that, in the course of performing the hadron efficiency correction for the 2015 data, an incorrect set of drift

chamber single-wire efficiency maps was used, causing a drastic difference between simulation and data, thus contaminating the corrected spectra used in the analysis. Though the focus of the paper is on the widths of the angular distributions which should, in principle, be immune to the overall normalization, the per-trigger yields cannot be used as a baseline currently until the efficiency corrections are redone. With higher statistics in the 2015 data set, the overall statistical error of $\sqrt{6} \approx 2.4$.

A.3 2016 200 *GeV* $Au + Au$ *Data*

Lastly, there is the 200 GeV $Au + Au$ data set that was taken in 2016. While there are results from the small systems scan done in Run 16, the $Au + Au$ data set remains largely untouched, which was initially due to the lack of technical support in developing all the necessary calibrations for it. In the early days of technical training for this PhD, I performed the centrality recalibration for this data set. Additional person power has recently resulted in a complete suite of calibrations for Run 16, however, and there are current efforts underway to extract direct photon-hadron correlations from it.

B Embedding Efficiencies for Runs 10 and Run 11

Below are distributions of S and R-Type tracks as well as the resultant occupancy corrections for Runs 10 and 11.

B.1 Run 10

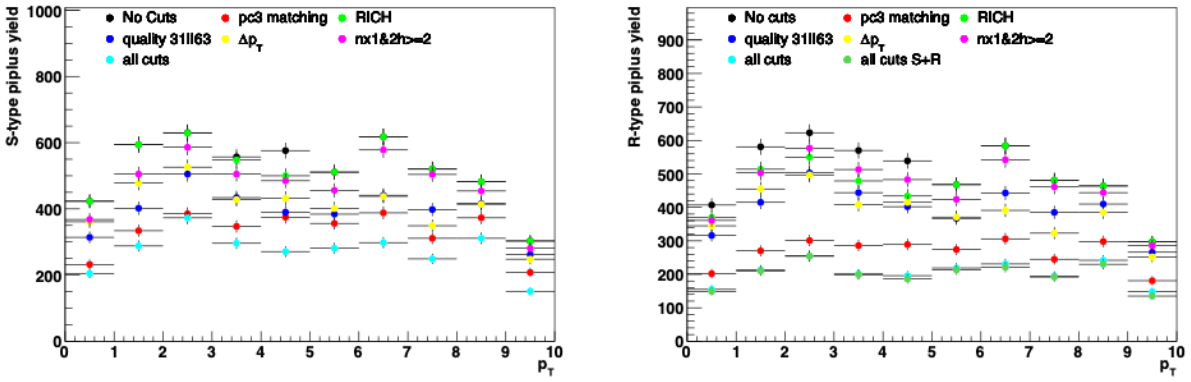

Figure 2: Left: Yield of S-Type tracks from the Run 10 embedding procedure in the 0–20% centrality bin. Right: Yield of R-Type tracks from the Run 10 embedding procedure in the 0–20% centrality bin.

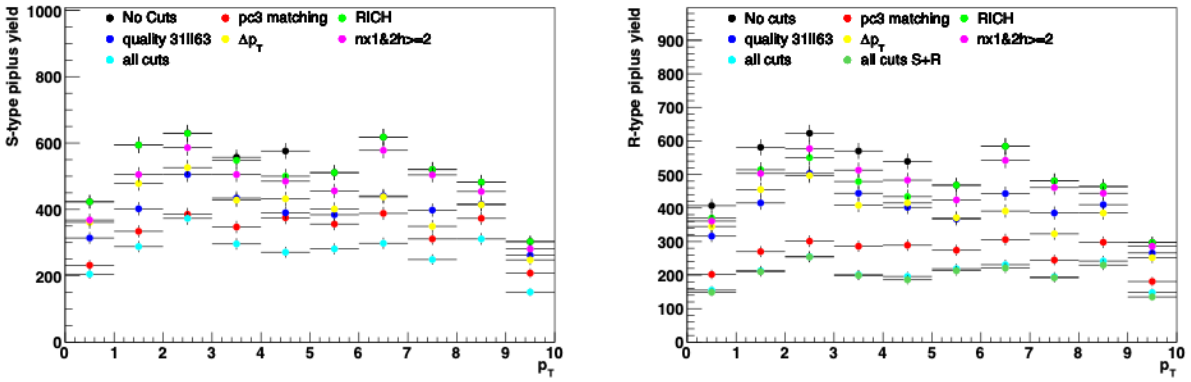

Figure 3: Left: Yield of S-Type tracks from the Run 10 embedding procedure in the 20–40% centrality bin. Right: Yield of R-Type tracks from the Run 10 embedding procedure in the 20–40% centrality bin.

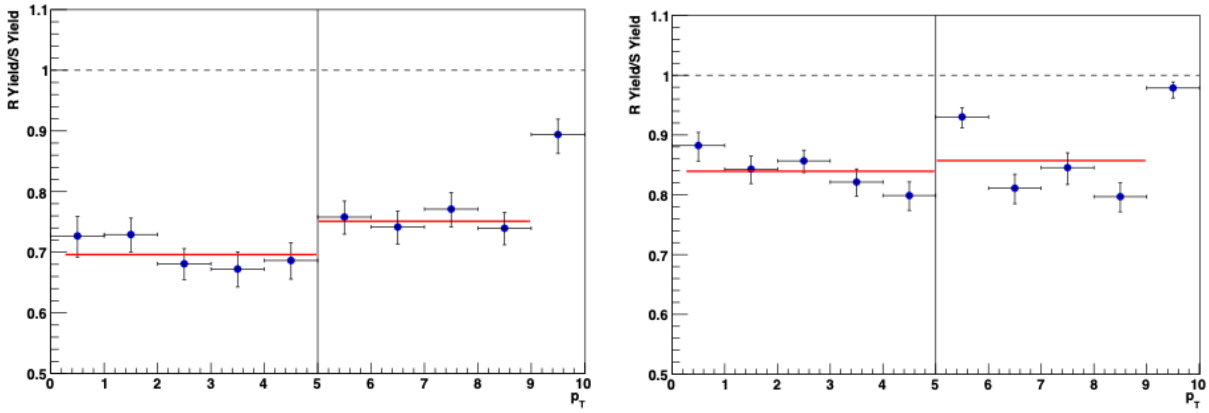

Figure 4: Left: Run 10 embedding efficiency in the 0–40% centrality bin. Right: Run 10 embedding efficiency in the 20–20% centrality bin.

B.2 Run 11

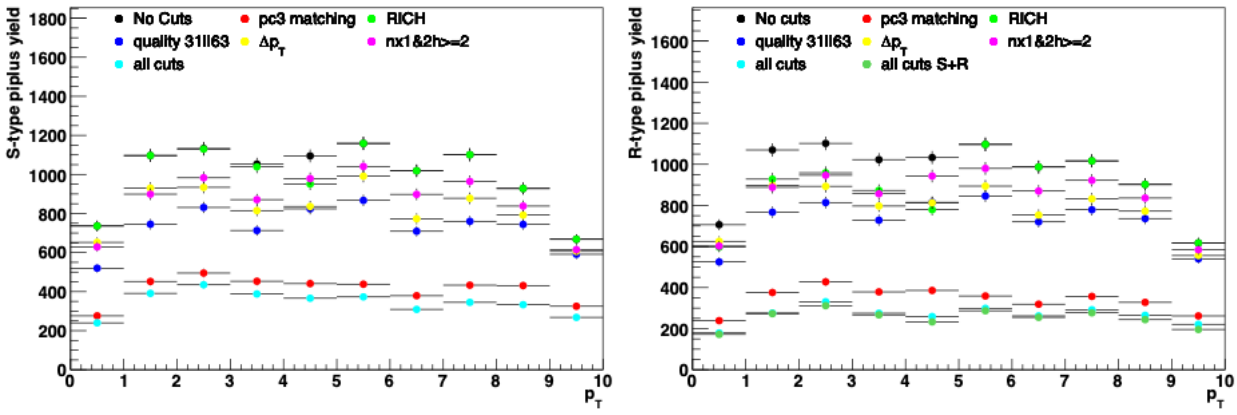

Figure 5: Left: Yield of S-Type tracks from the Run 11 embedding procedure in the 0–20% centrality bin. Right: Yield of R-Type tracks from the Run 11 embedding procedure in the 0–20% centrality bin.

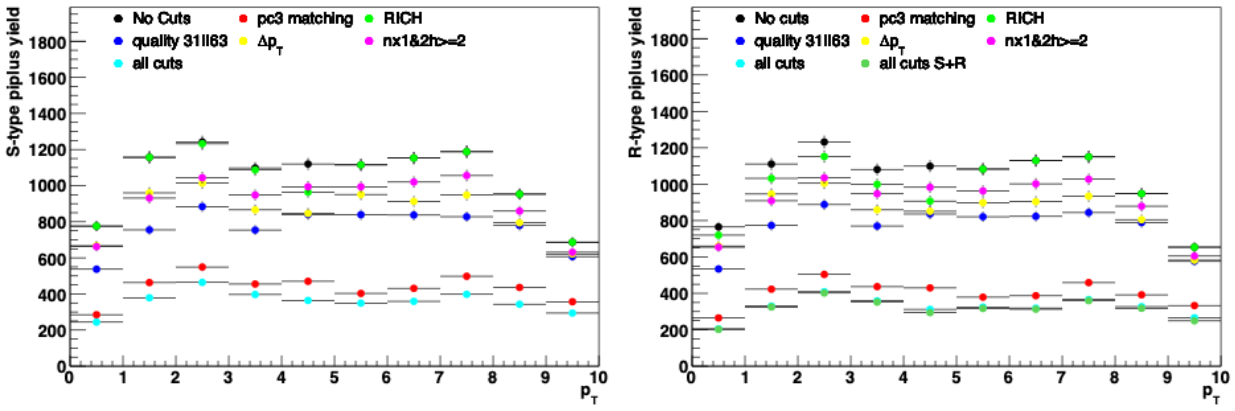

Figure 6: Left: Yield of S-Type tracks from the Run 11 embedding procedure in the 20–40% centrality bin. Right: Yield of R-Type tracks from the Run 11 embedding procedure in the 20–40% centrality bin.

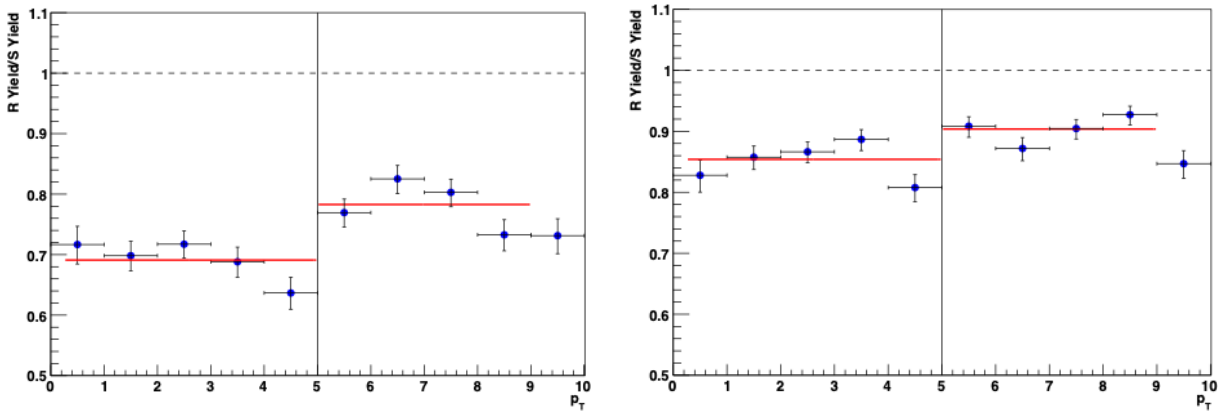

Figure 7: Left: Run 11 embedding efficiency in the 0–40% centrality bin. Right: Run 11 embedding efficiency in the 20–40% centrality bin.

C Run 10 PC3 Matching Recalibrator in Real Data

As discussed throughout the dissertation, Run 10 was not included in this analysis because a problem was found with its PC3 track matching recalibrator. This bug essentially caused it let in background tracks across all p_T analyzed in this analysis. The malfunction was deduced by analyzing distributions of the circular sigma cut in real data as was done in Sec 3.2.1 for the same values in simulation. The distribution for real data in Runs 10 and 14 (whose track matching recalibration has documentation showing its functionality) are shown in Fig. 8. As one can see, the distribution for Run 10 has a mean of approximately zero like that of the uncalibrated distribution shown in Fig. 3.26, whereas the mean of the Run 14 distribution is at approximately $\sqrt{\pi/2}$, as it should be for a distribution that is the quadrature convolution of two Gaussian distributions with mean 0 and standard deviation 0.

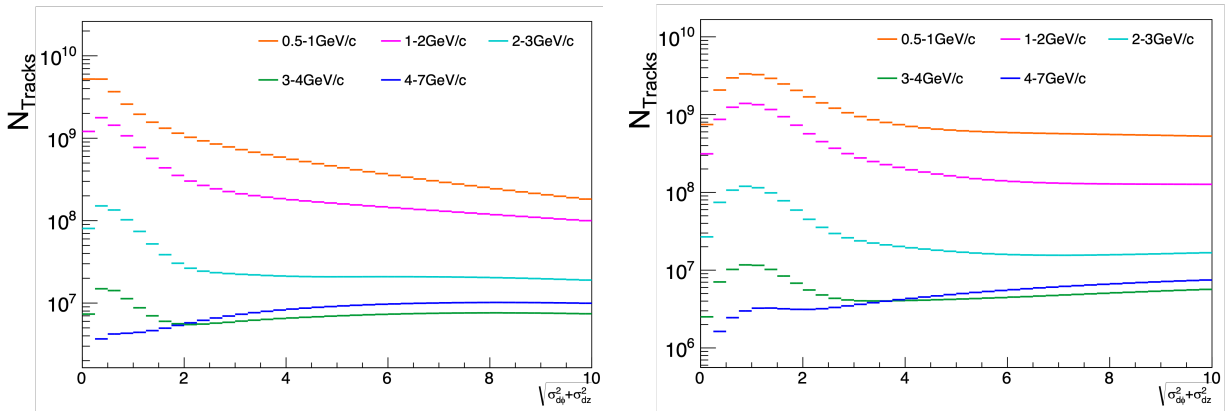

Figure 8: Number of tracks within a given circular sigma for Run 10 (Left) and for Run 14 (Right)

D Data Table: Coefficients of Flow Harmonics

Table 1: Interpolated charged hadron v_n

0–20%									
assoc p_T (GeV/c)	v_2	$\sigma^+_{v_2}$	$\sigma^-_{v_2}$	v_3	$\sigma^+_{v_3}$	$\sigma^-_{v_3}$	v_4	$\sigma^+_{v_4}$	$\sigma^-_{v_4}$
0.5–1.0	0.03648	0.00128	0.00128	0.01584	0.00085	0.00085	0.00767	0.00148	0.00148
1.0–2.0	0.06866	0.00167	0.00167	0.04074	0.00215	0.00215	0.02495	0.00458	0.00458
2.0–3.0	0.10240	0.00310	0.00310	0.07524	0.00301	0.00301	0.05482	0.00697	0.00697
3.0–5.0	0.10565	0.00401	0.00401	0.08484	0.00365	0.00365	0.07006	0.00931	0.00931
5.0–7.0	0.07678	0.00564	0.00564	0.04785	0.01684	0.01684	0.03972	0.02540	0.02540
20–40%									
assoc p_T (GeV/c)	v_2	$\sigma^+_{v_2}$	$\sigma^-_{v_2}$	v_3	$\sigma^+_{v_3}$	$\sigma^-_{v_3}$	v_4	$\sigma^+_{v_4}$	$\sigma^-_{v_4}$
0.5–1.0	0.07753	0.00148	0.00148	0.02280	0.00178	0.00178	0.01516	0.00407	0.00407
1.0–2.0	0.13623	0.00241	0.00241	0.05332	0.00499	0.00499	0.03929	0.00965	0.00965
2.0–3.0	0.19085	0.00399	0.00399	0.08970	0.00639	0.00639	0.07385	0.01813	0.01813
3.0–5.0	0.19341	0.00354	0.00354	0.09542	0.00693	0.00693	0.08715	0.02059	0.02059
5.0–7.0	0.14710	0.00541	0.00541	0.05137	0.02863	0.02863	0.05324	0.04081	0.04081

Table 2: Interpolated π^0 v_2

0–20%			
trigger p_T (GeV/c)	v_2	$\sigma^+_{v_2}$	$\sigma^-_{v_2}$
4–5	0.08875	0.00251	0.00251
5–7	0.07625	0.00585	0.00585
7–9	0.06262	0.00916	0.01324
9–12	0.05878	0.01256	0.02244
12–15	0.05832	0.01301	0.03909
20–40%			
trigger p_T (GeV/c)	v_2	$\sigma^+_{v_2}$	$\sigma^-_{v_2}$
4–5	0.15378	0.00283	0.00283
5–7	0.12754	0.00404	0.00404
7–9	0.09896	0.01060	0.00869
9–12	0.09177	0.01436	0.02469
12–15	0.09116	0.01491	0.05459

Table 3: Scaling factor g^h_n

centrality	g_3	σ_{g_3}	g_4	σ_{g_4}
0–20%	2.30	0.03	5.56	0.23
20–40%	1.07	0.02	2.20	0.15

E Data Table: ξ

Table 4: ξ in Run 14

Trigger p_T 4–5 GeV/c				
assoc p_T GeV/c	0–20%		20–40%	
	ξ	σ	ξ	σ
0.5–1	1.00225	0.00061	1.00911	0.00262
1.0–2	1.00205	0.00059	1.00988	0.00287
2.0–3	1.00179	0.00054	1.01012	0.00300
3.0–5	1.00189	0.00054	1.00917	0.00269
5.0–7	1.00363	0.00104	1.01164	0.00419
Trigger p_T 5–7 GeV/c				
assoc p_T GeV/c	0–20%		20–40%	
	ξ	σ	ξ	σ
0.5–1	1.00169	0.00048	1.00825	0.00242
1.0–2	1.00156	0.00046	1.00897	0.00267
2.0–3	1.00137	0.00042	1.00922	0.00280
3.0–5	1.00144	0.00043	1.00833	0.00250
5.0–7	1.00272	0.00079	1.01050	0.00380
Trigger p_T 7–9 GeV/c				
assoc p_T GeV/c	0–20%		20–40%	
	ξ	σ	ξ	σ
0.5–1	1.00161	0.00046	1.00794	0.00233
1.0–2	1.00148	0.00044	1.00863	0.00257
2.0–3	1.00130	0.00040	1.00887	0.00270
3.0–5	1.00137	0.00041	1.00802	0.00241
5.0–7	1.00257	0.00075	1.01009	0.00365
Trigger p_T 9–12 GeV/c				
assoc p_T GeV/c	0–20%		20–40%	
	ξ	σ	ξ	σ
0.5–1	1.00163	0.00047	1.00860	0.00259
1.0–2	1.00150	0.00045	1.00936	0.00286
2.0–3	1.00132	0.00042	1.00961	0.00300
3.0–5	1.00138	0.00042	1.00869	0.00268
5.0–7	1.00259	0.00078	1.01094	0.00399
Trigger p_T 12–15 GeV/c				
assoc p_T GeV/c	0–20%		20–40%	
	ξ	σ	ξ	σ
0.5–1	1.00191	0.00053	1.00831	0.00242
1.0–2	1.00174	0.00050	1.00902	0.00267
2.0–3	1.00153	0.00046	1.00925	0.00279
3.0–5	1.00161	0.00047	1.00838	0.00250
5.0–7	1.00308	0.00089	1.01060	0.00383

F Data Table: Jet Functions

Table 5: 0–20%, 4.0–5.0 $\otimes$ 0.5–1.0 GeV/c Jet Function

ϕ	per trig yield	σ_{stat}/y	systematic errors											
			$+\sigma_{f2}/y$	$-\sigma_{f2}/y$	$+\sigma_{f3}/y$	$-\sigma_{f3}/y$	$+\sigma_{f4}/y$	$-\sigma_{f4}/y$	$+\sigma_{\xi/ZYAM}/y$	$-\sigma_{\xi/ZYAM}/y$	$+\sigma_{\pi^0}/y$	$-\sigma_{\pi^0}/y$	$+\sigma_{total}/y$	$-\sigma_{total}/y$
-1.47	0.10650	0.29709	0.02809	-0.02506	0.01509	-0.01615	0.02578	-0.02926	0.09959	-0.09960	0.16802	-0.16802	0.19958	-0.19974
-1.26	-0.00241	-12.24127	0.85852	-0.73627	0.13477	-0.14534	0.56852	-0.64099	4.40700	-4.40742	0.16802	-0.16802	4.53082	-4.51969
-1.05	-0.02349	-1.09573	0.01579	-0.00548	0.00726	-0.00693	0.02394	-0.02023	0.45189	-0.45193	0.16802	-0.16802	0.48302	-0.48266
-0.84	-0.01984	-1.16344	0.09963	-0.09075	0.01679	-0.01810	0.09095	-0.07878	0.53637	-0.53642	0.16802	-0.16802	0.57827	-0.57511
-0.63	0.02470	0.81054	0.16927	-0.16493	0.06577	-0.07036	0.05513	-0.04758	0.43249	-0.43253	0.16802	-0.16802	0.50129	-0.49973
-0.42	0.06150	0.28748	0.09923	-0.09846	0.05234	-0.05594	0.00704	-0.00772	0.17440	-0.17441	0.16802	-0.16802	0.26698	-0.26746
-0.21	0.18184	0.09413	0.04074	-0.04070	0.02480	-0.02649	0.01209	-0.01369	0.05917	-0.05917	0.16802	-0.16802	0.18480	-0.18514
-0.00	0.21144	0.08050	0.03722	-0.03726	0.02365	-0.02527	0.01397	-0.01585	0.05094	-0.05095	0.16802	-0.16802	0.18156	-0.18194
0.21	0.15715	0.10725	0.04714	-0.04710	0.02869	-0.03066	0.01399	-0.01585	0.06846	-0.06847	0.16802	-0.16802	0.19015	-0.19060
0.42	0.05651	0.31010	0.10799	-0.10716	0.05697	-0.06089	0.00766	-0.00840	0.18981	-0.18982	0.16802	-0.16802	0.28147	-0.28200
0.63	0.03642	0.52694	0.11481	-0.11187	0.04461	-0.04772	0.03739	-0.03227	0.29334	-0.29337	0.16802	-0.16802	0.36173	-0.36073
0.84	0.01606	1.31491	0.12307	-0.11210	0.02074	-0.02236	0.11234	-0.09732	0.66257	-0.66263	0.16802	-0.16802	0.70386	-0.69989
1.05	0.00406	6.18464	0.09133	-0.03168	0.04196	-0.04011	0.13843	-0.11701	2.61344	-2.61369	0.16802	-0.16802	2.62442	-2.62219
1.26	-0.07417	-0.38537	0.02785	-0.02388	0.00437	-0.00471	0.01844	-0.02079	0.14297	-0.14298	0.16802	-0.16802	0.22317	-0.22293
1.47	0.04505	0.67264	0.06639	-0.05923	0.03568	-0.03817	0.06095	-0.06916	0.23543	-0.23545	0.16802	-0.16802	0.30505	-0.30564
1.68	-0.02800	-1.09076	0.10674	-0.09520	0.11412	-0.12197	0.09811	-0.11132	0.37930	-0.37934	0.06056	-0.06056	0.42612	-0.42883
1.88	0.07144	0.41088	0.02881	-0.02469	0.06273	-0.06702	0.01918	-0.02162	0.14888	-0.14890	0.06056	-0.06056	0.17597	-0.17722
2.09	0.11518	0.21948	0.00314	-0.00103	0.04320	-0.04616	0.00486	-0.00410	0.09252	-0.09253	0.06056	-0.06056	0.11886	-0.11991
2.30	0.11389	0.19261	0.01743	-0.01588	0.03943	-0.04213	0.01582	-0.01371	0.09374	-0.09375	0.06056	-0.06056	0.12068	-0.12112
2.51	0.13192	0.15415	0.03172	-0.03091	0.02435	-0.02603	0.01032	-0.00890	0.08108	-0.08109	0.06056	-0.06056	0.10930	-0.10934
2.72	0.13198	0.14788	0.04622	-0.04586	0.01236	-0.01322	0.00327	-0.00359	0.08117	-0.08118	0.06056	-0.06056	0.11206	-0.11202
2.93	0.14249	0.12943	0.05193	-0.05189	0.00247	-0.00266	0.01541	-0.01746	0.07527	-0.07528	0.06056	-0.06056	0.11079	-0.11108
3.14	0.16253	0.11071	0.04836	-0.04841	0.00088	-0.00084	0.01815	-0.02061	0.06602	-0.06602	0.06056	-0.06056	0.10341	-0.10390
3.35	0.14253	0.12932	0.05192	-0.05188	0.00247	-0.00266	0.01541	-0.01746	0.07525	-0.07526	0.06056	-0.06056	0.11077	-0.11106
3.56	0.17024	0.11199	0.03583	-0.03555	0.00958	-0.01025	0.00254	-0.00278	0.06293	-0.06293	0.06056	-0.06056	0.09492	-0.09489
3.77	0.14789	0.13748	0.02829	-0.02757	0.02172	-0.02322	0.00920	-0.00794	0.07232	-0.07233	0.06056	-0.06056	0.10127	-0.10130
3.98	0.12344	0.17935	0.01608	-0.01465	0.03638	-0.03887	0.01460	-0.01265	0.08649	-0.08650	0.06056	-0.06056	0.11377	-0.11417
4.19	0.07646	0.31777	0.00473	-0.00155	0.06508	-0.06953	0.00732	-0.00618	0.13938	-0.13939	0.06056	-0.06056	0.16555	-0.16725
4.40	0.06883	0.40619	0.02990	-0.02562	0.06510	-0.06956	0.01990	-0.02244	0.15453	-0.15454	0.06056	-0.06056	0.18187	-0.18317
4.61	0.11234	0.28124	0.02660	-0.02373	0.02844	-0.03040	0.02445	-0.02774	0.09452	-0.09453	0.06056	-0.06056	0.12131	-0.12190

Table 6: 0–20%, 4.0–5.0 $\otimes$ 1.0–2.0 GeV/c Jet Function

ϕ	per trig yield	σ_{stat}/y	systematic errors											
			$+\sigma_{f2}/y$	$-\sigma_{f2}/y$	$+\sigma_{f3}/y$	$-\sigma_{f3}/y$	$+\sigma_{f4}/y$	$-\sigma_{f4}/y$	$+\sigma_{\xi/ZYAM}/y$	$-\sigma_{\xi}/y$	$+\sigma_{\pi^0}/y$	$-\sigma_{\pi^0}/y$	$+\sigma_{total}/y$	$-\sigma_{total}/y$
-1.47	-0.00376	-5.64942	0.86495	-0.84261	0.22397	-0.20995	0.67794	-0.77345	0.78589	-0.78589	0.00985	-0.00985	1.36953	-1.40357
-1.26	-0.01418	-1.43175	0.18944	-0.18455	0.15527	-0.14555	0.06073	-0.06928	0.20774	-0.20774	0.00985	-0.00985	0.32702	-0.32140
-1.05	0.01119	1.42084	0.14843	-0.14459	0.24332	-0.22808	0.14211	-0.12456	0.26364	-0.26364	0.00985	-0.00985	0.41356	-0.39755
-0.84	0.01855	0.79856	0.01872	-0.01823	0.11874	-0.11130	0.16769	-0.14699	0.15979	-0.15979	0.00985	-0.00985	0.26115	-0.24486
-0.63	0.02774	0.43532	0.03604	-0.03700	0.03032	-0.02842	0.09274	-0.08128	0.10769	-0.10769	0.00985	-0.00985	0.15004	-0.14310
-0.42	0.07955	0.14499	0.02721	-0.02794	0.00991	-0.01057	0.00418	-0.00366	0.03789	-0.03789	0.00985	-0.00985	0.04888	-0.04938
-0.21	0.12969	0.07743	0.02279	-0.02339	0.01592	-0.01698	0.01438	-0.01641	0.02341	-0.02341	0.00985	-0.00985	0.04031	-0.04183
-0.00	0.22945	0.04494	0.01410	-0.01448	0.01112	-0.01186	0.01215	-0.01386	0.01327	-0.01327	0.00985	-0.00985	0.02726	-0.02856
0.21	0.14254	0.06981	0.02074	-0.02129	0.01448	-0.01545	0.01308	-0.01493	0.02130	-0.02130	0.00985	-0.00985	0.03690	-0.03828
0.42	0.07426	0.14968	0.02916	-0.02993	0.01062	-0.01133	0.00448	-0.00392	0.04059	-0.04059	0.00985	-0.00985	0.05223	-0.05277
0.63	0.02273	0.50692	0.04400	-0.04516	0.03702	-0.03470	0.11321	-0.09923	0.13146	-0.13146	0.00985	-0.00985	0.18303	-0.17455
0.84	0.01816	0.73573	0.01912	-0.01862	0.12127	-0.11367	0.17127	-0.15012	0.16319	-0.16319	0.00985	-0.00985	0.26670	-0.25006
1.05	-0.00283	-5.22091	0.58581	-0.57068	0.96032	-0.90017	0.56088	-0.49162	1.04055	-1.04055	0.00985	-0.00985	1.63181	-1.56860
1.26	0.00823	2.24484	0.32633	-0.31790	0.26748	-0.25072	0.10461	-0.11934	0.35786	-0.35786	0.00985	-0.00985	0.56315	-0.55347
1.47	0.01118	1.91628	0.29047	-0.28297	0.07522	-0.07050	0.22767	-0.25974	0.26392	-0.26392	0.00985	-0.00985	0.46002	-0.47145
1.68	-0.02025	-1.01027	0.16042	-0.15628	0.03894	-0.04154	0.12574	-0.14345	0.14621	-0.14621	0.04080	-0.04080	0.25711	-0.26414
1.88	-0.00601	-3.21488	0.44733	-0.43578	0.34369	-0.36666	0.14339	-0.16360	0.49454	-0.49454	0.04080	-0.04080	0.76487	-0.77288
2.09	0.03530	0.43307	0.04704	-0.04582	0.07228	-0.07711	0.04504	-0.03948	0.08439	-0.08439	0.04080	-0.04080	0.13510	-0.13561
2.30	0.05911	0.24158	0.00587	-0.00572	0.03493	-0.03726	0.05262	-0.04612	0.05055	-0.05055	0.04080	-0.04080	0.09079	-0.08814
2.51	0.07017	0.17110	0.01425	-0.01463	0.01124	-0.01199	0.03666	-0.03214	0.04270	-0.04270	0.04080	-0.04080	0.07185	-0.06985
2.72	0.05107	0.23360	0.04240	-0.04352	0.01647	-0.01544	0.00651	-0.00571	0.05885	-0.05885	0.04080	-0.04080	0.08508	-0.08540
2.93	0.04189	0.26132	0.07056	-0.07243	0.05257	-0.04928	0.04452	-0.05079	0.07189	-0.07189	0.04080	-0.04080	0.12867	-0.13072
3.14	0.06278	0.18295	0.05154	-0.05290	0.04336	-0.04065	0.04440	-0.05065	0.04801	-0.04801	0.04080	-0.04080	0.10236	-0.10482
3.35	0.06828	0.15988	0.04329	-0.04444	0.03226	-0.03024	0.02732	-0.03116	0.04411	-0.04411	0.04080	-0.04080	0.08527	-0.08643
3.56	0.05929	0.19752	0.03652	-0.03749	0.01419	-0.01330	0.00561	-0.00491	0.05069	-0.05069	0.04080	-0.04080	0.07616	-0.07642
3.77	0.05098	0.23249	0.01961	-0.02013	0.01547	-0.01650	0.05046	-0.04423	0.05877	-0.05877	0.04080	-0.04080	0.09105	-0.08805
3.98	0.05377	0.25753	0.00646	-0.00629	0.03839	-0.04096	0.05785	-0.05070	0.05557	-0.05557	0.04080	-0.04080	0.09805	-0.09508
4.19	0.02827	0.53001	0.05875	-0.05723	0.09027	-0.09630	0.05625	-0.04930	0.10540	-0.10540	0.04080	-0.04080	0.16594	-0.16659
4.40	0.01917	0.94018	0.14019	-0.13657	0.10771	-0.11490	0.04494	-0.05127	0.15498	-0.15498	0.04080	-0.04080	0.24281	-0.24529
4.61	-0.00723	-2.80272	0.44922	-0.43762	0.10904	-0.11632	0.35209	-0.40170	0.40942	-0.40942	0.04080	-0.04080	0.71200	-0.73191

Table 7: 0–20%, 4.0–5.0 $\otimes$ 2.0–3.0 GeV/c Jet Function

ϕ	per trig yield	σ_{stat}/y	systematic errors											
			$+\sigma_{f2}/y$	$-\sigma_{f2}/y$	$+\sigma_{f3}/y$	$-\sigma_{f3}/y$	$+\sigma_{f4}/y$	$-\sigma_{f4}/y$	$+\sigma_{\xi/ZYAM}/y$	$-\sigma_{\xi}/y$	$+\sigma_{\pi^0}/y$	$-\sigma_{\pi^0}/y$	$+\sigma_{total}/y$	$-\sigma_{total}/y$
-1.47	0.00928	0.67508	0.04782	-0.04645	0.01204	-0.01135	0.03929	-0.04441	0.02396	-0.02396	0.05744	-0.05744	0.08860	-0.09018
-1.26	0.00497	1.13338	0.07380	-0.07168	0.05884	-0.05543	0.02480	-0.02803	0.04451	-0.04451	0.05744	-0.05744	0.12167	-0.11949
-1.05	0.00402	1.20284	0.05636	-0.05473	0.08986	-0.08466	0.05603	-0.04958	0.05500	-0.05500	0.05744	-0.05744	0.14393	-0.13764
-0.84	0.00627	0.62916	0.00756	-0.00734	0.04663	-0.04393	0.07031	-0.06220	0.03551	-0.03551	0.05744	-0.05744	0.10833	-0.10205
-0.63	0.01304	0.27497	0.01044	-0.01075	0.00857	-0.00807	0.02797	-0.02475	0.01731	-0.01731	0.05744	-0.05744	0.06756	-0.06628
-0.42	0.02126	0.15180	0.01387	-0.01428	0.00495	-0.00526	0.00222	-0.00196	0.01079	-0.01079	0.05744	-0.05744	0.06031	-0.06043
-0.21	0.05679	0.05404	0.00709	-0.00730	0.00485	-0.00515	0.00470	-0.00531	0.00409	-0.00409	0.05744	-0.05744	0.05842	-0.05852
-0.00	0.08794	0.03368	0.00501	-0.00516	0.00387	-0.00411	0.00454	-0.00513	0.00265	-0.00265	0.05744	-0.05744	0.05803	-0.05811
0.21	0.05574	0.05434	0.00722	-0.00743	0.00494	-0.00525	0.00479	-0.00541	0.00416	-0.00416	0.05744	-0.05744	0.05845	-0.05856
0.42	0.02228	0.13830	0.01323	-0.01362	0.00473	-0.00502	0.00212	-0.00187	0.01029	-0.01029	0.05744	-0.05744	0.06006	-0.06017
0.63	0.00925	0.36106	0.01471	-0.01515	0.01208	-0.01138	0.03943	-0.03489	0.02440	-0.02440	0.05744	-0.05744	0.07624	-0.07397
0.84	0.00616	0.59914	0.00770	-0.00748	0.04752	-0.04477	0.07166	-0.06340	0.03620	-0.03620	0.05744	-0.05744	0.10983	-0.10339
1.05	0.00078	5.42151	0.28919	-0.28087	0.46112	-0.43440	0.28753	-0.25440	0.28221	-0.28221	0.05744	-0.05744	0.67961	-0.64440
1.26	0.00106	4.74198	0.34598	-0.33601	0.27583	-0.25985	0.11625	-0.13139	0.20866	-0.20866	0.05744	-0.05744	0.50610	-0.49450
1.47	0.00515	1.22354	0.08608	-0.08360	0.02168	-0.02042	0.07072	-0.07993	0.04313	-0.04313	0.05744	-0.05744	0.13431	-0.13767
1.68	0.00019	34.03142	2.35850	-2.29060	0.55962	-0.59403	1.93771	-2.19006	1.18859	-1.18859	0.12763	-0.12763	3.32557	-3.43877
1.88	0.00222	2.34630	0.16559	-0.16082	0.12437	-0.13202	0.05564	-0.06289	0.10138	-0.10138	0.12763	-0.12763	0.26936	-0.27169
2.09	0.00255	1.77456	0.08879	-0.08624	0.13338	-0.14158	0.08828	-0.07811	0.08827	-0.08827	0.12763	-0.12763	0.23989	-0.24013
2.30	0.01019	0.38579	0.00466	-0.00452	0.02706	-0.02872	0.04331	-0.03832	0.02221	-0.02221	0.12763	-0.12763	0.13933	-0.13819
2.51	0.00117	2.99393	0.11621	-0.11965	0.08986	-0.09539	0.31145	-0.27556	0.19379	-0.19379	0.12763	-0.12763	0.41524	-0.39140
2.72	0.01406	0.22973	0.02097	-0.02159	0.00795	-0.00749	0.00335	-0.00297	0.01622	-0.01622	0.12763	-0.12763	0.13064	-0.13070
2.93	0.00699	0.45769	0.05758	-0.05928	0.04186	-0.03943	0.03820	-0.04317	0.03273	-0.03273	0.12763	-0.12763	0.15455	-0.15587
3.14	0.01283	0.24743	0.03434	-0.03536	0.02819	-0.02656	0.03111	-0.03516	0.01786	-0.01786	0.12763	-0.12763	0.13982	-0.14071
3.35	0.01082	0.29360	0.03719	-0.03829	0.02704	-0.02547	0.02467	-0.02789	0.02114	-0.02114	0.12763	-0.12763	0.13950	-0.14010
3.56	0.00818	0.38678	0.03604	-0.03710	0.01366	-0.01287	0.00576	-0.00510	0.02787	-0.02787	0.12763	-0.12763	0.13632	-0.13651
3.77	0.00456	0.74810	0.02984	-0.03073	0.02308	-0.02450	0.07998	-0.07076	0.04976	-0.04976	0.12763	-0.12763	0.16305	-0.15911
3.98	0.00678	0.54940	0.00700	-0.00679	0.04067	-0.04317	0.06509	-0.05759	0.03337	-0.03337	0.12763	-0.12763	0.15278	-0.15043
4.19	0.00574	0.76205	0.03954	-0.03841	0.05940	-0.06305	0.03932	-0.03479	0.03931	-0.03931	0.12763	-0.12763	0.15644	-0.15651
4.40	-0.00502	-0.98742	0.07314	-0.07104	0.05494	-0.05831	0.02458	-0.02778	0.04478	-0.04478	0.12763	-0.12763	0.16513	-0.16587
4.61	-0.00359	-1.63726	0.12372	-0.12016	0.02936	-0.03116	0.10165	-0.11488	0.06235	-0.06235	0.12763	-0.12763	0.21605	-0.22087

Table 8: 0–20%, 4.0–5.0 $\otimes$ 3.0–5.0 GeV/c Jet Function

ϕ	per trig yield	σ_{stat}/y	systematic errors											
			$+\sigma_{f2}/y$	$-\sigma_{f2}/y$	$+\sigma_{f3}/y$	$-\sigma_{f3}/y$	$+\sigma_{f4}/y$	$-\sigma_{f4}/y$	$+\sigma_{\xi/ZYAM}/y$	$-\sigma_{\xi}/y$	$+\sigma_{\pi^0}/y$	$-\sigma_{\pi^0}/y$	$+\sigma_{total}/y$	$-\sigma_{total}/y$
-1.47	-0.00028	-7.71837	0.23018	-0.22285	0.05778	-0.05435	0.21209	-0.24001	0.10125	-0.09776	0.01480	-0.01480	0.33433	-0.34641
-1.26	-0.00260	-0.71468	0.02067	-0.02001	0.01642	-0.01545	0.00779	-0.00881	0.01093	-0.01055	0.01480	-0.01480	0.03311	-0.03236
-1.05	-0.00026	-6.43801	0.12723	-0.12318	0.20217	-0.19017	0.14204	-0.12552	0.10873	-0.10498	0.01480	-0.01480	0.29879	-0.27988
-0.84	0.00437	0.31428	0.00159	-0.00154	0.00977	-0.00919	0.01659	-0.01466	0.00653	-0.00631	0.01480	-0.01480	0.02520	-0.02368
-0.63	0.00072	1.71844	0.02738	-0.02828	0.02247	-0.02114	0.08267	-0.07305	0.03993	-0.03855	0.01480	-0.01480	0.09951	-0.09104
-0.42	0.00583	0.19475	0.00737	-0.00761	0.00263	-0.00279	0.00133	-0.00117	0.00505	-0.00488	0.01480	-0.01480	0.01754	-0.01761
-0.21	0.02167	0.05536	0.00271	-0.00280	0.00185	-0.00197	0.00202	-0.00229	0.00138	-0.00133	0.01480	-0.01480	0.01536	-0.01542
-0.00	0.04569	0.02742	0.00141	-0.00145	0.00108	-0.00115	0.00143	-0.00162	0.00066	-0.00063	0.01480	-0.01480	0.01499	-0.01502
0.21	0.02190	0.05414	0.00268	-0.00277	0.00183	-0.00195	0.00200	-0.00226	0.00136	-0.00132	0.01480	-0.01480	0.01535	-0.01541
0.42	0.00636	0.17337	0.00675	-0.00698	0.00241	-0.00256	0.00122	-0.00108	0.00463	-0.00447	0.01480	-0.01480	0.01713	-0.01719
0.63	0.00271	0.44279	0.00732	-0.00756	0.00600	-0.00565	0.02209	-0.01952	0.01067	-0.01030	0.01480	-0.01480	0.03017	-0.02820
0.84	0.00257	0.50576	0.00270	-0.00261	0.01658	-0.01559	0.02816	-0.02488	0.01109	-0.01071	0.01480	-0.01480	0.03765	-0.03468
1.05	0.00169	0.90127	0.01964	-0.01902	0.03121	-0.02936	0.02193	-0.01938	0.01679	-0.01621	0.01480	-0.01480	0.04840	-0.04562
1.26	0.00287	0.62211	0.01870	-0.01810	0.01486	-0.01398	0.00705	-0.00797	0.00989	-0.00955	0.01480	-0.01480	0.03061	-0.02995
1.47	0.00052	4.23719	0.12465	-0.12067	0.03129	-0.02943	0.11485	-0.12997	0.05483	-0.05294	0.01480	-0.01480	0.18147	-0.18799
1.68	0.00091	2.52877	0.07119	-0.06892	0.01681	-0.01787	0.06559	-0.07423	0.03152	-0.03043	0.22809	-0.22809	0.25035	-0.25205
1.88	-0.00233	-0.74427	0.02302	-0.02229	0.01721	-0.01829	0.00868	-0.00982	0.01238	-0.01196	0.22809	-0.22809	0.23040	-0.23043
2.09	0.00119	1.37510	0.02793	-0.02704	0.04175	-0.04438	0.03118	-0.02756	0.02437	-0.02353	0.22809	-0.22809	0.23689	-0.23673
2.30	0.00128	1.05190	0.00540	-0.00523	0.03124	-0.03321	0.05643	-0.04986	0.02260	-0.02182	0.22809	-0.22809	0.23818	-0.23690
2.51	0.00157	0.80073	0.01265	-0.01307	0.00977	-0.01039	0.03820	-0.03376	0.01857	-0.01793	0.22809	-0.22809	0.23257	-0.23188
2.72	0.00271	0.41063	0.01587	-0.01639	0.00601	-0.00566	0.00286	-0.00253	0.01080	-0.01043	0.22809	-0.22809	0.22900	-0.22900
2.93	0.00155	0.73061	0.03780	-0.03905	0.02747	-0.02584	0.02822	-0.03193	0.01893	-0.01828	0.22809	-0.22809	0.23530	-0.23574
3.14	0.00473	0.23742	0.01356	-0.01401	0.01113	-0.01047	0.01382	-0.01564	0.00621	-0.00600	0.22809	-0.22809	0.22927	-0.22938
3.35	0.00257	0.43855	0.02284	-0.02360	0.01660	-0.01562	0.01705	-0.01930	0.01144	-0.01104	0.22809	-0.22809	0.23075	-0.23092
3.56	0.00078	1.37965	0.05480	-0.05661	0.02077	-0.01954	0.00987	-0.00872	0.03731	-0.03602	0.22809	-0.22809	0.23864	-0.23872
3.77	0.00169	0.71033	0.01172	-0.01210	0.00905	-0.00962	0.03538	-0.03126	0.01719	-0.01660	0.22809	-0.22809	0.23193	-0.23134
3.98	0.00275	0.47344	0.00252	-0.00244	0.01460	-0.01552	0.02637	-0.02330	0.01056	-0.01020	0.22809	-0.22809	0.23033	-0.23005
4.19	-0.00142	-1.06136	0.02340	-0.02266	0.03498	-0.03719	0.02613	-0.02309	0.02042	-0.01972	0.22809	-0.22809	0.23430	-0.23419
4.40	0.00119	1.44815	0.04508	-0.04364	0.03369	-0.03582	0.01699	-0.01922	0.02424	-0.02341	0.22809	-0.22809	0.23679	-0.23692
4.61	0.00111	1.85625	0.05843	-0.05657	0.01380	-0.01467	0.05384	-0.06093	0.02587	-0.02498	0.22809	-0.22809	0.24331	-0.24450

Table 9: 0–20%, 4.0–5.0 $\otimes$ 5.0–7.0 GeV/c Jet Function

ϕ	per trig yield	σ_{stat}/y	systematic errors											
			$+\sigma_{f2}/y$	$-\sigma_{f2}/y$	$+\sigma_{f3}/y$	$-\sigma_{f3}/y$	$+\sigma_{f4}/y$	$-\sigma_{f4}/y$	$+\sigma_{\xi/ZYAM}/y$	$-\sigma_{\xi}/y$	$+\sigma_{\pi^0}/y$	$-\sigma_{\pi^0}/y$	$+\sigma_{total}/y$	$-\sigma_{total}/y$
-1.47	0.00022	4.45048	0.02904	-0.02788	0.01595	-0.01454	0.04460	-0.05201	0.02238	-0.02238	0.06311	-0.06311	0.08701	-0.09043
-1.26	0.00080	1.08301	0.00667	-0.00640	0.01159	-0.01056	0.00419	-0.00488	0.00620	-0.00620	0.06311	-0.06311	0.06494	-0.06479
-1.05	-0.00007	-10.17888	0.04958	-0.04759	0.17234	-0.15709	0.09507	-0.08153	0.07456	-0.07456	0.06311	-0.06311	0.22525	-0.20768
-0.84	0.00062	0.95302	0.00111	-0.00107	0.01495	-0.01363	0.01994	-0.01710	0.00803	-0.00803	0.06311	-0.06311	0.06834	-0.06728
-0.63	0.00015	3.46383	0.01271	-0.01324	0.02301	-0.02097	0.06646	-0.05699	0.03267	-0.03267	0.06311	-0.06311	0.10079	-0.09441
-0.42	0.00062	0.78460	0.00677	-0.00705	0.00516	-0.00566	0.00211	-0.00181	0.00813	-0.00813	0.06311	-0.06311	0.06423	-0.06430
-0.21	0.00418	0.14002	0.00138	-0.00143	0.00201	-0.00221	0.00173	-0.00201	0.00122	-0.00122	0.06311	-0.06311	0.06319	-0.06321
-0.00	0.01050	0.06674	0.00060	-0.00062	0.00099	-0.00109	0.00103	-0.00120	0.00049	-0.00049	0.06311	-0.06311	0.06313	-0.06314
0.21	0.00316	0.17251	0.00182	-0.00189	0.00266	-0.00292	0.00228	-0.00266	0.00161	-0.00161	0.06311	-0.06311	0.06325	-0.06328
0.42	0.00000	96.36617	0.89275	-0.93004	0.68044	-0.74647	0.27858	-0.23890	1.07152	-1.07152	0.06311	-0.06311	1.57789	-1.62216
0.63	-0.00004	-12.52693	0.04790	-0.04990	0.08673	-0.07906	0.25051	-0.21482	0.12314	-0.12314	0.06311	-0.06311	0.30285	-0.27210
0.84	-0.00010	-5.22266	0.00656	-0.00630	0.08825	-0.08044	0.11772	-0.10095	0.04742	-0.04742	0.06311	-0.06311	0.16710	-0.15144
1.05	-0.00021	-3.00656	0.01562	-0.01500	0.05431	-0.04951	0.02996	-0.02569	0.02350	-0.02350	0.06311	-0.06311	0.09288	-0.08872
1.26	0.00102	0.83579	0.00518	-0.00498	0.00901	-0.00821	0.00326	-0.00380	0.00482	-0.00482	0.06311	-0.06311	0.06422	-0.06413
1.47	-0.00088	-0.97031	0.00731	-0.00702	0.00401	-0.00366	0.01122	-0.01309	0.00563	-0.00563	0.06311	-0.06311	0.06489	-0.06518
1.68	0.00135	0.80850	0.00476	-0.00457	0.00238	-0.00261	0.00731	-0.00853	0.00368	-0.00368	0.17621	-0.17621	0.17648	-0.17654
1.88	0.00086	0.96055	0.00616	-0.00591	0.00975	-0.01070	0.00387	-0.00451	0.00577	-0.00577	0.17621	-0.17621	0.17673	-0.17679
2.09	-0.00073	-0.88427	0.00451	-0.00433	0.01430	-0.01569	0.00866	-0.00742	0.00687	-0.00687	0.17621	-0.17621	0.17720	-0.17725
2.30	0.00047	1.28102	0.00145	-0.00140	0.01784	-0.01957	0.02610	-0.02238	0.01061	-0.01061	0.17621	-0.17621	0.17935	-0.17902
2.51	0.00016	3.31801	0.01204	-0.01254	0.01986	-0.02179	0.06294	-0.05397	0.03105	-0.03105	0.17621	-0.17621	0.19109	-0.18858
2.72	0.00049	0.99647	0.00863	-0.00899	0.00721	-0.00657	0.00269	-0.00231	0.01032	-0.01032	0.17621	-0.17621	0.17689	-0.17688
2.93	0.00077	0.66906	0.00744	-0.00775	0.01193	-0.01087	0.00933	-0.01088	0.00654	-0.00654	0.17621	-0.17621	0.17714	-0.17717
3.14	0.00134	0.39425	0.00469	-0.00489	0.00850	-0.00775	0.00804	-0.00938	0.00377	-0.00377	0.17621	-0.17621	0.17670	-0.17674
3.35	0.00089	0.57283	0.00645	-0.00672	0.01035	-0.00943	0.00810	-0.00944	0.00567	-0.00567	0.17621	-0.17621	0.17691	-0.17694
3.56	0.00076	0.65207	0.00555	-0.00578	0.00464	-0.00423	0.00173	-0.00148	0.00664	-0.00664	0.17621	-0.17621	0.17650	-0.17649
3.77	0.00028	1.82064	0.00686	-0.00715	0.01133	-0.01243	0.03590	-0.03078	0.01771	-0.01771	0.17621	-0.17621	0.18119	-0.18033
3.98	0.00034	1.65088	0.00202	-0.00193	0.02471	-0.02711	0.03616	-0.03101	0.01471	-0.01471	0.17621	-0.17621	0.18218	-0.18157
4.19	-0.00105	-0.53906	0.00312	-0.00300	0.00989	-0.01085	0.00599	-0.00513	0.00475	-0.00475	0.17621	-0.17621	0.17668	-0.17671
4.40	-0.00004	-18.55267	0.13908	-0.13351	0.22034	-0.24172	0.08735	-0.10186	0.13046	-0.13046	0.17621	-0.17621	0.35156	-0.36702
4.61	-0.00068	-1.13083	0.00942	-0.00904	0.00471	-0.00517	0.01447	-0.01687	0.00729	-0.00729	0.17621	-0.17621	0.17727	-0.17748

Table 10: 0–20%, 5.0–7.0 $\otimes$ 0.5–1.0 GeV/c Jet Function

ϕ	per trig yield	σ_{stat}/y	systematic errors											
			$+\sigma_{f2}/y$	$-\sigma_{f2}/y$	$+\sigma_{f3}/y$	$-\sigma_{f3}/y$	$+\sigma_{f4}/y$	$-\sigma_{f4}/y$	$+\sigma_{\xi/ZYAM}/y$	$-\sigma_{\xi}/y$	$+\sigma_{\pi^0}/y$	$-\sigma_{\pi^0}/y$	$+\sigma_{total}/y$	$-\sigma_{total}/y$
-1.47	-0.05096	-0.82482	0.13100	-0.11750	0.01328	-0.01321	0.05261	-0.06699	0.19473	-0.19469	0.02235	-0.02235	0.24191	-0.23848
-1.26	0.07436	0.52824	0.07076	-0.06241	0.01632	-0.01360	0.01859	-0.02372	0.13343	-0.13340	0.02235	-0.02235	0.15467	-0.15145
-1.05	0.01930	1.77396	0.13874	-0.11281	0.10009	-0.08570	0.02293	-0.01834	0.51451	-0.51441	0.02235	-0.02235	0.54315	-0.53435
-0.84	0.04434	0.69418	0.02202	-0.01421	0.02723	-0.02269	0.03936	-0.03111	0.22451	-0.22447	0.02235	-0.02235	0.23169	-0.22928
-0.63	0.02278	1.16983	0.18766	-0.17953	0.03017	-0.03005	0.05621	-0.04449	0.43825	-0.43817	0.02235	-0.02235	0.48151	-0.47708
-0.42	0.00303	7.76350	2.36052	-2.34566	0.91757	-0.99787	0.16558	-0.21282	3.30759	-3.30693	0.02235	-0.02235	4.16918	-4.18084
-0.21	0.17175	0.13281	0.05299	-0.05328	0.02603	-0.02861	0.01260	-0.01606	0.05848	-0.05846	0.02235	-0.02235	0.08697	-0.08850
-0.00	0.21540	0.10542	0.04546	-0.04584	0.02376	-0.02616	0.01335	-0.01700	0.04667	-0.04666	0.02235	-0.02235	0.07407	-0.07584
0.21	0.15235	0.14771	0.05974	-0.06007	0.02935	-0.03225	0.01421	-0.01810	0.06592	-0.06591	0.02235	-0.02235	0.09735	-0.09909
0.42	-0.01452	-1.60995	0.49251	-0.48941	0.19145	-0.20820	0.03455	-0.04440	0.69012	-0.68998	0.02235	-0.02235	0.87016	-0.87259
0.63	-0.00612	-4.19298	0.69900	-0.66874	0.11238	-0.11195	0.20938	-0.16571	1.63245	-1.63213	0.02235	-0.02235	1.79178	-1.77526
0.84	0.02256	1.25467	0.04328	-0.02793	0.05352	-0.04459	0.07737	-0.06114	0.44128	-0.44119	0.02235	-0.02235	0.45382	-0.44906
1.05	-0.00325	-10.35559	0.82336	-0.66946	0.59398	-0.50862	0.13607	-0.10883	3.05339	-3.05278	0.02235	-0.02235	3.22070	-3.16838
1.26	-0.01939	-1.98762	0.27139	-0.23934	0.06258	-0.05217	0.07131	-0.09098	0.51170	-0.51159	0.02235	-0.02235	0.58735	-0.57490
1.47	-0.01124	-3.62066	0.59391	-0.53272	0.06019	-0.05989	0.23852	-0.30374	0.88285	-0.88268	0.02235	-0.02235	1.09233	-1.07669
1.68	-0.03411	-1.20290	0.19563	-0.17547	0.08103	-0.08813	0.07861	-0.10010	0.29115	-0.29110	0.01164	-0.01164	0.36868	-0.36530
1.88	0.01838	2.13396	0.28616	-0.25230	0.24242	-0.26641	0.07534	-0.09613	0.54128	-0.54117	0.01164	-0.01164	0.66290	-0.66096
2.09	0.09657	0.34916	0.02768	-0.02249	0.05283	-0.05818	0.00455	-0.00364	0.10316	-0.10313	0.01164	-0.01164	0.11981	-0.12115
2.30	0.10409	0.28175	0.00942	-0.00609	0.04285	-0.04709	0.01674	-0.01323	0.09587	-0.09585	0.01164	-0.01164	0.10739	-0.10841
2.51	0.14425	0.18803	0.02965	-0.02837	0.01924	-0.02092	0.00887	-0.00702	0.06929	-0.06928	0.01164	-0.01164	0.07915	-0.07891
2.72	0.14460	0.17984	0.04943	-0.04912	0.00478	-0.00477	0.00346	-0.00445	0.06922	-0.06920	0.01164	-0.01164	0.08605	-0.08591
2.93	0.12382	0.19842	0.07347	-0.07388	0.00965	-0.00803	0.01747	-0.02226	0.08091	-0.08090	0.01164	-0.01164	0.11171	-0.11268
3.14	0.13373	0.17893	0.07317	-0.07381	0.01432	-0.01225	0.02149	-0.02736	0.07494	-0.07493	0.01164	-0.01164	0.10850	-0.10998
3.35	0.16641	0.14768	0.05466	-0.05497	0.00718	-0.00598	0.01300	-0.01656	0.06020	-0.06019	0.01164	-0.01164	0.08348	-0.08420
3.56	0.12510	0.20299	0.05714	-0.05678	0.00553	-0.00551	0.00400	-0.00515	0.08001	-0.07999	0.01164	-0.01164	0.09924	-0.09907
3.77	0.15328	0.17693	0.02791	-0.02670	0.01810	-0.01969	0.00835	-0.00661	0.06521	-0.06519	0.01164	-0.01164	0.07459	-0.07436
3.98	0.03965	0.74372	0.02474	-0.01599	0.11250	-0.12363	0.04396	-0.03474	0.25170	-0.25165	0.01164	-0.01164	0.28052	-0.28322
4.19	0.03033	1.07081	0.08813	-0.07160	0.16818	-0.18523	0.01450	-0.01160	0.32840	-0.32834	0.01164	-0.01164	0.37980	-0.38407
4.40	0.07364	0.50811	0.07140	-0.06295	0.06049	-0.06648	0.01880	-0.02399	0.13506	-0.13503	0.01164	-0.01164	0.16579	-0.16531
4.61	-0.02565	-1.63746	0.26016	-0.23334	0.10776	-0.11720	0.10453	-0.13312	0.38719	-0.38711	0.01164	-0.01164	0.49018	-0.48569

Table 11: 0–20%, 5.0–7.0 $\otimes$ 1.0–2.0 GeV/c Jet Function

ϕ	per trig yield	σ_{stat}/y	systematic errors											
			$+\sigma_{f2}/y$	$-\sigma_{f2}/y$	$+\sigma_{f3}/y$	$-\sigma_{f3}/y$	$+\sigma_{f4}/y$	$-\sigma_{f4}/y$	$+\sigma_{\xi/ZYAM}/y$	$-\sigma_{\xi}/y$	$+\sigma_{\pi^0}/y$	$-\sigma_{\pi^0}/y$	$+\sigma_{total}/y$	$-\sigma_{total}/y$
-1.47	0.06103	0.46602	0.08808	-0.08489	0.01902	-0.01703	0.03968	-0.05028	0.03812	-0.03810	0.00831	-0.00831	0.10591	-0.10745
-1.26	-0.02242	-1.20308	0.19831	-0.19113	0.13555	-0.12138	0.03654	-0.04630	0.10365	-0.10361	0.00831	-0.00831	0.26429	-0.25340
-1.05	-0.00280	-7.53850	0.98142	-0.94591	1.34164	-1.20143	0.59984	-0.47341	0.83098	-0.83062	0.00831	-0.00831	1.95284	-1.80341
-0.84	-0.01006	-1.94614	0.05709	-0.05502	0.30202	-0.27046	0.32653	-0.25770	0.23219	-0.23209	0.00831	-0.00831	0.50505	-0.44331
-0.63	0.04671	0.34474	0.03504	-0.03636	0.02485	-0.02225	0.05817	-0.04591	0.05035	-0.05032	0.00831	-0.00831	0.08851	-0.08079
-0.42	0.07772	0.19729	0.04560	-0.04731	0.01337	-0.01493	0.00452	-0.00357	0.03048	-0.03047	0.00831	-0.00831	0.05724	-0.05892
-0.21	0.14558	0.09214	0.03324	-0.03448	0.01869	-0.02087	0.01218	-0.01544	0.01637	-0.01636	0.00831	-0.00831	0.04404	-0.04690
-0.00	0.27746	0.04973	0.01909	-0.01981	0.01212	-0.01354	0.00955	-0.01211	0.00861	-0.00860	0.00831	-0.00831	0.02731	-0.02942
0.21	0.14805	0.08976	0.03268	-0.03391	0.01838	-0.02053	0.01198	-0.01518	0.01609	-0.01609	0.00831	-0.00831	0.04333	-0.04615
0.42	0.07535	0.19674	0.04704	-0.04880	0.01380	-0.01540	0.00466	-0.00368	0.03144	-0.03143	0.00831	-0.00831	0.05901	-0.06074
0.63	0.04813	0.32123	0.03400	-0.03528	0.02412	-0.02160	0.05646	-0.04456	0.04886	-0.04884	0.00831	-0.00831	0.08591	-0.07843
0.84	0.00288	6.20825	0.19927	-0.19206	1.05419	-0.94402	1.13972	-0.89949	0.81044	-0.81009	0.00831	-0.00831	1.76263	-1.54708
1.05	0.01052	1.89279	0.26108	-0.25163	0.35690	-0.31960	0.15957	-0.12593	0.22105	-0.22096	0.00831	-0.00831	0.51955	-0.47981
1.26	0.00116	21.49205	3.84533	-3.70616	2.62834	-2.35368	0.70849	-0.89772	2.00984	-2.00899	0.00831	-0.00831	5.12213	-4.91095
1.47	0.00089	32.54380	6.07262	-5.85285	1.31130	-1.17427	2.73577	-3.46643	2.62830	-2.62718	0.00831	-0.00831	7.27933	-7.38600
1.68	0.05362	0.51768	0.10024	-0.09662	0.01938	-0.02165	0.04516	-0.05722	0.04349	-0.04348	0.02750	-0.02750	0.12293	-0.12539
1.88	0.04562	0.57093	0.09747	-0.09394	0.05966	-0.06662	0.01796	-0.02275	0.05127	-0.05125	0.02750	-0.02750	0.12948	-0.13101
2.09	0.04472	0.45751	0.06144	-0.05921	0.07521	-0.08399	0.03755	-0.02964	0.05243	-0.05241	0.02750	-0.02750	0.11978	-0.12224
2.30	0.02882	0.65794	0.01993	-0.01921	0.09441	-0.10543	0.11398	-0.08995	0.08157	-0.08154	0.02750	-0.02750	0.17237	-0.16425
2.51	0.06483	0.24680	0.02525	-0.02619	0.01603	-0.01790	0.04191	-0.03308	0.03636	-0.03635	0.02750	-0.02750	0.06877	-0.06464
2.72	0.07148	0.22262	0.04959	-0.05145	0.01624	-0.01454	0.00491	-0.00388	0.03306	-0.03305	0.02750	-0.02750	0.06779	-0.06871
2.93	0.07869	0.18612	0.06149	-0.06380	0.03862	-0.03458	0.02254	-0.02856	0.03009	-0.03007	0.02750	-0.02750	0.08626	-0.08799
3.14	0.06401	0.23854	0.08274	-0.08585	0.05868	-0.05255	0.04141	-0.05247	0.03701	-0.03699	0.02750	-0.02750	0.11887	-0.12251
3.35	0.08156	0.17844	0.05932	-0.06155	0.03726	-0.03336	0.02175	-0.02755	0.02903	-0.02901	0.02750	-0.02750	0.08354	-0.08520
3.56	0.05522	0.28193	0.06419	-0.06660	0.02102	-0.01882	0.00636	-0.00502	0.04280	-0.04278	0.02750	-0.02750	0.08479	-0.08603
3.77	0.04416	0.35803	0.03707	-0.03846	0.02354	-0.02629	0.06154	-0.04857	0.05339	-0.05336	0.02750	-0.02750	0.09655	-0.09018
3.98	0.04487	0.41204	0.01280	-0.01234	0.06065	-0.06773	0.07322	-0.05779	0.05240	-0.05238	0.02750	-0.02750	0.11272	-0.10761
4.19	0.06607	0.30540	0.04159	-0.04009	0.05091	-0.05686	0.02542	-0.02006	0.03550	-0.03548	0.02750	-0.02750	0.08357	-0.08519
4.40	0.03199	0.75607	0.13896	-0.13393	0.08506	-0.09498	0.02560	-0.03244	0.07310	-0.07307	0.02750	-0.02750	0.18248	-0.18468
4.61	-0.03865	-0.69982	0.13910	-0.13406	0.02690	-0.03004	0.06266	-0.07940	0.06035	-0.06032	0.02750	-0.02750	0.16851	-0.17197

Table 12: 0–20%, 5.0–7.0 $\otimes$ 2.0–3.0 GeV/c Jet Function

ϕ	per trig yield	σ_{stat}/y	systematic errors											
			$+\sigma_{f2}/y$	$-\sigma_{f2}/y$	$+\sigma_{f3}/y$	$-\sigma_{f3}/y$	$+\sigma_{f4}/y$	$-\sigma_{f4}/y$	$+\sigma_{\xi/ZYAM}/y$	$-\sigma_{\xi}/y$	$+\sigma_{\pi^0}/y$	$-\sigma_{\pi^0}/y$	$+\sigma_{total}/y$	$-\sigma_{total}/y$
-1.47	0.00959	0.87049	0.07299	-0.06990	0.01697	-0.01535	0.03902	-0.04833	0.01829	-0.01829	0.00631	-0.00631	0.08667	-0.08849
-1.26	-0.00508	-1.45691	0.11395	-0.10913	0.08384	-0.07588	0.02491	-0.03086	0.03441	-0.03441	0.00631	-0.00631	0.14785	-0.14086
-1.05	0.00519	1.24244	0.06900	-0.06607	0.10153	-0.09188	0.04891	-0.03949	0.03373	-0.03373	0.00631	-0.00631	0.13652	-0.12468
-0.84	-0.00569	-0.90922	0.01316	-0.01260	0.07495	-0.06783	0.08731	-0.07049	0.03096	-0.03096	0.00631	-0.00631	0.12004	-0.10357
-0.63	0.02423	0.19913	0.00874	-0.00913	0.00672	-0.00608	0.01695	-0.01368	0.00734	-0.00734	0.00631	-0.00631	0.02242	-0.02003
-0.42	0.02631	0.16433	0.01743	-0.01821	0.00560	-0.00619	0.00202	-0.00163	0.00685	-0.00685	0.00631	-0.00631	0.02064	-0.02143
-0.21	0.07419	0.05607	0.00844	-0.00881	0.00520	-0.00574	0.00370	-0.00458	0.00245	-0.00245	0.00631	-0.00631	0.01256	-0.01332
-0.00	0.12605	0.03248	0.00544	-0.00568	0.00378	-0.00418	0.00325	-0.00403	0.00145	-0.00145	0.00631	-0.00631	0.00982	-0.01038
0.21	0.07907	0.05225	0.00792	-0.00827	0.00488	-0.00539	0.00347	-0.00430	0.00230	-0.00230	0.00631	-0.00631	0.01199	-0.01269
0.42	0.02929	0.14152	0.01566	-0.01635	0.00503	-0.00556	0.00181	-0.00146	0.00615	-0.00615	0.00631	-0.00631	0.01875	-0.01944
0.63	0.01175	0.38203	0.01803	-0.01882	0.01385	-0.01253	0.03494	-0.02821	0.01514	-0.01514	0.00631	-0.00631	0.04479	-0.03970
0.84	0.00605	0.81914	0.01237	-0.01184	0.07042	-0.06373	0.08203	-0.06623	0.02909	-0.02909	0.00631	-0.00631	0.11281	-0.09733
1.05	0.00258	2.22632	0.13891	-0.13303	0.20441	-0.18500	0.09848	-0.07951	0.06791	-0.06791	0.00631	-0.00631	0.27465	-0.25079
1.26	-0.00087	-7.74826	0.66475	-0.63659	0.48909	-0.44264	0.14533	-0.18000	0.20073	-0.20073	0.00631	-0.00631	0.86172	-0.82092
1.47	0.01304	0.65789	0.05371	-0.05143	0.01248	-0.01130	0.02871	-0.03556	0.01346	-0.01346	0.00631	-0.00631	0.06392	-0.06526
1.68	0.00705	1.23244	0.09931	-0.09511	0.02089	-0.02308	0.05309	-0.06575	0.02500	-0.02500	0.00737	-0.00737	0.11746	-0.12075
1.88	0.00148	4.71297	0.39071	-0.37416	0.26017	-0.28747	0.08542	-0.10580	0.11940	-0.11940	0.00737	-0.00737	0.49188	-0.49814
2.09	0.01276	0.48131	0.02805	-0.02686	0.03735	-0.04127	0.01988	-0.01605	0.01391	-0.01391	0.00737	-0.00737	0.05315	-0.05413
2.30	0.00417	1.24594	0.01795	-0.01719	0.09248	-0.10219	0.11904	-0.09612	0.04272	-0.04272	0.00737	-0.00737	0.15788	-0.14784
2.51	0.00199	2.34553	0.10623	-0.11093	0.07387	-0.08162	0.20588	-0.16623	0.08963	-0.08963	0.00737	-0.00737	0.25927	-0.23386
2.72	0.01361	0.31635	0.03372	-0.03521	0.01196	-0.01083	0.00390	-0.00315	0.01319	-0.01319	0.00737	-0.00737	0.03903	-0.03994
2.93	0.01711	0.25191	0.03661	-0.03823	0.02491	-0.02254	0.01603	-0.01985	0.01052	-0.01052	0.00737	-0.00737	0.04881	-0.05029
3.14	0.01711	0.24804	0.04008	-0.04185	0.03079	-0.02787	0.02395	-0.02967	0.01053	-0.01053	0.00737	-0.00737	0.05739	-0.05978
3.35	0.00837	0.50301	0.07481	-0.07811	0.05090	-0.04606	0.03275	-0.04056	0.02149	-0.02149	0.00737	-0.00737	0.09887	-0.10191
3.56	0.01630	0.26072	0.02815	-0.02939	0.00999	-0.00904	0.00325	-0.00263	0.01101	-0.01101	0.00737	-0.00737	0.03283	-0.03358
3.77	0.01673	0.27607	0.01266	-0.01322	0.00881	-0.00973	0.02454	-0.01982	0.01069	-0.01069	0.00737	-0.00737	0.03176	-0.02882
3.98	0.00958	0.52212	0.00781	-0.00748	0.04027	-0.04449	0.05183	-0.04185	0.01860	-0.01860	0.00737	-0.00737	0.06906	-0.06471
4.19	0.00498	1.17533	0.07187	-0.06883	0.09572	-0.10576	0.05095	-0.04114	0.03566	-0.03566	0.00737	-0.00737	0.13509	-0.13763
4.40	0.01006	0.67391	0.05759	-0.05515	0.03835	-0.04237	0.01259	-0.01559	0.01760	-0.01760	0.00737	-0.00737	0.07287	-0.07378
4.61	0.00186	4.26097	0.37691	-0.36094	0.07929	-0.08761	0.20148	-0.24954	0.09487	-0.09487	0.00737	-0.00737	0.44497	-0.45747

Table 13: 0–20%, 5.0–7.0 $\otimes$ 3.0–5.0 GeV/c Jet Function

ϕ	per trig yield	σ_{stat}/y	systematic errors											
			$+\sigma_{f2}/y$	$-\sigma_{f2}/y$	$+\sigma_{f3}/y$	$-\sigma_{f3}/y$	$+\sigma_{f4}/y$	$-\sigma_{f4}/y$	$+\sigma_{\xi/ZYAM}/y$	$-\sigma_{\xi}/y$	$+\sigma_{\pi^0}/y$	$-\sigma_{\pi^0}/y$	$+\sigma_{total}/y$	$-\sigma_{total}/y$
-1.47	-0.00161	-1.77743	0.06024	-0.05727	0.01450	-0.01309	0.03771	-0.04683	0.01406	-0.01344	0.01310	-0.01310	0.07504	-0.07743
-1.26	0.00168	1.53248	0.04786	-0.04549	0.03647	-0.03292	0.01225	-0.01522	0.01344	-0.01286	0.01310	-0.01310	0.06421	-0.06101
-1.05	0.00323	0.71358	0.01539	-0.01463	0.02346	-0.02117	0.01281	-0.01032	0.00699	-0.00669	0.01310	-0.01310	0.03423	-0.03139
-0.84	0.00147	1.21348	0.00709	-0.00674	0.04179	-0.03772	0.05519	-0.04444	0.01549	-0.01482	0.01310	-0.01310	0.07249	-0.06192
-0.63	0.00247	0.68139	0.01182	-0.01243	0.00947	-0.00855	0.02709	-0.02181	0.00930	-0.00890	0.01310	-0.01310	0.03495	-0.03089
-0.42	0.00583	0.25989	0.01084	-0.01140	0.00362	-0.00401	0.00148	-0.00119	0.00400	-0.00382	0.01310	-0.01310	0.01790	-0.01827
-0.21	0.03234	0.05278	0.00267	-0.00281	0.00171	-0.00189	0.00138	-0.00171	0.00073	-0.00070	0.01310	-0.01310	0.01356	-0.01365
-0.00	0.09295	0.02190	0.00102	-0.00107	0.00074	-0.00081	0.00072	-0.00089	0.00025	-0.00024	0.01310	-0.01310	0.01318	-0.01320
0.21	0.03421	0.04972	0.00252	-0.00265	0.00162	-0.00179	0.00130	-0.00162	0.00069	-0.00066	0.01310	-0.01310	0.01352	-0.01359
0.42	0.00702	0.21036	0.00900	-0.00947	0.00301	-0.00333	0.00123	-0.00099	0.00332	-0.00317	0.01310	-0.01310	0.01655	-0.01683
0.63	0.00208	0.76535	0.01402	-0.01475	0.01124	-0.01014	0.03213	-0.02587	0.01103	-0.01055	0.01310	-0.01310	0.04060	-0.03568
0.84	0.00041	4.20092	0.02544	-0.02419	0.15007	-0.13544	0.19817	-0.15957	0.05563	-0.05321	0.01310	-0.01310	0.25633	-0.21770
1.05	0.00112	1.82053	0.04434	-0.04215	0.06758	-0.06099	0.03691	-0.02972	0.02015	-0.01927	0.01310	-0.01310	0.09205	-0.08321
1.26	0.00151	1.57481	0.05328	-0.05064	0.04060	-0.03664	0.01364	-0.01694	0.01497	-0.01432	0.01310	-0.01310	0.07119	-0.06761
1.47	0.00518	0.59739	0.01876	-0.01783	0.00452	-0.00408	0.01174	-0.01458	0.00438	-0.00419	0.01310	-0.01310	0.02648	-0.02714
1.68	0.00141	2.22076	0.06911	-0.06569	0.01501	-0.01664	0.04325	-0.05372	0.01621	-0.01550	0.20576	-0.20576	0.22242	-0.22373
1.88	-0.00162	-1.44816	0.04952	-0.04707	0.03406	-0.03774	0.01268	-0.01574	0.01410	-0.01349	0.20576	-0.20576	0.21519	-0.21542
2.09	-0.00187	-1.13527	0.02660	-0.02528	0.03658	-0.04053	0.02214	-0.01782	0.01229	-0.01175	0.20576	-0.20576	0.21219	-0.21231
2.30	-0.00051	-3.48929	0.02046	-0.01944	0.10889	-0.12065	0.15932	-0.12828	0.04533	-0.04336	0.20576	-0.20576	0.28644	-0.27497
2.51	-0.00107	-1.53032	0.02737	-0.02879	0.01980	-0.02194	0.06274	-0.05051	0.02165	-0.02071	0.20576	-0.20576	0.21882	-0.21593
2.72	0.00450	0.33515	0.01405	-0.01478	0.00520	-0.00469	0.00192	-0.00155	0.00515	-0.00493	0.20576	-0.20576	0.20638	-0.20641
2.93	0.00332	0.46045	0.02596	-0.02731	0.01843	-0.01663	0.01340	-0.01665	0.00700	-0.00669	0.20576	-0.20576	0.20875	-0.20900
3.14	0.00706	0.21649	0.01337	-0.01407	0.01072	-0.00968	0.00943	-0.01171	0.00330	-0.00315	0.20576	-0.20576	0.20671	-0.20682
3.35	0.00544	0.28261	0.01587	-0.01670	0.01127	-0.01017	0.00820	-0.01018	0.00428	-0.00409	0.20576	-0.20576	0.20688	-0.20698
3.56	0.00141	1.02956	0.04496	-0.04730	0.01664	-0.01502	0.00615	-0.00495	0.01649	-0.01577	0.20576	-0.20576	0.21200	-0.21230
3.77	0.00163	0.98462	0.01793	-0.01887	0.01298	-0.01438	0.04111	-0.03310	0.01419	-0.01357	0.20576	-0.20576	0.21147	-0.21019
3.98	0.00421	0.41859	0.00247	-0.00234	0.01313	-0.01455	0.01921	-0.01547	0.00547	-0.00523	0.20576	-0.20576	0.20716	-0.20693
4.19	-0.00113	-1.79264	0.04414	-0.04195	0.06071	-0.06726	0.03673	-0.02958	0.02039	-0.01950	0.20576	-0.20576	0.22301	-0.22333
4.40	0.00019	12.14572	0.42567	-0.40462	0.29275	-0.32437	0.10896	-0.13532	0.12119	-0.11592	0.20576	-0.20576	0.57948	-0.58568
4.61	-0.00215	-1.24619	0.04522	-0.04299	0.00983	-0.01089	0.02830	-0.03515	0.01061	-0.01014	0.20576	-0.20576	0.21305	-0.21364

Table 14: 0–20%, 5.0–7.0 $\otimes$ 5.0–7.0 GeV/c Jet Function

ϕ	per trig yield	σ_{stat}/y	systematic errors											
			$+\sigma_{f2}/y$	$-\sigma_{f2}/y$	$+\sigma_{f3}/y$	$-\sigma_{f3}/y$	$+\sigma_{f4}/y$	$-\sigma_{f4}/y$	$+\sigma_{\xi/ZYAM}/y$	$-\sigma_{\xi}/y$	$+\sigma_{\pi^0}/y$	$-\sigma_{\pi^0}/y$	$+\sigma_{total}/y$	$-\sigma_{total}/y$
-1.47	-0.00028	-4.35711	0.02898	-0.02688	0.01219	-0.01001	0.02669	-0.03623	0.01403	-0.01052	0.00282	-0.00282	0.04365	-0.04748
-1.26	-0.00085	-1.11993	0.00797	-0.00739	0.01061	-0.00871	0.00300	-0.00407	0.00465	-0.00349	0.00282	-0.00282	0.01465	-0.01293
-1.05	-0.00020	-4.33754	0.02051	-0.01902	0.05460	-0.04484	0.02745	-0.02022	0.01939	-0.01455	0.00282	-0.00282	0.06738	-0.05478
-0.84	-0.00022	-3.20283	0.00393	-0.00365	0.04049	-0.03325	0.04922	-0.03625	0.01785	-0.01339	0.00282	-0.00282	0.06636	-0.05119
-0.63	0.00003	21.38109	0.07435	-0.08015	0.10671	-0.08764	0.28088	-0.20689	0.12413	-0.09310	0.00282	-0.00282	0.33351	-0.25609
-0.42	-0.00002	-32.71521	0.28027	-0.30212	0.15257	-0.18577	0.06318	-0.04654	0.21801	-0.16351	0.00282	-0.00282	0.39161	-0.39332
-0.21	0.00595	0.14375	0.00119	-0.00128	0.00124	-0.00151	0.00093	-0.00126	0.00068	-0.00051	0.00282	-0.00282	0.00350	-0.00370
-0.00	0.03066	0.04706	0.00025	-0.00027	0.00030	-0.00036	0.00027	-0.00036	0.00013	-0.00010	0.00282	-0.00282	0.00286	-0.00288
0.21	0.00521	0.15669	0.00136	-0.00146	0.00142	-0.00173	0.00106	-0.00144	0.00078	-0.00058	0.00282	-0.00282	0.00368	-0.00393
0.42	0.00133	0.51012	0.00389	-0.00419	0.00212	-0.00258	0.00088	-0.00065	0.00303	-0.00227	0.00282	-0.00282	0.00612	-0.00614
0.63	-0.00016	-4.30996	0.01545	-0.01665	0.02217	-0.01821	0.05836	-0.04299	0.02579	-0.01934	0.00282	-0.00282	0.06935	-0.05328
0.84	0.00023	3.26406	0.00382	-0.00354	0.03933	-0.03230	0.04781	-0.03521	0.01734	-0.01301	0.00282	-0.00282	0.06446	-0.04973
1.05	-0.00082	-0.96599	0.00510	-0.00473	0.01358	-0.01115	0.00683	-0.00503	0.00482	-0.00362	0.00282	-0.00282	0.01698	-0.01389
1.26	0.00211	0.59665	0.00321	-0.00298	0.00428	-0.00351	0.00121	-0.00164	0.00188	-0.00141	0.00282	-0.00282	0.00644	-0.00582
1.47	0.00090	1.55552	0.00904	-0.00839	0.00380	-0.00312	0.00832	-0.01130	0.00438	-0.00328	0.00282	-0.00282	0.01388	-0.01505
1.68	0.00112	1.26710	0.00730	-0.00677	0.00252	-0.00307	0.00672	-0.00912	0.00354	-0.00266	0.03614	-0.03614	0.03773	-0.03810
1.88	-0.00096	-0.94397	0.00708	-0.00656	0.00774	-0.00942	0.00267	-0.00362	0.00416	-0.00312	0.03614	-0.03614	0.03796	-0.03822
2.09	0.00139	0.76064	0.00301	-0.00279	0.00659	-0.00802	0.00403	-0.00297	0.00288	-0.00216	0.03614	-0.03614	0.03719	-0.03731
2.30	0.00103	0.81111	0.00084	-0.00078	0.00715	-0.00870	0.01058	-0.00779	0.00387	-0.00290	0.03614	-0.03614	0.03854	-0.03810
2.51	0.00110	0.69986	0.00218	-0.00235	0.00257	-0.00313	0.00823	-0.00606	0.00365	-0.00274	0.03614	-0.03614	0.03740	-0.03696
2.72	0.00112	0.61342	0.00464	-0.00500	0.00307	-0.00253	0.00105	-0.00077	0.00360	-0.00270	0.03614	-0.03614	0.03676	-0.03668
2.93	0.00141	0.51322	0.00503	-0.00543	0.00640	-0.00525	0.00392	-0.00532	0.00287	-0.00215	0.03614	-0.03614	0.03737	-0.03737
3.14	0.00328	0.24679	0.00237	-0.00255	0.00339	-0.00279	0.00251	-0.00341	0.00123	-0.00092	0.03614	-0.03614	0.03649	-0.03651
3.35	0.00180	0.40761	0.00394	-0.00424	0.00500	-0.00411	0.00306	-0.00416	0.00224	-0.00168	0.03614	-0.03614	0.03690	-0.03690
3.56	0.00093	0.72120	0.00560	-0.00604	0.00371	-0.00305	0.00126	-0.00093	0.00435	-0.00326	0.03614	-0.03614	0.03704	-0.03693
3.77	0.00055	1.27894	0.00437	-0.00471	0.00515	-0.00627	0.01651	-0.01216	0.00732	-0.00549	0.03614	-0.03614	0.04096	-0.03932
3.98	-0.00020	-3.48633	0.00434	-0.00402	0.03669	-0.04468	0.05431	-0.04000	0.01985	-0.01489	0.03614	-0.03614	0.07756	-0.07170
4.19	0.00117	0.83278	0.00358	-0.00332	0.00783	-0.00954	0.00479	-0.00353	0.00342	-0.00256	0.03614	-0.03614	0.03762	-0.03778
4.40	0.00009	10.78699	0.07512	-0.06968	0.08214	-0.10001	0.02829	-0.03841	0.04421	-0.03316	0.03614	-0.03614	0.12826	-0.13689
4.61	-0.00096	-1.03486	0.00850	-0.00788	0.00294	-0.00357	0.00783	-0.01063	0.00413	-0.00309	0.03614	-0.03614	0.03828	-0.03878

Table 15: 0–20%, 7.0–9.0 $\otimes$ 0.5–1.0 GeV/c Jet Function

ϕ	per trig yield	σ_{stat}/y	systematic errors											
			$+\sigma_{f2}/y$	$-\sigma_{f2}/y$	$+\sigma_{f3}/y$	$-\sigma_{f3}/y$	$+\sigma_{f4}/y$	$-\sigma_{f4}/y$	$+\sigma_{\xi/ZYAM}/y$	$-\sigma_{\xi}/y$	$+\sigma_{\pi^0}/y$	$-\sigma_{\pi^0}/y$	$+\sigma_{total}/y$	$-\sigma_{total}/y$
-1.47	0.32359	0.36469	0.03359	-0.04366	0.00837	-0.00764	0.00927	-0.01102	0.11886	-0.11886	0.12958	-0.12958	0.17945	-0.18167
-1.26	-0.00973	-11.13807	0.92432	-1.20505	0.01602	-0.02138	0.16988	-0.20184	3.95389	-3.95379	0.12958	-0.12958	4.06615	-4.14036
-1.05	-0.07166	-1.31942	0.07760	-0.10223	0.00912	-0.01137	0.00253	-0.00206	0.53725	-0.53723	0.12958	-0.12958	0.55816	-0.56214
-0.84	0.02316	3.67462	0.05055	-0.07337	0.00725	-0.00945	0.06250	-0.05225	1.66569	-1.66565	0.12958	-0.12958	1.67267	-1.67314
-0.63	-0.04519	-1.62637	0.09260	-0.07570	0.06041	-0.05518	0.02203	-0.01839	0.85567	-0.85565	0.12958	-0.12958	0.87274	-0.87065
-0.42	-0.04083	-1.59052	0.22797	-0.18169	0.14436	-0.12988	0.01811	-0.02145	0.94946	-0.94943	0.12958	-0.12958	0.99569	-0.98415
-0.21	0.29954	0.21128	0.04268	-0.03382	0.02822	-0.02529	0.00822	-0.00978	0.12967	-0.12967	0.12958	-0.12958	0.19051	-0.18837
-0.00	0.27271	0.23033	0.05139	-0.04067	0.03458	-0.03096	0.01174	-0.01396	0.14253	-0.14253	0.12958	-0.12958	0.20268	-0.19978
0.21	0.24354	0.25544	0.05250	-0.04160	0.03471	-0.03110	0.01012	-0.01203	0.15948	-0.15948	0.12958	-0.12958	0.21515	-0.21229
0.42	0.06938	0.93053	0.13415	-0.10692	0.08495	-0.07643	0.01066	-0.01262	0.55874	-0.55872	0.12958	-0.12958	0.59524	-0.58855
0.63	0.09799	0.72421	0.04271	-0.03491	0.02786	-0.02545	0.01016	-0.00848	0.39461	-0.39460	0.12958	-0.12958	0.41859	-0.41766
0.84	0.05287	1.47690	0.02214	-0.03213	0.00317	-0.00414	0.02737	-0.02289	0.72953	-0.72951	0.12958	-0.12958	0.74179	-0.74199
1.05	-0.08512	-1.08392	0.06533	-0.08607	0.00768	-0.00957	0.00213	-0.00173	0.45230	-0.45228	0.12958	-0.12958	0.47507	-0.47839
1.26	0.04114	2.58620	0.21858	-0.28496	0.00379	-0.00506	0.04017	-0.04773	0.93499	-0.93497	0.12958	-0.12958	0.96975	-0.98715
1.47	0.22362	0.50580	0.04860	-0.06318	0.01210	-0.01106	0.01341	-0.01595	0.17199	-0.17199	0.12958	-0.12958	0.22150	-0.22526
1.68	0.01831	6.17699	0.59356	-0.77158	0.32020	-0.28807	0.16377	-0.19482	2.10190	-2.10185	0.11716	-0.11716	2.21662	-2.26887
1.88	0.18038	0.59961	0.04985	-0.06499	0.04668	-0.04182	0.00917	-0.01090	0.21362	-0.21362	0.11716	-0.11716	0.25320	-0.25583
2.09	0.16848	0.55095	0.03301	-0.04348	0.05579	-0.04994	0.00106	-0.00086	0.22903	-0.22902	0.11716	-0.11716	0.26530	-0.26564
2.30	0.26706	0.30397	0.00438	-0.00636	0.03157	-0.02829	0.00541	-0.00452	0.14469	-0.14469	0.11716	-0.11716	0.18896	-0.18847
2.51	0.12041	0.61839	0.03475	-0.02841	0.04888	-0.04398	0.00826	-0.00690	0.32135	-0.32134	0.11716	-0.11716	0.34736	-0.34609
2.72	0.14957	0.47818	0.06223	-0.04960	0.01831	-0.01672	0.00494	-0.00585	0.25901	-0.25900	0.11716	-0.11716	0.29162	-0.28911
2.93	0.33013	0.20656	0.03873	-0.03069	0.00058	-0.00072	0.00746	-0.00887	0.11744	-0.11744	0.11716	-0.11716	0.17051	-0.16893
3.14	0.32169	0.20662	0.04357	-0.03448	0.00194	-0.00243	0.00994	-0.01183	0.12056	-0.12055	0.11716	-0.11716	0.17396	-0.17203
3.35	0.26243	0.25979	0.04872	-0.03861	0.00072	-0.00091	0.00938	-0.01116	0.14774	-0.14773	0.11716	-0.11716	0.19497	-0.19279
3.56	0.22753	0.31012	0.04091	-0.03260	0.01203	-0.01099	0.00325	-0.00384	0.17026	-0.17026	0.11716	-0.11716	0.21105	-0.20955
3.77	0.29693	0.25400	0.01409	-0.01152	0.01982	-0.01783	0.00335	-0.00280	0.13031	-0.13031	0.11716	-0.11716	0.17695	-0.17654
3.98	0.33285	0.24806	0.00352	-0.00511	0.02533	-0.02270	0.00434	-0.00363	0.11609	-0.11609	0.11716	-0.11716	0.16696	-0.16660
4.19	0.04866	1.85281	0.11428	-0.15056	0.19318	-0.17293	0.00367	-0.00298	0.79300	-0.79298	0.11716	-0.11716	0.83244	-0.83374
4.40	0.25037	0.41654	0.03591	-0.04682	0.03363	-0.03013	0.00661	-0.00785	0.15390	-0.15390	0.11716	-0.11716	0.19969	-0.20143
4.61	0.22760	0.51422	0.04775	-0.06208	0.02576	-0.02318	0.01318	-0.01567	0.16911	-0.16910	0.11716	-0.11716	0.21317	-0.21670

Table 16: 0–20%, 7.0–9.0 $\otimes$ 1.0–2.0 GeV/c Jet Function

ϕ	per trig yield	σ_{stat}/y	systematic errors											
			$+\sigma_{f2}/y$	$-\sigma_{f2}/y$	$+\sigma_{f3}/y$	$-\sigma_{f3}/y$	$+\sigma_{f4}/y$	$-\sigma_{f4}/y$	$+\sigma_{\xi/ZYAM}/y$	$-\sigma_{\xi}/y$	$+\sigma_{\pi^0}/y$	$-\sigma_{\pi^0}/y$	$+\sigma_{total}/y$	$-\sigma_{total}/y$
-1.47	-0.03437	-2.27178	0.21717	-0.28737	0.04084	-0.04608	0.07442	-0.08781	0.06452	-0.06449	0.00411	-0.00411	0.24197	-0.31080
-1.26	0.07171	1.04945	0.08608	-0.11390	0.05123	-0.05782	0.01206	-0.01423	0.03090	-0.03088	0.00411	-0.00411	0.10560	-0.13225
-1.05	-0.03855	-1.52155	0.09896	-0.13095	0.11780	-0.13294	0.04284	-0.03631	0.05755	-0.05752	0.00411	-0.00411	0.16981	-0.19866
-0.84	0.02033	2.67955	0.03923	-0.05191	0.18070	-0.20393	0.15892	-0.13468	0.10949	-0.10944	0.00411	-0.00411	0.26730	-0.27279
-0.63	0.11067	0.40770	0.02819	-0.02131	0.01268	-0.01431	0.02415	-0.02047	0.02022	-0.02021	0.00411	-0.00411	0.04433	-0.03877
-0.42	0.08592	0.49362	0.07864	-0.05943	0.01843	-0.01633	0.00402	-0.00341	0.02620	-0.02618	0.00411	-0.00411	0.08511	-0.06718
-0.21	0.20256	0.18449	0.04554	-0.03441	0.02047	-0.01814	0.00925	-0.01091	0.01116	-0.01115	0.00411	-0.00411	0.05215	-0.04212
-0.00	0.41740	0.09252	0.02419	-0.01828	0.01228	-0.01088	0.00671	-0.00791	0.00542	-0.00542	0.00411	-0.00411	0.02876	-0.02370
0.21	0.27060	0.13742	0.03409	-0.02576	0.01532	-0.01358	0.00692	-0.00817	0.00835	-0.00835	0.00411	-0.00411	0.03913	-0.03164
0.42	0.08026	0.50920	0.08418	-0.06361	0.01973	-0.01749	0.00430	-0.00365	0.02804	-0.02803	0.00411	-0.00411	0.09109	-0.07189
0.63	0.04960	0.86122	0.06291	-0.04754	0.02830	-0.03193	0.05389	-0.04567	0.04512	-0.04510	0.00411	-0.00411	0.09857	-0.08612
0.84	0.11290	0.44176	0.00706	-0.00935	0.03254	-0.03673	0.02862	-0.02426	0.01972	-0.01971	0.00411	-0.00411	0.04831	-0.04930
1.05	0.03677	1.50327	0.10377	-0.13731	0.12352	-0.13940	0.04493	-0.03807	0.06034	-0.06032	0.00411	-0.00411	0.17805	-0.20831
1.26	-0.09182	-0.74158	0.06723	-0.08896	0.04001	-0.04516	0.00942	-0.01112	0.02413	-0.02412	0.00411	-0.00411	0.08252	-0.10332
1.47	-0.09466	-0.83266	0.07885	-0.10433	0.01483	-0.01673	0.02702	-0.03188	0.02342	-0.02341	0.00411	-0.00411	0.08793	-0.11290
1.68	-0.01542	-4.95110	0.48410	-0.64059	0.10273	-0.09103	0.16589	-0.19575	0.14409	-0.14402	0.00603	-0.00603	0.54150	-0.69119
1.88	-0.02989	-2.37390	0.20655	-0.27332	0.13874	-0.12294	0.02895	-0.03416	0.07450	-0.07446	0.00603	-0.00603	0.26141	-0.31075
2.09	0.06403	0.88193	0.05958	-0.07885	0.08005	-0.07093	0.02580	-0.02186	0.03485	-0.03484	0.00603	-0.00603	0.10897	-0.11391
2.30	0.01507	3.45124	0.05292	-0.07002	0.27510	-0.24376	0.21438	-0.18168	0.14841	-0.14834	0.00603	-0.00603	0.38275	-0.34551
2.51	0.03190	1.38053	0.09782	-0.07392	0.04965	-0.04400	0.08379	-0.07101	0.07029	-0.07026	0.00603	-0.00603	0.15502	-0.13197
2.72	0.11259	0.39115	0.06001	-0.04535	0.01247	-0.01407	0.00307	-0.00260	0.01995	-0.01994	0.00603	-0.00603	0.06481	-0.05192
2.93	0.08719	0.46510	0.10579	-0.07994	0.04214	-0.04755	0.02148	-0.02535	0.02580	-0.02579	0.00603	-0.00603	0.11887	-0.09998
3.14	0.18774	0.22713	0.05378	-0.04064	0.02419	-0.02730	0.01491	-0.01760	0.01199	-0.01198	0.00603	-0.00603	0.06229	-0.05373
3.35	0.03063	1.31132	0.30118	-0.22761	0.11997	-0.13539	0.06117	-0.07218	0.07346	-0.07343	0.00603	-0.00603	0.33805	-0.28421
3.56	0.05909	0.73052	0.11434	-0.08641	0.02375	-0.02680	0.00584	-0.00495	0.03802	-0.03800	0.00603	-0.00603	0.12310	-0.09844
3.77	0.10175	0.43489	0.03066	-0.02317	0.01557	-0.01379	0.02627	-0.02226	0.02203	-0.02202	0.00603	-0.00603	0.04893	-0.04176
3.98	0.01829	2.80139	0.04361	-0.05771	0.22671	-0.20089	0.17668	-0.14973	0.12231	-0.12225	0.00603	-0.00603	0.31545	-0.28476
4.19	0.03006	1.86066	0.12693	-0.16797	0.17052	-0.15110	0.05496	-0.04657	0.07425	-0.07422	0.00603	-0.00603	0.23186	-0.24240
4.40	0.08500	0.79239	0.07263	-0.09611	0.04878	-0.04323	0.01018	-0.01201	0.02620	-0.02618	0.00603	-0.00603	0.09209	-0.10941
4.61	-0.02463	-3.04555	0.30303	-0.40098	0.06430	-0.05698	0.10384	-0.12253	0.09019	-0.09015	0.00603	-0.00603	0.33899	-0.43268

Table 17: 0–20%, 7.0–9.0 $\otimes$ 2.0–3.0 GeV/c Jet Function

ϕ	per trig yield	σ_{stat}/y	systematic errors											
			$+\sigma_{f2}/y$	$-\sigma_{f2}/y$	$+\sigma_{f3}/y$	$-\sigma_{f3}/y$	$+\sigma_{f4}/y$	$-\sigma_{f4}/y$	$+\sigma_{\xi/ZYAM}/y$	$-\sigma_{\xi}/y$	$+\sigma_{\pi^0}/y$	$-\sigma_{\pi^0}/y$	$+\sigma_{total}/y$	$-\sigma_{total}/y$
-1.47	-0.00968	-2.33128	0.09830	-0.12775	0.02089	-0.02422	0.04455	-0.04919	0.01736	-0.01725	0.02268	-0.02268	0.11358	-0.14191
-1.26	0.01567	1.34516	0.05021	-0.06525	0.03377	-0.03916	0.00931	-0.01027	0.01070	-0.01063	0.02268	-0.02268	0.06615	-0.08077
-1.05	-0.00926	-1.90608	0.05251	-0.06824	0.07063	-0.08191	0.02813	-0.02548	0.01812	-0.01801	0.02268	-0.02268	0.09685	-0.11338
-0.84	-0.00903	-1.59372	0.01126	-0.01464	0.05862	-0.06799	0.05646	-0.05114	0.01868	-0.01857	0.02268	-0.02268	0.08726	-0.09117
-0.63	0.00828	1.58638	0.04719	-0.03631	0.02442	-0.02832	0.05094	-0.04614	0.02055	-0.02043	0.02268	-0.02268	0.07972	-0.07198
-0.42	0.05268	0.23409	0.01605	-0.01235	0.00445	-0.00384	0.00103	-0.00094	0.00326	-0.00324	0.02268	-0.02268	0.02835	-0.02633
-0.21	0.09568	0.12268	0.01207	-0.00929	0.00641	-0.00553	0.00330	-0.00364	0.00181	-0.00180	0.02268	-0.02268	0.02675	-0.02545
-0.00	0.23239	0.05320	0.00544	-0.00418	0.00326	-0.00281	0.00203	-0.00224	0.00075	-0.00074	0.02268	-0.02268	0.02365	-0.02336
0.21	0.08960	0.12883	0.01289	-0.00992	0.00685	-0.00591	0.00352	-0.00389	0.00193	-0.00192	0.02268	-0.02268	0.02727	-0.02582
0.42	0.02332	0.48713	0.03627	-0.02791	0.01005	-0.00867	0.00234	-0.00212	0.00736	-0.00732	0.02268	-0.02268	0.04462	-0.03777
0.63	0.01590	0.78144	0.02456	-0.01890	0.01271	-0.01474	0.02650	-0.02401	0.01069	-0.01063	0.02268	-0.02268	0.04578	-0.04217
0.84	-0.00549	-2.45404	0.01851	-0.02406	0.09637	-0.11177	0.09282	-0.08408	0.03071	-0.03053	0.02268	-0.02268	0.14037	-0.14693
1.05	-0.00917	-1.70633	0.05300	-0.06888	0.07129	-0.08268	0.02840	-0.02572	0.01829	-0.01818	0.02268	-0.02268	0.09771	-0.11440
1.26	0.01241	1.52942	0.06339	-0.08238	0.04264	-0.04945	0.01175	-0.01297	0.01350	-0.01343	0.02268	-0.02268	0.08168	-0.10047
1.47	0.00371	6.30803	0.25623	-0.33299	0.05445	-0.06314	0.11614	-0.12822	0.04524	-0.04497	0.02268	-0.02268	0.29098	-0.36585
1.68	0.01441	1.68082	0.06604	-0.08582	0.01627	-0.01403	0.02993	-0.03304	0.01170	-0.01163	0.00566	-0.00566	0.07544	-0.09392
1.88	0.00173	11.12380	0.45414	-0.59018	0.35423	-0.30544	0.08418	-0.09294	0.09761	-0.09703	0.00566	-0.00566	0.59023	-0.67801
2.09	-0.00528	-3.12668	0.09217	-0.11978	0.14378	-0.12398	0.04938	-0.04473	0.03215	-0.03196	0.00566	-0.00566	0.18075	-0.18103
2.30	-0.00622	-2.26563	0.01635	-0.02124	0.09869	-0.08509	0.08196	-0.07424	0.02736	-0.02719	0.00566	-0.00566	0.13230	-0.11822
2.51	-0.00747	-1.70686	0.05229	-0.04024	0.03139	-0.02706	0.05644	-0.05113	0.02285	-0.02271	0.00566	-0.00566	0.08637	-0.07425
2.72	0.01749	0.68293	0.04836	-0.03721	0.01156	-0.01340	0.00311	-0.00282	0.00979	-0.00973	0.00566	-0.00566	0.05108	-0.04122
2.93	0.02666	0.45081	0.04332	-0.03333	0.01985	-0.02302	0.01185	-0.01308	0.00643	-0.00640	0.00566	-0.00566	0.04984	-0.04342
3.14	0.02451	0.48337	0.05157	-0.03968	0.02669	-0.03095	0.01926	-0.02126	0.00700	-0.00696	0.00566	-0.00566	0.06183	-0.05536
3.35	0.03870	0.31116	0.02983	-0.02296	0.01367	-0.01586	0.00816	-0.00901	0.00443	-0.00441	0.00566	-0.00566	0.03457	-0.03018
3.56	0.02352	0.50528	0.03595	-0.02766	0.00859	-0.00996	0.00232	-0.00210	0.00727	-0.00723	0.00566	-0.00566	0.03816	-0.03087
3.77	0.02216	0.58346	0.01762	-0.01356	0.01058	-0.00912	0.01902	-0.01723	0.00770	-0.00765	0.00566	-0.00566	0.02959	-0.02558
3.98	0.00311	4.43715	0.03264	-0.04242	0.19705	-0.16990	0.16364	-0.14823	0.05462	-0.05430	0.00566	-0.00566	0.26398	-0.23584
4.19	0.00720	2.26523	0.06754	-0.08777	0.10536	-0.09085	0.03619	-0.03278	0.02356	-0.02342	0.00566	-0.00566	0.13251	-0.13271
4.40	-0.01587	-1.14778	0.04959	-0.06444	0.03868	-0.03335	0.00919	-0.01015	0.01066	-0.01060	0.00566	-0.00566	0.06469	-0.07425
4.61	-0.01676	-1.27635	0.05675	-0.07375	0.01398	-0.01206	0.02572	-0.02840	0.01005	-0.00999	0.00566	-0.00566	0.06489	-0.08076

Table 18: 0–20%, 7.0–9.0 $\otimes$ 3.0–5.0 GeV/c Jet Function

ϕ	per trig yield	σ_{stat}/y	systematic errors											
			$+\sigma_{f2}/y$	$-\sigma_{f2}/y$	$+\sigma_{f3}/y$	$-\sigma_{f3}/y$	$+\sigma_{f4}/y$	$-\sigma_{f4}/y$	$+\sigma_{\xi/ZYAM}/y$	$-\sigma_{\xi}/y$	$+\sigma_{\pi^0}/y$	$-\sigma_{\pi^0}/y$	$+\sigma_{total}/y$	$-\sigma_{total}/y$
-1.47	0.00422	1.97936	0.03048	-0.03875	0.00684	-0.00788	0.01643	-0.01828	0.00492	-0.00492	0.01189	-0.01189	0.03757	-0.04542
-1.26	-0.01049	-0.59758	0.01014	-0.01288	0.00720	-0.00829	0.00223	-0.00249	0.00197	-0.00197	0.01189	-0.01189	0.01746	-0.01965
-1.05	0.00043	14.36547	0.15165	-0.19275	0.21530	-0.24802	0.09737	-0.08754	0.04775	-0.04775	0.01189	-0.01189	0.28505	-0.32977
-0.84	0.00252	1.99157	0.00546	-0.00694	0.03000	-0.03456	0.03281	-0.02950	0.00827	-0.00827	0.01189	-0.01189	0.04707	-0.04819
-0.63	0.00119	3.86608	0.04344	-0.03418	0.02426	-0.02795	0.05745	-0.05165	0.01766	-0.01766	0.01189	-0.01189	0.07892	-0.07120
-0.42	0.00901	0.47832	0.01241	-0.00976	0.00369	-0.00320	0.00098	-0.00088	0.00235	-0.00235	0.01189	-0.01189	0.01776	-0.01592
-0.21	0.06632	0.08417	0.00230	-0.00181	0.00131	-0.00114	0.00077	-0.00085	0.00032	-0.00032	0.01189	-0.01189	0.01221	-0.01212
-0.00	0.17988	0.03972	0.00093	-0.00073	0.00060	-0.00052	0.00042	-0.00047	0.00012	-0.00012	0.01189	-0.01189	0.01195	-0.01193
0.21	0.06604	0.08317	0.00231	-0.00182	0.00132	-0.00114	0.00077	-0.00086	0.00032	-0.00032	0.01189	-0.01189	0.01221	-0.01212
0.42	0.00785	0.52402	0.01425	-0.01121	0.00423	-0.00368	0.00112	-0.00101	0.00270	-0.00270	0.01189	-0.01189	0.01926	-0.01700
0.63	0.00092	4.72590	0.05605	-0.04410	0.03130	-0.03606	0.07413	-0.06665	0.02279	-0.02279	0.01189	-0.01189	0.10138	-0.09136
0.84	0.00400	1.23144	0.00344	-0.00437	0.01888	-0.02175	0.02064	-0.01856	0.00520	-0.00520	0.01189	-0.01189	0.03103	-0.03170
1.05	0.00160	3.54533	0.04104	-0.05216	0.05827	-0.06712	0.02635	-0.02369	0.01292	-0.01292	0.01189	-0.01189	0.07799	-0.08998
1.26	-0.00886	-0.66285	0.01200	-0.01526	0.00852	-0.00982	0.00265	-0.00294	0.00234	-0.00234	0.01189	-0.01189	0.01925	-0.02202
1.47	-0.00359	-2.20901	0.03586	-0.04558	0.00804	-0.00926	0.01933	-0.02150	0.00579	-0.00579	0.01189	-0.01189	0.04358	-0.05292
1.68	-0.01746	-0.39482	0.00736	-0.00936	0.00190	-0.00165	0.00397	-0.00442	0.00119	-0.00119	0.05457	-0.05457	0.05526	-0.05558
1.88	0.01296	0.57319	0.00821	-0.01043	0.00671	-0.00583	0.00181	-0.00201	0.00161	-0.00161	0.05457	-0.05457	0.05565	-0.05593
2.09	-0.00208	-2.81233	0.03166	-0.04024	0.05178	-0.04495	0.02033	-0.01828	0.01009	-0.01009	0.05457	-0.05457	0.08472	-0.08399
2.30	0.00593	0.86700	0.00232	-0.00295	0.01467	-0.01273	0.01392	-0.01252	0.00354	-0.00354	0.05457	-0.05457	0.05835	-0.05761
2.51	0.01445	0.35614	0.00357	-0.00281	0.00230	-0.00200	0.00473	-0.00425	0.00146	-0.00146	0.05457	-0.05457	0.05496	-0.05487
2.72	0.01102	0.39878	0.01015	-0.00798	0.00262	-0.00302	0.00080	-0.00072	0.00192	-0.00192	0.05457	-0.05457	0.05561	-0.05528
2.93	0.02175	0.22420	0.00702	-0.00552	0.00347	-0.00400	0.00234	-0.00260	0.00097	-0.00097	0.05457	-0.05457	0.05519	-0.05507
3.14	0.02049	0.22790	0.00816	-0.00642	0.00456	-0.00525	0.00370	-0.00412	0.00104	-0.00104	0.05457	-0.05457	0.05550	-0.05536
3.35	0.00894	0.48676	0.01707	-0.01343	0.00844	-0.00972	0.00568	-0.00632	0.00237	-0.00237	0.05457	-0.05457	0.05813	-0.05743
3.56	0.01234	0.35527	0.00906	-0.00713	0.00234	-0.00269	0.00072	-0.00064	0.00171	-0.00171	0.05457	-0.05457	0.05540	-0.05513
3.77	0.01124	0.43087	0.00459	-0.00361	0.00296	-0.00257	0.00608	-0.00546	0.00187	-0.00187	0.05457	-0.05457	0.05521	-0.05506
3.98	0.00304	1.59323	0.00452	-0.00574	0.02858	-0.02481	0.02713	-0.02439	0.00690	-0.00690	0.05457	-0.05457	0.06782	-0.06534
4.19	-0.00058	-9.67347	0.11332	-0.14404	0.18534	-0.16089	0.07276	-0.06542	0.03613	-0.03613	0.05457	-0.05457	0.23827	-0.23493
4.40	0.00111	5.78806	0.09599	-0.12200	0.07849	-0.06814	0.02117	-0.02354	0.01886	-0.01886	0.05457	-0.05457	0.13841	-0.15302
4.61	0.00585	1.37174	0.02199	-0.02795	0.00568	-0.00493	0.01186	-0.01319	0.00356	-0.00356	0.05457	-0.05457	0.06039	-0.06301

Table 19: 0–20%, 7.0–9.0 $\otimes$ 5.0–7.0 GeV/c Jet Function

ϕ	per trig yield	σ_{stat}/y	systematic errors											
			$+\sigma_{f2}/y$	$-\sigma_{f2}/y$	$+\sigma_{f3}/y$	$-\sigma_{f3}/y$	$+\sigma_{f4}/y$	$-\sigma_{f4}/y$	$+\sigma_{\xi/ZYAM}/y$	$-\sigma_{\xi}/y$	$+\sigma_{\pi^0}/y$	$-\sigma_{\pi^0}/y$	$+\sigma_{total}/y$	$-\sigma_{total}/y$
-1.47	-0.00177	-1.54109	0.00556	-0.00649	0.00184	-0.00150	0.00317	-0.00491	0.00168	-0.00168	0.02962	-0.02962	0.03040	-0.03080
-1.26	-0.00070	-3.83904	0.01163	-0.01359	0.01221	-0.00997	0.00271	-0.00421	0.00424	-0.00424	0.02962	-0.02962	0.03445	-0.03460
-1.05	-0.00184	-1.02253	0.00273	-0.00319	0.00574	-0.00469	0.00259	-0.00167	0.00161	-0.00161	0.02962	-0.02962	0.03045	-0.03025
-0.84	-0.00089	-2.04583	0.00119	-0.00138	0.00962	-0.00786	0.01050	-0.00677	0.00336	-0.00336	0.02962	-0.02962	0.03306	-0.03159
-0.63	-0.00220	-0.61588	0.00165	-0.00141	0.00148	-0.00121	0.00350	-0.00226	0.00136	-0.00136	0.02962	-0.02962	0.02994	-0.02979
-0.42	-0.00031	-5.12127	0.02499	-0.02140	0.00846	-0.01037	0.00316	-0.00204	0.00959	-0.00959	0.02962	-0.02962	0.04094	-0.03923
-0.21	0.00876	0.30063	0.00123	-0.00105	0.00080	-0.00098	0.00047	-0.00073	0.00035	-0.00035	0.02962	-0.02962	0.02966	-0.02966
-0.00	0.08551	0.07601	0.00014	-0.00012	0.00010	-0.00012	0.00007	-0.00011	0.00004	-0.00004	0.02962	-0.02962	0.02962	-0.02962
0.21	0.01956	0.17987	0.00055	-0.00047	0.00036	-0.00044	0.00021	-0.00033	0.00016	-0.00016	0.02962	-0.02962	0.02963	-0.02963
0.42	0.00085	2.12401	0.00922	-0.00789	0.00312	-0.00382	0.00117	-0.00075	0.00354	-0.00354	0.02962	-0.02962	0.03140	-0.03110
0.63	-0.00302	-0.35595	0.00120	-0.00103	0.00108	-0.00088	0.00255	-0.00164	0.00099	-0.00099	0.02962	-0.02962	0.02979	-0.02971
0.84	0.00121	1.93729	0.00087	-0.00102	0.00707	-0.00577	0.00771	-0.00497	0.00247	-0.00247	0.02962	-0.02962	0.03152	-0.03070
1.05	0.00195	1.48472	0.00259	-0.00302	0.00543	-0.00443	0.00245	-0.00158	0.00153	-0.00153	0.02962	-0.02962	0.03036	-0.03018
1.26	-0.00087	-2.96211	0.00939	-0.01097	0.00985	-0.00804	0.00219	-0.00339	0.00342	-0.00342	0.02962	-0.02962	0.03285	-0.03295
1.47	-0.00450	-0.00000	0.00219	-0.00256	0.00073	-0.00059	0.00125	-0.00193	0.00066	-0.00066	0.02962	-0.02962	0.02974	-0.02981
1.68	0.00378	1.27107	0.00261	-0.00305	0.00071	-0.00086	0.00149	-0.00231	0.00079	-0.00079	0.11150	-0.11150	0.11154	-0.11157
1.88	-0.00122	-1.92661	0.00670	-0.00783	0.00574	-0.00703	0.00156	-0.00242	0.00246	-0.00246	0.11150	-0.11150	0.11188	-0.11204
2.09	0.00263	1.22148	0.00192	-0.00224	0.00328	-0.00402	0.00181	-0.00117	0.00114	-0.00114	0.11150	-0.11150	0.11158	-0.11160
2.30	-0.00163	-1.03046	0.00064	-0.00075	0.00427	-0.00524	0.00571	-0.00368	0.00184	-0.00184	0.11150	-0.11150	0.11174	-0.11170
2.51	0.00033	6.12399	0.01115	-0.00955	0.00818	-0.01002	0.02366	-0.01526	0.00923	-0.00923	0.11150	-0.11150	0.11518	-0.11376
2.72	0.00301	0.72867	0.00262	-0.00224	0.00108	-0.00089	0.00033	-0.00021	0.00100	-0.00100	0.11150	-0.11150	0.11154	-0.11153
2.93	0.00284	0.78978	0.00379	-0.00324	0.00301	-0.00246	0.00145	-0.00225	0.00106	-0.00106	0.11150	-0.11150	0.11161	-0.11160
3.14	0.00577	0.45016	0.00204	-0.00175	0.00183	-0.00150	0.00107	-0.00165	0.00052	-0.00052	0.11150	-0.11150	0.11154	-0.11153
3.35	0.00684	0.39509	0.00157	-0.00135	0.00125	-0.00102	0.00060	-0.00093	0.00044	-0.00044	0.11150	-0.11150	0.11152	-0.11151
3.56	0.00089	2.04734	0.00884	-0.00757	0.00367	-0.00299	0.00112	-0.00072	0.00339	-0.00339	0.11150	-0.11150	0.11196	-0.11185
3.77	0.00206	1.07241	0.00176	-0.00151	0.00129	-0.00158	0.00374	-0.00241	0.00146	-0.00146	0.11150	-0.11150	0.11159	-0.11155
3.98	-0.00276	-0.45692	0.00038	-0.00045	0.00253	-0.00310	0.00338	-0.00218	0.00109	-0.00109	0.11150	-0.11150	0.11158	-0.11157
4.19	-0.00331	-0.36988	0.00152	-0.00178	0.00261	-0.00319	0.00144	-0.00093	0.00090	-0.00090	0.11150	-0.11150	0.11155	-0.11156
4.40	-0.00159	-1.30970	0.00513	-0.00600	0.00440	-0.00539	0.00120	-0.00186	0.00188	-0.00188	0.11150	-0.11150	0.11172	-0.11182
4.61	-0.00021	-14.46793	0.04678	-0.05465	0.01266	-0.01551	0.02667	-0.04135	0.01415	-0.01415	0.11150	-0.11150	0.12527	-0.13255

Table 20: 0–20%, 9.0–12.0 $\otimes$ 0.5–1.0 GeV/c Jet Function

ϕ	per trig yield	σ_{stat}/y	systematic errors											
			$+\sigma_{f2}/y$	$-\sigma_{f2}/y$	$+\sigma_{f3}/y$	$-\sigma_{f3}/y$	$+\sigma_{f4}/y$	$-\sigma_{f4}/y$	$+\sigma_{\xi/ZYAM}/y$	$-\sigma_{\xi}/y$	$+\sigma_{\pi^0}/y$	$-\sigma_{\pi^0}/y$	$+\sigma_{total}/y$	$-\sigma_{total}/y$
-1.47	-0.13642	-1.63721	0.06141	-0.08858	0.01715	-0.01311	0.02560	-0.02921	0.45678	-0.45679	0.01479	-0.01479	0.46216	-0.46663
-1.26	0.07963	2.63256	0.07472	-0.10380	0.01339	-0.01694	0.02344	-0.02659	0.78259	-0.78260	0.01479	-0.01479	0.78675	-0.79022
-1.05	0.12874	1.42584	0.01173	-0.00994	0.01673	-0.02139	0.00297	-0.00240	0.48449	-0.48450	0.01479	-0.01479	0.48515	-0.48530
-0.84	0.17195	0.95808	0.04458	-0.02429	0.00615	-0.00777	0.01081	-0.00926	0.36338	-0.36339	0.01479	-0.01479	0.36662	-0.36470
-0.63	0.10675	1.33131	0.15948	-0.09485	0.02213	-0.01693	0.01248	-0.01063	0.58667	-0.58668	0.01479	-0.01479	0.60867	-0.59482
-0.42	0.11448	1.09735	0.21995	-0.13372	0.06057	-0.04669	0.00666	-0.00740	0.54840	-0.54841	0.01479	-0.01479	0.59418	-0.56665
-0.21	0.33237	0.36601	0.09241	-0.05664	0.03198	-0.02469	0.00856	-0.00975	0.18922	-0.18922	0.01479	-0.01479	0.21368	-0.19984
-0.00	0.45091	0.26940	0.07246	-0.04451	0.02671	-0.02063	0.00828	-0.00946	0.13957	-0.13957	0.01479	-0.01479	0.16041	-0.14898
0.21	0.36511	0.32834	0.08412	-0.05156	0.02912	-0.02248	0.00779	-0.00888	0.17225	-0.17226	0.01479	-0.01479	0.19462	-0.18203
0.42	0.08857	1.39889	0.28427	-0.17283	0.07828	-0.06035	0.00860	-0.00957	0.70879	-0.70880	0.01479	-0.01479	0.76786	-0.73227
0.63	-0.08099	-1.66778	0.21020	-0.12502	0.02917	-0.02231	0.01645	-0.01402	0.77325	-0.77326	0.01479	-0.01479	0.80214	-0.78388
0.84	-0.15537	-0.95591	0.04934	-0.02688	0.00680	-0.00860	0.01196	-0.01025	0.40216	-0.40217	0.01479	-0.01479	0.40568	-0.40356
1.05	0.00171	103.49941	0.88218	-0.74808	1.25889	-1.60924	0.22337	-0.18020	36.44978	-36.45036	0.01479	-0.01479	36.48287	-36.49398
1.26	0.02841	7.15983	0.20946	-0.29097	0.03755	-0.04749	0.06572	-0.07453	2.19379	-2.19382	0.01479	-0.01479	2.20511	-2.21485
1.47	-0.15347	-1.38870	0.05459	-0.07873	0.01524	-0.01166	0.02276	-0.02597	0.40603	-0.40604	0.01479	-0.01479	0.41087	-0.41484
1.68	0.03123	6.94263	0.26815	-0.38673	0.22101	-0.17039	0.11187	-0.12764	1.99669	-1.99672	0.04323	-0.04323	2.03025	-2.04540
1.88	-0.00726	-28.36098	0.81850	-1.13648	1.45990	-1.12714	0.25746	-0.29198	8.60076	-8.60089	0.04323	-0.04323	8.76598	-8.75354
2.09	0.22055	0.80967	0.00679	-0.00571	0.05446	-0.04206	0.00172	-0.00139	0.28339	-0.28340	0.04323	-0.04323	0.29188	-0.28980
2.30	0.23265	0.67024	0.03302	-0.01799	0.04560	-0.03520	0.00798	-0.00684	0.26902	-0.26903	0.04323	-0.04323	0.27834	-0.27542
2.51	0.27287	0.52796	0.06241	-0.03712	0.02538	-0.01957	0.00488	-0.00416	0.22966	-0.22967	0.04323	-0.04323	0.24326	-0.23747
2.72	-0.02224	-6.13236	1.13161	-0.68802	0.10659	-0.08151	0.03423	-0.03807	2.82042	-2.82046	0.04323	-0.04323	3.04133	-2.90488
2.93	0.32397	0.40473	0.09475	-0.05808	0.00321	-0.00406	0.00878	-0.01000	0.19380	-0.19380	0.04323	-0.04323	0.22021	-0.20717
3.14	0.27875	0.45863	0.11714	-0.07196	0.00764	-0.00976	0.01339	-0.01529	0.22530	-0.22530	0.04323	-0.04323	0.25804	-0.24112
3.35	0.38918	0.33806	0.07888	-0.04835	0.00267	-0.00338	0.00731	-0.00832	0.16133	-0.16133	0.04323	-0.04323	0.18487	-0.17411
3.56	0.26096	0.52007	0.09646	-0.05865	0.00909	-0.00695	0.00292	-0.00325	0.24041	-0.24042	0.04323	-0.04323	0.26280	-0.25133
3.77	0.49318	0.29655	0.03453	-0.02054	0.01404	-0.01083	0.00270	-0.00230	0.12707	-0.12707	0.04323	-0.04323	0.13933	-0.13624
3.98	0.07617	2.06235	0.10086	-0.05496	0.13927	-0.10752	0.02437	-0.02089	0.82170	-0.82171	0.04323	-0.04323	0.84097	-0.83193
4.19	0.19494	0.89437	0.00768	-0.00646	0.06161	-0.04758	0.00195	-0.00157	0.32063	-0.32064	0.04323	-0.04323	0.32944	-0.32709
4.40	0.42790	0.47198	0.01388	-0.01928	0.02476	-0.01912	0.00437	-0.00495	0.14588	-0.14588	0.04323	-0.04323	0.15484	-0.15464
4.61	0.03651	6.11492	0.22938	-0.33082	0.18906	-0.14575	0.09569	-0.10919	1.70802	-1.70805	0.04323	-0.04323	1.73687	-1.74983

Table 21: 0–20%, 9.0–12.0 $\otimes$ 1.0–2.0 GeV/c Jet Function

ϕ	per trig yield	σ_{stat}/y	systematic errors											
			$+\sigma_{f2}/y$	$-\sigma_{f2}/y$	$+\sigma_{f3}/y$	$-\sigma_{f3}/y$	$+\sigma_{f4}/y$	$-\sigma_{f4}/y$	$+\sigma_{\xi/ZYAM}/y$	$-\sigma_{\xi}/y$	$+\sigma_{\pi^0}/y$	$-\sigma_{\pi^0}/y$	$+\sigma_{total}/y$	$-\sigma_{total}/y$
-1.47	0.11000	1.38624	0.08897	-0.14515	0.01607	-0.02080	0.02823	-0.03202	0.02083	-0.02082	0.00659	-0.00659	0.09720	-0.15166
-1.26	-0.04725	-3.02622	0.17130	-0.27948	0.09795	-0.12678	0.02223	-0.02522	0.04846	-0.04844	0.00659	-0.00659	0.20451	-0.31178
-1.05	-0.05824	-1.94327	0.08589	-0.14013	0.09823	-0.12714	0.03311	-0.02918	0.03936	-0.03935	0.00659	-0.00659	0.14041	-0.19556
-0.84	0.09514	1.10815	0.01099	-0.01793	0.04864	-0.06296	0.03964	-0.03494	0.02417	-0.02416	0.00659	-0.00659	0.06846	-0.07832
-0.63	0.07378	1.17479	0.06837	-0.04190	0.02396	-0.03101	0.04228	-0.03727	0.03133	-0.03131	0.00659	-0.00659	0.08978	-0.07163
-0.42	0.00798	10.09848	1.36799	-0.83850	0.28659	-0.22143	0.05048	-0.04450	0.29099	-0.29086	0.00659	-0.00659	1.42856	-0.91582
-0.21	0.31766	0.22875	0.04694	-0.02877	0.01886	-0.01457	0.00716	-0.00812	0.00734	-0.00734	0.00659	-0.00659	0.05203	-0.03469
-0.00	0.53423	0.13979	0.03055	-0.01873	0.01386	-0.01071	0.00636	-0.00722	0.00437	-0.00437	0.00659	-0.00659	0.03505	-0.02408
0.21	0.32952	0.21780	0.04525	-0.02774	0.01818	-0.01405	0.00690	-0.00783	0.00708	-0.00708	0.00659	-0.00659	0.05019	-0.03349
0.42	0.08190	0.95564	0.13335	-0.08174	0.02794	-0.02158	0.00492	-0.00434	0.02837	-0.02835	0.00659	-0.00659	0.13941	-0.08952
0.63	0.11803	0.69884	0.04273	-0.02619	0.01498	-0.01939	0.02643	-0.02330	0.01958	-0.01957	0.00659	-0.00659	0.05635	-0.04507
0.84	-0.09696	-0.96268	0.01079	-0.01760	0.04773	-0.06178	0.03890	-0.03429	0.02372	-0.02371	0.00659	-0.00659	0.06719	-0.07686
1.05	-0.05149	-2.03495	0.09714	-0.15848	0.11109	-0.14379	0.03744	-0.03300	0.04452	-0.04450	0.00659	-0.00659	0.15876	-0.22115
1.26	0.01920	6.83402	0.42163	-0.68788	0.24110	-0.31205	0.05471	-0.06207	0.11927	-0.11922	0.00659	-0.00659	0.50315	-0.76724
1.47	-0.22147	-0.67260	0.04419	-0.07209	0.00798	-0.01033	0.01402	-0.01591	0.01034	-0.01034	0.00659	-0.00659	0.04861	-0.07554
1.68	-0.33081	-0.42714	0.02958	-0.04826	0.00692	-0.00534	0.00939	-0.01065	0.00694	-0.00693	0.03055	-0.03055	0.04463	-0.05876
1.88	-0.01458	-9.31756	0.55504	-0.90554	0.41078	-0.31738	0.07202	-0.08171	0.15770	-0.15763	0.03055	-0.03055	0.71260	-0.97631
2.09	0.03205	3.37192	0.15606	-0.25461	0.23100	-0.17847	0.06015	-0.05302	0.07190	-0.07187	0.03055	-0.03055	0.29570	-0.32494
2.30	0.11289	0.89187	0.00926	-0.01511	0.05306	-0.04100	0.03341	-0.02945	0.02046	-0.02045	0.03055	-0.03055	0.07328	-0.06425
2.51	0.00274	30.82087	1.83909	-1.12725	0.83428	-0.64458	1.13746	-1.00256	0.84407	-0.84370	0.03055	-0.03055	2.46687	-1.84502
2.72	0.07431	1.13174	0.14698	-0.09009	0.02379	-0.03079	0.00542	-0.00478	0.03121	-0.03120	0.03055	-0.03055	0.15526	-0.10485
2.93	0.16633	0.47244	0.08964	-0.05495	0.02782	-0.03601	0.01367	-0.01551	0.01396	-0.01396	0.03055	-0.03055	0.10062	-0.07540
3.14	0.08106	0.99692	0.20135	-0.12342	0.07057	-0.09134	0.04193	-0.04757	0.02867	-0.02865	0.03055	-0.03055	0.22144	-0.16611
3.35	0.24209	0.32602	0.06159	-0.03775	0.01912	-0.02474	0.00939	-0.01066	0.00959	-0.00959	0.03055	-0.03055	0.07261	-0.05636
3.56	0.24615	0.34277	0.04437	-0.02720	0.00718	-0.00930	0.00164	-0.00144	0.00942	-0.00942	0.03055	-0.03055	0.05518	-0.04301
3.77	0.11855	0.71946	0.04255	-0.02608	0.01930	-0.01491	0.02631	-0.02319	0.01953	-0.01952	0.03055	-0.03055	0.06473	-0.05248
3.98	-0.01030	-9.49420	0.10155	-0.16567	0.58167	-0.44942	0.36625	-0.32281	0.22430	-0.22420	0.03055	-0.03055	0.73078	-0.62035
4.19	0.03398	3.16871	0.14722	-0.24018	0.21791	-0.16836	0.05674	-0.05001	0.06783	-0.06780	0.03055	-0.03055	0.27912	-0.30670
4.40	0.14439	0.90105	0.05605	-0.09145	0.04149	-0.03205	0.00727	-0.00825	0.01593	-0.01592	0.03055	-0.03055	0.07812	-0.10318
4.61	0.28252	0.52687	0.03464	-0.05651	0.00810	-0.00626	0.01099	-0.01247	0.00812	-0.00812	0.03055	-0.03055	0.04884	-0.06623

Table 22: 0–20%, 9.0–12.0 $\otimes$ 2.0–3.0 GeV/c Jet Function

ϕ	per trig yield	σ_{stat}/y	systematic errors											
			$+\sigma_{f2}/y$	$-\sigma_{f2}/y$	$+\sigma_{f3}/y$	$-\sigma_{f3}/y$	$+\sigma_{f4}/y$	$-\sigma_{f4}/y$	$+\sigma_{\xi/ZYAM}/y$	$-\sigma_{\xi}/y$	$+\sigma_{\pi^0}/y$	$-\sigma_{\pi^0}/y$	$+\sigma_{total}/y$	$-\sigma_{total}/y$
-1.47	-0.04826	-0.85466	0.02561	-0.04096	0.00534	-0.00712	0.01128	-0.01177	0.00359	-0.00359	0.02288	-0.02288	0.03671	-0.04902
-1.26	0.01039	3.89775	0.09839	-0.15737	0.06490	-0.08661	0.01772	-0.01849	0.01663	-0.01663	0.02288	-0.02288	0.12250	-0.18278
-1.05	-0.01110	-3.04128	0.05692	-0.09105	0.07510	-0.10022	0.02801	-0.02685	0.01558	-0.01558	0.02288	-0.02288	0.10214	-0.14078
-0.84	-0.03608	-0.74197	0.00366	-0.00585	0.01869	-0.02493	0.01685	-0.01615	0.00481	-0.00481	0.02288	-0.02288	0.03454	-0.03826
-0.63	-0.00092	-27.07273	0.67747	-0.42356	0.27941	-0.37284	0.54565	-0.52294	0.18997	-0.18997	0.02288	-0.02288	0.93348	-0.79278
-0.42	0.02927	0.78782	0.04619	-0.02888	0.01174	-0.00880	0.00222	-0.00213	0.00604	-0.00604	0.02288	-0.02288	0.05326	-0.03842
-0.21	0.15760	0.15098	0.01171	-0.00732	0.00571	-0.00428	0.00253	-0.00264	0.00113	-0.00113	0.02288	-0.02288	0.02647	-0.02457
-0.00	0.30488	0.08189	0.00663	-0.00414	0.00365	-0.00273	0.00195	-0.00204	0.00058	-0.00058	0.02288	-0.02288	0.02418	-0.02351
0.21	0.13339	0.17240	0.01384	-0.00865	0.00674	-0.00505	0.00299	-0.00312	0.00133	-0.00133	0.02288	-0.02288	0.02777	-0.02521
0.42	0.03051	0.71969	0.04431	-0.02771	0.01126	-0.00844	0.00213	-0.00204	0.00579	-0.00579	0.02288	-0.02288	0.05150	-0.03742
0.63	0.01178	2.01418	0.05300	-0.03313	0.02186	-0.02917	0.04268	-0.04091	0.01486	-0.01486	0.02288	-0.02288	0.07650	-0.06608
0.84	0.03758	0.72249	0.00351	-0.00562	0.01794	-0.02394	0.01618	-0.01551	0.00462	-0.00462	0.02288	-0.02288	0.03377	-0.03728
1.05	0.02880	1.08367	0.02193	-0.03508	0.02894	-0.03861	0.01079	-0.01034	0.00600	-0.00600	0.02288	-0.02288	0.04466	-0.05821
1.26	-0.04865	-0.69149	0.02101	-0.03360	0.01386	-0.01849	0.00378	-0.00395	0.00355	-0.00355	0.02288	-0.02288	0.03440	-0.04497
1.47	-0.01405	-3.11355	0.08797	-0.14070	0.01833	-0.02446	0.03874	-0.04043	0.01232	-0.01232	0.02288	-0.02288	0.10124	-0.15068
1.68	0.05321	0.91025	0.02322	-0.03714	0.00646	-0.00484	0.01023	-0.01067	0.00326	-0.00326	0.01790	-0.01790	0.03189	-0.04299
1.88	0.01357	2.76519	0.07530	-0.12044	0.06628	-0.04967	0.01356	-0.01415	0.01283	-0.01283	0.01790	-0.01790	0.10360	-0.13289
2.09	0.00312	10.28509	0.20251	-0.32390	0.35651	-0.26717	0.09965	-0.09550	0.05598	-0.05598	0.01790	-0.01790	0.42602	-0.43459
2.30	0.04722	0.60922	0.00280	-0.00447	0.01905	-0.01428	0.01288	-0.01234	0.00371	-0.00371	0.01790	-0.01790	0.02951	-0.02666
2.51	0.03315	0.77492	0.01884	-0.01178	0.01037	-0.00777	0.01517	-0.01454	0.00530	-0.00530	0.01790	-0.01790	0.03227	-0.02755
2.72	0.03031	0.76926	0.04460	-0.02788	0.00849	-0.01134	0.00214	-0.00205	0.00581	-0.00581	0.01790	-0.01790	0.04920	-0.03556
2.93	0.05562	0.42743	0.03319	-0.02075	0.01212	-0.01617	0.00717	-0.00748	0.00317	-0.00317	0.01790	-0.01790	0.04038	-0.03284
3.14	0.08214	0.29401	0.02460	-0.01538	0.01015	-0.01354	0.00725	-0.00757	0.00215	-0.00215	0.01790	-0.01790	0.03295	-0.02832
3.35	0.01249	1.80235	0.14784	-0.09243	0.05400	-0.07205	0.03193	-0.03331	0.01413	-0.01413	0.01790	-0.01790	0.16221	-0.12396
3.56	0.05361	0.44030	0.02522	-0.01577	0.00480	-0.00641	0.00121	-0.00116	0.00329	-0.00329	0.01790	-0.01790	0.03150	-0.02495
3.77	0.03352	0.74921	0.01863	-0.01165	0.01025	-0.00768	0.01500	-0.01438	0.00524	-0.00524	0.01790	-0.01790	0.03202	-0.02738
3.98	0.00905	2.94712	0.01460	-0.02335	0.09944	-0.07452	0.06721	-0.06441	0.01936	-0.01936	0.01790	-0.01790	0.12375	-0.10461
4.19	-0.00409	-7.56238	0.15453	-0.24716	0.27205	-0.20387	0.07604	-0.07287	0.04272	-0.04272	0.01790	-0.01790	0.32529	-0.33183
4.40	-0.05848	-0.56263	0.01748	-0.02795	0.01538	-0.01153	0.00315	-0.00328	0.00298	-0.00298	0.01790	-0.01790	0.02969	-0.03542
4.61	-0.02428	-1.69214	0.05090	-0.08141	0.01415	-0.01061	0.02242	-0.02339	0.00715	-0.00715	0.01790	-0.01790	0.06054	-0.08752

Table 23: 0–20%, 9.0–12.0 $\otimes$ 3.0–5.0 GeV/c Jet Function

ϕ	per trig yield	σ_{stat}/y	systematic errors											
			$+\sigma_{f2}/y$	$-\sigma_{f2}/y$	$+\sigma_{f3}/y$	$-\sigma_{f3}/y$	$+\sigma_{f4}/y$	$-\sigma_{f4}/y$	$+\sigma_{\xi/ZYAM}/y$	$-\sigma_{\xi}/y$	$+\sigma_{\pi^0}/y$	$-\sigma_{\pi^0}/y$	$+\sigma_{total}/y$	$-\sigma_{total}/y$
-1.47	-0.00529	-2.79142	0.03134	-0.04889	0.00695	-0.00920	0.01653	-0.01741	0.00411	-0.00411	0.00836	-0.00836	0.03728	-0.05352
-1.26	-0.00849	-1.47447	0.01614	-0.02519	0.01133	-0.01501	0.00348	-0.00367	0.00256	-0.00256	0.00836	-0.00836	0.02185	-0.03081
-1.05	0.01252	1.07323	0.00676	-0.01055	0.00950	-0.01258	0.00402	-0.00382	0.00173	-0.00173	0.00836	-0.00836	0.01500	-0.01889
-0.84	-0.00391	-2.33020	0.00453	-0.00706	0.02460	-0.03258	0.02520	-0.02393	0.00558	-0.00558	0.00836	-0.00836	0.03690	-0.04225
-0.63	-0.01287	-0.59347	0.00635	-0.00407	0.00286	-0.00378	0.00633	-0.00602	0.00171	-0.00171	0.00836	-0.00836	0.01270	-0.01182
-0.42	0.01475	0.58966	0.01199	-0.00769	0.00330	-0.00249	0.00071	-0.00068	0.00151	-0.00151	0.00836	-0.00836	0.01508	-0.01174
-0.21	0.07605	0.14654	0.00318	-0.00204	0.00168	-0.00127	0.00084	-0.00089	0.00029	-0.00029	0.00836	-0.00836	0.00914	-0.00874
-0.00	0.25329	0.06187	0.00104	-0.00067	0.00062	-0.00047	0.00038	-0.00040	0.00009	-0.00009	0.00836	-0.00836	0.00845	-0.00841
0.21	0.09258	0.12599	0.00261	-0.00167	0.00138	-0.00104	0.00069	-0.00073	0.00024	-0.00024	0.00836	-0.00836	0.00889	-0.00862
0.42	0.00632	1.23519	0.02799	-0.01794	0.00770	-0.00582	0.00167	-0.00158	0.00352	-0.00352	0.00836	-0.00836	0.03046	-0.02099
0.63	-0.01630	-0.42034	0.00501	-0.00321	0.00225	-0.00299	0.00500	-0.00475	0.00135	-0.00135	0.00836	-0.00836	0.01126	-0.01065
0.84	0.01358	0.74731	0.00130	-0.00203	0.00708	-0.00938	0.00726	-0.00689	0.00161	-0.00161	0.00836	-0.00836	0.01330	-0.01456
1.05	-0.01075	-0.87804	0.00788	-0.01230	0.01107	-0.01466	0.00469	-0.00445	0.00202	-0.00202	0.00836	-0.00836	0.01675	-0.02145
1.26	0.01062	1.28497	0.01291	-0.02014	0.00906	-0.01200	0.00278	-0.00293	0.00204	-0.00204	0.00836	-0.00836	0.01818	-0.02514
1.47	0.01965	0.94268	0.00844	-0.01316	0.00187	-0.00248	0.00445	-0.00469	0.00111	-0.00111	0.00836	-0.00836	0.01286	-0.01650
1.68	0.00349	4.81532	0.04755	-0.07418	0.01397	-0.01054	0.02508	-0.02641	0.00626	-0.00626	0.03916	-0.03916	0.06825	-0.08879
1.88	0.00239	5.39688	0.05734	-0.08945	0.05331	-0.04025	0.01237	-0.01302	0.00916	-0.00916	0.03916	-0.03916	0.08888	-0.10681
2.09	-0.00098	-11.45997	0.08638	-0.13477	0.16063	-0.12127	0.05137	-0.04879	0.02239	-0.02239	0.03916	-0.03916	0.19477	-0.19309
2.30	0.01070	0.96079	0.00166	-0.00258	0.01191	-0.00899	0.00921	-0.00875	0.00206	-0.00206	0.03916	-0.03916	0.04204	-0.04126
2.51	0.00812	1.15780	0.01006	-0.00645	0.00600	-0.00453	0.01004	-0.00954	0.00272	-0.00272	0.03916	-0.03916	0.04218	-0.04116
2.72	0.00613	1.32434	0.02887	-0.01850	0.00600	-0.00794	0.00172	-0.00163	0.00361	-0.00361	0.03916	-0.03916	0.04918	-0.04422
2.93	0.04742	0.22895	0.00509	-0.00326	0.00203	-0.00269	0.00135	-0.00142	0.00047	-0.00047	0.03916	-0.03916	0.03957	-0.03942
3.14	0.05703	0.19166	0.00463	-0.00297	0.00209	-0.00276	0.00168	-0.00177	0.00039	-0.00039	0.03916	-0.03916	0.03953	-0.03942
3.35	0.04431	0.23879	0.00545	-0.00349	0.00217	-0.00288	0.00145	-0.00152	0.00050	-0.00050	0.03916	-0.03916	0.03963	-0.03946
3.56	0.01840	0.48496	0.00961	-0.00616	0.00200	-0.00265	0.00057	-0.00054	0.00120	-0.00120	0.03916	-0.03916	0.04040	-0.03976
3.77	0.00099	8.46003	0.08229	-0.05275	0.04904	-0.03703	0.08213	-0.07799	0.02224	-0.02224	0.03916	-0.03916	0.13398	-0.11075
3.98	-0.00512	-1.69403	0.00346	-0.00540	0.02490	-0.01880	0.01926	-0.01829	0.00430	-0.00430	0.03916	-0.03916	0.05055	-0.04764
4.19	-0.01691	-0.52545	0.00501	-0.00782	0.00932	-0.00703	0.00298	-0.00283	0.00130	-0.00130	0.03916	-0.03916	0.04070	-0.04067
4.40	-0.01158	-0.93986	0.01184	-0.01846	0.01100	-0.00831	0.00255	-0.00269	0.00189	-0.00189	0.03916	-0.03916	0.04249	-0.04421
4.61	-0.01100	-1.18334	0.01507	-0.02351	0.00443	-0.00334	0.00795	-0.00837	0.00198	-0.00198	0.03916	-0.03916	0.04299	-0.04660

Table 24: 0–20%, 9.0–12.0 $\otimes$ 5.0–7.0 GeV/c Jet Function

ϕ	per trig yield	σ_{stat}/y	systematic errors											
			$+\sigma_{f2}/y$	$-\sigma_{f2}/y$	$+\sigma_{f3}/y$	$-\sigma_{f3}/y$	$+\sigma_{f4}/y$	$-\sigma_{f4}/y$	$+\sigma_{\xi/ZYAM}/y$	$-\sigma_{\xi}/y$	$+\sigma_{\pi^0}/y$	$-\sigma_{\pi^0}/y$	$+\sigma_{total}/y$	$-\sigma_{total}/y$
-1.47	-0.00453	-0.00000	0.00270	-0.00380	0.00081	-0.00067	0.00122	-0.00208	0.00088	-0.00066	0.02068	-0.02068	0.02092	-0.02115
-1.26	0.00892	1.06989	0.00113	-0.00160	0.00107	-0.00089	0.00021	-0.00036	0.00044	-0.00033	0.02068	-0.02068	0.02074	-0.02076
-1.05	0.00080	6.65055	0.00777	-0.01097	0.01470	-0.01228	0.00642	-0.00376	0.00494	-0.00371	0.02068	-0.02068	0.02774	-0.02695
-0.84	-0.00454	-0.00000	0.00029	-0.00041	0.00210	-0.00176	0.00222	-0.00130	0.00088	-0.00066	0.02068	-0.02068	0.02092	-0.02081
-0.63	0.00123	3.34618	0.00443	-0.00314	0.00297	-0.00248	0.00679	-0.00398	0.00326	-0.00245	0.02068	-0.02068	0.02265	-0.02157
-0.42	-0.00235	-0.95488	0.00501	-0.00355	0.00130	-0.00155	0.00046	-0.00027	0.00171	-0.00128	0.02068	-0.02068	0.02139	-0.02108
-0.21	0.01803	0.36517	0.00089	-0.00063	0.00044	-0.00053	0.00022	-0.00038	0.00022	-0.00017	0.02068	-0.02068	0.02070	-0.02070
-0.00	0.15276	0.10909	0.00012	-0.00008	0.00006	-0.00008	0.00004	-0.00007	0.00003	-0.00002	0.02068	-0.02068	0.02068	-0.02068
0.21	0.01297	0.45446	0.00124	-0.00088	0.00061	-0.00074	0.00031	-0.00053	0.00031	-0.00023	0.02068	-0.02068	0.02073	-0.02072
0.42	0.00177	2.08158	0.00666	-0.00472	0.00172	-0.00206	0.00061	-0.00036	0.00228	-0.00171	0.02068	-0.02068	0.02192	-0.02138
0.63	0.00078	4.85894	0.00698	-0.00495	0.00468	-0.00391	0.01069	-0.00626	0.00514	-0.00385	0.02068	-0.02068	0.02527	-0.02283
0.84	-0.00454	-0.00000	0.00029	-0.00041	0.00210	-0.00176	0.00222	-0.00130	0.00088	-0.00066	0.02068	-0.02068	0.02092	-0.02081
1.05	-0.00453	-0.00000	0.00138	-0.00194	0.00261	-0.00218	0.00114	-0.00067	0.00088	-0.00066	0.02068	-0.02068	0.02093	-0.02090
1.26	0.00183	3.48326	0.00553	-0.00780	0.00523	-0.00437	0.00102	-0.00174	0.00217	-0.00163	0.02068	-0.02068	0.02216	-0.02265
1.47	-0.00453	-0.00000	0.00270	-0.00380	0.00081	-0.00067	0.00122	-0.00208	0.00088	-0.00066	0.02068	-0.02068	0.02092	-0.02115
1.68	-0.00453	-0.00000	0.00269	-0.00380	0.00067	-0.00080	0.00121	-0.00208	0.00088	-0.00066	0.00997	-0.00997	0.01046	-0.01092
1.88	0.00270	2.69113	0.00374	-0.00528	0.00296	-0.00354	0.00069	-0.00118	0.00148	-0.00111	0.00997	-0.00997	0.01117	-0.01194
2.09	0.00490	1.36832	0.00127	-0.00180	0.00201	-0.00241	0.00105	-0.00062	0.00081	-0.00061	0.00997	-0.00997	0.01034	-0.01045
2.30	0.00253	1.98637	0.00052	-0.00073	0.00315	-0.00377	0.00398	-0.00233	0.00158	-0.00119	0.00997	-0.00997	0.01131	-0.01100
2.51	-0.00158	-1.90625	0.00345	-0.00245	0.00193	-0.00231	0.00529	-0.00310	0.00255	-0.00191	0.00997	-0.00997	0.01223	-0.01114
2.72	0.00257	1.61202	0.00459	-0.00325	0.00142	-0.00119	0.00042	-0.00025	0.00157	-0.00117	0.00997	-0.00997	0.01118	-0.01062
2.93	0.02698	0.32779	0.00060	-0.00042	0.00035	-0.00030	0.00015	-0.00026	0.00015	-0.00011	0.00997	-0.00997	0.01000	-0.00999
3.14	0.02791	0.31444	0.00063	-0.00045	0.00042	-0.00035	0.00022	-0.00037	0.00014	-0.00011	0.00997	-0.00997	0.01000	-0.01000
3.35	0.01677	0.42748	0.00096	-0.00068	0.00057	-0.00048	0.00024	-0.00041	0.00024	-0.00018	0.00997	-0.00997	0.01004	-0.01002
3.56	0.00865	0.62724	0.00136	-0.00096	0.00042	-0.00035	0.00012	-0.00007	0.00046	-0.00035	0.00997	-0.00997	0.01008	-0.01003
3.77	-0.00458	-0.00000	0.00119	-0.00084	0.00067	-0.00080	0.00182	-0.00107	0.00088	-0.00066	0.00997	-0.00997	0.01027	-0.01012
3.98	0.00182	2.48481	0.00072	-0.00101	0.00438	-0.00524	0.00553	-0.00324	0.00220	-0.00165	0.00997	-0.00997	0.01243	-0.01188
4.19	0.00035	14.12438	0.01795	-0.02532	0.02835	-0.03395	0.01482	-0.00867	0.01148	-0.00861	0.00997	-0.00997	0.03971	-0.04519
4.40	-0.00454	-0.00000	0.00222	-0.00313	0.00175	-0.00210	0.00041	-0.00070	0.00088	-0.00066	0.00997	-0.00997	0.01041	-0.01070
4.61	-0.00453	-0.00000	0.00269	-0.00380	0.00067	-0.00080	0.00121	-0.00208	0.00088	-0.00066	0.00997	-0.00997	0.01046	-0.01092

Table 25: 0–20%, 12.0–15.0 $\otimes$ 0.5–1.0 GeV/c Jet Function

ϕ	per trig yield	σ_{stat}/y	systematic errors											
			$+\sigma_{f2}/y$	$-\sigma_{f2}/y$	$+\sigma_{f3}/y$	$-\sigma_{f3}/y$	$+\sigma_{f4}/y$	$-\sigma_{f4}/y$	$+\sigma_{\xi/ZYAM}/y$	$-\sigma_{\xi}/y$	$+\sigma_{\pi^0}/y$	$-\sigma_{\pi^0}/y$	$+\sigma_{total}/y$	$-\sigma_{total}/y$
-1.47	-0.03636	-15.30015	1.40941	-1.40941	9.16781	-9.16781	9.24997	-9.24997	6.30920	-6.30925	0.03648	-0.03648	14.53976	-14.53978
-1.26	0.02210	23.30624	2.02700	-2.02700	15.21670	-15.21670	15.12869	-15.12869	10.38232	-10.38241	0.03648	-0.03648	23.92338	-23.92341
-1.05	-0.00188	-239.49646	17.59899	-17.59899	180.04120	-180.04120	176.95332	-176.95332	122.44313	-122.44419	0.03648	-0.03648	281.12161	-281.12207
-0.84	0.16892	2.40581	0.18824	-0.18824	1.99576	-1.99576	1.97582	-1.97582	1.36175	-1.36176	0.03648	-0.03648	3.12699	-3.12699
-0.63	-0.05614	-6.20260	0.67770	-0.67770	5.96761	-5.96761	5.94950	-5.94950	4.10696	-4.10699	0.03648	-0.03648	9.39875	-9.39877
-0.42	0.17913	1.74137	0.06446	-0.24283	1.87683	-1.87683	1.87209	-1.87209	1.29016	-1.29017	0.03648	-0.03648	2.94910	-2.95838
-0.21	0.50844	0.59763	0.04102	-0.09284	0.67304	-0.67304	0.66591	-0.66591	0.45535	-0.45536	0.03648	-0.03648	1.05203	-1.05533
-0.00	0.31610	0.94954	0.07639	-0.15348	1.08979	-1.08979	1.07533	-1.07533	0.73289	-0.73290	0.03648	-0.03648	1.69949	-1.70470
0.21	-0.09263	-3.17222	0.22513	-0.50958	3.69410	-3.69410	3.65494	-3.65494	2.49927	-2.49930	0.03648	-0.03648	5.77091	-5.78900
0.42	0.12019	2.57826	0.09607	-0.36191	2.79720	-2.79720	2.79014	-2.79014	1.92285	-1.92286	0.03648	-0.03648	4.39513	-4.40896
0.63	-0.31845	-1.05065	0.11947	-0.11947	1.05204	-1.05204	1.04885	-1.04885	0.72402	-0.72403	0.03648	-0.03648	1.65731	-1.65731
0.84	-0.09324	-3.98893	0.34103	-0.34103	3.61570	-3.61570	3.57957	-3.57957	2.46707	-2.46710	0.03648	-0.03648	5.66487	-5.66488
1.05	-0.29903	-1.46446	0.11037	-0.11037	1.12912	-1.12912	1.10976	-1.10976	0.76790	-0.76791	0.03648	-0.03648	1.76342	-1.76343
1.26	0.57981	0.89752	0.07725	-0.07725	0.57993	-0.57993	0.57658	-0.57658	0.39569	-0.39569	0.03648	-0.03648	0.91249	-0.91249
1.47	-0.20367	-2.64666	0.25163	-0.25163	1.63676	-1.63676	1.65143	-1.65143	1.12640	-1.12641	0.03648	-0.03648	2.59608	-2.59608
1.68	0.85951	0.65523	0.05964	-0.05964	0.38856	-0.38856	0.39157	-0.39157	0.26709	-0.26709	0.05075	-0.05075	0.61788	-0.61788
1.88	-0.28073	-1.82635	0.15964	-0.15964	1.21018	-1.21018	1.19282	-1.19282	0.81860	-0.81861	0.05075	-0.05075	1.89355	-1.89355
2.09	0.89650	0.51209	0.03685	-0.03685	0.38173	-0.38173	0.37093	-0.37093	0.25666	-0.25667	0.05075	-0.05075	0.59424	-0.59424
2.30	0.28147	1.38254	0.11317	-0.11317	1.21008	-1.21008	1.18770	-1.18770	0.81859	-0.81860	0.05075	-0.05075	1.88691	-1.88691
2.51	0.13927	2.54723	0.27332	-0.27332	2.40982	-2.40982	2.39969	-2.39969	1.65652	-1.65654	0.05075	-0.05075	3.79303	-3.79304
2.72	0.04995	6.77489	0.23133	-0.87036	6.71827	-6.71827	6.70908	-6.70908	4.62361	-4.62365	0.05075	-0.05075	10.56318	-10.59647
2.93	0.39959	0.81120	0.05225	-0.11799	0.84768	-0.84768	0.84590	-0.84590	0.57843	-0.57843	0.05075	-0.05075	1.33191	-1.33611
3.14	0.38768	0.81286	0.06236	-0.12497	0.87678	-0.87678	0.87502	-0.87502	0.59636	-0.59636	0.05075	-0.05075	1.37714	-1.38139
3.35	0.21996	1.46504	0.09492	-0.21435	1.53995	-1.53995	1.53673	-1.53673	1.05081	-1.05082	0.05075	-0.05075	2.41842	-2.42605
3.56	0.27739	1.20313	0.04166	-0.15673	1.20982	-1.20982	1.20817	-1.20817	0.83262	-0.83263	0.05075	-0.05075	1.90287	-1.90886
3.77	0.33106	1.08170	0.11498	-0.11498	1.01379	-1.01379	1.00953	-1.00953	0.69688	-0.69689	0.05075	-0.05075	1.59635	-1.59636
3.98	-0.68021	-0.55738	0.04683	-0.04683	0.50074	-0.50074	0.49148	-0.49148	0.33873	-0.33874	0.05075	-0.05075	0.78217	-0.78217
4.19	-0.26441	-1.60705	0.12493	-0.12493	1.29427	-1.29427	1.25765	-1.25765	0.87022	-0.87023	0.05075	-0.05075	2.00805	-2.00806
4.40	0.06563	7.55161	0.68289	-0.68289	5.17687	-5.17687	5.10263	-5.10263	3.50179	-3.50182	0.05075	-0.05075	8.09743	-8.09744
4.61	0.55489	1.02934	0.09238	-0.09238	0.60187	-0.60187	0.60654	-0.60654	0.41371	-0.41371	0.05075	-0.05075	0.95520	-0.95520

Table 26: 0–20%, 12.0–15.0 $\otimes$ 1.0–2.0 GeV/c Jet Function

ϕ	per trig yield	σ_{stat}/y	systematic errors											
			$+\sigma_{f2}/y$	$-\sigma_{f2}/y$	$+\sigma_{f3}/y$	$-\sigma_{f3}/y$	$+\sigma_{f4}/y$	$-\sigma_{f4}/y$	$+\sigma_{\xi/ZYAM}/y$	$-\sigma_{\xi}/y$	$+\sigma_{\pi^0}/y$	$-\sigma_{\pi^0}/y$	$+\sigma_{total}/y$	$-\sigma_{total}/y$
-1.47	0.15131	2.50875	0.06697	-0.17957	0.01205	-0.02268	0.02660	-0.02382	0.01685	-0.01686	0.00186	-0.00186	0.07500	-0.18334
-1.26	0.08237	4.32316	0.10175	-0.27281	0.05794	-0.10909	0.01653	-0.01480	0.03094	-0.03095	0.00186	-0.00186	0.12224	-0.29581
-1.05	-0.04175	-6.62801	0.12406	-0.33265	0.14130	-0.26603	0.04725	-0.05276	0.06112	-0.06114	0.00186	-0.00186	0.20329	-0.43353
-0.84	0.14318	1.80890	0.00756	-0.02028	0.03333	-0.06276	0.02695	-0.03010	0.01788	-0.01789	0.00186	-0.00186	0.04710	-0.07470
-0.63	0.06574	3.24252	0.13056	-0.04869	0.02773	-0.05221	0.04855	-0.05422	0.03913	-0.03914	0.00186	-0.00186	0.14733	-0.09784
-0.42	-0.00186	-106.86382	9.96831	-3.71776	1.84078	-0.97772	0.22117	-0.24700	1.38671	-1.38725	0.00186	-0.00186	10.23365	-4.09429
-0.21	0.14386	1.23256	0.17639	-0.06579	0.06246	-0.03318	0.02049	-0.01835	0.01804	-0.01805	0.00186	-0.00186	0.18911	-0.07807
-0.00	0.51149	0.36245	0.05431	-0.02025	0.02172	-0.01153	0.00861	-0.00771	0.00508	-0.00508	0.00186	-0.00186	0.05937	-0.02514
0.21	0.34801	0.51338	0.07292	-0.02719	0.02582	-0.01371	0.00847	-0.00759	0.00746	-0.00746	0.00186	-0.00186	0.07819	-0.03232
0.42	0.25688	0.76995	0.07236	-0.02699	0.01336	-0.00710	0.00161	-0.00179	0.01007	-0.01007	0.00186	-0.00186	0.07430	-0.02978
0.63	0.08465	2.42350	0.10140	-0.03782	0.02154	-0.04055	0.03771	-0.04211	0.03039	-0.03040	0.00186	-0.00186	0.11443	-0.07599
0.84	0.15095	1.58308	0.00717	-0.01923	0.03162	-0.05953	0.02556	-0.02855	0.01696	-0.01697	0.00186	-0.00186	0.04467	-0.07085
1.05	-0.27121	-0.94306	0.01910	-0.05121	0.02175	-0.04095	0.00727	-0.00812	0.00941	-0.00941	0.00186	-0.00186	0.03135	-0.06677
1.26	-0.21989	-1.45659	0.03811	-0.10220	0.02170	-0.04086	0.00619	-0.00554	0.01159	-0.01159	0.00186	-0.00186	0.04583	-0.11083
1.47	-0.45384	-0.80328	0.02233	-0.05987	0.00402	-0.00756	0.00887	-0.00794	0.00562	-0.00562	0.00186	-0.00186	0.02507	-0.06115
1.68	0.45158	0.86133	0.02244	-0.06017	0.00760	-0.00404	0.00891	-0.00798	0.00566	-0.00566	0.00707	-0.00707	0.02688	-0.06150
1.88	-0.13270	-2.57053	0.06316	-0.16934	0.06771	-0.03597	0.01026	-0.00919	0.01929	-0.01930	0.00707	-0.00707	0.09540	-0.17457
2.09	-0.55844	-0.45849	0.00928	-0.02487	0.01989	-0.01056	0.00353	-0.00394	0.00459	-0.00460	0.00707	-0.00707	0.02377	-0.02858
2.30	0.08407	2.96611	0.01288	-0.03454	0.10688	-0.05677	0.04590	-0.05126	0.03058	-0.03059	0.00707	-0.00707	0.12117	-0.08961
2.51	-0.03983	-5.22453	0.21548	-0.08036	0.08616	-0.04576	0.08012	-0.08948	0.06468	-0.06470	0.00707	-0.00707	0.25399	-0.14421
2.72	0.70998	0.30973	0.02618	-0.00976	0.00257	-0.00483	0.00058	-0.00065	0.00364	-0.00364	0.00707	-0.00707	0.02749	-0.01350
2.93	0.45953	0.43225	0.05522	-0.02060	0.01039	-0.01955	0.00642	-0.00574	0.00563	-0.00563	0.00707	-0.00707	0.05727	-0.03035
3.14	0.10536	1.88776	0.26364	-0.09832	0.05599	-0.10542	0.04182	-0.03744	0.02455	-0.02456	0.00707	-0.00707	0.27393	-0.15111
3.35	0.28098	0.69222	0.09031	-0.03368	0.01699	-0.03198	0.01049	-0.00939	0.00920	-0.00920	0.00707	-0.00707	0.09322	-0.04879
3.56	0.20792	0.99002	0.08939	-0.03334	0.00877	-0.01651	0.00198	-0.00222	0.01242	-0.01242	0.00707	-0.00707	0.09097	-0.03992
3.77	-0.11689	-1.75343	0.07343	-0.02739	0.02936	-0.01560	0.02730	-0.03049	0.02204	-0.02205	0.00707	-0.00707	0.08681	-0.04959
3.98	0.45793	0.55009	0.00236	-0.00634	0.01962	-0.01042	0.00843	-0.00941	0.00561	-0.00562	0.00707	-0.00707	0.02331	-0.01786
4.19	0.04143	6.49191	0.12502	-0.33522	0.26808	-0.14239	0.04761	-0.05317	0.06192	-0.06194	0.00707	-0.00707	0.30602	-0.37331
4.40	0.16891	1.94208	0.04962	-0.13304	0.05320	-0.02826	0.00806	-0.00722	0.01515	-0.01516	0.00707	-0.00707	0.07508	-0.13722
4.61	0.24639	1.50894	0.04113	-0.11028	0.01393	-0.00740	0.01634	-0.01463	0.01037	-0.01037	0.00707	-0.00707	0.04806	-0.11219

Table 27: 0–20%, 12.0–15.0 $\otimes$ 2.0–3.0 GeV/c Jet Function

ϕ	per trig yield	σ_{stat}/y	systematic errors											
			$+\sigma_{f2}/y$	$-\sigma_{f2}/y$	$+\sigma_{f3}/y$	$-\sigma_{f3}/y$	$+\sigma_{f4}/y$	$-\sigma_{f4}/y$	$+\sigma_{\xi/ZYAM}/y$	$-\sigma_{\xi}/y$	$+\sigma_{\pi^0}/y$	$-\sigma_{\pi^0}/y$	$+\sigma_{total}/y$	$-\sigma_{total}/y$
-1.47	0.12048	1.02035	0.01058	-0.02765	0.00220	-0.00430	0.00598	-0.00482	0.00159	-0.00159	0.00828	-0.00828	0.01495	-0.02962
-1.26	0.21057	0.57174	0.00501	-0.01309	0.00329	-0.00644	0.00116	-0.00093	0.00091	-0.00091	0.00828	-0.00828	0.01032	-0.01682
-1.05	0.11395	0.83389	0.00572	-0.01494	0.00753	-0.01472	0.00279	-0.00346	0.00168	-0.00168	0.00828	-0.00828	0.01298	-0.02287
-0.84	-0.07026	-0.88532	0.00194	-0.00507	0.00987	-0.01931	0.00885	-0.01098	0.00274	-0.00274	0.00828	-0.00828	0.01598	-0.02439
-0.63	-0.03699	-1.57855	0.02845	-0.01088	0.00716	-0.01401	0.01390	-0.01724	0.00525	-0.00525	0.00828	-0.00828	0.03391	-0.02661
-0.42	0.08952	0.67597	0.02546	-0.00974	0.00579	-0.00296	0.00074	-0.00092	0.00219	-0.00219	0.00828	-0.00828	0.02748	-0.01333
-0.21	0.07326	0.74477	0.04247	-0.01624	0.01852	-0.00947	0.00720	-0.00580	0.00269	-0.00269	0.00828	-0.00828	0.04769	-0.02152
-0.00	0.37889	0.17185	0.00899	-0.00344	0.00443	-0.00226	0.00208	-0.00168	0.00052	-0.00052	0.00828	-0.00828	0.01317	-0.00941
0.21	0.14371	0.40119	0.02165	-0.00828	0.00944	-0.00483	0.00367	-0.00296	0.00137	-0.00137	0.00828	-0.00828	0.02533	-0.01308
0.42	-0.00653	-7.97902	0.34873	-0.13338	0.07929	-0.04055	0.01016	-0.01261	0.02996	-0.02996	0.00828	-0.00828	0.35913	-0.14339
0.63	-0.01459	-3.92840	0.07212	-0.02758	0.01816	-0.03551	0.03522	-0.04371	0.01330	-0.01330	0.00828	-0.00828	0.08377	-0.06464
0.84	0.09505	0.75434	0.00143	-0.00375	0.00730	-0.01427	0.00654	-0.00811	0.00203	-0.00203	0.00828	-0.00828	0.01306	-0.01887
1.05	-0.05735	-1.22198	0.01136	-0.02970	0.01495	-0.02924	0.00554	-0.00687	0.00334	-0.00334	0.00828	-0.00828	0.02152	-0.04317
1.26	-0.01124	-7.82833	0.09380	-0.24523	0.06174	-0.12073	0.02169	-0.01747	0.01704	-0.01704	0.00828	-0.00828	0.11593	-0.27455
1.47	0.29459	0.49242	0.00433	-0.01131	0.00090	-0.00176	0.00245	-0.00197	0.00065	-0.00065	0.00828	-0.00828	0.00972	-0.01427
1.68	0.15652	0.86330	0.00814	-0.02128	0.00331	-0.00169	0.00460	-0.00371	0.00123	-0.00123	0.01115	-0.01115	0.01497	-0.02440
1.88	0.10996	0.96022	0.00958	-0.02506	0.01234	-0.00631	0.00222	-0.00179	0.00176	-0.00176	0.01115	-0.01115	0.01940	-0.02825
2.09	0.21309	0.46367	0.00306	-0.00799	0.00787	-0.00402	0.00149	-0.00185	0.00091	-0.00091	0.01115	-0.01115	0.01409	-0.01444
2.30	-0.00874	-7.63279	0.01558	-0.04073	0.15518	-0.07936	0.07109	-0.08823	0.02221	-0.02221	0.01115	-0.01115	0.17319	-0.12790
2.51	0.02602	2.43141	0.04045	-0.01547	0.01991	-0.01018	0.01975	-0.02452	0.00748	-0.00748	0.01115	-0.01115	0.05102	-0.03353
2.72	0.03032	1.88189	0.07518	-0.02875	0.00874	-0.01709	0.00219	-0.00272	0.00644	-0.00644	0.01115	-0.01115	0.07680	-0.03594
2.93	0.21408	0.31593	0.01453	-0.00556	0.00324	-0.00634	0.00246	-0.00199	0.00091	-0.00091	0.01115	-0.01115	0.01879	-0.01414
3.14	0.15788	0.40222	0.02157	-0.00825	0.00543	-0.01062	0.00499	-0.00402	0.00124	-0.00124	0.01115	-0.01115	0.02541	-0.01797
3.35	0.16003	0.40287	0.01944	-0.00744	0.00434	-0.00848	0.00330	-0.00266	0.00122	-0.00122	0.01115	-0.01115	0.02310	-0.01612
3.56	0.05520	1.04965	0.04129	-0.01579	0.00480	-0.00939	0.00120	-0.00149	0.00354	-0.00354	0.01115	-0.01115	0.04320	-0.02183
3.77	0.09604	0.68441	0.01096	-0.00419	0.00540	-0.00276	0.00535	-0.00664	0.00203	-0.00203	0.01115	-0.01115	0.01750	-0.01406
3.98	0.06874	1.01620	0.00198	-0.00518	0.01973	-0.01009	0.00904	-0.01122	0.00282	-0.00282	0.01115	-0.01115	0.02464	-0.01967
4.19	-0.04886	-1.48476	0.01333	-0.03485	0.03432	-0.01755	0.00650	-0.00807	0.00396	-0.00396	0.01115	-0.01115	0.03921	-0.04157
4.40	-0.00079	-112.69247	1.33631	-3.49378	1.72009	-0.87967	0.30895	-0.24896	0.24474	-0.24474	0.01115	-0.01115	2.21357	-3.61971
4.61	0.06940	1.65021	0.01836	-0.04800	0.00747	-0.00382	0.01038	-0.00836	0.00277	-0.00277	0.01115	-0.01115	0.02515	-0.05021

Table 28: 0–20%, 12.0–15.0 $\otimes$ 3.0–5.0 GeV/c Jet Function

ϕ	per trig yield	σ_{stat}/y	systematic errors											
			$+\sigma_{f2}/y$	$-\sigma_{f2}/y$	$+\sigma_{f3}/y$	$-\sigma_{f3}/y$	$+\sigma_{f4}/y$	$-\sigma_{f4}/y$	$+\sigma_{\xi/ZYAM}/y$	$-\sigma_{\xi}/y$	$+\sigma_{\pi^0}/y$	$-\sigma_{\pi^0}/y$	$+\sigma_{total}/y$	$-\sigma_{total}/y$
-1.47	-0.02323	-1.23289	0.00734	-0.01858	0.00162	-0.00315	0.00496	-0.00404	0.00102	-0.00102	0.00872	-0.00872	0.01257	-0.02118
-1.26	-0.03137	-0.64951	0.00449	-0.01138	0.00315	-0.00610	0.00124	-0.00101	0.00075	-0.00075	0.00872	-0.00872	0.01040	-0.01563
-1.05	-0.03518	-0.47160	0.00248	-0.00627	0.00347	-0.00673	0.00146	-0.00179	0.00067	-0.00067	0.00872	-0.00872	0.00984	-0.01282
-0.84	0.02930	0.98302	0.00062	-0.00157	0.00337	-0.00653	0.00343	-0.00421	0.00081	-0.00081	0.00872	-0.00872	0.01001	-0.01181
-0.63	0.00956	2.45635	0.01426	-0.00563	0.00395	-0.00765	0.00870	-0.01067	0.00251	-0.00251	0.00872	-0.00872	0.01942	-0.01693
-0.42	-0.00649	-2.70693	0.04546	-0.01795	0.01126	-0.00581	0.00165	-0.00203	0.00373	-0.00373	0.00872	-0.00872	0.04782	-0.02122
-0.21	0.12464	0.26188	0.00323	-0.00128	0.00154	-0.00079	0.00068	-0.00055	0.00020	-0.00020	0.00872	-0.00872	0.00945	-0.00887
-0.00	0.33817	0.13155	0.00130	-0.00052	0.00070	-0.00036	0.00037	-0.00030	0.00007	-0.00007	0.00872	-0.00872	0.00885	-0.00875
0.21	0.06474	0.39929	0.00623	-0.00246	0.00296	-0.00153	0.00130	-0.00106	0.00038	-0.00038	0.00872	-0.00872	0.01120	-0.00925
0.42	0.04698	0.55067	0.00628	-0.00248	0.00156	-0.00080	0.00023	-0.00028	0.00052	-0.00052	0.00872	-0.00872	0.01087	-0.00912
0.63	0.00177	11.58612	0.07699	-0.03040	0.02131	-0.04130	0.04696	-0.05762	0.01355	-0.01355	0.00872	-0.00872	0.09406	-0.07880
0.84	-0.01340	-1.44234	0.00136	-0.00344	0.00738	-0.01429	0.00751	-0.00921	0.00178	-0.00178	0.00872	-0.00872	0.01385	-0.01949
1.05	-0.01051	-2.26912	0.00829	-0.02099	0.01162	-0.02252	0.00489	-0.00600	0.00225	-0.00225	0.00872	-0.00872	0.01757	-0.03264
1.26	0.00382	8.40673	0.03690	-0.09343	0.02586	-0.05011	0.01020	-0.00831	0.00620	-0.00620	0.00872	-0.00872	0.04742	-0.10689
1.47	0.00849	5.03198	0.02007	-0.05082	0.00444	-0.00861	0.01357	-0.01106	0.00279	-0.00279	0.00872	-0.00872	0.02628	-0.05351
1.68	-0.01919	-1.71210	0.00888	-0.02249	0.00381	-0.00197	0.00600	-0.00489	0.00124	-0.00124	0.00803	-0.00803	0.01398	-0.02448
1.88	0.00753	4.58540	0.01871	-0.04739	0.02542	-0.01312	0.00517	-0.00422	0.00317	-0.00317	0.00803	-0.00803	0.03313	-0.05010
2.09	-0.00852	-2.97195	0.01022	-0.02589	0.02777	-0.01433	0.00603	-0.00740	0.00281	-0.00281	0.00803	-0.00803	0.03138	-0.03167
2.30	-0.00284	-7.82874	0.00642	-0.01625	0.06744	-0.03481	0.03542	-0.04346	0.00846	-0.00846	0.00803	-0.00803	0.07733	-0.05916
2.51	0.02010	1.28126	0.00678	-0.00268	0.00364	-0.00188	0.00414	-0.00508	0.00120	-0.00120	0.00803	-0.00803	0.01193	-0.01012
2.72	0.05324	0.49909	0.00555	-0.00219	0.00071	-0.00137	0.00020	-0.00025	0.00045	-0.00045	0.00803	-0.00803	0.00980	-0.00845
2.93	0.10704	0.31284	0.00377	-0.00149	0.00092	-0.00179	0.00079	-0.00064	0.00023	-0.00023	0.00803	-0.00803	0.00895	-0.00839
3.14	0.11815	0.28516	0.00373	-0.00147	0.00103	-0.00200	0.00107	-0.00087	0.00021	-0.00021	0.00803	-0.00803	0.00898	-0.00845
3.35	0.11485	0.30578	0.00351	-0.00139	0.00086	-0.00167	0.00073	-0.00060	0.00021	-0.00021	0.00803	-0.00803	0.00884	-0.00834
3.56	0.01971	1.11078	0.01498	-0.00592	0.00192	-0.00371	0.00055	-0.00067	0.00123	-0.00123	0.00803	-0.00803	0.01716	-0.01073
3.77	0.01988	1.21791	0.00686	-0.00271	0.00368	-0.00190	0.00418	-0.00513	0.00121	-0.00121	0.00803	-0.00803	0.01200	-0.01016
3.98	-0.03348	-0.40127	0.00054	-0.00138	0.00572	-0.00295	0.00300	-0.00368	0.00072	-0.00072	0.00803	-0.00803	0.01034	-0.00944
4.19	-0.01250	-1.84251	0.00697	-0.01765	0.01894	-0.00977	0.00411	-0.00505	0.00192	-0.00192	0.00803	-0.00803	0.02219	-0.02238
4.40	-0.05220	-0.00000	0.00270	-0.00684	0.00367	-0.00189	0.00075	-0.00061	0.00046	-0.00046	0.00803	-0.00803	0.00927	-0.01074
4.61	0.00135	28.09168	0.12668	-0.32080	0.05436	-0.02806	0.08565	-0.06980	0.01770	-0.01770	0.00803	-0.00803	0.16345	-0.33008

Table 29: 0–20%, 12.0–15.0 $\otimes$ 5.0–7.0 GeV/c Jet Function

ϕ	per trig yield	σ_{stat}/y	systematic errors											
			$+\sigma_{f2}/y$	$-\sigma_{f2}/y$	$+\sigma_{f3}/y$	$-\sigma_{f3}/y$	$+\sigma_{f4}/y$	$-\sigma_{f4}/y$	$+\sigma_{\xi/ZYAM}/y$	$-\sigma_{\xi}/y$	$+\sigma_{\pi^0}/y$	$-\sigma_{\pi^0}/y$	$+\sigma_{total}/y$	$-\sigma_{total}/y$
-1.47	-0.00459	-0.00000	0.00276	-0.00613	0.00082	-0.00085	0.00133	-0.00210	0.00086	-0.00108	0.01561	-0.01561	0.01595	-0.01696
-1.26	-0.00458	-0.00000	0.00229	-0.00508	0.00214	-0.00223	0.00045	-0.00071	0.00086	-0.00108	0.01561	-0.01561	0.01595	-0.01662
-1.05	-0.00459	-0.00000	0.00141	-0.00314	0.00264	-0.00275	0.00115	-0.00073	0.00086	-0.00108	0.01561	-0.01561	0.01596	-0.01621
-0.84	-0.00460	-0.00000	0.00029	-0.00065	0.00213	-0.00222	0.00224	-0.00142	0.00086	-0.00108	0.01561	-0.01561	0.01594	-0.01588
-0.63	-0.00463	-0.00000	0.00192	-0.00087	0.00081	-0.00084	0.00184	-0.00117	0.00086	-0.00108	0.01561	-0.01561	0.01588	-0.01574
-0.42	0.00852	1.55213	0.00226	-0.00102	0.00046	-0.00044	0.00013	-0.00008	0.00047	-0.00059	0.01561	-0.01561	0.01579	-0.01566
-0.21	0.02886	0.67704	0.00091	-0.00041	0.00035	-0.00034	0.00015	-0.00024	0.00014	-0.00018	0.01561	-0.01561	0.01564	-0.01562
-0.00	0.18303	0.22447	0.00016	-0.00007	0.00007	-0.00007	0.00004	-0.00006	0.00002	-0.00003	0.01561	-0.01561	0.01561	-0.01561
0.21	0.01897	0.88717	0.00139	-0.00062	0.00054	-0.00052	0.00024	-0.00037	0.00021	-0.00027	0.01561	-0.01561	0.01568	-0.01564
0.42	-0.00466	-0.00000	0.00413	-0.00186	0.00084	-0.00080	0.00024	-0.00015	0.00086	-0.00108	0.01561	-0.01561	0.01620	-0.01578
0.63	-0.00463	-0.00000	0.00192	-0.00087	0.00081	-0.00084	0.00184	-0.00117	0.00086	-0.00108	0.01561	-0.01561	0.01588	-0.01574
0.84	-0.00460	-0.00000	0.00029	-0.00065	0.00213	-0.00222	0.00224	-0.00142	0.00086	-0.00108	0.01561	-0.01561	0.01594	-0.01588
1.05	-0.00459	-0.00000	0.00141	-0.00314	0.00264	-0.00275	0.00115	-0.00073	0.00086	-0.00108	0.01561	-0.01561	0.01596	-0.01621
1.26	-0.00458	-0.00000	0.00229	-0.00508	0.00214	-0.00223	0.00045	-0.00071	0.00086	-0.00108	0.01561	-0.01561	0.01595	-0.01662
1.47	-0.00459	-0.00000	0.00276	-0.00613	0.00082	-0.00085	0.00133	-0.00210	0.00086	-0.00108	0.01561	-0.01561	0.01595	-0.01696
1.68	-0.00460	-0.00000	0.00276	-0.00612	0.00085	-0.00082	0.00133	-0.00210	0.00086	-0.00108	0.00342	-0.00342	0.00475	-0.00745
1.88	0.03087	1.16020	0.00034	-0.00075	0.00033	-0.00032	0.00007	-0.00011	0.00013	-0.00016	0.00342	-0.00342	0.00346	-0.00352
2.09	-0.00462	-0.00000	0.00140	-0.00312	0.00273	-0.00263	0.00114	-0.00072	0.00086	-0.00108	0.00342	-0.00342	0.00482	-0.00548
2.30	-0.00463	-0.00000	0.00029	-0.00065	0.00220	-0.00212	0.00223	-0.00141	0.00086	-0.00108	0.00342	-0.00342	0.00473	-0.00445
2.51	-0.00464	-0.00000	0.00192	-0.00086	0.00084	-0.00081	0.00184	-0.00117	0.00086	-0.00108	0.00342	-0.00342	0.00450	-0.00395
2.72	0.03117	0.82040	0.00062	-0.00028	0.00012	-0.00012	0.00004	-0.00002	0.00013	-0.00016	0.00342	-0.00342	0.00348	-0.00344
2.93	0.02329	0.85486	0.00113	-0.00051	0.00042	-0.00044	0.00019	-0.00030	0.00017	-0.00022	0.00342	-0.00342	0.00364	-0.00351
3.14	0.04767	0.55660	0.00060	-0.00027	0.00025	-0.00026	0.00014	-0.00022	0.00008	-0.00011	0.00342	-0.00342	0.00349	-0.00345
3.35	0.02509	0.84503	0.00105	-0.00047	0.00039	-0.00041	0.00018	-0.00028	0.00016	-0.00020	0.00342	-0.00342	0.00361	-0.00350
3.56	0.00862	1.54455	0.00223	-0.00101	0.00043	-0.00045	0.00013	-0.00008	0.00047	-0.00058	0.00342	-0.00342	0.00414	-0.00364
3.77	-0.00464	-0.00000	0.00192	-0.00086	0.00084	-0.00081	0.00184	-0.00117	0.00086	-0.00108	0.00342	-0.00342	0.00450	-0.00395
3.98	-0.00463	-0.00000	0.00029	-0.00065	0.00220	-0.00212	0.00223	-0.00141	0.00086	-0.00108	0.00342	-0.00342	0.00473	-0.00445
4.19	-0.00462	-0.00000	0.00140	-0.00312	0.00273	-0.00263	0.00114	-0.00072	0.00086	-0.00108	0.00342	-0.00342	0.00482	-0.00548
4.40	-0.00461	-0.00000	0.00228	-0.00505	0.00221	-0.00213	0.00045	-0.00071	0.00086	-0.00108	0.00342	-0.00342	0.00477	-0.00659
4.61	-0.00460	-0.00000	0.00276	-0.00612	0.00085	-0.00082	0.00133	-0.00210	0.00086	-0.00108	0.00342	-0.00342	0.00475	-0.00745

Table 30: 20–40%, 4.0–5.0 $\otimes$ 0.5–1.0 GeV/c Jet Function

ϕ	per trig yield	σ_{stat}/y	systematic errors											
			$+\sigma_{f2}/y$	$-\sigma_{f2}/y$	$+\sigma_{f3}/y$	$-\sigma_{f3}/y$	$+\sigma_{f4}/y$	$-\sigma_{f4}/y$	$+\sigma_{\xi/ZYAM}/y$	$-\sigma_{\xi}/y$	$+\sigma_{\pi^0}/y$	$-\sigma_{\pi^0}/y$	$+\sigma_{total}/y$	$-\sigma_{total}/y$
-1.47	-0.03079	-0.79593	0.06220	-0.04668	0.06131	-0.06679	0.10549	-0.11300	0.31016	-0.31013	0.04724	-0.04724	0.34233	-0.34325
-1.26	0.01813	1.29021	0.05021	-0.02491	0.03602	-0.03973	0.05239	-0.03618	0.52770	-0.52765	0.04724	-0.04724	0.53597	-0.53306
-1.05	-0.01621	-1.27402	0.08395	-0.05775	0.01201	-0.01384	0.19280	-0.13121	0.59340	-0.59334	0.04724	-0.04724	0.63144	-0.61239
-0.84	0.02614	0.71092	0.14117	-0.12656	0.02652	-0.02922	0.20528	-0.15101	0.37151	-0.37147	0.04724	-0.04724	0.45058	-0.42415
-0.63	0.05687	0.28453	0.10785	-0.10192	0.03453	-0.03762	0.08063	-0.05815	0.17274	-0.17272	0.04724	-0.04724	0.22671	-0.21737
-0.42	0.06733	0.21270	0.12281	-0.11835	0.05239	-0.05690	0.01939	-0.00938	0.14759	-0.14758	0.04724	-0.04724	0.20547	-0.20333
-0.21	0.17652	0.07884	0.05506	-0.05351	0.02713	-0.02944	0.01308	-0.01303	0.05677	-0.05676	0.04724	-0.04724	0.09692	-0.09672
-0.00	0.18304	0.07587	0.05591	-0.05446	0.02880	-0.03125	0.01948	-0.02099	0.05491	-0.05491	0.04724	-0.04724	0.09789	-0.09813
0.21	0.15959	0.08574	0.06091	-0.05919	0.03001	-0.03257	0.01446	-0.01441	0.06279	-0.06278	0.04724	-0.04724	0.10485	-0.10462
0.42	0.06685	0.21004	0.12368	-0.11919	0.05276	-0.05731	0.01953	-0.00944	0.14864	-0.14863	0.04724	-0.04724	0.20685	-0.20470
0.63	0.02243	0.68094	0.27344	-0.25838	0.08755	-0.09537	0.20441	-0.14742	0.43795	-0.43791	0.04724	-0.04724	0.56414	-0.53998
0.84	0.02282	0.73414	0.16172	-0.14498	0.03038	-0.03348	0.23516	-0.17299	0.42558	-0.42554	0.04724	-0.04724	0.51549	-0.48516
1.05	0.00670	2.94051	0.20324	-0.13983	0.02908	-0.03350	0.46679	-0.31767	1.43665	-1.43650	0.04724	-0.04724	1.52520	-1.47897
1.26	-0.00972	-2.26947	0.09366	-0.04646	0.06720	-0.07411	0.09772	-0.06748	0.98431	-0.98420	0.04724	-0.04724	0.99696	-0.99151
1.47	0.00076	30.76381	2.53454	-1.90207	2.49836	-2.72153	4.29843	-4.60450	12.63817	-12.63687	0.04724	-0.04724	13.81549	-13.85348
1.68	0.02074	1.14011	0.09202	-0.06894	0.16516	-0.17939	0.15663	-0.16773	0.46144	-0.46139	0.04024	-0.04024	0.52424	-0.52874
1.88	0.06791	0.33701	0.01313	-0.00635	0.06887	-0.07473	0.01397	-0.00960	0.14156	-0.14155	0.04024	-0.04024	0.16362	-0.16545
2.09	0.06324	0.31205	0.02193	-0.01518	0.08173	-0.08866	0.04951	-0.03366	0.15305	-0.15304	0.04024	-0.04024	0.18616	-0.18511
2.30	0.06397	0.27056	0.05801	-0.05201	0.07373	-0.08001	0.08394	-0.06172	0.15253	-0.15251	0.04024	-0.04024	0.20182	-0.19441
2.51	0.09638	0.16881	0.06373	-0.06022	0.03632	-0.03945	0.04759	-0.03432	0.10212	-0.10211	0.04024	-0.04024	0.14033	-0.13567
2.72	0.15234	0.10345	0.05422	-0.05226	0.01307	-0.01423	0.00856	-0.00414	0.06511	-0.06511	0.04024	-0.04024	0.09510	-0.09386
2.93	0.13412	0.11164	0.07232	-0.07028	0.00571	-0.00629	0.01722	-0.01718	0.07436	-0.07436	0.04024	-0.04024	0.11273	-0.11146
3.14	0.12822	0.11406	0.07962	-0.07757	0.00233	-0.00263	0.02782	-0.03000	0.07794	-0.07794	0.04024	-0.04024	0.12171	-0.12090
3.35	0.12645	0.11872	0.07671	-0.07455	0.00606	-0.00667	0.01826	-0.01822	0.07888	-0.07887	0.04024	-0.04024	0.11872	-0.11736
3.56	0.12265	0.12659	0.06735	-0.06491	0.01623	-0.01768	0.01063	-0.00514	0.08088	-0.08087	0.04024	-0.04024	0.11434	-0.11275
3.77	0.09905	0.16677	0.06201	-0.05859	0.03534	-0.03839	0.04631	-0.03339	0.09937	-0.09936	0.04024	-0.04024	0.13686	-0.13233
3.98	0.09573	0.18561	0.03876	-0.03476	0.04927	-0.05347	0.05609	-0.04125	0.10193	-0.10192	0.04024	-0.04024	0.13816	-0.13333
4.19	0.10690	0.18245	0.01297	-0.00898	0.04835	-0.05245	0.02929	-0.01991	0.09054	-0.09053	0.04024	-0.04024	0.11480	-0.11420
4.40	0.02018	1.10025	0.04418	-0.02135	0.23175	-0.25146	0.04701	-0.03231	0.47638	-0.47633	0.04024	-0.04024	0.53519	-0.54152
4.61	0.02982	0.83286	0.06399	-0.04794	0.11485	-0.12474	0.10892	-0.11664	0.32087	-0.32084	0.04024	-0.04024	0.36569	-0.36881

Table 31: 20–40%, 4.0–5.0 $\otimes$ 1.0–2.0 GeV/c Jet Function

ϕ	per trig yield	σ_{stat}/y	systematic errors											
			$+\sigma_{f2}/y$	$-\sigma_{f2}/y$	$+\sigma_{f3}/y$	$-\sigma_{f3}/y$	$+\sigma_{f4}/y$	$-\sigma_{f4}/y$	$+\sigma_{\xi/ZYAM}/y$	$-\sigma_{\xi}/y$	$+\sigma_{\pi^0}/y$	$-\sigma_{\pi^0}/y$	$+\sigma_{total}/y$	$-\sigma_{total}/y$
-1.47	0.00084	19.81246	4.53100	-4.45000	1.00560	-0.92662	3.95704	-4.83714	8.29264	-8.29378	0.00043	-0.00043	10.29404	-10.62289
-1.26	-0.03148	-0.50321	0.10015	-0.09836	0.07036	-0.06483	0.03577	-0.04373	0.22189	-0.22192	0.00043	-0.00043	0.25592	-0.25502
-1.05	0.03360	0.38269	0.05800	-0.05696	0.08149	-0.07509	0.06630	-0.05424	0.20972	-0.20975	0.00043	-0.00043	0.24163	-0.23626
-0.84	0.02137	0.55812	0.01907	-0.01873	0.10367	-0.09553	0.20395	-0.16684	0.33520	-0.33524	0.00043	-0.00043	0.40628	-0.38691
-0.63	0.04011	0.24585	0.02949	-0.03002	0.02109	-0.01944	0.08985	-0.07350	0.18243	-0.18245	0.00043	-0.00043	0.20656	-0.19993
-0.42	0.09148	0.10344	0.02800	-0.02851	0.00852	-0.00925	0.00509	-0.00416	0.08176	-0.08177	0.00043	-0.00043	0.08699	-0.08719
-0.21	0.14178	0.05837	0.02466	-0.02511	0.01440	-0.01562	0.01720	-0.02103	0.05362	-0.05362	0.00043	-0.00043	0.06314	-0.06475
-0.00	0.22117	0.03865	0.01731	-0.01762	0.01141	-0.01238	0.01648	-0.02014	0.03458	-0.03458	0.00043	-0.00043	0.04355	-0.04545
0.21	0.16635	0.04940	0.02102	-0.02140	0.01227	-0.01332	0.01466	-0.01792	0.04570	-0.04570	0.00043	-0.00043	0.05381	-0.05518
0.42	0.10531	0.08631	0.02432	-0.02476	0.00740	-0.00803	0.00442	-0.00362	0.07102	-0.07103	0.00043	-0.00043	0.07556	-0.07574
0.63	0.03343	0.27677	0.03538	-0.03603	0.02531	-0.02332	0.10781	-0.08820	0.21889	-0.21892	0.00043	-0.00043	0.24785	-0.23989
0.84	0.02002	0.52868	0.02035	-0.01999	0.11066	-0.10197	0.21771	-0.17809	0.35780	-0.35785	0.00043	-0.00043	0.43368	-0.41300
1.05	0.00237	4.90007	0.82355	-0.80882	1.15710	-1.06622	0.94136	-0.77008	2.97775	-2.97816	0.00043	-0.00043	3.43078	-3.35462
1.26	0.00114	12.51122	2.75563	-2.70637	1.93587	-1.78382	0.98423	-1.20314	6.10510	-6.10594	0.00043	-0.00043	7.04145	-7.01687
1.47	0.00464	3.52952	0.82120	-0.80652	0.18226	-0.16794	0.71718	-0.87669	1.50297	-1.50317	0.00043	-0.00043	1.86570	-1.92530
1.68	0.00108	14.66673	3.53963	-3.47635	0.72388	-0.78558	3.09125	-3.77879	6.50700	-6.50790	0.01248	-0.01248	8.05916	-8.32672
1.88	0.03164	0.47510	0.09965	-0.09787	0.06451	-0.07000	0.03559	-0.04351	0.22334	-0.22337	0.01248	-0.01248	0.25572	-0.25772
2.09	0.03165	0.37929	0.06156	-0.06046	0.07971	-0.08650	0.07037	-0.05757	0.22577	-0.22580	0.01248	-0.01248	0.25734	-0.25611
2.30	0.06206	0.18302	0.00656	-0.00645	0.03289	-0.03569	0.07022	-0.05744	0.11671	-0.11673	0.01248	-0.01248	0.14083	-0.13563
2.51	0.07034	0.13737	0.01682	-0.01712	0.01108	-0.01203	0.05124	-0.04192	0.10447	-0.10449	0.01248	-0.01248	0.11875	-0.11519
2.72	0.07057	0.13724	0.03629	-0.03695	0.01199	-0.01105	0.00660	-0.00540	0.10554	-0.10555	0.01248	-0.01248	0.11313	-0.11320
2.93	0.07518	0.11961	0.04651	-0.04736	0.02946	-0.02715	0.03244	-0.03965	0.10003	-0.10005	0.01248	-0.01248	0.11936	-0.12132
3.14	0.07097	0.13311	0.05394	-0.05492	0.03858	-0.03555	0.05135	-0.06277	0.10634	-0.10636	0.01248	-0.01248	0.13601	-0.14031
3.35	0.06348	0.14137	0.05509	-0.05609	0.03490	-0.03216	0.03842	-0.04696	0.11848	-0.11849	0.01248	-0.01248	0.14114	-0.14346
3.56	0.06622	0.14539	0.03867	-0.03938	0.01278	-0.01177	0.00703	-0.00575	0.11247	-0.11248	0.01248	-0.01248	0.12047	-0.12054
3.77	0.06141	0.15777	0.01926	-0.01961	0.01269	-0.01378	0.05868	-0.04801	0.11965	-0.11967	0.01248	-0.01248	0.13583	-0.13174
3.98	0.05093	0.22008	0.00800	-0.00786	0.04008	-0.04349	0.08556	-0.06999	0.14221	-0.14223	0.01248	-0.01248	0.17138	-0.16504
4.19	0.05307	0.22699	0.03672	-0.03607	0.04754	-0.05159	0.04197	-0.03434	0.13467	-0.13468	0.01248	-0.01248	0.15382	-0.15309
4.40	0.03457	0.41348	0.09120	-0.08957	0.05904	-0.06407	0.03257	-0.03982	0.20439	-0.20442	0.01248	-0.01248	0.23409	-0.23592
4.61	0.06221	0.25917	0.06128	-0.06019	0.01253	-0.01360	0.05352	-0.06542	0.11266	-0.11267	0.01248	-0.01248	0.14009	-0.14470

Table 32: 20–40%, 4.0–5.0 $\otimes$ 2.0–3.0 GeV/c Jet Function

ϕ	per trig yield	σ_{stat}/y	systematic errors											
			$+\sigma_{f2}/y$	$-\sigma_{f2}/y$	$+\sigma_{f3}/y$	$-\sigma_{f3}/y$	$+\sigma_{f4}/y$	$-\sigma_{f4}/y$	$+\sigma_{\xi/ZYAM}/y$	$-\sigma_{\xi}/y$	$+\sigma_{\pi^0}/y$	$-\sigma_{\pi^0}/y$	$+\sigma_{total}/y$	$-\sigma_{total}/y$
-1.47	0.00343	1.45052	0.14304	-0.14028	0.02965	-0.02746	0.15365	-0.18782	0.17660	-0.17660	0.00727	-0.00727	0.27602	-0.29487
-1.26	0.00727	0.62619	0.05589	-0.05481	0.03666	-0.03396	0.02455	-0.03001	0.08338	-0.08338	0.00727	-0.00727	0.10988	-0.10983
-1.05	0.00205	1.90204	0.12231	-0.11995	0.16048	-0.14864	0.17196	-0.14067	0.29828	-0.29828	0.00727	-0.00727	0.39913	-0.38118
-0.84	0.00680	0.47898	0.00772	-0.00757	0.03919	-0.03630	0.10153	-0.08306	0.09208	-0.09208	0.00727	-0.00727	0.14295	-0.12964
-0.63	0.00786	0.37595	0.01935	-0.01973	0.01295	-0.01199	0.07264	-0.05942	0.08221	-0.08221	0.00727	-0.00727	0.11238	-0.10428
-0.42	0.01786	0.15150	0.01845	-0.01882	0.00528	-0.00570	0.00413	-0.00338	0.03741	-0.03741	0.00727	-0.00727	0.04287	-0.04301
-0.21	0.05784	0.04623	0.00778	-0.00793	0.00427	-0.00461	0.00668	-0.00817	0.01184	-0.01184	0.00727	-0.00727	0.01778	-0.01854
-0.00	0.09620	0.02761	0.00512	-0.00522	0.00317	-0.00342	0.00600	-0.00734	0.00718	-0.00718	0.00727	-0.00727	0.01329	-0.01404
0.21	0.05885	0.04483	0.00764	-0.00779	0.00419	-0.00453	0.00657	-0.00803	0.01163	-0.01163	0.00727	-0.00727	0.01753	-0.01827
0.42	0.02650	0.09866	0.01244	-0.01268	0.00356	-0.00384	0.00278	-0.00228	0.02521	-0.02521	0.00727	-0.00727	0.02938	-0.02948
0.63	0.00956	0.28643	0.01591	-0.01623	0.01065	-0.00986	0.05972	-0.04886	0.06759	-0.06759	0.00727	-0.00727	0.09249	-0.08584
0.84	0.00410	0.71899	0.01280	-0.01256	0.06501	-0.06021	0.16844	-0.13780	0.15276	-0.15276	0.00727	-0.00727	0.23696	-0.21485
1.05	0.00688	0.49535	0.03650	-0.03579	0.04789	-0.04435	0.05131	-0.04198	0.08901	-0.08901	0.00727	-0.00727	0.11930	-0.11396
1.26	0.00709	0.56598	0.05733	-0.05622	0.03761	-0.03483	0.02518	-0.03079	0.08553	-0.08553	0.00727	-0.00727	0.11271	-0.11265
1.47	0.00390	1.25663	0.12603	-0.12361	0.02612	-0.02419	0.13539	-0.16549	0.15561	-0.15561	0.00727	-0.00727	0.24323	-0.25984
1.68	-0.00267	-1.83438	0.18385	-0.18031	0.03529	-0.03810	0.19749	-0.24141	0.22871	-0.22871	0.02424	-0.02424	0.35629	-0.38097
1.88	0.00335	1.22022	0.12135	-0.11901	0.07374	-0.07961	0.05331	-0.06517	0.18464	-0.18464	0.02424	-0.02424	0.24017	-0.24378
2.09	0.01017	0.36060	0.02470	-0.02422	0.03001	-0.03240	0.03472	-0.02840	0.06169	-0.06169	0.02424	-0.02424	0.08432	-0.08269
2.30	0.00478	0.65579	0.01097	-0.01076	0.05160	-0.05571	0.14434	-0.11808	0.13342	-0.13342	0.02424	-0.02424	0.20495	-0.18855
2.51	0.01393	0.20951	0.01093	-0.01114	0.00677	-0.00731	0.04101	-0.03355	0.04674	-0.04674	0.02424	-0.02424	0.06796	-0.06383
2.72	0.01676	0.16068	0.01966	-0.02004	0.00607	-0.00562	0.00440	-0.00360	0.03957	-0.03957	0.02424	-0.02424	0.05095	-0.05098
2.93	0.01628	0.16656	0.02764	-0.02818	0.01637	-0.01517	0.02374	-0.02902	0.04133	-0.04133	0.02424	-0.02424	0.06238	-0.06451
3.14	0.01784	0.15142	0.02761	-0.02815	0.01847	-0.01710	0.03238	-0.03957	0.03790	-0.03790	0.02424	-0.02424	0.06462	-0.06837
3.35	0.01238	0.21666	0.03633	-0.03705	0.02152	-0.01994	0.03121	-0.03815	0.05432	-0.05432	0.02424	-0.02424	0.07935	-0.08224
3.56	0.01587	0.16941	0.02077	-0.02117	0.00642	-0.00594	0.00465	-0.00380	0.04180	-0.04180	0.02424	-0.02424	0.05319	-0.05323
3.77	0.00908	0.31341	0.01675	-0.01708	0.01038	-0.01121	0.06287	-0.05143	0.07165	-0.07165	0.02424	-0.02424	0.10031	-0.09372
3.98	0.00526	0.58193	0.00998	-0.00979	0.04693	-0.05066	0.13127	-0.10739	0.12134	-0.12134	0.02424	-0.02424	0.18667	-0.17177
4.19	0.00193	1.82661	0.13036	-0.12785	0.15843	-0.17105	0.18328	-0.14994	0.32565	-0.32565	0.02424	-0.02424	0.42699	-0.41800
4.40	0.00276	1.44802	0.14699	-0.14416	0.08932	-0.09643	0.06457	-0.07893	0.22365	-0.22365	0.02424	-0.02424	0.29045	-0.29482
4.61	0.00849	0.56101	0.05782	-0.05671	0.01110	-0.01198	0.06211	-0.07592	0.07193	-0.07193	0.02424	-0.02424	0.11439	-0.12200

Table 33: 20–40%, 4.0–5.0 $\otimes$ 3.0–5.0 GeV/c Jet Function

ϕ	per trig yield	σ_{stat}/y	systematic errors											
			$+\sigma_{f2}/y$	$-\sigma_{f2}/y$	$+\sigma_{f3}/y$	$-\sigma_{f3}/y$	$+\sigma_{f4}/y$	$-\sigma_{f4}/y$	$+\sigma_{\xi/ZYAM}/y$	$-\sigma_{\xi}/y$	$+\sigma_{\pi^0}/y$	$-\sigma_{\pi^0}/y$	$+\sigma_{total}/y$	$-\sigma_{total}/y$
-1.47	0.00101	1.76413	0.05808	-0.05704	0.01370	-0.01269	0.07614	-0.09289	0.06725	-0.06818	0.00920	-0.00920	0.11818	-0.12952
-1.26	0.00146	1.08294	0.03340	-0.03280	0.02494	-0.02309	0.01791	-0.02185	0.04668	-0.04733	0.00920	-0.00920	0.06574	-0.06642
-1.05	-0.00126	-1.06263	0.02393	-0.02350	0.03574	-0.03309	0.04098	-0.03359	0.05461	-0.05537	0.00920	-0.00920	0.08122	-0.07698
-0.84	0.00171	0.65828	0.00367	-0.00361	0.02123	-0.01966	0.05887	-0.04825	0.04101	-0.04158	0.00920	-0.00920	0.07547	-0.06739
-0.63	0.00294	0.36700	0.00621	-0.00632	0.00472	-0.00437	0.02833	-0.02322	0.02465	-0.02499	0.00920	-0.00920	0.03944	-0.03616
-0.42	0.00501	0.19438	0.00789	-0.00803	0.00256	-0.00277	0.00215	-0.00176	0.01498	-0.01519	0.00920	-0.00920	0.01955	-0.01976
-0.21	0.02180	0.05147	0.00248	-0.00252	0.00154	-0.00167	0.00259	-0.00316	0.00353	-0.00358	0.00920	-0.00920	0.01060	-0.01080
-0.00	0.04588	0.02678	0.00129	-0.00131	0.00091	-0.00098	0.00184	-0.00225	0.00170	-0.00172	0.00920	-0.00920	0.00966	-0.00976
0.21	0.02169	0.05063	0.00249	-0.00253	0.00155	-0.00168	0.00260	-0.00318	0.00355	-0.00360	0.00920	-0.00920	0.01061	-0.01081
0.42	0.00371	0.24609	0.01064	-0.01084	0.00346	-0.00374	0.00290	-0.00238	0.02021	-0.02049	0.00920	-0.00920	0.02504	-0.02533
0.63	0.00156	0.62581	0.01172	-0.01193	0.00891	-0.00825	0.05350	-0.04385	0.04655	-0.04720	0.00920	-0.00920	0.07301	-0.06668
0.84	0.00205	0.51303	0.00306	-0.00301	0.01770	-0.01638	0.04906	-0.04022	0.03417	-0.03465	0.00920	-0.00920	0.06310	-0.05639
1.05	0.00033	3.62286	0.09115	-0.08951	0.13613	-0.12604	0.15609	-0.12794	0.20800	-0.21089	0.00920	-0.00920	0.30749	-0.29125
1.26	0.00198	0.71944	0.02460	-0.02416	0.01837	-0.01701	0.01319	-0.01609	0.03438	-0.03486	0.00920	-0.00920	0.04882	-0.04931
1.47	0.00259	0.69155	0.02275	-0.02234	0.00537	-0.00497	0.02982	-0.03638	0.02634	-0.02670	0.00920	-0.00920	0.04705	-0.05143
1.68	0.00111	1.63210	0.05289	-0.05194	0.01155	-0.01248	0.06934	-0.08459	0.06173	-0.06259	0.00157	-0.00157	0.10748	-0.11802
1.88	0.00034	4.13323	0.14404	-0.14144	0.09958	-0.10756	0.07722	-0.09421	0.20554	-0.20840	0.00157	-0.00157	0.28085	-0.28963
2.09	0.00041	3.12227	0.07268	-0.07137	0.10049	-0.10854	0.12445	-0.10201	0.17013	-0.17249	0.00157	-0.00157	0.24457	-0.23882
2.30	0.00124	0.88366	0.00507	-0.00498	0.02716	-0.02933	0.08132	-0.06666	0.05781	-0.05861	0.00157	-0.00157	0.10354	-0.09362
2.51	0.00292	0.36312	0.00626	-0.00637	0.00441	-0.00476	0.02856	-0.02341	0.02504	-0.02539	0.00157	-0.00157	0.03878	-0.03548
2.72	0.00305	0.30890	0.01298	-0.01321	0.00456	-0.00422	0.00353	-0.00290	0.02446	-0.02480	0.00157	-0.00157	0.02833	-0.02861
2.93	0.00408	0.24296	0.01323	-0.01347	0.00891	-0.00825	0.01385	-0.01690	0.01854	-0.01880	0.00157	-0.00157	0.02815	-0.02985
3.14	0.00567	0.17368	0.01041	-0.01060	0.00792	-0.00733	0.01488	-0.01816	0.01340	-0.01359	0.00157	-0.00157	0.02397	-0.02613
3.35	0.00380	0.25876	0.01421	-0.01447	0.00957	-0.00886	0.01487	-0.01815	0.01991	-0.02018	0.00157	-0.00157	0.03022	-0.03205
3.56	0.00252	0.37075	0.01569	-0.01598	0.00551	-0.00510	0.00427	-0.00350	0.02958	-0.02999	0.00157	-0.00157	0.03424	-0.03458
3.77	0.00281	0.36875	0.00650	-0.00662	0.00458	-0.00495	0.02970	-0.02434	0.02603	-0.02640	0.00157	-0.00157	0.04032	-0.03688
3.98	0.00178	0.60754	0.00353	-0.00347	0.01891	-0.02042	0.05662	-0.04641	0.04025	-0.04081	0.00157	-0.00157	0.07210	-0.06520
4.19	0.00261	0.50112	0.01153	-0.01132	0.01595	-0.01722	0.01975	-0.01619	0.02700	-0.02737	0.00157	-0.00157	0.03884	-0.03793
4.40	0.00171	0.83284	0.02849	-0.02798	0.01970	-0.02127	0.01527	-0.01864	0.04066	-0.04122	0.00157	-0.00157	0.05557	-0.05731
4.61	0.00146	1.15364	0.04021	-0.03948	0.00878	-0.00948	0.05271	-0.06430	0.04692	-0.04758	0.00157	-0.00157	0.08171	-0.08972

Table 34: 20–40%, 4.0–5.0 $\otimes$ 5.0–7.0 GeV/c Jet Function

ϕ	per trig yield	σ_{stat}/y	systematic errors											
			$+\sigma_{f2}/y$	$-\sigma_{f2}/y$	$+\sigma_{f3}/y$	$-\sigma_{f3}/y$	$+\sigma_{f4}/y$	$-\sigma_{f4}/y$	$+\sigma_{\xi/ZYAM}/y$	$-\sigma_{\xi}/y$	$+\sigma_{\pi^0}/y$	$-\sigma_{\pi^0}/y$	$+\sigma_{total}/y$	$-\sigma_{total}/y$
-1.47	-0.00044	-1.50309	0.01122	-0.01095	0.00602	-0.00543	0.01836	-0.02352	0.01735	-0.01735	0.05239	-0.05239	0.05954	-0.06122
-1.26	-0.00057	-0.89288	0.00715	-0.00698	0.01215	-0.01095	0.00478	-0.00613	0.01338	-0.01338	0.05239	-0.05239	0.05608	-0.05595
-1.05	-0.00047	-0.98022	0.00534	-0.00521	0.01815	-0.01636	0.01199	-0.00936	0.01631	-0.01631	0.05239	-0.05239	0.05927	-0.05825
-0.84	0.00041	1.17297	0.00130	-0.00127	0.01710	-0.01541	0.02731	-0.02132	0.01931	-0.01931	0.05239	-0.05239	0.06448	-0.06174
-0.63	0.00047	0.96803	0.00324	-0.00332	0.00564	-0.00509	0.01951	-0.01523	0.01708	-0.01708	0.05239	-0.05239	0.05882	-0.05749
-0.42	0.00100	0.44114	0.00332	-0.00340	0.00241	-0.00267	0.00119	-0.00093	0.00827	-0.00827	0.05239	-0.05239	0.05321	-0.05323
-0.21	0.00323	0.16709	0.00140	-0.00143	0.00195	-0.00216	0.00184	-0.00236	0.00260	-0.00260	0.05239	-0.05239	0.05254	-0.05257
-0.00	0.01131	0.06920	0.00044	-0.00045	0.00069	-0.00076	0.00079	-0.00101	0.00075	-0.00075	0.05239	-0.05239	0.05241	-0.05241
0.21	0.00534	0.11843	0.00085	-0.00087	0.00118	-0.00131	0.00111	-0.00143	0.00157	-0.00157	0.05239	-0.05239	0.05245	-0.05246
0.42	0.00024	1.54425	0.01358	-0.01391	0.00984	-0.01092	0.00488	-0.00381	0.03383	-0.03383	0.05239	-0.05239	0.06477	-0.06494
0.63	-0.00020	-1.93259	0.00775	-0.00794	0.01349	-0.01216	0.04665	-0.03641	0.04082	-0.04082	0.05239	-0.05239	0.08264	-0.07712
0.84	0.00001	29.14281	0.03631	-0.03543	0.47731	-0.43022	0.76242	-0.59510	0.53920	-0.53920	0.05239	-0.05239	1.05067	-0.91322
1.05	-0.00028	-1.63145	0.00896	-0.00875	0.03045	-0.02745	0.02012	-0.01570	0.02737	-0.02737	0.05239	-0.05239	0.07004	-0.06760
1.26	-0.00019	-2.91212	0.02170	-0.02117	0.03685	-0.03322	0.01452	-0.01860	0.04059	-0.04059	0.05239	-0.05239	0.08020	-0.07931
1.47	-0.00086	-0.61690	0.00575	-0.00561	0.00309	-0.00278	0.00941	-0.01205	0.00889	-0.00889	0.05239	-0.05239	0.05436	-0.05485
1.68	-0.00014	-5.01734	0.03655	-0.03567	0.01768	-0.01962	0.05980	-0.07662	0.05674	-0.05674	0.22121	-0.22121	0.23954	-0.24429
1.88	-0.00033	-1.53850	0.01233	-0.01203	0.01888	-0.02094	0.00825	-0.01057	0.02332	-0.02332	0.22121	-0.22121	0.22372	-0.22399
2.09	0.00001	82.62853	0.39571	-0.38617	1.21172	-1.34432	0.88802	-0.69313	1.22460	-1.22460	0.22121	-0.22121	1.99048	-1.99633
2.30	0.00061	0.80726	0.00086	-0.00084	0.01025	-0.01137	0.01816	-0.01417	0.01298	-0.01298	0.22121	-0.22121	0.22257	-0.22233
2.51	0.00006	6.40592	0.02378	-0.02437	0.03731	-0.04140	0.14319	-0.11176	0.12580	-0.12580	0.22121	-0.22121	0.29533	-0.28206
2.72	0.00028	1.36642	0.01188	-0.01217	0.00955	-0.00861	0.00427	-0.00333	0.02948	-0.02948	0.22121	-0.22121	0.22372	-0.22368
2.93	0.00089	0.50132	0.00509	-0.00522	0.00785	-0.00708	0.00670	-0.00858	0.00937	-0.00937	0.22121	-0.22121	0.22170	-0.22175
3.14	0.00249	0.21957	0.00199	-0.00203	0.00346	-0.00312	0.00356	-0.00457	0.00335	-0.00335	0.22121	-0.22121	0.22130	-0.22131
3.35	0.00084	0.53461	0.00540	-0.00554	0.00833	-0.00751	0.00710	-0.00910	0.00994	-0.00994	0.22121	-0.22121	0.22177	-0.22181
3.56	0.00043	0.92490	0.00776	-0.00795	0.00624	-0.00562	0.00279	-0.00218	0.01925	-0.01925	0.22121	-0.22121	0.22228	-0.22227
3.77	0.00055	0.82483	0.00280	-0.00287	0.00440	-0.00488	0.01689	-0.01318	0.01484	-0.01484	0.22121	-0.22121	0.22241	-0.22217
3.98	0.00001	67.70822	0.08185	-0.07988	0.96999	-1.07614	1.71896	-1.34171	1.22898	-1.22898	0.22121	-0.22121	2.33703	-2.12696
4.19	0.00016	3.44087	0.01582	-0.01544	0.04845	-0.05375	0.03551	-0.02772	0.04897	-0.04897	0.22121	-0.22121	0.23492	-0.23500
4.40	-0.00064	-0.73095	0.00645	-0.00630	0.00988	-0.01096	0.00432	-0.00553	0.01220	-0.01220	0.22121	-0.22121	0.22190	-0.22197
4.61	-0.00057	-0.98992	0.00878	-0.00857	0.00425	-0.00471	0.01436	-0.01840	0.01362	-0.01362	0.22121	-0.22121	0.22230	-0.22260

Table 35: 20–40%, 5.0–7.0 $\otimes$ 0.5–1.0 GeV/c Jet Function

ϕ	per trig yield	σ_{stat}/y	systematic errors											
			$+\sigma_{f2}/y$	$-\sigma_{f2}/y$	$+\sigma_{f3}/y$	$-\sigma_{f3}/y$	$+\sigma_{f4}/y$	$-\sigma_{f4}/y$	$+\sigma_{\xi/ZYAM}/y$	$-\sigma_{\xi}/y$	$+\sigma_{\pi^0}/y$	$-\sigma_{\pi^0}/y$	$+\sigma_{total}/y$	$-\sigma_{total}/y$
-1.47	0.02829	1.11574	0.17198	-0.15296	0.04770	-0.05073	0.11245	-0.14381	0.33068	-0.33068	0.00179	-0.00179	0.39223	-0.39497
-1.26	-0.04411	-0.67208	0.08482	-0.07322	0.00661	-0.00604	0.03478	-0.04468	0.21239	-0.21239	0.00179	-0.00179	0.23144	-0.22915
-1.05	-0.00628	-4.18842	0.26854	-0.19463	0.02716	-0.01658	0.13273	-0.10637	1.49956	-1.49956	0.00179	-0.00179	1.52942	-1.51596
-0.84	0.00146	16.17376	0.92536	-0.64879	0.21713	-0.20142	1.70274	-1.34630	6.49847	-6.49847	0.00179	-0.00179	6.78475	-6.67114
-0.63	0.03405	0.60332	0.11876	-0.10874	0.04104	-0.04366	0.05551	-0.04399	0.28126	-0.28126	0.00179	-0.00179	0.31302	-0.30786
-0.42	0.06206	0.29378	0.10300	-0.09837	0.04396	-0.04763	0.00691	-0.00908	0.15578	-0.15578	0.00179	-0.00179	0.19199	-0.19052
-0.21	0.18848	0.09407	0.04237	-0.04104	0.02018	-0.02198	0.01349	-0.01727	0.05163	-0.05163	0.00179	-0.00179	0.07109	-0.07166
-0.00	0.21017	0.08422	0.04068	-0.03955	0.02005	-0.02187	0.01640	-0.02097	0.04642	-0.04642	0.00179	-0.00179	0.06696	-0.06811
0.21	0.20675	0.08464	0.03863	-0.03741	0.01839	-0.02004	0.01230	-0.01575	0.04707	-0.04707	0.00179	-0.00179	0.06481	-0.06533
0.42	0.01171	1.52561	0.54605	-0.52150	0.23305	-0.25250	0.03663	-0.04816	0.82582	-0.82582	0.00179	-0.00179	1.01774	-1.00996
0.63	0.00770	2.53320	0.52500	-0.48069	0.18141	-0.19300	0.24537	-0.19445	1.24335	-1.24335	0.00179	-0.00179	1.38372	-1.36090
0.84	0.03243	0.66235	0.04166	-0.02921	0.00978	-0.00907	0.07667	-0.06062	0.29260	-0.29260	0.00179	-0.00179	0.30549	-0.30038
1.05	-0.01103	-2.29082	0.15289	-0.11081	0.01547	-0.00944	0.07557	-0.06056	0.85376	-0.85376	0.00179	-0.00179	0.87077	-0.86311
1.26	0.03032	0.94031	0.12342	-0.10654	0.00961	-0.00879	0.05060	-0.06501	0.30903	-0.30903	0.00179	-0.00179	0.33673	-0.33340
1.47	0.01212	2.47394	0.40132	-0.35694	0.11131	-0.11837	0.26240	-0.33559	0.77164	-0.77164	0.00179	-0.00179	0.91528	-0.92167
1.68	0.01414	2.15337	0.34375	-0.30568	0.18831	-0.20406	0.22493	-0.28767	0.66218	-0.66218	0.01214	-0.01214	0.80178	-0.81023
1.88	0.08314	0.35329	0.04493	-0.03876	0.04489	-0.04891	0.01848	-0.02374	0.11309	-0.11309	0.01214	-0.01214	0.13158	-0.13189
2.09	0.07503	0.33689	0.02237	-0.01616	0.05530	-0.06033	0.01105	-0.00886	0.12604	-0.12604	0.01214	-0.01214	0.14041	-0.14146
2.30	0.08365	0.26549	0.01624	-0.01140	0.04493	-0.04894	0.02968	-0.02347	0.11384	-0.11384	0.01214	-0.01214	0.12755	-0.12721
2.51	0.12220	0.16998	0.03312	-0.03032	0.02219	-0.02404	0.01546	-0.01225	0.07849	-0.07849	0.01214	-0.01214	0.09020	-0.08919
2.72	0.15283	0.13132	0.04181	-0.03993	0.00925	-0.00984	0.00280	-0.00368	0.06317	-0.06317	0.01214	-0.01214	0.07732	-0.07643
2.93	0.16763	0.11400	0.04760	-0.04611	0.00216	-0.00204	0.01515	-0.01940	0.05785	-0.05785	0.01214	-0.01214	0.07742	-0.07746
3.14	0.14578	0.12765	0.05859	-0.05697	0.00070	-0.00028	0.02362	-0.03020	0.06663	-0.06663	0.01214	-0.01214	0.09262	-0.09351
3.35	0.21184	0.09068	0.03766	-0.03649	0.00171	-0.00162	0.01199	-0.01535	0.04577	-0.04577	0.01214	-0.01214	0.06171	-0.06174
3.56	0.11954	0.16532	0.05345	-0.05105	0.01183	-0.01258	0.00358	-0.00471	0.08076	-0.08076	0.01214	-0.01214	0.09838	-0.09724
3.77	0.14974	0.14093	0.02703	-0.02474	0.01811	-0.01962	0.01261	-0.01000	0.06405	-0.06405	0.01214	-0.01214	0.07394	-0.07313
3.98	0.09675	0.23448	0.01404	-0.00985	0.03884	-0.04232	0.02566	-0.02029	0.09842	-0.09842	0.01214	-0.01214	0.11045	-0.11015
4.19	0.07655	0.32524	0.02193	-0.01584	0.05421	-0.05913	0.01083	-0.00868	0.12354	-0.12354	0.01214	-0.01214	0.13764	-0.13868
4.40	0.04084	0.69663	0.09146	-0.07890	0.09139	-0.09956	0.03762	-0.04833	0.23021	-0.23021	0.01214	-0.01214	0.26698	-0.26762
4.61	0.02084	1.52496	0.23334	-0.20750	0.12783	-0.13851	0.15268	-0.19527	0.44949	-0.44949	0.01214	-0.01214	0.54433	-0.55006

Table 36: 20–40%, 5.0–7.0 $\otimes$ 1.0–2.0 GeV/c Jet Function

ϕ	per trig yield	σ_{stat}/y	systematic errors											
			$+\sigma_{f2}/y$	$-\sigma_{f2}/y$	$+\sigma_{f3}/y$	$-\sigma_{f3}/y$	$+\sigma_{f4}/y$	$-\sigma_{f4}/y$	$+\sigma_{\xi/ZYAM}/y$	$-\sigma_{\xi}/y$	$+\sigma_{\pi^0}/y$	$-\sigma_{\pi^0}/y$	$+\sigma_{total}/y$	$-\sigma_{total}/y$
-1.47	0.00677	3.15477	0.63831	-0.62397	0.10778	-0.09717	0.35394	-0.44821	0.96252	-0.96252	0.01312	-0.01312	1.21282	-1.23543
-1.26	-0.01325	-1.53377	0.26958	-0.26353	0.14409	-0.12991	0.06114	-0.07742	0.49229	-0.49229	0.01312	-0.01312	0.58283	-0.57865
-1.05	-0.00240	-6.77815	0.92011	-0.89944	0.98360	-0.88676	0.69178	-0.54628	2.73962	-2.73962	0.01312	-0.01312	3.13023	-3.06585
-0.84	0.00239	6.32832	0.19352	-0.18917	0.80055	-0.72173	1.36149	-1.07513	2.79398	-2.79398	0.01312	-0.01312	3.21535	-3.08530
-0.63	0.05115	0.24567	0.02608	-0.02668	0.01426	-0.01286	0.05252	-0.04147	0.13260	-0.13260	0.01312	-0.01312	0.14628	-0.14266
-0.42	0.10430	0.11542	0.02769	-0.02833	0.00630	-0.00699	0.00333	-0.00263	0.06617	-0.06617	0.01312	-0.01312	0.07327	-0.07354
-0.21	0.20197	0.05269	0.01953	-0.01997	0.00852	-0.00945	0.00869	-0.01100	0.03461	-0.03461	0.01312	-0.01312	0.04358	-0.04449
-0.00	0.29504	0.03726	0.01463	-0.01497	0.00721	-0.00800	0.00889	-0.01125	0.02381	-0.02381	0.01312	-0.01312	0.03292	-0.03396
0.21	0.19947	0.05273	0.01977	-0.02022	0.00863	-0.00957	0.00880	-0.01114	0.03505	-0.03505	0.01312	-0.01312	0.04408	-0.04500
0.42	0.05105	0.22425	0.05658	-0.05788	0.01288	-0.01429	0.00680	-0.00537	0.13519	-0.13519	0.01312	-0.01312	0.14786	-0.14843
0.63	0.02550	0.46329	0.05231	-0.05351	0.02860	-0.02579	0.10533	-0.08317	0.26594	-0.26594	0.01312	-0.01312	0.29248	-0.28520
0.84	0.02174	0.62486	0.02123	-0.02075	0.08783	-0.07918	0.14937	-0.11795	0.30652	-0.30652	0.01312	-0.01312	0.35299	-0.33873
1.05	-0.01696	-0.87715	0.13020	-0.12727	0.13918	-0.12548	0.09789	-0.07730	0.38766	-0.38766	0.01312	-0.01312	0.44312	-0.43402
1.26	0.02692	0.68998	0.13272	-0.12974	0.07094	-0.06395	0.03010	-0.03811	0.24236	-0.24236	0.01312	-0.01312	0.28716	-0.28510
1.47	0.00415	5.10267	1.04073	-1.01735	0.17574	-0.15843	0.57708	-0.73079	1.56932	-1.56932	0.01312	-0.01312	1.97736	-2.01422
1.68	0.01421	1.44003	0.30400	-0.29717	0.04628	-0.05133	0.16857	-0.21347	0.45994	-0.45994	0.00241	-0.00241	0.57838	-0.58997
1.88	0.01144	1.68424	0.31238	-0.30536	0.15053	-0.16696	0.07084	-0.08971	0.57540	-0.57540	0.00241	-0.00241	0.67553	-0.67843
2.09	0.05597	0.27617	0.03945	-0.03856	0.03802	-0.04217	0.02966	-0.02342	0.11871	-0.11871	0.00241	-0.00241	0.13409	-0.13383
2.30	0.08288	0.17561	0.00557	-0.00544	0.02077	-0.02304	0.03918	-0.03094	0.08110	-0.08110	0.00241	-0.00241	0.09263	-0.09000
2.51	0.08443	0.14636	0.01580	-0.01616	0.00779	-0.00864	0.03181	-0.02512	0.08058	-0.08058	0.00241	-0.00241	0.08844	-0.08641
2.72	0.08382	0.14732	0.03446	-0.03525	0.00870	-0.00785	0.00414	-0.00327	0.08208	-0.08208	0.00241	-0.00241	0.08958	-0.08977
2.93	0.09840	0.11670	0.04008	-0.04100	0.01941	-0.01749	0.01783	-0.02258	0.07046	-0.07046	0.00241	-0.00241	0.08527	-0.08642
3.14	0.11944	0.10118	0.03614	-0.03697	0.01976	-0.01782	0.02195	-0.02780	0.05822	-0.05822	0.00241	-0.00241	0.07466	-0.07651
3.35	0.09347	0.12260	0.04219	-0.04316	0.02043	-0.01842	0.01877	-0.02377	0.07419	-0.07419	0.00241	-0.00241	0.08978	-0.09098
3.56	0.07165	0.17066	0.04032	-0.04124	0.01018	-0.00918	0.00484	-0.00383	0.09602	-0.09602	0.00241	-0.00241	0.10478	-0.10501
3.77	0.09795	0.12689	0.01362	-0.01393	0.00671	-0.00745	0.02742	-0.02166	0.06946	-0.06946	0.00241	-0.00241	0.07625	-0.07450
3.98	0.04950	0.28863	0.00932	-0.00912	0.03478	-0.03858	0.06561	-0.05181	0.13578	-0.13578	0.00241	-0.00241	0.15506	-0.15066
4.19	0.03197	0.48096	0.06906	-0.06751	0.06655	-0.07382	0.05192	-0.04100	0.20781	-0.20781	0.00241	-0.00241	0.23470	-0.23426
4.40	0.07066	0.26119	0.05056	-0.04943	0.02436	-0.02703	0.01147	-0.01452	0.09314	-0.09314	0.00241	-0.00241	0.10937	-0.10984
4.61	0.04691	0.43972	0.09208	-0.09001	0.01402	-0.01555	0.05106	-0.06466	0.13931	-0.13931	0.00241	-0.00241	0.17520	-0.17871

Table 37: 20–40%, 5.0–7.0 $\otimes$ 2.0–3.0 GeV/c Jet Function

ϕ	per trig yield	σ_{stat}/y	systematic errors											
			$+\sigma_{f2}/y$	$-\sigma_{f2}/y$	$+\sigma_{f3}/y$	$-\sigma_{f3}/y$	$+\sigma_{f4}/y$	$-\sigma_{f4}/y$	$+\sigma_{\xi/ZYAM}/y$	$-\sigma_{\xi}/y$	$+\sigma_{\pi^0}/y$	$-\sigma_{\pi^0}/y$	$+\sigma_{total}/y$	$-\sigma_{total}/y$
-1.47	-0.00229	-2.75444	0.23832	-0.23241	0.03917	-0.03557	0.16614	-0.21038	0.24937	-0.24937	0.00101	-0.00101	0.38486	-0.40215
-1.26	-0.00461	-1.22614	0.09761	-0.09519	0.05078	-0.04611	0.02783	-0.03524	0.12357	-0.12357	0.00101	-0.00101	0.16778	-0.16643
-1.05	0.00925	0.54839	0.03009	-0.02935	0.03131	-0.02843	0.02844	-0.02246	0.06223	-0.06223	0.00101	-0.00101	0.08104	-0.07776
-0.84	-0.00089	-4.55710	0.06515	-0.06354	0.26235	-0.23824	0.57625	-0.45506	0.65675	-0.65675	0.00101	-0.00101	0.91458	-0.83618
-0.63	0.01194	0.31750	0.01406	-0.01441	0.00750	-0.00681	0.03567	-0.02817	0.05042	-0.05042	0.00101	-0.00101	0.06379	-0.05992
-0.42	0.01906	0.18080	0.01906	-0.01955	0.00427	-0.00470	0.00289	-0.00228	0.03241	-0.03241	0.00101	-0.00101	0.03797	-0.03822
-0.21	0.08125	0.04347	0.00610	-0.00626	0.00262	-0.00288	0.00342	-0.00433	0.00775	-0.00775	0.00101	-0.00101	0.01081	-0.01129
-0.00	0.13706	0.02616	0.00396	-0.00406	0.00192	-0.00211	0.00303	-0.00384	0.00463	-0.00463	0.00101	-0.00101	0.00714	-0.00763
0.21	0.07949	0.04362	0.00624	-0.00640	0.00268	-0.00295	0.00350	-0.00443	0.00792	-0.00792	0.00101	-0.00101	0.01105	-0.01154
0.42	0.02461	0.13467	0.01476	-0.01513	0.00330	-0.00364	0.00223	-0.00176	0.02510	-0.02510	0.00101	-0.00101	0.02940	-0.02960
0.63	0.01128	0.31163	0.01487	-0.01525	0.00793	-0.00720	0.03773	-0.02980	0.05334	-0.05334	0.00101	-0.00101	0.06749	-0.06339
0.84	0.00349	1.08633	0.01669	-0.01627	0.06719	-0.06101	0.14758	-0.11655	0.16820	-0.16820	0.00101	-0.00101	0.23424	-0.21416
1.05	0.00214	2.03207	0.13022	-0.12699	0.13550	-0.12305	0.12308	-0.09720	0.26928	-0.26928	0.00101	-0.00101	0.35069	-0.33650
1.26	0.00372	1.38233	0.12110	-0.11809	0.06300	-0.05721	0.03452	-0.04372	0.15331	-0.15331	0.00101	-0.00101	0.20816	-0.20648
1.47	0.00312	2.03110	0.17475	-0.17042	0.02872	-0.02608	0.12182	-0.15426	0.18286	-0.18286	0.00101	-0.00101	0.28221	-0.29489
1.68	0.00093	6.88334	0.58575	-0.57122	0.08743	-0.09628	0.40833	-0.51707	0.61639	-0.61639	0.01228	-0.01228	0.94740	-0.99147
1.88	0.00385	1.36531	0.11695	-0.11405	0.05525	-0.06085	0.03334	-0.04222	0.15026	-0.15026	0.01228	-0.01228	0.20142	-0.20303
2.09	0.00650	0.71772	0.04285	-0.04179	0.04049	-0.04459	0.04050	-0.03198	0.09022	-0.09022	0.01228	-0.01228	0.11578	-0.11422
2.30	0.00193	2.06349	0.03021	-0.02946	0.11047	-0.12166	0.26722	-0.21102	0.30894	-0.30894	0.01228	-0.01228	0.42440	-0.39471
2.51	0.01724	0.21743	0.00973	-0.00998	0.00471	-0.00519	0.02469	-0.01950	0.03509	-0.03509	0.01228	-0.01228	0.04592	-0.04346
2.72	0.01971	0.17506	0.01843	-0.01890	0.00454	-0.00412	0.00279	-0.00220	0.03117	-0.03117	0.01228	-0.01228	0.03861	-0.03875
2.93	0.02281	0.15287	0.02175	-0.02230	0.01028	-0.00933	0.01219	-0.01544	0.02725	-0.02725	0.01228	-0.01228	0.04025	-0.04142
3.14	0.02972	0.11801	0.01827	-0.01874	0.00975	-0.00885	0.01398	-0.01771	0.02100	-0.02100	0.01228	-0.01228	0.03487	-0.03653
3.35	0.02450	0.14224	0.02025	-0.02076	0.00957	-0.00869	0.01135	-0.01437	0.02537	-0.02537	0.01228	-0.01228	0.03775	-0.03883
3.56	0.01366	0.24836	0.02660	-0.02727	0.00655	-0.00595	0.00403	-0.00318	0.04498	-0.04498	0.01228	-0.01228	0.05423	-0.05444
3.77	0.01289	0.28350	0.01301	-0.01335	0.00631	-0.00694	0.03302	-0.02608	0.04693	-0.04693	0.01228	-0.01228	0.06044	-0.05710
3.98	0.00668	0.58708	0.00871	-0.00849	0.03185	-0.03507	0.07703	-0.06083	0.08906	-0.08906	0.01228	-0.01228	0.12290	-0.11439
4.19	0.01101	0.41792	0.02527	-0.02465	0.02388	-0.02630	0.02389	-0.01887	0.05322	-0.05322	0.01228	-0.01228	0.06901	-0.06810
4.40	0.00949	0.55045	0.04747	-0.04629	0.02243	-0.02470	0.01353	-0.01714	0.06098	-0.06098	0.01228	-0.01228	0.08252	-0.08316
4.61	0.00024	25.37245	2.30251	-2.24542	0.34367	-0.37846	1.60512	-2.03257	2.42297	-2.42297	0.01228	-0.01228	3.72384	-3.89710

Table 38: 20–40%, 5.0–7.0 $\otimes$ 3.0–5.0 GeV/c Jet Function

ϕ	per trig yield	σ_{stat}/y	systematic errors											
			$+\sigma_{f2}/y$	$-\sigma_{f2}/y$	$+\sigma_{f3}/y$	$-\sigma_{f3}/y$	$+\sigma_{f4}/y$	$-\sigma_{f4}/y$	$+\sigma_{\xi/ZYAM}/y$	$-\sigma_{\xi}/y$	$+\sigma_{\pi^0}/y$	$-\sigma_{\pi^0}/y$	$+\sigma_{total}/y$	$-\sigma_{total}/y$
-1.47	0.00250	0.93928	0.02651	-0.02590	0.00487	-0.00442	0.02220	-0.02805	0.02593	-0.02555	0.00005	-0.00005	0.04349	-0.04615
-1.26	0.00143	1.41731	0.03847	-0.03760	0.02235	-0.02029	0.01318	-0.01665	0.04550	-0.04483	0.00005	-0.00005	0.06499	-0.06413
-1.05	-0.00194	-0.86860	0.01746	-0.01706	0.02029	-0.01842	0.01978	-0.01566	0.03371	-0.03321	0.00005	-0.00005	0.04737	-0.04448
-0.84	0.00141	1.01274	0.00503	-0.00492	0.02264	-0.02055	0.05336	-0.04224	0.04737	-0.04667	0.00005	-0.00005	0.07503	-0.06640
-0.63	0.00148	0.90178	0.01380	-0.01412	0.00821	-0.00745	0.04189	-0.03315	0.04615	-0.04548	0.00005	-0.00005	0.06436	-0.05850
-0.42	0.00716	0.17814	0.00620	-0.00634	0.00154	-0.00170	0.00112	-0.00089	0.00984	-0.00969	0.00005	-0.00005	0.01178	-0.01174
-0.21	0.03700	0.04397	0.00164	-0.00167	0.00078	-0.00086	0.00110	-0.00139	0.00194	-0.00191	0.00005	-0.00005	0.00288	-0.00302
-0.00	0.09421	0.02140	0.00070	-0.00072	0.00038	-0.00042	0.00065	-0.00082	0.00077	-0.00076	0.00005	-0.00005	0.00128	-0.00139
0.21	0.04042	0.04049	0.00150	-0.00153	0.00072	-0.00079	0.00101	-0.00127	0.00178	-0.00175	0.00005	-0.00005	0.00263	-0.00277
0.42	0.00617	0.19534	0.00718	-0.00735	0.00179	-0.00197	0.00130	-0.00103	0.01140	-0.01123	0.00005	-0.00005	0.01366	-0.01361
0.63	0.00101	1.22143	0.02025	-0.02072	0.01204	-0.01093	0.06145	-0.04863	0.06771	-0.06671	0.00005	-0.00005	0.09442	-0.08582
0.84	0.00107	1.24688	0.00663	-0.00648	0.02980	-0.02705	0.07024	-0.05560	0.06236	-0.06144	0.00005	-0.00005	0.09876	-0.08740
1.05	0.00159	0.99118	0.02131	-0.02083	0.02477	-0.02248	0.02414	-0.01911	0.04114	-0.04054	0.00005	-0.00005	0.05782	-0.05429
1.26	-0.00362	-0.45454	0.01517	-0.01482	0.00881	-0.00800	0.00520	-0.00656	0.01794	-0.01768	0.00005	-0.00005	0.02563	-0.02528
1.47	0.00204	1.12488	0.03249	-0.03175	0.00596	-0.00541	0.02720	-0.03437	0.03178	-0.03132	0.00005	-0.00005	0.05330	-0.05656
1.68	-0.00296	-0.72963	0.02240	-0.02188	0.00373	-0.00411	0.01875	-0.02369	0.02204	-0.02172	0.00671	-0.00671	0.03739	-0.03967
1.88	-0.00102	-1.72342	0.05375	-0.05252	0.02834	-0.03123	0.01841	-0.02325	0.06457	-0.06362	0.00671	-0.00671	0.09080	-0.09147
2.09	0.00254	0.67777	0.01337	-0.01307	0.01410	-0.01554	0.01515	-0.01199	0.02632	-0.02593	0.00671	-0.00671	0.03667	-0.03568
2.30	0.00040	3.43160	0.01772	-0.01731	0.07232	-0.07968	0.18782	-0.14865	0.16929	-0.16680	0.00671	-0.00671	0.26367	-0.23794
2.51	0.00191	0.69204	0.01071	-0.01096	0.00578	-0.00637	0.03250	-0.02572	0.03602	-0.03549	0.00671	-0.00671	0.05046	-0.04612
2.72	0.00647	0.19490	0.00686	-0.00702	0.00188	-0.00171	0.00124	-0.00098	0.01082	-0.01066	0.00671	-0.00671	0.01464	-0.01455
2.93	0.01046	0.13142	0.00579	-0.00593	0.00305	-0.00277	0.00389	-0.00492	0.00678	-0.00668	0.00671	-0.00671	0.01220	-0.01251
3.14	0.01337	0.10329	0.00496	-0.00507	0.00295	-0.00268	0.00455	-0.00575	0.00532	-0.00524	0.00671	-0.00671	0.01128	-0.01176
3.35	0.00837	0.15911	0.00724	-0.00741	0.00381	-0.00346	0.00486	-0.00615	0.00847	-0.00834	0.00671	-0.00671	0.01440	-0.01481
3.56	0.00686	0.18486	0.00646	-0.00662	0.00178	-0.00161	0.00117	-0.00093	0.01020	-0.01005	0.00671	-0.00671	0.01398	-0.01390
3.77	0.00510	0.26774	0.00402	-0.00411	0.00217	-0.00239	0.01219	-0.00965	0.01351	-0.01331	0.00671	-0.00671	0.01993	-0.01838
3.98	-0.00008	-16.86750	0.08963	-0.08758	0.36582	-0.40306	0.95005	-0.75193	0.85634	-0.84374	0.00671	-0.00671	1.33335	-1.20311
4.19	-0.00075	-2.09899	0.04536	-0.04432	0.04784	-0.05271	0.05138	-0.04067	0.08926	-0.08795	0.00671	-0.00671	0.12247	-0.11906
4.40	-0.00040	-4.39157	0.13717	-0.13404	0.07234	-0.07970	0.04697	-0.05935	0.16478	-0.16236	0.00671	-0.00671	0.23120	-0.23291
4.61	-0.00078	-2.67977	0.08554	-0.08359	0.01425	-0.01570	0.07163	-0.09050	0.08419	-0.08295	0.00671	-0.00671	0.14065	-0.14949

Table 39: 20–40%, 5.0–7.0 $\otimes$ 5.0–7.0 GeV/c Jet Function

ϕ	per trig yield	σ_{stat}/y	systematic errors											
			$+\sigma_{f2}/y$	$-\sigma_{f2}/y$	$+\sigma_{f3}/y$	$-\sigma_{f3}/y$	$+\sigma_{f4}/y$	$-\sigma_{f4}/y$	$+\sigma_{\xi/ZYAM}/y$	$-\sigma_{\xi}/y$	$+\sigma_{\pi^0}/y$	$-\sigma_{\pi^0}/y$	$+\sigma_{total}/y$	$-\sigma_{total}/y$
-1.47	0.00194	0.70659	0.00263	-0.00254	0.00108	-0.00094	0.00288	-0.00385	0.00398	-0.00348	0.00674	-0.00674	0.00881	-0.00893
-1.26	-0.00034	-2.09965	0.01244	-0.01202	0.01620	-0.01411	0.00557	-0.00746	0.02279	-0.01994	0.00674	-0.00674	0.03183	-0.02902
-1.05	0.00038	1.94024	0.00687	-0.00664	0.01790	-0.01559	0.01079	-0.00806	0.02053	-0.01797	0.00674	-0.00674	0.03084	-0.02684
-0.84	0.00079	0.82886	0.00069	-0.00067	0.00699	-0.00609	0.01019	-0.00761	0.01005	-0.00880	0.00674	-0.00674	0.01731	-0.01477
-0.63	0.00004	11.93937	0.03500	-0.03621	0.04717	-0.04108	0.14885	-0.11119	0.18097	-0.15835	0.00674	-0.00674	0.24166	-0.20120
-0.42	0.00072	0.74086	0.00468	-0.00484	0.00254	-0.00291	0.00119	-0.00089	0.01139	-0.00996	0.00674	-0.00674	0.01431	-0.01332
-0.21	0.00692	0.13022	0.00067	-0.00069	0.00069	-0.00079	0.00059	-0.00079	0.00120	-0.00105	0.00674	-0.00674	0.00694	-0.00695
-0.00	0.02986	0.05232	0.00017	-0.00017	0.00020	-0.00023	0.00020	-0.00027	0.00028	-0.00025	0.00674	-0.00674	0.00675	-0.00675
0.21	0.00777	0.12061	0.00059	-0.00061	0.00062	-0.00071	0.00053	-0.00071	0.00107	-0.00094	0.00674	-0.00674	0.00690	-0.00690
0.42	0.00033	1.47486	0.01023	-0.01058	0.00554	-0.00637	0.00260	-0.00194	0.02489	-0.02178	0.00674	-0.00674	0.02841	-0.02600
0.63	0.00045	1.25183	0.00345	-0.00356	0.00464	-0.00404	0.01465	-0.01095	0.01782	-0.01559	0.00674	-0.00674	0.02472	-0.02091
0.84	-0.00001	-95.26999	0.09505	-0.09187	0.95817	-0.83446	1.39642	-1.04309	1.37817	-1.20590	0.00674	-0.00674	2.18552	-1.80196
1.05	-0.00003	-18.37356	0.07513	-0.07262	0.19572	-0.17045	0.11796	-0.08811	0.22452	-0.19646	0.00674	-0.00674	0.32912	-0.28413
1.26	-0.00018	-3.99155	0.02353	-0.02275	0.03065	-0.02669	0.01054	-0.01411	0.04313	-0.03773	0.00674	-0.00674	0.05924	-0.05384
1.47	0.00111	1.03739	0.00460	-0.00445	0.00189	-0.00165	0.00504	-0.00675	0.00697	-0.00610	0.00674	-0.00674	0.01201	-0.01227
1.68	0.00328	0.46068	0.00156	-0.00150	0.00056	-0.00064	0.00171	-0.00228	0.00236	-0.00207	0.00487	-0.00487	0.00591	-0.00599
1.88	-0.00002	-31.80281	0.18432	-0.17817	0.20908	-0.24008	0.08257	-0.11053	0.34063	-0.29805	0.00487	-0.00487	0.44783	-0.43641
2.09	0.00061	1.27449	0.00427	-0.00413	0.00969	-0.01113	0.00671	-0.00501	0.01290	-0.01128	0.00487	-0.00487	0.01863	-0.01780
2.30	0.00025	2.28417	0.00215	-0.00207	0.01884	-0.02164	0.03153	-0.02356	0.03138	-0.02746	0.00487	-0.00487	0.04860	-0.04248
2.51	0.00046	1.23563	0.00338	-0.00350	0.00397	-0.00456	0.01438	-0.01074	0.01753	-0.01534	0.00487	-0.00487	0.02377	-0.02018
2.72	0.00033	1.48662	0.01010	-0.01045	0.00629	-0.00547	0.00256	-0.00191	0.02451	-0.02144	0.00487	-0.00487	0.02779	-0.02503
2.93	0.00226	0.30732	0.00204	-0.00211	0.00243	-0.00212	0.00181	-0.00243	0.00366	-0.00320	0.00487	-0.00487	0.00710	-0.00698
3.14	0.00462	0.18040	0.00109	-0.00113	0.00147	-0.00128	0.00132	-0.00177	0.00179	-0.00157	0.00487	-0.00487	0.00566	-0.00567
3.35	0.00234	0.29467	0.00197	-0.00204	0.00235	-0.00204	0.00175	-0.00234	0.00353	-0.00309	0.00487	-0.00487	0.00697	-0.00686
3.56	0.00235	0.28600	0.00144	-0.00149	0.00089	-0.00078	0.00036	-0.00027	0.00348	-0.00305	0.00487	-0.00487	0.00623	-0.00599
3.77	0.00129	0.50447	0.00121	-0.00125	0.00142	-0.00163	0.00515	-0.00384	0.00627	-0.00549	0.00487	-0.00487	0.00964	-0.00853
3.98	-0.00027	-1.88473	0.00198	-0.00192	0.01743	-0.02001	0.02916	-0.02178	0.02902	-0.02539	0.00487	-0.00487	0.04499	-0.03933
4.19	-0.00064	-0.83704	0.00404	-0.00391	0.00918	-0.01054	0.00635	-0.00474	0.01221	-0.01069	0.00487	-0.00487	0.01771	-0.01693
4.40	0.00054	1.54585	0.00787	-0.00761	0.00892	-0.01025	0.00352	-0.00472	0.01454	-0.01272	0.00487	-0.00487	0.01972	-0.01925
4.61	0.00073	1.38131	0.00699	-0.00675	0.00250	-0.00287	0.00765	-0.01024	0.01061	-0.00928	0.00487	-0.00487	0.01581	-0.01639

Table 40: 20–40%, 7.0–9.0 $\otimes$ 0.5–1.0 GeV/c Jet Function

ϕ	per trig yield	σ_{stat}/y	systematic errors											
			$+\sigma_{f2}/y$	$-\sigma_{f2}/y$	$+\sigma_{f3}/y$	$-\sigma_{f3}/y$	$+\sigma_{f4}/y$	$-\sigma_{f4}/y$	$+\sigma_{\xi/ZYAM}/y$	$-\sigma_{\xi}/y$	$+\sigma_{\pi^0}/y$	$-\sigma_{\pi^0}/y$	$+\sigma_{total}/y$	$-\sigma_{total}/y$
-1.47	-0.08599	-1.00378	0.11782	-0.09249	0.00564	-0.00748	0.02795	-0.04417	0.24483	-0.24483	0.01190	-0.01190	0.27346	-0.26579
-1.26	0.11072	0.74421	0.07189	-0.05575	0.00720	-0.00543	0.01116	-0.01768	0.19042	-0.19042	0.01190	-0.01190	0.20432	-0.19963
-1.05	0.08021	0.90582	0.04976	-0.03636	0.01673	-0.01261	0.00629	-0.00406	0.26388	-0.26388	0.01190	-0.01190	0.26939	-0.26697
-0.84	0.12839	0.51012	0.00976	-0.00849	0.00609	-0.00459	0.01524	-0.00971	0.16587	-0.16587	0.01190	-0.01190	0.16739	-0.16686
-0.63	0.03247	1.73483	0.17296	-0.19731	0.01560	-0.02070	0.04414	-0.02816	0.66064	-0.66064	0.01190	-0.01190	0.68462	-0.69047
-0.42	0.01954	2.54941	0.48182	-0.56476	0.09510	-0.12620	0.02312	-0.03691	1.10517	-1.10517	0.01190	-0.01190	1.20966	-1.24811
-0.21	0.27263	0.17908	0.04400	-0.05201	0.01083	-0.01437	0.00715	-0.01131	0.07961	-0.07961	0.01190	-0.01190	0.09265	-0.09757
-0.00	0.26794	0.18163	0.04818	-0.05707	0.01257	-0.01668	0.00967	-0.01528	0.08115	-0.08115	0.01190	-0.01190	0.09644	-0.10245
0.21	0.24759	0.19430	0.04845	-0.05727	0.01192	-0.01582	0.00788	-0.01246	0.08766	-0.08766	0.01190	-0.01190	0.10187	-0.10730
0.42	-0.05525	-0.88189	0.17042	-0.19975	0.03363	-0.04463	0.00818	-0.01306	0.39089	-0.39089	0.01190	-0.01190	0.42800	-0.44159
0.63	-0.00406	-13.16237	1.38315	-1.57784	0.12475	-0.16557	0.35296	-0.22522	5.28305	-5.28305	0.01190	-0.01190	5.47394	-5.52074
0.84	-0.06492	-0.90279	0.01931	-0.01679	0.01204	-0.00907	0.03013	-0.01919	0.32803	-0.32803	0.01190	-0.01190	0.33041	-0.32936
1.05	0.03752	1.85869	0.10639	-0.07773	0.03577	-0.02696	0.01346	-0.00868	0.56419	-0.56419	0.01190	-0.01190	0.57552	-0.57034
1.26	-0.13047	-0.59415	0.06101	-0.04731	0.00611	-0.00461	0.00947	-0.01500	0.16159	-0.16159	0.01190	-0.01190	0.17350	-0.16952
1.47	-0.00398	-20.70790	2.54538	-1.99827	0.12177	-0.16162	0.60385	-0.95434	5.28956	-5.28956	0.01190	-0.01190	5.90237	-5.73668
1.68	0.14244	0.59455	0.07110	-0.05582	0.01284	-0.01704	0.01688	-0.02667	0.14793	-0.14793	0.02212	-0.02212	0.16697	-0.16276
1.88	0.11801	0.68555	0.06740	-0.05226	0.02475	-0.03284	0.01048	-0.01661	0.17910	-0.17910	0.02212	-0.02212	0.19450	-0.19144
2.09	0.15304	0.45545	0.02603	-0.01901	0.02183	-0.02897	0.00328	-0.00212	0.13873	-0.13873	0.02212	-0.02212	0.14457	-0.14471
2.30	0.13383	0.45627	0.00941	-0.00819	0.02191	-0.02907	0.01460	-0.00930	0.15951	-0.15951	0.02212	-0.02212	0.16345	-0.16411
2.51	0.16723	0.34094	0.03359	-0.03832	0.01107	-0.01469	0.00856	-0.00546	0.12838	-0.12838	0.02212	-0.02212	0.13526	-0.13670
2.72	0.14367	0.38137	0.06552	-0.07681	0.00357	-0.00474	0.00314	-0.00501	0.15019	-0.15019	0.02212	-0.02212	0.16542	-0.17028
2.93	0.21614	0.24261	0.05547	-0.06558	0.00350	-0.00263	0.00902	-0.01426	0.10018	-0.10018	0.02212	-0.02212	0.11703	-0.12262
3.14	0.17985	0.28372	0.07173	-0.08499	0.00725	-0.00547	0.01440	-0.02275	0.12054	-0.12054	0.02212	-0.02212	0.14291	-0.15096
3.35	0.18032	0.29084	0.06649	-0.07861	0.00419	-0.00316	0.01081	-0.01709	0.12008	-0.12008	0.02212	-0.02212	0.13951	-0.14625
3.56	0.26801	0.20452	0.03512	-0.04117	0.00192	-0.00254	0.00168	-0.00269	0.08051	-0.08051	0.02212	-0.02212	0.09062	-0.09317
3.77	0.12920	0.44811	0.04348	-0.04960	0.01433	-0.01902	0.01108	-0.00707	0.16618	-0.16618	0.02212	-0.02212	0.17413	-0.17600
3.98	0.03995	1.55604	0.03152	-0.02744	0.07340	-0.09740	0.04890	-0.03115	0.53443	-0.53443	0.02212	-0.02212	0.54303	-0.54527
4.19	0.05246	1.30570	0.07594	-0.05545	0.06368	-0.08451	0.00956	-0.00617	0.40472	-0.40472	0.02212	-0.02212	0.41737	-0.41778
4.40	0.07449	1.05831	0.10678	-0.08279	0.03920	-0.05202	0.01661	-0.02631	0.28374	-0.28374	0.02212	-0.02212	0.30694	-0.30208
4.61	-0.08374	-1.03788	0.12095	-0.09495	0.02185	-0.02899	0.02871	-0.04537	0.25164	-0.25164	0.02212	-0.02212	0.28239	-0.27518

Table 41: 20–40%, 7.0–9.0 $\otimes$ 1.0–2.0 GeV/c Jet Function

ϕ	per trig yield	σ_{stat}/y	systematic errors											
			$+\sigma_{f2}/y$	$-\sigma_{f2}/y$	$+\sigma_{f3}/y$	$-\sigma_{f3}/y$	$+\sigma_{f4}/y$	$-\sigma_{f4}/y$	$+\sigma_{\xi/ZYAM}/y$	$-\sigma_{\xi}/y$	$+\sigma_{\pi^0}/y$	$-\sigma_{\pi^0}/y$	$+\sigma_{total}/y$	$-\sigma_{total}/y$
-1.47	0.11938	0.50537	0.07111	-0.05836	0.00725	-0.00545	0.01441	-0.02258	0.05288	-0.05288	0.00095	-0.00095	0.09008	-0.08211
-1.26	-0.04818	-1.15280	0.14575	-0.11961	0.04704	-0.03533	0.01208	-0.01893	0.13127	-0.13127	0.00095	-0.00095	0.20208	-0.18206
-1.05	0.03279	1.37545	0.13234	-0.10861	0.08543	-0.06415	0.04499	-0.02871	0.19411	-0.19411	0.00095	-0.00095	0.25400	-0.23327
-0.84	0.05005	0.83389	0.01813	-0.01488	0.04528	-0.03400	0.05766	-0.03680	0.12854	-0.12854	0.00095	-0.00095	0.14908	-0.13876
-0.63	0.06247	0.55390	0.03524	-0.04294	0.01386	-0.01041	0.03821	-0.02439	0.10436	-0.10436	0.00095	-0.00095	0.11741	-0.11592
-0.42	0.18510	0.18042	0.02575	-0.03138	0.00351	-0.00468	0.00167	-0.00106	0.03568	-0.03568	0.00095	-0.00095	0.04418	-0.04776
-0.21	0.26762	0.11019	0.02432	-0.02963	0.00636	-0.00847	0.00471	-0.00738	0.02491	-0.02491	0.00095	-0.00095	0.03571	-0.04032
-0.00	0.37114	0.08188	0.01919	-0.02339	0.00567	-0.00755	0.00507	-0.00795	0.01803	-0.01803	0.00095	-0.00095	0.02742	-0.03151
0.21	0.32870	0.08956	0.01980	-0.02412	0.00518	-0.00689	0.00383	-0.00601	0.02028	-0.02028	0.00095	-0.00095	0.02908	-0.03283
0.42	0.04046	0.77192	0.11779	-0.14352	0.01607	-0.02139	0.00762	-0.00486	0.16320	-0.16320	0.00095	-0.00095	0.20206	-0.21844
0.63	0.09416	0.34891	0.02338	-0.02848	0.00919	-0.00690	0.02535	-0.01618	0.06923	-0.06923	0.00095	-0.00095	0.07790	-0.07691
0.84	0.02704	1.38110	0.03355	-0.02753	0.08381	-0.06294	0.10673	-0.06812	0.23790	-0.23790	0.00095	-0.00095	0.27593	-0.25682
1.05	-0.00026	-156.38022	16.48995	-13.53303	10.64420	-7.99385	5.60585	-3.57788	24.18617	-24.18617	0.00095	-0.00095	31.64828	-29.06573
1.26	0.00366	13.91500	1.91846	-1.57445	0.61918	-0.46501	0.15900	-0.24911	1.72793	-1.72793	0.00095	-0.00095	2.65987	-2.39644
1.47	-0.04761	-1.21437	0.17832	-0.14634	0.01818	-0.01365	0.03614	-0.05662	0.13260	-0.13260	0.00095	-0.00095	0.22587	-0.20589
1.68	-0.00382	-14.76299	2.22495	-1.82598	0.17037	-0.22686	0.45087	-0.70643	1.65823	-1.65823	0.00281	-0.00281	2.81646	-2.57574
1.88	0.02224	2.38430	0.31568	-0.25908	0.07652	-0.10189	0.02616	-0.04099	0.28601	-0.28601	0.00281	-0.00281	0.43360	-0.40124
2.09	0.05953	0.71406	0.07289	-0.05982	0.03534	-0.04705	0.02478	-0.01582	0.10769	-0.10769	0.00281	-0.00281	0.13705	-0.13285
2.30	0.09198	0.43317	0.00986	-0.00809	0.01850	-0.02464	0.03138	-0.02003	0.07035	-0.07035	0.00281	-0.00281	0.07988	-0.07766
2.51	0.08478	0.39871	0.02596	-0.03163	0.00767	-0.01021	0.02815	-0.01797	0.07706	-0.07706	0.00281	-0.00281	0.08644	-0.08587
2.72	0.12893	0.26335	0.03697	-0.04504	0.00671	-0.00504	0.00239	-0.00153	0.05111	-0.05111	0.00281	-0.00281	0.06354	-0.06839
2.93	0.18020	0.17695	0.03611	-0.04400	0.01258	-0.00944	0.00699	-0.01096	0.03679	-0.03679	0.00281	-0.00281	0.05359	-0.05922
3.14	0.14673	0.22577	0.04854	-0.05915	0.01909	-0.01434	0.01283	-0.02011	0.04528	-0.04528	0.00281	-0.00281	0.07031	-0.07853
3.35	0.19825	0.16115	0.03282	-0.03999	0.01143	-0.00858	0.00636	-0.00996	0.03344	-0.03344	0.00281	-0.00281	0.04873	-0.05384
3.56	0.14077	0.24052	0.03386	-0.04126	0.00615	-0.00462	0.00219	-0.00140	0.04681	-0.04681	0.00281	-0.00281	0.05821	-0.06265
3.77	0.07018	0.48418	0.03137	-0.03822	0.00926	-0.01234	0.03402	-0.02171	0.09310	-0.09310	0.00281	-0.00281	0.10441	-0.10373
3.98	0.07545	0.52352	0.01202	-0.00987	0.02256	-0.03004	0.03825	-0.02441	0.08576	-0.08576	0.00281	-0.00281	0.09736	-0.09465
4.19	-0.00490	-8.60913	0.88549	-0.72671	0.42926	-0.57158	0.30103	-0.19213	1.30819	-1.30819	0.00281	-0.00281	1.66443	-1.61341
4.40	-0.02778	-1.80086	0.25279	-0.20746	0.06127	-0.08159	0.02095	-0.03283	0.22903	-0.22903	0.00281	-0.00281	0.34722	-0.32131
4.61	-0.00226	-24.94551	3.75236	-3.07950	0.28734	-0.38260	0.76039	-1.19139	2.79660	-2.79660	0.00281	-0.00281	4.74994	-4.34397

Table 42: 20–40%, 7.0–9.0 $\otimes$ 2.0–3.0 GeV/c Jet Function

ϕ	per trig yield	σ_{stat}/y	systematic errors											
			$+\sigma_{f2}/y$	$-\sigma_{f2}/y$	$+\sigma_{f3}/y$	$-\sigma_{f3}/y$	$+\sigma_{f4}/y$	$-\sigma_{f4}/y$	$+\sigma_{\xi/ZYAM}/y$	$-\sigma_{\xi}/y$	$+\sigma_{\pi^0}/y$	$-\sigma_{\pi^0}/y$	$+\sigma_{total}/y$	$-\sigma_{total}/y$
-1.47	-0.02055	-0.80399	0.05017	-0.04118	0.00546	-0.00412	0.01326	-0.02078	0.02693	-0.02693	0.00140	-0.00140	0.05874	-0.05359
-1.26	-0.02542	-0.58150	0.03355	-0.02754	0.01155	-0.00872	0.00363	-0.00568	0.02181	-0.02181	0.00140	-0.00140	0.04183	-0.03666
-1.05	0.01401	1.00397	0.03761	-0.03087	0.02590	-0.01956	0.01668	-0.01064	0.03988	-0.03988	0.00140	-0.00140	0.06290	-0.05515
-0.84	0.01560	0.74732	0.00706	-0.00580	0.01882	-0.01421	0.02930	-0.01870	0.03635	-0.03635	0.00140	-0.00140	0.05085	-0.04369
-0.63	0.03439	0.31709	0.00777	-0.00947	0.00326	-0.00246	0.01099	-0.00702	0.01681	-0.01681	0.00140	-0.00140	0.02183	-0.02073
-0.42	0.02920	0.32946	0.01983	-0.02416	0.00290	-0.00384	0.00167	-0.00107	0.02019	-0.02019	0.00140	-0.00140	0.02853	-0.03176
-0.21	0.12082	0.08483	0.00654	-0.00797	0.00184	-0.00243	0.00165	-0.00259	0.00495	-0.00495	0.00140	-0.00140	0.00868	-0.01013
-0.00	0.21727	0.04987	0.00398	-0.00485	0.00126	-0.00167	0.00137	-0.00215	0.00277	-0.00277	0.00140	-0.00140	0.00538	-0.00637
0.21	0.10516	0.09376	0.00752	-0.00916	0.00211	-0.00279	0.00190	-0.00297	0.00568	-0.00568	0.00140	-0.00140	0.00994	-0.01161
0.42	0.04227	0.22179	0.01370	-0.01669	0.00200	-0.00265	0.00116	-0.00074	0.01394	-0.01394	0.00140	-0.00140	0.01973	-0.02196
0.63	-0.00045	-21.11688	0.59995	-0.73093	0.25166	-0.19005	0.84843	-0.54153	1.29743	-1.29743	0.00140	-0.00140	1.68121	-1.59592
0.84	-0.00175	-5.86504	0.06278	-0.05153	0.16730	-0.12634	0.26048	-0.16625	0.32318	-0.32318	0.00140	-0.00140	0.45192	-0.38821
1.05	0.00525	2.29664	0.10034	-0.08236	0.06910	-0.05218	0.04449	-0.02840	0.10640	-0.10640	0.00140	-0.00140	0.16777	-0.14709
1.26	-0.00393	-3.53853	0.21676	-0.17792	0.07463	-0.05636	0.02343	-0.03671	0.14089	-0.14089	0.00140	-0.00140	0.27010	-0.23671
1.47	-0.00219	-7.92924	0.47108	-0.38667	0.05124	-0.03870	0.12451	-0.19507	0.25286	-0.25286	0.00140	-0.00140	0.55135	-0.50299
1.68	0.01917	0.95958	0.05378	-0.04414	0.00442	-0.00585	0.01421	-0.02227	0.02898	-0.02898	0.00267	-0.00267	0.06293	-0.05766
1.88	-0.00277	-5.13737	0.30756	-0.25245	0.07997	-0.10590	0.03325	-0.05209	0.20191	-0.20191	0.00267	-0.00267	0.37798	-0.34414
2.09	0.01045	1.23363	0.05041	-0.04138	0.02622	-0.03472	0.02235	-0.01427	0.05411	-0.05411	0.00267	-0.00267	0.08163	-0.07782
2.30	0.04299	0.27649	0.00256	-0.00210	0.00516	-0.00683	0.01063	-0.00679	0.01332	-0.01332	0.00267	-0.00267	0.01819	-0.01679
2.51	0.00353	2.80262	0.07564	-0.09215	0.02396	-0.03173	0.10696	-0.06827	0.16417	-0.16417	0.00267	-0.00267	0.21141	-0.20278
2.72	0.02373	0.40051	0.02439	-0.02972	0.00473	-0.00357	0.00206	-0.00131	0.02474	-0.02474	0.00267	-0.00267	0.03523	-0.03895
2.93	0.06280	0.16307	0.01259	-0.01533	0.00468	-0.00353	0.00318	-0.00498	0.00943	-0.00943	0.00267	-0.00267	0.01693	-0.01920
3.14	0.06741	0.15211	0.01283	-0.01564	0.00538	-0.00407	0.00442	-0.00693	0.00881	-0.00881	0.00267	-0.00267	0.01727	-0.01985
3.35	0.05738	0.17655	0.01377	-0.01678	0.00512	-0.00386	0.00348	-0.00545	0.01032	-0.01032	0.00267	-0.00267	0.01849	-0.02097
3.56	0.03845	0.25402	0.01506	-0.01834	0.00292	-0.00220	0.00127	-0.00081	0.01527	-0.01527	0.00267	-0.00267	0.02185	-0.02413
3.77	0.02707	0.38193	0.00988	-0.01203	0.00313	-0.00414	0.01397	-0.00891	0.02144	-0.02144	0.00267	-0.00267	0.02773	-0.02661
3.98	0.03296	0.34761	0.00334	-0.00274	0.00673	-0.00891	0.01387	-0.00885	0.01737	-0.01737	0.00267	-0.00267	0.02362	-0.02178
4.19	0.03171	0.42031	0.01662	-0.01364	0.00864	-0.01145	0.00737	-0.00470	0.01784	-0.01784	0.00267	-0.00267	0.02703	-0.02578
4.40	-0.00929	-1.48772	0.09176	-0.07532	0.02386	-0.03159	0.00992	-0.01554	0.06024	-0.06024	0.00267	-0.00267	0.11280	-0.10270
4.61	0.00521	3.21126	0.19802	-0.16253	0.01627	-0.02154	0.05234	-0.08200	0.10670	-0.10670	0.00267	-0.00267	0.23153	-0.21212

Table 43: 20–40%, 7.0–9.0 $\otimes$ 3.0–5.0 GeV/c Jet Function

ϕ	per trig yield	σ_{stat}/y	systematic errors											
			$+\sigma_{f2}/y$	$-\sigma_{f2}/y$	$+\sigma_{f3}/y$	$-\sigma_{f3}/y$	$+\sigma_{f4}/y$	$-\sigma_{f4}/y$	$+\sigma_{\xi/ZYAM}/y$	$-\sigma_{\xi}/y$	$+\sigma_{\pi^0}/y$	$-\sigma_{\pi^0}/y$	$+\sigma_{total}/y$	$-\sigma_{total}/y$
-1.47	0.00678	1.03715	0.01908	-0.01566	0.00224	-0.00169	0.00591	-0.00924	0.00924	-0.00910	0.00486	-0.00486	0.02265	-0.02097
-1.26	-0.00733	-0.62456	0.01460	-0.01198	0.00543	-0.00410	0.00185	-0.00289	0.00856	-0.00843	0.00486	-0.00486	0.01852	-0.01623
-1.05	-0.00180	-2.57873	0.03666	-0.03009	0.02727	-0.02058	0.01901	-0.01216	0.03505	-0.03451	0.00486	-0.00486	0.06083	-0.05188
-0.84	0.00208	1.91120	0.00666	-0.00546	0.01915	-0.01446	0.03229	-0.02066	0.03089	-0.03041	0.00486	-0.00486	0.04931	-0.04018
-0.63	-0.00560	-0.56637	0.00599	-0.00730	0.00271	-0.00205	0.00991	-0.00634	0.01169	-0.01151	0.00486	-0.00486	0.01737	-0.01593
-0.42	0.00680	0.51072	0.01068	-0.01301	0.00169	-0.00223	0.00105	-0.00067	0.00982	-0.00967	0.00486	-0.00486	0.01543	-0.01708
-0.21	0.06462	0.08219	0.00153	-0.00187	0.00046	-0.00062	0.00045	-0.00071	0.00105	-0.00103	0.00486	-0.00486	0.00524	-0.00539
-0.00	0.17953	0.04033	0.00060	-0.00074	0.00021	-0.00027	0.00024	-0.00038	0.00038	-0.00037	0.00486	-0.00486	0.00492	-0.00495
0.21	0.06559	0.07967	0.00151	-0.00184	0.00046	-0.00061	0.00045	-0.00070	0.00103	-0.00102	0.00486	-0.00486	0.00523	-0.00537
0.42	0.01018	0.34318	0.00713	-0.00869	0.00113	-0.00149	0.00070	-0.00045	0.00656	-0.00645	0.00486	-0.00486	0.01092	-0.01197
0.63	-0.00059	-5.60798	0.05710	-0.06957	0.02587	-0.01953	0.09444	-0.06043	0.11138	-0.10967	0.00486	-0.00486	0.15899	-0.14465
0.84	-0.00094	-3.73390	0.01466	-0.01203	0.04220	-0.03185	0.07114	-0.04552	0.06805	-0.06700	0.00486	-0.00486	0.10822	-0.08800
1.05	0.00250	1.76158	0.02640	-0.02167	0.01963	-0.01482	0.01369	-0.00876	0.02524	-0.02485	0.00486	-0.00486	0.04394	-0.03751
1.26	-0.00044	-10.98181	0.24127	-0.19802	0.08972	-0.06773	0.03058	-0.04779	0.14143	-0.13926	0.00486	-0.00486	0.29534	-0.25593
1.47	-0.00651	-0.80688	0.01987	-0.01630	0.00233	-0.00176	0.00616	-0.00962	0.00962	-0.00947	0.00486	-0.00486	0.02354	-0.02179
1.68	-0.00246	-2.50300	0.05263	-0.04319	0.00467	-0.00618	0.01631	-0.02549	0.02559	-0.02520	0.00845	-0.00845	0.06151	-0.05710
1.88	0.00104	4.81548	0.10246	-0.08409	0.02876	-0.03810	0.01299	-0.02029	0.06070	-0.05977	0.00845	-0.00845	0.12349	-0.11216
2.09	-0.00340	-1.23593	0.01948	-0.01598	0.01093	-0.01448	0.01010	-0.00646	0.01886	-0.01857	0.00845	-0.00845	0.03206	-0.03039
2.30	0.00312	1.26201	0.00443	-0.00364	0.00963	-0.01276	0.02151	-0.01377	0.02079	-0.02047	0.00845	-0.00845	0.03284	-0.02926
2.51	0.00882	0.45473	0.00380	-0.00464	0.00130	-0.00172	0.00629	-0.00403	0.00745	-0.00734	0.00845	-0.00845	0.01351	-0.01288
2.72	0.01548	0.24939	0.00469	-0.00572	0.00098	-0.00074	0.00046	-0.00030	0.00430	-0.00423	0.00845	-0.00845	0.01063	-0.01107
2.93	0.02527	0.17438	0.00392	-0.00478	0.00157	-0.00119	0.00116	-0.00182	0.00266	-0.00261	0.00845	-0.00845	0.00988	-0.01028
3.14	0.04955	0.10467	0.00219	-0.00267	0.00099	-0.00075	0.00089	-0.00138	0.00136	-0.00134	0.00845	-0.00845	0.00893	-0.00909
3.35	0.02585	0.17117	0.00384	-0.00467	0.00154	-0.00116	0.00114	-0.00178	0.00260	-0.00256	0.00845	-0.00845	0.00982	-0.01021
3.56	0.00613	0.55974	0.01186	-0.01445	0.00248	-0.00187	0.00117	-0.00075	0.01086	-0.01069	0.00845	-0.00845	0.01836	-0.01996
3.77	-0.00180	-1.83810	0.01862	-0.02268	0.00637	-0.00844	0.03079	-0.01970	0.03646	-0.03590	0.00845	-0.00845	0.05231	-0.04831
3.98	-0.00004	-91.69386	0.34107	-0.27993	0.74101	-0.98163	1.65501	-1.05900	1.59948	-1.57487	0.00845	-0.00845	2.44191	-2.15493
4.19	-0.00509	-0.77802	0.01300	-0.01067	0.00730	-0.00967	0.00674	-0.00431	0.01259	-0.01240	0.00845	-0.00845	0.02231	-0.02124
4.40	0.00277	1.86709	0.03860	-0.03168	0.01084	-0.01435	0.00489	-0.00765	0.02287	-0.02252	0.00845	-0.00845	0.04718	-0.04297
4.61	0.00225	2.70249	0.05743	-0.04713	0.00509	-0.00675	0.01780	-0.02781	0.02793	-0.02750	0.00845	-0.00845	0.06702	-0.06219

Table 44: 20–40%, 7.0–9.0 $\otimes$ 5.0–7.0 GeV/c Jet Function

ϕ	per trig yield	σ_{stat}/y	systematic errors											
			$+\sigma_{f2}/y$	$-\sigma_{f2}/y$	$+\sigma_{f3}/y$	$-\sigma_{f3}/y$	$+\sigma_{f4}/y$	$-\sigma_{f4}/y$	$+\sigma_{\xi/ZYAM}/y$	$-\sigma_{\xi}/y$	$+\sigma_{\pi^0}/y$	$-\sigma_{\pi^0}/y$	$+\sigma_{total}/y$	$-\sigma_{total}/y$
-1.47	-0.00194	-0.00000	0.00433	-0.00355	0.00094	-0.00068	0.00178	-0.00300	0.00351	-0.00401	0.00435	-0.00435	0.00735	-0.00755
-1.26	0.00051	4.83216	0.01366	-0.01122	0.00942	-0.00681	0.00230	-0.00387	0.01341	-0.01533	0.00435	-0.00435	0.02190	-0.02100
-1.05	0.00330	0.92331	0.00130	-0.00107	0.00180	-0.00130	0.00097	-0.00057	0.00208	-0.00238	0.00435	-0.00435	0.00539	-0.00526
-0.84	-0.00082	-1.42362	0.00110	-0.00090	0.00586	-0.00424	0.00762	-0.00453	0.00850	-0.00971	0.00435	-0.00435	0.01359	-0.01235
-0.63	0.00003	43.16813	0.06508	-0.07926	0.05466	-0.03952	0.15385	-0.09137	0.21029	-0.24033	0.00435	-0.00435	0.27410	-0.27197
-0.42	0.00256	0.73553	0.00184	-0.00225	0.00052	-0.00072	0.00026	-0.00015	0.00279	-0.00319	0.00435	-0.00435	0.00551	-0.00589
-0.21	0.01274	0.24470	0.00051	-0.00062	0.00027	-0.00038	0.00020	-0.00033	0.00057	-0.00065	0.00435	-0.00435	0.00442	-0.00446
-0.00	0.08204	0.08911	0.00009	-0.00010	0.00005	-0.00007	0.00005	-0.00008	0.00009	-0.00010	0.00435	-0.00435	0.00435	-0.00435
0.21	0.01068	0.26906	0.00060	-0.00073	0.00032	-0.00045	0.00024	-0.00040	0.00068	-0.00077	0.00435	-0.00435	0.00446	-0.00451
0.42	-0.00053	-2.02500	0.00895	-0.01090	0.00251	-0.00347	0.00126	-0.00075	0.01354	-0.01547	0.00435	-0.00435	0.01703	-0.01974
0.63	0.00089	1.88667	0.00245	-0.00299	0.00206	-0.00149	0.00580	-0.00345	0.00793	-0.00906	0.00435	-0.00435	0.01121	-0.01114
0.84	0.00144	1.37705	0.00063	-0.00051	0.00334	-0.00241	0.00434	-0.00258	0.00484	-0.00553	0.00435	-0.00435	0.00852	-0.00789
1.05	-0.00051	-2.85149	0.00844	-0.00693	0.01165	-0.00842	0.00626	-0.00372	0.01350	-0.01543	0.00435	-0.00435	0.02115	-0.01974
1.26	0.00020	10.51649	0.03395	-0.02788	0.02341	-0.01693	0.00571	-0.00961	0.03332	-0.03808	0.00435	-0.00435	0.05350	-0.05123
1.47	-0.00194	-0.00000	0.00433	-0.00355	0.00094	-0.00068	0.00178	-0.00300	0.00351	-0.00401	0.00435	-0.00435	0.00735	-0.00755
1.68	-0.00195	-0.00000	0.00432	-0.00355	0.00068	-0.00094	0.00178	-0.00299	0.00351	-0.00401	0.01628	-0.01628	0.01731	-0.01742
1.88	0.00019	11.46854	0.03713	-0.03049	0.01851	-0.02561	0.00625	-0.01052	0.03665	-0.04189	0.01628	-0.01628	0.05804	-0.06096
2.09	0.00150	1.64093	0.00286	-0.00235	0.00286	-0.00395	0.00212	-0.00126	0.00461	-0.00527	0.01628	-0.01628	0.01753	-0.01777
2.30	0.00031	5.23335	0.00288	-0.00237	0.01112	-0.01538	0.01999	-0.01187	0.02241	-0.02561	0.01628	-0.01628	0.03604	-0.03611
2.51	0.00176	1.07382	0.00124	-0.00151	0.00075	-0.00104	0.00292	-0.00174	0.00400	-0.00458	0.01628	-0.01628	0.01708	-0.01710
2.72	0.00488	0.47456	0.00097	-0.00118	0.00038	-0.00027	0.00014	-0.00008	0.00146	-0.00167	0.01628	-0.01628	0.01638	-0.01641
2.93	0.01113	0.30850	0.00058	-0.00071	0.00043	-0.00031	0.00023	-0.00038	0.00064	-0.00074	0.01628	-0.01628	0.01631	-0.01632
3.14	0.01102	0.29927	0.00064	-0.00078	0.00054	-0.00039	0.00034	-0.00058	0.00065	-0.00075	0.01628	-0.01628	0.01632	-0.01633
3.35	0.00524	0.46593	0.00123	-0.00150	0.00091	-0.00066	0.00048	-0.00081	0.00137	-0.00157	0.01628	-0.01628	0.01642	-0.01646
3.56	0.00420	0.52684	0.00112	-0.00137	0.00044	-0.00031	0.00016	-0.00009	0.00170	-0.00194	0.01628	-0.01628	0.01642	-0.01646
3.77	0.00605	0.47381	0.00036	-0.00044	0.00022	-0.00030	0.00085	-0.00051	0.00117	-0.00133	0.01628	-0.01628	0.01635	-0.01635
3.98	0.00153	1.33415	0.00059	-0.00048	0.00227	-0.00314	0.00408	-0.00243	0.00458	-0.00523	0.01628	-0.01628	0.01756	-0.01756
4.19	0.00499	0.70107	0.00086	-0.00071	0.00086	-0.00119	0.00064	-0.00038	0.00139	-0.00158	0.01628	-0.01628	0.01640	-0.01642
4.40	0.00005	41.55404	0.14387	-0.11815	0.07174	-0.09923	0.02420	-0.04075	0.14202	-0.16231	0.01628	-0.01628	0.21648	-0.22820
4.61	-0.00195	-0.00000	0.00432	-0.00355	0.00068	-0.00094	0.00178	-0.00299	0.00351	-0.00401	0.01628	-0.01628	0.01731	-0.01742

Table 45: 20–40%, 9.0–12.0 $\otimes$ 0.5–1.0 GeV/c Jet Function

ϕ	per trig yield	σ_{stat}/y	systematic errors											
			$+\sigma_{f2}/y$	$-\sigma_{f2}/y$	$+\sigma_{f3}/y$	$-\sigma_{f3}/y$	$+\sigma_{f4}/y$	$-\sigma_{f4}/y$	$+\sigma_{\xi/ZYAM}/y$	$-\sigma_{\xi}/y$	$+\sigma_{\pi^0}/y$	$-\sigma_{\pi^0}/y$	$+\sigma_{total}/y$	$-\sigma_{total}/y$
-1.47	0.16718	0.99954	0.17119	-0.14549	0.07098	-0.10653	0.01187	-0.01474	1.12018	-1.12018	0.00562	-0.00562	1.13548	-1.13471
-1.26	0.08974	1.74412	0.36720	-0.30207	0.15045	-0.21981	0.04302	-0.04306	2.08978	-2.08978	0.00562	-0.00562	2.12756	-2.12335
-1.05	0.14609	0.95512	0.28018	-0.22071	0.09694	-0.14040	0.04368	-0.03933	1.28853	-1.28853	0.00562	-0.00562	1.32293	-1.31541
-0.84	0.29673	0.42702	0.17252	-0.13093	0.04585	-0.06701	0.02658	-0.02316	0.63797	-0.63797	0.00562	-0.00562	0.66303	-0.65514
-0.63	0.16999	0.63995	0.36450	-0.26938	0.07093	-0.10649	0.04351	-0.03832	1.12105	-1.12105	0.00562	-0.00562	1.18176	-1.15851
-0.42	0.27233	0.35583	0.26208	-0.19043	0.03718	-0.05828	0.01927	-0.01807	0.70420	-0.70420	0.00562	-0.00562	0.75258	-0.73207
-0.21	0.41427	0.22702	0.18773	-0.13515	0.02065	-0.03393	0.00695	-0.00763	0.46503	-0.46503	0.00562	-0.00562	0.50200	-0.48555
-0.00	0.52403	0.18033	0.15274	-0.10963	0.01518	-0.02549	0.00356	-0.00459	0.36823	-0.36823	0.00562	-0.00562	0.39900	-0.38512
0.21	0.44080	0.21039	0.17644	-0.12702	0.01941	-0.03189	0.00653	-0.00717	0.43704	-0.43704	0.00562	-0.00562	0.47179	-0.45633
0.42	0.39624	0.24201	0.18012	-0.13088	0.02555	-0.04005	0.01325	-0.01242	0.48399	-0.48399	0.00562	-0.00562	0.51725	-0.50315
0.63	0.40634	0.25782	0.15249	-0.11269	0.02967	-0.04455	0.01820	-0.01603	0.46899	-0.46899	0.00562	-0.00562	0.49442	-0.48469
0.84	0.33587	0.34052	0.15241	-0.11567	0.04050	-0.05920	0.02348	-0.02046	0.56362	-0.56362	0.00562	-0.00562	0.58577	-0.57880
1.05	0.32684	0.41321	0.12523	-0.09865	0.04333	-0.06275	0.01952	-0.01758	0.57593	-0.57593	0.00562	-0.00562	0.59133	-0.58797
1.26	0.31763	0.48112	0.10375	-0.08535	0.04251	-0.06210	0.01215	-0.01217	0.59043	-0.59043	0.00562	-0.00562	0.60113	-0.59994
1.47	0.47478	0.34277	0.06028	-0.05123	0.02499	-0.03751	0.00418	-0.00519	0.39444	-0.39444	0.00562	-0.00562	0.39986	-0.39959
1.68	-0.02012	-7.89587	1.42437	-1.21035	0.49057	-0.76942	0.09881	-0.12267	9.31368	-9.31368	0.00434	-0.00434	9.43524	-9.42426
1.88	0.49215	0.32380	0.06720	-0.05526	0.01683	-0.02771	0.00787	-0.00787	0.38190	-0.38190	0.00434	-0.00434	0.38824	-0.38698
2.09	0.05601	2.36344	0.73344	-0.57766	0.13766	-0.23186	0.11416	-0.10281	3.37017	-3.37017	0.00434	-0.00434	3.45369	-3.42872
2.30	0.50714	0.23740	0.10117	-0.07678	0.01653	-0.02720	0.01557	-0.01357	0.37410	-0.37410	0.00434	-0.00434	0.38823	-0.38313
2.51	0.29297	0.37537	0.21165	-0.15642	0.03435	-0.05385	0.02526	-0.02225	0.65101	-0.65101	0.00434	-0.00434	0.68590	-0.67209
2.72	0.34639	0.30692	0.20592	-0.14962	0.03498	-0.05253	0.01514	-0.01419	0.55319	-0.55319	0.00434	-0.00434	0.59151	-0.57566
2.93	0.33893	0.29844	0.22911	-0.16493	0.04064	-0.05943	0.00846	-0.00929	0.56716	-0.56716	0.00434	-0.00434	0.61311	-0.59372
3.14	0.50151	0.19866	0.15931	-0.11434	0.02872	-0.04164	0.00369	-0.00477	0.38374	-0.38374	0.00434	-0.00434	0.41652	-0.40262
3.35	0.41394	0.24557	0.18760	-0.13504	0.03327	-0.04866	0.00693	-0.00761	0.46439	-0.46439	0.00434	-0.00434	0.50202	-0.48615
3.56	0.28245	0.36953	0.25252	-0.18348	0.04290	-0.06442	0.01857	-0.01741	0.67840	-0.67840	0.00434	-0.00434	0.72539	-0.70594
3.77	0.27962	0.39750	0.22176	-0.16389	0.03599	-0.05642	0.02647	-0.02331	0.68210	-0.68210	0.00434	-0.00434	0.71865	-0.70418
3.98	0.54192	0.22615	0.09468	-0.07186	0.01547	-0.02546	0.01457	-0.01270	0.35009	-0.35009	0.00434	-0.00434	0.36332	-0.35854
4.19	0.19009	0.68962	0.21610	-0.17020	0.04056	-0.06831	0.03364	-0.03029	0.99297	-0.99297	0.00434	-0.00434	1.01759	-1.01023
4.40	0.26504	0.56870	0.12478	-0.10262	0.03125	-0.05146	0.01461	-0.01462	0.70915	-0.70915	0.00434	-0.00434	0.72088	-0.71854
4.61	0.25249	0.66941	0.11353	-0.09647	0.03910	-0.06133	0.00788	-0.00978	0.74234	-0.74234	0.00434	-0.00434	0.75205	-0.75117

Table 46: 20–40%, 9.0–12.0 $\otimes$ 1.0–2.0 GeV/c Jet Function

ϕ	per trig yield	σ_{stat}/y	systematic errors											
			$+\sigma_{f2}/y$	$-\sigma_{f2}/y$	$+\sigma_{f3}/y$	$-\sigma_{f3}/y$	$+\sigma_{f4}/y$	$-\sigma_{f4}/y$	$+\sigma_{\xi/ZYAM}/y$	$-\sigma_{\xi}/y$	$+\sigma_{\pi^0}/y$	$-\sigma_{\pi^0}/y$	$+\sigma_{total}/y$	$-\sigma_{total}/y$
-1.47	0.12082	0.95940	0.09125	-0.14538	0.00825	-0.00931	0.01792	-0.02355	0.05833	-0.05832	0.00183	-0.00183	0.11010	-0.15869
-1.26	0.14648	0.75900	0.06225	-0.09918	0.01782	-0.02011	0.00500	-0.00657	0.04820	-0.04820	0.00183	-0.00183	0.08090	-0.11230
-1.05	0.07554	1.17549	0.07460	-0.11886	0.04271	-0.04821	0.02061	-0.01569	0.09403	-0.09402	0.00183	-0.00183	0.12907	-0.15981
-0.84	0.08046	1.01047	0.01464	-0.02333	0.03244	-0.03662	0.03786	-0.02882	0.08917	-0.08915	0.00183	-0.00183	0.10322	-0.10328
-0.63	0.19429	0.35542	0.02856	-0.01793	0.00513	-0.00579	0.01297	-0.00987	0.03738	-0.03737	0.00183	-0.00183	0.04910	-0.04304
-0.42	0.07412	0.85441	0.16211	-0.10175	0.01518	-0.01345	0.00439	-0.00334	0.09914	-0.09913	0.00183	-0.00183	0.19069	-0.14274
-0.21	0.32383	0.17839	0.05066	-0.03180	0.00910	-0.00806	0.00490	-0.00644	0.02289	-0.02289	0.00183	-0.00183	0.05657	-0.04055
-0.00	0.49841	0.12022	0.03603	-0.02261	0.00731	-0.00647	0.00476	-0.00625	0.01492	-0.01492	0.00183	-0.00183	0.04000	-0.02861
0.21	0.34970	0.16340	0.04691	-0.02944	0.00842	-0.00746	0.00454	-0.00596	0.02120	-0.02119	0.00183	-0.00183	0.05239	-0.03756
0.42	0.07523	0.80599	0.15972	-0.10025	0.01496	-0.01325	0.00433	-0.00329	0.09768	-0.09767	0.00183	-0.00183	0.18788	-0.14063
0.63	0.03459	1.81421	0.16044	-0.10070	0.02882	-0.03254	0.07285	-0.05544	0.20996	-0.20993	0.00183	-0.00183	0.27561	-0.24155
0.84	-0.03423	-2.08038	0.03442	-0.05484	0.07626	-0.08608	0.08901	-0.06774	0.20960	-0.20957	0.00183	-0.00183	0.24261	-0.24275
1.05	-0.00471	-16.79603	1.19545	-1.90465	0.68437	-0.77249	0.33034	-0.25139	1.50680	-1.50659	0.00183	-0.00183	2.06810	-2.56075
1.26	0.14545	0.69331	0.06269	-0.09988	0.01795	-0.02026	0.00504	-0.00662	0.04854	-0.04854	0.00183	-0.00183	0.08147	-0.11309
1.47	0.21932	0.53599	0.05027	-0.08009	0.00455	-0.00513	0.00987	-0.01297	0.03213	-0.03213	0.00183	-0.00183	0.06067	-0.08743
1.68	-0.00402	-27.29708	2.74019	-4.36583	0.27970	-0.24779	0.53819	-0.70719	1.75523	-1.75499	0.00590	-0.00590	3.31020	-4.76467
1.88	0.04810	2.15075	0.18959	-0.30207	0.06126	-0.05427	0.01523	-0.02001	0.14757	-0.14755	0.00590	-0.00590	0.24848	-0.34117
2.09	-0.04174	-1.94768	0.13503	-0.21513	0.08725	-0.07730	0.03731	-0.02839	0.17129	-0.17127	0.00590	-0.00590	0.23793	-0.28711
2.30	0.09028	0.85662	0.01305	-0.02079	0.03263	-0.02891	0.03375	-0.02568	0.07988	-0.07987	0.00590	-0.00590	0.09375	-0.09133
2.51	0.05462	1.20013	0.10160	-0.06377	0.02060	-0.01825	0.04613	-0.03511	0.13321	-0.13320	0.00590	-0.00590	0.17509	-0.15300
2.72	0.19948	0.33467	0.06024	-0.03781	0.00500	-0.00564	0.00163	-0.00124	0.03677	-0.03676	0.00590	-0.00590	0.07101	-0.05338
2.93	0.23176	0.26992	0.07079	-0.04443	0.01126	-0.01271	0.00684	-0.00899	0.03182	-0.03182	0.00590	-0.00590	0.07894	-0.05713
3.14	0.33029	0.20007	0.05437	-0.03413	0.00977	-0.01103	0.00718	-0.00943	0.02237	-0.02237	0.00590	-0.00590	0.06032	-0.04371
3.35	0.23930	0.26065	0.06856	-0.04303	0.01091	-0.01231	0.00663	-0.00871	0.03082	-0.03082	0.00590	-0.00590	0.07647	-0.05535
3.56	0.22303	0.29772	0.05388	-0.03382	0.00447	-0.00505	0.00146	-0.00111	0.03289	-0.03288	0.00590	-0.00590	0.06357	-0.04781
3.77	0.00305	21.25393	1.81700	-1.14043	0.36847	-0.32644	0.82503	-0.62787	2.38246	-2.38213	0.00590	-0.00590	3.12955	-2.73422
3.98	0.13606	0.56555	0.00866	-0.01380	0.02165	-0.01918	0.02239	-0.01704	0.05300	-0.05300	0.00590	-0.00590	0.06236	-0.06076
4.19	0.12223	0.68389	0.04611	-0.07346	0.02979	-0.02639	0.01274	-0.00970	0.05849	-0.05848	0.00590	-0.00590	0.08143	-0.09819
4.40	-0.03346	-2.86824	0.27252	-0.43419	0.08805	-0.07801	0.02189	-0.02876	0.21212	-0.21209	0.00590	-0.00590	0.35711	-0.49036
4.61	-0.11619	-0.90790	0.09489	-0.15118	0.00969	-0.00858	0.01864	-0.02449	0.06078	-0.06077	0.00590	-0.00590	0.11478	-0.16510

Table 47: 20–40%, 9.0–12.0 $\otimes$ 2.0–3.0 GeV/c Jet Function

ϕ	per trig yield	σ_{stat}/y	systematic errors											
			$+\sigma_{f2}/y$	$-\sigma_{f2}/y$	$+\sigma_{f3}/y$	$-\sigma_{f3}/y$	$+\sigma_{f4}/y$	$-\sigma_{f4}/y$	$+\sigma_{\xi/ZYAM}/y$	$-\sigma_{\xi}/y$	$+\sigma_{\pi^0}/y$	$-\sigma_{\pi^0}/y$	$+\sigma_{total}/y$	$-\sigma_{total}/y$
-1.47	0.00841	4.07246	0.15836	-0.24918	0.01563	-0.01844	0.04086	-0.05368	0.07348	-0.07337	0.00355	-0.00355	0.18001	-0.26591
-1.26	-0.02997	-0.94091	0.03673	-0.05779	0.01148	-0.01353	0.00388	-0.00509	0.02064	-0.02061	0.00355	-0.00355	0.04398	-0.06314
-1.05	-0.00693	-3.78475	0.09821	-0.15453	0.06137	-0.07238	0.03564	-0.02713	0.09000	-0.08986	0.00355	-0.00355	0.15098	-0.19479
-0.84	0.03209	0.73171	0.00443	-0.00697	0.01072	-0.01264	0.01505	-0.01146	0.01970	-0.01967	0.00355	-0.00355	0.02760	-0.02719
-0.63	0.02941	0.71285	0.02250	-0.01430	0.00447	-0.00527	0.01359	-0.01034	0.02188	-0.02185	0.00355	-0.00355	0.03467	-0.02879
-0.42	0.01859	0.98118	0.07706	-0.04897	0.00833	-0.00707	0.00278	-0.00211	0.03522	-0.03516	0.00355	-0.00355	0.08525	-0.06084
-0.21	0.15290	0.13590	0.01279	-0.00813	0.00265	-0.00225	0.00165	-0.00216	0.00434	-0.00433	0.00355	-0.00355	0.01431	-0.01035
-0.00	0.34562	0.06887	0.00620	-0.00394	0.00145	-0.00123	0.00109	-0.00143	0.00193	-0.00193	0.00355	-0.00355	0.00761	-0.00595
0.21	0.19799	0.10882	0.00988	-0.00628	0.00205	-0.00174	0.00127	-0.00167	0.00335	-0.00335	0.00355	-0.00355	0.01128	-0.00831
0.42	0.03937	0.45702	0.03640	-0.02313	0.00394	-0.00334	0.00131	-0.00100	0.01664	-0.01661	0.00355	-0.00355	0.04039	-0.02891
0.63	0.00105	17.25025	0.62879	-0.39961	0.12485	-0.14726	0.37968	-0.28902	0.61148	-0.61053	0.00355	-0.00355	0.96387	-0.79854
0.84	-0.02368	-0.79924	0.00601	-0.00945	0.01453	-0.01713	0.02040	-0.01553	0.02670	-0.02666	0.00355	-0.00355	0.03727	-0.03671
1.05	-0.00083	-27.65360	0.81933	-1.28921	0.51198	-0.60384	0.29735	-0.22634	0.75085	-0.74967	0.00355	-0.00355	1.25922	-1.62479
1.26	-0.03327	-0.74428	0.03309	-0.05207	0.01034	-0.01219	0.00349	-0.00459	0.01860	-0.01857	0.00355	-0.00355	0.03966	-0.05691
1.47	-0.03741	-0.80590	0.03558	-0.05598	0.00351	-0.00414	0.00918	-0.01206	0.01651	-0.01648	0.00355	-0.00355	0.04059	-0.05984
1.68	-0.00066	-52.11973	2.02760	-3.19041	0.23604	-0.20014	0.52314	-0.68724	0.94410	-0.94262	0.00627	-0.00627	2.30909	-3.40288
1.88	-0.01661	-1.63206	0.06627	-0.10427	0.02442	-0.02070	0.00699	-0.00919	0.03757	-0.03752	0.00627	-0.00627	0.08055	-0.11328
2.09	-0.00047	-52.39543	1.44737	-2.27743	1.06671	-0.90443	0.52527	-0.39985	1.34095	-1.33885	0.00627	-0.00627	2.30366	-2.82083
2.30	0.01837	1.19452	0.00774	-0.01218	0.02208	-0.01872	0.02630	-0.02002	0.03472	-0.03466	0.00627	-0.00627	0.04984	-0.04627
2.51	-0.00435	-4.36631	0.15216	-0.09670	0.03563	-0.03021	0.09188	-0.06994	0.14846	-0.14823	0.00627	-0.00627	0.23440	-0.19279
2.72	0.01893	0.96479	0.07567	-0.04809	0.00694	-0.00818	0.00273	-0.00208	0.03447	-0.03442	0.00627	-0.00627	0.08372	-0.06006
2.93	0.08572	0.24138	0.02282	-0.01450	0.00401	-0.00473	0.00293	-0.00385	0.00767	-0.00766	0.00627	-0.00627	0.02537	-0.01859
3.14	0.12446	0.17499	0.01720	-0.01093	0.00342	-0.00403	0.00302	-0.00397	0.00530	-0.00529	0.00627	-0.00627	0.01960	-0.01479
3.35	0.09845	0.21320	0.01987	-0.01263	0.00349	-0.00412	0.00256	-0.00336	0.00668	-0.00667	0.00627	-0.00627	0.02231	-0.01648
3.56	0.01169	1.53275	0.12252	-0.07786	0.01124	-0.01325	0.00441	-0.00336	0.05582	-0.05573	0.00627	-0.00627	0.13532	-0.09693
3.77	0.01747	1.12122	0.03788	-0.02408	0.00887	-0.00752	0.02288	-0.01741	0.03696	-0.03690	0.00627	-0.00627	0.05868	-0.04838
3.98	-0.00962	-2.08063	0.01478	-0.02326	0.04215	-0.03574	0.05019	-0.03821	0.06626	-0.06616	0.00627	-0.00627	0.09458	-0.08772
4.19	-0.00652	-3.59939	0.10441	-0.16429	0.07695	-0.06524	0.03789	-0.02884	0.09673	-0.09658	0.00627	-0.00627	0.16630	-0.20358
4.40	0.02032	1.40776	0.05417	-0.08524	0.01996	-0.01693	0.00572	-0.00751	0.03072	-0.03067	0.00627	-0.00627	0.06594	-0.09267
4.61	-0.04128	-0.68550	0.03224	-0.05074	0.00375	-0.00318	0.00832	-0.01093	0.01501	-0.01499	0.00627	-0.00627	0.03725	-0.05448

Table 48: 20–40%, 9.0–12.0 $\otimes$ 3.0–5.0 GeV/c Jet Function

ϕ	per trig yield	σ_{stat}/y	systematic errors											
			$+\sigma_{f2}/y$	$-\sigma_{f2}/y$	$+\sigma_{f3}/y$	$-\sigma_{f3}/y$	$+\sigma_{f4}/y$	$-\sigma_{f4}/y$	$+\sigma_{\xi/ZYAM}/y$	$-\sigma_{\xi}/y$	$+\sigma_{\pi^0}/y$	$-\sigma_{\pi^0}/y$	$+\sigma_{total}/y$	$-\sigma_{total}/y$
-1.47	-0.00035	-32.92609	0.47572	-0.75621	0.05038	-0.05924	0.14438	-0.18790	0.19914	-0.19641	0.00039	-0.00039	0.53791	-0.80576
-1.26	-0.00973	-0.85941	0.01433	-0.02277	0.00480	-0.00565	0.00178	-0.00231	0.00726	-0.00716	0.00039	-0.00039	0.01686	-0.02464
-1.05	-0.00976	-0.77413	0.00883	-0.01403	0.00592	-0.00696	0.00373	-0.00287	0.00729	-0.00719	0.00039	-0.00039	0.01343	-0.01748
-0.84	-0.00634	-1.03264	0.00284	-0.00452	0.00737	-0.00867	0.01125	-0.00864	0.01139	-0.01123	0.00039	-0.00039	0.01785	-0.01722
-0.63	0.00717	1.08273	0.01180	-0.00742	0.00249	-0.00293	0.00822	-0.00632	0.01024	-0.01010	0.00039	-0.00039	0.01783	-0.01435
-0.42	0.00082	7.52664	0.22413	-0.14100	0.02567	-0.02183	0.00931	-0.00716	0.09152	-0.09027	0.00039	-0.00039	0.24363	-0.16899
-0.21	0.10355	0.11901	0.00242	-0.00152	0.00053	-0.00045	0.00036	-0.00047	0.00073	-0.00072	0.00039	-0.00039	0.00263	-0.00185
-0.00	0.29423	0.05922	0.00093	-0.00059	0.00023	-0.00020	0.00019	-0.00025	0.00026	-0.00026	0.00039	-0.00039	0.00108	-0.00081
0.21	0.08150	0.13416	0.00307	-0.00193	0.00067	-0.00057	0.00046	-0.00060	0.00093	-0.00092	0.00039	-0.00039	0.00333	-0.00233
0.42	0.01942	0.38702	0.00944	-0.00594	0.00108	-0.00092	0.00039	-0.00030	0.00385	-0.00380	0.00039	-0.00039	0.01027	-0.00713
0.63	0.00685	1.04725	0.01235	-0.00777	0.00261	-0.00306	0.00860	-0.00661	0.01073	-0.01058	0.00039	-0.00039	0.01867	-0.01502
0.84	0.00513	1.47979	0.00351	-0.00558	0.00911	-0.01072	0.01390	-0.01068	0.01408	-0.01388	0.00039	-0.00039	0.02207	-0.02129
1.05	-0.00646	-1.10569	0.01334	-0.02120	0.00894	-0.01051	0.00564	-0.00433	0.01102	-0.01087	0.00039	-0.00039	0.02027	-0.02640
1.26	-0.00004	-245.95695	3.66854	-5.83153	1.22964	-1.44614	0.45534	-0.59260	1.85900	-1.83353	0.00039	-0.00039	4.31664	-6.30960
1.47	0.01597	0.93981	0.01055	-0.01677	0.00112	-0.00131	0.00320	-0.00417	0.00442	-0.00436	0.00039	-0.00039	0.01194	-0.01787
1.68	0.00697	1.96265	0.02417	-0.03842	0.00301	-0.00256	0.00733	-0.00955	0.01015	-0.01001	0.00050	-0.00050	0.02739	-0.04091
1.88	0.01377	0.88751	0.01012	-0.01609	0.00399	-0.00339	0.00126	-0.00164	0.00518	-0.00511	0.00050	-0.00050	0.01212	-0.01730
2.09	0.01532	0.71367	0.00562	-0.00894	0.00443	-0.00377	0.00238	-0.00183	0.00470	-0.00463	0.00050	-0.00050	0.00890	-0.01091
2.30	0.00914	0.91533	0.00197	-0.00313	0.00601	-0.00511	0.00780	-0.00599	0.00797	-0.00786	0.00050	-0.00050	0.01283	-0.01157
2.51	0.00596	1.26024	0.01419	-0.00893	0.00352	-0.00299	0.00988	-0.00759	0.01236	-0.01219	0.00050	-0.00050	0.02155	-0.01718
2.72	0.02073	0.38667	0.00884	-0.00556	0.00086	-0.00101	0.00037	-0.00028	0.00360	-0.00355	0.00050	-0.00050	0.00960	-0.00670
2.93	0.04922	0.20892	0.00508	-0.00320	0.00095	-0.00112	0.00076	-0.00099	0.00153	-0.00151	0.00050	-0.00050	0.00547	-0.00387
3.14	0.07354	0.15642	0.00372	-0.00234	0.00079	-0.00092	0.00076	-0.00099	0.00103	-0.00101	0.00050	-0.00050	0.00405	-0.00293
3.35	0.05832	0.18752	0.00429	-0.00270	0.00080	-0.00094	0.00064	-0.00084	0.00129	-0.00127	0.00050	-0.00050	0.00462	-0.00328
3.56	0.01387	0.53345	0.01321	-0.00831	0.00129	-0.00151	0.00055	-0.00042	0.00538	-0.00530	0.00050	-0.00050	0.01434	-0.00999
3.77	-0.00678	-0.85197	0.01248	-0.00785	0.00309	-0.00263	0.00869	-0.00668	0.01087	-0.01072	0.00050	-0.00050	0.01895	-0.01511
3.98	0.00244	3.04687	0.00738	-0.01173	0.02252	-0.01915	0.02921	-0.02244	0.02984	-0.02944	0.00050	-0.00050	0.04801	-0.04330
4.19	-0.00178	-4.46749	0.04831	-0.07679	0.03808	-0.03238	0.02043	-0.01570	0.04037	-0.03982	0.00050	-0.00050	0.07636	-0.09369
4.40	0.00564	1.81445	0.02470	-0.03926	0.00974	-0.00828	0.00307	-0.00399	0.01263	-0.01246	0.00050	-0.00050	0.02956	-0.04221
4.61	-0.00704	-1.38463	0.02395	-0.03808	0.00298	-0.00254	0.00727	-0.00946	0.01006	-0.00993	0.00050	-0.00050	0.02715	-0.04055

Table 49: 20–40%, 9.0–12.0 $\otimes$ 5.0–7.0 GeV/c Jet Function

ϕ	per trig yield	σ_{stat}/y	systematic errors											
			$+\sigma_{f2}/y$	$-\sigma_{f2}/y$	$+\sigma_{f3}/y$	$-\sigma_{f3}/y$	$+\sigma_{f4}/y$	$-\sigma_{f4}/y$	$+\sigma_{\xi/ZYAM}/y$	$-\sigma_{\xi}/y$	$+\sigma_{\pi^0}/y$	$-\sigma_{\pi^0}/y$	$+\sigma_{total}/y$	$-\sigma_{total}/y$
-1.47	-0.00192	-0.00000	0.00539	-0.00802	0.00096	-0.00071	0.00164	-0.00298	0.00406	-0.00406	0.00062	-0.00062	0.00704	-0.00952
-1.26	-0.00192	-0.00000	0.00445	-0.00662	0.00252	-0.00186	0.00055	-0.00100	0.00406	-0.00406	0.00062	-0.00062	0.00659	-0.00807
-1.05	-0.00193	-0.00000	0.00273	-0.00407	0.00309	-0.00228	0.00162	-0.00089	0.00406	-0.00406	0.00062	-0.00062	0.00604	-0.00628
-0.84	-0.00195	-0.00000	0.00057	-0.00084	0.00248	-0.00183	0.00313	-0.00173	0.00406	-0.00406	0.00062	-0.00062	0.00576	-0.00489
-0.63	-0.00198	-0.00000	0.00245	-0.00165	0.00093	-0.00069	0.00255	-0.00141	0.00406	-0.00406	0.00062	-0.00062	0.00551	-0.00470
-0.42	-0.00201	-0.00000	0.00525	-0.00353	0.00068	-0.00092	0.00033	-0.00018	0.00406	-0.00406	0.00062	-0.00062	0.00671	-0.00550
-0.21	0.02082	0.35180	0.00069	-0.00046	0.00017	-0.00023	0.00011	-0.00020	0.00040	-0.00040	0.00062	-0.00062	0.00103	-0.00092
-0.00	0.12671	0.13256	0.00012	-0.00008	0.00003	-0.00005	0.00003	-0.00005	0.00007	-0.00007	0.00062	-0.00062	0.00064	-0.00064
0.21	0.01859	0.37427	0.00077	-0.00052	0.00019	-0.00026	0.00012	-0.00022	0.00044	-0.00044	0.00062	-0.00062	0.00111	-0.00099
0.42	0.00079	3.56049	0.01340	-0.00901	0.00174	-0.00235	0.00083	-0.00046	0.01038	-0.01038	0.00062	-0.00062	0.01707	-0.01397
0.63	-0.00198	-0.00000	0.00245	-0.00165	0.00093	-0.00069	0.00255	-0.00141	0.00406	-0.00406	0.00062	-0.00062	0.00551	-0.00470
0.84	-0.00195	-0.00000	0.00057	-0.00084	0.00248	-0.00183	0.00313	-0.00173	0.00406	-0.00406	0.00062	-0.00062	0.00576	-0.00489
1.05	-0.00193	-0.00000	0.00273	-0.00407	0.00309	-0.00228	0.00162	-0.00089	0.00406	-0.00406	0.00062	-0.00062	0.00604	-0.00628
1.26	0.00759	1.26061	0.00113	-0.00168	0.00064	-0.00047	0.00014	-0.00025	0.00103	-0.00103	0.00062	-0.00062	0.00177	-0.00213
1.47	-0.00192	-0.00000	0.00539	-0.00802	0.00096	-0.00071	0.00164	-0.00298	0.00406	-0.00406	0.00062	-0.00062	0.00704	-0.00952
1.68	-0.00192	-0.00000	0.00538	-0.00800	0.00071	-0.00096	0.00164	-0.00297	0.00406	-0.00406	0.00229	-0.00229	0.00734	-0.00977
1.88	-0.00193	-0.00000	0.00443	-0.00659	0.00185	-0.00250	0.00055	-0.00100	0.00406	-0.00406	0.00229	-0.00229	0.00671	-0.00851
2.09	0.00498	1.39639	0.00106	-0.00158	0.00089	-0.00120	0.00063	-0.00035	0.00159	-0.00159	0.00229	-0.00229	0.00317	-0.00344
2.30	0.00246	1.80463	0.00045	-0.00067	0.00145	-0.00197	0.00249	-0.00137	0.00325	-0.00325	0.00229	-0.00229	0.00493	-0.00469
2.51	0.00197	2.01362	0.00247	-0.00166	0.00069	-0.00094	0.00257	-0.00142	0.00410	-0.00410	0.00229	-0.00229	0.00594	-0.00526
2.72	0.01732	0.46080	0.00061	-0.00041	0.00011	-0.00008	0.00004	-0.00002	0.00047	-0.00047	0.00229	-0.00229	0.00242	-0.00237
2.93	0.02495	0.36615	0.00058	-0.00039	0.00019	-0.00014	0.00009	-0.00017	0.00033	-0.00033	0.00229	-0.00229	0.00239	-0.00236
3.14	0.02709	0.34581	0.00058	-0.00039	0.00022	-0.00016	0.00013	-0.00023	0.00030	-0.00030	0.00229	-0.00229	0.00239	-0.00236
3.35	0.00437	1.03691	0.00329	-0.00221	0.00111	-0.00082	0.00053	-0.00096	0.00187	-0.00187	0.00229	-0.00229	0.00459	-0.00390
3.56	0.01631	0.46348	0.00065	-0.00043	0.00011	-0.00008	0.00004	-0.00002	0.00050	-0.00050	0.00229	-0.00229	0.00243	-0.00238
3.77	0.00187	2.06380	0.00259	-0.00174	0.00073	-0.00099	0.00270	-0.00149	0.00430	-0.00430	0.00229	-0.00229	0.00619	-0.00548
3.98	0.00266	1.74451	0.00042	-0.00062	0.00134	-0.00182	0.00230	-0.00127	0.00301	-0.00301	0.00229	-0.00229	0.00464	-0.00443
4.19	0.00377	1.52122	0.00140	-0.00208	0.00117	-0.00159	0.00083	-0.00046	0.00210	-0.00210	0.00229	-0.00229	0.00370	-0.00409
4.40	-0.00193	-0.00000	0.00443	-0.00659	0.00185	-0.00250	0.00055	-0.00100	0.00406	-0.00406	0.00229	-0.00229	0.00671	-0.00851
4.61	0.00759	1.26063	0.00136	-0.00203	0.00018	-0.00024	0.00042	-0.00075	0.00103	-0.00103	0.00229	-0.00229	0.00289	-0.00332

Table 50: 20–40%, 12.0–15.0 $\otimes$ 0.5–1.0 GeV/c Jet Function

ϕ	per trig yield	σ_{stat}/y	systematic errors											
			$+\sigma_{f2}/y$	$-\sigma_{f2}/y$	$+\sigma_{f3}/y$	$-\sigma_{f3}/y$	$+\sigma_{f4}/y$	$-\sigma_{f4}/y$	$+\sigma_{\xi/ZYAM}/y$	$-\sigma_{\xi}/y$	$+\sigma_{\pi^0}/y$	$-\sigma_{\pi^0}/y$	$+\sigma_{total}/y$	$-\sigma_{total}/y$
-1.47	-0.63868	-0.61339	0.05661	-0.01850	0.00933	-0.04439	0.00136	-0.00136	0.44958	-0.44958	0.02739	-0.02739	0.45405	-0.45298
-1.26	0.60438	0.66537	0.07556	-0.02446	0.01273	-0.05264	0.00183	-0.00458	0.47575	-0.47576	0.02739	-0.02739	0.48267	-0.48009
-1.05	0.49555	0.71506	0.12741	-0.04084	0.01689	-0.06704	0.00757	-0.01092	0.58239	-0.58239	0.02739	-0.02739	0.59708	-0.58840
-0.84	0.11352	2.74167	0.75389	-0.24000	0.06815	-0.28244	0.04688	-0.06159	2.55665	-2.55667	0.02739	-0.02739	2.66691	-2.58427
-0.63	0.53032	0.52756	0.20576	-0.06523	0.01140	-0.05433	0.00902	-0.01219	0.55090	-0.55090	0.02739	-0.02739	0.58889	-0.55821
-0.42	0.08438	2.84625	1.53666	-0.48599	0.04670	-0.29323	0.02965	-0.04973	3.48396	-3.48398	0.02739	-0.02739	3.80829	-3.53037
-0.21	0.15364	1.51987	0.93496	-0.29533	0.01456	-0.13954	0.01104	-0.01104	1.92220	-1.92222	0.02739	-0.02739	2.13778	-1.94999
-0.00	0.40044	0.59316	0.37107	-0.11716	0.00396	-0.05038	0.00271	-0.00271	0.73869	-0.73870	0.02739	-0.02739	0.82712	-0.75013
0.21	0.05479	4.20259	2.62184	-0.82817	0.04083	-0.39132	0.03095	-0.03095	5.39032	-5.39036	0.02739	-0.02739	5.99441	-5.46778
0.42	-0.33971	-0.68547	0.38172	-0.12072	0.01160	-0.07284	0.00736	-0.01235	0.86543	-0.86544	0.02739	-0.02739	0.94637	-0.87736
0.63	-0.21656	-1.18387	0.50389	-0.15975	0.02791	-0.13305	0.02209	-0.02986	1.34909	-1.34910	0.02739	-0.02739	1.44082	-1.36563
0.84	0.29534	0.99614	0.28977	-0.09225	0.02620	-0.10856	0.01802	-0.02367	0.98270	-0.98271	0.02739	-0.02739	1.02540	-0.99364
1.05	-0.17442	-1.94426	0.36198	-0.11603	0.04798	-0.19047	0.02151	-0.03104	1.65461	-1.65462	0.02739	-0.02739	1.69478	-1.67010
1.26	-0.33280	-1.12511	0.13721	-0.04442	0.02311	-0.09560	0.00332	-0.00831	0.86399	-0.86400	0.02739	-0.02739	0.87556	-0.87087
1.47	-0.11816	-3.38334	0.30602	-0.10000	0.05042	-0.23996	0.00734	-0.00734	2.43013	-2.43015	0.02739	-0.02739	2.45001	-2.44418
1.68	0.23277	1.78243	0.15567	-0.05087	0.01645	-0.10371	0.00372	-0.00372	1.23458	-1.23459	0.00237	-0.00237	1.24447	-1.23999
1.88	0.14750	2.67931	0.31095	-0.10066	0.01434	-0.14092	0.00753	-0.01881	1.95371	-1.95372	0.00237	-0.00237	1.97837	-1.96148
2.09	0.21523	1.58658	0.29450	-0.09439	0.00686	-0.09101	0.01746	-0.02520	1.34457	-1.34458	0.00237	-0.00237	1.37657	-1.35119
2.30	0.75060	0.41622	0.11428	-0.03638	0.00288	-0.02802	0.00710	-0.00933	0.38751	-0.38751	0.00237	-0.00237	0.40409	-0.39034
2.51	0.13544	2.03763	0.80627	-0.25561	0.02890	-0.18163	0.03534	-0.04777	2.15893	-2.15895	0.00237	-0.00237	2.30503	-2.18213
2.72	-0.01094	-24.12970	11.84564	-3.74633	0.55487	-2.64689	0.22851	-0.38332	26.85041	-26.85059	0.00237	-0.00237	29.35343	-27.24229
2.93	0.05729	4.40452	2.50372	-0.79085	0.13637	-0.56674	0.02945	-0.02945	5.14356	-5.14360	0.00237	-0.00237	5.72227	-5.23489
3.14	0.80889	0.32017	0.18339	-0.05791	0.01048	-0.04180	0.00135	-0.00135	0.36472	-0.36472	0.00237	-0.00237	0.40838	-0.37166
3.35	0.20630	1.23562	0.69530	-0.21962	0.03787	-0.15739	0.00818	-0.00818	1.42840	-1.42841	0.00237	-0.00237	1.58911	-1.45377
3.56	0.15112	1.74184	0.85755	-0.27121	0.04017	-0.19162	0.01654	-0.02775	1.94379	-1.94381	0.00237	-0.00237	2.12500	-1.97217
3.77	0.65166	0.44496	0.16757	-0.05312	0.00601	-0.03775	0.00734	-0.00993	0.44870	-0.44870	0.00237	-0.00237	0.47907	-0.45352
3.98	0.21506	1.41632	0.39887	-0.12698	0.01005	-0.09780	0.02477	-0.03255	1.35248	-1.35249	0.00237	-0.00237	1.41033	-1.36235
4.19	0.08700	3.80653	0.72856	-0.23352	0.01697	-0.22515	0.04318	-0.06234	3.32630	-3.32632	0.00237	-0.00237	3.40547	-3.34269
4.40	0.15295	2.47085	0.29988	-0.09707	0.01383	-0.13591	0.00726	-0.01814	1.88415	-1.88416	0.00237	-0.00237	1.90793	-1.89164
4.61	-0.11457	-3.64108	0.31627	-0.10334	0.03341	-0.21070	0.00755	-0.00755	2.50830	-2.50832	0.00237	-0.00237	2.52839	-2.51928

Table 51: 20–40%, 12.0–15.0 $\otimes$ 1.0–2.0 GeV/c Jet Function

ϕ	per trig yield	σ_{stat}/y	systematic errors											
			$+\sigma_{f2}/y$	$-\sigma_{f2}/y$	$+\sigma_{f3}/y$	$-\sigma_{f3}/y$	$+\sigma_{f4}/y$	$-\sigma_{f4}/y$	$+\sigma_{\xi/ZYAM}/y$	$-\sigma_{\xi}/y$	$+\sigma_{\pi^0}/y$	$-\sigma_{\pi^0}/y$	$+\sigma_{total}/y$	$-\sigma_{total}/y$
-1.47	0.23665	1.22848	0.04818	-0.15853	0.00431	-0.00813	0.01260	-0.01219	0.02778	-0.02778	0.00511	-0.00511	0.05741	-0.16169
-1.26	0.05549	4.76550	0.16993	-0.55918	0.04809	-0.09083	0.01817	-0.01758	0.11870	-0.11868	0.00511	-0.00511	0.21362	-0.57909
-1.05	0.10028	2.14683	0.05812	-0.19124	0.03289	-0.06213	0.01574	-0.01627	0.06608	-0.06607	0.00511	-0.00511	0.09539	-0.21234
-0.84	0.18171	1.10211	0.00670	-0.02206	0.01469	-0.02774	0.01699	-0.01757	0.03683	-0.03682	0.00511	-0.00511	0.04395	-0.05428
-0.63	-0.28211	-0.54802	0.04201	-0.01277	0.00361	-0.00682	0.00905	-0.00936	0.02401	-0.02401	0.00511	-0.00511	0.04963	-0.02999
-0.42	0.03311	4.67904	0.77516	-0.23557	0.05815	-0.03079	0.00997	-0.01030	0.20701	-0.20698	0.00511	-0.00511	0.80450	-0.31530
-0.21	0.55590	0.26927	0.06303	-0.01915	0.00907	-0.00480	0.00393	-0.00380	0.01243	-0.01243	0.00511	-0.00511	0.06520	-0.02419
-0.00	0.64395	0.23690	0.05956	-0.01810	0.00967	-0.00512	0.00507	-0.00490	0.01077	-0.01077	0.00511	-0.00511	0.06171	-0.02280
0.21	0.43158	0.33547	0.08118	-0.02467	0.01168	-0.00618	0.00506	-0.00489	0.01602	-0.01601	0.00511	-0.00511	0.08388	-0.03088
0.42	0.13639	1.12876	0.18816	-0.05718	0.01411	-0.00747	0.00242	-0.00250	0.05025	-0.05024	0.00511	-0.00511	0.19534	-0.07669
0.63	-0.17582	-0.86995	0.06741	-0.02049	0.00580	-0.01095	0.01453	-0.01502	0.03853	-0.03852	0.00511	-0.00511	0.07937	-0.04770
0.84	-0.21600	-0.80665	0.00564	-0.01856	0.01235	-0.02333	0.01430	-0.01478	0.03098	-0.03098	0.00511	-0.00511	0.03708	-0.04575
1.05	-0.08417	-2.36858	0.06924	-0.22784	0.03919	-0.07402	0.01876	-0.01939	0.07873	-0.07872	0.00511	-0.00511	0.11361	-0.25296
1.26	0.25754	1.00993	0.03661	-0.12048	0.01036	-0.01957	0.00392	-0.00379	0.02557	-0.02557	0.00511	-0.00511	0.04630	-0.12487
1.47	0.03787	7.55907	0.30108	-0.99072	0.02692	-0.05084	0.07874	-0.07617	0.17363	-0.17360	0.00511	-0.00511	0.35741	-1.00999
1.68	0.14304	1.97743	0.07970	-0.26226	0.01346	-0.00713	0.02084	-0.02016	0.04605	-0.04605	0.02533	-0.02533	0.09864	-0.26833
1.88	-0.18529	-1.32090	0.05089	-0.16746	0.02720	-0.01440	0.00544	-0.00527	0.03573	-0.03573	0.02533	-0.02533	0.07265	-0.17377
2.09	-0.04888	-4.16485	0.11922	-0.39231	0.12745	-0.06748	0.03229	-0.03338	0.13643	-0.13641	0.02533	-0.02533	0.22529	-0.42288
2.30	0.04604	4.15288	0.02646	-0.08707	0.10947	-0.05796	0.06707	-0.06933	0.14609	-0.14607	0.02533	-0.02533	0.19790	-0.19423
2.51	0.44803	0.39438	0.02645	-0.00804	0.00430	-0.00228	0.00570	-0.00589	0.01515	-0.01514	0.02533	-0.02533	0.04027	-0.03123
2.72	0.16213	1.01670	0.15829	-0.04810	0.00629	-0.01187	0.00204	-0.00210	0.04219	-0.04219	0.02533	-0.02533	0.16590	-0.06986
2.93	0.45765	0.35683	0.07656	-0.02327	0.00583	-0.01101	0.00477	-0.00462	0.01503	-0.01503	0.02533	-0.02533	0.08238	-0.03939
3.14	0.82431	0.21616	0.04653	-0.01414	0.00400	-0.00756	0.00396	-0.00383	0.00836	-0.00836	0.02533	-0.02533	0.05393	-0.03136
3.35	0.33578	0.47234	0.10435	-0.03171	0.00795	-0.01501	0.00650	-0.00629	0.02048	-0.02048	0.02533	-0.02533	0.10979	-0.04829
3.56	-0.04964	-3.16861	0.51701	-0.15712	0.02053	-0.03878	0.00665	-0.00687	0.13780	-0.13778	0.02533	-0.02533	0.53609	-0.21416
3.77	-0.09408	-1.68493	0.12598	-0.03829	0.02046	-0.01083	0.02715	-0.02807	0.07214	-0.07213	0.02533	-0.02533	0.15124	-0.09064
3.98	-0.00518	-36.07358	0.23513	-0.77373	0.97272	-0.51501	0.59600	-0.61610	1.29814	-1.29794	0.02533	-0.02533	1.74427	-1.71137
4.19	0.13808	1.52055	0.04221	-0.13888	0.04512	-0.02389	0.01143	-0.01182	0.04830	-0.04829	0.02533	-0.02533	0.08320	-0.15157
4.40	-0.20510	-1.12235	0.04597	-0.15128	0.02457	-0.01301	0.00492	-0.00476	0.03228	-0.03228	0.02533	-0.02533	0.06652	-0.15736
4.61	0.21526	1.30583	0.05296	-0.17428	0.00894	-0.00474	0.01385	-0.01340	0.03060	-0.03060	0.02533	-0.02533	0.06823	-0.17931

Table 52: 20–40%, 12.0–15.0 $\otimes$ 2.0–3.0 GeV/c Jet Function

ϕ	per trig yield	σ_{stat}/y	systematic errors											
			$+\sigma_{f2}/y$	$-\sigma_{f2}/y$	$+\sigma_{f3}/y$	$-\sigma_{f3}/y$	$+\sigma_{f4}/y$	$-\sigma_{f4}/y$	$+\sigma_{\xi/ZYAM}/y$	$-\sigma_{\xi}/y$	$+\sigma_{\pi^0}/y$	$-\sigma_{\pi^0}/y$	$+\sigma_{total}/y$	$-\sigma_{total}/y$
-1.47	-0.01590	-4.94211	0.08661	-0.27992	0.00847	-0.01709	0.02978	-0.02880	0.03612	-0.03618	0.00398	-0.00398	0.09890	-0.28425
-1.26	-0.07696	-0.76498	0.01480	-0.04783	0.00458	-0.00924	0.00208	-0.00201	0.00747	-0.00749	0.00398	-0.00398	0.01778	-0.04949
-1.05	0.00389	16.60808	0.18095	-0.58481	0.11206	-0.22604	0.06441	-0.06662	0.14904	-0.14929	0.00398	-0.00398	0.26772	-0.64795
-0.84	0.07666	0.80687	0.00192	-0.00620	0.00460	-0.00928	0.00639	-0.00661	0.00767	-0.00768	0.00398	-0.00398	0.01185	-0.01559
-0.63	-0.01352	-3.45176	0.10395	-0.03216	0.00996	-0.02009	0.02998	-0.03100	0.04422	-0.04430	0.00398	-0.00398	0.11737	-0.06616
-0.42	0.02818	1.64129	0.10801	-0.03342	0.00964	-0.00478	0.00186	-0.00192	0.02159	-0.02163	0.00398	-0.00398	0.11065	-0.04034
-0.21	0.20691	0.26689	0.02009	-0.00622	0.00344	-0.00170	0.00168	-0.00162	0.00298	-0.00298	0.00398	-0.00398	0.02104	-0.00830
-0.00	0.55479	0.12563	0.00820	-0.00254	0.00158	-0.00079	0.00093	-0.00090	0.00112	-0.00112	0.00398	-0.00398	0.00936	-0.00499
0.21	0.21743	0.25403	0.01912	-0.00591	0.00327	-0.00162	0.00159	-0.00154	0.00284	-0.00284	0.00398	-0.00398	0.02006	-0.00799
0.42	0.02442	1.80423	0.12465	-0.03857	0.01112	-0.00552	0.00214	-0.00222	0.02492	-0.02496	0.00398	-0.00398	0.12768	-0.04649
0.63	0.02945	1.67451	0.04774	-0.01477	0.00457	-0.00923	0.01377	-0.01424	0.02031	-0.02034	0.00398	-0.00398	0.05402	-0.03059
0.84	0.01783	2.97335	0.00825	-0.02666	0.01977	-0.03988	0.02748	-0.02842	0.03295	-0.03301	0.00398	-0.00398	0.04813	-0.06492
1.05	-0.09630	-0.44703	0.00731	-0.02362	0.00453	-0.00913	0.00260	-0.00269	0.00602	-0.00603	0.00398	-0.00398	0.01152	-0.02647
1.26	-0.09555	-0.52902	0.01192	-0.03852	0.00369	-0.00744	0.00168	-0.00162	0.00602	-0.00603	0.00398	-0.00398	0.01451	-0.03993
1.47	-0.03915	-1.93239	0.03517	-0.11367	0.00344	-0.00694	0.01209	-0.01169	0.01467	-0.01469	0.00398	-0.00398	0.04033	-0.11549
1.68	0.07424	1.35014	0.01855	-0.05994	0.00366	-0.00181	0.00638	-0.00617	0.00776	-0.00777	0.00742	-0.00742	0.02266	-0.06123
1.88	-0.01792	-3.80080	0.06356	-0.20541	0.03970	-0.01968	0.00894	-0.00864	0.03239	-0.03244	0.00742	-0.00742	0.08246	-0.20920
2.09	0.08373	0.85912	0.00841	-0.02717	0.01050	-0.00521	0.00299	-0.00309	0.00700	-0.00701	0.00742	-0.00742	0.01715	-0.02965
2.30	0.04359	1.32773	0.00338	-0.01091	0.01632	-0.00809	0.01125	-0.01163	0.01360	-0.01362	0.00742	-0.00742	0.02538	-0.02367
2.51	-0.01118	-4.13030	0.12572	-0.03890	0.02430	-0.01205	0.03626	-0.03749	0.05366	-0.05375	0.00742	-0.00742	0.14369	-0.07752
2.72	0.04478	1.08053	0.06798	-0.02103	0.00301	-0.00607	0.00117	-0.00121	0.01355	-0.01357	0.00742	-0.00742	0.06978	-0.02683
2.93	0.15812	0.36275	0.02629	-0.00813	0.00223	-0.00450	0.00219	-0.00212	0.00387	-0.00387	0.00742	-0.00742	0.02776	-0.01269
3.14	0.22550	0.27596	0.02018	-0.00624	0.00193	-0.00390	0.00230	-0.00222	0.00272	-0.00272	0.00742	-0.00742	0.02188	-0.01103
3.35	0.13925	0.40062	0.02985	-0.00924	0.00253	-0.00511	0.00249	-0.00241	0.00439	-0.00440	0.00742	-0.00742	0.03127	-0.01384
3.56	0.05920	0.82188	0.05142	-0.01591	0.00228	-0.00459	0.00088	-0.00092	0.01025	-0.01027	0.00742	-0.00742	0.05301	-0.02087
3.77	-0.05781	-0.69116	0.02432	-0.00752	0.00470	-0.00233	0.00701	-0.00725	0.01038	-0.01040	0.00742	-0.00742	0.02873	-0.01667
3.98	0.00467	11.08811	0.03149	-0.10178	0.15224	-0.07547	0.10491	-0.10849	0.12688	-0.12709	0.00742	-0.00742	0.22655	-0.20984
4.19	0.01518	4.01171	0.04637	-0.14985	0.05792	-0.02871	0.01651	-0.01707	0.03860	-0.03867	0.00742	-0.00742	0.08557	-0.15850
4.40	-0.07696	-0.70806	0.01480	-0.04782	0.00924	-0.00458	0.00208	-0.00201	0.00754	-0.00755	0.00742	-0.00742	0.02051	-0.04924
4.61	0.06247	1.44972	0.02204	-0.07123	0.00435	-0.00216	0.00758	-0.00733	0.00922	-0.00924	0.00742	-0.00742	0.02650	-0.07261

Table 53: 20–40%, 12.0–15.0 $\otimes$ 3.0–5.0 GeV/c Jet Function

ϕ	per trig yield	σ_{stat}/y	systematic errors											
			$+\sigma_{f2}/y$	$-\sigma_{f2}/y$	$+\sigma_{f3}/y$	$-\sigma_{f3}/y$	$+\sigma_{f4}/y$	$-\sigma_{f4}/y$	$+\sigma_{\xi/ZYAM}/y$	$-\sigma_{\xi}/y$	$+\sigma_{\pi^0}/y$	$-\sigma_{\pi^0}/y$	$+\sigma_{total}/y$	$-\sigma_{total}/y$
-1.47	-0.02646	-0.00000	0.00659	-0.02163	0.00069	-0.00139	0.00268	-0.00255	0.00248	-0.00248	0.00595	-0.00595	0.00963	-0.02276
-1.26	-0.02650	-0.00000	0.00545	-0.01787	0.00181	-0.00363	0.00091	-0.00086	0.00248	-0.00248	0.00595	-0.00595	0.00868	-0.01936
-1.05	-0.00639	-3.18095	0.01396	-0.04580	0.00927	-0.01862	0.00579	-0.00608	0.01038	-0.01038	0.00595	-0.00595	0.02139	-0.05123
-0.84	0.04441	0.65884	0.00042	-0.00138	0.00108	-0.00217	0.00163	-0.00171	0.00151	-0.00151	0.00595	-0.00595	0.00646	-0.00687
-0.63	0.01279	1.57975	0.01414	-0.00431	0.00143	-0.00287	0.00468	-0.00491	0.00535	-0.00535	0.00595	-0.00595	0.01697	-0.01073
-0.42	-0.01198	-0.95020	0.03269	-0.00997	0.00307	-0.00153	0.00065	-0.00068	0.00582	-0.00582	0.00595	-0.00595	0.03388	-0.01310
-0.21	0.10642	0.29225	0.00502	-0.00153	0.00090	-0.00045	0.00049	-0.00047	0.00066	-0.00066	0.00595	-0.00595	0.00789	-0.00622
-0.00	0.36334	0.13379	0.00161	-0.00049	0.00033	-0.00016	0.00021	-0.00020	0.00020	-0.00020	0.00595	-0.00595	0.00618	-0.00598
0.21	0.09711	0.29811	0.00551	-0.00168	0.00099	-0.00049	0.00054	-0.00051	0.00073	-0.00073	0.00595	-0.00595	0.00822	-0.00627
0.42	0.00260	5.90956	0.15078	-0.04597	0.01416	-0.00705	0.00298	-0.00313	0.02684	-0.02684	0.00595	-0.00595	0.15395	-0.05412
0.63	0.00207	8.28197	0.08746	-0.02667	0.00885	-0.01778	0.02895	-0.03038	0.03310	-0.03310	0.00595	-0.00595	0.09847	-0.05551
0.84	-0.02706	-0.00000	0.00069	-0.00226	0.00177	-0.00356	0.00267	-0.00281	0.00248	-0.00248	0.00595	-0.00595	0.00724	-0.00820
1.05	0.00527	4.29423	0.01693	-0.05552	0.01124	-0.02258	0.00702	-0.00737	0.01258	-0.01258	0.00595	-0.00595	0.02561	-0.06197
1.26	-0.02650	-0.00000	0.00545	-0.01787	0.00181	-0.00363	0.00091	-0.00086	0.00248	-0.00248	0.00595	-0.00595	0.00868	-0.01936
1.47	0.00826	4.20994	0.02113	-0.06931	0.00222	-0.00445	0.00859	-0.00819	0.00796	-0.00796	0.00595	-0.00595	0.02498	-0.07064
1.68	0.01304	3.04187	0.01339	-0.04391	0.00282	-0.00140	0.00544	-0.00519	0.00506	-0.00506	0.00698	-0.00698	0.01706	-0.04507
1.88	-0.02675	-0.00000	0.00540	-0.01770	0.00360	-0.00179	0.00090	-0.00085	0.00248	-0.00248	0.00698	-0.00698	0.00989	-0.01929
2.09	-0.02700	-0.00000	0.00330	-0.01084	0.00441	-0.00219	0.00137	-0.00144	0.00248	-0.00248	0.00698	-0.00698	0.00933	-0.01338
2.30	-0.00319	-5.35844	0.00585	-0.01919	0.03020	-0.01504	0.02271	-0.02383	0.02129	-0.02129	0.00698	-0.00698	0.04432	-0.04079
2.51	0.03373	0.74468	0.00536	-0.00163	0.00109	-0.00054	0.00177	-0.00186	0.00204	-0.00204	0.00698	-0.00698	0.00927	-0.00770
2.72	0.03826	0.61361	0.01024	-0.00312	0.00048	-0.00096	0.00020	-0.00021	0.00182	-0.00182	0.00698	-0.00698	0.01253	-0.00792
2.93	0.05699	0.47424	0.00938	-0.00286	0.00084	-0.00169	0.00091	-0.00087	0.00123	-0.00123	0.00698	-0.00698	0.01182	-0.00787
3.14	0.13925	0.27080	0.00420	-0.00128	0.00043	-0.00085	0.00056	-0.00053	0.00050	-0.00050	0.00698	-0.00698	0.00819	-0.00718
3.35	0.12033	0.29260	0.00444	-0.00135	0.00040	-0.00080	0.00043	-0.00041	0.00058	-0.00058	0.00698	-0.00698	0.00831	-0.00719
3.56	0.03697	0.62258	0.01059	-0.00323	0.00050	-0.00099	0.00021	-0.00022	0.00188	-0.00188	0.00698	-0.00698	0.01283	-0.00798
3.77	-0.00825	-1.66289	0.02191	-0.00668	0.00445	-0.00222	0.00725	-0.00761	0.00832	-0.00832	0.00698	-0.00698	0.02589	-0.01501
3.98	0.01984	1.19066	0.00094	-0.00308	0.00485	-0.00242	0.00365	-0.00383	0.00342	-0.00342	0.00698	-0.00698	0.00991	-0.00951
4.19	0.00526	4.34265	0.01696	-0.05563	0.02262	-0.01126	0.00703	-0.00738	0.01275	-0.01275	0.00698	-0.00698	0.03256	-0.05905
4.40	-0.00568	-3.70936	0.02540	-0.08331	0.01694	-0.00843	0.00422	-0.00402	0.01169	-0.01169	0.00698	-0.00698	0.03369	-0.08493
4.61	-0.02656	-0.00000	0.00657	-0.02155	0.00138	-0.00069	0.00267	-0.00255	0.00248	-0.00248	0.00698	-0.00698	0.01035	-0.02294

Table 54: 20–40%, 12.0–15.0 $\otimes$ 5.0–7.0 GeV/c Jet Function

ϕ	per trig yield	σ_{stat}/y	systematic errors											
			$+\sigma_{f2}/y$	$-\sigma_{f2}/y$	$+\sigma_{f3}/y$	$-\sigma_{f3}/y$	$+\sigma_{f4}/y$	$-\sigma_{f4}/y$	$+\sigma_{\xi/ZYAM}/y$	$-\sigma_{\xi}/y$	$+\sigma_{\pi^0}/y$	$-\sigma_{\pi^0}/y$	$+\sigma_{total}/y$	$-\sigma_{total}/y$
-1.47	-0.00192	-0.00000	0.00555	-0.01652	0.00097	-0.00086	0.00176	-0.00299	0.00354	-0.00405	0.00638	-0.00638	0.00939	-0.01843
-1.26	-0.00193	-0.00000	0.00458	-0.01363	0.00254	-0.00224	0.00060	-0.00101	0.00354	-0.00405	0.00638	-0.00638	0.00900	-0.01578
-1.05	-0.00194	-0.00000	0.00282	-0.00837	0.00312	-0.00275	0.00163	-0.00096	0.00354	-0.00405	0.00638	-0.00638	0.00857	-0.01165
-0.84	-0.00196	-0.00000	0.00058	-0.00173	0.00250	-0.00220	0.00315	-0.00185	0.00354	-0.00405	0.00638	-0.00638	0.00835	-0.00827
-0.63	-0.00199	-0.00000	0.00506	-0.00170	0.00094	-0.00083	0.00257	-0.00151	0.00354	-0.00405	0.00638	-0.00638	0.00929	-0.00793
-0.42	0.03791	0.76031	0.00057	-0.00019	0.00004	-0.00005	0.00002	-0.00001	0.00019	-0.00021	0.00638	-0.00638	0.00640	-0.00638
-0.21	0.01286	1.16708	0.00231	-0.00078	0.00034	-0.00038	0.00019	-0.00033	0.00056	-0.00064	0.00638	-0.00638	0.00681	-0.00647
-0.00	0.13741	0.32794	0.00024	-0.00008	0.00004	-0.00004	0.00003	-0.00005	0.00005	-0.00006	0.00638	-0.00638	0.00638	-0.00638
0.21	0.02775	0.77081	0.00107	-0.00036	0.00016	-0.00018	0.00009	-0.00015	0.00026	-0.00030	0.00638	-0.00638	0.00647	-0.00640
0.42	-0.00201	-0.00000	0.01081	-0.00363	0.00082	-0.00093	0.00033	-0.00019	0.00354	-0.00405	0.00638	-0.00638	0.01307	-0.00844
0.63	-0.00199	-0.00000	0.00506	-0.00170	0.00094	-0.00083	0.00257	-0.00151	0.00354	-0.00405	0.00638	-0.00638	0.00929	-0.00793
0.84	-0.00196	-0.00000	0.00058	-0.00173	0.00250	-0.00220	0.00315	-0.00185	0.00354	-0.00405	0.00638	-0.00638	0.00835	-0.00827
1.05	-0.00194	-0.00000	0.00282	-0.00837	0.00312	-0.00275	0.00163	-0.00096	0.00354	-0.00405	0.00638	-0.00638	0.00857	-0.01165
1.26	-0.00193	-0.00000	0.00458	-0.01363	0.00254	-0.00224	0.00060	-0.00101	0.00354	-0.00405	0.00638	-0.00638	0.00900	-0.01578
1.47	-0.00192	-0.00000	0.00555	-0.01652	0.00097	-0.00086	0.00176	-0.00299	0.00354	-0.00405	0.00638	-0.00638	0.00939	-0.01843
1.68	-0.00193	-0.00000	0.00554	-0.01648	0.00086	-0.00097	0.00176	-0.00299	0.00354	-0.00405	0.00950	-0.00950	0.01172	-0.01970
1.88	-0.00194	-0.00000	0.00456	-0.01357	0.00223	-0.00252	0.00059	-0.00101	0.00354	-0.00405	0.00950	-0.00950	0.01135	-0.01726
2.09	-0.00195	-0.00000	0.00280	-0.00832	0.00273	-0.00310	0.00162	-0.00095	0.00354	-0.00405	0.00950	-0.00950	0.01098	-0.01365
2.30	-0.00197	-0.00000	0.00058	-0.00172	0.00219	-0.00248	0.00313	-0.00184	0.00354	-0.00405	0.00950	-0.00950	0.01085	-0.01091
2.51	-0.00199	-0.00000	0.00505	-0.00170	0.00083	-0.00094	0.00256	-0.00151	0.00354	-0.00405	0.00950	-0.00950	0.01164	-0.01061
2.72	0.01639	1.13351	0.00133	-0.00045	0.00011	-0.00010	0.00004	-0.00002	0.00043	-0.00050	0.00950	-0.00950	0.00960	-0.00952
2.93	0.08732	0.53538	0.00034	-0.00011	0.00006	-0.00005	0.00003	-0.00005	0.00008	-0.00009	0.00950	-0.00950	0.00950	-0.00950
3.14	0.03967	0.75956	0.00082	-0.00028	0.00015	-0.00013	0.00009	-0.00016	0.00018	-0.00021	0.00950	-0.00950	0.00953	-0.00950
3.35	0.05009	0.61710	0.00059	-0.00020	0.00010	-0.00009	0.00005	-0.00008	0.00014	-0.00016	0.00950	-0.00950	0.00952	-0.00950
3.56	-0.00201	-0.00000	0.01083	-0.00364	0.00093	-0.00082	0.00033	-0.00019	0.00354	-0.00405	0.00950	-0.00950	0.01487	-0.01098
3.77	-0.00199	-0.00000	0.00505	-0.00170	0.00083	-0.00094	0.00256	-0.00151	0.00354	-0.00405	0.00950	-0.00950	0.01164	-0.01061
3.98	-0.00197	-0.00000	0.00058	-0.00172	0.00219	-0.00248	0.00313	-0.00184	0.00354	-0.00405	0.00950	-0.00950	0.01085	-0.01091
4.19	-0.00195	-0.00000	0.00280	-0.00832	0.00273	-0.00310	0.00162	-0.00095	0.00354	-0.00405	0.00950	-0.00950	0.01098	-0.01365
4.40	-0.00194	-0.00000	0.00456	-0.01357	0.00223	-0.00252	0.00059	-0.00101	0.00354	-0.00405	0.00950	-0.00950	0.01135	-0.01726
4.61	-0.00193	-0.00000	0.00554	-0.01648	0.00086	-0.00097	0.00176	-0.00299	0.00354	-0.00405	0.00950	-0.00950	0.01172	-0.01970

G Data Table: Per Trigger Yields

Table 55: Away side yield, 0–20%

trig p_T 4–5 GeV/c													
assoc p_T (GeV/c)	yield	σ_{stat}/Y	systematic error										
			$+\sigma_{f2}/Y$	$-\sigma_{f2}/Y$	$+\sigma_{f3}/Y$	$-\sigma_{f3}/Y$	$+\sigma_{f4}/Y$	$-\sigma_{f4}/Y$	$+\sigma_{\xi/ZYAM}/Y$	$-\sigma_{\xi}/Y$	σ_{π^0}	$-\sigma_{\pi^0}$	$+\sigma_{total}/Y$	$-\sigma_{total}/Y$
0.5–1.0	0.70505	0.05429	0.02264	-0.02122	0.02646	-0.02828	0.00596	-0.00662	0.09516	-0.09517	0.06056	-0.06056	0.11820	-0.11840
1.0–2.0	0.11867	0.10163	0.00000	-0.00000	0.01457	-0.01555	0.00000	-0.00000	0.07914	-0.07914	0.04080	-0.04080	0.09022	-0.09038
2.0–3.0	0.01627	0.21188	0.00000	-0.00000	0.01420	-0.01507	0.00000	-0.00000	0.04373	-0.04373	0.12763	-0.12763	0.13566	-0.13575
3.0–5.0	0.00212	0.28410	0.00000	-0.00000	0.00791	-0.00840	0.00000	-0.00000	0.02149	-0.02075	0.22809	-0.22809	0.22924	-0.22919
5.0–7.0	0.00055	0.47765	0.00000	-0.00000	0.00644	-0.00706	0.00000	-0.00000	0.01439	-0.01439	0.17621	-0.17621	0.17692	-0.17694
trig p_T 5–7 GeV/c													
assoc p_T (GeV/c)	yield	σ_{stat}/Y	systematic error										
			$+\sigma_{f2}/Y$	$-\sigma_{f2}/Y$	$+\sigma_{f3}/Y$	$-\sigma_{f3}/Y$	$+\sigma_{f4}/Y$	$-\sigma_{f4}/Y$	$+\sigma_{\xi/ZYAM}/Y$	$-\sigma_{\xi}/Y$	σ_{π^0}	$-\sigma_{\pi^0}$	$+\sigma_{total}/Y$	$-\sigma_{total}/Y$
0.5–1.0	0.54207	0.09426	0.02102	-0.01747	0.02849	-0.03087	0.00838	-0.01074	0.11568	-0.11566	0.01164	-0.01164	0.12183	-0.12201
1.0–2.0	0.15436	0.10469	0.00000	-0.00000	0.01477	-0.01649	0.00000	-0.00000	0.04787	-0.04785	0.02750	-0.02750	0.05714	-0.05760
2.0–3.0	0.02998	0.15480	0.00000	-0.00000	0.01078	-0.01191	0.00000	-0.00000	0.01868	-0.01868	0.00737	-0.00737	0.02279	-0.02335
3.0–5.0	0.00218	0.36945	0.00000	-0.00000	0.01062	-0.01177	0.00000	-0.00000	0.01660	-0.01588	0.20576	-0.20576	0.20670	-0.20671
5.0–7.0	0.00135	0.26642	0.00000	-0.00000	0.00230	-0.00280	0.00000	-0.00000	0.00467	-0.00350	0.03614	-0.03614	0.03652	-0.03642
trig p_T 7–9 GeV/c													
assoc p_T (GeV/c)	yield	σ_{stat}/Y	systematic error										
			$+\sigma_{f2}/Y$	$-\sigma_{f2}/Y$	$+\sigma_{f3}/Y$	$-\sigma_{f3}/Y$	$+\sigma_{f4}/Y$	$-\sigma_{f4}/Y$	$+\sigma_{\xi/ZYAM}/Y$	$-\sigma_{\xi}/Y$	σ_{π^0}	$-\sigma_{\pi^0}$	$+\sigma_{total}/Y$	$-\sigma_{total}/Y$
0.5–1.0	1.34141	0.10555	0.00005	-0.00099	0.02532	-0.02280	0.00454	-0.00538	0.18102	-0.18101	0.11716	-0.11716	0.21715	-0.21689
1.0–2.0	0.15779	0.28296	0.00000	-0.00000	0.02201	-0.01951	0.00000	-0.00000	0.04455	-0.04453	0.00603	-0.00603	0.05005	-0.04898
2.0–3.0	0.02679	0.47676	0.00000	-0.00000	0.01919	-0.01655	0.00000	-0.00000	0.01996	-0.01984	0.00566	-0.00566	0.02826	-0.02645
3.0–5.0	0.01141	0.20032	0.00000	-0.00000	0.00319	-0.00277	0.00000	-0.00000	0.00289	-0.00289	0.05457	-0.05457	0.05474	-0.05472
5.0–7.0	0.00182	0.55779	0.00000	-0.00000	0.00160	-0.00196	0.00000	-0.00000	0.00259	-0.00259	0.11150	-0.11150	0.11154	-0.11154
trig p_T 9–12 GeV/c													
assoc p_T (GeV/c)	yield	σ_{stat}/Y	systematic error										
			$+\sigma_{f2}/Y$	$-\sigma_{f2}/Y$	$+\sigma_{f3}/Y$	$-\sigma_{f3}/Y$	$+\sigma_{f4}/Y$	$-\sigma_{f4}/Y$	$+\sigma_{\xi/ZYAM}/Y$	$-\sigma_{\xi}/Y$	σ_{π^0}	$-\sigma_{\pi^0}$	$+\sigma_{total}/Y$	$-\sigma_{total}/Y$
0.5–1.0	1.34433	0.20224	0.04694	-0.02658	0.02913	-0.02244	0.00486	-0.00546	0.29256	-0.29256	0.04323	-0.04323	0.30089	-0.29783
1.0–2.0	0.24742	0.34698	0.00000	-0.00000	0.02028	-0.01567	0.00000	-0.00000	0.02933	-0.02932	0.03055	-0.03055	0.04696	-0.04515
2.0–3.0	0.07124	0.34901	0.00000	-0.00000	0.01058	-0.00793	0.00000	-0.00000	0.00773	-0.00773	0.01790	-0.01790	0.02219	-0.02105
3.0–5.0	0.01606	0.27474	0.00000	-0.00000	0.00332	-0.00251	0.00000	-0.00000	0.00215	-0.00215	0.03916	-0.03916	0.03936	-0.03930
5.0–7.0	0.00790	0.27488	0.00000	-0.00000	0.00042	-0.00051	0.00000	-0.00000	0.00080	-0.00060	0.00997	-0.00997	0.01001	-0.01000
trig p_T 12–15 GeV/c													
assoc p_T (GeV/c)	yield	σ_{stat}/Y	systematic error										
			$+\sigma_{f2}/Y$	$-\sigma_{f2}/Y$	$+\sigma_{f3}/Y$	$-\sigma_{f3}/Y$	$+\sigma_{f4}/Y$	$-\sigma_{f4}/Y$	$+\sigma_{\xi/ZYAM}/Y$	$-\sigma_{\xi}/Y$	σ_{π^0}	$-\sigma_{\pi^0}$	$+\sigma_{total}/Y$	$-\sigma_{total}/Y$
0.5–1.0	1.35614	0.50059	0.15482	-0.15482	1.54849	-1.54849	1.55085	-1.55085	1.06765	-1.06766	0.05075	-0.05075	2.44323	-2.44323
1.0–2.0	0.49558	0.43714	0.00000	-0.00000	0.01519	-0.00807	0.00000	-0.00000	0.01630	-0.01631	0.00707	-0.00707	0.02338	-0.01952
2.0–3.0	0.27204	0.24646	0.00000	-0.00000	0.00418	-0.00214	0.00000	-0.00000	0.00224	-0.00224	0.01115	-0.01115	0.01211	-0.01157
3.0–5.0	0.03488	0.32152	0.00000	-0.00000	0.00230	-0.00119	0.00000	-0.00000	0.00108	-0.00108	0.00803	-0.00803	0.00842	-0.00819
5.0–7.0	0.01311	0.48361	0.00000	-0.00000	0.00033	-0.00031	0.00000	-0.00000	0.00048	-0.00060	0.00342	-0.00342	0.00347	-0.00349

Table 56: Away side yield, 20–40%

assoc p_T (GeV/c)	yield	σ_{stat}/Y	systematic error											
			$+\sigma_{f2}/Y$	$-\sigma_{f2}/Y$	$+\sigma_{f3}/Y$	$-\sigma_{f3}/Y$	$+\sigma_{f4}/Y$	$-\sigma_{f4}/Y$	$+\sigma_{\xi/ZYAM}/Y$	$-\sigma_{\xi}/Y$	σ_{π^0}	$-\sigma_{\pi^0}$	$+\sigma_{total}/Y$	$-\sigma_{total}/Y$
trig p_T 4–5 GeV/c														
0.5–1.0	0.55615	0.05467	0.04887	-0.04467	0.03675	-0.03992	0.00909	-0.00260	0.11049	-0.11048	0.04024	-0.04024	0.13285	-0.13199
1.0–2.0	0.16868	0.05701	0.00000	-0.00000	0.01014	-0.01100	0.00000	-0.00000	0.13547	-0.13549	0.01248	-0.01248	0.13643	-0.13651
2.0–3.0	0.02853	0.09778	0.00000	-0.00000	0.00725	-0.00783	0.00000	-0.00000	0.07076	-0.07076	0.02424	-0.02424	0.07515	-0.07521
3.0–5.0	0.00372	0.13431	0.00000	-0.00000	0.00379	-0.00409	0.00000	-0.00000	0.03050	-0.03092	0.00157	-0.00157	0.03077	-0.03123
5.0–7.0	0.00049	0.41080	0.00000	-0.00000	0.00540	-0.00600	0.00000	-0.00000	0.02584	-0.02584	0.22121	-0.22121	0.22278	-0.22279
trig p_T 5–7 GeV/c														
0.5–1.0	0.65366	0.05952	0.01959	-0.01585	0.02406	-0.02603	0.00677	-0.00879	0.09170	-0.09170	0.01214	-0.01214	0.09780	-0.09778
1.0–2.0	0.21210	0.05813	0.00000	-0.00000	0.00680	-0.00754	0.00000	-0.00000	0.09989	-0.09989	0.00241	-0.00241	0.10015	-0.10020
2.0–3.0	0.03794	0.09456	0.00000	-0.00000	0.00470	-0.00517	0.00000	-0.00000	0.04953	-0.04953	0.01228	-0.01228	0.05124	-0.05129
3.0–5.0	0.00518	0.12233	0.00000	-0.00000	0.00234	-0.00258	0.00000	-0.00000	0.02065	-0.02035	0.00671	-0.00671	0.02184	-0.02158
5.0–7.0	0.00190	0.16660	0.00000	-0.00000	0.00106	-0.00121	0.00000	-0.00000	0.00663	-0.00580	0.00487	-0.00487	0.00829	-0.00767
trig p_T 7–9 GeV/c														
0.5–1.0	0.80212	0.13349	0.01849	-0.01910	0.01287	-0.01708	0.00507	-0.00806	0.16745	-0.16745	0.02212	-0.02212	0.17048	-0.17103
1.0–2.0	0.24301	0.13934	0.00000	-0.00000	0.00587	-0.00781	0.00000	-0.00000	0.08385	-0.08385	0.00281	-0.00281	0.08410	-0.08426
2.0–3.0	0.08604	0.11755	0.00000	-0.00000	0.00216	-0.00286	0.00000	-0.00000	0.02099	-0.02099	0.00267	-0.00267	0.02127	-0.02135
3.0–5.0	0.01335	0.13791	0.00000	-0.00000	0.00094	-0.00125	0.00000	-0.00000	0.00766	-0.00754	0.00845	-0.00845	0.01144	-0.01139
5.0–7.0	0.00513	0.18769	0.00000	-0.00000	0.00028	-0.00039	0.00000	-0.00000	0.00215	-0.00245	0.01628	-0.01628	0.01643	-0.01647
trig p_T 9–12 GeV/c														
0.5–1.0	1.98571	0.10405	0.17089	-0.12871	0.03266	-0.05082	0.01544	-0.01467	0.60106	-0.60106	0.00434	-0.00434	0.62594	-0.61697
1.0–2.0	0.31056	0.21128	0.00000	-0.00000	0.00795	-0.00704	0.00000	-0.00000	0.07311	-0.07310	0.00590	-0.00590	0.07377	-0.07367
2.0–3.0	0.06616	0.28849	0.00000	-0.00000	0.00514	-0.00436	0.00000	-0.00000	0.03038	-0.03033	0.00627	-0.00627	0.03144	-0.03128
3.0–5.0	0.02716	0.14487	0.00000	-0.00000	0.00085	-0.00072	0.00000	-0.00000	0.00423	-0.00417	0.00050	-0.00050	0.00434	-0.00426
5.0–7.0	0.01147	0.21548	0.00000	-0.00000	0.00013	-0.00018	0.00000	-0.00000	0.00110	-0.00110	0.00229	-0.00229	0.00254	-0.00254
trig p_T 12–15 GeV/c														
0.5–1.0	1.54411	0.33847	0.37310	-0.11862	0.01715	-0.10226	0.00871	-0.01554	1.18501	-1.18502	0.00237	-0.00237	1.24251	-1.19542
1.0–2.0	0.45703	0.36106	0.00000	-0.00000	0.00924	-0.00489	0.00000	-0.00000	0.04633	-0.04633	0.02533	-0.02533	0.05361	-0.05303
2.0–3.0	0.15642	0.32657	0.00000	-0.00000	0.00381	-0.00189	0.00000	-0.00000	0.01194	-0.01196	0.00742	-0.00742	0.01457	-0.01421
3.0–5.0	0.03835	0.25440	0.00000	-0.00000	0.00105	-0.00052	0.00000	-0.00000	0.00279	-0.00279	0.00698	-0.00698	0.00759	-0.00753
5.0–7.0	0.01800	0.38561	0.00000	-0.00000	0.00010	-0.00011	0.00000	-0.00000	0.00061	-0.00070	0.00950	-0.00950	0.00952	-0.00952

H Data Table: $I_{AA}(p_T)$

Table 57: 0–20%, Away side $I_{AA}(p_T)$

trig p_T 4–5 GeV/c															
assoc p_T (GeV/c)	$I_{AA}(p_T)$	σ_{stat}/I	systematic error												
			$+\sigma_{f2}/I$	$-\sigma_{f2}/I$	$+\sigma_{f3}/I$	$-\sigma_{f3}/I$	$+\sigma_{f4}/I$	$-\sigma_{f4}/I$	$+\sigma_{\xi/ZYAM}/I$	$-\sigma_{\xi}/I$	σ_{π^0}	$-\sigma_{\pi^0}$	$+\sigma_{pp}/I$	$-\sigma_{pp}/I$	$+\sigma_{total}/I$	$-\sigma_{total}/I$
0.5–1.0	2.09628	0.05550	0.02264	-0.02122	0.02646	-0.02828	0.00596	-0.00662	0.09516	-0.09517	0.06056	-0.06056	1.23310	-0.03727	0.12394	-0.12506
1.0–2.0	1.02563	0.10214	0.00000	-0.00000	0.01457	-0.01555	0.00000	-0.00000	0.07914	-0.07914	0.04080	-0.04080	1.57145	-0.03620	0.09721	-0.09845
2.0–3.0	0.54710	0.21245	0.00000	-0.00000	0.01420	-0.01507	0.00000	-0.00000	0.04373	-0.04373	0.12763	-0.12763	1.61005	-0.04064	0.14162	-0.14278
3.0–5.0	0.29443	0.28480	0.00000	-0.00000	0.00791	-0.00840	0.00000	-0.00000	0.02149	-0.02075	0.22809	-0.22809	0.62219	-0.04874	0.23437	-0.23395
5.0–7.0	0.44576	0.48016	0.00000	-0.00000	0.00644	-0.00706	0.00000	-0.00000	0.01439	-0.01439	0.17621	-0.17621	2.76426	-0.07981	0.19409	-0.19049
trig p_T 5–7 GeV/c																
assoc p_T (GeV/c)	$I_{AA}(p_T)$	σ_{stat}/I	systematic error												
			$+\sigma_{f2}/I$	$-\sigma_{f2}/I$	$+\sigma_{f3}/I$	$-\sigma_{f3}/I$	$+\sigma_{f4}/I$	$-\sigma_{f4}/I$	$+\sigma_{\xi/ZYAM}/I$	$-\sigma_{\xi}/I$	σ_{π^0}	$-\sigma_{\pi^0}$	$+\sigma_{pp}/I$	$-\sigma_{pp}/I$	$+\sigma_{total}/I$	$-\sigma_{total}/I$
0.5–1.0	1.27957	0.09535	0.02102	-0.01747	0.02849	-0.03087	0.00838	-0.01074	0.11568	-0.11566	0.01164	-0.01164	1.31251	-0.03497	0.12675	-0.12767
1.0–2.0	0.95302	0.10535	0.00000	-0.00000	0.01477	-0.01649	0.00000	-0.00000	0.04787	-0.04785	0.02750	-0.02750	0.77473	-0.03289	0.06593	-0.06751
2.0–3.0	0.60537	0.15575	0.00000	-0.00000	0.01078	-0.01191	0.00000	-0.00000	0.01868	-0.01868	0.00737	-0.00737	0.58813	-0.03663	0.04314	-0.04590
3.0–5.0	0.16904	0.37016	0.00000	-0.00000	0.01062	-0.01177	0.00000	-0.00000	0.01660	-0.01588	0.20576	-0.20576	0.27325	-0.04661	0.21189	-0.21117
5.0–7.0	0.48212	0.27185	0.00000	-0.00000	0.00230	-0.00280	0.00000	-0.00000	0.00467	-0.00350	0.03614	-0.03614	0.47576	-0.07751	0.08568	-0.07436
trig p_T 7–9 GeV/c																
assoc p_T (GeV/c)	$I_{AA}(p_T)$	σ_{stat}/I	systematic error												
			$+\sigma_{f2}/I$	$-\sigma_{f2}/I$	$+\sigma_{f3}/I$	$-\sigma_{f3}/I$	$+\sigma_{f4}/I$	$-\sigma_{f4}/I$	$+\sigma_{\xi/ZYAM}/I$	$-\sigma_{\xi}/I$	σ_{π^0}	$-\sigma_{\pi^0}$	$+\sigma_{pp}/I$	$-\sigma_{pp}/I$	$+\sigma_{total}/I$	$-\sigma_{total}/I$
0.5–1.0	2.50730	0.11008	0.00005	-0.00099	0.02532	-0.02280	0.00454	-0.00538	0.18102	-0.18101	0.11716	-0.11716	1.42999	-0.05018	0.22287	-0.22395
1.0–2.0	0.68916	0.28405	0.00000	-0.00000	0.02201	-0.01951	0.00000	-0.00000	0.04455	-0.04453	0.00603	-0.00603	0.44678	-0.04453	0.06700	-0.06920
2.0–3.0	0.30594	0.47807	0.00000	-0.00000	0.01919	-0.01655	0.00000	-0.00000	0.01996	-0.01984	0.00566	-0.00566	0.26499	-0.04968	0.05716	-0.06118
3.0–5.0	0.42681	0.20621	0.00000	-0.00000	0.00319	-0.00277	0.00000	-0.00000	0.00289	-0.00289	0.05457	-0.05457	0.11545	-0.06069	0.08173	-0.08185
5.0–7.0	0.25463	0.57235	0.00000	-0.00000	0.00160	-0.00196	0.00000	-0.00000	0.00259	-0.00259	0.11150	-0.11150	0.14373	-0.10627	0.15406	-0.15422
trig p_T 9–12 GeV/c																
assoc p_T (GeV/c)	$I_{AA}(p_T)$	σ_{stat}/I	systematic error												
			$+\sigma_{f2}/I$	$-\sigma_{f2}/I$	$+\sigma_{f3}/I$	$-\sigma_{f3}/I$	$+\sigma_{f4}/I$	$-\sigma_{f4}/I$	$+\sigma_{\xi/ZYAM}/I$	$-\sigma_{\xi}/I$	σ_{π^0}	$-\sigma_{\pi^0}$	$+\sigma_{pp}/I$	$-\sigma_{pp}/I$	$+\sigma_{total}/I$	$-\sigma_{total}/I$
0.5–1.0	2.00404	0.20831	0.04694	-0.02658	0.02913	-0.02244	0.00486	-0.00546	0.29256	-0.29256	0.04323	-0.04323	1.60520	-0.06612	0.30807	-0.30742
1.0–2.0	0.77064	0.34925	0.00000	-0.00000	0.02028	-0.01567	0.00000	-0.00000	0.02933	-0.02932	0.03055	-0.03055	0.28242	-0.05548	0.07268	-0.07702
2.0–3.0	0.65118	0.35468	0.00000	-0.00000	0.01058	-0.00793	0.00000	-0.00000	0.00773	-0.00773	0.01790	-0.01790	0.20141	-0.06933	0.07279	-0.08320
3.0–5.0	0.39261	0.28599	0.00000	-0.00000	0.00332	-0.00251	0.00000	-0.00000	0.00215	-0.00215	0.03916	-0.03916	0.07256	-0.07503	0.08473	-0.08917
5.0–7.0	0.56547	0.38516	0.00000	-0.00000	0.00042	-0.00051	0.00000	-0.00000	0.00080	-0.00060	0.00997	-0.00997	0.06891	-0.15245	0.15278	-0.18750

Table 58: 20–40%, Away side $I_{AA}(p_T)$

trig p_T 4–5 GeV/c																
assoc p_T (GeV/c)	$I_{AA}(p_T)$	σ_{stat}/I	systematic error													
			$+\sigma_{f2}/I$	$-\sigma_{f2}/I$	$+\sigma_{f3}/I$	$-\sigma_{f3}/I$	$+\sigma_{f4}/I$	$-\sigma_{f4}/I$	$+\sigma_{\xi/ZYAM}/I$	$-\sigma_{\xi}/I$	σ_{π^0}	$-\sigma_{\pi^0}$	$+\sigma_{pp}/I$	$-\sigma_{pp}/I$	$+\sigma_{total}/I$	$-\sigma_{total}/I$
0.5–1.0	1.65356	0.05587	0.04887	-0.04467	0.03675	-0.03992	0.00909	-0.00260	0.11049	-0.11048	0.04024	-0.04024	1.23310	-0.03727	0.13798	-0.13800
1.0–2.0	1.45788	0.05790	0.00000	-0.00000	0.01014	-0.01100	0.00000	-0.00000	0.13547	-0.13549	0.01248	-0.01248	1.57145	-0.03620	0.14115	-0.14198
2.0–3.0	0.95948	0.09902	0.00000	-0.00000	0.00725	-0.00783	0.00000	-0.00000	0.07076	-0.07076	0.02424	-0.02424	1.61005	-0.04064	0.08544	-0.08726
3.0–5.0	0.51525	0.13578	0.00000	-0.00000	0.00379	-0.00409	0.00000	-0.00000	0.03050	-0.03092	0.00157	-0.00157	0.62219	-0.04874	0.05764	-0.05638
5.0–7.0	0.39721	0.41371	0.00000	-0.00000	0.00540	-0.00600	0.00000	-0.00000	0.02584	-0.02584	0.22121	-0.22121	2.76426	-0.07981	0.23664	-0.23370
trig p_T 5–7 GeV/c																
assoc p_T (GeV/c)	$I_{AA}(p_T)$	σ_{stat}/I	systematic error													
			$+\sigma_{f2}/I$	$-\sigma_{f2}/I$	$+\sigma_{f3}/I$	$-\sigma_{f3}/I$	$+\sigma_{f4}/I$	$-\sigma_{f4}/I$	$+\sigma_{\xi/ZYAM}/I$	$-\sigma_{\xi}/I$	σ_{π^0}	$-\sigma_{\pi^0}$	$+\sigma_{pp}/I$	$-\sigma_{pp}/I$	$+\sigma_{total}/I$	$-\sigma_{total}/I$
0.5–1.0	1.54300	0.06123	0.01959	-0.01585	0.02406	-0.02603	0.00677	-0.00879	0.09170	-0.09170	0.01214	-0.01214	1.31251	-0.03497	0.10386	-0.10476
1.0–2.0	1.30948	0.05931	0.00000	-0.00000	0.00680	-0.00754	0.00000	-0.00000	0.09989	-0.09989	0.00241	-0.00241	0.77473	-0.03289	0.10541	-0.10620
2.0–3.0	0.76605	0.09612	0.00000	-0.00000	0.00470	-0.00517	0.00000	-0.00000	0.04953	-0.04953	0.01228	-0.01228	0.58813	-0.03663	0.06299	-0.06475
3.0–5.0	0.40179	0.12445	0.00000	-0.00000	0.00234	-0.00258	0.00000	-0.00000	0.02065	-0.02035	0.00671	-0.00671	0.27325	-0.04661	0.05148	-0.04829
5.0–7.0	0.67947	0.17515	0.00000	-0.00000	0.00106	-0.00121	0.00000	-0.00000	0.00663	-0.00580	0.00487	-0.00487	0.47576	-0.07751	0.07795	-0.06528
trig p_T 7–9 GeV/c																
assoc p_T (GeV/c)	$I_{AA}(p_T)$	σ_{stat}/I	systematic error													
			$+\sigma_{f2}/I$	$-\sigma_{f2}/I$	$+\sigma_{f3}/I$	$-\sigma_{f3}/I$	$+\sigma_{f4}/I$	$-\sigma_{f4}/I$	$+\sigma_{\xi/ZYAM}/I$	$-\sigma_{\xi}/I$	σ_{π^0}	$-\sigma_{\pi^0}$	$+\sigma_{pp}/I$	$-\sigma_{pp}/I$	$+\sigma_{total}/I$	$-\sigma_{total}/I$
0.5–1.0	1.49927	0.13710	0.01849	-0.01910	0.01287	-0.01708	0.00507	-0.00806	0.16745	-0.16745	0.02212	-0.02212	1.42999	-0.05018	0.17771	-0.17989
1.0–2.0	1.06137	0.14153	0.00000	-0.00000	0.00587	-0.00781	0.00000	-0.00000	0.08385	-0.08385	0.00281	-0.00281	0.44678	-0.04453	0.09516	-0.09741
2.0–3.0	0.98264	0.12279	0.00000	-0.00000	0.00216	-0.00286	0.00000	-0.00000	0.02099	-0.02099	0.00267	-0.00267	0.26499	-0.04968	0.05404	-0.05915
3.0–5.0	0.49929	0.14633	0.00000	-0.00000	0.00094	-0.00125	0.00000	-0.00000	0.00766	-0.00754	0.00845	-0.00845	0.11545	-0.06069	0.06176	-0.06192
5.0–7.0	0.71539	0.22733	0.00000	-0.00000	0.00028	-0.00039	0.00000	-0.00000	0.00215	-0.00245	0.01628	-0.01628	0.14373	-0.10627	0.10753	-0.10777
trig p_T 9–12 GeV/c																
assoc p_T (GeV/c)	$I_{AA}(p_T)$	σ_{stat}/I	systematic error													
			$+\sigma_{f2}/I$	$-\sigma_{f2}/I$	$+\sigma_{f3}/I$	$-\sigma_{f3}/I$	$+\sigma_{f4}/I$	$-\sigma_{f4}/I$	$+\sigma_{\xi/ZYAM}/I$	$-\sigma_{\xi}/I$	σ_{π^0}	$-\sigma_{\pi^0}$	$+\sigma_{pp}/I$	$-\sigma_{pp}/I$	$+\sigma_{total}/I$	$-\sigma_{total}/I$
0.5–1.0	2.96016	0.11540	0.17089	-0.12871	0.03266	-0.05082	0.01544	-0.01467	0.60106	-0.60106	0.00434	-0.00434	1.60520	-0.06612	0.62942	-0.62165
1.0–2.0	0.96728	0.21499	0.00000	-0.00000	0.00795	-0.00704	0.00000	-0.00000	0.07311	-0.07310	0.00590	-0.00590	0.28242	-0.05548	0.09231	-0.09655
2.0–3.0	0.60476	0.29533	0.00000	-0.00000	0.00514	-0.00436	0.00000	-0.00000	0.03038	-0.03033	0.00627	-0.00627	0.20141	-0.06933	0.07613	-0.08635
3.0–5.0	0.66382	0.16521	0.00000	-0.00000	0.00085	-0.00072	0.00000	-0.00000	0.00423	-0.00417	0.00050	-0.00050	0.07256	-0.07503	0.07516	-0.08015
5.0–7.0	0.82135	0.34529	0.00000	-0.00000	0.00013	-0.00018	0.00000	-0.00000	0.00110	-0.00110	0.00229	-0.00229	0.06891	-0.15245	0.15247	-0.18725

I Data Table: I_{AA} vs. $\Delta\phi$

Table 59: 0–20%, trigger p_T 4.0–5.0 Away–side $I_{AA}(\Delta\phi)$

ϕ	$I_{AA}(\Delta\phi)$	σ_{stat}/I	systematic errors													
			$+\sigma_{f2}/I$	$-\sigma_{f2}/I$	$+\sigma_{f3}/I$	$-\sigma_{f3}/I$	$+\sigma_{f4}/I$	$-\sigma_{f4}/I$	$+\sigma_{\xi/ZYAM}/I$	$-\sigma_{\xi}/I$	$+\sigma_{\pi^0}/I$	$-\sigma_{\pi^0}/I$	$+\sigma_{pp}/I$	$-\sigma_{pp}/I$	$+\sigma_{total}/I$	$-\sigma_{total}/I$
associate p_T 0.5–1.0 GeV/c																
1.68	6.44369	0.60010	0.10243	-0.08799	0.10417	-0.09499	0.10051	-0.09206	0.19920	-0.19352	0.12203	-0.11249	0.08934	-0.07579	0.23258	-0.22884
1.88	4.53977	0.31373	0.05259	-0.04751	0.06615	-0.06536	0.05025	-0.04673	0.11762	-0.11594	0.06457	-0.06145	0.04832	-0.04406	0.13539	-0.13478
2.09	3.38932	0.19244	0.03532	-0.03303	0.05088	-0.05128	0.03546	-0.03320	0.08617	-0.08530	0.05612	-0.05476	0.03522	-0.03302	0.10347	-0.10362
2.30	2.63065	0.13595	0.03189	-0.02997	0.03991	-0.03999	0.03151	-0.02947	0.07017	-0.06950	0.05210	-0.05117	0.02962	-0.02796	0.08793	-0.08767
2.51	2.13174	0.10563	0.03399	-0.03264	0.03117	-0.03069	0.02748	-0.02600	0.06025	-0.05970	0.05048	-0.04980	0.02661	-0.02531	0.07892	-0.07851
2.72	1.75516	0.09210	0.03800	-0.03708	0.02623	-0.02529	0.02517	-0.02403	0.05606	-0.05555	0.04993	-0.04935	0.02509	-0.02393	0.07670	-0.07631
2.93	1.42480	0.09282	0.04405	-0.04348	0.02439	-0.02341	0.02666	-0.02640	0.05852	-0.05811	0.04925	-0.04877	0.02433	-0.02334	0.08202	-0.08193
3.14	1.49522	0.07959	0.04216	-0.04118	0.02467	-0.02289	0.02780	-0.02713	0.05280	-0.05199	0.04942	-0.04855	0.02466	-0.02288	0.07717	-0.07695
associate p_T 1.0–2.0 GeV/c																
1.68	-10.84137	1.35401	0.32248	-0.24108	0.27874	-0.18295	0.30531	-0.23226	0.31506	-0.23412	0.27761	-0.18060	0.27577	-0.17776	0.38346	-0.32646
1.88	1.51235	2.02074	0.30056	-0.29025	0.23702	-0.24725	0.12462	-0.12757	0.32994	-0.32714	0.10412	-0.09488	0.08344	-0.07158	0.50388	-0.50713
2.09	2.01688	0.34219	0.05214	-0.04984	0.06765	-0.06968	0.05104	-0.04636	0.07581	-0.07471	0.04687	-0.04507	0.03680	-0.03447	0.11148	-0.11112
2.30	2.41715	0.18079	0.03169	-0.02984	0.04068	-0.04042	0.05004	-0.04516	0.04885	-0.04768	0.04266	-0.04131	0.03139	-0.02954	0.07367	-0.07109
2.51	1.36635	0.14091	0.02859	-0.02748	0.02768	-0.02661	0.03979	-0.03612	0.04365	-0.04284	0.03918	-0.03828	0.02610	-0.02473	0.06230	-0.06018
2.72	0.88550	0.15239	0.03696	-0.03675	0.02669	-0.02533	0.02478	-0.02352	0.04560	-0.04497	0.03786	-0.03710	0.02442	-0.02323	0.06181	-0.06154
2.93	0.67734	0.14094	0.04458	-0.04489	0.03670	-0.03464	0.03348	-0.03527	0.04519	-0.04464	0.03779	-0.03712	0.02340	-0.02231	0.07573	-0.07641
3.14	0.72129	0.13002	0.04320	-0.04348	0.03844	-0.03629	0.03903	-0.04212	0.04111	-0.04054	0.03702	-0.03638	0.02319	-0.02216	0.07600	-0.07736
associate p_T 2.0–3.0 GeV/c																
1.68	10.26994	3.33597	0.40460	-1.29817	0.36266	-1.28657	0.39066	-1.29711	0.37183	-1.28909	0.38444	-1.29278	0.36000	-1.28572	0.46420	-1.32048
1.88	-2.52834	2.62824	0.30362	-0.24237	0.27789	-0.21950	0.24846	-0.17696	0.26594	-0.19807	0.34686	-0.29803	0.24053	-0.16236	0.43675	-0.40105
2.09	1.86754	0.77388	0.07766	-0.07036	0.08895	-0.08570	0.07755	-0.06853	0.07754	-0.07084	0.11780	-0.11350	0.06733	-0.05948	0.14735	-0.14401
2.30	1.74021	0.32692	0.04150	-0.03828	0.04727	-0.04523	0.05531	-0.05010	0.04541	-0.04250	0.10090	-0.09962	0.04131	-0.03809	0.11150	-0.10931
2.51	0.30501	0.85451	0.04568	-0.04518	0.04041	-0.04007	0.09517	-0.08477	0.06399	-0.06310	0.10932	-0.10881	0.03096	-0.02909	0.15808	-0.15254
2.72	0.68140	0.20512	0.03225	-0.03169	0.02718	-0.02601	0.02641	-0.02527	0.02998	-0.02901	0.09696	-0.09667	0.02624	-0.02513	0.10012	-0.09990
2.93	0.38166	0.25411	0.04028	-0.04036	0.03378	-0.03203	0.03242	-0.03348	0.03052	-0.02961	0.09552	-0.09523	0.02453	-0.02338	0.10707	-0.10740
3.14	0.44404	0.17608	0.03401	-0.03363	0.03105	-0.02930	0.03241	-0.03352	0.02695	-0.02579	0.09333	-0.09301	0.02381	-0.02249	0.10169	-0.10201
associate p_T 3.0–5.0 GeV/c																
1.68	-38.48538	6.37514	0.67500	-1.94373	0.67356	-1.94326	0.67477	-1.94381	0.67378	-1.94333	0.69270	-1.94998	0.67348	-1.94323	0.69582	-1.95117
1.88	8.76926	2.90991	0.45578	-4.45722	0.45363	-4.45706	0.45159	-4.45684	0.45231	-4.45688	0.69092	-4.48739	0.45089	-4.45675	0.69727	-4.48839
2.09	-0.10383	9.66121	0.21734	-0.20927	0.31408	-0.33155	0.23980	-0.21282	0.19314	-0.18526	1.83652	-1.83629	0.07473	-0.06895	1.89503	-1.89375
2.30	1.00181	0.47476	0.04930	-0.04904	0.05121	-0.05121	0.05542	-0.05388	0.05028	-0.04996	0.17851	-0.17844	0.04924	-0.04898	0.18116	-0.18075
2.51	0.47544	0.53674	0.03808	-0.03966	0.03769	-0.03929	0.04529	-0.04495	0.03919	-0.04053	0.16561	-0.16597	0.03710	-0.03865	0.16846	-0.16837
2.72	0.24415	0.44588	0.03315	-0.03584	0.02898	-0.03162	0.02839	-0.03113	0.03060	-0.03305	0.18630	-0.18674	0.02822	-0.03100	0.18763	-0.18807
2.93	0.16111	0.38907	0.03186	-0.03469	0.02870	-0.03098	0.02891	-0.03255	0.02667	-0.02941	0.16795	-0.16842	0.02469	-0.02776	0.17074	-0.17139
3.14	0.29370	0.16989	0.02524	-0.02905	0.02463	-0.02829	0.02531	-0.02946	0.02375	-0.02763	0.16297	-0.16358	0.02334	-0.02731	0.16379	-0.16448
associate p_T 5.0–7.0 GeV/c																
1.68	-7.57509	2.33063	0.31429	-0.80955	0.31407	-0.80948	0.31469	-0.80981	0.31417	-0.80952	0.50797	-0.90258	0.31400	-0.80945	0.50874	-0.90309
1.88	-10.45127	1.70442	0.33852	-0.98803	0.33870	-0.98812	0.33844	-0.98802	0.33850	-0.98803	0.38545	-1.00508	0.33839	-0.98800	0.38596	-1.00531
2.09	-90.75068	4.95809	1.86305	-0.68493	1.86306	-0.68498	1.86305	-0.68494	1.86305	-0.68494	1.86735	-0.69654	1.86305	-0.68492	1.86738	-0.69662
2.30	1.69010	1.05397	0.11982	-0.10853	0.12071	-0.10971	0.12172	-0.11007	0.12014	-0.10888	0.17403	-0.16646	0.11982	-0.10853	0.17618	-0.16847
2.51	0.61758	1.68417	0.08466	-0.08507	0.08505	-0.08557	0.09041	-0.08925	0.08593	-0.08632	0.15433	-0.15455	0.08444	-0.08483	0.15893	-0.15835
2.72	0.54371	0.56462	0.04007	-0.05067	0.03998	-0.05055	0.03981	-0.05044	0.04019	-0.05074	0.13357	-0.13711	0.03978	-0.05042	0.13384	-0.13737
2.93	0.30835	0.44245	0.02898	-0.04112	0.02962	-0.04142	0.02922	-0.04142	0.02889	-0.04103	0.12814	-0.13141	0.02857	-0.04080	0.12869	-0.13197
3.14	0.45152	0.28556	0.02786	-0.04017	0.02831	-0.04040	0.02824	-0.04057	0.02779	-0.04011	0.12764	-0.13087	0.02767	-0.04002	0.12798	-0.13123

Table 60: 0–20%, trigger p_T 5.0–7.0 Away–side $I_{AA}(\Delta\phi)$

ϕ	$I_{AA}(\Delta\phi)$	σ_{stat}/I	systematic errors													
			$+\sigma_{f2}/I$	$-\sigma_{f2}/I$	$+\sigma_{f3}/I$	$-\sigma_{f3}/I$	$+\sigma_{f4}/I$	$-\sigma_{f4}/I$	$+\sigma_{\xi/ZYAM}/I$	$-\sigma_{\xi}/I$	$+\sigma_{\pi^0}/I$	$-\sigma_{\pi^0}/I$	$+\sigma_{pp}/I$	$-\sigma_{pp}/I$	$+\sigma_{total}/I$	$-\sigma_{total}/I$
associate p_T 0.5–1.0 GeV/c																
1.68	-4.27037	1.07017	0.19820	-0.17123	0.13646	-0.11966	0.13553	-0.12564	0.26378	-0.25391	0.12005	-0.09657	0.11976	-0.09622	0.32077	-0.31015
1.88	2.26194	0.60651	0.09484	-0.08435	0.08456	-0.08774	0.05400	-0.05268	0.16072	-0.15936	0.05055	-0.04616	0.04963	-0.04515	0.19389	-0.19226
2.09	2.40768	0.38136	0.05145	-0.04554	0.07065	-0.07354	0.04223	-0.03877	0.11867	-0.11750	0.04296	-0.03968	0.04195	-0.03857	0.13533	-0.13570
2.30	1.34770	0.29300	0.03049	-0.02810	0.05256	-0.05547	0.03363	-0.03057	0.10236	-0.10192	0.03030	-0.02885	0.02892	-0.02740	0.11345	-0.11409
2.51	1.82243	0.13262	0.03190	-0.03045	0.02790	-0.02748	0.02533	-0.02392	0.05349	-0.05296	0.02593	-0.02484	0.02459	-0.02343	0.05961	-0.05899
2.72	1.21435	0.13668	0.04370	-0.04301	0.02275	-0.02180	0.02262	-0.02176	0.05709	-0.05670	0.02393	-0.02303	0.02246	-0.02150	0.06893	-0.06852
2.93	1.09520	0.12127	0.04928	-0.04901	0.02231	-0.02096	0.02398	-0.02441	0.05336	-0.05290	0.02309	-0.02202	0.02154	-0.02039	0.07089	-0.07112
3.14	0.90974	0.12773	0.05589	-0.05599	0.02342	-0.02204	0.02602	-0.02802	0.05705	-0.05672	0.02267	-0.02187	0.02112	-0.02026	0.07958	-0.08036
associate p_T 1.0–2.0 GeV/c																
ϕ	$I_{AA}(\Delta\phi)$	σ_{stat}/I	systematic errors													
			$+\sigma_{f2}/I$	$-\sigma_{f2}/I$	$+\sigma_{f3}/I$	$-\sigma_{f3}/I$	$+\sigma_{f4}/I$	$-\sigma_{f4}/I$	$+\sigma_{\xi/ZYAM}/I$	$-\sigma_{\xi}/I$	$+\sigma_{\pi^0}/I$	$-\sigma_{\pi^0}/I$	$+\sigma_{pp}/I$	$-\sigma_{pp}/I$	$+\sigma_{total}/I$	$-\sigma_{total}/I$
1.68	-52.36984	11.67527	0.89421	-1.63210	0.74273	-1.56091	0.77091	-1.58379	0.76845	-1.57254	0.74615	-1.56178	0.73622	-1.55706	0.96164	-1.68014
1.88	11.54912	0.64856	0.17712	-0.14294	0.16513	-0.13191	0.15821	-0.12121	0.16317	-0.12708	0.15874	-0.12134	0.15750	-0.11973	0.19042	-0.16143
2.09	3.73156	0.27697	0.05731	-0.05340	0.06243	-0.06330	0.05014	-0.04466	0.05431	-0.05103	0.04946	-0.04583	0.04532	-0.04133	0.08292	-0.08200
2.30	1.16768	0.36263	0.03186	-0.03004	0.06017	-0.06473	0.06977	-0.05714	0.05412	-0.05314	0.03590	-0.03443	0.02989	-0.02810	0.10074	-0.09597
2.51	0.96518	0.20821	0.03199	-0.03177	0.02746	-0.02740	0.04261	-0.03603	0.03883	-0.03819	0.03104	-0.03025	0.02392	-0.02289	0.06145	-0.05777
2.72	0.71312	0.17684	0.04489	-0.04582	0.02486	-0.02343	0.02158	-0.02059	0.03385	-0.03331	0.02889	-0.02826	0.02122	-0.02036	0.05726	-0.05764
2.93	0.65225	0.12976	0.04713	-0.04828	0.03343	-0.03074	0.02537	-0.02760	0.02889	-0.02836	0.02787	-0.02732	0.01996	-0.01919	0.06325	-0.06415
3.14	0.46421	0.16934	0.06179	-0.06349	0.04600	-0.04156	0.03539	-0.04151	0.03286	-0.03211	0.02780	-0.02692	0.01987	-0.01862	0.08637	-0.08860
associate p_T 2.0–3.0 GeV/c																
ϕ	$I_{AA}(\Delta\phi)$	σ_{stat}/I	systematic errors													
			$+\sigma_{f2}/I$	$-\sigma_{f2}/I$	$+\sigma_{f3}/I$	$-\sigma_{f3}/I$	$+\sigma_{f4}/I$	$-\sigma_{f4}/I$	$+\sigma_{\xi/ZYAM}/I$	$-\sigma_{\xi}/I$	$+\sigma_{\pi^0}/I$	$-\sigma_{\pi^0}/I$	$+\sigma_{pp}/I$	$-\sigma_{pp}/I$	$+\sigma_{total}/I$	$-\sigma_{total}/I$
1.68	-748.66809	94.00685	0.97213	-1.04218	0.96603	-1.03705	0.96758	-1.03934	0.96616	-1.03710	0.96577	-1.03674	0.96575	-1.03673	0.97464	-1.04548
1.88	16.04957	1.59416	0.93606	-0.33284	0.93456	-0.32998	0.93349	-0.32639	0.93361	-0.32654	0.93338	-0.32589	0.93336	-0.32582	0.93765	-0.33822
2.09	3.18392	0.51539	0.08775	-0.07624	0.09127	-0.08263	0.08541	-0.07302	0.08418	-0.07257	0.08318	-0.07140	0.08298	-0.07117	0.09892	-0.08985
2.30	0.91283	0.53057	0.04089	-0.03781	0.05645	-0.05742	0.06496	-0.05546	0.04414	-0.04137	0.04055	-0.03751	0.04016	-0.03709	0.07887	-0.07361
2.51	0.68157	0.35445	0.03349	-0.03221	0.03146	-0.03016	0.04275	-0.03722	0.03237	-0.03067	0.03016	-0.02833	0.02942	-0.02754	0.04933	-0.04519
2.72	0.58407	0.20478	0.03185	-0.03177	0.02456	-0.02334	0.02346	-0.02237	0.02482	-0.02384	0.02390	-0.02289	0.02332	-0.02228	0.03434	-0.03408
2.93	0.29439	0.23778	0.04036	-0.04138	0.03131	-0.02920	0.02554	-0.02738	0.02281	-0.02223	0.02124	-0.02061	0.02051	-0.01986	0.05050	-0.05153
3.14	0.34267	0.17692	0.03474	-0.03526	0.02962	-0.02749	0.02627	-0.02842	0.02142	-0.02057	0.02075	-0.01987	0.02008	-0.01917	0.04528	-0.04642
associate p_T 3.0–5.0 GeV/c																
ϕ	$I_{AA}(\Delta\phi)$	σ_{stat}/I	systematic errors													
			$+\sigma_{f2}/I$	$-\sigma_{f2}/I$	$+\sigma_{f3}/I$	$-\sigma_{f3}/I$	$+\sigma_{f4}/I$	$-\sigma_{f4}/I$	$+\sigma_{\xi/ZYAM}/I$	$-\sigma_{\xi}/I$	$+\sigma_{\pi^0}/I$	$-\sigma_{\pi^0}/I$	$+\sigma_{pp}/I$	$-\sigma_{pp}/I$	$+\sigma_{total}/I$	$-\sigma_{total}/I$
1.68	1.05535	5.58550	0.29003	-0.43075	0.22692	-0.39571	0.25157	-0.41868	0.22751	-0.39538	0.74569	-0.81289	0.22333	-0.39320	0.77924	-0.84624
1.88	2.50570	2.40412	0.27492	-0.54837	0.26883	-0.54652	0.26402	-0.54376	0.26421	-0.54360	0.35249	-0.59160	0.26324	-0.54317	0.36664	-0.60035
2.09	-2.83764	1.09565	0.28142	-0.18454	0.28229	-0.18665	0.28112	-0.18386	0.28065	-0.18348	0.31799	-0.23670	0.28044	-0.18319	0.32126	-0.24116
2.30	0.73386	0.68769	0.06254	-0.06010	0.06589	-0.06438	0.06964	-0.06493	0.06303	-0.06057	0.24379	-0.24318	0.06241	-0.05998	0.24684	-0.24574
2.51	0.05717	4.07819	0.08356	-0.08787	0.06635	-0.07216	0.17327	-0.14204	0.07041	-0.06949	0.71481	-0.71492	0.03960	-0.04157	0.74232	-0.73630
2.72	0.22716	0.35677	0.02907	-0.03314	0.02544	-0.02950	0.02490	-0.02911	0.02543	-0.02954	0.16611	-0.16680	0.02482	-0.02906	0.16700	-0.16772
2.93	0.17451	0.24991	0.02507	-0.02909	0.02308	-0.02667	0.02206	-0.02667	0.02119	-0.02538	0.15111	-0.15176	0.02085	-0.02513	0.15229	-0.15303
3.14	0.21842	0.15601	0.02220	-0.02609	0.02146	-0.02507	0.02116	-0.02550	0.02021	-0.02422	0.14687	-0.14748	0.02008	-0.02412	0.14754	-0.14822
associate p_T 5.0–7.0 GeV/c																
ϕ	$I_{AA}(\Delta\phi)$	σ_{stat}/I	systematic errors													
			$+\sigma_{f2}/I$	$-\sigma_{f2}/I$	$+\sigma_{f3}/I$	$-\sigma_{f3}/I$	$+\sigma_{f4}/I$	$-\sigma_{f4}/I$	$+\sigma_{\xi/ZYAM}/I$	$-\sigma_{\xi}/I$	$+\sigma_{\pi^0}/I$	$-\sigma_{\pi^0}/I$	$+\sigma_{pp}/I$	$-\sigma_{pp}/I$	$+\sigma_{total}/I$	$-\sigma_{total}/I$
1.68	0.35496	10.97265	0.30793	-0.21035	0.30022	-0.20151	0.30661	-0.21906	0.30125	-0.20092	0.45052	-0.39133	0.29916	-0.19916	0.46336	-0.40950
1.88	-2.78484	1.75546	0.47693	-0.25401	0.47696	-0.25423	0.47682	-0.25387	0.47685	-0.25385	0.47848	-0.25695	0.47680	-0.25381	0.47883	-0.25768
2.09	20.34020	1.29529	3.43900	-0.44176	3.43901	-0.44179	3.43901	-0.44176	3.43900	-0.44175	3.43910	-0.44250	3.43900	-0.44175	3.43911	-0.44255
2.30	0.78767	1.34272	0.11905	-0.10938	0.11970	-0.11044	0.12048	-0.11023	0.11923	-0.10949	0.12752	-0.11855	0.11904	-0.10937	0.12967	-0.12043
2.51	0.81644	0.65388	0.06791	-0.07391	0.06793	-0.07393	0.06833	-0.07410	0.06797	-0.07392	0.07304	-0.07864	0.06788	-0.07387	0.07360	-0.07897
2.72	0.42294	0.48130	0.03765	-0.05015	0.03756	-0.05004	0.03749	-0.05001	0.03759	-0.05005	0.04543	-0.05621	0.03748	-0.05000	0.04573	-0.05642
2.93	0.30930	0.33156	0.02629	-0.04028	0.02641	-0.04027	0.02622	-0.04027	0.02617	-0.04016	0.03667	-0.04769	0.02611	-0.04014	0.03714	-0.04805
3.14	0.43654	0.18974	0.02318	-0.03756	0.02324	-0.03757	0.02319	-0.03760	0.02314	-0.03752	0.03446	-0.04540	0.02312	-0.03752	0.03464	-0.04554

Table 61: 0–20%, trigger p_T 7.0–9.0 Away–side $I_{AA}(\Delta\phi)$

ϕ	$I_{AA}(\Delta\phi)$	σ_{stat}/I	systematic errors													
			$+\sigma_{f2}/I$	$-\sigma_{f2}/I$	$+\sigma_{f3}/I$	$-\sigma_{f3}/I$	$+\sigma_{f4}/I$	$-\sigma_{f4}/I$	$+\sigma_{\xi/ZYAM}/I$	$-\sigma_{\xi}/I$	$+\sigma_{\pi^0}/I$	$-\sigma_{\pi^0}/I$	$+\sigma_{pp}/I$	$-\sigma_{pp}/I$	$+\sigma_{total}/I$	$-\sigma_{total}/I$
associate p_T 0.5–1.0 GeV/c																
1.68	321.87057	20.06902	1.28196	-0.82437	1.28088	-0.82092	1.28056	-0.82062	1.29943	-0.84970	1.28505	-0.82754	1.28044	-0.82036	1.30602	-0.86126
1.88	13.51583	0.59509	0.14719	-0.11819	0.14682	-0.11446	0.14430	-0.11193	0.19183	-0.16879	0.16685	-0.13976	0.14420	-0.11175	0.21333	-0.19409
2.09	4.18775	0.65225	0.09862	-0.09082	0.11028	-0.09474	0.09174	-0.07728	0.26753	-0.26292	0.13179	-0.12217	0.09173	-0.07728	0.29255	-0.28872
2.30	5.13186	0.22388	0.04901	-0.04480	0.05281	-0.04805	0.04905	-0.04471	0.10340	-0.10143	0.09664	-0.09454	0.04893	-0.04462	0.13436	-0.13257
2.51	2.33594	0.26537	0.04038	-0.03698	0.04275	-0.03943	0.03796	-0.03523	0.13646	-0.13574	0.09757	-0.09656	0.03781	-0.03512	0.16530	-0.16426
2.72	1.28352	0.27102	0.04569	-0.03952	0.03122	-0.02960	0.02962	-0.02827	0.14824	-0.14797	0.08959	-0.08913	0.02949	-0.02807	0.17454	-0.17298
2.93	1.55649	0.16759	0.04069	-0.03505	0.02691	-0.02537	0.02754	-0.02631	0.09636	-0.09594	0.08762	-0.08716	0.02691	-0.02537	0.13117	-0.12958
3.14	1.44513	0.15026	0.03993	-0.03434	0.02544	-0.02424	0.02636	-0.02558	0.08895	-0.08861	0.08665	-0.08630	0.02541	-0.02418	0.12560	-0.12402
associate p_T 1.0–2.0 GeV/c																
ϕ	$I_{AA}(\Delta\phi)$	σ_{stat}/I	systematic errors													
			$+\sigma_{f2}/I$	$-\sigma_{f2}/I$	$+\sigma_{f3}/I$	$-\sigma_{f3}/I$	$+\sigma_{f4}/I$	$-\sigma_{f4}/I$	$+\sigma_{\xi/ZYAM}/I$	$-\sigma_{\xi}/I$	$+\sigma_{\pi^0}/I$	$-\sigma_{\pi^0}/I$	$+\sigma_{pp}/I$	$-\sigma_{pp}/I$	$+\sigma_{total}/I$	$-\sigma_{total}/I$
1.68	4.75345	2.86160	0.33459	-0.49458	0.21357	-0.35416	0.22503	-0.36651	0.22054	-0.35933	0.20616	-0.35070	0.20612	-0.35068	0.35973	-0.51438
1.88	6.45535	2.03773	0.43842	-0.30744	0.42243	-0.24386	0.40941	-0.22641	0.41278	-0.23203	0.40892	-0.22510	0.40880	-0.22489	0.45540	-0.32780
2.09	2.86587	0.88030	0.11213	-0.11097	0.12337	-0.10590	0.09950	-0.08366	0.10203	-0.08763	0.09646	-0.08109	0.09635	-0.08097	0.14237	-0.13624
2.30	0.44776	2.19157	0.06102	-0.06419	0.18296	-0.16241	0.14609	-0.12488	0.10757	-0.10537	0.05098	-0.04623	0.05080	-0.04603	0.24978	-0.22551
2.51	0.96066	0.47157	0.04806	-0.04105	0.03874	-0.03582	0.04494	-0.04046	0.04222	-0.04031	0.03526	-0.03295	0.03493	-0.03260	0.06306	-0.05537
2.72	0.66671	0.36179	0.06165	-0.04915	0.02893	-0.02859	0.02667	-0.02555	0.03234	-0.03145	0.02689	-0.02583	0.02652	-0.02544	0.06561	-0.05435
2.93	0.31145	0.48551	0.11319	-0.08668	0.04999	-0.05468	0.03255	-0.03489	0.03582	-0.03524	0.02400	-0.02314	0.02353	-0.02265	0.12655	-0.10699
3.14	0.89061	0.16380	0.04444	-0.03618	0.02866	-0.02925	0.02529	-0.02526	0.02450	-0.02356	0.02338	-0.02239	0.02299	-0.02198	0.04969	-0.04389
associate p_T 2.0–3.0 GeV/c																
ϕ	$I_{AA}(\Delta\phi)$	σ_{stat}/I	systematic errors													
			$+\sigma_{f2}/I$	$-\sigma_{f2}/I$	$+\sigma_{f3}/I$	$-\sigma_{f3}/I$	$+\sigma_{f4}/I$	$-\sigma_{f4}/I$	$+\sigma_{\xi/ZYAM}/I$	$-\sigma_{\xi}/I$	$+\sigma_{\pi^0}/I$	$-\sigma_{\pi^0}/I$	$+\sigma_{pp}/I$	$-\sigma_{pp}/I$	$+\sigma_{total}/I$	$-\sigma_{total}/I$
1.68	1.64723	13.90088	0.71583	-3.28163	0.45471	-3.19909	0.50384	-3.20952	0.44409	-3.19837	0.43567	-3.19724	0.43244	-3.19680	0.78234	-3.29821
1.88	-9.19488	2.68032	2.87748	-0.43806	2.87705	-0.42922	2.87644	-0.42625	2.87645	-0.42628	2.87641	-0.42599	2.87640	-0.42594	2.87823	-0.44191
2.09	0.61436	12.09709	0.69494	-0.53826	0.81617	-0.55239	0.62597	-0.32252	0.60886	-0.29882	0.59653	-0.27316	0.59595	-0.27190	0.92024	-0.75305
2.30	-0.16774	6.36070	0.09574	-0.09369	0.29188	-0.25155	0.24685	-0.22224	0.11414	-0.10532	0.08475	-0.07291	0.08379	-0.07180	0.38395	-0.34239
2.51	0.37347	1.24087	0.06069	-0.05197	0.05272	-0.04735	0.06258	-0.05670	0.05040	-0.04616	0.04849	-0.04410	0.04764	-0.04317	0.07867	-0.06912
2.72	0.49652	0.41683	0.04294	-0.03706	0.03229	-0.03058	0.03158	-0.02954	0.03207	-0.03007	0.03178	-0.02977	0.03152	-0.02949	0.04413	-0.03863
2.93	0.43706	0.26549	0.03535	-0.03064	0.02751	-0.02731	0.02593	-0.02503	0.02528	-0.02415	0.02534	-0.02421	0.02501	-0.02386	0.03818	-0.03468
3.14	0.19639	0.34477	0.04229	-0.03509	0.02854	-0.03038	0.02538	-0.02589	0.02198	-0.02164	0.02178	-0.02145	0.02141	-0.02108	0.04868	-0.04446
associate p_T 3.0–5.0 GeV/c																
ϕ	$I_{AA}(\Delta\phi)$	σ_{stat}/I	systematic errors													
			$+\sigma_{f2}/I$	$-\sigma_{f2}/I$	$+\sigma_{f3}/I$	$-\sigma_{f3}/I$	$+\sigma_{f4}/I$	$-\sigma_{f4}/I$	$+\sigma_{\xi/ZYAM}/I$	$-\sigma_{\xi}/I$	$+\sigma_{\pi^0}/I$	$-\sigma_{\pi^0}/I$	$+\sigma_{pp}/I$	$-\sigma_{pp}/I$	$+\sigma_{total}/I$	$-\sigma_{total}/I$
1.68	-5.59458	1.57115	0.67974	-0.29117	0.67957	-0.29051	0.67962	-0.29064	0.67957	-0.29050	0.68505	-0.30311	0.67956	-0.29049	0.68530	-0.30394
1.88	-4.52658	0.74562	0.19489	-0.30986	0.19480	-0.30965	0.19461	-0.30957	0.19461	-0.30957	0.20103	-0.31365	0.19460	-0.30956	0.20153	-0.31405
2.09	5.83780	4.42647	0.63711	-2.34474	0.63872	-2.34484	0.63655	-2.34440	0.63625	-2.34434	0.63769	-2.34473	0.63615	-2.34431	0.64170	-2.34580
2.30	0.92424	0.82421	0.11086	-0.09491	0.11169	-0.09561	0.11160	-0.09559	0.11089	-0.09493	0.11802	-0.10317	0.11084	-0.09487	0.11959	-0.10460
2.51	1.68653	0.32195	0.07499	-0.06965	0.07496	-0.06963	0.07503	-0.06970	0.07495	-0.06962	0.08443	-0.07974	0.07494	-0.06961	0.08459	-0.07987
2.72	0.50627	0.28166	0.03620	-0.03841	0.03560	-0.03810	0.03556	-0.03805	0.03558	-0.03806	0.05252	-0.05423	0.03556	-0.03804	0.05300	-0.05455
2.93	0.28928	0.22514	0.02613	-0.02936	0.02540	-0.02911	0.02527	-0.02895	0.02518	-0.02885	0.04880	-0.05079	0.02516	-0.02883	0.04949	-0.05132
3.14	0.25708	0.17423	0.02323	-0.02682	0.02273	-0.02669	0.02265	-0.02659	0.02251	-0.02644	0.04467	-0.04678	0.02250	-0.02643	0.04524	-0.04724
associate p_T 5.0–7.0 GeV/c																
ϕ	$I_{AA}(\Delta\phi)$	σ_{stat}/I	systematic errors													
			$+\sigma_{f2}/I$	$-\sigma_{f2}/I$	$+\sigma_{f3}/I$	$-\sigma_{f3}/I$	$+\sigma_{f4}/I$	$-\sigma_{f4}/I$	$+\sigma_{\xi/ZYAM}/I$	$-\sigma_{\xi}/I$	$+\sigma_{\pi^0}/I$	$-\sigma_{\pi^0}/I$	$+\sigma_{pp}/I$	$-\sigma_{pp}/I$	$+\sigma_{total}/I$	$-\sigma_{total}/I$
1.68	4.65511	2.23431	1.67601	-0.39211	1.67600	-0.39208	1.67600	-0.39210	1.67600	-0.39208	1.68017	-0.40953	1.67600	-0.39208	1.68018	-0.40957
2.09	-0.94133	5.20735	1.95715	-0.40426	1.95721	-0.40467	1.95715	-0.40412	1.95713	-0.40412	2.07609	-0.80194	1.95712	-0.40407	2.07623	-0.80238
2.30	-3.67487	0.92001	0.68576	-0.29720	0.68576	-0.29721	0.68576	-0.29721	0.68576	-0.29720	0.69057	-0.30815	0.68576	-0.29720	0.69058	-0.30817
2.51	0.84756	1.32884	0.22331	-0.16562	0.22330	-0.16562	0.22334	-0.16564	0.22330	-0.16562	0.24364	-0.19217	0.22330	-0.16561	0.24371	-0.19222
2.72	0.38150	0.77143	0.06714	-0.07357	0.06709	-0.07354	0.06708	-0.07353	0.06709	-0.07354	0.11203	-0.11601	0.06708	-0.07353	0.11208	-0.11605
2.93	0.35780	0.41729	0.03544	-0.04824	0.03542	-0.04823	0.03541	-0.04823	0.03541	-0.04823	0.09236	-0.09800	0.03540	-0.04822	0.09239	-0.09802
3.14	0.22488	0.35744	0.02664	-0.04049	0.02663	-0.04049	0.02661	-0.04049	0.02661	-0.04047	0.08321	-0.08862	0.02660	-0.04047	0.08323	-0.08864

Table 62: 0–20%, trigger p_T 9.0–12.0 Away–side $I_{AA}(\Delta\phi)$

ϕ	$I_{AA}(\Delta\phi)$	σ_{stat}/I	systematic errors													
associate p_T 0.5–1.0 GeV/c																
			$+\sigma_{f2}/I$	$-\sigma_{f2}/I$	$+\sigma_{f3}/I$	$-\sigma_{f3}/I$	$+\sigma_{f4}/I$	$-\sigma_{f4}/I$	$+\sigma_{\xi/ZYAM}/I$	$-\sigma_{\xi}/I$	$+\sigma_{\pi^0}/I$	$-\sigma_{\pi^0}/I$	$+\sigma_{pp}/I$	$-\sigma_{pp}/I$	$+\sigma_{total}/I$	$-\sigma_{total}/I$
1.68	-16.62250	8.32524	0.65068	-2.48513	0.64311	-2.47480	0.63099	-2.47370	1.44488	-2.79413	0.62750	-2.47249	0.62676	-2.47230	1.46467	-2.80909
1.88	87.81606	5.74039	3.15548	-0.59506	3.15562	-0.59505	3.15542	-0.59446	3.16239	-0.63038	3.15572	-0.59604	3.15541	-0.59442	3.16296	-0.63316
2.09	4.26097	0.66570	0.09739	-0.08147	0.10550	-0.08727	0.09727	-0.08137	0.23392	-0.22777	0.10197	-0.08693	0.09726	-0.08136	0.23949	-0.23202
2.30	2.16031	0.74023	0.07902	-0.06488	0.08582	-0.07245	0.07126	-0.06241	0.29522	-0.29325	0.07861	-0.07082	0.07075	-0.06198	0.30331	-0.29832
2.51	2.60210	0.28771	0.05338	-0.04369	0.04500	-0.04069	0.04321	-0.03954	0.12347	-0.12225	0.05360	-0.05070	0.04314	-0.03948	0.13197	-0.12809
2.72	0.69903	0.81079	0.15430	-0.09781	0.04202	-0.03824	0.03986	-0.03704	0.37378	-0.37349	0.06179	-0.05997	0.03961	-0.03670	0.40549	-0.38744
2.93	1.52514	0.26910	0.06954	-0.04873	0.03367	-0.03146	0.03408	-0.03200	0.12896	-0.12839	0.04552	-0.04387	0.03361	-0.03135	0.14600	-0.13736
3.14	1.08549	0.33035	0.08884	-0.05929	0.03257	-0.03121	0.03348	-0.03230	0.16252	-0.16219	0.04434	-0.04314	0.03211	-0.03043	0.18527	-0.17319
associate p_T 1.0–2.0 GeV/c																
			systematic errors													
ϕ	$I_{AA}(\Delta\phi)$	σ_{stat}/I	$+\sigma_{f2}/I$	$-\sigma_{f2}/I$	$+\sigma_{f3}/I$	$-\sigma_{f3}/I$	$+\sigma_{f4}/I$	$-\sigma_{f4}/I$	$+\sigma_{\xi/ZYAM}/I$	$-\sigma_{\xi}/I$	$+\sigma_{\pi^0}/I$	$-\sigma_{\pi^0}/I$	$+\sigma_{pp}/I$	$-\sigma_{pp}/I$	$+\sigma_{total}/I$	$-\sigma_{total}/I$
1.68	-5.44622	4.75938	1.35331	-0.59196	1.32432	-0.36674	1.32575	-0.37744	1.32433	-0.36923	1.35095	-0.45557	1.32262	-0.36307	1.38725	-0.66631
1.88	5.54219	1.63738	0.30492	-0.23395	0.29910	-0.19126	0.29211	-0.18495	0.29296	-0.18618	0.29388	-0.18762	0.29189	-0.18449	0.31489	-0.24339
2.09	2.02944	2.36105	0.22805	-0.22626	0.25628	-0.18883	0.20552	-0.14822	0.20729	-0.15192	0.20248	-0.14530	0.20132	-0.14368	0.28594	-0.26539
2.30	1.23070	1.38406	0.08440	-0.07522	0.11719	-0.09579	0.09808	-0.08488	0.08905	-0.07822	0.08975	-0.07902	0.08316	-0.07145	0.13711	-0.11824
2.51	0.66610	0.99594	0.07498	-0.05582	0.05362	-0.04735	0.05904	-0.05333	0.05377	-0.05045	0.05527	-0.05205	0.04651	-0.04262	0.09632	-0.07867
2.72	0.85568	0.37833	0.05761	-0.04201	0.03251	-0.03153	0.03161	-0.02991	0.03318	-0.03157	0.03996	-0.03864	0.03156	-0.02987	0.06394	-0.05074
2.93	0.81733	0.27857	0.05886	-0.04134	0.03248	-0.03373	0.02933	-0.02806	0.02937	-0.02779	0.03579	-0.03450	0.02825	-0.02660	0.06580	-0.05260
3.14	0.24677	0.70686	0.14470	-0.09060	0.05619	-0.06903	0.03932	-0.04153	0.03284	-0.03169	0.03368	-0.03256	0.02584	-0.02436	0.15870	-0.11995
associate p_T 2.0–3.0 GeV/c																
			systematic errors													
ϕ	$I_{AA}(\Delta\phi)$	σ_{stat}/I	$+\sigma_{f2}/I$	$-\sigma_{f2}/I$	$+\sigma_{f3}/I$	$-\sigma_{f3}/I$	$+\sigma_{f4}/I$	$-\sigma_{f4}/I$	$+\sigma_{\xi/ZYAM}/I$	$-\sigma_{\xi}/I$	$+\sigma_{\pi^0}/I$	$-\sigma_{\pi^0}/I$	$+\sigma_{pp}/I$	$-\sigma_{pp}/I$	$+\sigma_{total}/I$	$-\sigma_{total}/I$
1.68	-7.22814	2.73804	0.37675	-1.45441	0.37226	-1.45125	0.37283	-1.45146	0.37198	-1.45122	0.37364	-1.45165	0.37188	-1.45120	0.37989	-1.45520
1.88	3.74349	1.14807	0.15974	-0.23356	0.15901	-0.22880	0.15657	-0.22789	0.15656	-0.22788	0.15828	-0.22907	0.15646	-0.22781	0.16418	-0.23588
2.09	4.89113	55.15962	1.30618	-1.83341	1.86878	-1.63272	1.03020	-1.17218	0.95934	-1.11796	0.92970	-1.09263	0.92482	-1.08848	2.15017	-2.25957
2.30	4.33689	0.88472	0.25886	-0.17059	0.25982	-0.17135	0.25929	-0.17114	0.25887	-0.17057	0.25929	-0.17120	0.25884	-0.17051	0.26078	-0.17279
2.51	1.58100	0.58313	0.08336	-0.07105	0.08262	-0.07077	0.08299	-0.07130	0.08238	-0.07066	0.08326	-0.07169	0.08230	-0.07056	0.08538	-0.07319
2.72	0.89267	0.41611	0.05099	-0.04416	0.04582	-0.04220	0.04563	-0.04182	0.04571	-0.04191	0.04747	-0.04382	0.04562	-0.04180	0.05293	-0.04655
2.93	0.28052	0.48844	0.04792	-0.03604	0.03199	-0.03277	0.02993	-0.02827	0.02899	-0.02717	0.03243	-0.03081	0.02876	-0.02692	0.05290	-0.04428
3.14	0.56032	0.22225	0.03190	-0.02762	0.02769	-0.02713	0.02723	-0.02594	0.02679	-0.02543	0.02959	-0.02837	0.02674	-0.02539	0.03547	-0.03233
associate p_T 3.0–5.0 GeV/c																
			systematic errors													
ϕ	$I_{AA}(\Delta\phi)$	σ_{stat}/I	$+\sigma_{f2}/I$	$-\sigma_{f2}/I$	$+\sigma_{f3}/I$	$-\sigma_{f3}/I$	$+\sigma_{f4}/I$	$-\sigma_{f4}/I$	$+\sigma_{\xi/ZYAM}/I$	$-\sigma_{\xi}/I$	$+\sigma_{\pi^0}/I$	$-\sigma_{\pi^0}/I$	$+\sigma_{pp}/I$	$-\sigma_{pp}/I$	$+\sigma_{total}/I$	$-\sigma_{total}/I$
2.09	-6.46794	1.55377	2.04484	-0.40373	2.04487	-0.40370	2.04483	-0.40361	2.04483	-0.40360	2.04516	-0.40529	2.04483	-0.40359	2.04522	-0.40556
2.30	0.50207	2.44572	0.22021	-0.15656	0.22252	-0.15829	0.22158	-0.15819	0.22024	-0.15650	0.23537	-0.17718	0.22016	-0.15640	0.23900	-0.18063
2.51	0.40242	1.41136	0.10892	-0.09330	0.10844	-0.09312	0.10891	-0.09372	0.10823	-0.09301	0.11375	-0.09938	0.10818	-0.09295	0.11545	-0.10065
2.72	0.32990	0.51565	0.04507	-0.04529	0.04396	-0.04490	0.04391	-0.04482	0.04392	-0.04483	0.05373	-0.05447	0.04390	-0.04481	0.05475	-0.05495
2.93	0.60207	0.20983	0.03066	-0.03349	0.03047	-0.03346	0.03045	-0.03342	0.03044	-0.03340	0.04116	-0.04340	0.03044	-0.03340	0.04137	-0.04352
3.14	0.44142	0.17129	0.02546	-0.02878	0.02529	-0.02877	0.02528	-0.02873	0.02525	-0.02871	0.03748	-0.03989	0.02525	-0.02871	0.03767	-0.04001
associate p_T 5.0–7.0 GeV/c																
			systematic errors													
ϕ	$I_{AA}(\Delta\phi)$	σ_{stat}/I	$+\sigma_{f2}/I$	$-\sigma_{f2}/I$	$+\sigma_{f3}/I$	$-\sigma_{f3}/I$	$+\sigma_{f4}/I$	$-\sigma_{f4}/I$	$+\sigma_{\xi/ZYAM}/I$	$-\sigma_{\xi}/I$	$+\sigma_{\pi^0}/I$	$-\sigma_{\pi^0}/I$	$+\sigma_{pp}/I$	$-\sigma_{pp}/I$	$+\sigma_{total}/I$	$-\sigma_{total}/I$
1.88	-0.32879	4.22316	0.46013	-0.24950	0.46010	-0.24936	0.46007	-0.24927	0.46007	-0.24927	0.46095	-0.25088	0.46006	-0.24926	0.46106	-0.25125
2.09	3.46625	2.22668	9.32861	-0.53181	9.32861	-0.53182	9.32861	-0.53181	9.32861	-0.53181	9.32861	-0.53189	9.32861	-0.53181	9.32861	-0.53190
2.51	-0.71530	0.74870	0.26861	-0.18541	0.26861	-0.18541	0.26861	-0.18541	0.26861	-0.18540	0.26872	-0.18557	0.26861	-0.18540	0.26873	-0.18558
2.72	0.71749	0.71246	0.14232	-0.12300	0.14231	-0.12300	0.14231	-0.12300	0.14231	-0.12300	0.14253	-0.12326	0.14231	-0.12300	0.14254	-0.12326
2.93	1.28258	0.41295	0.07129	-0.07606	0.07129	-0.07606	0.07129	-0.07606	0.07129	-0.07606	0.07166	-0.07640	0.07129	-0.07606	0.07166	-0.07640
3.14	0.40793	0.40010	0.03079	-0.04358	0.03078	-0.04358	0.03078	-0.04358	0.03078	-0.04358	0.03158	-0.04415	0.03078	-0.04358	0.03158	-0.04415

Table 63: 20–40%, trigger p_T 4.0–5.0 Away–side $I_{AA}(\Delta\phi)$

ϕ	$I_{AA}(\Delta\phi)$	σ_{stat}/I	systematic errors													
			$+\sigma_{f2}/I$	$-\sigma_{f2}/I$	$+\sigma_{f3}/I$	$-\sigma_{f3}/I$	$+\sigma_{f4}/I$	$-\sigma_{f4}/I$	$+\sigma_{\xi/ZYAM}/I$	$-\sigma_{\xi}/I$	$+\sigma_{\pi^0}/I$	$-\sigma_{\pi^0}/I$	$+\sigma_{pp}/I$	$-\sigma_{pp}/I$	$+\sigma_{total}/I$	$-\sigma_{total}/I$
associate p_T 0.5–1.0 GeV/c																
1.68	3.86241	0.74077	0.10407	-0.08570	0.13099	-0.12873	0.12742	-0.12333	0.28218	-0.27816	0.09390	-0.08112	0.08934	-0.07579	0.31740	-0.31639
1.88	2.85081	0.38202	0.05039	-0.04460	0.08929	-0.09262	0.05066	-0.04529	0.16173	-0.16049	0.05816	-0.05467	0.04832	-0.04406	0.18242	-0.18330
2.09	3.00919	0.17364	0.03706	-0.03397	0.05555	-0.05711	0.04379	-0.03746	0.08782	-0.08695	0.04586	-0.04419	0.03522	-0.03302	0.10598	-0.10475
2.30	1.77014	0.15925	0.04424	-0.04062	0.05120	-0.05326	0.05602	-0.04477	0.09134	-0.09081	0.04146	-0.04030	0.02962	-0.02796	0.11946	-0.11504
2.51	1.48890	0.12113	0.05180	-0.04904	0.03674	-0.03739	0.04254	-0.03484	0.07603	-0.07558	0.03896	-0.03809	0.02661	-0.02531	0.10154	-0.09806
2.72	1.59702	0.08249	0.04934	-0.04742	0.02710	-0.02640	0.02597	-0.02415	0.05685	-0.05634	0.03806	-0.03731	0.02509	-0.02393	0.07750	-0.07619
2.93	1.30261	0.08287	0.05799	-0.05623	0.02468	-0.02378	0.02737	-0.02648	0.05935	-0.05894	0.03745	-0.03681	0.02433	-0.02334	0.08531	-0.08414
3.14	1.17954	0.08192	0.06147	-0.05943	0.02472	-0.02296	0.03155	-0.03121	0.06038	-0.05967	0.03766	-0.03651	0.02466	-0.02288	0.08953	-0.08850
associate p_T 1.0–2.0 GeV/c																
1.68	24.96403	0.92867	0.28863	-0.19646	0.27632	-0.17876	0.28563	-0.19967	0.31713	-0.23692	0.27604	-0.17818	0.27577	-0.17776	0.33737	-0.26816
1.88	7.60906	0.39179	0.10723	-0.09745	0.09414	-0.08580	0.08684	-0.07738	0.17246	-0.16706	0.08391	-0.07212	0.08344	-0.07158	0.19192	-0.18832
2.09	2.68776	0.20979	0.04911	-0.04700	0.05593	-0.05725	0.05231	-0.04597	0.12484	-0.12419	0.03791	-0.03566	0.03680	-0.03447	0.14100	-0.13979
2.30	2.41942	0.14690	0.03180	-0.02996	0.04047	-0.04051	0.06293	-0.05351	0.09594	-0.09536	0.03262	-0.03084	0.03139	-0.02954	0.11374	-0.10934
2.51	1.48589	0.10607	0.02903	-0.02791	0.02741	-0.02635	0.04667	-0.04017	0.08308	-0.08267	0.02756	-0.02627	0.02610	-0.02473	0.09332	-0.09036
2.72	1.09771	0.10121	0.03602	-0.03558	0.02593	-0.02458	0.02489	-0.02356	0.08078	-0.08043	0.02596	-0.02485	0.02442	-0.02323	0.08604	-0.08576
2.93	0.85246	0.09255	0.04266	-0.04262	0.03253	-0.03052	0.03415	-0.03771	0.08020	-0.07989	0.02502	-0.02401	0.02340	-0.02231	0.09440	-0.09559
3.14	0.81534	0.09503	0.04464	-0.04471	0.03581	-0.03351	0.04309	-0.04961	0.07869	-0.07840	0.02481	-0.02386	0.02319	-0.02216	0.09893	-0.10166
associate p_T 2.0–3.0 GeV/c																
1.68	-17.59724	2.44370	0.37925	-1.29104	0.36073	-1.28596	0.38213	-1.29523	0.38939	-1.29426	0.36190	-1.28626	0.36000	-1.28572	0.42915	-1.30970
1.88	5.51612	1.09958	0.25825	-0.18671	0.24722	-0.17368	0.24405	-0.17003	0.27985	-0.21638	0.24115	-0.16327	0.24053	-0.16236	0.30400	-0.24894
2.09	2.72400	0.44550	0.07346	-0.06609	0.07620	-0.07087	0.07898	-0.06840	0.09957	-0.09444	0.07045	-0.06299	0.06733	-0.05948	0.11910	-0.11315
2.30	1.03038	0.44213	0.04197	-0.03877	0.05399	-0.05347	0.10564	-0.08819	0.09891	-0.09761	0.04473	-0.04177	0.04131	-0.03809	0.14420	-0.13270
2.51	1.22416	0.18176	0.03235	-0.03061	0.03150	-0.02975	0.04680	-0.04087	0.05059	-0.04946	0.03557	-0.03395	0.03096	-0.02909	0.06495	-0.06089
2.72	0.99978	0.11976	0.02987	-0.02905	0.02661	-0.02546	0.02643	-0.02527	0.03892	-0.03819	0.03134	-0.03042	0.02624	-0.02513	0.04519	-0.04458
2.93	0.61407	0.13491	0.03308	-0.03254	0.02783	-0.02636	0.03107	-0.03302	0.04127	-0.04060	0.03001	-0.02908	0.02453	-0.02338	0.05506	-0.05614
3.14	0.61746	0.10889	0.03079	-0.03003	0.02715	-0.02554	0.03303	-0.03590	0.03585	-0.03499	0.02933	-0.02828	0.02381	-0.02249	0.05152	-0.05332
associate p_T 3.0–5.0 GeV/c																
1.68	-49.04481	6.26338	0.67425	-1.94349	0.67351	-1.94324	0.67481	-1.94392	0.67453	-1.94361	0.67348	-1.94323	0.67348	-1.94323	0.67667	-1.94457
1.88	-15.73847	2.19472	0.45214	-4.45687	0.45149	-4.45682	0.45125	-4.45680	0.45344	-4.45702	0.45089	-4.45675	0.45089	-4.45675	0.45564	-4.45726
2.09	1.36566	0.62988	0.07605	-0.07032	0.07723	-0.07208	0.07853	-0.07172	0.08168	-0.07662	0.07475	-0.06896	0.07473	-0.06895	0.08849	-0.08304
2.30	0.75045	0.51856	0.04933	-0.04906	0.05171	-0.05185	0.06821	-0.06242	0.05959	-0.05964	0.04926	-0.04899	0.04924	-0.04898	0.07770	-0.07316
2.51	0.83449	0.26608	0.03737	-0.03892	0.03723	-0.03880	0.04243	-0.04217	0.04125	-0.04276	0.03711	-0.03866	0.03710	-0.03865	0.04645	-0.04634
2.72	0.38914	0.24127	0.02995	-0.03265	0.02844	-0.03117	0.02835	-0.03108	0.03398	-0.03647	0.02824	-0.03102	0.02822	-0.03100	0.03573	-0.03810
2.93	0.30810	0.17975	0.02653	-0.02946	0.02554	-0.02841	0.02670	-0.03039	0.02818	-0.03098	0.02472	-0.02778	0.02469	-0.02776	0.03217	-0.03533
3.14	0.35199	0.12554	0.02448	-0.02832	0.02400	-0.02779	0.02561	-0.03017	0.02519	-0.02895	0.02337	-0.02733	0.02334	-0.02731	0.02885	-0.03297
associate p_T 5.0–7.0 GeV/c																
1.68	7.97840	1.73292	0.31416	-0.80951	0.31403	-0.80946	0.31442	-0.80972	0.31438	-0.80960	0.36366	-0.82997	0.31400	-0.80945	0.36453	-0.83046
1.88	12.30283	1.29087	0.33845	-0.98801	0.33852	-0.98805	0.33842	-0.98801	0.33858	-0.98806	0.37600	-1.00150	0.33839	-0.98800	0.37635	-1.00164
2.09	8.52028	6.73721	1.86317	-0.68525	1.86421	-0.68881	1.86367	-0.68596	1.86424	-0.68815	1.87517	-0.71724	1.86305	-0.68492	1.87825	-0.72531
2.30	1.29180	1.10333	0.11982	-0.10854	0.12067	-0.10969	0.12248	-0.11033	0.12119	-0.11004	0.24955	-0.24433	0.11982	-0.10853	0.25191	-0.24633
2.51	0.84673	1.02031	0.08451	-0.08491	0.08462	-0.08506	0.08710	-0.08645	0.08650	-0.08688	0.21640	-0.21655	0.08444	-0.08483	0.21836	-0.21812
2.72	0.30787	0.78335	0.04033	-0.05088	0.04014	-0.05065	0.03985	-0.05046	0.04305	-0.05304	0.16470	-0.16759	0.03978	-0.05042	0.16576	-0.16861
2.93	0.31980	0.37279	0.02881	-0.04098	0.02913	-0.04113	0.02898	-0.04128	0.02937	-0.04137	0.15907	-0.16172	0.02857	-0.04080	0.15944	-0.16211
3.14	0.84013	0.16714	0.02770	-0.04005	0.02777	-0.04008	0.02778	-0.04015	0.02777	-0.04009	0.15884	-0.16146	0.02767	-0.04002	0.15891	-0.16153

Table 64: 20–40%, trigger p_T 5.0–7.0 Away–side $I_{AA}(\Delta\phi)$

ϕ	$I_{AA}(\Delta\phi)$	σ_{stat}/I	systematic errors													
			$+\sigma_{f2}/I$	$-\sigma_{f2}/I$	$+\sigma_{f3}/I$	$-\sigma_{f3}/I$	$+\sigma_{f4}/I$	$-\sigma_{f4}/I$	$+\sigma_{\xi/ZYAM}/I$	$-\sigma_{\xi}/I$	$+\sigma_{\pi^0}/I$	$-\sigma_{\pi^0}/I$	$+\sigma_{pp}/I$	$-\sigma_{pp}/I$	$+\sigma_{total}/I$	$-\sigma_{total}/I$
associate p_T 0.5–1.0 GeV/c																
1.68	2.49968	1.32783	0.23018	-0.19953	0.16106	-0.15124	0.17575	-0.19057	0.39714	-0.39068	0.12008	-0.09661	0.11976	-0.09622	0.47389	-0.47322
1.88	3.04786	0.36012	0.06541	-0.05822	0.06539	-0.06473	0.05263	-0.05045	0.11818	-0.11636	0.05045	-0.04605	0.04963	-0.04515	0.13410	-0.13279
2.09	2.87576	0.25319	0.04478	-0.04020	0.05708	-0.05720	0.04266	-0.03907	0.09769	-0.09629	0.04282	-0.03952	0.04195	-0.03857	0.10687	-0.10628
2.30	1.69150	0.18196	0.03082	-0.02840	0.04129	-0.04220	0.03486	-0.03143	0.08006	-0.07952	0.03018	-0.02872	0.02892	-0.02740	0.08856	-0.08787
2.51	1.66572	0.11325	0.03236	-0.03034	0.02834	-0.02798	0.02648	-0.02469	0.05561	-0.05511	0.02606	-0.02497	0.02459	-0.02343	0.06249	-0.06146
2.72	1.22632	0.10588	0.04006	-0.03829	0.02363	-0.02287	0.02257	-0.02170	0.05493	-0.05454	0.02407	-0.02317	0.02246	-0.02150	0.06520	-0.06421
2.93	1.43195	0.07395	0.03671	-0.03529	0.02158	-0.02043	0.02352	-0.02372	0.04207	-0.04149	0.02321	-0.02215	0.02154	-0.02039	0.05311	-0.05268
3.14	0.99168	0.09194	0.04650	-0.04509	0.02113	-0.02027	0.02693	-0.02944	0.05163	-0.05129	0.02280	-0.02201	0.02112	-0.02026	0.06881	-0.06916
associate p_T 1.0–2.0 GeV/c																
1.68	-213.70418	11.39484	0.74297	-1.56012	0.73637	-1.55715	0.73830	-1.55864	0.75159	-1.56439	0.73622	-1.55706	0.73622	-1.55706	0.76038	-1.56910
1.88	12.21659	0.56255	0.16910	-0.13399	0.16027	-0.12417	0.15812	-0.12103	0.19406	-0.16488	0.15752	-0.11975	0.15750	-0.11973	0.20622	-0.17946
2.09	2.96219	0.26629	0.05757	-0.05397	0.05679	-0.05612	0.05260	-0.04640	0.11606	-0.11456	0.04536	-0.04137	0.04532	-0.04133	0.12891	-0.12735
2.30	2.09764	0.16147	0.03029	-0.02851	0.03509	-0.03472	0.04579	-0.03924	0.07778	-0.07710	0.02994	-0.02815	0.02989	-0.02810	0.08728	-0.08449
2.51	1.61512	0.09996	0.02606	-0.02521	0.02445	-0.02357	0.03171	-0.02818	0.05793	-0.05751	0.02398	-0.02295	0.02392	-0.02289	0.06265	-0.06103
2.72	0.87505	0.11356	0.03377	-0.03372	0.02223	-0.02122	0.02145	-0.02051	0.06608	-0.06581	0.02129	-0.02043	0.02122	-0.02036	0.07152	-0.07140
2.93	0.78091	0.08595	0.03526	-0.03539	0.02442	-0.02301	0.02378	-0.02523	0.05487	-0.05459	0.02003	-0.01927	0.01996	-0.01919	0.06499	-0.06555
3.14	0.86610	0.07311	0.03237	-0.03210	0.02429	-0.02248	0.02522	-0.02708	0.04572	-0.04518	0.01995	-0.01870	0.01987	-0.01862	0.05641	-0.05721
associate p_T 2.0–3.0 GeV/c																
1.68	-98.00385	94.29812	1.16994	-1.22047	0.97077	-1.04239	1.06986	-1.18938	1.18979	-1.24809	0.96580	-1.03678	0.96575	-1.03673	1.43994	-1.52452
1.88	18.55459	1.46235	0.93458	-0.32913	0.93363	-0.32677	0.93346	-0.32628	0.93538	-0.33155	0.93341	-0.32596	0.93336	-0.32582	0.93701	-0.33630
2.09	3.14208	0.42065	0.08597	-0.07447	0.08566	-0.07492	0.08566	-0.07312	0.09554	-0.08548	0.08347	-0.07173	0.08298	-0.07117	0.10303	-0.09325
2.30	0.57159	0.65363	0.04128	-0.03824	0.05324	-0.05346	0.09361	-0.07638	0.10569	-0.10456	0.04137	-0.03839	0.04016	-0.03709	0.14047	-0.13061
2.51	1.09692	0.18046	0.03046	-0.02870	0.02967	-0.02786	0.03557	-0.03174	0.04089	-0.03956	0.03070	-0.02890	0.02942	-0.02754	0.04717	-0.04443
2.72	0.65182	0.14851	0.02795	-0.02731	0.02363	-0.02254	0.02344	-0.02236	0.03496	-0.03427	0.02494	-0.02396	0.02332	-0.02228	0.03946	-0.03895
2.93	0.54654	0.10711	0.02531	-0.02501	0.02167	-0.02085	0.02213	-0.02248	0.02767	-0.02719	0.02228	-0.02168	0.02051	-0.01986	0.03434	-0.03461
3.14	0.59529	0.08662	0.02388	-0.02330	0.02123	-0.02017	0.02239	-0.02290	0.02498	-0.02425	0.02188	-0.02105	0.02008	-0.01917	0.03180	-0.03217
associate p_T 3.0–5.0 GeV/c																
1.68	5.31175	1.07771	0.22474	-0.39396	0.22337	-0.39323	0.22432	-0.39410	0.22469	-0.39395	0.22340	-0.39324	0.22333	-0.39320	0.22717	-0.39567
1.88	2.48287	1.89702	0.26885	-0.54579	0.26481	-0.54410	0.26391	-0.54369	0.27130	-0.54701	0.26329	-0.54320	0.26324	-0.54317	0.27891	-0.55105
2.09	1.69552	1.39216	0.28172	-0.18505	0.28186	-0.18582	0.28208	-0.18476	0.28536	-0.19042	0.28061	-0.18346	0.28044	-0.18319	0.28978	-0.19646
2.30	0.06364	5.96535	0.06979	-0.06730	0.14194	-0.15272	0.33689	-0.26880	0.30486	-0.30007	0.06299	-0.06058	0.06241	-0.05998	0.46887	-0.42359
2.51	0.71469	0.28243	0.03981	-0.04178	0.03966	-0.04164	0.04154	-0.04274	0.04197	-0.04376	0.03994	-0.04189	0.03960	-0.04157	0.04436	-0.04544
2.72	0.51291	0.14138	0.02526	-0.02946	0.02485	-0.02909	0.02483	-0.02907	0.02590	-0.02997	0.02527	-0.02945	0.02482	-0.02906	0.02680	-0.03075
2.93	0.37491	0.10726	0.02134	-0.02556	0.02099	-0.02522	0.02107	-0.02542	0.02152	-0.02567	0.02139	-0.02558	0.02085	-0.02513	0.02284	-0.02689
3.14	0.41361	0.07900	0.02038	-0.02438	0.02019	-0.02419	0.02034	-0.02446	0.02043	-0.02440	0.02063	-0.02458	0.02008	-0.02412	0.02161	-0.02551
associate p_T 5.0–7.0 GeV/c																
1.68	8.97749	0.92524	0.29916	-0.19917	0.29916	-0.19916	0.29916	-0.19918	0.29917	-0.19917	0.29918	-0.19920	0.29916	-0.19916	0.29921	-0.19924
1.88	1.65198	2.31417	0.47694	-0.25406	0.47699	-0.25426	0.47683	-0.25390	0.47729	-0.25450	0.47683	-0.25386	0.47680	-0.25381	0.47767	-0.25534
2.09	-0.27262	27.68389	3.44069	-0.45386	3.44768	-0.52335	3.44316	-0.45946	3.45435	-0.52549	3.44132	-0.45944	3.43900	-0.44175	3.47108	-0.63058
2.30	-0.01955	37.63343	0.12475	-0.11517	0.34856	-0.39175	0.56100	-0.42387	0.55835	-0.48969	0.14811	-0.14046	0.11904	-0.10937	0.85369	-0.74704
2.51	0.86636	0.52197	0.06789	-0.07389	0.06790	-0.07389	0.06809	-0.07398	0.06820	-0.07409	0.06799	-0.07397	0.06788	-0.07387	0.06854	-0.07433
2.72	0.55512	0.33056	0.03752	-0.05004	0.03750	-0.05001	0.03748	-0.05000	0.03773	-0.05014	0.03773	-0.05019	0.03748	-0.05000	0.03803	-0.05037
2.93	0.44361	0.22837	0.02614	-0.04016	0.02616	-0.04016	0.02614	-0.04017	0.02623	-0.04020	0.02633	-0.04028	0.02611	-0.04014	0.02658	-0.04043
3.14	0.61564	0.14771	0.02313	-0.03753	0.02314	-0.03753	0.02314	-0.03754	0.02315	-0.03753	0.02337	-0.03768	0.02312	-0.03752	0.02346	-0.03773

Table 65: 20–40%, trigger p_T 7.0–9.0 Away–side $I_{AA}(\Delta\phi)$

ϕ	$I_{AA}(\Delta\phi)$	σ_{stat}/I	systematic errors													
			$+\sigma_{f2}/I$	$-\sigma_{f2}/I$	$+\sigma_{f3}/I$	$-\sigma_{f3}/I$	$+\sigma_{f4}/I$	$-\sigma_{f4}/I$	$+\sigma_{\xi/ZYAM}/I$	$-\sigma_{\xi}/I$	$+\sigma_{\pi^0}/I$	$-\sigma_{\pi^0}/I$	$+\sigma_{pp}/I$	$-\sigma_{pp}/I$	$+\sigma_{total}/I$	$-\sigma_{total}/I$
associate p_T 0.5–1.0 GeV/c																
1.68	76.83758	20.16434	1.30348	-0.84242	1.28120	-0.82244	1.28175	-0.82545	1.37740	-0.96472	1.28195	-0.82272	1.28044	-0.82036	1.40212	-0.99149
1.88	6.04005	0.75947	0.15559	-0.12058	0.14579	-0.11532	0.14449	-0.11267	0.21191	-0.19131	0.14509	-0.11289	0.14420	-0.11175	0.22163	-0.19981
2.09	3.96332	0.54447	0.09574	-0.07983	0.09457	-0.08308	0.09180	-0.07731	0.17252	-0.16529	0.09337	-0.07922	0.09173	-0.07728	0.17708	-0.17018
2.30	1.48657	0.51408	0.04999	-0.04551	0.05444	-0.05471	0.05145	-0.04576	0.18049	-0.17937	0.05206	-0.04803	0.04893	-0.04462	0.18390	-0.18351
2.51	1.65921	0.28474	0.04635	-0.04656	0.03883	-0.03702	0.03842	-0.03538	0.10918	-0.10828	0.04096	-0.03849	0.03781	-0.03512	0.11407	-0.11430
2.72	1.40122	0.19470	0.04376	-0.04717	0.02954	-0.02817	0.02953	-0.02818	0.07977	-0.07926	0.03371	-0.03248	0.02949	-0.02807	0.08765	-0.08943
2.93	1.04141	0.19131	0.05053	-0.05657	0.02705	-0.02545	0.02779	-0.02765	0.08179	-0.08130	0.03116	-0.02983	0.02691	-0.02537	0.09392	-0.09766
3.14	0.80797	0.20367	0.05673	-0.06478	0.02592	-0.02449	0.02737	-0.02904	0.08894	-0.08860	0.02983	-0.02879	0.02541	-0.02418	0.10420	-0.10945
associate p_T 1.0–2.0 GeV/c																
1.68	0.72144	13.15899	1.98603	-1.65859	0.25566	-0.40440	0.45023	-0.71855	1.48653	-1.51336	0.20613	-0.35068	0.20612	-0.35068	2.50893	-2.31347
1.88	-0.64819	13.21235	1.84050	-1.48981	0.59692	-0.62131	0.43502	-0.32384	1.67646	-1.64133	0.40920	-0.22562	0.40880	-0.22489	2.49850	-2.29194
2.09	1.66411	1.12396	0.14800	-0.12270	0.11068	-0.10869	0.10365	-0.08455	0.19190	-0.18466	0.09640	-0.08102	0.09635	-0.08097	0.23212	-0.22013
2.30	2.24708	0.35425	0.05138	-0.04646	0.05280	-0.04985	0.05635	-0.04859	0.07462	-0.07146	0.05084	-0.04608	0.05080	-0.04603	0.08020	-0.07588
2.51	1.11386	0.31601	0.04029	-0.04077	0.03543	-0.03354	0.04117	-0.03544	0.06910	-0.06795	0.03499	-0.03266	0.03493	-0.03260	0.07545	-0.07400
2.72	1.04739	0.18297	0.03644	-0.03968	0.02691	-0.02566	0.02657	-0.02546	0.04356	-0.04291	0.02660	-0.02551	0.02652	-0.02544	0.05049	-0.05277
2.93	1.00039	0.12360	0.03384	-0.03730	0.02501	-0.02353	0.02400	-0.02382	0.03417	-0.03357	0.02362	-0.02274	0.02353	-0.02265	0.04309	-0.04586
3.14	0.69608	0.16286	0.04131	-0.04725	0.02666	-0.02421	0.02472	-0.02618	0.03942	-0.03883	0.02308	-0.02207	0.02299	-0.02198	0.05478	-0.05972
associate p_T 2.0–3.0 GeV/c																
1.68	-17.02795	2.56070	0.43655	-3.19717	0.43246	-3.19680	0.43272	-3.19689	0.43364	-3.19696	0.43244	-3.19680	0.43244	-3.19680	0.43806	-3.19744
1.88	-7.84908	2.52417	2.87814	-0.43377	2.87652	-0.42733	2.87642	-0.42628	2.87715	-0.43097	2.87640	-0.42595	2.87640	-0.42594	2.87902	-0.44038
2.09	13.46390	1.06533	0.59622	-0.27228	0.59603	-0.27217	0.59601	-0.27194	0.59626	-0.27256	0.59596	-0.27190	0.59595	-0.27190	0.59664	-0.27327
2.30	4.10439	0.29225	0.08382	-0.07182	0.08389	-0.07201	0.08422	-0.07201	0.08447	-0.07259	0.08381	-0.07183	0.08379	-0.07180	0.08504	-0.07304
2.51	0.77796	0.48093	0.04922	-0.04572	0.04781	-0.04348	0.05075	-0.04459	0.05467	-0.05082	0.04770	-0.04324	0.04764	-0.04317	0.05889	-0.05446
2.72	0.75280	0.23019	0.03416	-0.03357	0.03163	-0.02956	0.03154	-0.02950	0.03424	-0.03238	0.03158	-0.02956	0.03152	-0.02949	0.03684	-0.03624
2.93	0.80362	0.13075	0.02668	-0.02642	0.02525	-0.02401	0.02512	-0.02415	0.02596	-0.02486	0.02508	-0.02394	0.02501	-0.02386	0.02796	-0.02776
3.14	0.54015	0.11668	0.02326	-0.02380	0.02175	-0.02127	0.02164	-0.02164	0.02230	-0.02198	0.02150	-0.02116	0.02141	-0.02108	0.02465	-0.02532
associate p_T 3.0–5.0 GeV/c																
1.68	-0.09894	42.15858	1.12034	-0.78663	0.68414	-0.30876	0.73348	-0.52006	0.80587	-0.51602	0.69325	-0.32122	0.67956	-0.29049	1.24258	-1.00822
1.88	-1.22795	1.90917	0.19860	-0.31127	0.19492	-0.30991	0.19466	-0.30966	0.19601	-0.31042	0.19471	-0.30963	0.19460	-0.30956	0.20046	-0.31264
2.09	18.64047	3.28046	0.63624	-2.34433	0.63618	-2.34433	0.63617	-2.34432	0.63624	-2.34434	0.63618	-2.34432	0.63615	-2.34431	0.63642	-2.34438
2.30	0.31699	1.77544	0.11102	-0.09501	0.11170	-0.09661	0.11505	-0.09690	0.11478	-0.09930	0.11117	-0.09525	0.11084	-0.09487	0.12011	-0.10336
2.51	0.46054	0.75989	0.07524	-0.07010	0.07498	-0.06968	0.07577	-0.06998	0.07610	-0.07082	0.07572	-0.07045	0.07494	-0.06961	0.07801	-0.07254
2.72	0.46846	0.25658	0.03587	-0.03848	0.03557	-0.03805	0.03556	-0.03804	0.03582	-0.03828	0.03615	-0.03860	0.03556	-0.03804	0.03673	-0.03927
2.93	0.48188	0.14229	0.02531	-0.02902	0.02519	-0.02884	0.02518	-0.02886	0.02523	-0.02889	0.02586	-0.02944	0.02516	-0.02883	0.02611	-0.02973
3.14	0.62178	0.09932	0.02255	-0.02650	0.02251	-0.02644	0.02251	-0.02645	0.02252	-0.02645	0.02328	-0.02710	0.02250	-0.02643	0.02337	-0.02721
associate p_T 5.0–7.0 GeV/c																
2.09	8.97503	1.42479	1.95712	-0.40407	1.95712	-0.40407	1.95712	-0.40407	1.95712	-0.40407	1.95717	-0.40428	1.95712	-0.40407	1.95717	-0.40429
2.30	1.53671	1.62255	0.68576	-0.29720	0.68576	-0.29722	0.68577	-0.29721	0.68578	-0.29726	0.68590	-0.29752	0.68576	-0.29720	0.68594	-0.29762
2.51	2.77325	0.63452	0.22330	-0.16561	0.22330	-0.16561	0.22330	-0.16561	0.22330	-0.16562	0.22368	-0.16613	0.22330	-0.16561	0.22369	-0.16614
2.72	0.88797	0.43004	0.06708	-0.07354	0.06708	-0.07353	0.06708	-0.07353	0.06709	-0.07354	0.06806	-0.07443	0.06708	-0.07353	0.06808	-0.07445
2.93	0.60532	0.32977	0.03541	-0.04823	0.03540	-0.04822	0.03540	-0.04823	0.03541	-0.04823	0.03746	-0.04975	0.03540	-0.04822	0.03747	-0.04976
3.14	0.42956	0.26688	0.02661	-0.04048	0.02661	-0.04047	0.02660	-0.04047	0.02661	-0.04047	0.02899	-0.04208	0.02660	-0.04047	0.02900	-0.04209

Table 66: 20–40%, trigger p_T 9.0–12.0 Away–side $I_{AA}(\Delta\phi)$

ϕ	$I_{AA}(\Delta\phi)$	σ_{stat}/I	systematic errors													
			$+\sigma_{f2}/I$	$-\sigma_{f2}/I$	$+\sigma_{f3}/I$	$-\sigma_{f3}/I$	$+\sigma_{f4}/I$	$-\sigma_{f4}/I$	$+\sigma_{\xi/ZYAM}/I$	$-\sigma_{\xi}/I$	$+\sigma_{\pi^0}/I$	$-\sigma_{\pi^0}/I$	$+\sigma_{pp}/I$	$-\sigma_{pp}/I$	$+\sigma_{total}/I$	$-\sigma_{total}/I$
associate p_T 0.5–1.0 GeV/c																
1.68	-57.02176	7.01423	0.65058	-2.47674	0.62963	-2.47410	0.62687	-2.47235	1.30159	-2.72279	0.62677	-2.47231	0.62676	-2.47230	1.31467	-2.72850
1.88	158.07826	5.70666	3.15602	-0.59658	3.15545	-0.59496	3.15542	-0.59446	3.17488	-0.69034	3.15542	-0.59443	3.15541	-0.59442	3.17553	-0.69272
2.09	2.52380	0.80957	0.25531	-0.20294	0.10688	-0.11040	0.10397	-0.08783	1.08904	-1.08774	0.09732	-0.08143	0.09726	-0.08136	1.11582	-1.10653
2.30	7.33867	0.24712	0.09895	-0.08122	0.07165	-0.06471	0.07155	-0.06267	0.26536	-0.26316	0.07082	-0.06206	0.07075	-0.06198	0.27469	-0.26917
2.51	1.94493	0.29246	0.15911	-0.11987	0.04979	-0.05547	0.04685	-0.04264	0.47304	-0.47272	0.04325	-0.03960	0.04314	-0.03948	0.49818	-0.48792
2.72	1.84141	0.25247	0.16523	-0.12219	0.04808	-0.05497	0.04133	-0.03833	0.43275	-0.43249	0.03973	-0.03683	0.03961	-0.03670	0.46248	-0.44993
2.93	1.61008	0.20213	0.14969	-0.10958	0.04241	-0.04914	0.03404	-0.03190	0.36265	-0.36245	0.03375	-0.03150	0.03361	-0.03135	0.39179	-0.37930
3.14	1.95293	0.15392	0.11713	-0.08639	0.03800	-0.04235	0.03222	-0.03062	0.27324	-0.27305	0.03226	-0.03059	0.03211	-0.03043	0.29627	-0.28632
associate p_T 1.0–2.0 GeV/c																
1.68	-13.55737	2.48870	1.32897	-0.41776	1.32269	-0.36326	1.32287	-0.36461	1.32523	-0.37245	1.32264	-0.36311	1.32262	-0.36307	1.33188	-0.42745
1.88	0.62484	9.67188	0.92824	-1.41598	0.40774	-0.31250	0.30035	-0.20661	0.74540	-0.71016	0.29284	-0.18599	0.29189	-0.18449	1.19108	-1.59628
2.09	2.47399	1.52809	0.22435	-0.21338	0.21125	-0.15446	0.20318	-0.14518	0.23729	-0.19083	0.20155	-0.14399	0.20132	-0.14368	0.26654	-0.25503
2.30	2.71517	0.52588	0.08349	-0.07240	0.08518	-0.07329	0.08531	-0.07290	0.09459	-0.08447	0.08327	-0.07157	0.08316	-0.07145	0.09859	-0.08813
2.51	0.31674	1.60320	0.14380	-0.09545	0.05408	-0.04914	0.07733	-0.06346	0.18438	-0.18341	0.04684	-0.04299	0.04651	-0.04262	0.23900	-0.20922
2.72	1.12820	0.23368	0.05113	-0.03911	0.03174	-0.03011	0.03158	-0.02988	0.03999	-0.03866	0.03184	-0.03016	0.03156	-0.02987	0.05698	-0.04652
2.93	0.94269	0.19598	0.05678	-0.04078	0.02932	-0.02803	0.02865	-0.02733	0.03590	-0.03461	0.02856	-0.02693	0.02825	-0.02660	0.06177	-0.04784
3.14	1.00546	0.15079	0.04632	-0.03429	0.02674	-0.02558	0.02633	-0.02526	0.03029	-0.02905	0.02617	-0.02472	0.02584	-0.02436	0.04987	-0.03935
associate p_T 2.0–3.0 GeV/c																
1.68	10.47634	1.94928	0.37458	-1.45291	0.37192	-1.45120	0.37206	-1.45128	0.37247	-1.45135	0.37193	-1.45121	0.37188	-1.45120	0.37543	-1.45316
1.88	-0.30918	10.63004	0.44795	-0.69863	0.22001	-0.26286	0.16261	-0.23513	0.28481	-0.32918	0.16264	-0.23210	0.15646	-0.22781	0.53399	-0.75306
2.09	35.28559	30.82303	0.93502	-1.10985	0.93038	-1.09188	0.92617	-1.08915	0.93358	-1.09591	0.92484	-1.08850	0.92482	-1.08848	0.95046	-1.12110
2.30	0.67411	3.44020	0.25986	-0.17431	0.26702	-0.17935	0.27037	-0.18058	0.27863	-0.19919	0.25926	-0.17116	0.25884	-0.17051	0.29797	-0.21872
2.51	0.31105	2.09133	0.10891	-0.08387	0.08398	-0.07197	0.09289	-0.07781	0.10778	-0.09904	0.08275	-0.07109	0.08230	-0.07056	0.13753	-0.11495
2.72	0.32580	0.84559	0.08036	-0.05929	0.04602	-0.04241	0.04568	-0.04184	0.05467	-0.05151	0.04584	-0.04205	0.04562	-0.04180	0.08619	-0.06705
2.93	0.75853	0.18211	0.03245	-0.02857	0.02888	-0.02710	0.02883	-0.02704	0.02920	-0.02739	0.02910	-0.02729	0.02876	-0.02692	0.03330	-0.02962
3.14	0.84899	0.14658	0.02938	-0.02654	0.02685	-0.02554	0.02683	-0.02554	0.02700	-0.02566	0.02711	-0.02577	0.02674	-0.02539	0.03012	-0.02746
associate p_T 3.0–5.0 GeV/c																
2.09	4.89518	1.66478	2.04485	-0.40385	2.04484	-0.40364	2.04483	-0.40361	2.04484	-0.40366	2.04483	-0.40360	2.04483	-0.40359	2.04488	-0.40397
2.30	1.04182	1.05288	0.22018	-0.15644	0.22027	-0.15651	0.22034	-0.15655	0.22034	-0.15665	0.22017	-0.15641	0.22016	-0.15640	0.22063	-0.15694
2.51	-0.03617	11.58245	0.18185	-0.13075	0.11409	-0.09793	0.14856	-0.12149	0.16709	-0.15626	0.10832	-0.09311	0.10818	-0.09295	0.24698	-0.19993
2.72	0.46545	0.35141	0.04454	-0.04506	0.04391	-0.04482	0.04391	-0.04481	0.04401	-0.04491	0.04391	-0.04481	0.04390	-0.04481	0.04465	-0.04517
2.93	0.70587	0.19027	0.03061	-0.03347	0.03044	-0.03341	0.03044	-0.03341	0.03045	-0.03342	0.03044	-0.03340	0.03044	-0.03340	0.03064	-0.03350
3.14	0.56916	0.15234	0.02539	-0.02875	0.02526	-0.02871	0.02526	-0.02871	0.02526	-0.02871	0.02525	-0.02871	0.02525	-0.02871	0.02541	-0.02878
associate p_T 5.0–7.0 GeV/c																
2.09	5.78426	1.87394	9.32861	-0.53181	9.32861	-0.53181	9.32861	-0.53181	9.32861	-0.53181	9.32861	-0.53181	9.32861	-0.53181	9.32861	-0.53181
2.51	0.44663	1.54901	0.26861	-0.18541	0.26861	-0.18540	0.26861	-0.18541	0.26862	-0.18543	0.26861	-0.18541	0.26861	-0.18540	0.26864	-0.18544
2.72	2.15010	0.49435	0.14231	-0.12300	0.14231	-0.12300	0.14231	-0.12300	0.14231	-0.12300	0.14232	-0.12301	0.14231	-0.12300	0.14232	-0.12301
2.93	0.85962	0.47307	0.07129	-0.07606	0.07129	-0.07606	0.07129	-0.07606	0.07129	-0.07606	0.07132	-0.07608	0.07129	-0.07606	0.07132	-0.07609
3.14	0.39581	0.41283	0.03079	-0.04358	0.03078	-0.04358	0.03078	-0.04358	0.03078	-0.04358	0.03082	-0.04361	0.03078	-0.04358	0.03083	-0.04362

J Data Table: $\pi^0 D_{AA}$ vs. $\Delta\phi$

Table 67: 0–20%, trigger p_T 4.0–5.0 Away–side $D_{AA}(\Delta\phi)$

ϕ	$D_{AA}(\Delta\phi)$	σ_{stat}	systematic errors													
			$+\sigma_{f2}$	$-\sigma_{f2}$	$+\sigma_{f3}$	$-\sigma_{f3}$	$+\sigma_{f4}$	$-\sigma_{f4}$	$+\sigma_{\xi/ZYAM}$	$-\sigma_{\xi/ZYAM}$	$+\sigma_{\pi^0}$	$-\sigma_{\pi^0}$	$+\sigma_{pp}$	$-\sigma_{pp}$	$+\sigma_{total}$	$-\sigma_{total}$
associate p_T 0.5–1.0 GeV/c																
1.68	0.03563	0.02206	0.00218	-0.00196	0.00232	-0.00247	0.00202	-0.00227	0.00753	-0.00753	0.00355	-0.00355	0.00054	-0.00054	0.00907	-0.00912
1.88	0.05469	0.02036	0.00162	-0.00144	0.00325	-0.00346	0.00120	-0.00130	0.00756	-0.00756	0.00309	-0.00309	0.00071	-0.00071	0.00890	-0.00896
2.09	0.06755	0.01761	0.00100	-0.00097	0.00365	-0.00388	0.00104	-0.00102	0.00760	-0.00760	0.00430	-0.00430	0.00096	-0.00097	0.00937	-0.00946
2.30	0.07356	0.01566	0.00191	-0.00182	0.00343	-0.00363	0.00182	-0.00170	0.00766	-0.00766	0.00525	-0.00525	0.00130	-0.00130	0.00991	-0.00995
2.51	0.07428	0.01447	0.00341	-0.00335	0.00284	-0.00297	0.00195	-0.00190	0.00775	-0.00775	0.00624	-0.00624	0.00170	-0.00170	0.01053	-0.01054
2.72	0.06502	0.01373	0.00480	-0.00477	0.00240	-0.00245	0.00213	-0.00214	0.00786	-0.00786	0.00685	-0.00686	0.00211	-0.00211	0.01115	-0.01115
2.93	0.04249	0.01313	0.00575	-0.00575	0.00239	-0.00241	0.00284	-0.00297	0.00795	-0.00795	0.00655	-0.00655	0.00238	-0.00239	0.01141	-0.01144
3.14	0.05383	0.01282	0.00614	-0.00612	0.00262	-0.00255	0.00335	-0.00348	0.00803	-0.00800	0.00744	-0.00741	0.00262	-0.00255	0.01217	-0.01221
associate p_T 1.0–2.0 GeV/c																
1.68	-0.01501	0.01444	0.00231	-0.00225	0.00062	-0.00065	0.00182	-0.00207	0.00211	-0.00211	0.00052	-0.00052	0.00027	-0.00027	0.00367	-0.00377
1.88	0.00223	0.01325	0.00193	-0.00188	0.00150	-0.00159	0.00070	-0.00077	0.00213	-0.00213	0.00053	-0.00053	0.00034	-0.00034	0.00329	-0.00332
2.09	0.01603	0.01075	0.00130	-0.00127	0.00189	-0.00201	0.00126	-0.00113	0.00218	-0.00218	0.00108	-0.00108	0.00056	-0.00056	0.00339	-0.00340
2.30	0.03309	0.00999	0.00075	-0.00075	0.00162	-0.00171	0.00231	-0.00205	0.00223	-0.00223	0.00178	-0.00178	0.00071	-0.00071	0.00383	-0.00372
2.51	0.01624	0.00849	0.00133	-0.00134	0.00126	-0.00127	0.00214	-0.00195	0.00240	-0.00240	0.00210	-0.00210	0.00113	-0.00112	0.00361	-0.00351
2.72	-0.00713	0.00842	0.00213	-0.00216	0.00160	-0.00158	0.00150	-0.00150	0.00259	-0.00259	0.00218	-0.00218	0.00149	-0.00148	0.00347	-0.00348
2.93	-0.02624	0.00780	0.00280	-0.00284	0.00243	-0.00236	0.00228	-0.00239	0.00283	-0.00282	0.00248	-0.00247	0.00186	-0.00186	0.00438	-0.00443
3.14	-0.02426	0.00820	0.00302	-0.00307	0.00276	-0.00267	0.00279	-0.00299	0.00290	-0.00290	0.00268	-0.00268	0.00197	-0.00197	0.00495	-0.00505
associate p_T 2.0–3.0 GeV/c																
1.68	-0.00153	0.00436	0.00033	-0.00032	0.00012	-0.00012	0.00027	-0.00031	0.00018	-0.00018	0.00025	-0.00025	0.00009	-0.00009	0.00051	-0.00052
1.88	-0.00195	0.00361	0.00028	-0.00027	0.00022	-0.00023	0.00014	-0.00015	0.00019	-0.00019	0.00037	-0.00037	0.00011	-0.00011	0.00052	-0.00052
2.09	0.00193	0.00317	0.00021	-0.00021	0.00028	-0.00029	0.00021	-0.00020	0.00021	-0.00021	0.00042	-0.00042	0.00014	-0.00014	0.00056	-0.00056
2.30	0.00361	0.00273	0.00020	-0.00020	0.00027	-0.00028	0.00037	-0.00034	0.00025	-0.00025	0.00080	-0.00080	0.00019	-0.00019	0.00090	-0.00089
2.51	-0.00653	0.00248	0.00030	-0.00030	0.00029	-0.00029	0.00038	-0.00036	0.00032	-0.00032	0.00041	-0.00041	0.00028	-0.00028	0.00053	-0.00051
2.72	-0.00520	0.00230	0.00047	-0.00047	0.00042	-0.00043	0.00042	-0.00042	0.00045	-0.00045	0.00112	-0.00112	0.00042	-0.00042	0.00115	-0.00115
2.93	-0.01443	0.00231	0.00063	-0.00063	0.00060	-0.00059	0.00059	-0.00060	0.00058	-0.00058	0.00099	-0.00099	0.00056	-0.00056	0.00108	-0.00109
3.14	-0.01606	0.00232	0.00074	-0.00074	0.00072	-0.00071	0.00073	-0.00074	0.00069	-0.00068	0.00134	-0.00133	0.00067	-0.00066	0.00144	-0.00144
associate p_T 3.0–5.0 GeV/c																
1.68	0.00104	0.00155	0.00007	-0.00007	0.00006	-0.00006	0.00007	-0.00007	0.00006	-0.00006	0.00017	-0.00017	0.00005	-0.00005	0.00018	-0.00019
1.88	-0.00051	0.00123	0.00007	-0.00006	0.00006	-0.00006	0.00006	-0.00006	0.00006	-0.00006	0.00030	-0.00030	0.00005	-0.00005	0.00031	-0.00031
2.09	-0.00122	0.00112	0.00008	-0.00009	0.00008	-0.00009	0.00008	-0.00009	0.00008	-0.00008	0.00022	-0.00023	0.00008	-0.00008	0.00023	-0.00023
2.30	0.00000	0.00096	0.00009	-0.00010	0.00010	-0.00011	0.00011	-0.00011	0.00010	-0.00011	0.00036	-0.00036	0.00009	-0.00010	0.00036	-0.00037
2.51	-0.00180	0.00090	0.00012	-0.00014	0.00012	-0.00014	0.00013	-0.00014	0.00012	-0.00014	0.00029	-0.00030	0.00012	-0.00014	0.00029	-0.00030
2.72	-0.00541	0.00082	0.00020	-0.00023	0.00020	-0.00023	0.00020	-0.00023	0.00020	-0.00023	0.00038	-0.00039	0.00020	-0.00023	0.00038	-0.00040
2.93	-0.01073	0.00089	0.00031	-0.00037	0.00031	-0.00037	0.00031	-0.00037	0.00031	-0.00037	0.00046	-0.00050	0.00031	-0.00036	0.00046	-0.00050
3.14	-0.01139	0.00090	0.00037	-0.00045	0.00037	-0.00045	0.00037	-0.00046	0.00037	-0.00045	0.00085	-0.00089	0.00037	-0.00045	0.00085	-0.00089
associate p_T 5.0–7.0 GeV/c																
1.68	0.00038	0.00067	0.00002	-0.00002	0.00002	-0.00002	0.00002	-0.00002	0.00002	-0.00002	0.00013	-0.00013	0.00002	-0.00002	0.00013	-0.00013
1.88	0.00045	0.00055	0.00002	-0.00002	0.00002	-0.00002	0.00002	-0.00002	0.00002	-0.00002	0.00008	-0.00008	0.00002	-0.00002	0.00008	-0.00008
2.09	-0.00090	0.00043	0.00002	-0.00002	0.00002	-0.00002	0.00002	-0.00002	0.00002	-0.00002	0.00011	-0.00011	0.00002	-0.00002	0.00011	-0.00011
2.30	0.00017	0.00042	0.00003	-0.00003	0.00003	-0.00003	0.00003	-0.00003	0.00003	-0.00003	0.00006	-0.00006	0.00003	-0.00003	0.00006	-0.00006
2.51	-0.00014	0.00038	0.00003	-0.00003	0.00003	-0.00003	0.00003	-0.00003	0.00003	-0.00003	0.00004	-0.00004	0.00003	-0.00003	0.00004	-0.00004
2.72	-0.00052	0.00036	0.00004	-0.00006	0.00004	-0.00006	0.00004	-0.00006	0.00004	-0.00006	0.00009	-0.00010	0.00004	-0.00006	0.00009	-0.00010
2.93	-0.00187	0.00041	0.00008	-0.00011	0.00008	-0.00011	0.00008	-0.00011	0.00007	-0.00011	0.00013	-0.00015	0.00007	-0.00011	0.00013	-0.00016
3.14	-0.00163	0.00042	0.00008	-0.00012	0.00008	-0.00012	0.00008	-0.00012	0.00008	-0.00012	0.00019	-0.00021	0.00008	-0.00012	0.00019	-0.00021

Table 68: 0–20%, trigger p_T 5.0–7.0 Away–side $D_{AA}(\Delta\phi)$

ϕ	$D_{AA}(\Delta\phi)$	σ_{stat}	systematic errors													
			$+\sigma_{f2}$	$-\sigma_{f2}$	$+\sigma_{f3}$	$-\sigma_{f3}$	$+\sigma_{f4}$	$-\sigma_{f4}$	$+\sigma_{\xi/ZYAM}$	$-\sigma_{\xi/ZYAM}$	$+\sigma_{\pi^0}$	$-\sigma_{\pi^0}$	$+\sigma_{pp}$	$-\sigma_{pp}$	$+\sigma_{total}$	$-\sigma_{total}$
associate p_T 0.5–1.0 GeV/c																
1.68	-0.03688	0.02951	0.00478	-0.00430	0.00209	-0.00225	0.00204	-0.00253	0.00706	-0.00706	0.00079	-0.00079	0.00075	-0.00074	0.00892	-0.00884
1.88	0.02567	0.02726	0.00384	-0.00342	0.00329	-0.00359	0.00137	-0.00158	0.00710	-0.00710	0.00106	-0.00106	0.00096	-0.00096	0.00868	-0.00865
2.09	0.03710	0.02355	0.00217	-0.00186	0.00376	-0.00411	0.00111	-0.00109	0.00712	-0.00712	0.00121	-0.00121	0.00106	-0.00106	0.00823	-0.00832
2.30	0.01854	0.02094	0.00165	-0.00157	0.00349	-0.00378	0.00194	-0.00179	0.00721	-0.00721	0.00163	-0.00164	0.00150	-0.00150	0.00803	-0.00810
2.51	0.06713	0.01935	0.00360	-0.00349	0.00277	-0.00290	0.00216	-0.00209	0.00733	-0.00733	0.00231	-0.00231	0.00196	-0.00196	0.00831	-0.00829
2.72	0.02380	0.01835	0.00561	-0.00558	0.00249	-0.00249	0.00247	-0.00248	0.00749	-0.00748	0.00268	-0.00268	0.00244	-0.00244	0.00912	-0.00911
2.93	0.01261	0.01756	0.00701	-0.00703	0.00292	-0.00285	0.00318	-0.00338	0.00762	-0.00760	0.00304	-0.00301	0.00279	-0.00276	0.01019	-0.01026
3.14	-0.01327	0.01711	0.00756	-0.00761	0.00333	-0.00325	0.00366	-0.00399	0.00771	-0.00771	0.00323	-0.00323	0.00304	-0.00304	0.01070	-0.01084
associate p_T 1.0–2.0 GeV/c																
1.68	0.00763	0.01945	0.00382	-0.00369	0.00084	-0.00091	0.00176	-0.00221	0.00170	-0.00170	0.00099	-0.00099	0.00040	-0.00040	0.00465	-0.00474
1.88	0.03545	0.01784	0.00318	-0.00306	0.00198	-0.00220	0.00074	-0.00086	0.00172	-0.00172	0.00089	-0.00089	0.00046	-0.00046	0.00418	-0.00423
2.09	0.04055	0.01444	0.00205	-0.00198	0.00246	-0.00273	0.00135	-0.00113	0.00178	-0.00178	0.00127	-0.00127	0.00064	-0.00064	0.00390	-0.00397
2.30	0.00529	0.01333	0.00100	-0.00099	0.00213	-0.00233	0.00250	-0.00205	0.00190	-0.00190	0.00117	-0.00117	0.00092	-0.00091	0.00366	-0.00350
2.51	-0.00197	0.01135	0.00175	-0.00179	0.00151	-0.00156	0.00233	-0.00201	0.00213	-0.00213	0.00170	-0.00171	0.00132	-0.00132	0.00335	-0.00318
2.72	-0.02548	0.01127	0.00311	-0.00319	0.00202	-0.00199	0.00186	-0.00186	0.00249	-0.00249	0.00222	-0.00222	0.00185	-0.00185	0.00384	-0.00388
2.93	-0.04272	0.01050	0.00418	-0.00429	0.00322	-0.00308	0.00271	-0.00288	0.00293	-0.00293	0.00286	-0.00286	0.00240	-0.00240	0.00538	-0.00546
3.14	-0.07389	0.01099	0.00461	-0.00468	0.00378	-0.00354	0.00328	-0.00353	0.00317	-0.00311	0.00296	-0.00290	0.00269	-0.00262	0.00601	-0.00613
associate p_T 2.0–3.0 GeV/c																
1.68	0.00446	0.00590	0.00052	-0.00050	0.00020	-0.00020	0.00031	-0.00037	0.00021	-0.00021	0.00017	-0.00017	0.00017	-0.00017	0.00061	-0.00062
1.88	0.00541	0.00489	0.00044	-0.00043	0.00032	-0.00035	0.00020	-0.00021	0.00021	-0.00021	0.00018	-0.00018	0.00017	-0.00017	0.00055	-0.00055
2.09	0.00609	0.00428	0.00033	-0.00032	0.00040	-0.00043	0.00028	-0.00026	0.00025	-0.00025	0.00022	-0.00022	0.00021	-0.00021	0.00052	-0.00053
2.30	-0.00066	0.00366	0.00030	-0.00029	0.00040	-0.00042	0.00046	-0.00041	0.00032	-0.00032	0.00029	-0.00029	0.00029	-0.00029	0.00055	-0.00052
2.51	-0.00437	0.00335	0.00042	-0.00042	0.00041	-0.00041	0.00049	-0.00045	0.00041	-0.00041	0.00040	-0.00039	0.00039	-0.00039	0.00054	-0.00051
2.72	-0.01065	0.00313	0.00067	-0.00067	0.00059	-0.00059	0.00058	-0.00058	0.00060	-0.00060	0.00059	-0.00059	0.00058	-0.00058	0.00069	-0.00070
2.93	-0.03054	0.00320	0.00098	-0.00099	0.00092	-0.00092	0.00089	-0.00091	0.00088	-0.00089	0.00087	-0.00088	0.00087	-0.00088	0.00105	-0.00107
3.14	-0.03281	0.00322	0.00110	-0.00110	0.00105	-0.00103	0.00102	-0.00104	0.00099	-0.00098	0.00099	-0.00098	0.00098	-0.00098	0.00120	-0.00121
associate p_T 3.0–5.0 GeV/c																
1.68	-0.00002	0.00207	0.00012	-0.00012	0.00010	-0.00010	0.00011	-0.00011	0.00010	-0.00010	0.00028	-0.00028	0.00010	-0.00010	0.00030	-0.00030
1.88	-0.00043	0.00166	0.00012	-0.00011	0.00011	-0.00011	0.00010	-0.00010	0.00010	-0.00010	0.00020	-0.00020	0.00010	-0.00010	0.00021	-0.00021
2.09	-0.00202	0.00149	0.00012	-0.00012	0.00013	-0.00013	0.00012	-0.00012	0.00012	-0.00012	0.00025	-0.00025	0.00012	-0.00012	0.00026	-0.00026
2.30	-0.00067	0.00129	0.00015	-0.00016	0.00015	-0.00017	0.00016	-0.00017	0.00015	-0.00016	0.00046	-0.00047	0.00015	-0.00016	0.00047	-0.00047
2.51	-0.00462	0.00121	0.00019	-0.00021	0.00019	-0.00021	0.00019	-0.00022	0.00019	-0.00021	0.00027	-0.00029	0.00019	-0.00021	0.00028	-0.00030
2.72	-0.01004	0.00119	0.00032	-0.00039	0.00032	-0.00039	0.00031	-0.00039	0.00032	-0.00039	0.00058	-0.00062	0.00031	-0.00039	0.00058	-0.00062
2.93	-0.02072	0.00138	0.00052	-0.00065	0.00051	-0.00065	0.00051	-0.00065	0.00051	-0.00065	0.00083	-0.00092	0.00051	-0.00065	0.00084	-0.00093
3.14	-0.02527	0.00145	0.00064	-0.00080	0.00064	-0.00080	0.00064	-0.00080	0.00064	-0.00080	0.00121	-0.00130	0.00064	-0.00080	0.00121	-0.00131
associate p_T 5.0–7.0 GeV/c																
1.68	-0.00014	0.00089	0.00005	-0.00006	0.00005	-0.00006	0.00005	-0.00006	0.00005	-0.00006	0.00006	-0.00006	0.00005	-0.00006	0.00006	-0.00006
1.88	-0.00059	0.00068	0.00005	-0.00005	0.00005	-0.00005	0.00005	-0.00005	0.00005	-0.00005	0.00005	-0.00006	0.00005	-0.00005	0.00005	-0.00006
2.09	0.00121	0.00072	0.00005	-0.00005	0.00005	-0.00005	0.00005	-0.00005	0.00005	-0.00005	0.00006	-0.00006	0.00005	-0.00005	0.00006	-0.00006
2.30	-0.00011	0.00057	0.00006	-0.00006	0.00006	-0.00007	0.00006	-0.00007	0.00006	-0.00006	0.00006	-0.00007	0.00006	-0.00006	0.00006	-0.00007
2.51	-0.00019	0.00055	0.00006	-0.00008	0.00006	-0.00008	0.00006	-0.00008	0.00006	-0.00008	0.00007	-0.00008	0.00006	-0.00008	0.00007	-0.00008
2.72	-0.00139	0.00055	0.00009	-0.00013	0.00009	-0.00013	0.00009	-0.00013	0.00009	-0.00013	0.00009	-0.00013	0.00009	-0.00013	0.00009	-0.00013
2.93	-0.00358	0.00067	0.00013	-0.00022	0.00013	-0.00022	0.00013	-0.00022	0.00013	-0.00022	0.00014	-0.00022	0.00013	-0.00022	0.00014	-0.00022
3.14	-0.00423	0.00080	0.00017	-0.00029	0.00017	-0.00029	0.00017	-0.00029	0.00017	-0.00029	0.00019	-0.00030	0.00017	-0.00029	0.00019	-0.00030

Table 69: 0–20%, trigger p_T 7.0–9.0 Away–side $D_{AA}(\Delta\phi)$

ϕ	$D_{AA}(\Delta\phi)$	σ_{stat}	systematic errors													
			$+\sigma_{f2}$	$-\sigma_{f2}$	$+\sigma_{f3}$	$-\sigma_{f3}$	$+\sigma_{f4}$	$-\sigma_{f4}$	$+\sigma_{\xi/ZYAM}$	$-\sigma_{\xi/ZYAM}$	$+\sigma_{\pi^0}$	$-\sigma_{\pi^0}$	$+\sigma_{pp}$	$-\sigma_{pp}$	$+\sigma_{total}$	$-\sigma_{total}$
associate p_T 0.5–1.0 GeV/c																
1.68	0.12257	0.08174	0.00788	-0.01014	0.00450	-0.00412	0.00275	-0.00307	0.02727	-0.02727	0.01349	-0.01349	0.00174	-0.00174	0.03168	-0.03229
1.88	0.19944	0.07552	0.00667	-0.00853	0.00628	-0.00570	0.00232	-0.00244	0.02732	-0.02732	0.01819	-0.01819	0.00201	-0.00200	0.03392	-0.03424
2.09	0.08264	0.06506	0.00450	-0.00562	0.00699	-0.00633	0.00218	-0.00217	0.02737	-0.02737	0.01050	-0.01050	0.00218	-0.00217	0.03024	-0.03028
2.30	0.24151	0.05827	0.00285	-0.00298	0.00656	-0.00600	0.00291	-0.00286	0.02746	-0.02746	0.02515	-0.02515	0.00273	-0.00273	0.03763	-0.03754
2.51	0.11934	0.05344	0.00440	-0.00405	0.00528	-0.00496	0.00333	-0.00330	0.02755	-0.02755	0.01905	-0.01905	0.00325	-0.00325	0.03374	-0.03364
2.72	0.04165	0.05076	0.00781	-0.00675	0.00463	-0.00460	0.00424	-0.00429	0.02771	-0.02772	0.01650	-0.01651	0.00421	-0.00424	0.03271	-0.03246
2.93	0.10593	0.04881	0.01033	-0.00871	0.00499	-0.00496	0.00528	-0.00537	0.02786	-0.02786	0.02520	-0.02520	0.00499	-0.00495	0.03836	-0.03797
3.14	0.09909	0.04764	0.01134	-0.00959	0.00553	-0.00554	0.00596	-0.00614	0.02797	-0.02797	0.02721	-0.02721	0.00552	-0.00552	0.03995	-0.03952
associate p_T 1.0–2.0 GeV/c																
1.68	-0.01581	0.05368	0.00539	-0.00707	0.00157	-0.00148	0.00211	-0.00240	0.00191	-0.00191	0.00110	-0.00110	0.00109	-0.00109	0.00600	-0.00761
1.88	0.02329	0.04910	0.00454	-0.00591	0.00318	-0.00288	0.00138	-0.00143	0.00200	-0.00200	0.00127	-0.00127	0.00124	-0.00124	0.00567	-0.00669
2.09	0.03063	0.03995	0.00306	-0.00385	0.00390	-0.00352	0.00186	-0.00175	0.00214	-0.00214	0.00146	-0.00146	0.00144	-0.00145	0.00514	-0.00535
2.30	-0.02057	0.03676	0.00189	-0.00195	0.00344	-0.00316	0.00291	-0.00264	0.00240	-0.00239	0.00180	-0.00180	0.00180	-0.00180	0.00446	-0.00410
2.51	-0.00274	0.03154	0.00322	-0.00288	0.00260	-0.00255	0.00301	-0.00284	0.00283	-0.00283	0.00237	-0.00237	0.00235	-0.00234	0.00422	-0.00380
2.72	-0.04291	0.03133	0.00582	-0.00493	0.00347	-0.00354	0.00334	-0.00337	0.00369	-0.00372	0.00335	-0.00338	0.00333	-0.00336	0.00613	-0.00532
2.93	-0.13024	0.02919	0.00784	-0.00660	0.00507	-0.00527	0.00455	-0.00465	0.00463	-0.00466	0.00436	-0.00439	0.00435	-0.00438	0.00852	-0.00756
3.14	-0.02306	0.03091	0.00857	-0.00718	0.00572	-0.00596	0.00513	-0.00528	0.00500	-0.00500	0.00480	-0.00480	0.00474	-0.00474	0.00953	-0.00856
associate p_T 2.0–3.0 GeV/c																
1.68	-0.00046	0.01624	0.00087	-0.00103	0.00057	-0.00056	0.00062	-0.00064	0.00056	-0.00056	0.00055	-0.00055	0.00055	-0.00055	0.00094	-0.00110
1.88	-0.00784	0.01334	0.00080	-0.00092	0.00072	-0.00068	0.00058	-0.00058	0.00058	-0.00058	0.00057	-0.00057	0.00057	-0.00057	0.00092	-0.00101
2.09	-0.00060	0.01170	0.00068	-0.00074	0.00079	-0.00075	0.00061	-0.00061	0.00060	-0.00060	0.00059	-0.00059	0.00058	-0.00058	0.00089	-0.00089
2.30	-0.01081	0.01003	0.00072	-0.00072	0.00084	-0.00081	0.00080	-0.00079	0.00073	-0.00073	0.00072	-0.00072	0.00072	-0.00072	0.00092	-0.00088
2.51	-0.01232	0.00934	0.00094	-0.00091	0.00091	-0.00090	0.00094	-0.00093	0.00090	-0.00090	0.00090	-0.00089	0.00089	-0.00089	0.00101	-0.00097
2.72	-0.02079	0.00891	0.00140	-0.00134	0.00127	-0.00127	0.00126	-0.00126	0.00127	-0.00126	0.00126	-0.00126	0.00126	-0.00126	0.00141	-0.00136
2.93	-0.04209	0.00936	0.00200	-0.00193	0.00186	-0.00188	0.00184	-0.00184	0.00183	-0.00183	0.00183	-0.00183	0.00182	-0.00183	0.00205	-0.00200
3.14	-0.10029	0.01010	0.00276	-0.00277	0.00266	-0.00274	0.00264	-0.00271	0.00262	-0.00269	0.00262	-0.00269	0.00262	-0.00269	0.00283	-0.00285
associate p_T 3.0–5.0 GeV/c																
1.68	-0.00685	0.00545	0.00043	-0.00044	0.00042	-0.00043	0.00042	-0.00043	0.00042	-0.00043	0.00065	-0.00066	0.00042	-0.00043	0.00066	-0.00067
1.88	0.00859	0.00492	0.00038	-0.00038	0.00038	-0.00037	0.00038	-0.00037	0.00038	-0.00037	0.00052	-0.00051	0.00038	-0.00037	0.00053	-0.00052
2.09	-0.00110	0.00411	0.00040	-0.00040	0.00040	-0.00040	0.00040	-0.00040	0.00040	-0.00040	0.00040	-0.00040	0.00040	-0.00040	0.00041	-0.00041
2.30	-0.00037	0.00373	0.00048	-0.00051	0.00049	-0.00051	0.00049	-0.00051	0.00048	-0.00051	0.00052	-0.00054	0.00048	-0.00051	0.00052	-0.00055
2.51	0.00523	0.00376	0.00053	-0.00057	0.00053	-0.00057	0.00053	-0.00057	0.00053	-0.00057	0.00073	-0.00076	0.00053	-0.00057	0.00073	-0.00076
2.72	-0.01139	0.00378	0.00080	-0.00091	0.00079	-0.00091	0.00079	-0.00091	0.00079	-0.00091	0.00091	-0.00102	0.00079	-0.00091	0.00092	-0.00102
2.93	-0.03770	0.00507	0.00131	-0.00158	0.00130	-0.00158	0.00130	-0.00158	0.00130	-0.00157	0.00145	-0.00170	0.00130	-0.00157	0.00146	-0.00170
3.14	-0.05920	0.00623	0.00176	-0.00217	0.00175	-0.00217	0.00175	-0.00216	0.00175	-0.00216	0.00192	-0.00230	0.00175	-0.00216	0.00193	-0.00231
associate p_T 5.0–7.0 GeV/c																
1.68	0.00140	0.00291	0.00024	-0.00025	0.00024	-0.00025	0.00024	-0.00025	0.00024	-0.00025	0.00032	-0.00032	0.00024	-0.00025	0.00032	-0.00032
1.88	-0.00140	0.00157	0.00023	-0.00023	0.00023	-0.00023	0.00023	-0.00023	0.00023	-0.00023	0.00026	-0.00026	0.00023	-0.00023	0.00026	-0.00026
2.09	-0.00070	0.00178	0.00024	-0.00025	0.00024	-0.00025	0.00024	-0.00025	0.00024	-0.00025	0.00034	-0.00034	0.00024	-0.00025	0.00034	-0.00034
2.30	-0.00279	0.00115	0.00024	-0.00025	0.00024	-0.00025	0.00024	-0.00025	0.00024	-0.00025	0.00030	-0.00031	0.00024	-0.00025	0.00030	-0.00031
2.51	-0.00021	0.00162	0.00026	-0.00028	0.00026	-0.00028	0.00026	-0.00028	0.00026	-0.00028	0.00028	-0.00030	0.00026	-0.00028	0.00028	-0.00030
2.72	-0.00316	0.00190	0.00032	-0.00041	0.00032	-0.00041	0.00032	-0.00041	0.00032	-0.00041	0.00037	-0.00044	0.00032	-0.00041	0.00037	-0.00044
2.93	-0.00868	0.00329	0.00046	-0.00069	0.00046	-0.00069	0.00046	-0.00069	0.00046	-0.00069	0.00062	-0.00080	0.00046	-0.00069	0.00062	-0.00080
3.14	-0.01988	0.00456	0.00066	-0.00108	0.00066	-0.00108	0.00066	-0.00108	0.00066	-0.00108	0.00081	-0.00117	0.00066	-0.00108	0.00081	-0.00117

Table 70: 0–20%, trigger p_T 9.0–12.0 Away–side $D_{AA}(\Delta\phi)$

ϕ	$D_{AA}(\Delta\phi)$	σ_{stat}	systematic errors													
			$+\sigma_{f2}$	$-\sigma_{f2}$	$+\sigma_{f3}$	$-\sigma_{f3}$	$+\sigma_{f4}$	$-\sigma_{f4}$	$+\sigma_{\xi/ZYAM}$	$-\sigma_{\xi/ZYAM}$	$+\sigma_{\pi^0}$	$-\sigma_{\pi^0}$	$+\sigma_{pp}$	$-\sigma_{pp}$	$+\sigma_{total}$	$-\sigma_{total}$
associate p_T 0.5–1.0 GeV/c																
1.68	0.03591	0.15624	0.00684	-0.00920	0.00596	-0.00509	0.00422	-0.00443	0.04422	-0.04423	0.00358	-0.00358	0.00342	-0.00342	0.04497	-0.04530
1.88	0.20792	0.14483	0.00547	-0.00681	0.00827	-0.00677	0.00375	-0.00382	0.04428	-0.04428	0.00989	-0.00989	0.00351	-0.00351	0.04606	-0.04600
2.09	0.15899	0.12557	0.00445	-0.00441	0.00953	-0.00785	0.00433	-0.00432	0.04441	-0.04441	0.00769	-0.00769	0.00432	-0.00432	0.04567	-0.04535
2.30	0.08293	0.11146	0.00720	-0.00557	0.00886	-0.00747	0.00490	-0.00485	0.04451	-0.04451	0.00709	-0.00709	0.00472	-0.00472	0.04579	-0.04530
2.51	0.23583	0.10380	0.01349	-0.00938	0.00781	-0.00713	0.00616	-0.00610	0.04473	-0.04473	0.01362	-0.01360	0.00609	-0.00605	0.04816	-0.04706
2.72	-0.05139	0.09736	0.01895	-0.01263	0.00672	-0.00663	0.00653	-0.00653	0.04484	-0.04484	0.00862	-0.00862	0.00651	-0.00651	0.04860	-0.04649
2.93	0.12278	0.09421	0.02300	-0.01531	0.00764	-0.00762	0.00786	-0.00791	0.04504	-0.04504	0.01333	-0.01331	0.00760	-0.00757	0.05123	-0.04828
3.14	0.02195	0.09183	0.02443	-0.01631	0.00813	-0.00829	0.00842	-0.00861	0.04512	-0.04513	0.01168	-0.01173	0.00799	-0.00806	0.05149	-0.04820
associate p_T 1.0–2.0 GeV/c																
1.68	-0.02858	0.10306	0.00737	-0.01157	0.00300	-0.00282	0.00335	-0.00355	0.00300	-0.00300	0.00711	-0.00711	0.00252	-0.00253	0.01042	-0.01373
1.88	0.05319	0.09448	0.00631	-0.00971	0.00499	-0.00421	0.00275	-0.00278	0.00311	-0.00311	0.00345	-0.00345	0.00265	-0.00265	0.00811	-0.01064
2.09	0.01675	0.07669	0.00447	-0.00638	0.00590	-0.00488	0.00305	-0.00298	0.00318	-0.00318	0.00282	-0.00282	0.00273	-0.00273	0.00724	-0.00786
2.30	0.00962	0.07072	0.00328	-0.00343	0.00531	-0.00458	0.00417	-0.00398	0.00359	-0.00360	0.00364	-0.00364	0.00320	-0.00321	0.00644	-0.00580
2.51	-0.03040	0.06085	0.00539	-0.00461	0.00436	-0.00424	0.00461	-0.00450	0.00436	-0.00437	0.00443	-0.00444	0.00405	-0.00405	0.00652	-0.00570
2.72	-0.02702	0.06100	0.00962	-0.00746	0.00586	-0.00599	0.00574	-0.00577	0.00596	-0.00599	0.00695	-0.00698	0.00573	-0.00577	0.01059	-0.00874
2.93	-0.04564	0.05747	0.01258	-0.00940	0.00760	-0.00804	0.00705	-0.00707	0.00706	-0.00702	0.00820	-0.00817	0.00686	-0.00683	0.01394	-0.01151
3.14	-0.24744	0.05966	0.01420	-0.01083	0.00921	-0.00973	0.00862	-0.00864	0.00843	-0.00837	0.00846	-0.00839	0.00827	-0.00820	0.01515	-0.01257
associate p_T 2.0–3.0 GeV/c																
1.68	0.01647	0.03192	0.00147	-0.00183	0.00121	-0.00120	0.00125	-0.00125	0.00119	-0.00119	0.00130	-0.00130	0.00118	-0.00118	0.00163	-0.00196
1.88	-0.01646	0.02502	0.00133	-0.00160	0.00128	-0.00121	0.00112	-0.00112	0.00112	-0.00112	0.00124	-0.00124	0.00111	-0.00111	0.00158	-0.00177
2.09	-0.00039	0.02248	0.00130	-0.00141	0.00145	-0.00135	0.00124	-0.00124	0.00122	-0.00122	0.00122	-0.00122	0.00122	-0.00122	0.00154	-0.00155
2.30	0.02164	0.01993	0.00134	-0.00134	0.00148	-0.00142	0.00140	-0.00140	0.00134	-0.00134	0.00140	-0.00140	0.00133	-0.00133	0.00161	-0.00155
2.51	0.01225	0.01857	0.00166	-0.00162	0.00162	-0.00161	0.00164	-0.00164	0.00161	-0.00161	0.00166	-0.00166	0.00160	-0.00160	0.00177	-0.00173
2.72	-0.00505	0.01767	0.00226	-0.00214	0.00206	-0.00207	0.00205	-0.00205	0.00205	-0.00205	0.00212	-0.00212	0.00205	-0.00205	0.00234	-0.00222
2.93	-0.08735	0.01947	0.00364	-0.00346	0.00343	-0.00342	0.00341	-0.00337	0.00340	-0.00336	0.00343	-0.00340	0.00339	-0.00336	0.00372	-0.00357
3.14	-0.06446	0.02060	0.00408	-0.00392	0.00386	-0.00390	0.00384	-0.00384	0.00382	-0.00382	0.00396	-0.00396	0.00382	-0.00382	0.00427	-0.00416
associate p_T 3.0–5.0 GeV/c																
1.68	-0.00290	0.01062	0.00090	-0.00090	0.00089	-0.00089	0.00089	-0.00089	0.00089	-0.00089	0.00092	-0.00091	0.00089	-0.00089	0.00093	-0.00093
1.88	-0.00460	0.00844	0.00091	-0.00092	0.00091	-0.00091	0.00090	-0.00090	0.00090	-0.00090	0.00093	-0.00093	0.00090	-0.00090	0.00094	-0.00095
2.09	-0.01033	0.00740	0.00093	-0.00094	0.00094	-0.00094	0.00093	-0.00094	0.00093	-0.00094	0.00099	-0.00099	0.00093	-0.00094	0.00100	-0.00100
2.30	-0.00277	0.00711	0.00100	-0.00103	0.00101	-0.00103	0.00101	-0.00103	0.00100	-0.00103	0.00103	-0.00106	0.00100	-0.00103	0.00104	-0.00106
2.51	-0.00676	0.00705	0.00111	-0.00116	0.00111	-0.00116	0.00111	-0.00116	0.00111	-0.00116	0.00112	-0.00117	0.00111	-0.00116	0.00112	-0.00117
2.72	-0.02491	0.00835	0.00157	-0.00175	0.00156	-0.00174	0.00156	-0.00174	0.00156	-0.00174	0.00161	-0.00178	0.00156	-0.00174	0.00161	-0.00179
2.93	-0.03031	0.01243	0.00226	-0.00263	0.00225	-0.00263	0.00225	-0.00263	0.00225	-0.00263	0.00258	-0.00292	0.00225	-0.00263	0.00259	-0.00293
3.14	-0.07217	0.01559	0.00319	-0.00382	0.00318	-0.00382	0.00318	-0.00382	0.00318	-0.00382	0.00355	-0.00413	0.00318	-0.00382	0.00356	-0.00414
associate p_T 5.0–7.0 GeV/c																
1.68	-0.00427	0.00000	0.00083	-0.00083	0.00083	-0.00083	0.00083	-0.00083	0.00083	-0.00083	0.00083	-0.00083	0.00083	-0.00083	0.00083	-0.00083
1.88	-0.00373	0.00567	0.00089	-0.00093	0.00089	-0.00093	0.00089	-0.00093	0.00089	-0.00093	0.00089	-0.00093	0.00089	-0.00093	0.00089	-0.00093
2.09	0.00187	0.00432	0.00085	-0.00086	0.00085	-0.00086	0.00085	-0.00086	0.00085	-0.00086	0.00085	-0.00086	0.00085	-0.00086	0.00085	-0.00086
2.30	0.00218	0.00338	0.00083	-0.00083	0.00083	-0.00083	0.00083	-0.00083	0.00083	-0.00083	0.00083	-0.00083	0.00083	-0.00083	0.00083	-0.00083
2.51	-0.00737	0.00287	0.00091	-0.00098	0.00091	-0.00098	0.00091	-0.00098	0.00091	-0.00098	0.00091	-0.00098	0.00091	-0.00098	0.00091	-0.00098
2.72	-0.00221	0.00448	0.00097	-0.00110	0.00097	-0.00110	0.00097	-0.00110	0.00097	-0.00110	0.00098	-0.00110	0.00097	-0.00110	0.00098	-0.00110
2.93	0.00482	0.00789	0.00114	-0.00140	0.00113	-0.00140	0.00113	-0.00140	0.00113	-0.00140	0.00115	-0.00141	0.00113	-0.00140	0.00115	-0.00141
3.14	-0.04052	0.02359	0.00204	-0.00312	0.00204	-0.00312	0.00204	-0.00312	0.00204	-0.00312	0.00205	-0.00312	0.00204	-0.00312	0.00205	-0.00312

Table 71: 20–40%, trigger p_T 4.0–5.0 Away–side $D_{AA}(\Delta\phi)$

ϕ	$D_{AA}(\Delta\phi)$	σ_{stat}	systematic errors													
			$+\sigma_{f2}$	$-\sigma_{f2}$	$+\sigma_{f3}$	$-\sigma_{f3}$	$+\sigma_{f4}$	$-\sigma_{f4}$	$+\sigma_{\xi/ZYAM}$	$-\sigma_{\xi/ZYAM}$	$+\sigma_{\pi^0}$	$-\sigma_{\pi^0}$	$+\sigma_{pp}$	$-\sigma_{pp}$	$+\sigma_{total}$	$-\sigma_{total}$
associate p_T 0.5–1.0 GeV/c																
1.68	0.01873	0.01726	0.00145	-0.00114	0.00248	-0.00268	0.00236	-0.00252	0.00679	-0.00679	0.00091	-0.00091	0.00054	-0.00054	0.00772	-0.00778
1.88	0.02859	0.01605	0.00095	-0.00077	0.00338	-0.00366	0.00098	-0.00085	0.00684	-0.00683	0.00159	-0.00159	0.00071	-0.00071	0.00778	-0.00787
2.09	0.05680	0.01397	0.00137	-0.00118	0.00378	-0.00408	0.00241	-0.00179	0.00691	-0.00691	0.00268	-0.00268	0.00096	-0.00097	0.00856	-0.00851
2.30	0.03474	0.01250	0.00293	-0.00269	0.00358	-0.00384	0.00401	-0.00308	0.00702	-0.00702	0.00266	-0.00266	0.00130	-0.00130	0.00933	-0.00900
2.51	0.03209	0.01170	0.00466	-0.00444	0.00300	-0.00318	0.00366	-0.00289	0.00716	-0.00716	0.00326	-0.00326	0.00170	-0.00170	0.00972	-0.00941
2.72	0.05140	0.01117	0.00621	-0.00601	0.00253	-0.00261	0.00230	-0.00216	0.00732	-0.00732	0.00446	-0.00447	0.00211	-0.00211	0.01030	-0.01017
2.93	0.03027	0.01072	0.00726	-0.00708	0.00244	-0.00246	0.00288	-0.00289	0.00744	-0.00745	0.00440	-0.00441	0.00238	-0.00239	0.01092	-0.01080
3.14	0.01952	0.01046	0.00768	-0.00748	0.00262	-0.00256	0.00363	-0.00373	0.00754	-0.00751	0.00449	-0.00445	0.00262	-0.00255	0.01134	-0.01125
associate p_T 1.0–2.0 GeV/c																
1.68	0.03037	0.01134	0.00271	-0.00266	0.00062	-0.00066	0.00237	-0.00289	0.00496	-0.00496	0.00048	-0.00048	0.00027	-0.00027	0.00616	-0.00636
1.88	0.02876	0.01042	0.00225	-0.00222	0.00148	-0.00160	0.00086	-0.00103	0.00501	-0.00501	0.00044	-0.00045	0.00034	-0.00034	0.00573	-0.00578
2.09	0.02660	0.00856	0.00149	-0.00147	0.00187	-0.00202	0.00167	-0.00141	0.00508	-0.00508	0.00068	-0.00068	0.00056	-0.00056	0.00579	-0.00577
2.30	0.03314	0.00803	0.00077	-0.00076	0.00161	-0.00172	0.00316	-0.00262	0.00517	-0.00517	0.00087	-0.00087	0.00071	-0.00071	0.00622	-0.00599
2.51	0.02154	0.00691	0.00140	-0.00141	0.00126	-0.00127	0.00279	-0.00237	0.00532	-0.00532	0.00127	-0.00127	0.00113	-0.00112	0.00601	-0.00583
2.72	0.00609	0.00691	0.00234	-0.00237	0.00160	-0.00158	0.00152	-0.00151	0.00547	-0.00547	0.00160	-0.00160	0.00149	-0.00148	0.00584	-0.00584
2.93	-0.01200	0.00644	0.00309	-0.00313	0.00243	-0.00235	0.00254	-0.00281	0.00563	-0.00563	0.00196	-0.00196	0.00186	-0.00186	0.00661	-0.00671
3.14	-0.01607	0.00678	0.00335	-0.00339	0.00276	-0.00266	0.00325	-0.00372	0.00569	-0.00569	0.00207	-0.00207	0.00197	-0.00197	0.00710	-0.00731
associate p_T 2.0–3.0 GeV/c																
1.68	0.00308	0.00344	0.00036	-0.00035	0.00011	-0.00012	0.00038	-0.00047	0.00044	-0.00044	0.00014	-0.00014	0.00009	-0.00009	0.00069	-0.00073
1.88	0.00250	0.00288	0.00031	-0.00030	0.00020	-0.00022	0.00017	-0.00019	0.00045	-0.00045	0.00012	-0.00012	0.00011	-0.00011	0.00058	-0.00059
2.09	0.00383	0.00256	0.00023	-0.00022	0.00026	-0.00027	0.00029	-0.00025	0.00047	-0.00047	0.00019	-0.00019	0.00014	-0.00014	0.00061	-0.00060
2.30	0.00015	0.00222	0.00020	-0.00020	0.00026	-0.00027	0.00053	-0.00044	0.00049	-0.00049	0.00021	-0.00021	0.00019	-0.00019	0.00072	-0.00067
2.51	0.00211	0.00207	0.00030	-0.00030	0.00029	-0.00029	0.00049	-0.00043	0.00054	-0.00054	0.00035	-0.00035	0.00028	-0.00028	0.00072	-0.00068
2.72	-0.00000	0.00195	0.00048	-0.00048	0.00042	-0.00043	0.00042	-0.00042	0.00063	-0.00063	0.00050	-0.00051	0.00042	-0.00042	0.00073	-0.00073
2.93	-0.00901	0.00198	0.00064	-0.00065	0.00059	-0.00059	0.00062	-0.00065	0.00073	-0.00073	0.00061	-0.00061	0.00056	-0.00056	0.00090	-0.00092
3.14	-0.01105	0.00199	0.00076	-0.00075	0.00071	-0.00070	0.00079	-0.00083	0.00082	-0.00082	0.00074	-0.00073	0.00067	-0.00066	0.00106	-0.00109
associate p_T 3.0–5.0 GeV/c																
1.68	0.00131	0.00125	0.00007	-0.00007	0.00005	-0.00005	0.00008	-0.00009	0.00007	-0.00007	0.00005	-0.00005	0.00005	-0.00005	0.00010	-0.00011
1.88	0.00109	0.00101	0.00006	-0.00006	0.00006	-0.00006	0.00006	-0.00006	0.00007	-0.00007	0.00005	-0.00005	0.00005	-0.00005	0.00009	-0.00009
2.09	0.00040	0.00094	0.00008	-0.00008	0.00008	-0.00009	0.00009	-0.00009	0.00009	-0.00010	0.00008	-0.00008	0.00008	-0.00008	0.00011	-0.00011
2.30	-0.00050	0.00079	0.00009	-0.00010	0.00010	-0.00011	0.00012	-0.00012	0.00011	-0.00012	0.00009	-0.00010	0.00009	-0.00010	0.00013	-0.00013
2.51	-0.00057	0.00077	0.00012	-0.00014	0.00012	-0.00014	0.00014	-0.00015	0.00013	-0.00015	0.00012	-0.00014	0.00012	-0.00014	0.00015	-0.00016
2.72	-0.00437	0.00072	0.00020	-0.00023	0.00020	-0.00023	0.00020	-0.00023	0.00020	-0.00023	0.00020	-0.00023	0.00020	-0.00023	0.00021	-0.00024
2.93	-0.00885	0.00080	0.00031	-0.00037	0.00031	-0.00037	0.00031	-0.00037	0.00031	-0.00037	0.00031	-0.00037	0.00031	-0.00036	0.00032	-0.00038
3.14	-0.01045	0.00081	0.00037	-0.00045	0.00037	-0.00045	0.00037	-0.00046	0.00037	-0.00046	0.00037	-0.00045	0.00037	-0.00045	0.00038	-0.00046
associate p_T 5.0–7.0 GeV/c																
1.68	-0.00031	0.00044	0.00002	-0.00002	0.00002	-0.00002	0.00002	-0.00002	0.00002	-0.00002	0.00007	-0.00007	0.00002	-0.00002	0.00007	-0.00007
1.88	-0.00045	0.00035	0.00002	-0.00002	0.00002	-0.00002	0.00002	-0.00002	0.00002	-0.00002	0.00008	-0.00008	0.00002	-0.00002	0.00008	-0.00008
2.09	0.00007	0.00039	0.00002	-0.00002	0.00002	-0.00002	0.00002	-0.00002	0.00002	-0.00002	0.00003	-0.00003	0.00002	-0.00002	0.00003	-0.00003
2.30	0.00007	0.00034	0.00003	-0.00003	0.00003	-0.00003	0.00003	-0.00003	0.00003	-0.00003	0.00007	-0.00007	0.00003	-0.00003	0.00007	-0.00007
2.51	-0.00006	0.00031	0.00003	-0.00003	0.00003	-0.00003	0.00003	-0.00003	0.00003	-0.00003	0.00007	-0.00007	0.00003	-0.00003	0.00007	-0.00007
2.72	-0.00079	0.00030	0.00004	-0.00006	0.00004	-0.00006	0.00004	-0.00006	0.00004	-0.00006	0.00007	-0.00008	0.00004	-0.00006	0.00007	-0.00008
2.93	-0.00183	0.00037	0.00007	-0.00011	0.00008	-0.00011	0.00008	-0.00011	0.00008	-0.00011	0.00015	-0.00018	0.00007	-0.00011	0.00015	-0.00018
3.14	-0.00047	0.00043	0.00008	-0.00012	0.00008	-0.00012	0.00008	-0.00012	0.00008	-0.00012	0.00040	-0.00041	0.00008	-0.00012	0.00040	-0.00041

Table 72: 20–40%, trigger p_T 5.0–7.0 Away–side $D_{AA}(\Delta\phi)$

ϕ	$D_{AA}(\Delta\phi)$	σ_{stat}	systematic errors													
			$+\sigma_{f2}$	$-\sigma_{f2}$	$+\sigma_{f3}$	$-\sigma_{f3}$	$+\sigma_{f4}$	$-\sigma_{f4}$	$+\sigma_{\xi/ZYAM}$	$-\sigma_{\xi/ZYAM}$	$+\sigma_{\pi^0}$	$-\sigma_{\pi^0}$	$+\sigma_{pp}$	$-\sigma_{pp}$	$+\sigma_{total}$	$-\sigma_{total}$
associate p_T 0.5–1.0 GeV/c																
1.68	0.01049	0.02221	0.00352	-0.00315	0.00203	-0.00217	0.00237	-0.00297	0.00667	-0.00666	0.00076	-0.00076	0.00075	-0.00074	0.00805	-0.00814
1.88	0.04165	0.02066	0.00281	-0.00247	0.00281	-0.00303	0.00145	-0.00170	0.00672	-0.00672	0.00111	-0.00111	0.00096	-0.00096	0.00778	-0.00780
2.09	0.04944	0.01792	0.00159	-0.00136	0.00312	-0.00337	0.00121	-0.00116	0.00677	-0.00677	0.00124	-0.00124	0.00106	-0.00106	0.00753	-0.00758
2.30	0.03687	0.01606	0.00178	-0.00165	0.00305	-0.00326	0.00231	-0.00205	0.00690	-0.00690	0.00169	-0.00169	0.00150	-0.00150	0.00770	-0.00768
2.51	0.05434	0.01502	0.00347	-0.00327	0.00274	-0.00286	0.00237	-0.00223	0.00706	-0.00706	0.00228	-0.00228	0.00196	-0.00196	0.00805	-0.00797
2.72	0.02513	0.01431	0.00513	-0.00496	0.00264	-0.00266	0.00246	-0.00247	0.00725	-0.00725	0.00271	-0.00271	0.00244	-0.00244	0.00869	-0.00859
2.93	0.05723	0.01379	0.00630	-0.00612	0.00280	-0.00277	0.00332	-0.00359	0.00740	-0.00739	0.00324	-0.00321	0.00279	-0.00276	0.00962	-0.00962
3.14	-0.00122	0.01341	0.00676	-0.00661	0.00304	-0.00304	0.00390	-0.00435	0.00751	-0.00751	0.00329	-0.00329	0.00304	-0.00304	0.01002	-0.01011
associate p_T 1.0–2.0 GeV/c																
1.68	0.03070	0.01462	0.00308	-0.00301	0.00061	-0.00065	0.00174	-0.00218	0.00464	-0.00464	0.00040	-0.00040	0.00040	-0.00040	0.00583	-0.00594
1.88	0.03769	0.01343	0.00257	-0.00251	0.00130	-0.00143	0.00073	-0.00086	0.00468	-0.00468	0.00047	-0.00047	0.00046	-0.00046	0.00548	-0.00551
2.09	0.02913	0.01100	0.00169	-0.00166	0.00164	-0.00179	0.00134	-0.00113	0.00474	-0.00474	0.00065	-0.00064	0.00064	-0.00064	0.00535	-0.00534
2.30	0.03464	0.01031	0.00097	-0.00097	0.00152	-0.00163	0.00247	-0.00203	0.00484	-0.00484	0.00092	-0.00092	0.00092	-0.00091	0.00550	-0.00535
2.51	0.03473	0.00890	0.00162	-0.00164	0.00140	-0.00142	0.00231	-0.00200	0.00499	-0.00499	0.00133	-0.00133	0.00132	-0.00132	0.00544	-0.00533
2.72	-0.01110	0.00887	0.00275	-0.00279	0.00192	-0.00190	0.00186	-0.00186	0.00520	-0.00520	0.00185	-0.00185	0.00185	-0.00185	0.00562	-0.00563
2.93	-0.02691	0.00833	0.00368	-0.00373	0.00276	-0.00269	0.00271	-0.00287	0.00546	-0.00546	0.00241	-0.00241	0.00240	-0.00240	0.00640	-0.00648
3.14	-0.01846	0.00879	0.00407	-0.00407	0.00316	-0.00302	0.00326	-0.00352	0.00560	-0.00557	0.00269	-0.00262	0.00269	-0.00262	0.00685	-0.00697
associate p_T 2.0–3.0 GeV/c																
1.68	0.00059	0.00442	0.00042	-0.00041	0.00018	-0.00018	0.00032	-0.00038	0.00044	-0.00044	0.00017	-0.00017	0.00017	-0.00017	0.00065	-0.00067
1.88	0.00631	0.00374	0.00036	-0.00036	0.00023	-0.00024	0.00020	-0.00021	0.00044	-0.00044	0.00018	-0.00018	0.00017	-0.00017	0.00058	-0.00058
2.09	0.00597	0.00332	0.00029	-0.00029	0.00028	-0.00030	0.00028	-0.00026	0.00047	-0.00047	0.00023	-0.00023	0.00021	-0.00021	0.00058	-0.00057
2.30	-0.00323	0.00286	0.00029	-0.00029	0.00033	-0.00033	0.00047	-0.00041	0.00051	-0.00051	0.00029	-0.00029	0.00029	-0.00029	0.00065	-0.00061
2.51	0.00133	0.00270	0.00041	-0.00041	0.00040	-0.00039	0.00049	-0.00046	0.00058	-0.00058	0.00041	-0.00041	0.00039	-0.00039	0.00068	-0.00065
2.72	-0.00891	0.00256	0.00064	-0.00064	0.00059	-0.00059	0.00058	-0.00058	0.00073	-0.00073	0.00060	-0.00060	0.00058	-0.00058	0.00079	-0.00079
2.93	-0.01962	0.00269	0.00094	-0.00095	0.00089	-0.00089	0.00089	-0.00091	0.00097	-0.00098	0.00089	-0.00090	0.00087	-0.00088	0.00109	-0.00110
3.14	-0.02020	0.00274	0.00106	-0.00105	0.00100	-0.00099	0.00103	-0.00104	0.00108	-0.00107	0.00102	-0.00101	0.00098	-0.00098	0.00123	-0.00124
associate p_T 3.0–5.0 GeV/c																
1.68	-0.00152	0.00152	0.00011	-0.00011	0.00010	-0.00010	0.00011	-0.00011	0.00011	-0.00011	0.00010	-0.00010	0.00010	-0.00010	0.00013	-0.00013
1.88	-0.00042	0.00126	0.00011	-0.00011	0.00010	-0.00010	0.00010	-0.00010	0.00011	-0.00011	0.00010	-0.00010	0.00010	-0.00010	0.00012	-0.00012
2.09	0.00037	0.00119	0.00012	-0.00012	0.00012	-0.00012	0.00012	-0.00012	0.00012	-0.00013	0.00012	-0.00012	0.00012	-0.00012	0.00013	-0.00013
2.30	-0.00236	0.00101	0.00015	-0.00016	0.00015	-0.00016	0.00016	-0.00017	0.00016	-0.00017	0.00015	-0.00016	0.00015	-0.00016	0.00017	-0.00017
2.51	-0.00140	0.00103	0.00019	-0.00021	0.00019	-0.00021	0.00019	-0.00022	0.00019	-0.00022	0.00019	-0.00021	0.00019	-0.00021	0.00020	-0.00022
2.72	-0.00633	0.00107	0.00032	-0.00039	0.00031	-0.00039	0.00031	-0.00039	0.00032	-0.00039	0.00032	-0.00039	0.00031	-0.00039	0.00032	-0.00039
2.93	-0.01569	0.00129	0.00051	-0.00065	0.00051	-0.00065	0.00051	-0.00065	0.00052	-0.00065	0.00051	-0.00065	0.00051	-0.00065	0.00052	-0.00065
3.14	-0.01896	0.00138	0.00064	-0.00080	0.00064	-0.00080	0.00064	-0.00080	0.00064	-0.00080	0.00064	-0.00080	0.00064	-0.00080	0.00065	-0.00081
associate p_T 5.0–7.0 GeV/c																
1.68	0.00178	0.00093	0.00005	-0.00006	0.00005	-0.00006	0.00005	-0.00006	0.00005	-0.00006	0.00005	-0.00006	0.00005	-0.00006	0.00005	-0.00006
1.88	0.00010	0.00057	0.00005	-0.00005	0.00005	-0.00005	0.00005	-0.00005	0.00005	-0.00005	0.00005	-0.00005	0.00005	-0.00005	0.00005	-0.00005
2.09	-0.00008	0.00048	0.00005	-0.00005	0.00005	-0.00005	0.00005	-0.00005	0.00005	-0.00005	0.00005	-0.00005	0.00005	-0.00005	0.00005	-0.00005
2.30	-0.00054	0.00042	0.00006	-0.00006	0.00006	-0.00007	0.00006	-0.00007	0.00006	-0.00007	0.00006	-0.00006	0.00006	-0.00006	0.00006	-0.00007
2.51	-0.00013	0.00046	0.00006	-0.00008	0.00006	-0.00008	0.00006	-0.00008	0.00006	-0.00008	0.00006	-0.00008	0.00006	-0.00008	0.00006	-0.00008
2.72	-0.00108	0.00050	0.00009	-0.00013	0.00009	-0.00013	0.00009	-0.00013	0.00009	-0.00013	0.00009	-0.00013	0.00009	-0.00013	0.00009	-0.00013
2.93	-0.00288	0.00065	0.00013	-0.00022	0.00013	-0.00022	0.00013	-0.00022	0.00013	-0.00022	0.00013	-0.00022	0.00013	-0.00022	0.00013	-0.00022
3.14	-0.00289	0.00081	0.00017	-0.00029	0.00017	-0.00029	0.00017	-0.00029	0.00017	-0.00029	0.00017	-0.00029	0.00017	-0.00029	0.00017	-0.00029

Table 73: 20–40%, trigger p_T 7.0–9.0 Away–side $D_{AA}(\Delta\phi)$

ϕ	$D_{AA}(\Delta\phi)$	σ_{stat}	systematic errors													
			$+\sigma_{f2}$	$-\sigma_{f2}$	$+\sigma_{f3}$	$-\sigma_{f3}$	$+\sigma_{f4}$	$-\sigma_{f4}$	$+\sigma_{\xi/ZYAM}$	$-\sigma_{\xi/ZYAM}$	$+\sigma_{\pi^0}$	$-\sigma_{\pi^0}$	$+\sigma_{pp}$	$-\sigma_{pp}$	$+\sigma_{total}$	$-\sigma_{total}$
associate p_T 0.5–1.0 GeV/c																
1.68	0.02897	0.06116	0.00737	-0.00589	0.00217	-0.00245	0.00244	-0.00320	0.01500	-0.01500	0.00253	-0.00253	0.00174	-0.00174	0.01686	-0.01644
1.88	0.08031	0.05700	0.00597	-0.00480	0.00288	-0.00340	0.00219	-0.00244	0.01508	-0.01508	0.00253	-0.00253	0.00201	-0.00200	0.01632	-0.01607
2.09	0.07682	0.04934	0.00356	-0.00299	0.00321	-0.00381	0.00221	-0.00218	0.01517	-0.01517	0.00282	-0.00281	0.00218	-0.00217	0.01572	-0.01573
2.30	0.02844	0.04407	0.00287	-0.00284	0.00343	-0.00388	0.00306	-0.00287	0.01534	-0.01534	0.00313	-0.00314	0.00273	-0.00273	0.01564	-0.01571
2.51	0.05889	0.04121	0.00514	-0.00558	0.00351	-0.00369	0.00341	-0.00331	0.01553	-0.01553	0.00401	-0.00400	0.00325	-0.00325	0.01628	-0.01645
2.72	0.05894	0.03943	0.00787	-0.00888	0.00422	-0.00427	0.00422	-0.00427	0.01583	-0.01584	0.00539	-0.00541	0.00421	-0.00424	0.01750	-0.01799
2.93	0.00788	0.03786	0.00984	-0.01118	0.00502	-0.00497	0.00518	-0.00541	0.01610	-0.01609	0.00588	-0.00585	0.00499	-0.00495	0.01852	-0.01934
3.14	-0.04275	0.03692	0.01066	-0.01213	0.00559	-0.00556	0.00581	-0.00623	0.01629	-0.01629	0.00619	-0.00619	0.00552	-0.00552	0.01899	-0.01998
associate p_T 1.0–2.0 GeV/c																
1.68	0.00117	0.04010	0.00610	-0.00505	0.00119	-0.00125	0.00164	-0.00220	0.00461	-0.00461	0.00109	-0.00109	0.00109	-0.00109	0.00768	-0.00704
1.88	-0.00704	0.03670	0.00512	-0.00426	0.00173	-0.00203	0.00131	-0.00140	0.00467	-0.00467	0.00124	-0.00124	0.00124	-0.00124	0.00693	-0.00643
2.09	0.01090	0.03022	0.00339	-0.00290	0.00207	-0.00245	0.00178	-0.00159	0.00476	-0.00476	0.00145	-0.00145	0.00144	-0.00145	0.00595	-0.00578
2.30	0.04646	0.02838	0.00191	-0.00187	0.00217	-0.00241	0.00272	-0.00222	0.00492	-0.00492	0.00181	-0.00181	0.00180	-0.00180	0.00550	-0.00536
2.51	0.00792	0.02438	0.00282	-0.00302	0.00239	-0.00242	0.00289	-0.00258	0.00518	-0.00518	0.00235	-0.00235	0.00235	-0.00234	0.00569	-0.00566
2.72	0.00610	0.02461	0.00474	-0.00531	0.00338	-0.00339	0.00333	-0.00336	0.00573	-0.00574	0.00334	-0.00337	0.00333	-0.00336	0.00668	-0.00708
2.93	0.00007	0.02339	0.00633	-0.00712	0.00463	-0.00455	0.00444	-0.00460	0.00639	-0.00642	0.00437	-0.00440	0.00435	-0.00438	0.00810	-0.00873
3.14	-0.06407	0.02439	0.00691	-0.00775	0.00514	-0.00497	0.00492	-0.00518	0.00667	-0.00667	0.00475	-0.00475	0.00474	-0.00474	0.00870	-0.00942
associate p_T 2.0–3.0 GeV/c																
1.68	0.01291	0.01254	0.00091	-0.00081	0.00055	-0.00055	0.00058	-0.00062	0.00067	-0.00067	0.00055	-0.00055	0.00055	-0.00055	0.00101	-0.00095
1.88	-0.00680	0.01003	0.00083	-0.00076	0.00059	-0.00061	0.00057	-0.00058	0.00069	-0.00069	0.00057	-0.00057	0.00057	-0.00057	0.00094	-0.00088
2.09	0.01951	0.00940	0.00069	-0.00066	0.00062	-0.00064	0.00061	-0.00059	0.00071	-0.00071	0.00059	-0.00059	0.00058	-0.00058	0.00084	-0.00082
2.30	0.02872	0.00845	0.00072	-0.00072	0.00073	-0.00075	0.00079	-0.00074	0.00082	-0.00082	0.00072	-0.00072	0.00072	-0.00072	0.00090	-0.00088
2.51	-0.00437	0.00749	0.00091	-0.00092	0.00090	-0.00089	0.00093	-0.00090	0.00098	-0.00098	0.00090	-0.00089	0.00089	-0.00089	0.00104	-0.00102
2.72	-0.01021	0.00741	0.00133	-0.00135	0.00126	-0.00126	0.00126	-0.00126	0.00133	-0.00132	0.00126	-0.00126	0.00126	-0.00126	0.00139	-0.00142
2.93	-0.01468	0.00819	0.00191	-0.00195	0.00184	-0.00183	0.00183	-0.00184	0.00187	-0.00188	0.00183	-0.00183	0.00182	-0.00183	0.00197	-0.00202
3.14	-0.05739	0.00919	0.00269	-0.00279	0.00263	-0.00269	0.00262	-0.00271	0.00265	-0.00272	0.00262	-0.00269	0.00262	-0.00269	0.00274	-0.00285
associate p_T 3.0–5.0 GeV/c																
1.68	-0.00114	0.00453	0.00043	-0.00043	0.00042	-0.00043	0.00042	-0.00043	0.00042	-0.00043	0.00042	-0.00043	0.00042	-0.00043	0.00043	-0.00044
1.88	0.00346	0.00363	0.00038	-0.00037	0.00038	-0.00037	0.00038	-0.00037	0.00038	-0.00037	0.00038	-0.00037	0.00038	-0.00037	0.00039	-0.00038
2.09	-0.00401	0.00298	0.00040	-0.00040	0.00040	-0.00040	0.00040	-0.00040	0.00040	-0.00040	0.00040	-0.00040	0.00040	-0.00040	0.00041	-0.00040
2.30	-0.00332	0.00295	0.00048	-0.00051	0.00048	-0.00051	0.00049	-0.00051	0.00049	-0.00051	0.00048	-0.00051	0.00048	-0.00051	0.00049	-0.00051
2.51	-0.00411	0.00290	0.00053	-0.00057	0.00053	-0.00057	0.00053	-0.00057	0.00053	-0.00057	0.00053	-0.00057	0.00053	-0.00057	0.00054	-0.00057
2.72	-0.01226	0.00336	0.00079	-0.00091	0.00079	-0.00091	0.00079	-0.00091	0.00079	-0.00091	0.00080	-0.00091	0.00079	-0.00091	0.00080	-0.00092
2.93	-0.02748	0.00497	0.00130	-0.00158	0.00130	-0.00157	0.00130	-0.00158	0.00130	-0.00158	0.00131	-0.00158	0.00130	-0.00157	0.00131	-0.00159
3.14	-0.03014	0.00643	0.00176	-0.00217	0.00175	-0.00216	0.00175	-0.00216	0.00175	-0.00216	0.00178	-0.00218	0.00175	-0.00216	0.00178	-0.00219
associate p_T 5.0–7.0 GeV/c																
1.68	-0.00233	0.00060	0.00024	-0.00025	0.00024	-0.00025	0.00024	-0.00025	0.00024	-0.00025	0.00024	-0.00025	0.00024	-0.00025	0.00024	-0.00025
1.88	0.00012	0.00147	0.00023	-0.00023	0.00023	-0.00023	0.00023	-0.00023	0.00023	-0.00023	0.00023	-0.00023	0.00023	-0.00023	0.00023	-0.00023
2.09	0.00288	0.00219	0.00024	-0.00025	0.00024	-0.00025	0.00024	-0.00025	0.00024	-0.00025	0.00024	-0.00025	0.00024	-0.00025	0.00024	-0.00025
2.30	0.00032	0.00139	0.00024	-0.00025	0.00024	-0.00025	0.00024	-0.00025	0.00024	-0.00025	0.00024	-0.00025	0.00024	-0.00025	0.00024	-0.00025
2.51	0.00250	0.00183	0.00026	-0.00028	0.00026	-0.00028	0.00026	-0.00028	0.00026	-0.00028	0.00026	-0.00028	0.00026	-0.00028	0.00026	-0.00028
2.72	-0.00057	0.00204	0.00032	-0.00041	0.00032	-0.00041	0.00032	-0.00041	0.00032	-0.00041	0.00033	-0.00041	0.00032	-0.00041	0.00033	-0.00041
2.93	-0.00534	0.00349	0.00046	-0.00069	0.00046	-0.00069	0.00046	-0.00069	0.00046	-0.00069	0.00047	-0.00069	0.00046	-0.00069	0.00047	-0.00069
3.14	-0.01463	0.00478	0.00066	-0.00108	0.00066	-0.00108	0.00066	-0.00108	0.00066	-0.00108	0.00068	-0.00109	0.00066	-0.00108	0.00068	-0.00109

Table 74: 20–40%, trigger p_T 9.0–12.0 Away–side $D_{AA}(\Delta\phi)$

ϕ	$D_{AA}(\Delta\phi)$	σ_{stat}	systematic errors													
			$+\sigma_{f2}$	$-\sigma_{f2}$	$+\sigma_{f3}$	$-\sigma_{f3}$	$+\sigma_{f4}$	$-\sigma_{f4}$	$+\sigma_{\xi/ZYAM}$	$-\sigma_{\xi/ZYAM}$	$+\sigma_{\pi^0}$	$-\sigma_{\pi^0}$	$+\sigma_{pp}$	$-\sigma_{pp}$	$+\sigma_{total}$	$-\sigma_{total}$
associate p_T 0.5–1.0 GeV/c																
1.68	0.11822	0.11685	0.02056	-0.01756	0.00777	-0.01147	0.00370	-0.00384	0.13258	-0.13258	0.00347	-0.00347	0.00342	-0.00342	0.13431	-0.13415
1.88	0.37620	0.11052	0.02365	-0.01955	0.00683	-0.01026	0.00445	-0.00445	0.13295	-0.13295	0.00371	-0.00371	0.00351	-0.00351	0.13515	-0.13471
2.09	0.07429	0.09419	0.02937	-0.02328	0.00696	-0.01015	0.00625	-0.00593	0.13354	-0.13354	0.00434	-0.00434	0.00432	-0.00432	0.13685	-0.13586
2.30	0.45306	0.08691	0.03659	-0.02794	0.00758	-0.01084	0.00731	-0.00678	0.13424	-0.13424	0.00499	-0.00499	0.00472	-0.00472	0.13930	-0.13747
2.51	0.13909	0.07968	0.04427	-0.03296	0.00936	-0.01269	0.00803	-0.00761	0.13500	-0.13500	0.00615	-0.00611	0.00609	-0.00605	0.14222	-0.13936
2.72	0.14367	0.07597	0.05085	-0.03722	0.01076	-0.01442	0.00749	-0.00738	0.13565	-0.13565	0.00658	-0.00658	0.00651	-0.00651	0.14503	-0.14115
2.93	0.14264	0.07343	0.05543	-0.04024	0.01236	-0.01613	0.00787	-0.00789	0.13614	-0.13614	0.00769	-0.00765	0.00760	-0.00757	0.14714	-0.14250
3.14	0.24471	0.07228	0.05706	-0.04134	0.01295	-0.01682	0.00810	-0.00824	0.13632	-0.13632	0.00814	-0.00821	0.00799	-0.00806	0.14792	-0.14301
associate p_T 1.0–2.0 GeV/c																
1.68	-0.06454	0.07673	0.00819	-0.01268	0.00265	-0.00262	0.00295	-0.00323	0.00560	-0.00560	0.00255	-0.00255	0.00252	-0.00253	0.00976	-0.01379
1.88	-0.00439	0.07112	0.00697	-0.01061	0.00337	-0.00323	0.00270	-0.00274	0.00567	-0.00567	0.00265	-0.00265	0.00265	-0.00265	0.00885	-0.01190
2.09	0.02398	0.05884	0.00483	-0.00691	0.00375	-0.00356	0.00294	-0.00286	0.00574	-0.00574	0.00275	-0.00276	0.00273	-0.00273	0.00754	-0.00891
2.30	0.07149	0.05525	0.00331	-0.00347	0.00382	-0.00370	0.00386	-0.00360	0.00602	-0.00602	0.00324	-0.00324	0.00320	-0.00321	0.00679	-0.00666
2.51	-0.06221	0.04717	0.00564	-0.00474	0.00412	-0.00411	0.00442	-0.00427	0.00655	-0.00655	0.00405	-0.00406	0.00405	-0.00405	0.00788	-0.00716
2.72	0.02401	0.04889	0.01025	-0.00785	0.00577	-0.00582	0.00573	-0.00577	0.00773	-0.00775	0.00580	-0.00583	0.00573	-0.00577	0.01154	-0.00949
2.93	-0.01432	0.04640	0.01348	-0.00998	0.00711	-0.00714	0.00696	-0.00699	0.00862	-0.00859	0.00693	-0.00690	0.00686	-0.00683	0.01465	-0.01159
3.14	0.00179	0.04977	0.01516	-0.01144	0.00858	-0.00860	0.00844	-0.00849	0.00979	-0.00973	0.00839	-0.00832	0.00827	-0.00820	0.01634	-0.01309
associate p_T 2.0–3.0 GeV/c																
1.68	-0.01897	0.02244	0.00151	-0.00190	0.00119	-0.00119	0.00121	-0.00123	0.00126	-0.00126	0.00119	-0.00119	0.00118	-0.00118	0.00160	-0.00198
1.88	0.00785	0.01978	0.00136	-0.00166	0.00115	-0.00114	0.00112	-0.00112	0.00120	-0.00120	0.00112	-0.00112	0.00111	-0.00111	0.00146	-0.00174
2.09	-0.00339	0.01727	0.00131	-0.00143	0.00127	-0.00125	0.00123	-0.00123	0.00130	-0.00130	0.00122	-0.00122	0.00122	-0.00122	0.00144	-0.00154
2.30	-0.00211	0.01527	0.00134	-0.00134	0.00136	-0.00136	0.00138	-0.00136	0.00141	-0.00141	0.00134	-0.00133	0.00133	-0.00133	0.00148	-0.00146
2.51	-0.01453	0.01442	0.00167	-0.00163	0.00161	-0.00160	0.00163	-0.00162	0.00167	-0.00166	0.00160	-0.00160	0.00160	-0.00160	0.00176	-0.00171
2.72	-0.03169	0.01417	0.00229	-0.00215	0.00205	-0.00205	0.00205	-0.00205	0.00210	-0.00210	0.00205	-0.00205	0.00205	-0.00205	0.00234	-0.00220
2.93	-0.02931	0.01812	0.00367	-0.00347	0.00340	-0.00337	0.00340	-0.00337	0.00343	-0.00339	0.00342	-0.00338	0.00339	-0.00336	0.00373	-0.00355
3.14	-0.02214	0.01923	0.00411	-0.00394	0.00383	-0.00383	0.00383	-0.00383	0.00385	-0.00385	0.00386	-0.00386	0.00382	-0.00382	0.00419	-0.00403
associate p_T 3.0–5.0 GeV/c																
1.68	0.00083	0.00840	0.00090	-0.00091	0.00089	-0.00089	0.00089	-0.00089	0.00089	-0.00089	0.00089	-0.00089	0.00089	-0.00089	0.00090	-0.00091
1.88	0.00971	0.00797	0.00091	-0.00092	0.00091	-0.00090	0.00090	-0.00090	0.00091	-0.00091	0.00090	-0.00090	0.00090	-0.00090	0.00091	-0.00092
2.09	0.00539	0.00701	0.00093	-0.00094	0.00093	-0.00094	0.00093	-0.00094	0.00093	-0.00094	0.00093	-0.00094	0.00093	-0.00094	0.00093	-0.00094
2.30	0.00023	0.00606	0.00100	-0.00103	0.00100	-0.00103	0.00100	-0.00103	0.00100	-0.00103	0.00100	-0.00103	0.00100	-0.00103	0.00101	-0.00103
2.51	-0.01173	0.00570	0.00111	-0.00116	0.00111	-0.00116	0.00111	-0.00116	0.00111	-0.00116	0.00111	-0.00116	0.00111	-0.00116	0.00111	-0.00116
2.72	-0.01987	0.00794	0.00157	-0.00175	0.00156	-0.00174	0.00156	-0.00174	0.00156	-0.00174	0.00156	-0.00174	0.00156	-0.00174	0.00157	-0.00175
2.93	-0.02241	0.01238	0.00226	-0.00263	0.00225	-0.00263	0.00225	-0.00263	0.00225	-0.00263	0.00225	-0.00263	0.00225	-0.00263	0.00226	-0.00264
3.14	-0.05566	0.01579	0.00319	-0.00382	0.00318	-0.00382	0.00318	-0.00382	0.00318	-0.00382	0.00318	-0.00382	0.00318	-0.00382	0.00319	-0.00382
associate p_T 5.0–7.0 GeV/c																
1.68	0.00310	0.00478	0.00083	-0.00083	0.00083	-0.00083	0.00083	-0.00083	0.00083	-0.00083	0.00083	-0.00083	0.00083	-0.00083	0.00083	-0.00083
1.88	-0.00474	0.00435	0.00089	-0.00093	0.00089	-0.00093	0.00089	-0.00093	0.00089	-0.00093	0.00089	-0.00093	0.00089	-0.00093	0.00089	-0.00093
2.09	0.00362	0.00466	0.00085	-0.00086	0.00085	-0.00086	0.00085	-0.00086	0.00085	-0.00086	0.00085	-0.00086	0.00085	-0.00086	0.00085	-0.00086
2.30	0.00256	0.00321	0.00083	-0.00083	0.00083	-0.00083	0.00083	-0.00083	0.00083	-0.00083	0.00083	-0.00083	0.00083	-0.00083	0.00083	-0.00083
2.51	-0.00238	0.00369	0.00091	-0.00098	0.00091	-0.00098	0.00091	-0.00098	0.00091	-0.00098	0.00091	-0.00098	0.00091	-0.00098	0.00091	-0.00098
2.72	0.00899	0.00621	0.00097	-0.00110	0.00097	-0.00110	0.00097	-0.00110	0.00097	-0.00110	0.00097	-0.00110	0.00097	-0.00110	0.00097	-0.00110
2.93	-0.00239	0.00748	0.00114	-0.00140	0.00113	-0.00140	0.00113	-0.00140	0.00113	-0.00140	0.00114	-0.00140	0.00113	-0.00140	0.00114	-0.00140
3.14	-0.04134	0.02371	0.00204	-0.00312	0.00204	-0.00312	0.00204	-0.00312	0.00204	-0.00312	0.00204	-0.00312	0.00204	-0.00312	0.00204	-0.00312

K Data Table: Direct photon D_{AA} vs. $\Delta\phi$

$\Delta\phi$	D_{AA}	$\pm\sigma^{Stat}$	$\pm\sigma^{Sys}$
1.727	-0.0290514	0.0283025	0.049952
2.041	0.0815407	0.0343543	0.0410123
2.355	-0.00180095	0.0499545	0.0283371
2.669	-0.0245236	0.0492332	0.038112
2.983	-0.0951037	0.0358327	0.0544749

Table 75: D_{AA} vs. $\Delta\phi$ data points for $2 < \xi < 2.4$

$\Delta\phi$	D_{AA}	$\pm\sigma^{Stat}$	$\pm\sigma^{Sys}$
1.727	0.0234591	0.0161722	0.0313316
2.041	0.0852486	0.0230786	0.0271213
2.355	0.0386012	0.0321749	0.0188682
2.669	0.0266235	0.0299872	0.0262798
2.983	-0.00594106	0.0220763	0.0368902

Table 76: D_{AA} vs. $\Delta\phi$ data points for $1.6 < \xi < 2$

$\Delta\phi$	D_{AA}	$\pm\sigma^{Stat}$	$\pm\sigma^{Sys}$
1.727	0.0383709	0.0126072	0.0146818
2.041	0.0111165	0.0140437	0.0126074
2.355	0.00819576	0.0193102	0.0134055
2.669	-0.00224209	0.0207473	0.0146859
2.983	-0.00179446	0.0134086	0.0186718

Table 77: D_{AA} vs. $\Delta\phi$ data points for $1.2 < \xi < 1.6$

$\Delta\phi$	D_{AA}	$\pm\sigma^{Stat}$	$\pm\sigma^{Sys}$
1.727	0.00451746	0.00559099	0.00559099
2.041	0.0186738	0.00698476	0.00464587
2.355	-0.00555534	0.0116307	0.00325274
2.669	-0.000526201	0.0116469	0.00698714
2.983	-0.0188596	0.00791502	0.0088434

Table 78: D_{AA} vs. $\Delta\phi$ data points for $0.8 < \xi < 1.2$

$\Delta\phi$	D_{AA}	$\pm\sigma^{Stat}$	$\pm\sigma^{Sys}$
1.727	-0.00335354	0.00139599	0.00139599
2.041	0.00173341	0.00306826	0.00111971
2.355	-0.005172	0.0030683	0.00167237
2.669	-0.00895746	0.0038972	0.00168725
2.983	-0.0132129	0.00277788	0.00306861

Table 79: D_{AA} vs. $\Delta\phi$ data points for $0.4 < \xi < 0.8$

$\Delta\phi$	D_{AA}	$\pm\sigma^{Stat}$	$\pm\sigma^{Sys}$
1.727	-0.00187763	0.00112945	0.00112761
2.041	-0.000662702	0.000753583	0.0011313
2.355	-0.00103762	0.00169694	0.00113682
2.669	-0.00258071	0.00169879	0.00169695
2.983	-0.00529007	0.00150905	0.00188495

Table 80: D_{AA} vs. $\Delta\phi$ data points for $0.0 < \xi < 0.4$